SYNTHETIC APPROACHES TO NOVEL (OXA)CAGES FROM A POLYCYCLIC HYDROCARBON FRAMEWORK

by

Matthew James Faussett

A thesis submitted to the faculty of
The University of North Carolina at Charlotte
in partial fulfillment of the requirements
for the degree of Master of Science in
Chemistry

Charlotte

2022

Approved by:

_____
Dr. Markus Etzkorn

_____
Dr. Christopher Bejger

_____
Dr. Daniel Rabinovich

_____
Dr. Richard Chi

©2022

Matthew James Faussett

ALL RIGHTS RESERVED

ABSTRACT

MATTHEW JAMES FAUSSETT. Synthetic Approaches to Novel (Oxa)cages From a Polycyclic Hydrocarbon Framework. (Under the direction of MARKUS ETZKORN)

Organic cage chemistry, an incredibly diverse sect of organic synthesis, has always intrigued chemists to push the limits of synthetic knowledge, to explore novel structural elements, and to understand unique reactivity patterns. Organic cage compounds containing oxygen heteroatoms, known as oxacages, have been routinely investigated since the late 1990s as potential analogs to the highly researched crown ethers (and other cryptands) for use in molecular recognition. Crown ethers and cryptands are well known for their exceptional metal-chelation capacity and high affinity for specific metal ions. Oxacages, however, are expected to display different binding patterns and greater selectivity towards specific ions due to being more conformationally ridged.

The cage diene **1** is a literature known compound that was initially proposed as a model compound for the elusive bishomohexaprismane **10**. Further investigation into this scaffold lead some researchers to probe **1** as a building block for the tetraoxacage **183**. While initial attempts to prepare **183** through ozonolysis failed, we recognize the potential synthetic value of diene **1**. Utilizing selected functionalization methods, we attempted to prepare tetraoxacage **183** through a multi-step linear synthesis. This would avoid the issues cited with the initial ozonolysis and also provide access to many novel scaffolds that may prove useful in synthesizing other unique and elusive compounds. The preparation of a variety of hydrocarbon, halogenated, and oxygen-containing cages is detailed herein. Utilizing well understood methods such as carbene addition,

epoxidation, and *cis*-dihydroxylation, we prepared multiple novel scaffolds for further investigation into the effects of functionalization on cage systems. These scaffolds were also prepared as potential precursors to elusive and highly sought-after systems such as tetraoxacage **183**. We also utilized acid catalyzed rearrangements of prepared hydrocarbons and epoxides to target novel scaffolds such as the norpentaasterane **126** and investigated the interesting mechanisms observed.

ACKNOWLEDGEMENTS

Chemistry is not an endeavor of individuals. All the work done and that will ever be done is built upon the foundations that others laid before us. As such, many people helped me along the way giving guidance, teaching me the fundamentals of science, and occasionally to just bounce ideas off of. I first must acknowledge my mentor and advisor Dr. Markus Etzkorn who truly guided me to be the best I could and pushed me to excel whenever he could. I would also like to acknowledge many of the UNC Charlotte faculty who were invaluable in their assistance with many of the analytical techniques employed herein: Dr. Cliff Carlin, Dr. Jon Merkert, Dr. Michael Murphy, and Dr. Adam Fessler for their assistance with NMR and GC/MS techniques and Dr. Schmedake for his assistance with X-ray crystallography. I would also like to acknowledge Dr. Michael Gerken of the University of Lethbridge in Canada for his assistance with X-ray crystallography. Finally, I would like to acknowledge Dr. Thomas D. Walsh and the Walsh Graduate Research Fellowship. This fellowship was offered to all chemistry masters students at UNC Charlotte in which participants competed with a presentation on their research to a committee. One student is then selected for the fellowship and provided a research assistanceship. I was fortunate to be able to compete in this competition and was selected as a finalist and the winner of the fellowship in 2020. This allowed for me to pursue much of the interesting chemistry discussed below.

DEDICATION

To the best writing partners I could ask for

Marigold, Moose, and Muppet

And

To the ones who kept me going

TABLE OF CONTENTS

LIST OF TABLES

LIST OF FIGURES

LIST OF ABBREVIATIONS

9-BBN	9-Borabicyclo[3.3.1]nonane
ACN	Acetonitrile
BzBr	Benzyl Bromide
COD	Cyclooctadiene
COSY	Correlation Spectroscopy
COT	Cyclooctatetraene
DCM	Dichloromethane
DMSO	Dimethyl sulfoxide
Ea	Activation Energy
EtOAc	Ethyl Acetate
EtOH	Ethanol
FVP	Flash Vacuum Pyrolysis
GC/MS	Gas Chromatography/Mass spectrometry
HF*Py	Polyhydrogen Fluoride Pyridine
HMBC	Heteronuclear Multiple Bond Correlation
HMPA	*N*-(2-hydroxypropyl)methacrylamide
HMQC	Heteronuclear Multiple Quantum Coherence
IR	Infrared
LAH	Lithium Aluminum Hydride
MCPBA	*meta*-Chloroperoxybenzoic Acid
Me_3NO	Trimethylamine *N*-oxide
MeOH	Methanol

NMO	*N*-methylmorpholine *N*-oxide
NMR	Nuclear magnetic Resonance
Pd/C	Palladium on Carbon
Pt/C	Platinum on Carbon
PTC	Phase-Transfer Catalyst
SiO_2	Silicon Dioxide/Silica Gel
^{t}BuOH	*tert*-Butanol
TEBA-Cl	Triethylbenzylammonium Chloride
TFAA	Trifluoroacetic Anhydride
THF	Tetrahydrofuran
TLC	Thin-layer Chromatography
TMS	Tetramethylsilane
$TMSCF_3$	Trimethyl(trifluoromethyl)silane
TMSI	Trimethylsilyl Iodide
tROSEY	Transverse Relaxation Optimized Spectroscopy
ω	Dihedral angle
XRD	X-ray Diffraction

LIST OF EQUATIONS

1 INTRODUCTION

Organic cage compounds are structurally rigid polycyclic scaffolds. This rigidity often gives this class of compounds unique structural features and large amounts of inherent strain energy.[1, 2] Exploiting these structural moieties can often be challenging, but rewards with greater understanding of the fundamentals of chemistry; information on the impact on strain energy, electronic structure, transannular interactions, and reactivity.[1, 2] Cage compounds can also provide significant synthetic challenges for organic chemists as standard methods for functionalization and transformations often result in unexpected results with new methods needing be developed for even some well-established methods. Cage dienes, such as **1** (*Figure 1, pg. 1*) allow for a range of different chemistry to be explored due to the inherent reactivity of the cage scaffold and the two olefin units providing multiple reactivity sites.[3]

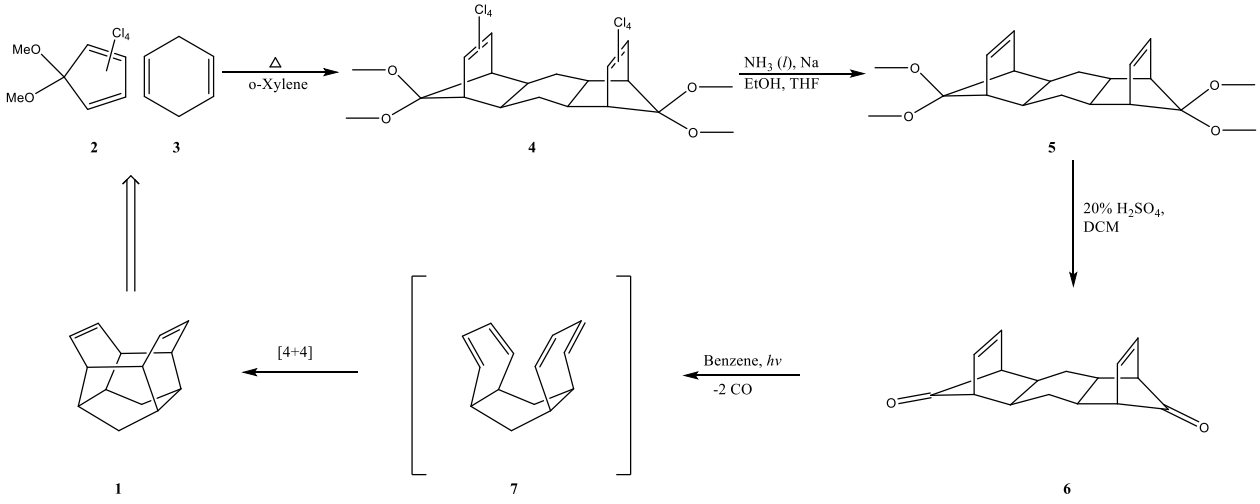

*Figure 1: The synthesis of **1**: 1) two-fold Diels-Alder with inverse electron demand. 2) Birch-type dehalogenation. 3) Deprotection. 4) [4+4] photocyclization.*

The cage diene **1** is a literature known compound prepared over four steps from the commercially available starting materials tetrachlorocyclopentadienone dimethyl ketal **2** and 1,4-

cyclopenatdiene **3** (*Figure 1, pg. 7*).[3] The preparation of octochloro-bisketal **4** proceeds through a two-fold Diels-Alder reaction with inverse electron demand due to the four halogens of the tetrachlorocyclopentadienone. Dienophile **3** is relatively electron rich when compared to the diene **2** which is electron poor switching the typical electron demands of a Diels-Alder reaction. Unsurprisingly, significantly worse yields of the octochloroketal **4** were observed when using shorter reaction times due to the dienophile having less electron density after the first addition. The inductive effect of the chlorines removes significant electron density from dienophile **3** resulting in slower conversion.[3] The dehalogenation of **4** can be accomplished *via* a Birch-type dehalogenation. This reaction, done with liquid ammonia, sodium metal, and ethanol (EtOH) as a proton source results in the protected species **5**.[3] Alternatively, this transformation can be carried out *via* a Gassmann dehalogenation. This method uses sodium metal and *tert*-butanol (^{t}BuOH) as a proton source in tetrahydrofuran (THF) at reflux to afford **5**.[4] Deprotection of the ketal by acid hydrolysis yields the dione **6**. This biphasic reaction was performed in dichloromethane (DCM) with 30% sulfuric acid (H_2SO_4) as a heterogenous mixture (time was dependent on scale and mixing efficiency). Finally, a [4+4] photocyclization was utilized to obtain the diene **1**. Mechanistically, this reaction begins with a photochemical two-fold decarbonylation to give tetraene **7** as a reactive intermediate. The two-fold extrusion of carbon monoxide is imperative to generating the tetraene **7**. This tetraene undergoes a [4+4] photocyclization to give the diene **1**.[3]

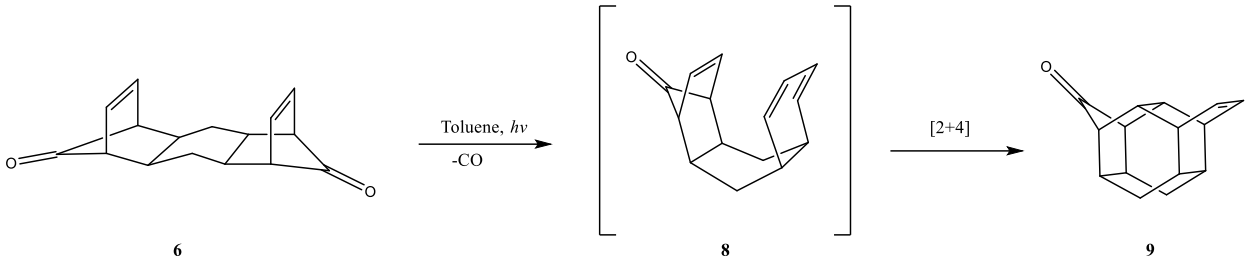

*Figure 2: The single decarbonylating of **6** was observed in toluene to give **9**.*

When the photochemical reaction is done using toluene as the solvent instead of benzene only the single decarbonylating was observed to the keto-olefin compound **9**. This was also observed under thermal activation conditions (200 °C neat or solution in toluene, sealed tube).[3]

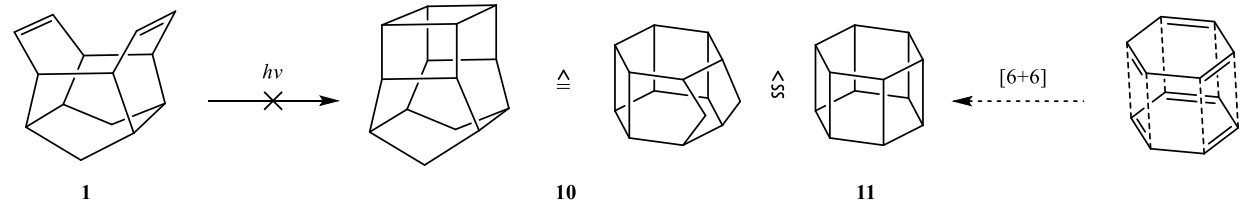

*Figure 3: The [2+2] photocyclization of **1** to the bishomohexaprismane **10** failed. The compound **10** was proposed as a model compound for **11**, a formal [6+6] dimer of benzene.*

Cage compound **1** was initially synthesized a potential precursor to the bishomohexaprismane **10** *via* the [2+2] photocyclization of the olefin units. This approach was not successful as the dihedral angle ($\omega > 105°$) is not favorable. In addition, as the final step in the preparation of **1** is a photochemical reaction, if this [2+2] was possible, the fully cyclized product **10** should have been available from the photoreaction used to obtain the cage **1**.[3] Bishomohexaprismane **10** was proposed as a model compound for the elusive hexaprismane **11**, the formal [6+6] dimer of benzene.[5, 6] Hexaprismane **11** is proposed to exhibit large amounts of

inherent strain energy making it a desirable scaffold to preparative organic chemists and material science.[2, 5]

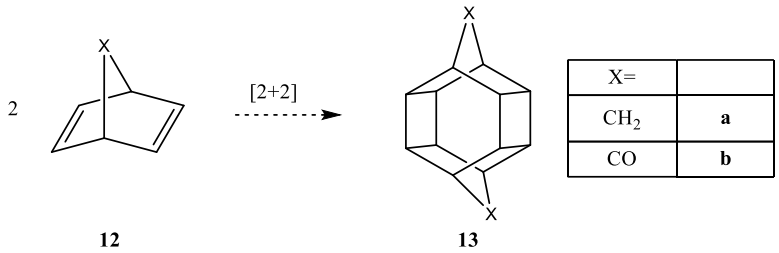

*Figure 4: Garudane **13a**, a true face-to-face dimer of norbornadiene, and Bishomohexaprismanedione **13b**, a dimer of norbornadieneone.*[7-9]

Other bishomohexaprismanes and equivalent scaffolds are known. Garudane, **13a**, is another bishomohexaprismane with a different connectivity to the proposed **10**.[7] Garudane differs form **10** as it can also be envisioned as a norbornadiene dimer, a transformation that is disfavored entropically as well as increasing in strain energy.[7] The ΔE_{strain} of norbornadiene to **13a** is +118.9 kJ/mol, a significant increase in strain energy.[10] The diketone derivative **13b** was also synthesized as the face-to-face dimer of norbornadieneone.[8, 9]

$$\mathbf{13a}\ E_{strain} - 2 * \mathbf{12a}\ E_{strain} = \Delta E_{strain}$$
$$389.12 - (2 * 135.1) = +118.9$$

*Equation 1: Calculation of ΔE_{strain} for the dimerization of **12a**. E_{strain} of **13a** was calculated by MM-2 calculatoins.*[7] *E_{strain} of **12a** was calculated by DFT calculations using a three-parameter hybrid functional combined with B3LYP functional and 6-31G(d) basis set.*[10]

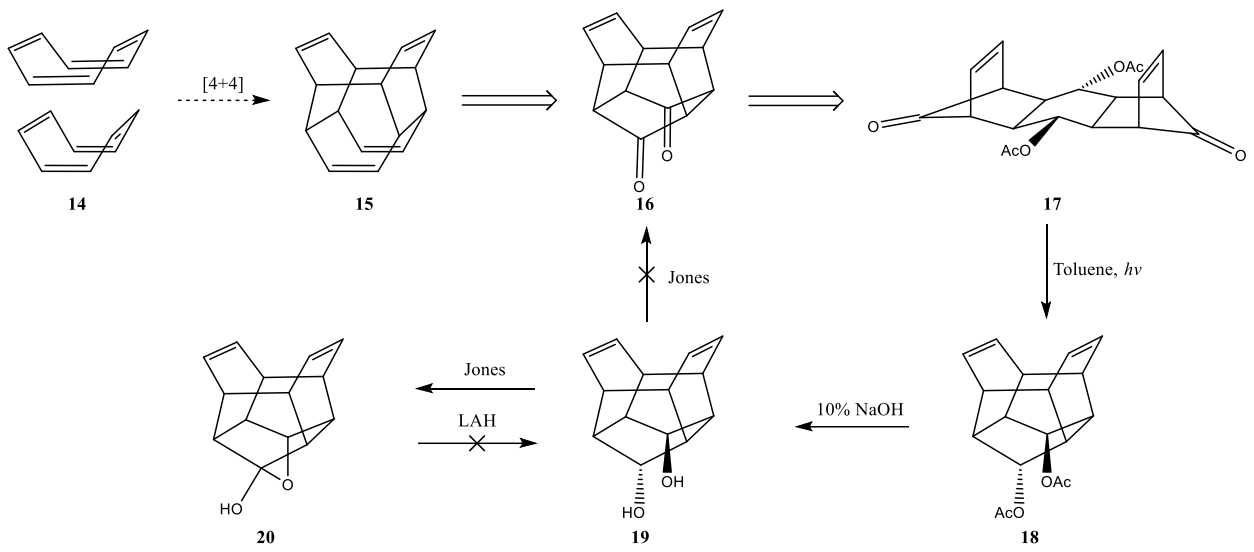

*Figure 5: Attempted synthesis of **16**, a potential precursor to the COT dimer **15**.*[4]

Scaffolds similar to diene **1** have been targeted as potential precursors to other elusive species. The diketone cage **16** was targeted as a way to access the tetraene **15**, the formal [4+4] dimer of cyclooctatetraene (COT) (*Figure 5, pg. 5*).[4] The diacetate species **17** was subjected to [4+4] photocyclization yielding the protected cage diene **18** with comparable success to the parent diene **1**.[3, 4] Deprotection by acid hydrolysis of diacetate protected cage diene **18** yielded the diol cage **19**. Diol cage **19** was then oxidized but did not deliver dione **16**. When subjected to Jones oxidation in acetone rapid oxidation followed by transannular reaction resulted in the hemiacetal **20**. Interestingly, **20**, was observed to be highly stable and could not be reduced with lithium aluminum hydride (LAH).[4]

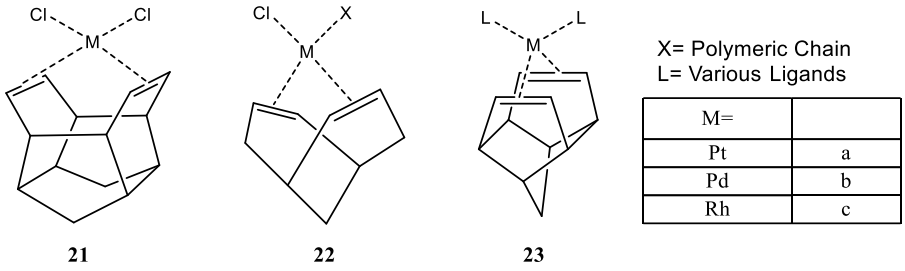

Figure 6: Known metal complexes of cage (and cage-like) compounds with COD subunits.[11-13]

Cage diene **1** has also been used as a metal complexing ligand (*Figure 6, pg. 6*).[11] This chemistry exploited the internal cyclooctadiene (COD) subunit of **1**. While metal complexes of COD are extremely common, very few examples of metal complexes of COD moieties within cage compounds are known. Metal complexes of bicyclononadiene **22**, a cage-like polycyclic compound with an internal COD unit, and the cage diene homohypostrophene **23** (**23** for metal complex, **76** for hydrocarbon) are the only cage-like compounds with metal complexes known (*Figure 6, pg. 6*).[12, 13]

2 RESEARCH GOALS

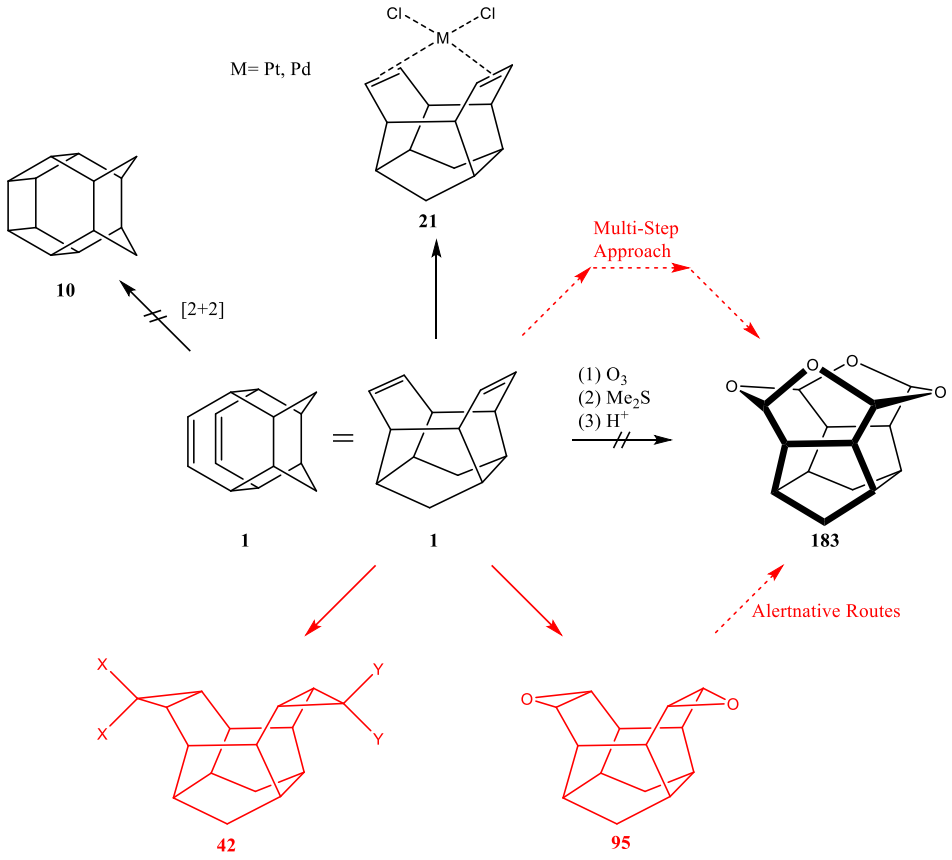

*Figure 7: General outline of thesis work (red) and known chemistry of diene **1**.*

2.1 Carbene Chemistry of Cage Compounds

Previously in the Etzkorn group the dichlorocarbene adducts **40c** and **41c** as well as the cyclopropane adducts **40a** and **41a** were prepared but not fully characterized (*Figure 15, pg. 17*). Full analytical data and x-ray crystallography data was obtained for these compounds as well as many other carbene adducts. Structural analysis was completed on several organic cages were single crystals suitable for X-ray diffraction (XRD) were obtained. Utilizing simple carbene generation reactions a large library of compounds was developed. Several patterns related to the molecular structure of these compounds were observed such as several compounds sharing identical point groups, space groups, and unit cells.

2.2 Preparation of Cage Hydrocarbons and Oxacages *Via* Rearrangement of Cage Scaffolds

Initial investigations into the viability of the epoxides **94**, **95**, and **96** (*Figure 60, pg. 83*) as precursors to the oxacage **183** (*Figure 7, pg. 7; Figure 108, pg. 146*) lead to the observation of acid catalyzed rearrangements of the epoxides. This same principle was then applied to other scaffolds such as diene **1** to investigate their lability in the presence of Brønsted acids. While the initial probing did not lead to compounds that could be utilized to prepare **183**, several compounds of unique and interesting structure were obtained. The rearrangements observed on these scaffolds were propagated using the sulfonic acid catalyst, Amberlyst-15. Several hydrocarbon cages and oxacage compounds were obtained from these acid catalyzed rearrangements and structures elucidated for characterization (sometimes from enriched material). Once structures were determined the mechanism for several products was elucidated with calculational support for the proposed mechanisms. The same mechanism was observed in the formation of at least one stable intermediate for each epoxide rearrangement and relied on a series of complex transannular reactions.

2.3 Multistep Synthetic Approach Towards the Preparation of a Novel Tetraoxacage

In an attempt to circumvent issues with well-established ozonolysis protocols for the development of oxacages, a multistep pathway towards the target tetraoxacage **183** was investigated. Ozonolysis of **1** resulted in failure to obtain the oxacage **183**. The cited reasons for this were due to the unfavorable formation of the two seven-membered ring acetals and the relative stereochemistry of the suspected tetraaldehyde intermediate. One of the main issues with this approach is the various equilibrium-driven reactions. The formation of primary and secondary ozonide as well as the cleavage of the ozonide to the aldehyde species are equilibrium driven. In addition, formation of the acetal units *via* acid treatment is also equilibrium driven. To combat the

issues of equilibrium driven reactions, we propose several stepwise strategies from diene **1** towards **183** utilizing a variety of oxidation techniques. Our approaches towards tetraoxacage **183** take advantage of the diene structure of **1**. Using methods such as *cis*-dihydroxylation, epoxidation (mentioned above), and others to introduce alcohol (oxygen) functionality we sought to oxidatively cleave these moieties or oxidize to higher oxidation state species as precursors to **183**. Once obtained the tetraoxacage **183** will be investigated for its affinity in metal complexation and potential for applications in materials and/or medicinal chemistry.

3 DISCUSSION

3.1 Preparation of Cage Diene **1** and Model Compounds

The preparation of the cage diene **1** proceeded similarly to descriptions in the literature (*Figure 1, pg. 1*).[3] Some minor alterations to rection conditions were needed to improve rate of reaction and yield. For instance, the Gassmann dehalogenation protocol was observed to be less effective than the Birch-type reduction.[3, 4] Under Gassmann conditions, significantly more partial dehalogenation products were observed by ^{1}H-NMR and GC/MS. In addition, deprotection of **5** to the bis ketone **6** was accomplished with 30% H_2SO_4 in DCM over five days rather than reported 20% H_2SO_4 for 16 hours. Reaction time occasionally varied due to the scale of the reaction (2g versus 5+g). As a heterogenous reaction, the physical properties of the reaction such as efficient stirring became very important.

To obtain the partially saturated cage **24** as a model compound, the diene **1** was subjected to hydrogenation yielding a mixture of monoene **24** and fully saturated cage **25**; hydrogen gas and a platinum (or palladium) catalyst or diimide reduction were both viable methods.

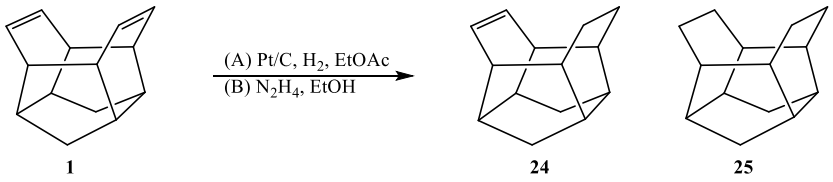

*Figure 8: Compounds **24** and **25** were prepared by the hydrogenation of **1**.*

While this reaction proceeded smoothly under both conditions, separation of the products proved challenging. Purification by repeated column chromatography (SiO_2, *n*-pentane) was ineffective at fully separating **24** and **25**. Reverse phase column chromatography (Si-C_{18}, MeOH gradient)

was also ineffective (at full separation). Peak shaving allowed for the isolation of an enriched 4:1 mixture of **24**/**25** (all chemistry of the monoene **24** was done on this mixture).

3.2 Carbene Chemistry of Cage Compounds

3.2.1 Introduction of Carbene Chemistry in Polycyclic Systems

Carbenes are highly reactive neutral carbon species that contain two valence electrons and exist in either a singlet or triplet state. Singlet carbenes have two spin-paired electrons while triplet carbenes have two spin-unpaired electrons in orthogonal orbitals.[14] The mechanism of the addition reactions of carbenes to alkenes is dependent on this structure. Reactions of singlet carbenes are stereospecific, reacting *via* a concerted, cyclic transition state, while triplet carbenes react stereoselectivly in a multistep sequence *via* radical-like intermediates. This is due to the diradical character of triplet carbenes and may result in the *cis* or *trans* product(s) (*Figure 9, pg. 11*).[15, 16]

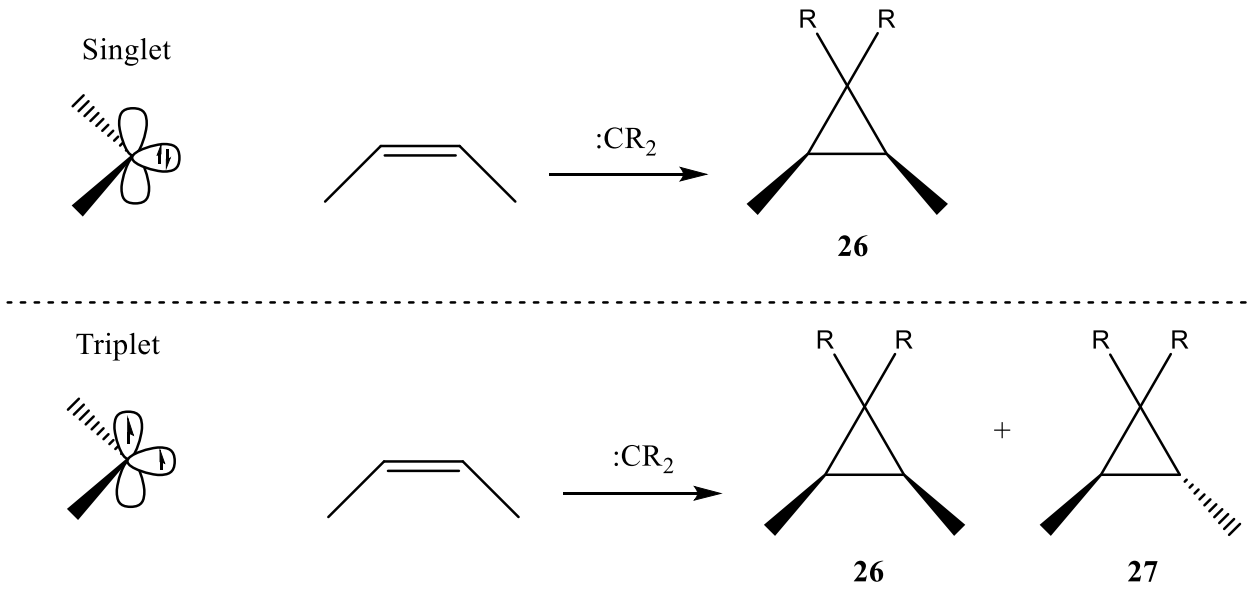

Figure 9: Orbital diagram and reactivity differences in singlet versus triplet carbenes.

Depending on the substituent pattern, triplet carbenes are often more stable than the singlet carbenes; such is the case for methylene carbene.[17, 18] However, when halides are bound to the divalent carbon the halides provide stabilization to the singlet state (

Table 1, pg. 12). Dihalocarbenes primarily exist as singlet carbenes (although can exist as triplet carbenes under certain circumstances), and the specific halide has a large impact on reactivity.[18] Difluorocarbene exhibits high stabilization of the singlet state giving it diminished reactivity towards addition reactions with electron deficient substraits.[19] Diiodocarbene has the lowest singlet state stabilization giving it occasionally uncontrollable reactivity towards both addition and insertion reactions.[18, 20] Diiodocarbene has the smallest singlet-triplet gap and is closest in energy to methylene carbene.[21] Dichlorocarbene and dibromocarbene both show moderate stabilization, with dibromocarbene being more reactive towards cheletropic addition and insertion reactions.[18, 20]

Table 1: Singlet-Triplet energy gaps for methylene (carbene) and the four dihalocarbenes. The energy gap of :CH_2 carbene was determined experiemtnaly.[21] The energy gap of :CF_2 carbene was calculated using ab initio methods (CCSD(T) level and triple- and quadruple-zeta basis sets). The energies of heavier dihalocarbenes were calculated using DTF calculations with multiple basis sets (e.g., CCSD(T) and B3LYP).[18]

Carbene	S-T gap (kJ/mol)		
:CH_2	-37.86	±	0.25
:CF_2	225.9	±	12.5
:CCl_2	83.7	±	4.2
:CBr_2	71.1	±	8.4

$:CI_2$	37.7	±	8.4

Carbene reactions have been performed on several cage(-like) dienes in the literature, but the libraries of compounds are limited, and little structural information can be gleaned.[22-26]

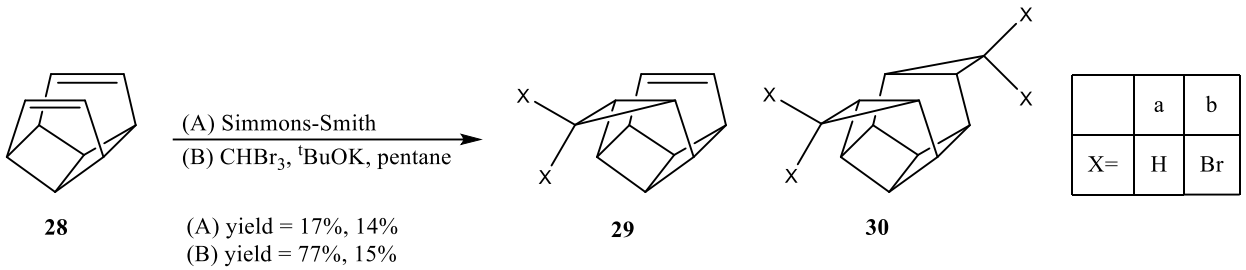

*Figure 10: Cyclopropanation of the cage diene hypostrophene **28**. (A) Simmons-Smith cyclopropanation. (B) dibromocarbene addition. Both approaches give a mixture of the one- and two-fold addition products of **28**.* [22]

One example of carbene addition and cyclopropanation of a cage compound is the synthesis of **29** and **30** (*Figure 10, pg. 13*). The dibromocarbene addition of hypostrophene **28** was carried out using potassium *tert*-butoxide and bromoform in pentane at -30 °C. This resulted in a product mixture of 77% **29b** and 15% **30b** (92% conversion, 8% **28** recovered by sublimation). The cyclopropane adducts were obtained through dehalogenation of the dibromo adducts or by Simmons-Smith cyclopropanation. It was observed that better yields of **29a** could be obtained by Gassmann dehalogenation of **29b** versus direct cyclopropanation to **29a** (76% versus 17%). This is likely due to the cyclopropanation resulting in a product mixture of **29a** and **30a**. Similarities in the physicochemical properties and polarity may result in issues with purification by chromatography, recrystallization, or sublimation. There were no reports of significant side product formation in these reactions.[22]

In addition to the typical carbene addition, carbenes are also known to undergo C-H and C-C bond insertion reactions.[16, 27-32] C-H bond insertion on cage systems has been reported for compounds such as adamantane **31** and dodecahedrane **33** (*Figure 11, pg. 14*).[31]

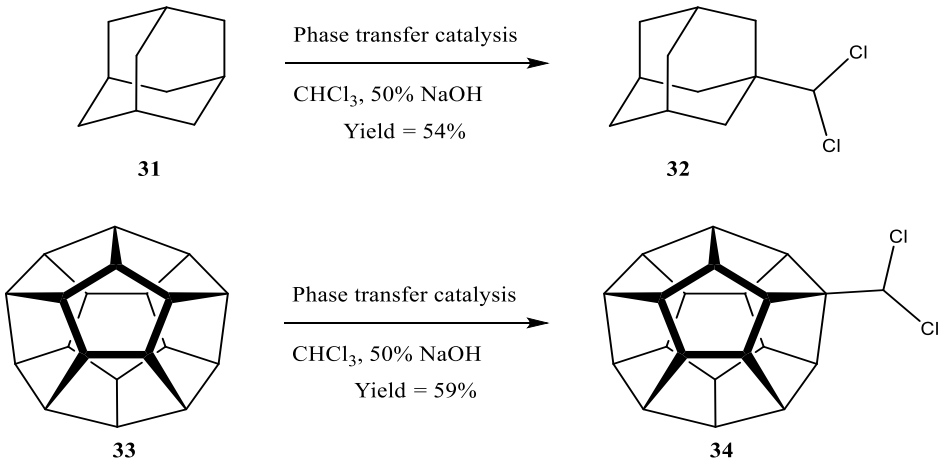

*Figure 11: C-H insertion reactions on cage systems adamantane and dodecahedrane under phase transfer conditions yielding **32** and **34**.*[31]

C-H insertion shows a high degree of regioselectivity towards tertiary positions and α-C-H bonds of ethers.[30] It has been shown that the more reactive methylene carbene has a 7:1 ratio of selectivity towards bridgehead insertion versus secondary bridge positions. This ratio expands to nearly infinite selectivity for bridgehead positions with dichlorocarbene on scaffolds like adamantane and similarly high selectivity for diamantane.[27, 29, 30] C-H insertion of dichlorocarbene (and partly dibromocarbene) is highly favored over C-C bond insertion due to the transition state and electrophilic character of the carbene (*Figure 12, pg. 15*).

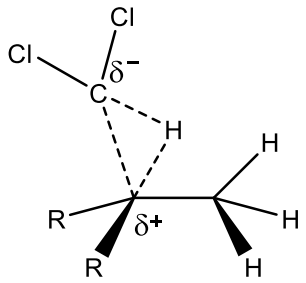

Figure 12: Transition state of C-H insertion by dichlorocarbene.[30]

In select polycyclic structures containing cyclopropane rings the degree of overlap of the delocalized Walsh orbitals has been shown to have a drastic effect on the regioselectivity of dihalocarbene insertion (*Figure 13, pg. 15*).[16, 31] A variety of polycyclic substrates have demonstrated that dichlorocarbene and dibromocarbene selectively insert into the C-H bonds adjacent to three-membered rings under phase-transfer conditoins.[16] In this scenario the electron donating Walsh orbitals stabilize the partial positive charge of the transition state and stabilizes the carbenium ion.

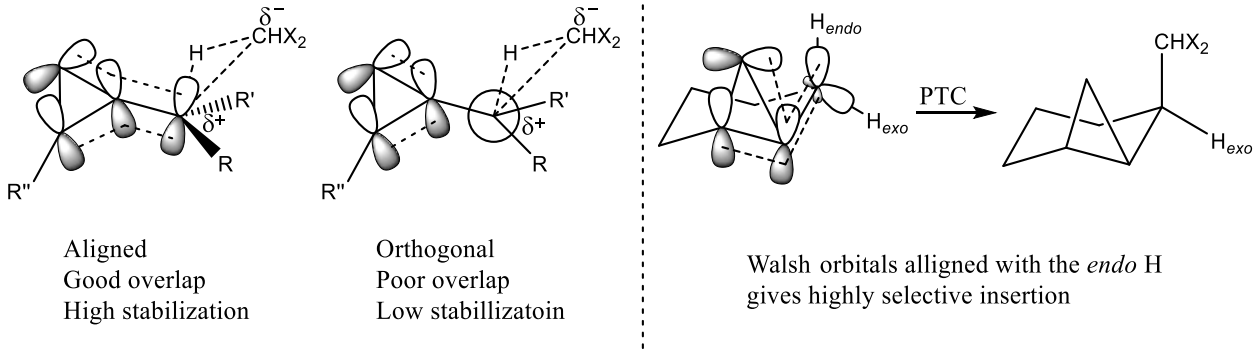

Figure 13: In bicyclic systems the bisected alignment provides stabilization to the carbenium transition state and high selectivity.[16, 31]

When the orbitals of the cyclopropane and the empty p orbital of the carbenium ion are aligned in a bisected conformation, the Walsh orbitals provide sufficient stabilization to act as a directing

group. It is only in this bisected alignment where significant directing effects were observed (*Figure 13, pg. 15*). Investigations into a variety of substrates revealed that when the orbitals are not in alignment the directing effect is non-existent and only low yields of insertion products were observed.[16, 31] The product distribution of *endo* and *exo* insertion was dependent on the degree of overlap based on the geometry of the substrate.[31]

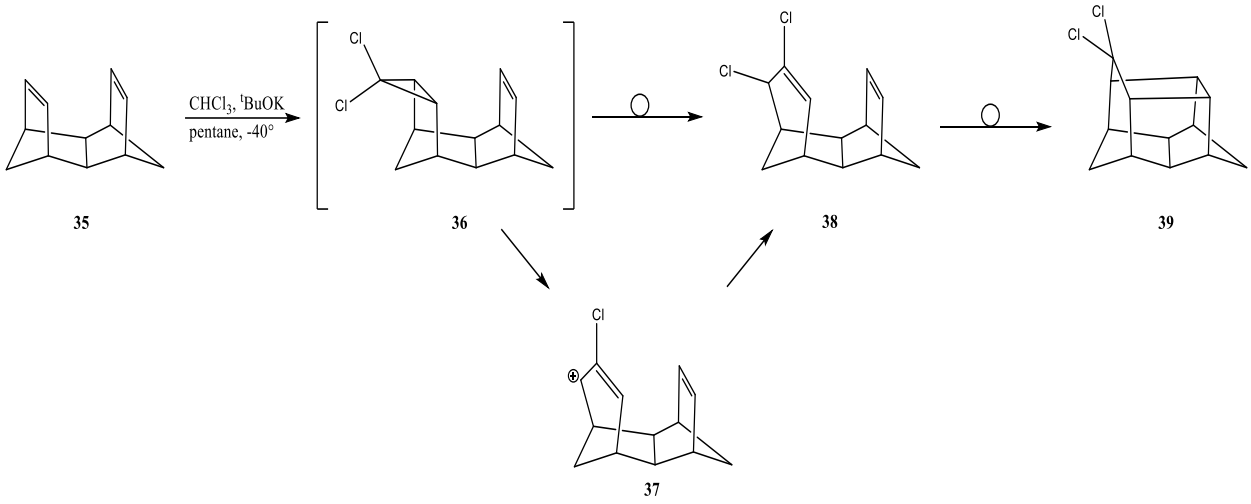

*Figure 14: Dichlorocarbene addition to the isodrin-derived scaffold, **35**. Rapid rearrangement through the allylic cation **37** gives **38** which in turn will decompose into cage compound **39**.*[24]

Under certain conditions, cyclopropanes can undergo ring-expansion in polycyclic systems.[24] To cleave the cyclopropane, typically heat and another reagent are needed, so the solvolysis would not likely occur under typically mild phase transfer conditions.[33, 34] In select cases opening can occur on highly strained systems where ring opening reactions are favorable. Dichlorocarbene addition was attempted on the polycyclic, isodrin-derived diene, **35** (*Figure 14, pg. 16*).[24] The reaction was carried out with potassium *tert*-butoxide and chloroform in pentane at -40 °C. This resulted in a compound different from the desired dihalocyclopropane **36**. The compound obtained, **38** ,was proposed to form by the ring expansion *via* the corresponding allylic

cation. This material was extremely unstable and readily rearranged to **39** making characterization of the intermediate and the carbene adduct impossible. This is an example of an unstable carbene adduct resulting in a ring-expansion without forcing conditions.[24]

3.2.2 Synthetic Outline

To expand the current library and investigate structural variations in cage systems, a series of carbene addition products were prepared from the diene **1** and the corresponding monoene, **24**.

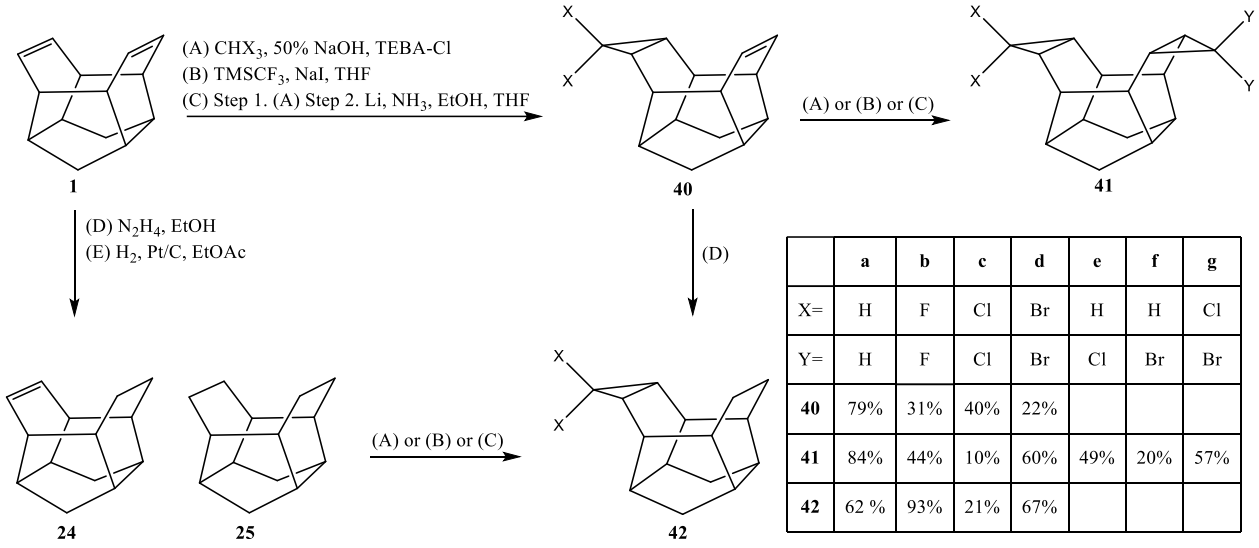

	a	b	c	d	e	f	g
X=	H	F	Cl	Br	H	H	Cl
Y=	H	F	Cl	Br	Cl	Br	Br
40	79%	31%	40%	22%			
41	84%	44%	10%	60%	49%	20%	57%
42	62 %	93%	21%	67%			

*Figure 15: Synthesis of carbene adducts **40a-d**, **41a-g**, and **42a-d**. Carbene adducts were synthesized along three protocols: (A) phase-transfer catalysis, (B) difluorocarbene generation from $TMSCF_3$, (C) Birch-type dehalogenation. Hydrogenation was used to obtain **24** as a precursor of **42a-d** or from **40a-d** using two methods: (D) alkene reduction by diimide, (E) hydrogenation by platinum catalyst.*

3.2.2.1 Synthesis of Cyclopropane Adducts of Cage Diene **1**

Cyclopropane adducts **40a, 41a,** and **42a** were obtained *via* Birch-type dehalogenation (*liq.* NH_3, Li, EtOH, -78 °C) of the respective dichlorocarbene adducts, **40c, 41c,** and **42c** (*Figure 15,*

pg. 17). Cyclopropanation can be achieved through methods such as the Simmons-Smith reaction or 1,3-dipolar cycloaddition of diazo compounds. While these methods have benefits, they also have significant drawbacks related to the diene **1**. The Simmons-Smith reaction is a one-step reaction that does not require the synthesis and separation of the dichlorocarbene adducts. However, this reaction may also result in a mixture the mono-cyclopropane **40a** and bis-cyclopropane **41a**. This would create a problem as the comparable structure, polarity, and solubility make most separation methods such as column chromatography or recrystallization challenging. The same benefits and challenges can be said of using diazo compounds (with the added drawback of diazomethane must be prepared fresh and can be dangerous if handled improperly) and would result in comparable product mixtures. Gassmann dehalogenation (Na, ^{t}BuOH, THF reflux) was also attempted but due to the small batch size did not give results comparable to the Birch-type dehalogenation. This observation was consistent with the reported outcome of the (formal) cyclopropanation of other cage systems (*e.g.*, hypostrophene **28**, *Figure 10, pg. 13*).[22]

The three adducts **40a, 41a,** and **42a** were all obtained in excellent yields (80-90%) with no cleavage of the cyclopropane or other side reactions in significant amounts. Each compound was purified and isolated by column chromatography (SiO_2, *n*-pentane). The mono-cyclopropane adduct **40a** and saturated mono-cyclopropane adduct **42a** were isolated as waxy, colorless solids. The bis-cyclopropane adduct **41a** was isolated as a colorless crystalline solid. Single crystals of **41a** suitable for XRD were crystalized from chloroform (structure discussed in *3.2.4 X-Ray Crystallography of Select Carbene Adducts*).

3.2.2.2 Synthesis of Difluorocarbene Adducts of Cage Diene **1**

While many methods for generating difluorocarbene have been detailed in the literature, one of the more convenient ways is through the activation of trimethyl(trifluoromethyl)silane ($TMSCF_3$).[19, 35] $TMSCF_3$ can be activated at low or high temperatures with an appropriate initiator. This method also serves to replace the more expensive and hazardous Seyferth reagents like trimethyl(trifluoromethyl) stannane or phenyl(trifluoromethyl)mercury and circumvent other less effective difluorocarbene equivalents/precursors.[19, 35] The mono-difluorocarbene adduct **40b** and bis-difluorocarbene adduct **41b** were prepared using $TMSCF_3$ as a difluorocarbene equivalent in the presence of sodium iodide (NaI) from diene **1** (*Figure 15, pg. 17*). This reaction resulted in mixtures containing both **40b** and **41b** with excellent conversion averaging approximately 90% (10% **1**, 70% **40b**, and 20% **41b**) based on ^{1}H-NMR data and GC/MS. The separation of these compounds was difficult due to the similar polarities. Purification by column chromatography (SiO_2, *n*-pentane) resulted in a large number of mixed fractions, mainly overlap of the mono adduct **40b** and starting material **1**, decreasing the amounts of materials isolated significantly. The isolated amounts of purified **40b** and **41b** were moderate to poor (31% and 44%, respectively).

The saturated mono-cyclopropane adduct **42b** was synthesized *via* the hydrogenation of precursor **40b** (*Figure 15, pg. 17*). While it was possible to produce **42b** *via* difluorocarbene addition of the monoene **24**, we observed low conversion (>50%) and were only able to isolate the product in small amounts due to difficulties in purification. The hydrogenation, however, proceeded smoothly with near quantitative conversion and high isolated yields (93%). Reduction of **40b** was carried out with diimide, generated from hydrazine in the presence of oxygen. Compound **42b** was isolated by filtration over silica gel using *n*-pentane as the eluting solvent. The three difluorocarbene adducts were obtained as colorless crystalline solids but no crystals

suitable for XRD could be grown; solvents such as hexanes, pentane, ethyl acetate, various hexanes/ethyl acetate mixtures, DCM, chloroform, and benzene were screened as crystallization medias.

In contrast to literature reports on the difluorocarbene addition (on various substrates) our reactions were observed to be significantly slower with reaction times exceeding multiple days.[19] This may be due to the alkene units of **1** and **24** being relatively electron poor compared to the highly conjugated systems found in the literarture.[19] In addition, it does not appear that the amount of NaI nor $TMSCF_3$ played an important role in conversion rates. When using up to 1.0 molar equivalents (up from 0.2 eq) of NaI and/or 5 molar equivalents (up from 2.5 eq) of $TMSCF_3$, no change in reaction rate nor conversion was observed.

3.2.2.3 Synthesis of Dichlorocarbene Adducts of Cage Diene **1**

A common method for the generation of dihalocarbenes is by α-elimination under phase transfer conditions.[16, 20, 27] Utilizing α-elimination for the generation of dihalocarbenes was first employed by Doering in 1954 while using phase transfer conditions came years later in 1969.[20, 36] This method was employed for the *in-situ* generation of dichlorocarbene, dibromocarbene, and diiodocarbene. It has been shown that different phase transfer catalysts (PTCs) can result in different yields and outcomes for reactions based on the structure and electronic environment of the PTC.[28] Different substituent patterns paired with some PTCs may yield significantly higher rations of insertion products rather than the standard cheletropic addition. The PTC used in the following experiments does not show selectivity towards insertion versus addition and does not show a strong directing effect. The prevalence of insertion reactions was therefore dependent on the capacity for carbene insertion of the substrate and reactivity of the carbene equivalent.[28]

The general method employed involved vigorously stirring the appropriate haloform with 50% sodium hydroxide (NaOH) in the presence of the PTC triethylbenzylammonium chloride (TEBA-Cl) and the substrate. The only variation of this was the use of carbon tetrachloride as a solvent for the generation of diiodocarbene from crystalline iodoform.[37]

Under phase transfer conditions the reaction of dichlorocarbene with diene **1** gave a mixture of **40c** and **41c** (*Figure 15, pg. 17*). Conversion to these adducts was close to 100% overall (65% **40c**, 35% **41c**) based on ^{1}H-NMR and GC/MS data. Conversion and product distribution was dependent on reaction time (*Table 2, pg. 21*).

Table 2: Relative concentration of compounds after different reaction times in the dichlorocarbene reaction determined by ^{1}H-NMR and GC/MS.

	Ratio		
Reaction time	**1**	**40c**	**41c**
6 hours	2	4	1
16 hours	0	3	2
24 hours	0	1	8

When the reaction was allowed to proceed for 24 hours, nearly all of **40c** was converted to **41c** and no significant side reactions were observed. Purification by column chromatography (SiO_2, *n*-pentane) resulted in some mixed fractions collected, diminishing the isolated yields slightly. When using the standard reaction time of 16 hours, isolated amounts of the mono adduct **40c** were moderate (40%) while isolated amounts of the bis adduct **41c** were poor (10%).

The synthesis of mono-dichlorocyclopropane adduct **42c** (*Figure 15, pg. 17*) did not proceed as smoothly. The dichlorocarbene addition to monoene **24** resulted in a complex mixture. Due to the difficulties of separating monoene **24** from the saturated cage **25**, the reaction was carried out on a mixture of **24** and **25** (4:1 distribution). Compound **42c** was obtained through purification by column chromatography (SiO_2, *n*-pentane). Overlap of some fractions resulted in lower-than-expected isolated amounts (21%) based on the conversion of starting material (60% by ^{1}H-NMR). Compound **42c** was more readily available through the hydrogenation of **40c** with diimide (*Figure 15, pg. 17*). The major side products observed in the dichlorocarbene addition of monoene **24** (and hydrocarbon **25**) appear to be the result of C-H insertion.

It was determined that two of the three major side products were derived from the saturated cage **25** and are therefore not technically side products of the dichlorocarbene addition to **24**. For simplicity these side products derived from **25**, **CI-1** and **CI-3** have been included in the following section(s). These compounds are specified to be derived from **25** (this is also the case for the dibromocarbene addition discussed in *3.2.2.4 Synthesis of Dibromocarbene Adducts of Cage Diene **1***)

Analysis of this reaction suggests four distinct products, **42c** and three unknowns, along with unreacted monoene **24** and saturated cage **25**. Due to similarities between the various suspected insertion products, purification was not possible and only enriched materials were isolated. While the structures of these compounds could not be unequivocally assigned, certain characteristic structural elements were observed, and possible structures are proposed. The proposed structures of the three major side products are supported by ^{1}H-NMR and GC/MS data.

The ^{1}H-NMR of the first side product, **CI-1a**, suggests a system with C_i symmetry displaying 18 independent protons. GC/MS data shows an $M^{\cdot+}$ peak of m/z = 270 ($C_{15}H_{20}{}^{35}Cl_2$)

with the appropriate isotope pattern for a dichloro compound. This suggests that a C-H insertion has occurred on **25** (*Figure 16, pg. 23*).

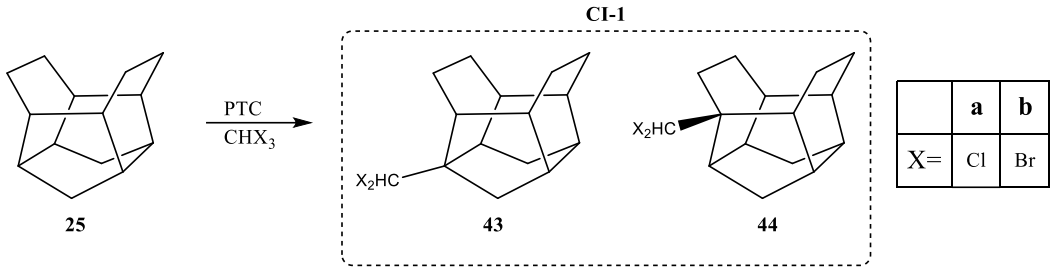

Figure 16: ***CI-1****, possible C-H insertion products of* ***25****.*

The low field singlet at 5.63 ppm in the ^{1}H-NMR is indicative of a H-CX_2 proton and supports the possibility of a C-H insertion (*Figure 17, pg. 24*). The insertion is likely to have reacted at any of the eight bridgehead positions (3° positions are more active towards insertion versus 2° positions), giving two possible products **43a** or **44a**. **CI-1** was the most abundant side product observed in this reaction.

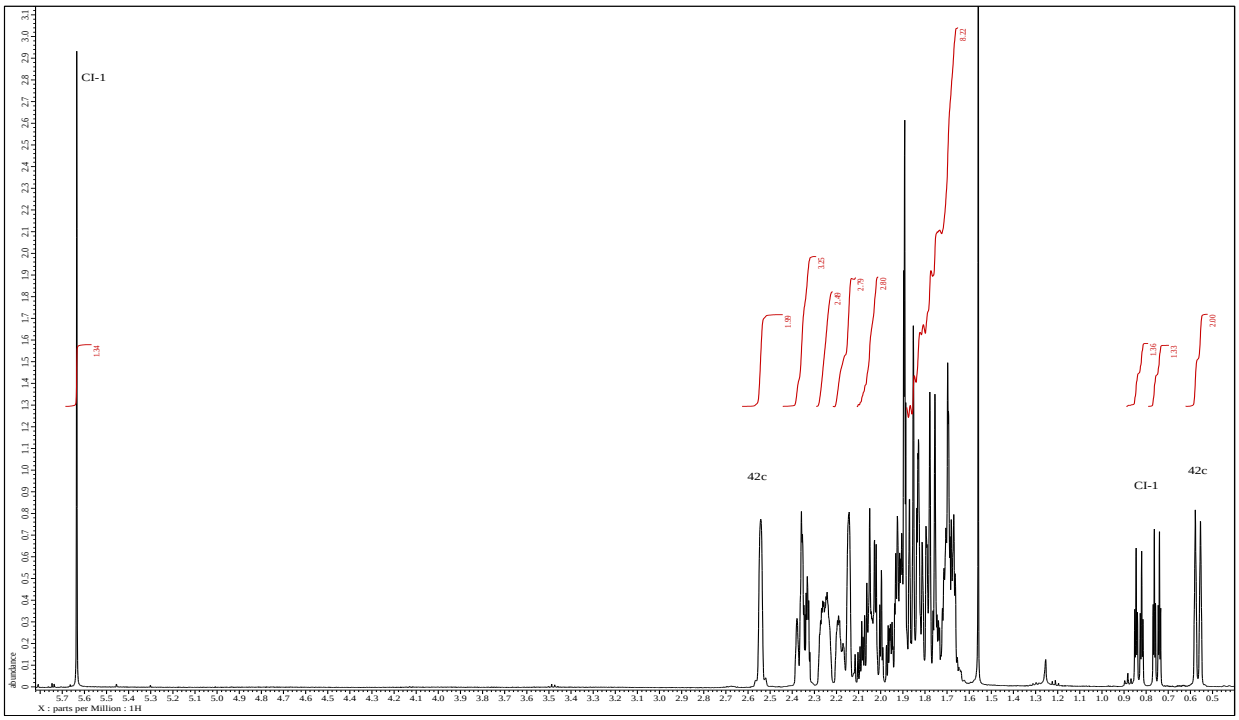

*Figure 17: ^{1}H-NMR of an enriched fraction of **CI-1a**. The spectrum shows a 1:2 mixture of saturated mono-dichlorocarbene adduct **42c** and **CI-1a**.*

The second side product, **C1-2a**, is also likely to be a bridgehead insertion but occurs on monoene **24** (*Figure 18, pg. 25*), GC/MS data shows an $M^{\cdot+}$ peak of *m/z* = 268 ($C_{15}H_{18}{}^{35}Cl_2$) with the appropriate isotope pattern for a dichloro compound.

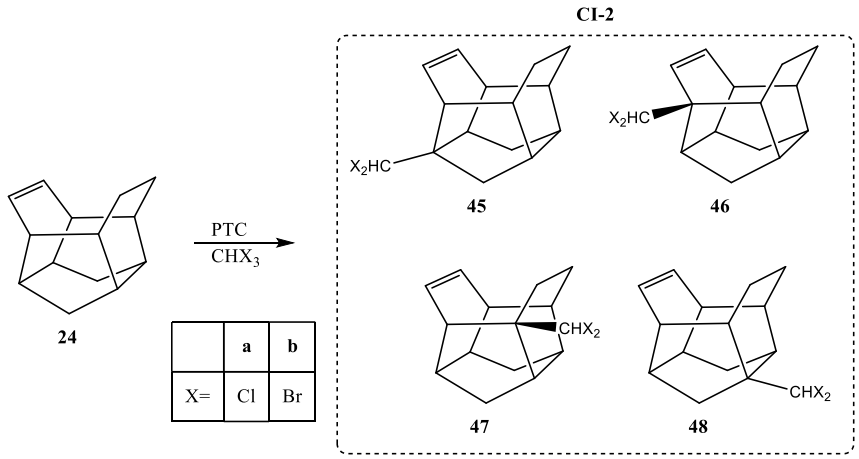

*Figure 18: **CI-2** possible structures of the C-H insertion of **24** by dichlorocarbene.*

The ^{1}H-NMR of the second side product shows two olefin signals each integrating to 1H, a low field singlet at 5.81 ppm integrating to 1H indicative of a H-CX_2 unit, and two signals at high field indicative of methylene protons each integrating to 1H *(Figure 19, pg. 26*). This suggests a system with C_i symmetry derived from the C-H carbene insertion to monoene **24**. The position of the insertion could occur at any of the bridgehead positions as none are sterically or conformationally hindered from forming the necessary transition state (*Figure 12, pg. 15*). **CI-2** was the second most abundant insertion product observed in this reaction and is likely not as abundant as **CI-1** due to the olefin being much more likely to react, rather than the C-H insertion.[31] Compounds **45a**, **46a**, **47a**, and **48a** all fit the relative assignments, thus, a specific structure cannot be assigned without further spectroscopic evidence (2-D NMR), however, **47a** and **48a** are more likely due to proximity of the olefin relative to the eight possible reaction sites.

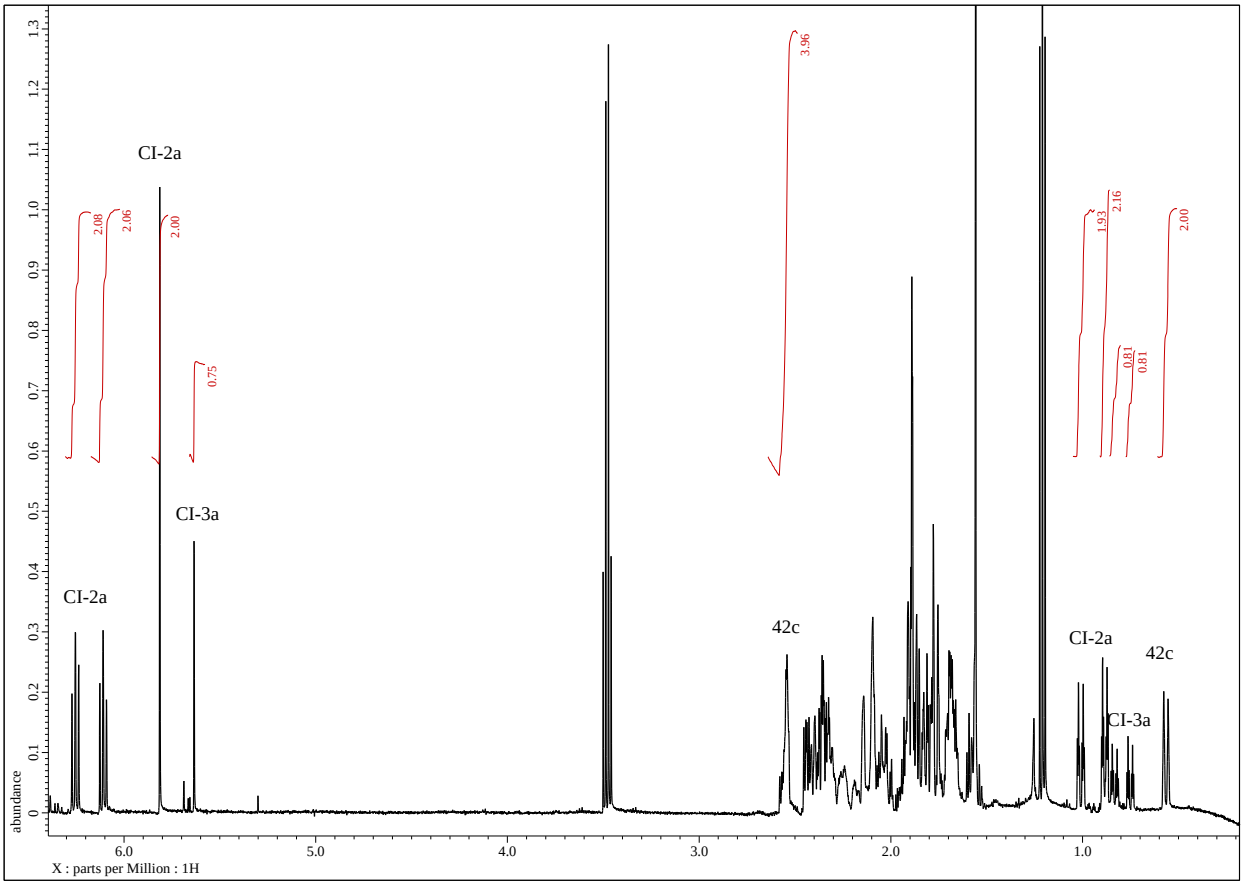

*Figure 19: [1]H-NMR of enriched fraction of **CI-2a** in a 4:2:1 ratio of **CI-2a/42c/CI-3**. The two olefin signals, low field singlet, and two methylene protons intergrate with a 1:1:1 ratio relative to the two methylene protons of **42c**. **CI-3a** is also visible in lower concentration with a 1:1 signal ration between the methylene protons and the low field signal.*

The last side product that could be isolated, **CI-3a**, is likely found by further reaction of the first side product, **CI-1a** (**43a/44a**, *Figure 16, pg. 23*). The ^{1}H-NMR (*Figure 21, pg. 28*) and GC/MS suggests a variety of high mass side products in trace amounts along with **CI-3**. The GC/MS shows an $M^{\cdot+}$ peak of *m/z* = 352 ($C_{16}H_{20}{}^{35}Cl_2{}^{37}Cl_2$). The appropriate isotope pattern was not observed likely due to the low intensity of the $M^{\cdot+}$ peak. This observed mass suggests two dichlorocarbene equivalents reacting with **25** (*Figure 20, pg. 27*).

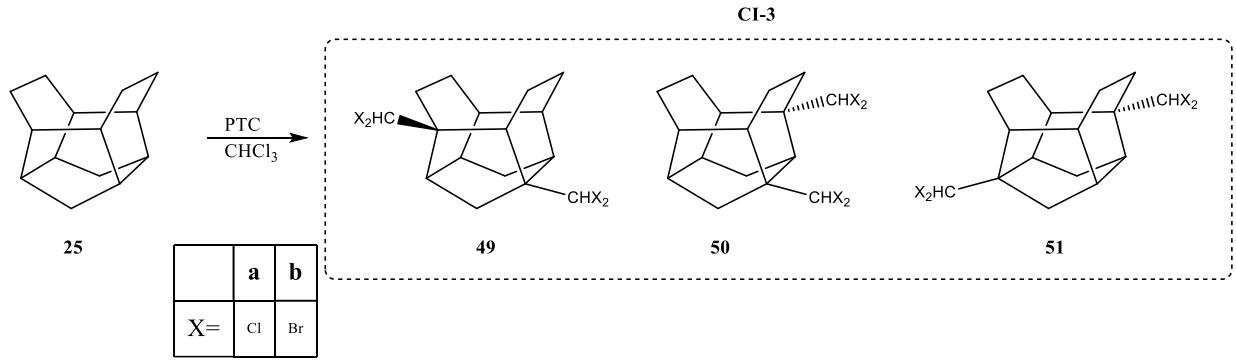

*Figure 20: Possible structures of **CI-3**, the two-fold C-H insertion product of **25** by dihalocarbene.*

^{1}H-NMR signal patterns allude to a cage scaffold with C_i symmetry. The ^{1}H-NMR spectrum shows two low field signals centered at 5.65 and 5.67 ppm each integrating to 1H. The identity of **CI-3** is likely **49**, **50**, or **51** when steric hinderance and symmetry are taken into consideration. Due to the ridged structure of the cage the bridgehead positions separated by one bond will result in steric crowding (see x-ray structure for various carbene adducts in *3.2.4 X-Ray Crystallography of Select Carbene Adducts*).

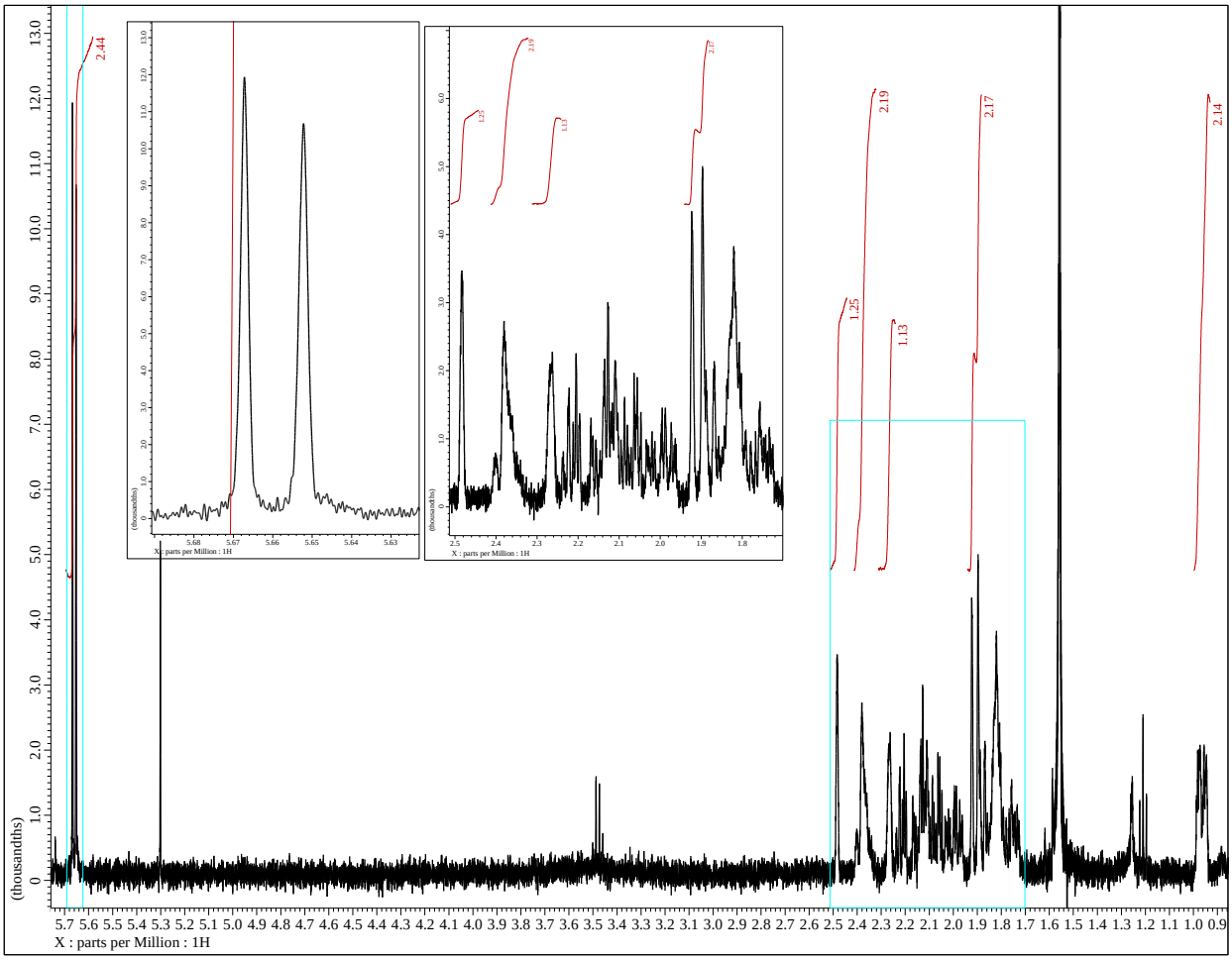

*Figure 21: ^{1}H-NMR spectrum of a highly enriched fraction (95+%) of **CI-3a**.*

3.2.2.4 Synthesis of Dibromocarbene Adducts of Cage Diene **1**

The synthesis of the dibromocarbene adducts of **1** were also accomplished under the above discussed conditions with bromoform as the carbene equivalent (*Figure 15, pg. 17*). This resulted in a mixture of the mono-dibromocarbene adduct **40d** and bis-dibromocarbene adduct **41d**. Unlike the dichlorocarbene addition to **1**, dibromocarbene addition gave rise to significant side product formation. A range of reaction times were attempted to optimize the reaction and minimize side product formation (*Table 3, pg. 29*). Reactions ranging from 4 to 6 hours favor formation of **40d** with only small amounts of **41d** are observed. Reactions over this time period begin to see larger

increases in insertion product concentration.[15, 18, 20] After 48 hours no trace of desired product was identifiable (*Figure 22, pg. 30*). Signals visible in the olefinic region of the ^{1}H-NMR (*Figure 22, pg. 30*) show multiple possible mono-insertion reactions on diene **1** or mono-dibromocarbene adduct **40d**. As the reaction progressed, the increasing number of side products suggest that some may be derived from the targeted compounds **40d** and **41d** or the insertion products themselves.

Table 3: Relative concentration of compounds after different reaction times in the dibromocarbene reaction.

	Relative Concentration (Ratio)			
Reaction Time	**1**	**40d**	**41d**	**Side Products**
4 hours	1	10	2	0
24 hours	0	2	2	1
48 hours	0	0	0	1

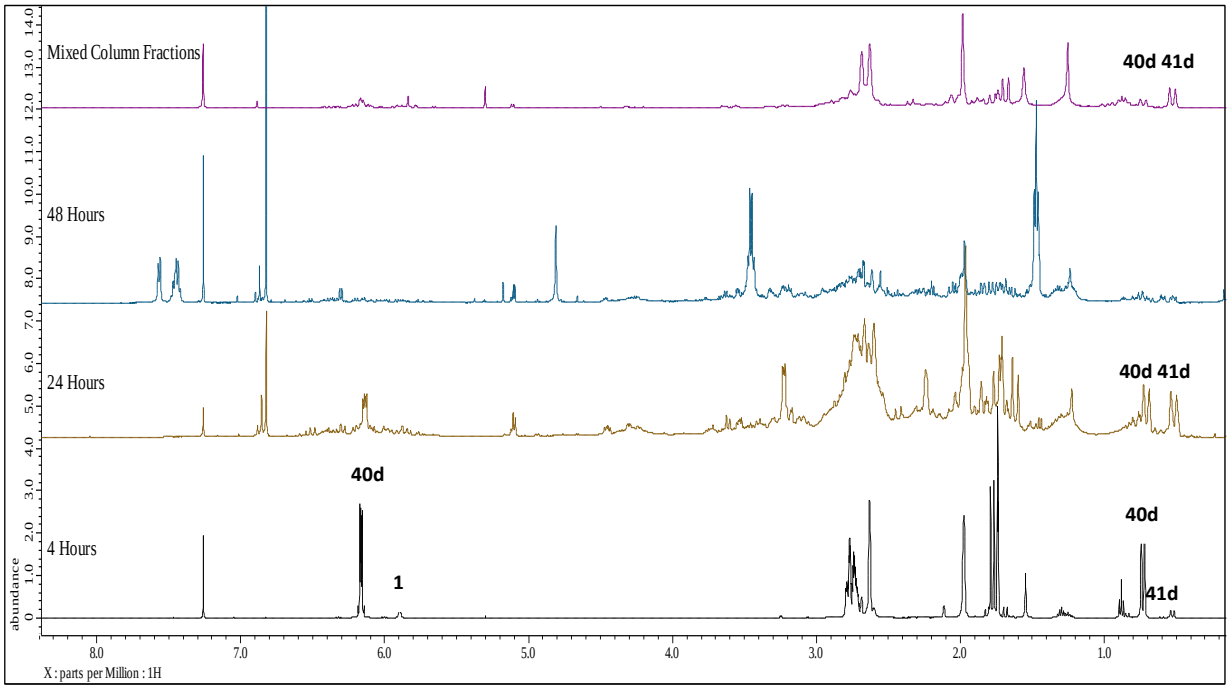

*Figure 22: [1]H-NMR of crude reaction mixtures at different reaction times used in the dibromocarbene addition to **1** and the mixed fraction containing product after purification. The same ratios are reported in Table 3 (pg. 29) above.*

The purification of the mono- and bis-dibromocarbene adducts **40d** and **41d** was challenging. Using column chromatography (SiO_2, *n*-pentane) allowed for separation of the hydrocarbon **1** from the desired products, however, the bulk of the products **40d** and **41d** eluted in mixed fraction. Trituration of the mixed fractions was effective at separating **40d** and **41d**. A mixture of mono and bis adduct (1:1) was crystallized from DCM then triturated with ethyl acetate (EtOAc). The mono adduct **40d** was solubilized, giving clean, colorless, crystalline material for both compounds **40d** and **41d**. Single crystals obtained from the purification were suitable for XRD. The side products were observed eluting late on the column requiring methanol (MeOH) to remove the mixture of multiple compounds; none of the side products could be isolated as pure or enriched materials. The low field ^{1}H-NMR region of the crude material obtained from the 24-hour

reaction (*Figure 22, pg. 30*) shows multiple signals and GC/MS data was unreliable due to decomposition.

The synthesis of the saturated mono-dibromocarbene adduct **42d**, much like the saturated mono-dichlorocarbene adduct **42c**, proved unruly (*Figure 15, pg. 17*). When monoene **24** was subjected to carbene addition a complex mixture of **42d** and several side products was observed. The desired product was isolated in low amounts (20%) by column chromatography (SiO_2, *n*-pentane). It was also possible to obtain this compound in moderate yields (67%) by hydrogenation of **40d** with diimide generated from hydrazine in the presence of oxygen and purification by column chromatography (SiO_2, *n*-pentane).

Based on ^{1}H-NMR and GC/MS data there appeared to be ten distinct side products observed in the dibromocarbene addition of monoene **24**, however, due to low concentrations, some side products could not be enriched sufficiently to gain significant structural detail. The characteristic 1:2:2:1 isotope pattern of dibromide compounds was not observed due to the low intensity of the $M^{\cdot+}$ peak, however, the 1:1 isotope pattern was distinguishable. Many of the observed side products of the dichlorocarbene and dibromocarbene additions share analogous structures. This may be in part due to the similar in structure and reactivity of the two carbene equivalents. Three side products of the dibromocarbene addition to **24** (and **25**) could be sufficiently enriched to obtain adequate spectra and all strongly resemble the side products observed in the dichlorocarbene addition.

The first side product, **CI-1b**, displayed the same low field singlet, slightly more downfield at 5.71 ppm, as well as integration equal to 18 hydrogen signals, same as seen in **CI-1a** (**43a**/**44a** *Figure 16, pg. 23*) in the ^{1}H-NMR (*Figure 23, pg. 32*). The GC/MS data also shows a $M^{\cdot+}$ peak of

m/z = 358 ($C_{15}H_{20}{}^{79}Br_2$) implying C-H insertion on hydrocarbon **25**. The identity of **CI-1b** is likely **43b** or **44b** (*Figure 16, pg. 23*).

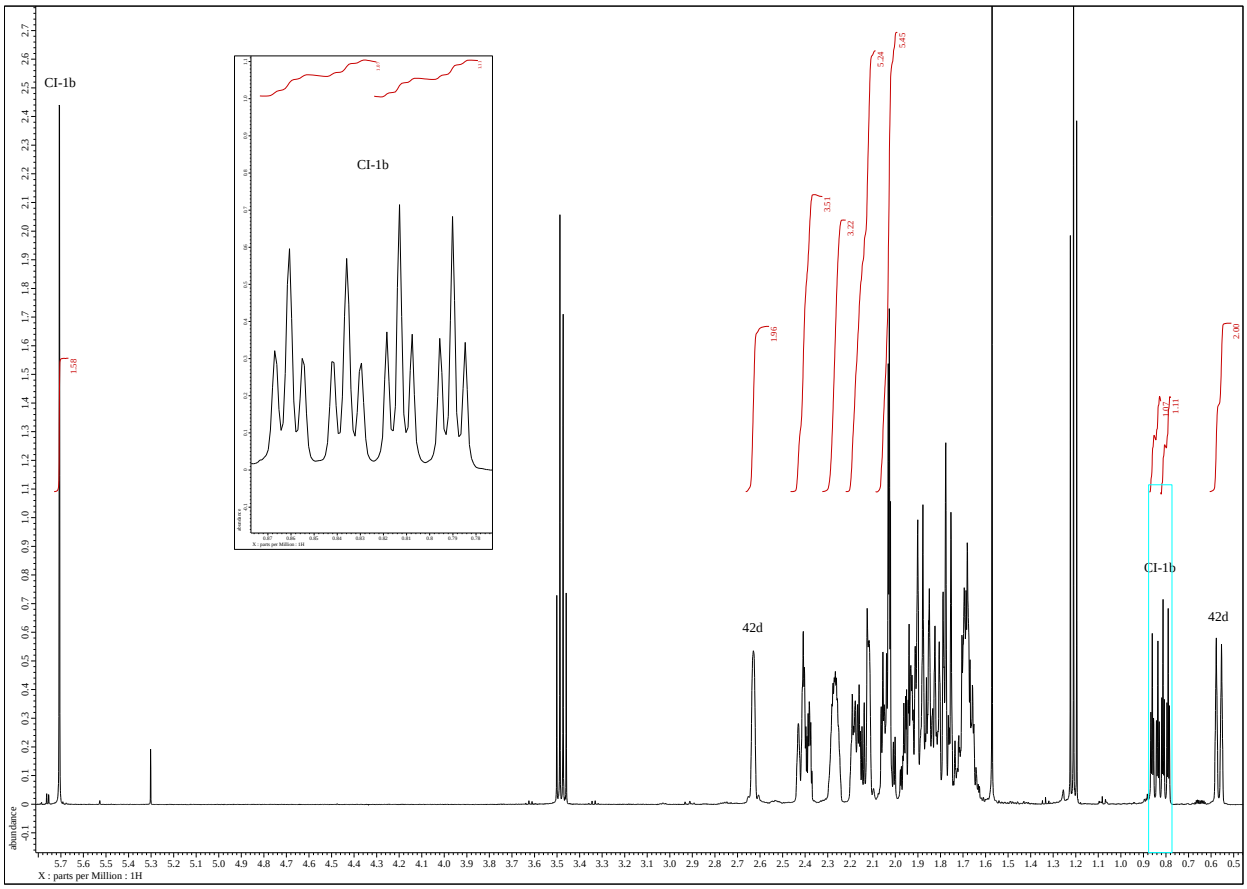

*Figure 23: ^{1}H-NMR of enriched fraction of C-H insertion product **CI-1b**. Spectrum shows a 1:1 mixture of **CI-1b** (**43b/44b**) and mono-dibromocarbene adduct **42d**.*

The second side product, **CI-2b**, could not be isolated cleanly and the obtained spectra also contains mono-dibromocarbene adduct **42d** and other impurities in low concentrations. However, certain characteristic signal can still be identified. This side product displays two inequivalent olefinic signals in the ^{1}H-NMR (*Figure 24, pg. 33*) and an $M^{\cdot+}$ peak of *m/z* = 356 ($C_{15}H_{18}{}^{79}Br_2$) in the GC/MS. The analytical data obtained for **CI-2b** mirrors the observed characteristics of **CI-2a** and implies the two materials are structurally analogous **(***Figure 18, pg. 25*).

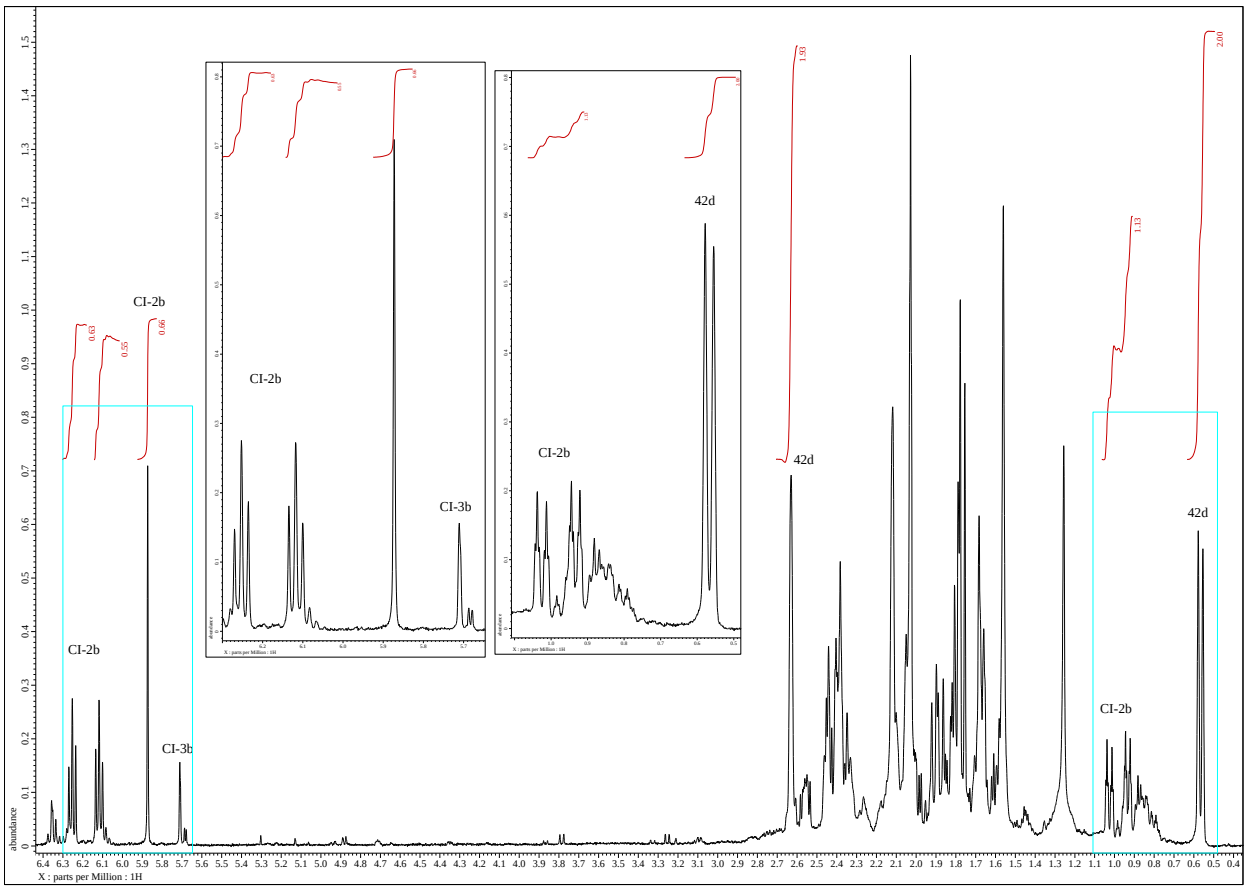

*Figure 24: ^{1}H-NMR depicting an enriched fraction of **CI-2b**. The defining olefin signals can be seen in this spectrum. **CI-2b** can likely be assigned the structure of **45b**, **46b**, **47b**, or **48b**.*

The third enriched side product, **CI-3b**, shares many of the same spectroscopic features as **CI-3b**. The mass observed by GC/MS shows an $M^{\cdot+}$ peak of *m/z* = 530 ($C_{16}H_{20}{}^{79}Br_2{}^{81}Br_2$). This is indicative of a two-fold reaction of dibromocarbene on hydrocarbon **25** (*Figure 20, pg. 27*). The observed mass is likely the $C_{16}H_{20}{}^{79}Br_2{}^{81}Br_2$ mass as the $^{79}Br_4$ isotope is much lower in concentration (*Figure 25, pg. 34*).

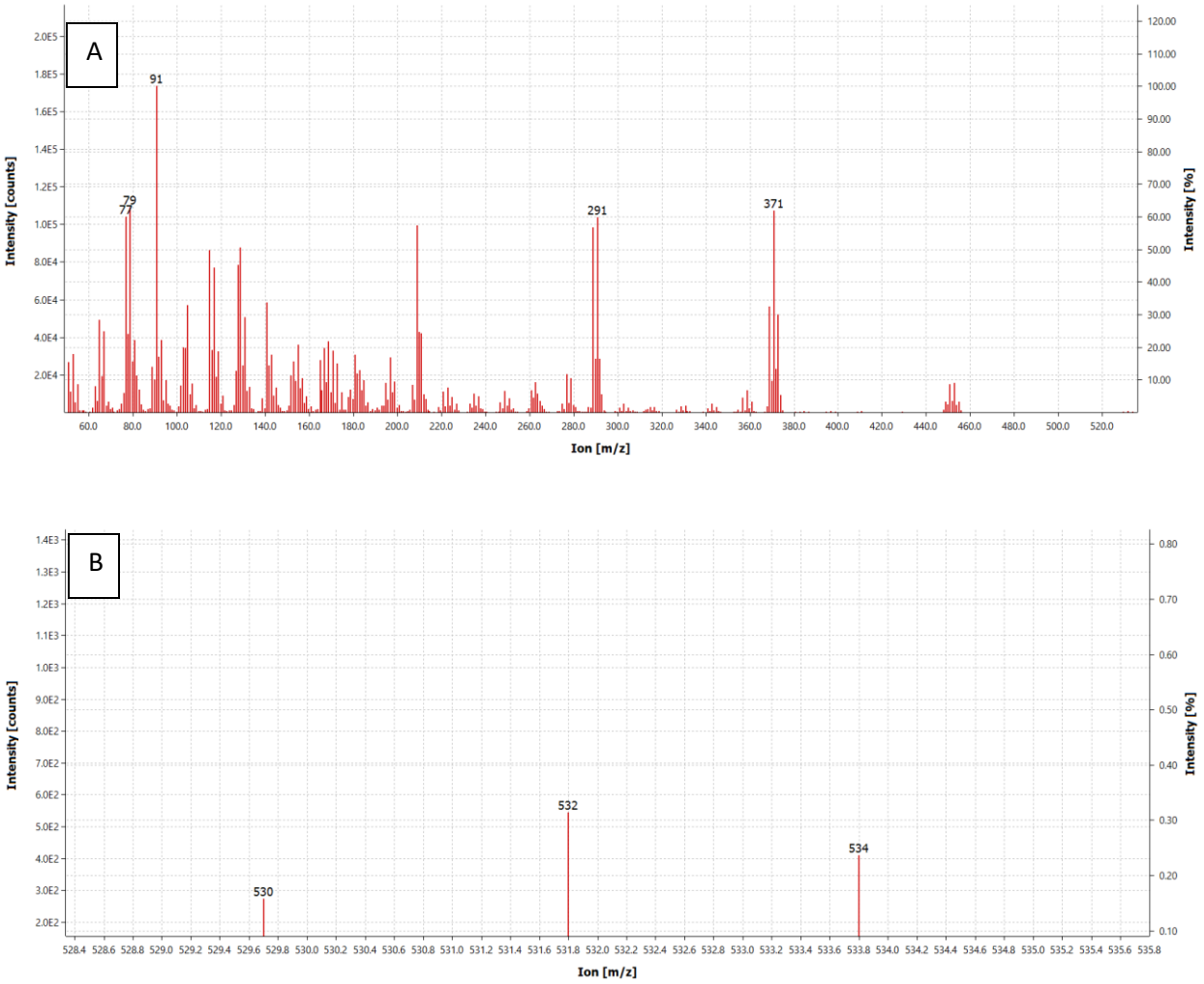

*Figure 25: (A) Mass spectrum of **CI-3b** obtained in the dibromocarbene addition to **24**. The $M^{\cdot+}$ peak and isotope pattern imply insertion on **25**. (B) Zoom of $M^{\cdot+}$ peak is also shown.*

The ^{1}H-NMR of **CI-3b** shows two low field singlets, each integrating to 1H and the ^{13}C-NMR displays 16 carbon signals suggesting a structure with no internal mirror plane. When considering steric demand of the dibromomethyl group and C_i symmetry implied by the NMR data, the structure of **CI-3b** is likely one of the isomers **49b**, **50b**, or **51b** (*Figure 20, pg. 27*).

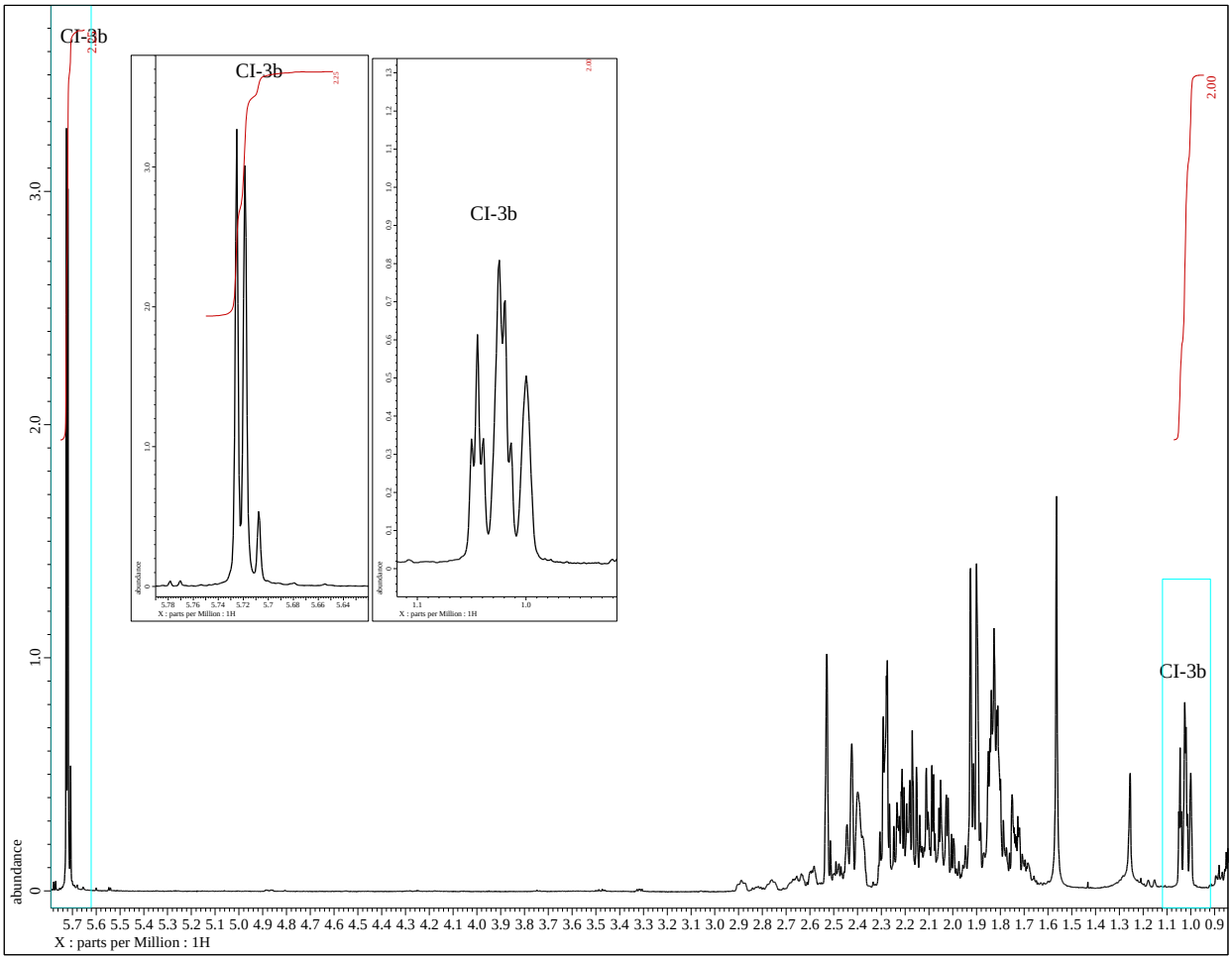

*Figure 26: [1]H-NMR of a highly enriched fraction (90+%) of **CI-3b** (**49b**/**50b**/**51b**) and small amounts of other side products.*

3.2.2.5 Attempted synthesis of Diiodocarbene Adducts of Cage Diene **1**

The synthesis of the diiodocarbene adducts of **1** was attempted along standard literature procedures.[37] Diiodocarbene is the least stabilized dihalocarbene with the smallest singlet-triplet gap.[18] This reactivity is the most likely cause of this reaction failing to deliver the desired product. In the [1]H-NMR spectrum of the crude reaction mixture, some signals resembling the cage scaffold were observed. However, the overly complex spectrum shows multiple overlapping signals preventing any unequivocal identification of a specific product. Furthermore, the product mixture

was observed to decompose rapidly over 24 hours, making isolation of any material unlikely. The decomposition may be facilitated by the weak C-I bond and trace water and/or base could lead to hydrolysis or elimination of the halogen (elimination would result in rearrangement as to not produce an anti-Bredt olefin).

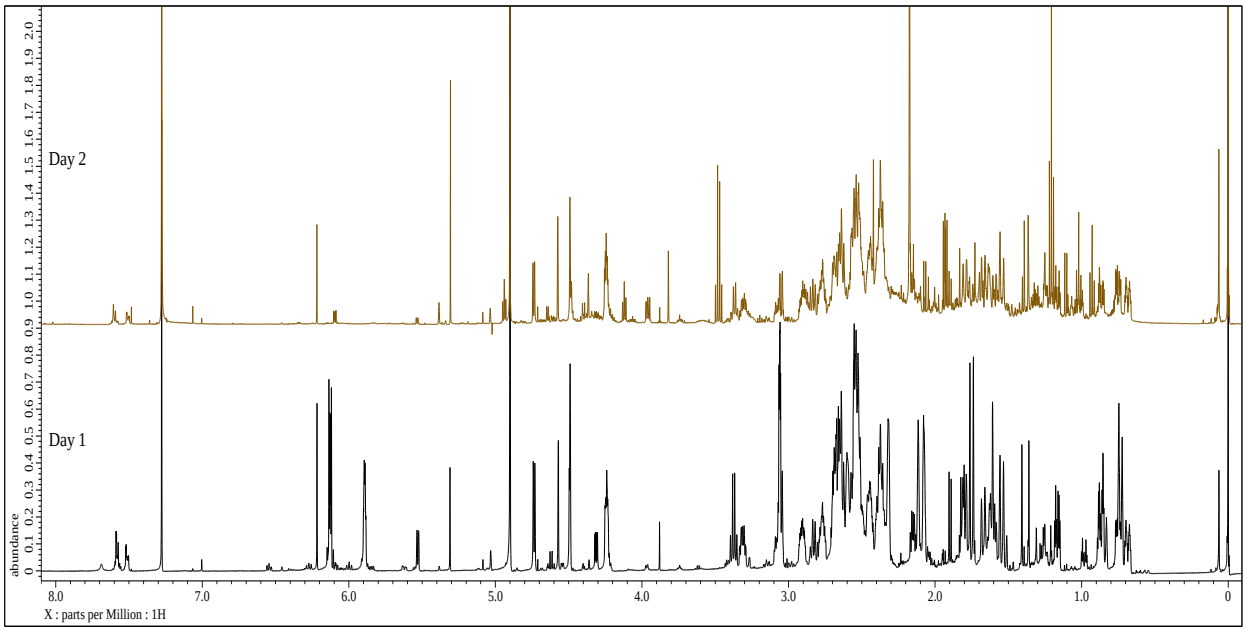

*Figure 27: ^{1}H-NMR spectrum of the crude product mixture obtained from the diiodocarbene addition to **1**. The mixture rapidly decomposed over 24 hours at ambient temperature. Day 1 was acquired immediately after workup. Day 2 was acquired less than 24 hours later from the same batch of material.*

3.2.2.6 Synthesis of Mixed Carbene Adducts of Cage Diene **1**

Three mixed carbene adducts **41e-g** were synthesized by dihalocarbene addition to previously prepared mono-(dichloro)cyclopropane adducts **40a** or **40c** (*Figure 15, pg. 17*). The mixed carbene **41e** was synthesized by dichlorocarbene addition of mono-cyclopropane **40a** under phase transfer conditions. This reaction proceeded slowly and did not reach full conversion after more than 88 hours (as followed by GC/MS). After 64 hours of reaction time significant side

product was observed forming by GC/MS. Conversion of 90% was achieved and isolation of the desired product was accomplished by trituration with *n*-pentane followed by column chromatography (SiO_2, *n*-pentane). Compound **41e** was isolated in moderate yield (49%) and crystals suitable for XRD were obtained from chloroform. Over the course of the reaction two side products could be observed by GC/MS: *m/z* =280 ($C_{16}H_{18}{}^{35}Cl_2$) and *m/z* =362 ($C_{17}H_{18}{}^{35}Cl_4$). These masses correspond to single and two-fold carbene reactions on the substrate **40a**.

The first side product, **CI-4a**, shows an $M^{\cdot+}$ peak of *m/z* =280 ($C_{16}H_{18}Cl_2$) and the appropriate isotope pattern in the GC/MS. In the ^{1}H-NMR spectrum, two olefin signals and multiple signals in the methylene region were observed suggesting a compound with C_i symmetry (*Figure 29, pg. 38*). The presence of the olefin signal in the ^{1}H-NMR also suggests **CI-4** is formed through a C-H insertion to one of the bridgehead positions of mono-cyclopropane **40a**.

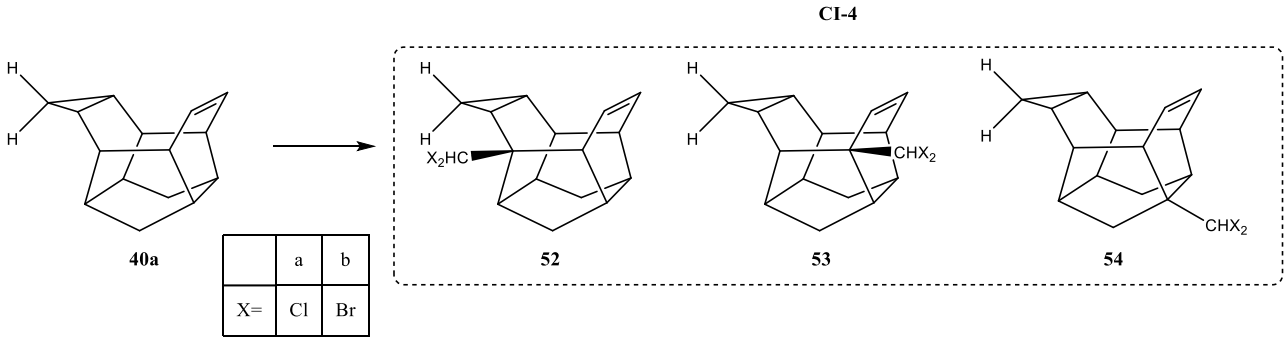

*Figure 28: Potential structures of **CI-4,** one of two identified C-H insertion products of **40a**.*

This is also supported by the low field singlet integrating to 1H at 5.82 ppm, characteristic of a C-CX_2-H moiety. The position of C-H insertion is likely to occur at a bridgehead position, however lower bridgehead proximate to the cyclopropane may be less available due to the steric requirements of the dichloromethyl group. The proximity of the olefin makes **53a** an unlikely candidate for the observed structure as the carbene addition is the more favored reaction.

In addition, cyclopropanes have been shown to have a directing effect in non-cage systems due to overlap of Walsh orbitals with the σ orbital of the α C-H (*Figure 13, pg. 15*).[16, 31] This phenomenon is based on the conformation of the rings and may directing force in this cage system if the overlap is significant. Further calculational data is required to determine if the orbital overlap in **40a** is significant enough to impact the regioselectivity of the C-H insertion. Based on current data the structure for the C-H insertion product of **40a** could be **52a** or **53a** or **54a**.

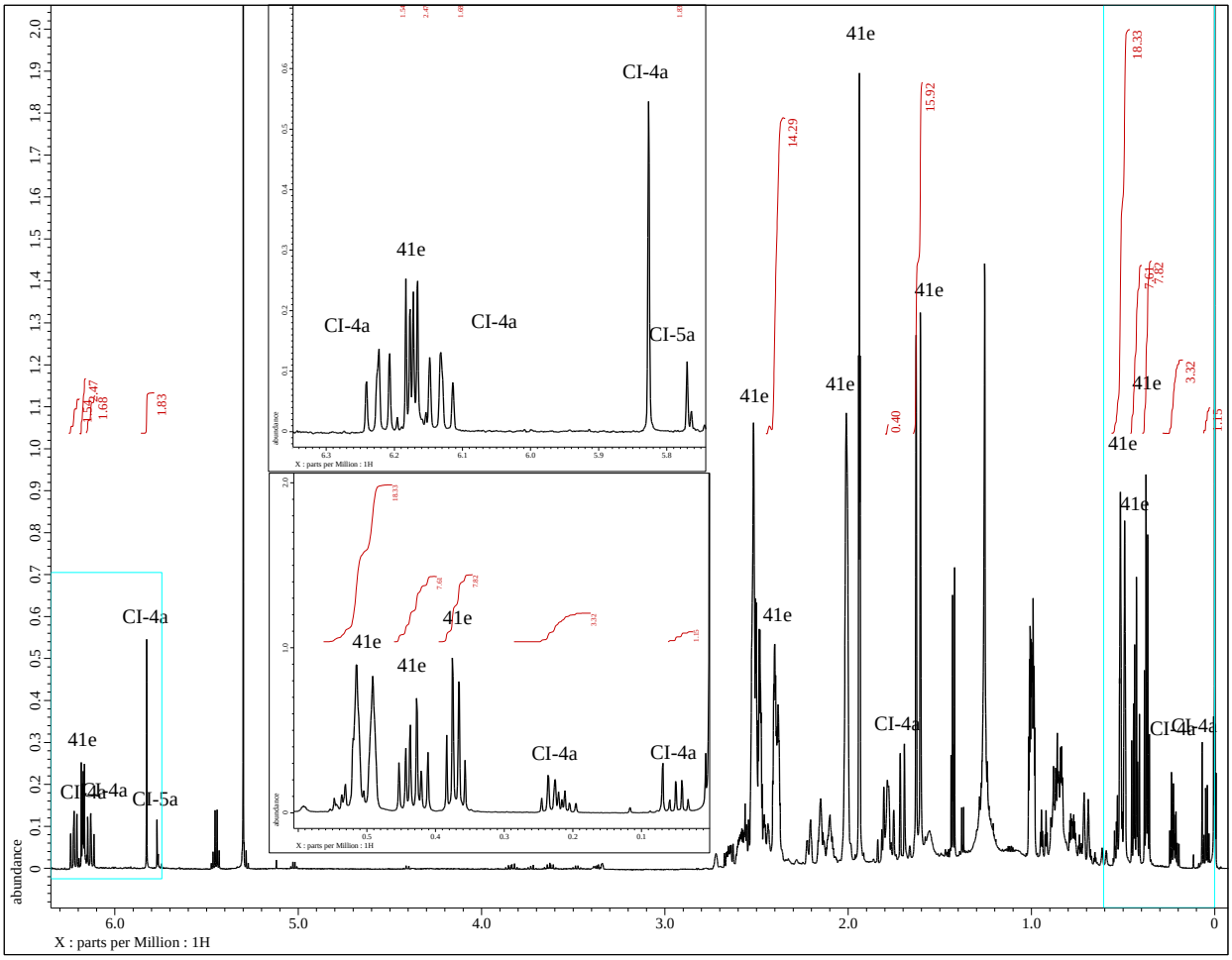

*Figure 29: [1]H-NMR of a fraction containing suspected mono insertion product **CI-4a**, enriched to approximately 30%. Trace amounts of **CI-5a** are visible.*

The second side product, **CI-5a**, shows a $M^{\cdot+}$ peak of *m/z* =362 ($C_{17}H_{18}{}^{35}Cl_4$) in the GC/MS and displays a characteristic low field singlet at 5.77 ppm in the ^{1}H-NMR. This implies a two-fold carbene reaction has occurred. The number of signals in the ^{1}H-NMR suggests a system with C_i symmetry and as there is no indication of an olefin it is reasonable to assume that the alkene has reacted with a carbene equivalent (*Figure 31, pg. 40*). These characteristics suggest that the mixed carbene **41** is present as a substructure of **CI-5** (*Figure 30, pg. 39*).

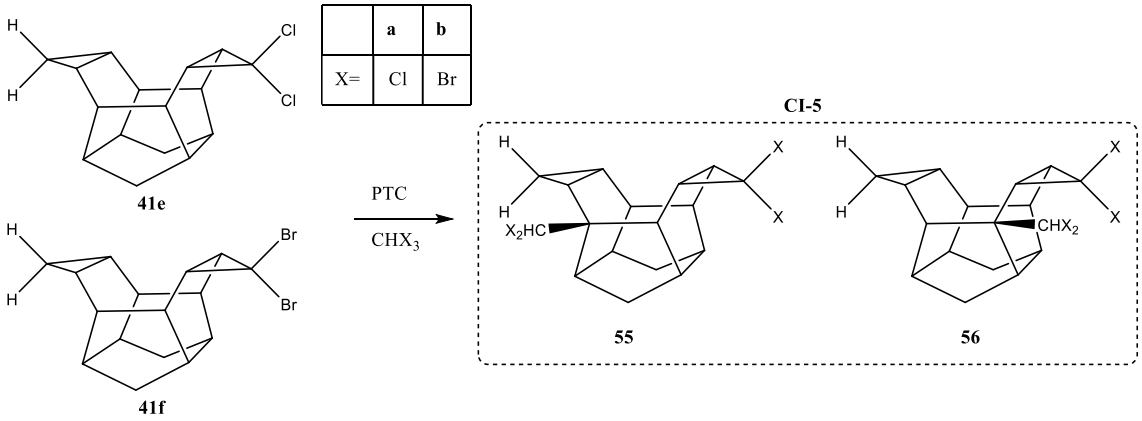

*Figure 30: Proposed structures of **CI-5**, the potential C-H insertion products of **41e-f**. The products are also available through the dihalocarbene addition of **CI-4**.*

Insertion of the lower bridgehead positions is unlikely due to the steric requirements of the dihalomethyl group and the (dihalo)cyclopropane (see X-ray structure of **41e** in *3.2.4 X-Ray Crystallography of Select Carbene Adducts*). **CI-5a** could be derived from one or both possible pathways; C-H insertion of dichlorocarbene on **41e** or carbene addition to **CI-4a** (specifically **52** or **53**).

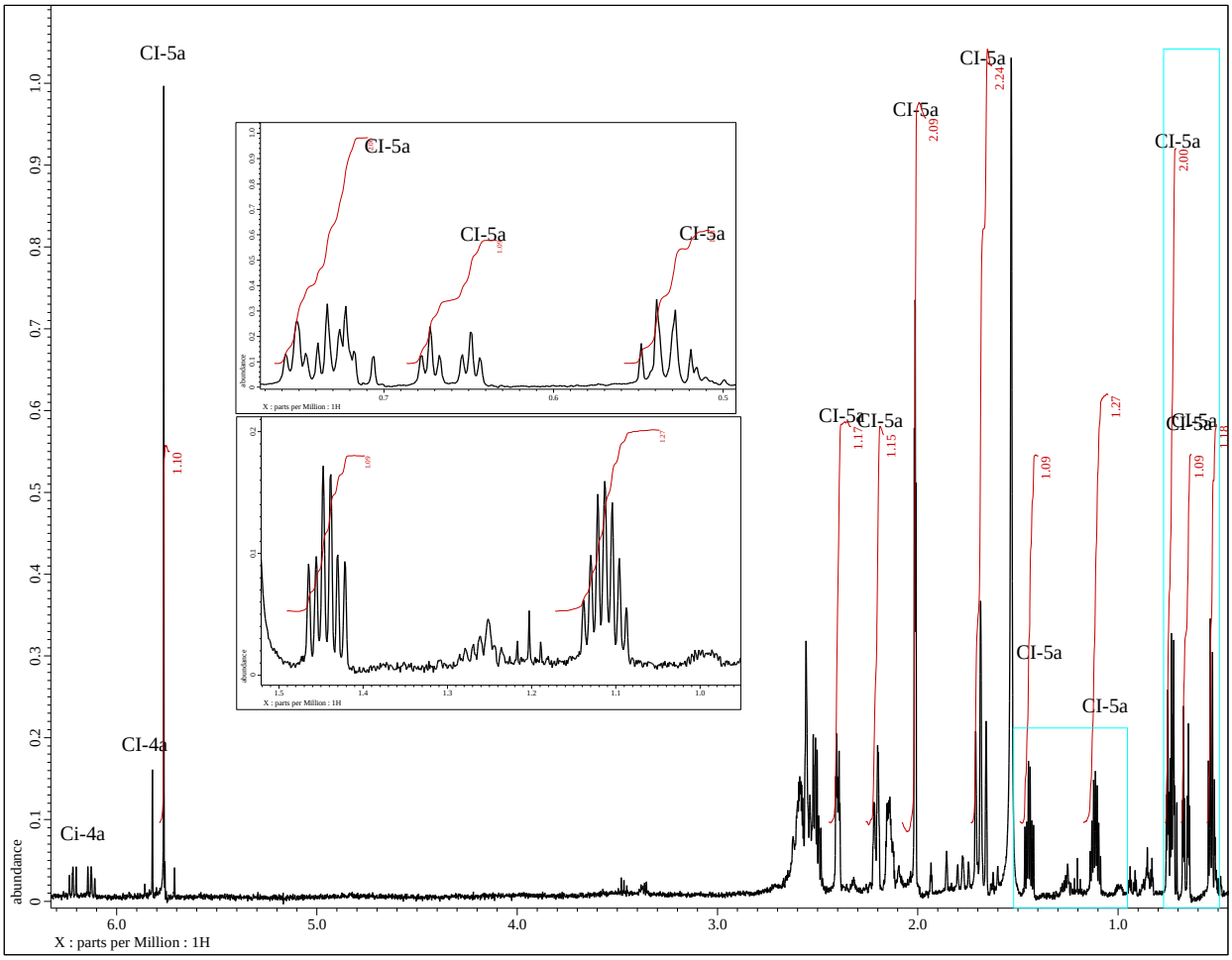

*Figure 31: [1]H-NMR of enriched fraction (90%) of **CI-5a**. This fraction contained approximately 10% of **CI-4a** and other impurities.*

The mixed carbene adduct **41f** was synthesized by dibromocarbene addition to mono-cyclopropane **40a**. Unlike the dichlorocarbene addition this reaction proceeded significantly faster leading to almost full conversion within 4 hours. However, this also gave rise to faster development of two distinct side products. The mixed carbene adduct **41f** was isolated by column chromatography (SiO_2, hexanes) in low amounts (20%).

The side products observed strongly resemble the ones identified in the dichlorocarbene reaction to mono-cyclopropane **40a**, however, due to decomposition, the use of GC/MS data for

identification was limited. The ^{1}H-NMR of the first insertion product displays two inequivalent olefin signals suggesting a system with C_i symmetry. This is the same signal pattern observed in **CI-4a** and indicates that the side product may be the larger homolog, **CI-5b** (*Figure 28, pg. 37*). Other signals such as a low field singlet at 5.85 ppm integrating to 1H suggest a C-H insertion analogous to that observed previously in the dichlorocarbene addition to mono-cyclopropane **40a**.

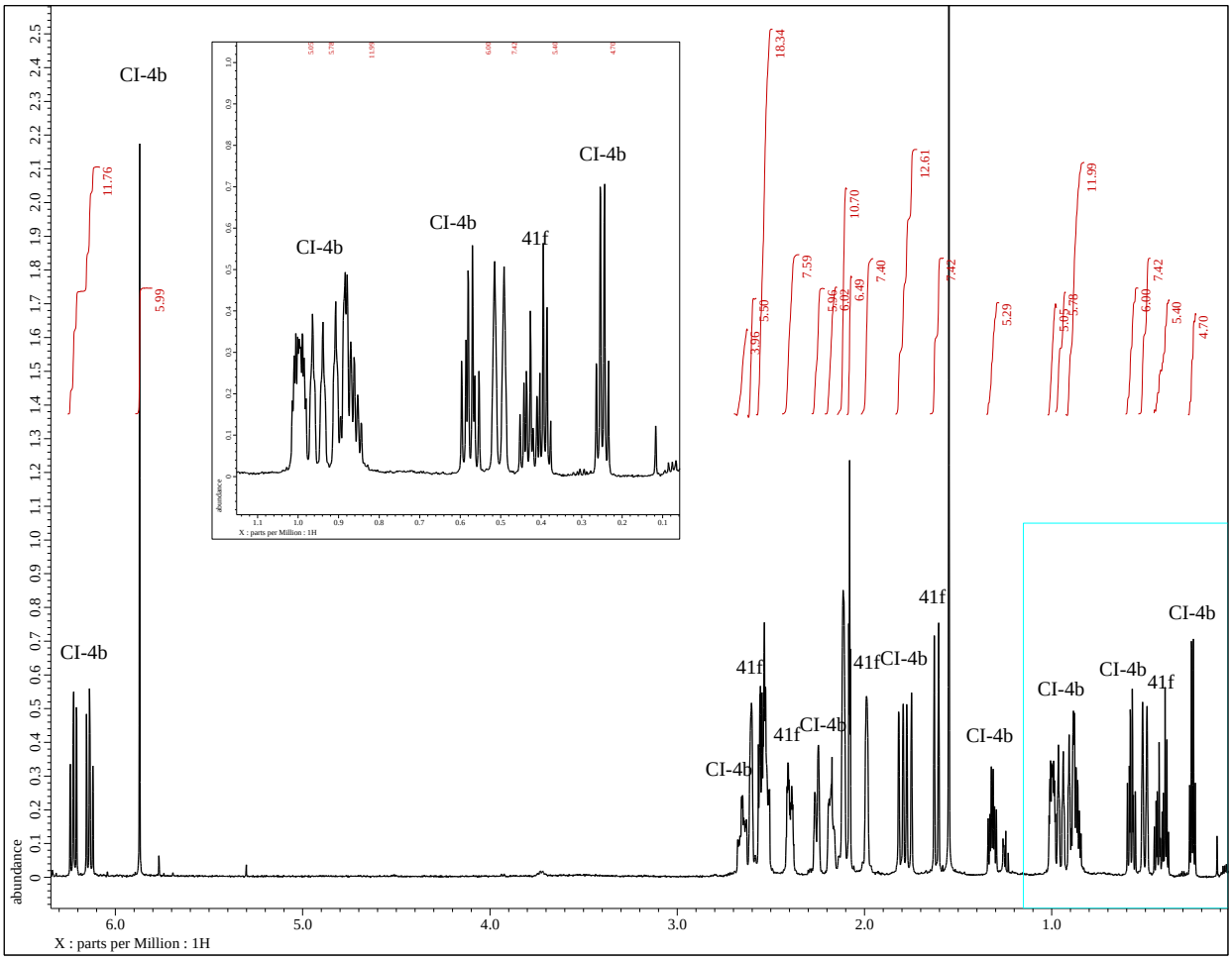

*Figure 32: ^{1}H-NMR of an enriched fraction of **CI-4b**. This fraction also contains starting material **41f** in approximately 1:1 ratio based on integration.*

The second side product of this reaction, **CI-5b**, also shows analogous signal patterns to **CI-5a** in the ^{1}H-NMR. The lack of an olefinic signal at low field paired with the unsymmetrical

methylene positions and the low field singlet integrating to 1H at 5.81 ppm suggest a C-H insertion on mono-dibromocarbene-mono-cyclopropane adduct **41f** or the carbene addition to **CI-4b** (**52** or **53**). This would give **CI-5b** the assigned structure **55b** or **56b** (*Figure 30, pg. 39*).

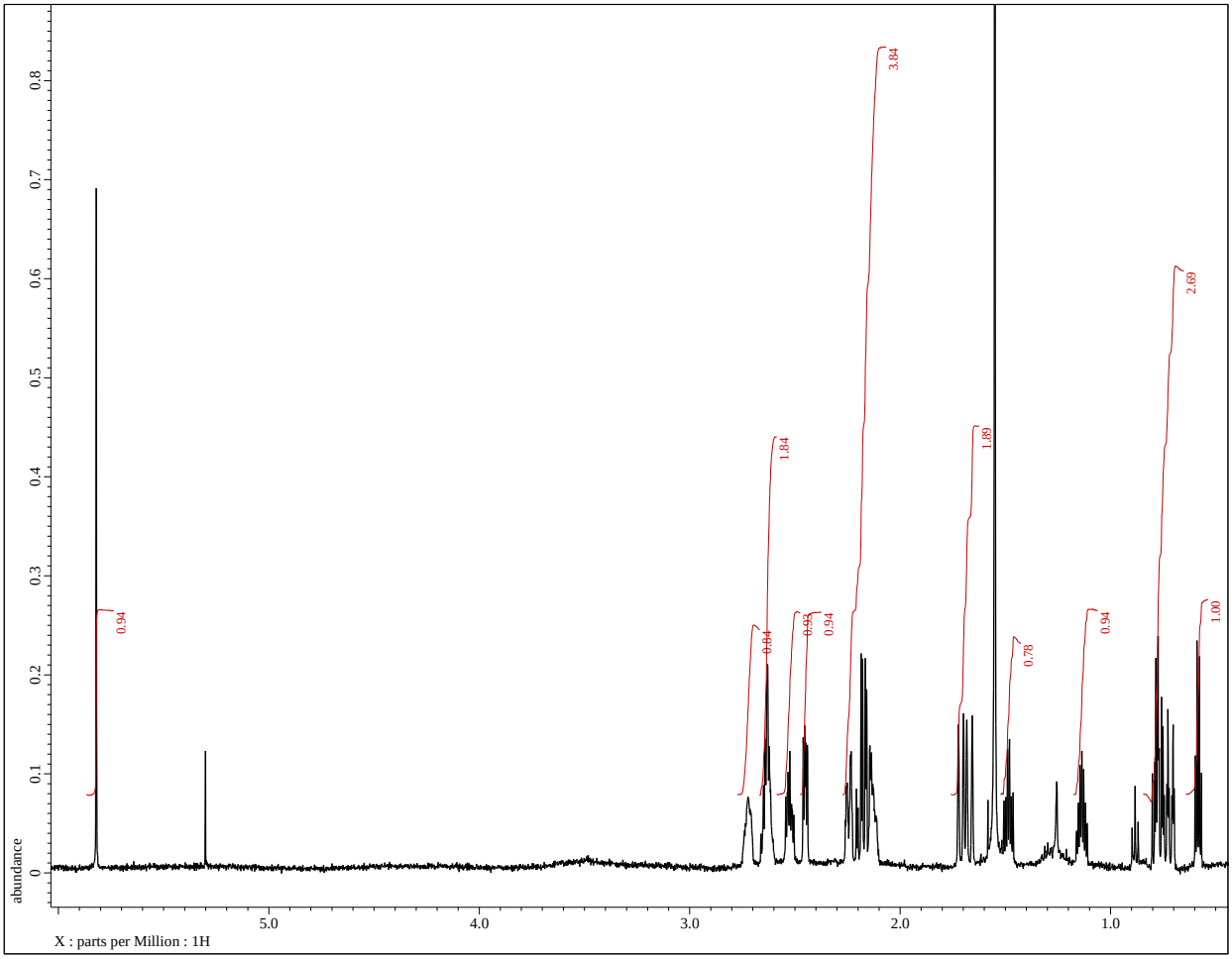

*Figure 33: ^{1}H-NMR of a highly enriched (98%) fraction of **CI-5b** (**55b** or **56b**).*

The final mixed carbene, **41g**, was obtained by the dibromocarbene addition of mono-dichlorocarbene adduct **40c**. This reaction proceeded slowly, taking multiple days to reach 50% conversion. Interestingly, despite these extended reaction times there was little to no side product formation or conversion past the 50% mark. The product **41g** was isolated in moderate yields (57%) by column chromatography (SiO_2, hexanes).

3.2.3 Physical Data and NMR Analysis of Select Carbene Adducts

Table 4: Table of the different carbene adducts detailing if x-ray diffraction data was collected, the solvent used for crystal growth, and the melting point obtained for each compound.

Product		XRD	Solvent	Melting Point (°C)
Mono CH_2	**40a**			242.3-243.2
Bis CH_2	**41a**	Yes	$CDCl_3$	178.3-179.6
Sat. CH_2	**42a**			210.0-211.0
Mono CF_2	**40b**			87.6-88.6
Bis CF_2	**41b**			137.4-137.8
Sat. CF_2	**42b**			104.5-106.3
Mono CCl_2	**40c**	Yes	$CHCl_3$	153.8-154.2
Bis CCl_2	**41c**	Yes	$CHCl_3$	237.1-239.5
Sat. CCl_2	**42c**	Yes	$CDCl_3$	184.1-184.9
Mono CBr_2	**40d**	Yes	Ethyl Acetate	164.6-164.8 (186.4 decomposition)
Bis CBr_2	**41d**	Yes	$CHCl_3/CH_2Cl_2$	189.7-190.6
Sat. CBr_2	**42d**	Yes	$CDCl_3$	191.9-192.5
CCl_2 CH_2	**41e**	Yes	$CHCl_3/CH_2Cl_2$	142.5-143.2 (147.9 full melt)
CBr_2 CH_2	**41f**			144.5-146.2
CBr_2 CCl_2	**41g**			193.6-195.0

The general trend of the three homogenously halogenated adducts show that the mono adducts have the lowest melting point, followed by the saturated systems, and the bis adducts

having the highest melting point (*Table 4, pg. 43*): **40b-d** < **42b-d** < **41b-d** (the only deviation of this is a slightly higher melting point of sat. mono-dibromocarbene **42d** compared to bis-dibromocarbene **41d**). Interestingly, this trend is revered for the hydrocarbon cages: **41a** < **42a** < **40a**. The overall melting point trend shows the melting points in order from lowest to highest CF_2<CCl_2<CBr_2<CH_2. The mixed carbene adducts support this trend as well. Only the mono-dibromocarbene adduct **40d** showed decomposition upon heating (186.4 °C) and only the dichloro-cyclopropane mixed carbene adduct **41e** showed a wide melting point range. The sample of compound **41e** melted 90% between 142.5-143.2 °C but did not fully melting until 147.9 °C.

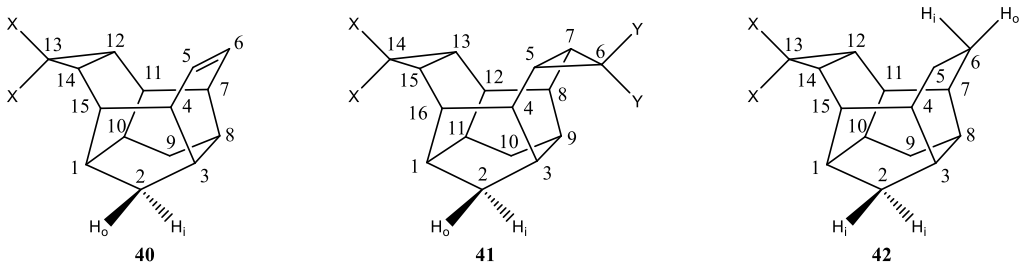

	a	b	c	d	e	f	g
X=	H	F	Cl	Br	H	H	Cl
Y=	H	F	Cl	Br	Cl	Br	Br

Figure 34: IUPAC numbering of each of the three base carbene scaffolds.

Trends in the ^{1}H-NMR and ^{13}C-NMR were also observed. One of the main ways to gauge the progress, purity, and identity of these compounds were by the higher order multiplets in the olefinic region (5.8-6.5 ppm) the double signals of the outer methylene position (0.1-1.0 ppm) with characteristic geminal couplings (^{2}J*=10.0-13.0 Hz*). The absolute assignment of all signals was accomplished using 2-D NMR spectroscopy (primarily ^{1}H-Corelation Spectroscopy (COSY) and Heteronuclear Multiple Quantum Coherence (HMQC)). Heteronuclear Multiple Bond Correlation (HMBC) was occasionally used, but not necessary for most compounds. All the carbene adducts

share the same ridged scaffold that impacts coupling. Most H-H coupling was clear in the 2-D COSY NMR; however, some coupling was weak. The dihedral angle, derived from the Karplus equation, shows the strong coupling of the outer methylene hydrogens located on carbons C-2/9 (or C-2/10) of all adducts and C-13/14 of the saturated systems (*Figure 34, pg. 44*). The dihedral angle of the outside hydrogens of the methylene position are all close to 54° while the interior hydrogens have a dihedral angle of 70°. Angles closer to 90° will show weak coupling to other protons. The inner methylene protons display large ^{2}J geminal couplings with the outer methylene protons but ^{3}J couplings could not clearly established.

Analytical data obtained for the four mono carbene adducts is consistent with their C_s point group. Each show eight signals (plus two additional signals for the cyclopropane **40a**) ^{1}H-NMR and eight signals in the ^{13}C-NMR. Only slight variations in proton chemical shifts were observed between the mono adducts. The H-12, -14 protons of the difluorocarbene adduct **40b** (*Figure 34, pg. 44*) displayed an apparent dt structure with a large coupling constant $^{3}J_{H\text{-}F}$ =15.77 Hz; these were the only proton noticeably split by fluorine. The mono-cyclopropane adduct **40a** has the largest variation in chemical shift trends with H-12, -14 being at 0.78 ppm, significantly lower that the dihalocarbenes (lowest being the difluorocarbene adduct **40b** centered at 1.42 ppm). The mono-cyclopropane also displayed characteristic signals for the cyclopropane unit; two ddd signals at high field (centered at 0.22 and 0.05 ppm) each integrating to one proton. ^{13}C-NMR also show similar consistence among the various adducts. The olefinic signals of the four mono adducts were withing a 1 ppm range of 133 to 134 ppm. Major differences between the various adducts stemmed from the position of the cyclopropane carbon. C-13 for adduct **40a** is at highest field (4.9 ppm) and was consistent with an unsubstituted CH_2 cyclopropane. Adduct **40d** had a C-13 chemical shift of 36 ppm. This carbon is slightly less shielded compared to the other dihalocyclopropane due to

the electronegativity of the halides. Adduct **40c** had a C-13 chemical shift of 66.2 ppm. The difluorocarbene adduct **40b** C-13 signal was at lowest field (centered at 116 ppm) of the series and clearly displayed a distinct dd coupling pattern, consistent with the inequivalent fluorine atoms.

Analytical data obtained for the four bis-carbene adducts **41a-d** was consistent with a C_{2v} point group, showing five proton (two additional signals for compound **41a**) and five carbon signals. Each compound showed the same signal pattern with only slight variation in chemical shift (numbering in *Figure 34, pg. 44*). Bis-cyclopropane adduct **41a** and its fluorinated derivative, **41b**, were slightly different from the other dihalides with the H-5, -7, -13, -15 signal observed at higher field than H-2_i, -10_i and the dichloro- and dibromo adducts **41c** and **41d** having H-2_i, -10_i being at higher field. Coupling of the geminal difluoride and H-5, -7, -13, -15 was not observed in the same significant fashion as **40b** due to overlap of ^{1}H signals, however, the C-6, -14 coupling was still observed as a triplet at 116 ppm.

Analytical data obtained for the four saturated mono-carbene adducts **41a-d** was consistent with a C_s point group. The saturated mono adducts **42a-d** share many similar signal patterns with their analogous mono adducts **40a-d**. The major difference between the saturated and unsaturated adducts is the change in chemical shifts at C-5/6 and H-5/6 (numbering in *Figure 34, pg. 44*). Conversion of the hydrogenation reactions can be tracked and quantified using the relative intensity of the olefin signal versus the new ethano signals at higher field. This structural change is also reflected in the ^{13}C-NMR, moving the olefinic signals of **40** near 133 ppm to the range of 20 ppm for the saturated adducts of **41**.

Analytical data for the three mixed carbene adducts **41e-g** was consistent with a C_s point group. The two dihalocyclopropane adducts **41e** and **41f** display many of same signal patterns with the only main difference being the chemical shift of CX_2 (C-6, -14) in the ^{13}C-NMR (numbering

in *Figure 34, pg. 44*). The mixed dichloro adduct **41e** has a CX_2 carbon shift of 53.5 ppm versus mixed dibromo adduct **41f** at 37 ppm. The mixed dibromo dichloro adduct **41g** shows the CCl_2 carbon at 52.8 ppm and the CBr_2 carbon at 28.5 ppm, both assigned as C-6, -14.

3.2.3.1 NMR Analysis of Mono-dibromocarbene Adduct **40d**

All ^{1}H-NMR and ^{13}C-NMR (and ^{19}F-NMR when applicable) chemical shifts were assigned using 2-D COSY and HMQC (and HMBC and tROESY where applicable) experiments.

The ^{1}H-NMR of mono-dibromocarbene adduct **40d** displays eight signals with equal integration, consistent with the compounds C_s symmetry. In the olefinic region, a multiplet of higher order centered at 6.16 ppm was observed for protons H-5, -6. The upper bridgehead protons proximate to the cyclopropane unit, H-11, -15 were observed as a broad multiplet centered at 2.78 ppm. The upper bridgehead protons proximate to the olefin unit, H-4, -7 were observed as a broad multiplet centered at 2.73 ppm. The lower bridgehead positions H-1, -10 had a higher chemical shift, displayed at 2.63 ppm, when compared to the protons assigned to H-3, -10, displayed at 1.97 ppm; both lower bridgehead positions are displayed as apparent singlets. The signals associated with the methylene positions H-2 and H-9 were delineated as H-2_i, -9_i and H-2_o, -9_o due to the mirror plane of the compound. These signals are characteristic due to the large geminal coupling observed; $^{2}J_{\text{H-9o, -9i}} = {}^{2}J_{\text{H-2o, -2i}} = 11.8$ Hz. The signal associated with the interior methylene protons, H-2_i, -9_i, were observed at a higher chemical shift, 1.74 ppm, versus the outer position at 0.73 ppm. This is consistent considering the rigid structure of the cage and the effect of steric environments on chemical shift. Between the two methylene signals at a chemical shift of 1.74 ppm, protons H-12, -14 can be observed.

The ^{13}C-NMR of mono-dibromocarbene adduct **40d** displayed eight signals, consistent with the C_s symmetry of the compound. The lowest field signal observed in the olefin region is

indicative of the carbons C-5, -6. At a chemical shift of 36.0 ppm the carbon C-13 was observed. This chemical shift is indicative of a CX_2 (X=Br, Cl) moiety in the molecule. The most intense signals in the ^{13}C spectrum are observed at highest field and are associated with the methylene positions C-2, -9. This higher intensity can be explained by the methylene carbons being secondary with a shorter relaxation time versus other carbons.

All signals were unequivocally assigned using common 2-D homonuclear and heteronuclear correlation experiments. The COSY spectrum displayed clear correlations between the olefinic protons H-5, -6 and the bridgehead protons H-4, -7 with an intense crosspeak. H-5, -6 showed no other couplings within the scaffold. The protons H-4, -7 displayed a cupoling to the upper bridgeheads H-11, -15 and lower bridgeheads H-3, -8. The dihedral angle between H-11, -15 and H-4, -7 is close to 0° and had the high intensity crosspeak. The lower bridgehead H-3, -8 shows correlation to the outer methylene protons H-2_o, -9_o which can be easily identified due to the doublet signal structure mentioned above. The methylene protons H-2_o, -9_o can also be observed coupling to the lower bridgehead protons H-1, -10. Methylene protons H-2_o, -9_o and H-2_i, -9_i show the typical intense crosspeak expected of geminal protons, however, due to a dihedral angel of nearly 70° between the inner methylene protons H-2_i, -9_i and all four lower bridgehead positions little to no coupling was observed. The lower bridgehead protons H-1, -10 displayed a strong coupling to the upper bridgehead protons H-11, -15. The upper bridgehead protons H-11, -15 also display coupling with the high field doublet of doublets associated with the dibromocyclopropane protons, H-12, -14.

HMQC data clearly supports these assignments with H-5, -6 showing correlation to the carbon signal in the olefinic region. The methylene protons H-2, -9 showed correlation to the highest field signal consistent with the above-mentioned observations. In addition, correlations between

respective bridgehead positions is clear allowing for unequivocal distinction. The dibromocyclopropane CX_2 carbon shows no correlation to protons.

3.2.3.2 NMR Analysis of Bis-dibromocarbene Adduct **41d**

The ^{1}H-NMR of bis-dibromocarbene adduct **41d** displays five signals, four integrating to four protons and one integrating to two protons, consistent with the compounds C_{2v} symmetry. At lowest field, integrating to four protons, is the signal assigned to the upper bridgehead positions, H-4, -8, -12, -16 at chemical shift of 2.69 ppm and displayed as a singlet. At slightly lower field, 2.63 ppm, is the signal assigned to the lower bridgehead positions H-1, -3, -9, -11, also integrating to four protons and displayed as a singlet. The protons associated with the cyclopropane moieties of **41d**, H-5, -7, -13, -15, were located at 1.99 ppm as a singlet and integrated to four protons. The only characteristic signals for this compound were those of the methylene units. Methylene positions H-2 and H-10 were delineated as H-2_i, -10_i and H-2_o, -10_o due to the mirror plane of the compound. These signals are characteristic due to the large geminal coupling observed; $^{2}J_{\text{H-10o, -10i}}$ = $^{2}J_{\text{H-2o, -2i}}$ = 11.9 Hz. The signal associated with the interior methylene protons, H-2_i, -9_i, were observed at a higher chemical shift, 1.69 ppm, versus the outer position at 0. 53 ppm. This is consistent considering the rigid structure of the cage and the effect of steric environments on chemical shift.

The ^{13}C-NMR of mono-dibromocarbene adduct **41d** displayed four signals, consistent with the C_{2v} symmetry of the compound. The two bridgehead positions of the cage and the bridgehead carbons of the cyclopropane moieties all share similar chemical shifts. The upper bridgehead was observed at lowest field followed by the lower bridgeheads, and then the cyclopropane carbons. At a chemical shift of 34.9 ppm the carbons C-6, -14 were observed. This chemical shift is

indicative of a CX_2 (X=Br, Cl) moiety in the molecule. At highest field the methylene positions C-2, -9 were observed and is consistent with other molecules with analogous structure.

All signals were unequivocally assigned using common 2-D homonuclear and heteronuclear correlation experiments. The COSY spectrum displayed clear coupling between the cyclopropane protons H-5, -7, -13, -15 and the upper bridgehead positions H-4, -8, -12, -16 with an intense crosspeak. The upper bridgeheads were also observed strongly coupling with the lower bridgehead positions H-1, -3, -9, -11. The lower bridgehead H-1, -3, -9, -11 shows correlation to the outer methylene protons H-2_o, -10_o which can be easily identified due to the doublet signal structure mentioned above. Methylene protons H-2_o, -9_o and H-2_i, -9_i show the typical intense crosspeak expected of geminal protons, however, due to a dihedral angel of nearly 70° between the inner methylene protons H-2_i, -9_i and the four lower bridgehead positions little to no coupling was observed.

HMQC data clearly supports these assignments with each clear correlations for each of the bridgehead positions. The methylene protons H-2, -9 showed correlation to the highest field signal consistent with the above-mentioned observations. The dibromocyclopropane CX_2 carbon shows no correlation to protons.

3.2.3.3 NMR Analysis of Saturated Mono-dibromocarbene Adduct **42d**

The assignment and NMR spectra for the saturated carbene adducts share many similarities with the mono adducts. The olefinic signal characteristic of **40d** was no longer present and two signals, both integrating to two protons can be observed at higher field. These new signals corresponded to the four ethano protons H-5_i, -6_i and H-5_o, -6_o and displayed a complex coupling pattern of higher order, AA'XX'. The ^{13}C-NMR no longer had a signal in the olefinic region and a new signal at highest field was observed corresponding to C-5, -6.

3.2.4 X-Ray Crystallography of Select Carbene Adducts

Table 5: X-ray crystallographic data obtained for the mono and saturated mono carbene adducts.

Parameter	Mono CCl_2	Mono CBr_2	Sat. Mono CCl_2	Sat. Mono CBr_2
Structure #	**42c**	**42d**	**40c**	**40d**
Empirical Formula	$C_{15}H_{16}Cl_2$	$C_{15}H_{16}Br_2$	$C_{15}H_{18}Cl_2$	$C_{15}H_{18}Br_2$
Formula Weight g/mol	267.2	356.1	269.2	358.1
Temperature, K	100	100	100	100
Color	Colorless	colorless	colorless	colorless
Crystal size, mm^3	?×?×?	?×?×?	?×?×?	0.285×0.188×0.051
Crystal system, space group	triclinic, $P\bar{1}$	triclinic, $P\bar{1}$	triclinic, $P\bar{1}$	triclinic, $P\bar{1}$
a, Å	6.8261 (2)	6.9111 (2)	6.8224 (2)	6.9111 (2)
b, Å	7.2483 (3)	7.3381 (1)	7.1892 (3)	7.3381 (1)
c, Å	11.8725 (5)	12.1058 (2)	12.4399 (5)	12.1058 (2)
α, °	88.011 (3)	89.279 (2)	81.348 (3)	81.016 (4)
β, °	84.934 (3)	85.367 (2)	80.021 (3)	80.122 (4)
γ, °	79.384 (3)	79.607 (2)	81.170 (3)	82.830 (4)
Volume, $Å^3$	575.01 (4)	601.89 (2)	588.97 (4)	615.56 (5)
Z	2	2	2	2
ρ_{calcd}, mg/m^3	1.543	1.54184	1.518	1.932
R_1[a] [$I > 2\sigma(I)$]	0.0285		0.0299	0.0321
R_1[a] (all)	0.0286		0.0350	0.0420
wR_2[b] [$I > 2\sigma(I)$]	0.0734		0.0717	0.0741
wR_2[a] (all)	0.0735		0.0752	0.0797
Largest diff. peak/hole, e $Å^{-3}$	039/-0.34		0.32/-0.23	1.11/-065

Table 6: X-ray crystallographic data obtained for the bis and mixed carbene adducts.

Parameter	Bis CH_2	Bis CCl_2	Bis CBr_2	CCl_2 CH_2
Structure #	**41a**	**41c**	**41d**	**41e**
Empirical Formula	$C_{16}H_{18}$	$C_{16}H_{16}Cl_2$	$C_{16}H_{16}Br_2$	$C_{16}H_{18}Cl_2$
Formula Weight, g/mol	212.3	350.1	527.9	281.2
Temperature, K	100	100	100	100
Color	colorless	colorless	colorless	colorless
Crystal size, mm^3	0.181×0.127×0.063	?×?×?	?×?×?	0.559×0.249×0.134
Crystal system, space group	orthorhombic, Cmcm	monoclinic, $P2_1/c$	monoclinic, $P2_1/c$	monoclinic, C2/m
a, Å	9.9098 (5)	8.3694(2)	8.5038 (2)	12.6905 (5)
b, Å	11.7445 (4)	12.9044(2)	13.3548 (2)	9.9152 (4)
c, Å	9.2126 (4)	13.4707(2)	13.5362 (3)	9.8811 (4)
α, °	90	90	90	90
β, °	90	104.447(2)	103.071 (2)	91.052 (3)
γ, °	90	90	90	90
Volume, $Å^3$	1072.21 (8)	1408.86(5)	1497.43 (5)	1243.12 (9)
Z	4	4	4	4
ρ_{calcd}, mg/m^3	1.315	1.651	1.54184	1.503
R_1[a] [$I > 2\sigma(I)$]	0.0386	0.0289		0.0333
R_1[a] (all)	0.0417	0.0298		0.0381
wR_2[b] [$I > 2\sigma(I)$]	0.1011	0.0723		0.0805
wR_2[a] (all)	0.1041	0.0728		0.0838
Largest diff. peak/hole, e $Å^{-3}$	0.28/-0.17	0.36/-0.34		0.30/-0.40

X-ray structures were obtained for eight of the fifteen carbene adducts. Some structural features are shared between the various adducts of each series. It was observed that each of the mono dihalocarbenes and saturated dihalocarbenes share the same triclinic, $P\bar{1}$ unit cell and space group (*Table 5, pg. 51*). This similarity in crystal packing is expected due to their similar structures. It can be inferred that the difluorocarbene adduct will also share this property, however the presence of fluorine substituents may cause drastic changes to crystal packing.

The trend of identical unit cell and space group extends to the bis-dihalocarbenes **41c-d** as both are monoclinic, $P2_1/c$ (*Table 6, pg. 52*). However, the bis-cyclopropane **41a** shows a variation on the trend and fills an orthorhombic crystal system. This variation in crystal packing may indicate that two mono-cyclopropane adducts **40a** and **42a** would follow not the same trends as the mono-dihalocarbene adducts **40c-d**. The mixed carbene **41e** is in the monoclinic crystal system but fills a different space group compared to the other bis adducts in the monoclinic system.

The mono-dihalocarbene adducts **40c** and **40d** crystalize in the triclinic space group, $P\bar{1}$, with typical bond distances. The longest bonds are the *exo* C-X (Br-1 and Cl-1) bond at 1.777 Å and 1.942 Å for **40c** and **40d**, respectively. These are slightly longer (0.016 and 0.014 Å) than the *endo* C-X (Br-2 and Cl-2) bond but within normal bounds of C-X bonds in a cyclopropane.[38] This is likely in part due to the decreased crowding the *exo* C-X bond experiences; increased crowding to the *endo* halide leads to bond shortening.

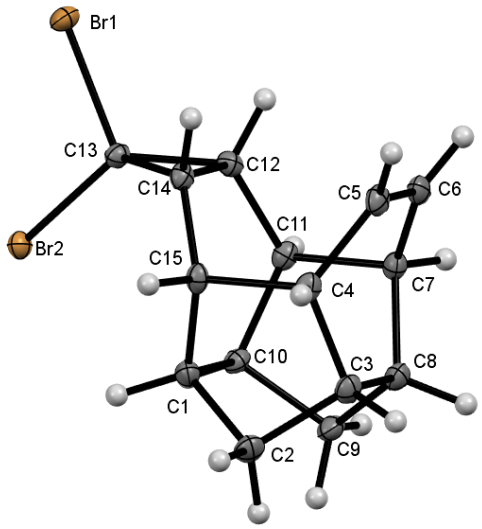

*Figure 35: Thermal ellipsoid plot of **40d**. Thermal ellipsoids are drawn at the 50 % probability level. Numbering is assigned through IUPAC conventions.*

The longest C-C bond spans the upper bridgehead positions C-4/7 and C-11/15 at 1.600 Å for both adducts, slightly longer than the average sp^3 bond length. The shortest bonds are found in the cyclopropane unit and the olefin. The C-12 to C-13 and C-13 to C-14 bonds of the dihalocyclopropane units average 1.502 Å. The C-5/6 bond average is 1.327 Å. Both these values are within normal ranges. Many of the bond angles deviate from the ideal geometry due to the conformationally ridged scaffold. The largest deviation from the ideal sp^3 geometry is located at C-12/14 with a C-C-C bond angle of 125.3° and C-13 with a X1-C-C bond angle of 124.9°. This is more pronounced in the dibromocarbene adduct due to the size of the bromine atoms. These larger deviations from ideal can be attributed to the cyclopropane ring. Interestingly, the sp^2 olefinic carbons are closest to ideal with an average C-C-C and C-C-H angle of 120.0°.

Carbene adducts **40c** and **40d** crystalized in a centrosymmetric pattern with two molecules occupying each discrete unit cell.

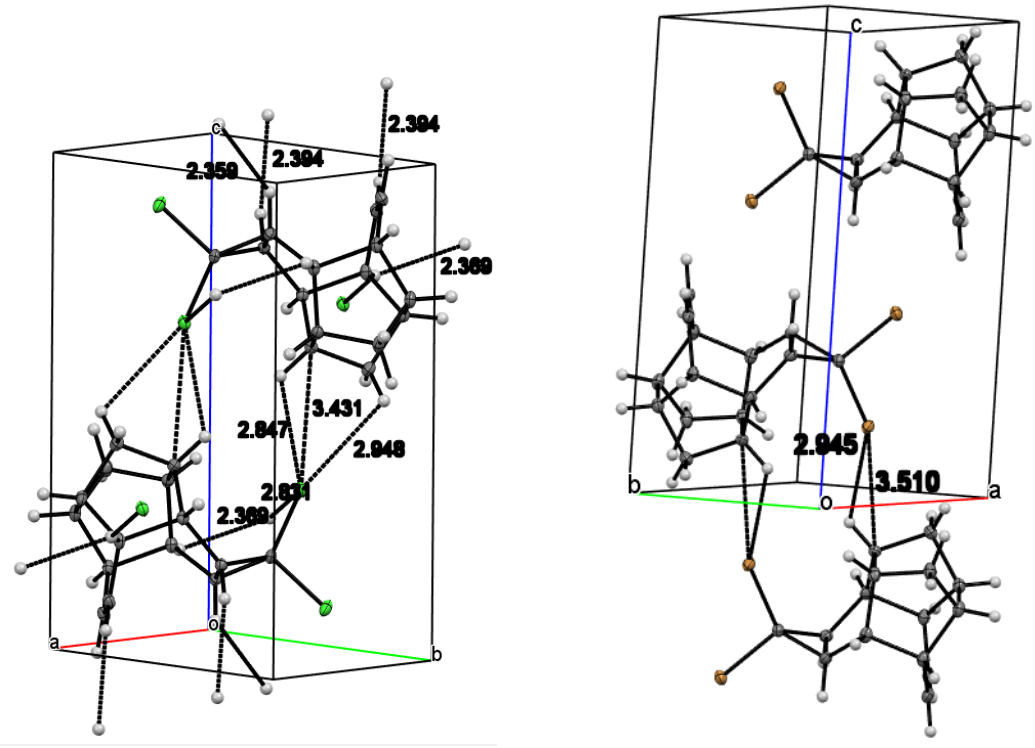

*Figure 36: Thermal ellipsoid plot of crystal packing within the monoclinic unit cell in the crystal structures of **40c** (left) and **40d** (right). This plot shows the difference in packing and short contact between molecules in each discrete unit cell. Distances and short contacts between adjacent cells were omitted for clarity. Thermal ellipsoids are drawn at the 50% probability level.*

Short contact interactions show three interactions between each molecule of the **40c** unit cell. Short contact distances for $Cl^{\delta-}\cdots H^{\delta+}_{bridgehead}$ and $Cl^{\delta-}\cdots H^{\delta+}_{methylene}$ are 2.847 and 2.948 Å, respectively. The $Cl^{\delta-}\cdots C^{\delta+}_{bridgehead}$ distance is shown to be longer at 3.431Å. Short contacts within the unit the unit cell of **40d** show two interactions. Short contact distances for $Br^{\delta-}\cdots H^{\delta+}_{bridgehead}$ and $Br^{\delta-}\cdots C^{\delta+}_{bridgehead}$ are 2.945 and 3.510 Å, respectively. Short contacts between the adjacent unit cells for **40c** show no interactions along the a-o-c planes. Interactions along the b-o-c plane is limited to one bridgehead hydrogen for each molecule. Short contacts for this bridgehead show a

$H_{bridgehead}\cdots H_{bridgehead}$ and a $Cl^{\delta-}\cdots H^{\delta+}{}_{bridgehead}$ interaction with distances of 2.369 and 2.831 Å. Interestingly, both interactions occur with the same molecule. Interactions between cell along the a-o-b plane are limited to H-H short contacts. Two interactions, both $H_{olefin}\cdots H_{cyclopropane}$, are inverse of the other, binding to the analogous position of the other molecule. Both have the same short contact distance of 2.394 Å. The third interaction along the a-o-b plane is a $H_{cyclopropane}\cdots H_{cyclopropane}$ short contact of 2.359 Å. Only one interaction between unit cells of **40d** was observed. The $Br^{\delta}{}_{exo}\cdots Br^{\delta}{}_{exo}$ interaction shows a short contact distance of 2.954 Å. This is the only interaction and is along the a-o-c plane.

The bis dihalocarbene adducts follow much of the same trends observed in the mono adducts. Both the dichloro- and dibromocarbene adducts, **41c** and **41d**, crystalize in the monoclinic, $P2_1/c$ space group. The longest bonds are the *exo* C-X (Br-1/3 and Cl-1/3) bond at 1.775 Å and 1.941 Å for the dichloro- and dibromo adducts, respectively. These are slightly longer (0.015 and 0.014 Å) than the *endo* C-X (Br-2/4 and Cl-2/4) bond but still within normal ranges for the C-X bond.

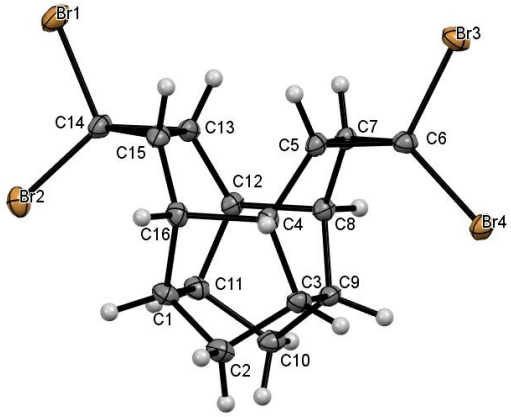

*Figure 37: Thermal ellipsoid plot of **41d**. Thermal ellipsoids are drawn at the 50 % probability level. Numbering is assigned through IUPAC conventions.*

The longest C-C bond spans the upper bridgehead positions C-4/8 and C-12/16 at 1.596 Å for both adducts, slightly longer than the average sp^3 bond length. The shortest bonds are found in the cyclopropane unit and the olefin. The C-5/13 to C-6/14 and C-6/14 to C-7/15 bonds of the dihalocyclopropane units average 1.501 Å. The largest deviation from the ideal sp^3 geometry is located at C-5/7/13/15 with a C-C-C bond angle of 125.02° for the dichlorocarbene adduct and 125.85° for the dibromocarbene adduct. This is more pronounced in the dibromocarbene adduct due to the size of the bromine atoms. The bis cyclopropane unit only shows some minor differences in bond angles. Due to the lack of halogens the large bond angels seen at C-5/7/13/15 are diminished and much closet to ideal at 119.99°.

The bis adduct **41a** is unique in that it does not fit the pattern established by the dihalocarbene adducts. **41a** crystalizes in an orthorhombic crystal system. **41**a crystalizes in a base-centered polar pattern with six molecules occupying each unit cell.

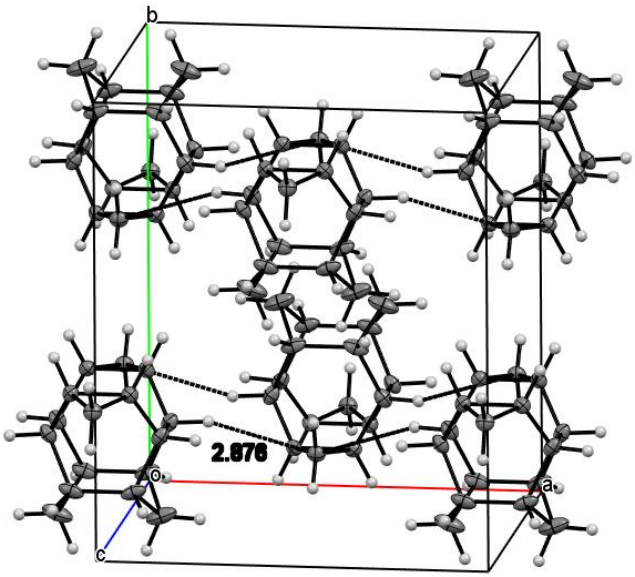

*Figure 38: Thermal ellipsoid plot of crystal packing within the orthorhombic unit cell in the crystal structures of **41a**. This plot shows the packing and short contacts between molecules in each discrete unit cell. Distances and short contacts between adjacent cells were omitted for clarity. Thermal ellipsoids are drawn at the 50% probability level.*

Short contacts within the unit cell are all the same showing a $C_{cyclopropane}\cdots H_{bridgehead}$ distance of 2.878 Å. This interaction acts as a repeating unit throughout the crystal branching through the a-o-b and b-o-c planes. There are not short contacts along the a-o-c plane, implying that these crystals form bimolecular sheets with strong interactions along two planes and only weak Van der Waals interactions along the third plane.

The bis carbene adducts **41c**, and **41d** both crystalized in a centrosymmetric pattern with four molecules occupying each unit cell. Each unit cell shows these four molecules grouped in such a way that the two molecules in the upper half (direction is relative to depiction in *Figure 37*,

pg. 56) of the unit cell interact with each other, the two molecules in the lower half interact, and the interior molecules of the upper and lower interact.

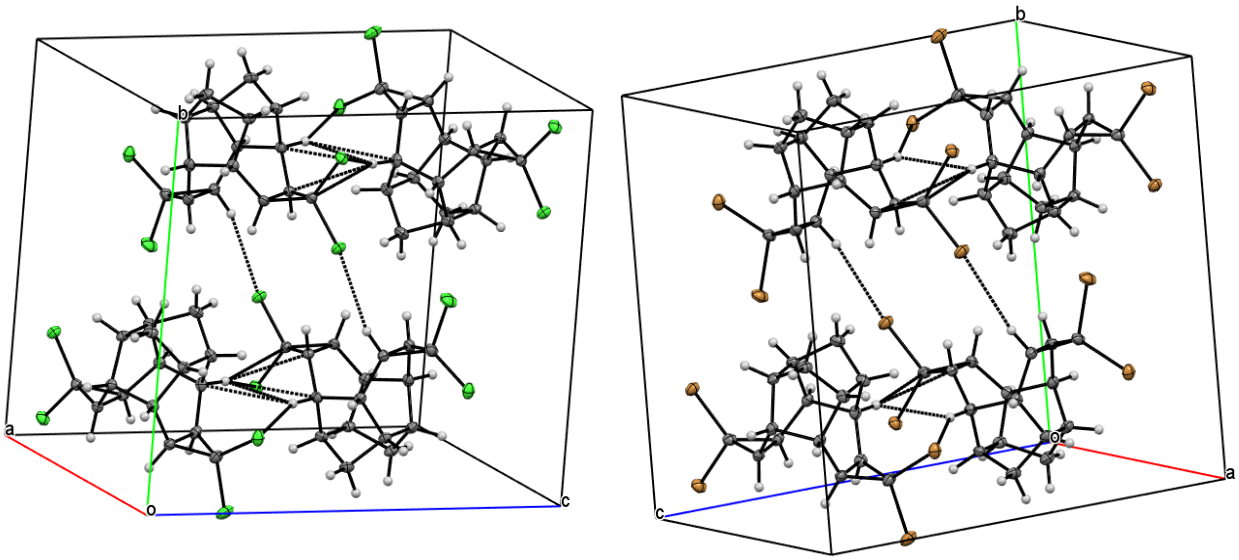

*Figure 39: Thermal ellipsoid plot of crystal packing within the monoclinic unit cell in the crystal structures of **41c** (left) and **41d** (right). This plot shows the difference in packing and short contact between molecules in each discrete unit cell. Distances and short contacts between adjacent cells were omitted for clarity. Thermal ellipsoids are drawn at the 50% probability level.*

Short contact distances in the upper and lower halves of **41c** show significant interactions in the plane. Three $C_{bridgehead}\cdots H_{bridgehead}$ distances of 2.893, 2.881 and 2.776 Å, Two $Cl^{\delta-}\cdots H^{\delta+}{}_{bridgehead}$ distances of 2.864 and 2.929 Å, one $C_{cyclopropane}\cdots H_{bridgehead}$ distance of 2.876 Å, and only one $H_{bridgehead}\cdots H_{bridgehead}$ distance of 2.296 Å were observed. Short contact distances in the upper and lower halves of **41d** show $H_{bridgehead}\cdots H_{bridgehead}$ distances of 2.342 Å and $C_{cylopropane}\cdots H_{bridgehead}$ interactions at 2.768 and 2.888 Å. The reduced interactions within the **41d** unit cell is likely due to the crystallization pattern and the larger Van der Waals raii of the bromide and larger distance between the upper and lower halves of the unit cell.[39] The only short contact between these sections

is a $X^{\delta-}\cdots H^{\delta+}_{bridgehead}$ interaction (X=Cl, Br) with a distance of 2.717Å in **41c** and 2.889 Å in **41d**. This tight binding along the lateral sections of the crystal forms the major component of the unit cell. Interactions between unit cells are strong showing the same interactions between the molecules in the same cell and in adjacent cells along the a-o-b plane. Short contacts along the b-o-c plane are limited to $X^{\delta-}\cdots H^{\delta+}_{bridgehead}$ interactions with one short contact at 2.934 Å for **41c** and three short contacts averaging 2.994 Å for **41d**. Along the a-o-c plane **41c** shows three $Cl^{\delta-}\cdots H^{\delta+}_{bridgehead}$ short contacts averaging 2.776 Å. Compound **41d** shows significantly more interaction with four different $Br^{\delta-}\cdots H^{\delta+}_{bridgehead}$ interactions averaging 2.906 Å and a $Br^{\delta-}\cdots C^{\delta+}_{bridgehead}$ short contact distance of 3.518 Å. These values and number of short contacts show that **41d** displays looser packing within the unit cell but tighter packing throughout the crystal system.

The saturated monocarbene adducts **42c** and **42d** crystalize in the triclinic space group $P\,\overline{1}$ with typical bond distances.[38] Thus, the longest bonds are the *exo* C-X (Br-2 and Cl-2) bond at 1.776 Å and 1.941 Å for the dichloro- and dibromo adducts, respectively. These are slightly longer (+0.018 and +0.026Å) than the *endo* C-X (Br-1 and Cl-1) bond but within normal bounds of C-X bonds in a cyclopropane.[38] This is likely in part due to the decreased crowding the *exo* C-X bond experiences; increased crowding to the *endo* halide leads to bond shortening.

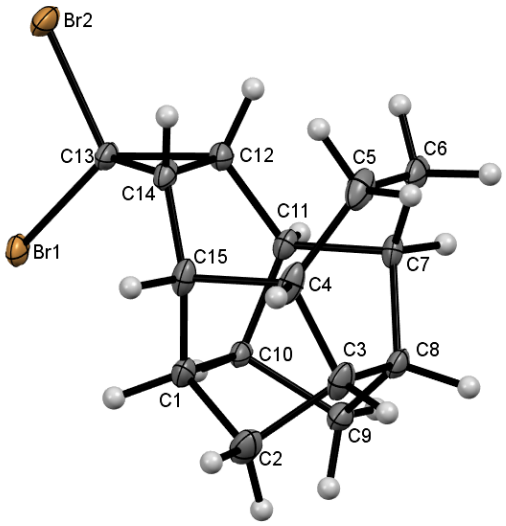

*Figure 40: Thermal ellipsoid plot of **42d**. Thermal ellipsoids are drawn at the 50 % probability level. Numbering is assigned through IUPAC conventions.*

The longest C-C bond spans the upper bridgehead positions C-4/7 and C-11/15 at 1.587 Å for **42c** and 1.585 for **42d**, slightly longer than the average sp^3 bond length but the shortest among the various carbene adducts.[38] The shortest bonds are found in the cyclopropane unit. The C-12 to C-13 and C-13 to C-14 bonds of the dihalocyclopropane units average 1.500 Å. Many of the bond angles deviate from the ideal geometry due to the conformationally ridged scaffold. The largest deviation from the ideal sp^3 geometry is located at C-12/14 with a C-C-C bond angle of 125.03° and at C-13 with a X1-C-C bond of 126.6°. This is more pronounced in **42d** due to the size of the bromine atoms. These larger deviations from ideal can be attributed to the cyclopropane ring.

In the solid state each adduct crystalized in a centrosymmetric pattern with two molecules occupying each unit cell.

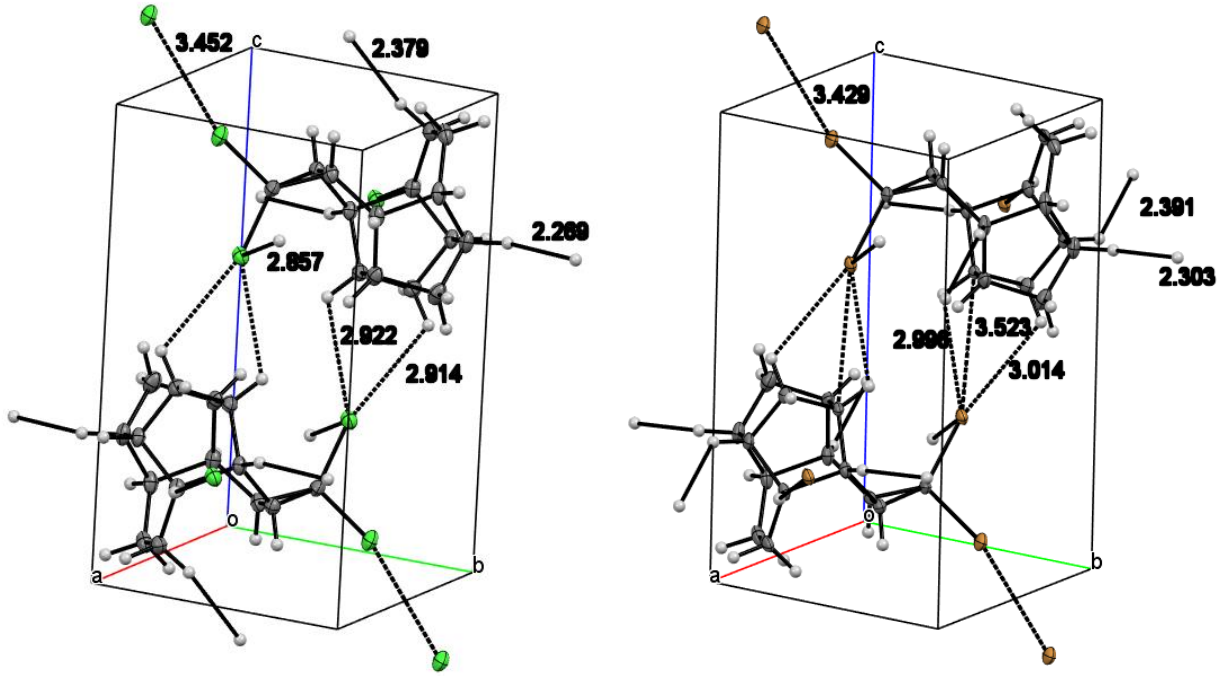

*Figure 41: Thermal ellipsoid plot of crystal packing within the triclinic unit cell in the crystal structures of **42c** (left) and **42d** (right). This plot shows the difference in packing and short contact between molecules in each discrete unit cell and short contacts between each unit cell. Thermal ellipsoids are drawn at the 50% probability level.*

Short contact distances between these two molecules in **42c** show $Cl^{\delta-}\cdots H^{\delta+}_{methylene}$ and $Cl^{\delta-}\cdots H^{\delta+}_{bridgehead}$ distances of 2.914 and 2.922 Å. These are shorter than the distances in **42d** with $Br^{\delta-}\cdots H^{\delta+}_{methylene}$ and $Br^{\delta-}\cdots H^{\delta+}_{bridgehead}$ distances of 3.014 and 2.996 Å. **42d** also has a short contact distance of 3.523 Å for a $Br^{\delta-}\cdots C^{\delta+}_{bridgehead}$ interaction. Interactions between adjacent unit cells can be measured by the short contact distances between molecules in each cell. Compound **42c** shows interactions $Cl^{\delta-}\cdots H^{\delta+}_{bridgehead}$, and Cl···Cl at 3.452 and 2.857 Å. There are two H-H interactions $H_{bridgehead}\cdots H_{bridgehead}$ and $H_{ethano}\cdots H_{ethano}$ at 2.268 and 2.379 Å. Compound **42d** shows only three interactions between cells. The $H_{ethano}\cdots H_{ethano}$ was not present in the solid state of **42d**, however, an additional $H_{bridgehead}\cdots H_{bridgehead}$ interaction can be observed. Short contact distances of Br···Br

and $Br^{\delta-}\cdots H^{\delta+}_{bridgehead}$ distances at 3.429 and 2.988 Å and two distinct $H_{bridgehead}\cdots H_{bridgehead}$ interactions at 2.391 and 2.303 Å were observed. The smaller distances within the unit cell of **42c** indicate tighter packing. This closer interaction is likely due to the smaller Van der Waals radii of the chlorides versus the bromides.[39] Despite this, there are some inter-unit-cell short contacts in **42d** that are shorter than those observed in **42c**. As such differences in packing patterns between the two adducts can be ascribed to packing effects of the halogens. The bromides cause a looser pack within each unit cell due to the Van der Waals radii but also to tighter packing along the a-o-c plane. The chlorides result in tighter intra-cell packing and a stronger interaction on the b-o-c plane. The interactions along the a-o-b plane of **42c** show two interactions, $H_{ethano}\cdots H_{ethano}$ and Cl···Cl, but the Br···Br interactions of **42d** are shorter.

The mixed carbene adduct **41e** crystalized in the monoclinic, C2/m space group. The longest bonds are the *exo* C-Cl (Cl-1') bond at 1.776 Å. This are slightly longer (0.014 Å) than the *endo* C-Cl (Cl-2') bond but still within normal ranges for the C-X bond.

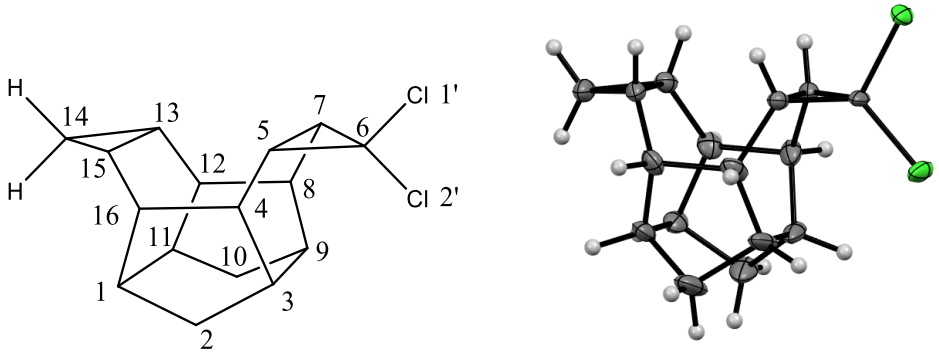

*Figure 42: Thermal ellipsoid plot of **41e**. Thermal ellipsoids are drawn at the 50 % probability level. Numbering is assigned through IUPAC conventions.*

The longest C-C bond spans the upper bridgehead positions C-4/8 and C-12/16 at 1.590 Å, slightly longer than the average sp^3 bond length. Bonds from C-1 to C-11 and C-3 to C-9 are both longer than average at 1.571 and 1.561 Å, respectively. The shortest bonds are found in the cyclopropane unit and the olefin. The C-5 to C-6 and C-6 to C-7 bonds of the dihalocyclopropane units both measure 1.494 Å. The C-13 to C-14 and C-14 to C-15 bonds are longer measuring at 1.508 Å. The largest deviation from the ideal sp^3 geometry is located at C-5/7 with a C-C-C bond angles of 124.92°. The cyclopropane unit shows some minor differences in bond angles. Due to the lack of halogens the large bond angels seen at C-5/7 are diminished and much closet to ideal at 119.87°. The other atoms within the scaffold are significantly closer to ideal with C-4/8 and C-12/16 having C-C-C bond angles averaging 103.78° and C-1/11 and C-3/9 having C-C-C bond angles averaging 110.29°.

41a crystalizes in a monoclinic crystal system. **41**a crystalizes in a centrosymmetric pattern with six molecules occupying each unit cell.

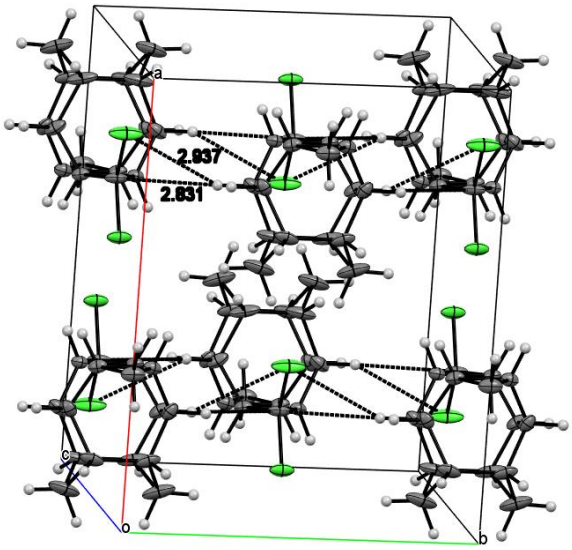

*Figure 43: Thermal ellipsoid plot of crystal packing within the orthorhombic unit cell in the crystal structures of **41e**. This plot shows the packing and short contacts between molecules in each discrete unit cell. Distances and short contacts between adjacent cells were omitted for clarity. Thermal ellipsoids are drawn at the 50% probability level.*

Interestingly, the packing pattern of **41e** most closely resembles that seen in **41a**. This is likely a packing effect driven by the cyclopropane units. The interactions within the unit cell and between each unit cell are identical. Two short contact distances can be observed in the unit cell. The $Cl^{\delta-}\cdots H^{\delta+}_{bridgehead}$ and $C_{dihalocyclopropane}\cdots H_{bridgehead}$ interactions measure at 2.937 and 2.831 Å, respectively. These are the only interactions observed between unit cells along the a-o-c plane. The a-o-b and b-o-c planes do not show interactions between unit cells. This is likely due to the similar packing pattern as observed with **41a** and decreased intermolecular interactions.

3.3 Preparation of Cage Hydrocarbons and Oxacages *Via* Rearrangement of Cage Compounds

3.3.1 Introduction to Rearrangement Chemistry of Polycyclic Systems

Rearrangement reactions are a powerful tool to access unique, new scaffolds by exploiting the inherent strain of cages and cage precursors; release of strain energy is a major driving force towards rearrangement.[2] Conditions for rearrangement reactions can vary greatly and can be used to synthesize novel cage structures from preexisting cages or from non-cage polycyclic compounds. Possibly the most well-known rearrangement reaction is the synthesis of adamantane **31** (*Figure 44, pg. 67*).[40, 41] By treating *endo*-tetrahydrodicyclopentadiene **57** with a Lewis acid, such as $AlCl_3$, a series of multiple rearrangements occur.[40, 41] Eventually, this will lead to the stabilomer, which is the most favorable configurational isomer possible. While further rearrangement is possible after the formation of adamantane, the stability of **31** will drive the equilibrium back the most stable isomer. Adamantane is significantly lower in strain energy, approximately 84-105 kJ/mol, due to the tetrahedral geometry and favorable chair conformations of the cyclohexane rings within the polycyclic scaffold.[42] *endo*-Tetrahydrodicyclopentadiene **57** will undergo a conformational flip to the *exo*-tetrahydrodicyclopentadiene **58** when exposed to a Brønsted acid (*Figure 44, pg. 67*).[41]This reaction proceeds through the deprotonation of **57** and a series of Wagner-Meerwein shifts. The *exo* conformer **58** is 12.55 kJ/mol less strained than **57**, making this a favorable reaction. The difference in products between the Lewis acid and Brønsted acid is based on the initial formation of the first carbocation species.[41]

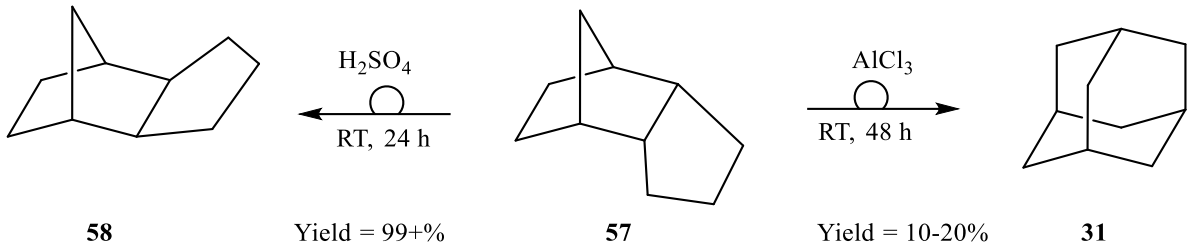

*Figure 44: : The isomerization of **57** to **31** proceeds through a series of Lewis acid catalyzed carbocation rearrangements. When isomerization is initiated by a Brønsted acid such as sulfuric acid, a conformational flip to exo-**58** is observed.*

Some Lewis acid catalyzed rearrangements may utilize metal ions such as silver, gold, platinum, and rhodium ions.[43-48] Silver (I) perchlorate and silver (I) nitrate have been used to obtain rearrangement products of cubane (*Figure 45, pg. 67*), homocubyl (*Figure 46, pg. 69*), and l,l'-bishomocubyl systems.[45, 46] These isomerization reactions may vary in mechanism as displayed by select functionalized cubane derivatives.

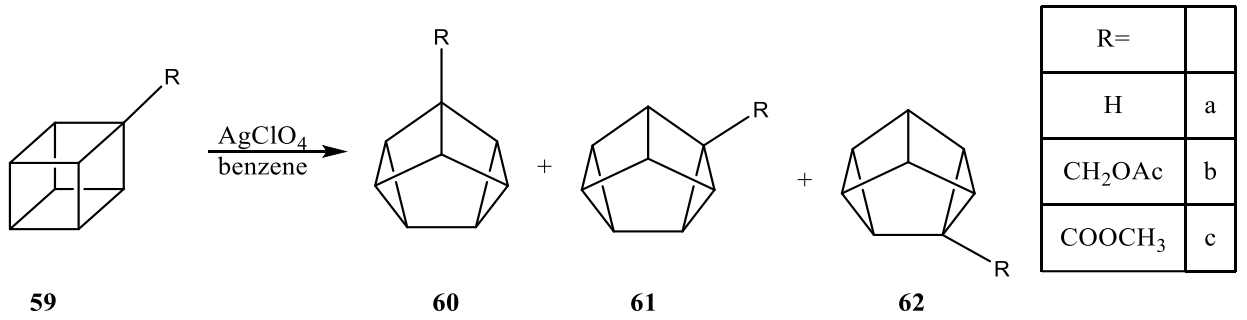

*Figure 45: Quantitative isomerization of cubane **59** to cuneane **60**. The potential for multiple pathways is highlitghed by the acetate (**b**) and ester (**c**) derivatives.*

It was also observed that the difference in substituent drastically impact the rate of reaction and product distribution (*Table 7, pg. 68*).[45]

Table 7: Rate constants at 40 °C of the isomerization of cubane and its derivatives. Rate law of second order: $\frac{-d[cubane]}{dt} = k_{Ag} * [cubane][AgClO_4]$.[45]

Substrate	k_{Ag}, M^{-1} sec^{-1}	Relative rate	Product(s)	Distribution **60**:**61**:**62**
59a	3.0×10^{-1}	17000	**60a**	N/A
59b	2.3×10^{-2}	1300	**60b-62b**	6:2:1
59c	5.5×10^{-3}	310	**60c-62c**	2:5:1

Silver ions can also be used to circumvent orbital symmetry requirements allowing isomerization that would be otherwise prohibited in a thermal conversion pathway (*Figure 46, pg. 69*) or require photochemical processes.[46] The rearrangement of homocubane **63** to homocuneane **66** is a symmetry disallowed $_{\sigma}2_a + _{\sigma}2_a$ electrocyclic reaction resulting in a decrease of 196.65 kJ/mol of strain energy.[10, 46] Paquette *et al*. originally calculates the decrease in strain to be approximately 188.3 kJ/mol. This was estimated using the assumption that the total strain energy should be approximately equal to the sum of the strain energy of the composite fused rings.[46, 49] Using more recent calculational data obtained using the B3LYP/6-31G* basis set, this value can be adjusted to the more accurate measurement of ΔE_{strain} = -196.65 kJ/mol (approximation).[10] Despite the favorable decrease in strain, the formation of the necessary transition state under thermal conversion is prevented by a sizeable activation barrier (E_A). This large E_A prevents isomerization of **63** to **66**, however, the addition of silver ions results in a complexation of metal orbitals with the strained σ orbitals of **63**. This gives a new set of occupied molecular orbitals with the correct symmetry properties for rearrangement to yield **66**.[46]

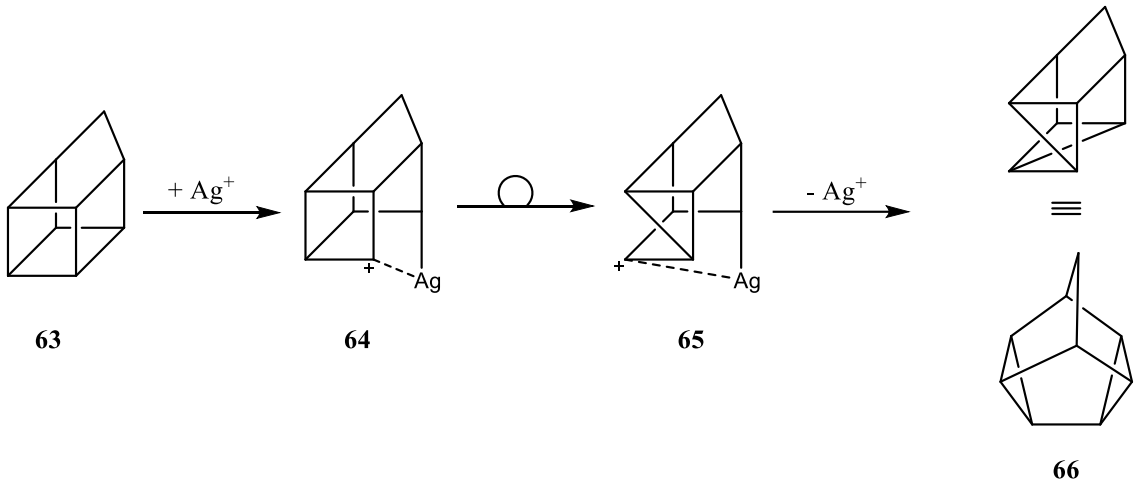

*Figure 46: Silver ion catalyzed isomerization of homocubane **63** to homocuneane **66**. The mechanism of this rearrangement is shown.*

The oxidative addition of silver to homocubane **63** removes two cyclobutane rings (ΔE_{strain} = -220.1 kJ/mol). The proximity of the metal to the carbocation of **64** allows for a carbocation-metal complex to form and stabilizes the activated species. This stabilization of the carbocation allows for the symmetry-disallowed transformation. A Wagner-Meerwein shift results in the formation of carbocation **65** with the loss of an additional two cyclobutane rings and the addition of a cyclopropane subunit and a net decrease in strain energy (ΔE_{strain} = -98.7 kJ/mol). The geometric arrangement of the carbocation-metal complex of **65** provides significantly less stabilization to the new molecular orbitals resulting in the reductive elimination of the silver and a Wagner-Meerwein shift forming a cyclopropane ring (ΔE_{strain} = 121.3 kJ/mol).[47] Overall, there is a decrease in strain due to the loss of four cyclobutane rings and addition of two cyclopropane rings making this reaction energetically favorable.[46, 47]

Not all cage systems will rearrange in the presence of silver salts. Systems such as pentaprismane **67a** and homopentaprismane **67b** do not isomerize when exposed to silver (I) salts

(*Figure 47, pg. 70*). It has also observed that many scaffolds obtained by rearrangement with silver salts will not react further even under more forcing conditions such as heat.[45, 47, 50] In systems such as homopentaprismane there is not a significant drop in the strain energy and prevents rearrangements analogous to those observed in the cubyl systems (*Figure 45, pg. 67*; *Figure 46, pg. 69*). Each intermediate also exhibits different levels of stabilization due to the geometrical arrangement of the carbocation-metal complex. The carbocation rearrangement after the addition of silver to homopentaprismane results in no further loss of strain energy. Therefore, the main driving force for this rearrangement is not present. Stabilization of the carbocation will also decrease upon further rearrangements thus eliminating the other driving force of the isomerization.[47]

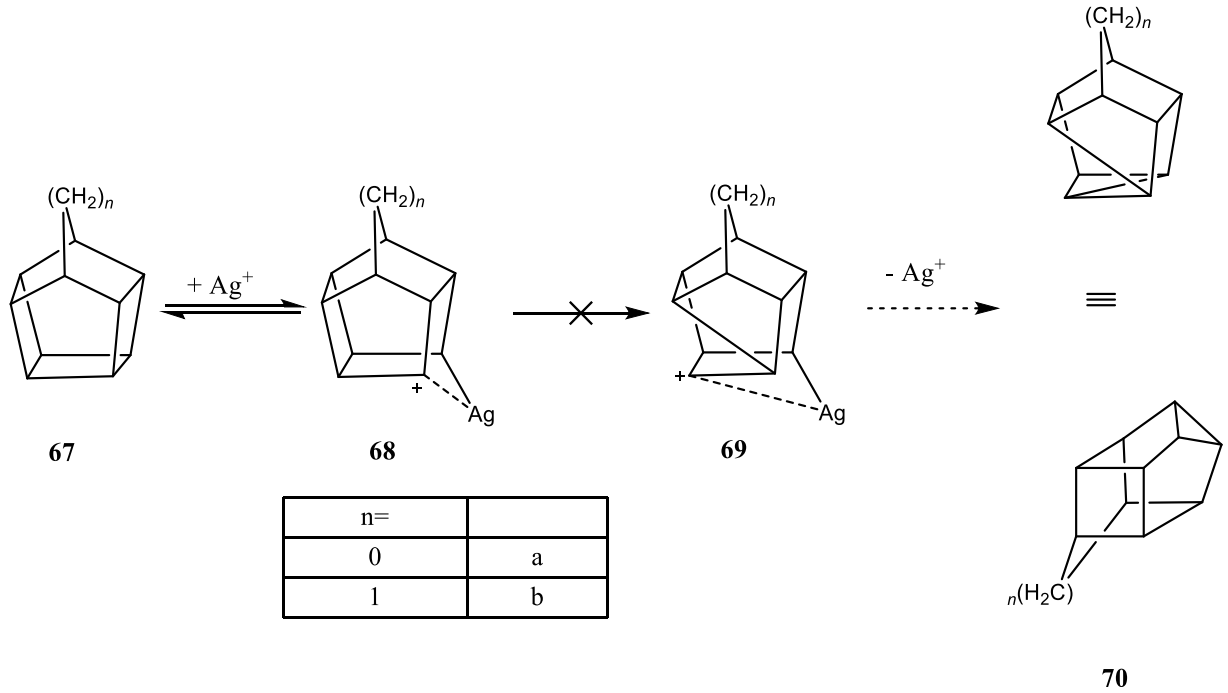

n=	
0	a
1	b

*Figure 47: Compound **67a-b** does not isomerize to **70a-b** by treatment with silver salts.*

The first carbocation species **68** is formed through the reversable oxidative addition of silver and is favorable as the number of cyclobutane rings is decreased by two. In addition, the silver ion

provides significant stabilization. The subsequent rearrangement to **69** does not occur as the number of rings stay stagnant. Carbocation **69** is less stable due to poor stabilization by the metal ion. The final rearrangement also results in an increase in overall strain energy with the addition of a cyclopropane and loss of a cyclopentane ring. The ΔE_{strain} for the isomerization of **67b** to **70b** was calculated to be +100.4 kJ/mol. Typically strain energy is reduced by 146-209 kJ/mol in transition metal catalyzed rearrangements and the lack of driving force prevents this isomerization.[51]

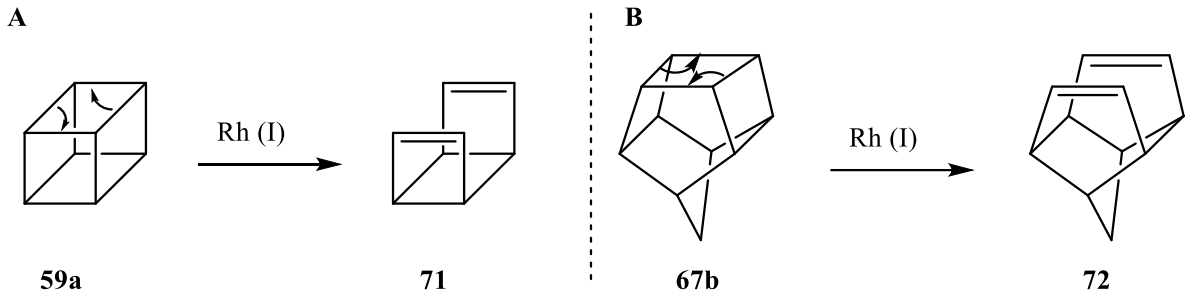

*Figure 48: Strained cages react differently based on the metal ion used. A) Cubane **59a** will undergo bond cleavage to the diene **71**. B) Homopentaprismane **67b** is cleaved to the homohypostrophene scaffold **72**.*[47]

While platinum ion catalyzed isomerization typically leads to the same products as silver ions, rhodium catalyzed isomerization often gives different results. Treating **59a** or **67b** with $(PH_3P)_2Rh(CO)Cl$ in chloroform at 75 °C for 20 hours (or $[Rh(norbornadiene)Cl]_2$ in benzene for 40 hours) resulted in the formal cycloreversion to diene **71** and homohypostrophene **72**, respectively (*Figure 48, pg. 71*).[45, 47, 51] Typically, silver, platinum, and rhodium metal salts used in these types reactions are all in the +1-oxidation state, however, a difference in the oxidative addition mechanism of Rh^+ to a C-C bond results in different reactivity that favors the homolytic

bond cleavage rather than carbocation rearrangement. The release of strain energy is still the main driving force in this isomserization.[47, 50]

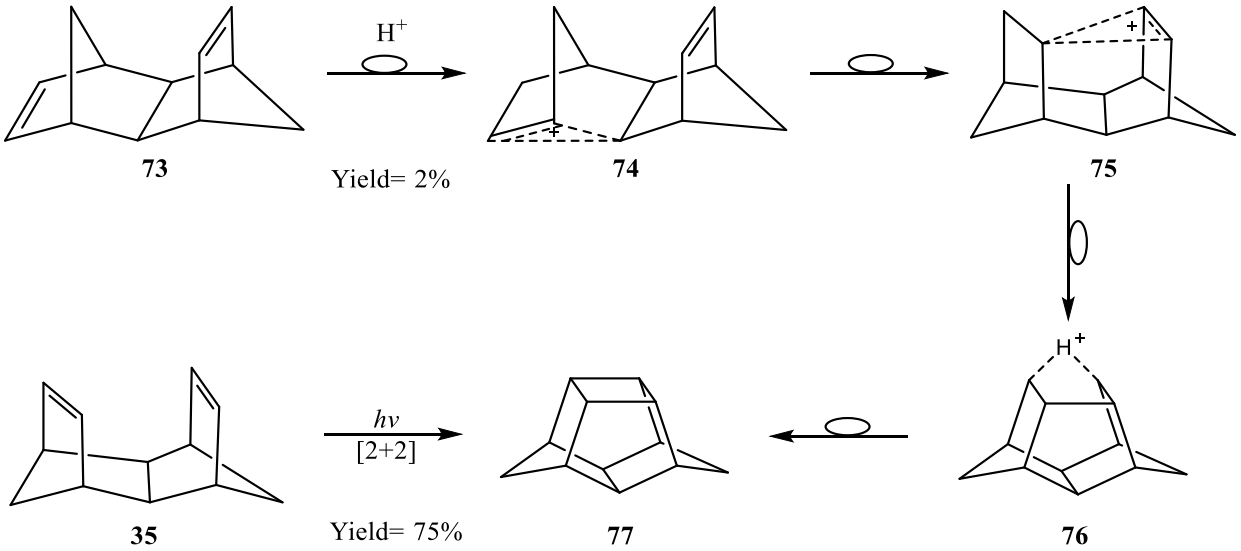

*Figure 49: The birdcage hydrocarbon **77** can be accessed through the isomerization of dehalogenated aldrin **73** through a series of carbocation rearrangements.*[52, 53]

Brønsted acid catalyzed rearrangement, unlike Lewis acid catalyzed rearrangements, can only be done on systems containing basic proton-accepting positions. Formic acid has been shown to react with certain scaffolds and generate cage compounds as a result.[53] Dehalogenated aldrin **73**, an isomer of the dehalogenated isodrin **35**, when exposed to formic acid can isomerize into the birdcage hydrocarbon **77** (2% yield) (*Figure 49, pg. 72*). This scaffold can also accessed through from **35** *via* a photochemical [2+2] cycloaddition.[52]

The epoxide **78** (derived from hypostrophene **28**) was subjected to rearrangement by Brønsted acid (*Figure 50, pg. 73*).[22] In the presence of 10% perchloric acid, protonation of epoxide **78** resulted in an electrophilic ring opening to generate a carbocation. This carbocation, **79a**, then rearranged over three steps to give carbocation **82a** before reacting with water from the aqueous

environment to give the known diol **83a**. This is an instance where the rearrangement of a cage compound results in the loss of the cage structure.[22]

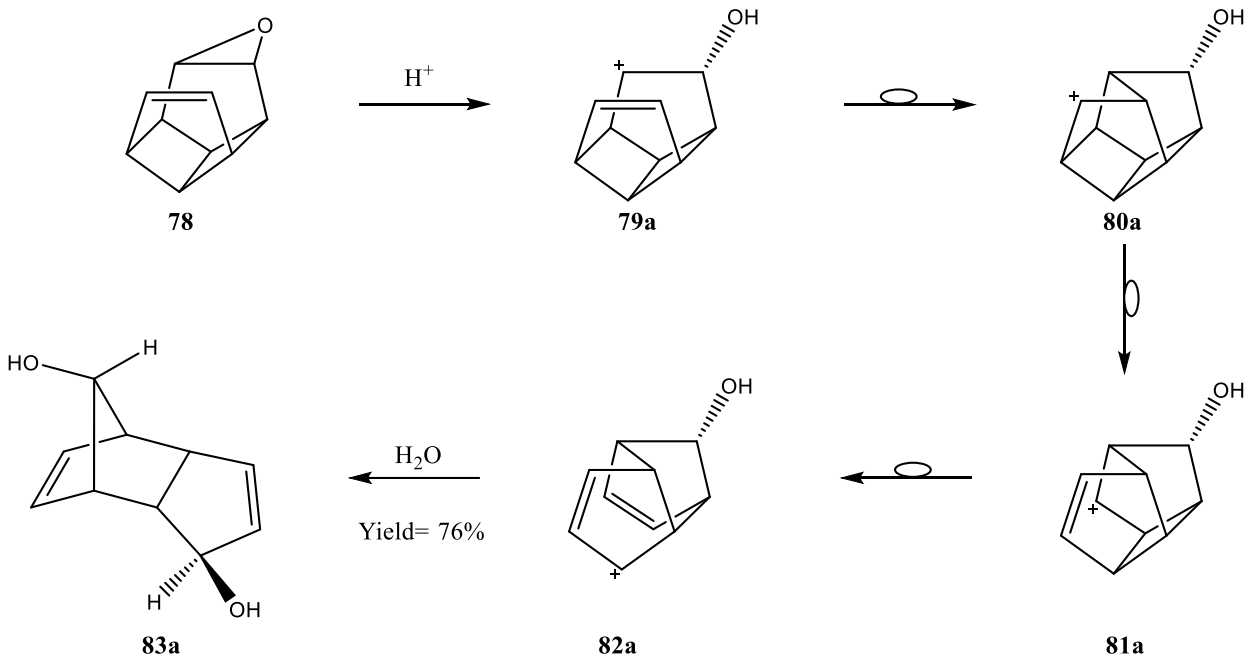

*Figure 50: The mechanism for the rearrangement and hydroxylation of **54** to the diol **83a**, formally the 2,4-cyclopentadien-1-ol dimer.*

This mechanism shares many similarities with other rearrangement reactions (*Figure 52, pg. 74*). Once protonated, the system undergoes several transannular reactions to furnish cationic diene **82a**. Once this intermediate was formed, no further isomerization was observed.[22]

Both Lewis and Brønsted acid catalyzed rearrangements display common mechanistic patters, such as carbocation formation followed by transannular reactions (*e.g.*, Wagner-Meerwein shifts) to afford the final scaffold. Ionic pathways accessed through S_N1 or E1-type mechanisms resulting in carbocations may use analogous mechanisms as acid catalyzed rearrangements.[23, 52, 54]

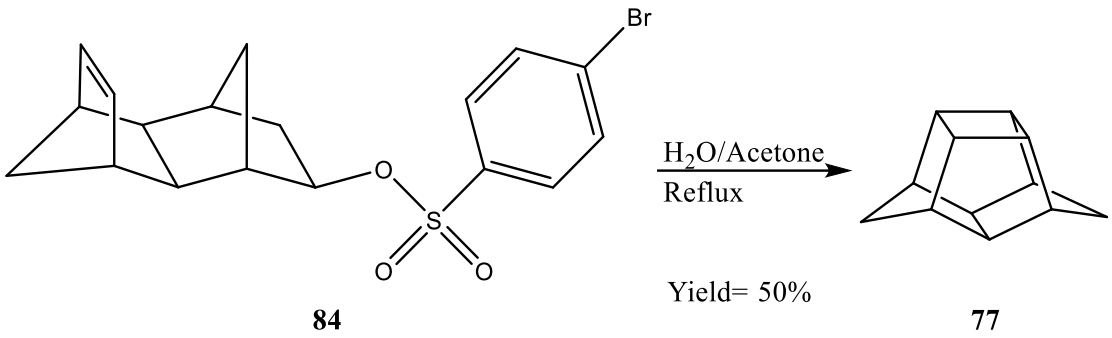

*Figure 51: Solvolysis of the brosylate in **84** proceeds through carbocation **74**, also observed in the formic acid treatemnt of **73** (Figure 49, pg. 72), to the final product, **77**.*[52, 54]

The solvolysis of the brosylate **84** resulted in the same carbocation **74** observed in the formic acid rearrangement of **73** (*Figure 49, pg. 72*) furnishing rearrangement product **77**.[54] This is an example of a formal elimination propagated rearrangement.

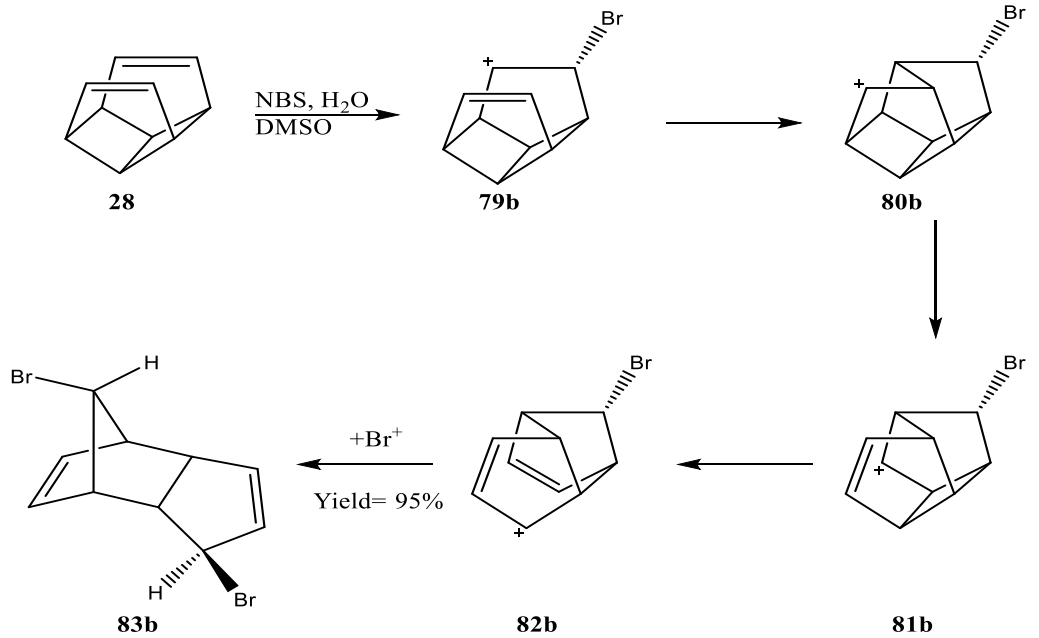

*Figure 52: The bromination and rearrangement of **28** to the dibromide **83b** shares mechanistic similarities to the rearrangement of epoxide **78** (Figure 50, pg. 73). Both mechanisms follow the same steps; the key difference between these two reactions being the nucleophile in the last step.*[22]

The NBS bromination to hypostrophene **28** (*Figure 52, pg. 74*) is an example of a S_N1-type mechanism resulting in rearrangement. Interestingly, this reaction results in a comparable scaffold as the rearrangement of epoxide **78**. Paquette *et al.* gives both rearrangement reactions comparable mechanisms (*Figure 50, pg. 73; Figure 52, pg. 74*).[22]

Dehalogenation reactions have also been shown to facilitate rearrangements of cage compounds. In the synthesis of homohypostrophene **72** (*Figure 53, pg. 75*), the cage compound **85** can be converted into the desired product **72** through heating in the presence of NaI in *N*-(2-hydroxypropyl)methacrylamide (HMPA); potassium iodide (KI) in polyhydrogen fluoride-pyridine (HF*py) has also been described.[51, 55] Some side reactions were observed in the dehalogenation/elimination steps of this reaction sequence, resulting in the formation of the unusual hydrocarbon **70b** and the iodocages **87** and **88** (*Figure 53, pg. 75*).

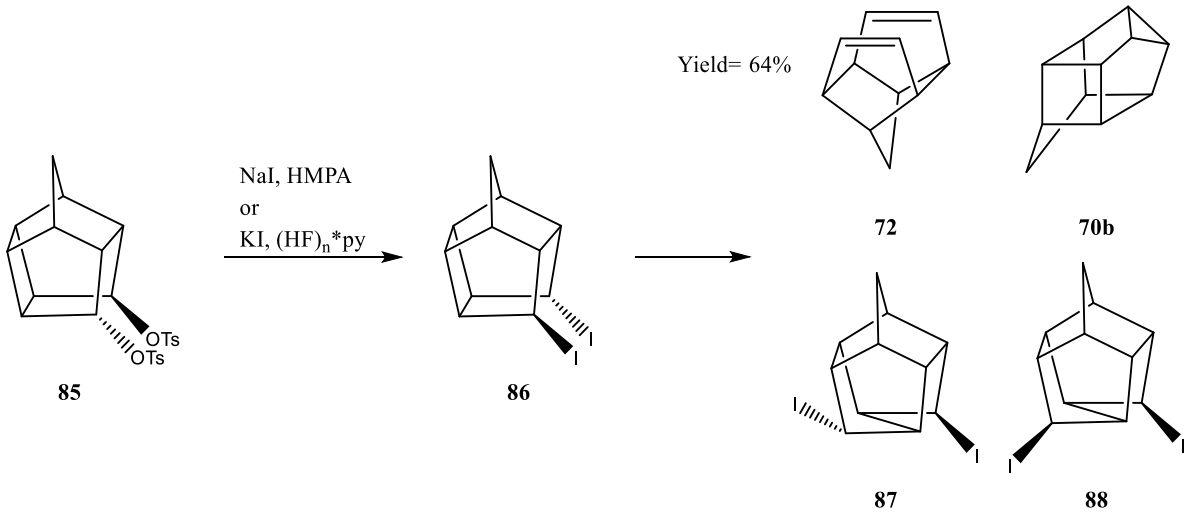

*Figure 53: When treated with NaI or KI, **85** will undergo two substitution reactions to the diiodide **86**. This intermediate undergoes dehalogenation when heated in the appropriate solvent(s) to **72**. Three side products were also observed **70b**, **87**, and **88**. Compound **70b** was not obtained through silver salt treatment of **67b** but can be synthesized from **85** in competition with **72**.*[47, 51, 55]

The proposed mechanism of the rearrangement to **70b** is a concerted pathway and relies on the abstraction of one iodide in **86** followed by a transannular attack to an electrophilic bridgehead position. A Wager-Meerwein shift, and loss of the second iodide gives the side product **70b**.[51]

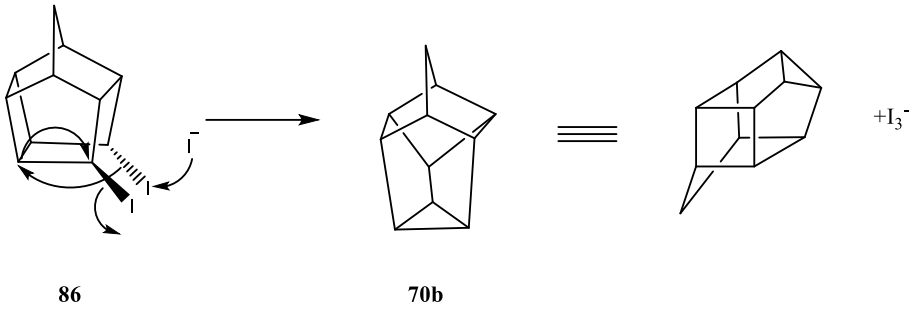

86 **70b**

*Figure 54: Proposed mechanism for obtaining **70b** from **86**.*[51]

Finally, rearrangement reactions can also be propagated through thermal pathways. Thermal isomerization is commonly observed the synthesis of cage scaffolds *via* thermal activation of two-fold homolytic bond cleavage (formally a cycloreversion).[56] Under pyrolysis conditions the birdcage hydrocarbon forms the Fukunaga diene **89** (*Figure 55, pg. 76*).[56]

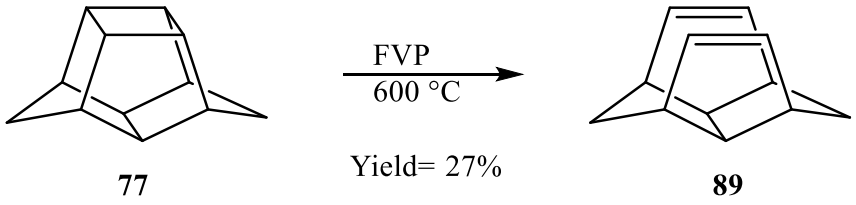

77 **89**

*Figure 55: Flash vacuum pyrolysis (FVP) of **77** at 600 °C in a graphite tube yielded the diene **89** via homolytic bond cleavage.*[56]

3.3.2 Rearrangement of the Diene **1**

Acid catalyzed rearrangement of cage diene **1** and select oxygen-containing derivatives were carried out under specific conditions. Rearrangement reactions initiated *via* silver salts,

periodic acid, and Amberlyst-15 (a solid polymer-bound sulfonic acid catalyst) were investigated. Herein, the rearrangement reactions of **1** and its derivatives are explored. *Note: Rearrangement arrows have been omitted for clarity.*

The diene **1** was exposed to silver salts in hopes to facilitate rearrangement.[45, 47, 48] These reactions were attempted along two different protocols. Protocol I was carried out by stirring compound **1** at room temperature with silver perchlorate in benzene for two days.[45] Protocol II was carried out by stirring **1** at room temperature with silver nitrate in a 4:3 solution of MeOH/water for two days in the dark.[48] Neither of these reactions resulted in any detectable isomerization (GC/MS and ^{1}H-NMR). Since no rearrangement was observed under these conditions, we can conclude that the oxidative addition of silver either does not occur or the resulting complex does not favor rearrangement.[47]

Interestingly, there was also no trace of silver-olefin metal complexes. Silver salts have been shown to form complexes with olefins under similar conditions and the diene **1** has been shown to form metal complexes to Pt and Pd metal centers (*Figure 6, pg. 6*).[11]

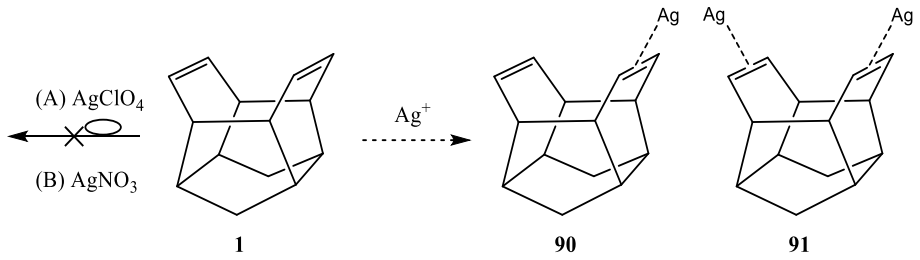

*Figure 56: Upon treatment of **1** with Ag^{+} salts no rearrangement was observed. In addition, neither **90** nor **91** were detected.*

While no rearrangement nor metal complexation occurred under the above conditions, however, diene **1** does rearrange in the presence the polymer-supported sulfonic acid catalyst,

Amberlyst-15 (*Figure 57, pg. 78*).[57, 58] This is likely due to the difference in mechanism and reversibility of the oxidative addition of silver versus the protonation of the olefin unit. Oxidative addition results in a partial positive charge on the bound carbon atoms as the charge is delocalized by the silver center. The protonation of the olefin *via* Brønsted acid results in a true carbocation that it not delocalized due to lack of conjugation and heavily favors carbocation rearrangements to more stable tertiary carbocation intermediates.

When diene **1** was stirred with 2 equivalents of Amberlyst-15 (catalyst loading in *5.1 General Comments*) over the course of 10 days rearrangement to two products were observed by GC/MS (*Figure 57, pg. 78*). To ensure consistent concentration of acid in the system, additional DCM was added when necessary to maintain solvent levels. The intermediate, hydrocarbon **92**, was observed as an isomer of diene **1** with an $M^{\cdot+}$ peak of *m/z*= 184 ($C_{14}H_{16}$) (data collected by Alyssa Feduik, undergraduate researcher) but could not be isolated pure for full characterization. Over time the signal intensity of **92** diminished while a second product signal increased. Full conversion to **93** was reached after 10 days of reaction time (may take as long as 20 days) and no further reaction was observed. This, along with the GC/MS data suggests that **92** is a precursor to **93** and that **93** is the final product in the isomerization of **1**.

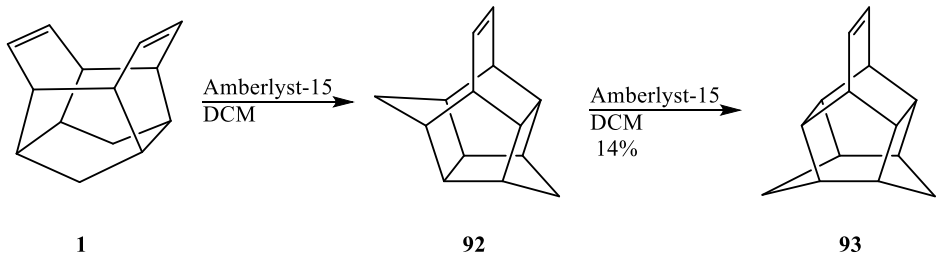

*Figure 57: The isomerization of **1** resulted in two hydrocarbons **92** and **93***

The slow rate of rearrangement was likely due to **92** being close in relative strain energy to **93** (*Table 8, pg. 79*). Compound **1** contains an eight-membered ring and is more strained than **92** which contains a seven-membered ring which in turn is more strained than **93** composed of only five-and six-membered rings (*Table 8, pg. 79*).

*Table 8: Change in enthalpy (H°) and heat of formation (E) in the rearrangement of **1** to **92**. Overall change in strain energy was ΔE_{strain} =-114.4125 kJ/mol Calculated by DFT using the B3-LPY 6-31J* basis set.*

	1	**92**	**93**
H° (E_h)	-542.83178	-543.10741	-543.10573
E (E_h)	-543.86831	-543.82603	-543.82734
ΔE_{strain} (kJ/mol)	0	110.982400	3.430088

The cage compound **93** was isolated in low yields (14%) by column chromatography (SiO_2, *n*-pentane). The low yield of this reaction was determined to be due, in part, to hydrolysis of the carbocation intermediates by trace amounts of water in the reaction solvent and/or atmosphere. No hydrolysis products were isolated for characterization, however, polar eluting materials observed by GC/MS suggest hydroxylation. The mechanism for the formation of **92** and **93** is unknown but is suspected to go through a non-classical carbocation intermediate. It can be inferred based on the rearrangements of the mono-epoxide **94** (*Figure 63, pg. 85*) and its rearrangement product oxacage **99** (*Figure 69, pg. 93*) that the rearrangement of diene **1** begins with protonation of the olefin generating a carbocation. This carbocation then undergoes a series of rearrangements to the intermediate **92** and to the final product **93**.

This reaction was also attempted on the monoene **24**. As rearrangement of diene **1** was observed it was hypothesized that the initial steps for the rearrangement of **1** and monoene **24** would share similar mechanisms and aid in determining the exact mechanism in which **92** and **93** form. While we have not yet been able to isolate distinct products from this reaction GC/MS data suggests two products (approximately 3:1 ratio), both with possible molecular ion peaks of *m/z*= 186 ($C_{14}H_{18}$) making them isomers of the monoene **24**. When the fully saturated cage **25** or the mono-cyclopropane **40a** are reacted under identical conditions no reaction was observed (*Figure 58, pg. 80*).

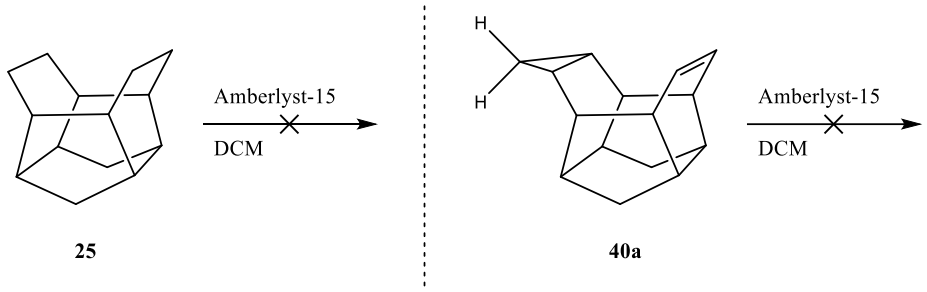

*Figure 58: When exposed to Amberlyst-15 compounds **25** and **40a** do not show any detectable conversion to rearrangement products.*

3.3.2.1 NMR Analysis of **93**

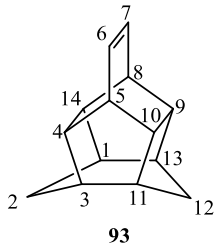

*Figure 59: IUPAC numbering of hydrocarbon **93**.*

The ^{1}H-NMR of hydrocarbon **93** displays six signals, four signals integrating to two protons and two signals integrating to four protons, consistent with the compounds C_{2v} symmetry. In the olefinic region, a multiplet of higher order integrating to two protons and centered at 6.16 ppm was observed for protons H-6, -7. The upper bridgehead protons at a chemical shift of 2.49 ppm, observed as an apparent singlet, were assigned as H-5, -8. These protons are shown at lower field compared to the lower bridgehead positions H-4, -9, -10, -14 and middle bridgehead positions H-1, -3, -11. -13 which have chemical shifts of 2.28 and 1.98 ppm, respectively. Both the middle and lower bridgehead positions integrate to four protons. The signals associated with the methylene positions H-2 and H-12 were delineated as H-2_i, -12_i and H-2_o, -12_o due to the mirror plane of the compound. These signals are characteristic due to the large geminal coupling observed; $^{2}J_{\text{H-2o, -2i}} = {}^{2}J_{\text{H-12o, -12i}}$ = 11.5 Hz. The signal associated with the interior methylene protons, H-2_i, -12_i, were observed at a higher chemical shift, 1.41 ppm, versus the outer position at 1.11 ppm. This is consistent considering the rigid structure of the cage and the effect of steric environments on chemical shift. The methylene signals for **93** were also found to have a narrower chemical shift range versus **1**.

The ^{13}C-NMR of hydrocarbon **93** displayed five signals, consistent with the C_{2v} symmetry of the compound. The lowest field signal observed in the olefin region is indicative of the carbons C-6, -7. The three bridgehead positions all show similar chemical shifts with the upper bridgeheads C-5, -8 being at highest field. The lower and middle bridgeheads can be observed at slightly lower fields at chemical shifts of 50.3 and 42.4 ppm, respectively. The lower and middle bridgehead positions also show the most intense signals in the ^{13}C spectrum due to the difference in abundance. At highest field, the methylene positions C-2, -12 were observed.

All signals were unequivocally assigned using common 2-D homonuclear and heteronuclear correlation experiments. The COSY spectrum displayed clear correlations between the olefinic protons H-6, -7 and the upper bridgehead protons H-5, -8 with an intense crosspeak. H-6, -7 showed no other couplings within the scaffold. The protons H-5, -8 displayed a coupling to the middle bridgehead positions H-4, -9, -10, -14. The lower bridgehead H-1, -3, -11, -13 shows coupling to the middle bridgeheads and to the outer methylene protons H-2_o, -12_o which can be easily identified due to the doublet signal structure mentioned above. Methylene protons H-2_o, -9_o and H-2_i, -9_i show the typical intense crosspeak expected of geminal protons, however, for the lower bridgehead positions little to no coupling was observed. This is likely due to the dihedral angel nearing 90° but without XRD data, the exact angle is unknown.

HMQC data clearly supports these assignments with H-6, -7 showing correlation to the carbon signal in the olefinic region. The methylene protons H-2, -9 showed correlation to the highest field signal consistent with the above-mentioned observations. In addition, correlations between respective bridgehead positions is clear allowing for unequivocal distinction.

3.3.3 Synthesis and Rearrangement of Epoxide Cages

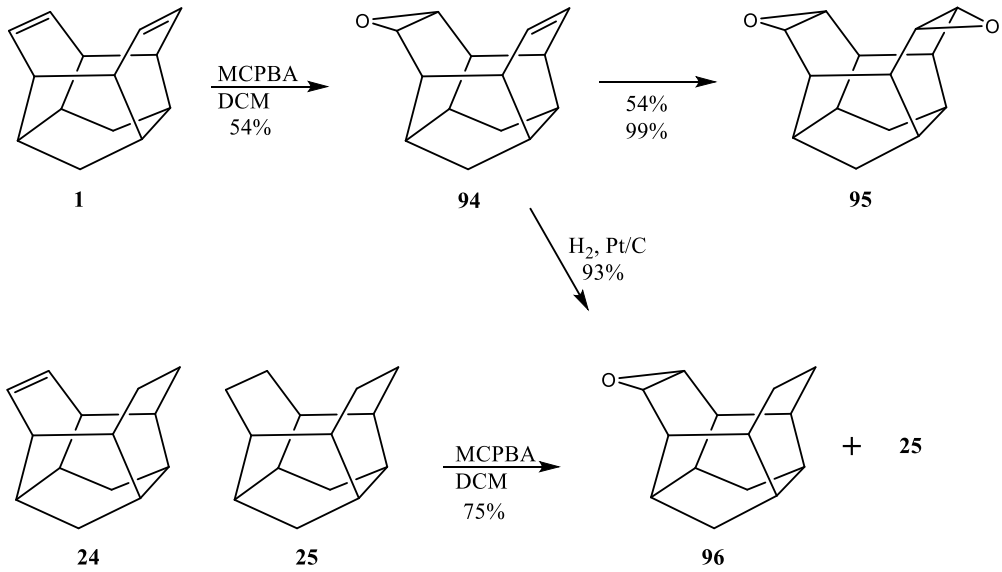

*Figure 60: The epoxidation of **1** yields epoxides **94** and **95**. Epoxide **96** can be accessed through hydrogenation of **94** or epoxidation of **24**. Compound **25** does not participate in these reactions under standard conditions but will undergo hydroxylation under forcing conditions.*

The epoxides **94** and **95** were synthesized through epoxidation of **1** with MCPBA (*Figure 60, pg. 83*). When diene **1** was reacted with 1.2 molar equivalents of MCPBA over the course of 16 hours, a mixture of **94** and **95** was obtained with nearly 100% conversion of **1**. The products were then purified by column chromatography (SiO_2, 5:1 hexanes/EtOAc). Both **94** and **95** were isolated in moderate yields (both 54%). Single crystals for XRD were grown from chloroform for both compounds. Bis-epoxide **95** was prepared using 2.2 molar equivalents of MCPBA giving full conversion with no further purification necessary and excellent isolated yields (95%).

The saturated mono-epoxide **96** was synthesized by epoxidation of **24** (in mixture with **25**) with MCPBA (*Figure 60, pg. 83*). Reacting 1.2 molar equivalents of MCPBA with the mixture of **24** and **25** over 16 hours gave a mixture of **96** and unreacted **25**. The product was then purified by

column chromatography (SiO_2, 5:1 hexanes/EtOAc). **96** was isolated in moderate to good yields (75%). **96** can also be synthesized by catalytic hydrogenation of **94**. This afforded clean **96** in good yields (93%) without further purification.

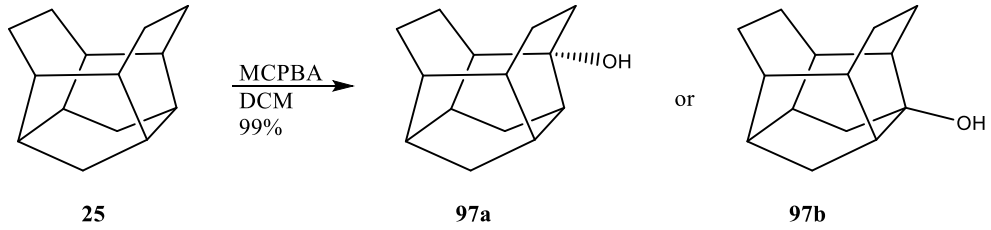

*Figure 61: Treating the fully saturated cage **25** with MCPBA results in hydroxylation of a bridgehead position. The position of hydroxylation could not be determined by NMR. Data suggests **97a** as the more likely structure.*

When a large excess of MCPBA (4.0 molar equivalents or more) was added to the mixture of **24** and **25**, hydroxylation of **25** was observed alongside epoxidation of **24**. In a control experiment the fully saturated cage **25** was subjected to oxidation with 5.0 molar equivalents of MCPBA resulting in full conversion to a hydroxylated species, likely **97a** or **97b** (*Figure 61, pg. 84*). This compound displayed C_i symmetry in the ^{1}H-NMR and a molecular ion peak of *m/z*= 204 ($C_{14}H_{20}O$) in the GC/MS with a characteristic loss of water (-18) giving a *m/z* = 186 ($C_{14}H_{18}$) as the second most intense fragment. Infrared spectroscopy (IR) showed a strong broad signal at $\tilde{\nu}$ = 3293 cm^{-1} (br, m, O-H), clearly indicating an alcohol functionality. While the structure of this compound could not be unequivocally assigned by NMR due to overlapping signals data suggests the assigned structures of **97a** and **97b**. The compound formed single crystals in a variety of solvents (chloroform, DCM, benzene, 5:1 hexanes/EtOAc), however, none were viable for XDR. Frames of the diffraction pattern were recorded as well diffracting and poorly diffracting in an alternating fashion leading to half of the data set being unusable.

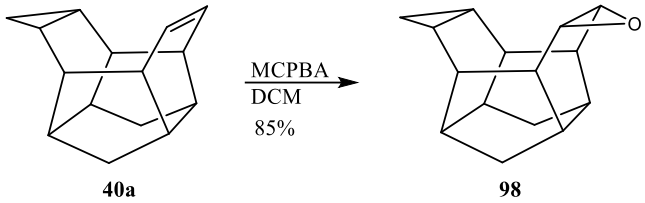

*Figure 62: The mono-cyclopropane adduct **40a** was epoxidized with MCPBA to give epoxide **98**.*

The mono-cyclopropane **40a** was also subjected to MCPBA oxidation under the above conditions resulting in compound **98**, which was isolated in good yield (85%) without further purification (*Figure 62, pg. 85*). Once obtained in sufficient quantities the rearrangement of **98** will be investigated.

3.3.3.1 Rearrangement Reactions of the Mono-epoxide Cage **94**

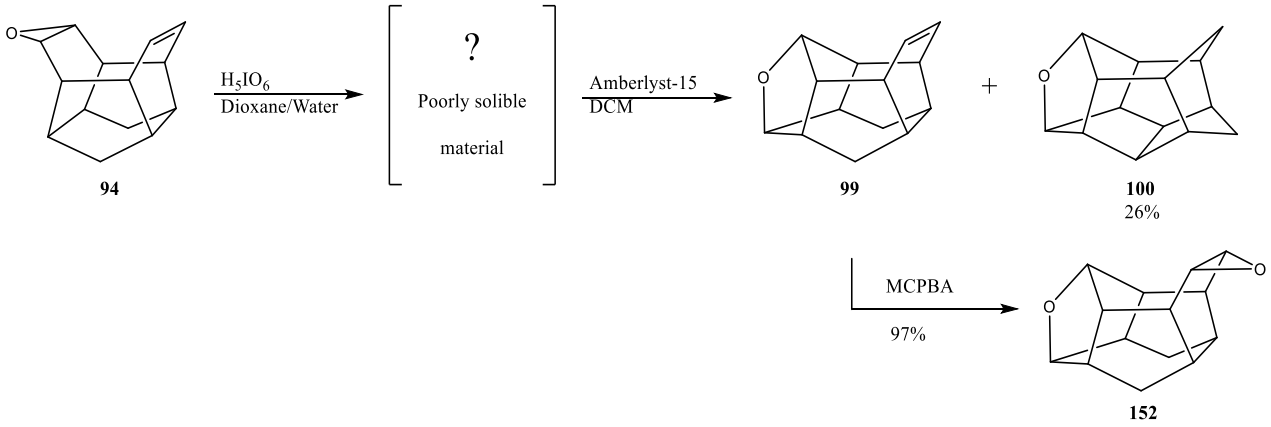

*Figure 63: Reaction scheme of the rearrangement of **94** using Protocol **R-A**. Trace amounts of water are necessary to propagate the second rearrangement to **99** and **100**. Oxacage **99** can be epoxidized with MCPBA.*

The rearrangement of mono-epoxide **94** furnished two novel oxacages **99** and **100** (*Figure 63, pg. 85*); bis-epoxide **95** and saturated mono-epoxide **96** were also subjected to rearrangements resulting in novel oxacages. It was observed that the rearrangements propagated by Amberlyst-15

required trace amounts of water to activate the catalyst. Reactions performed in distilled and dried DCM resulted in no conversion while reactions run in DCM containing trace amounts of moisture resulted in rearrangement.

The mono-epoxide **94** was subjected to rearrangement conditions following two protocols, resulting in slightly different product distributions. Protocol **R-A** was carried out over two steps. The first step involved treating **94** with periodic acid in a 2:1 solution of 1,4-dioxane/water. The crude, poorly soluble material was then treated with Amberlyst-15 in a suspension of DCM for 16 to 20 hours and resulted in a mixture of the two products **99** and **100** in a 1:3 ratio. Purification by column chromatography (SiO_2, 13:1 cyclohexane/EtOAc) was ineffective at isolating **99** and resulted in low amounts of pure **100** (26% isolated yield). Compound **100** was more easily purified after epoxidation of **99** (*Figure 63, pg. 85*) in mixture with **100** and separating by column chromatography (SiO_2, 13:1 cyclohexane/EtOAc) as the resulting epoxide **93** is much more polar. This gave quantitative yields of epoxide **152** and isolation of pure **100** (column yield of 97%).

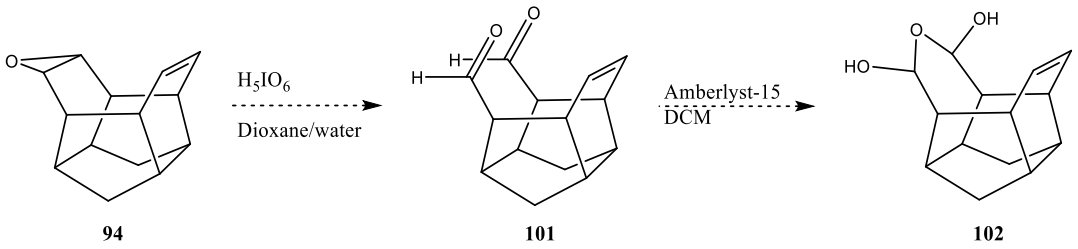

*Figure 64: Epoxides have been shown to cleave to dialdehydes when treated with periodic acid, however, the oxidative cleavage of **94** to the dial **101** was not observed.*[59]

Originally, the purpose for the periodic acid treatment was to facilitate an oxidative cleavage to a dialdehyde species (*Figure 64, pg. 86*).[59] From dial **101**, in accordance with literature precedent, Amberlyst-15 was intended to facilitate an intramolecular acetalization to the lactol

102.[60] As the desired lactol **102** was not observed, the scaffold may be too susceptible towards rearrangement under acidic conditions for the oxidative cleavage to proceed smoothly.

Reacting the mono-epoxide **94** with periodic acid resulted in an extremely poorly soluble material. The colorless solid showed little to no solubility in common organic solvents (DCM, chloroform, hexanes, benzene, EtOAc, diethyl ether (Et_2O), diglyme, acetone, dimethylsulfoxide (DMSO), acetonitrile (ACN), THF, MeOH, and EtOH) and water. A small amount of the material was dissolved in acetone-D_6 as a heterogenous sample allowing for preliminary ^{1}H-NMR analysis (*Figure 65, pg. 88*). Notable signals include two small signals at low field that may indicate aldehyde or carboxylic acid functionality, the single prominent olefin signal associated with the starting material, and signals in the range of 3.4 to 4.5 ppm that resemble the ether signals of the rearrangement products. The material(s) in this crude mixture could not be identified and do not correspond to the observed products.

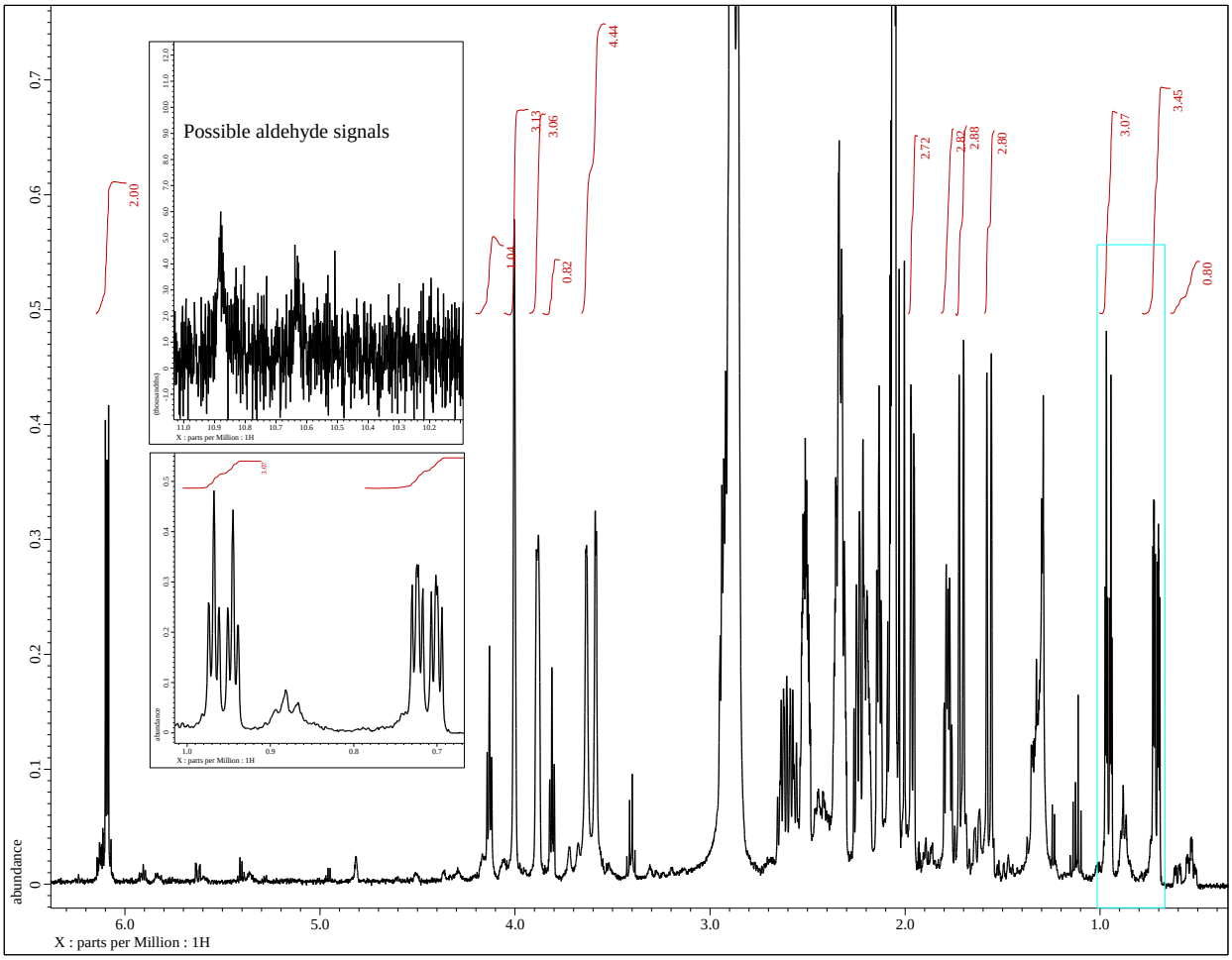

Figure 65: ^{1}H-NMR in acetone-D_6 (heterogenous sample) of the poorly soluble material obtained by periodic acid treatment.

The second protocol, Protocol **R-B**, involved stirring the substrate and 1.0 molar equivalents of Amberlyst-15 (2.0 used of bis-epoxide) and was allowed to react for multiple days. During this time, the DCM was replenished to account for evaporation and additional catalyst may be added to increase the rate of reaction. This reaction was worked up by filtration and washing of the catalyst with DCM once the conversion of **94** reached at least 90%. GC/MS timepoints revealed that **99** was an intermediate to **100** and a third product **103** (*Figure 66, pg. 90*), forms in this reaction (*Table 9, pg. 89*).

*Table 9: Ratios obtained by GC/MS tracking the progress of the rearrangement of **94** to **99**, **100**, and **103**. No additional Amberlyst added over time. DCM replenished every 24 hours.*

	Product Distribution (Ratio by GC/MS integration)				
Time (Hours)	**94**	**99**	**100**	**103**	Conversion %
1	100	0	0	0	0
2	94	3	trace	trace	5
4	85	10	trace	5	15
20	0	60	40	10	100
26	0	37	42	21	100
48	0	29	57	14	100

Compound **103** was confirmed to originate from **99** and is not as a precursor to **100** (*Table 9, pg. 89*). Carbonyl-cage **103** was not shown to form **100** when subjected to acid treatment suggesting that it is a competing product in this reaction. It was also observed that no further rearrangement of **100** occurs under acidic conditions.

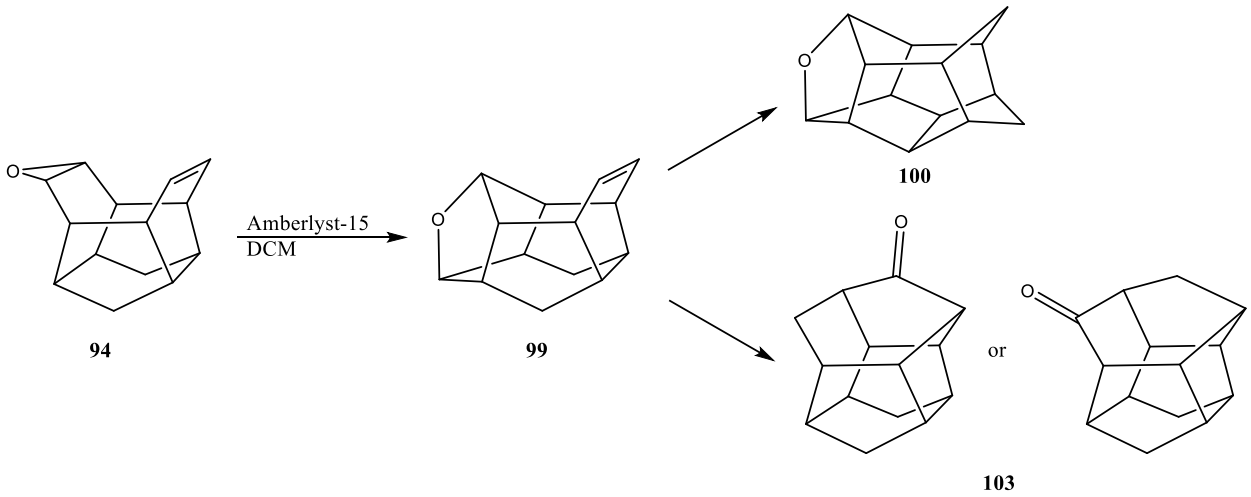

*Figure 66: Rearrangement of **94** using protocol **R-B**. This resulted in a mixture of **99** and **100** (as seen in protocol **R-A**), but also formed **103** in an unexpected side reaction.*

This third product, carbonyl-cage **103**, was only observed under Protocol **R-B**. Interestingly, while the overall oxidation state of **103** remained the same as **94**, **99**, and **100** the oxidation state of the carbonyl carbon and one other carbon atom in **103** changed. This observation is consistent with sulfonic acids not acting as redox reagent, however, poses some challenging mechanistic implcations.[61] The periodic acid route was explicitly meant to perform an oxidative cleavage of the epoxide, yet no change in oxidation state was observed.[59] The exact mechanism for the formation of **103** still unknown and will require further investigation such as elucidation of the exact structure and theoretical support.

The mechanism for the conversion of **94** to **99** and **100** was postulated after complete structural elucidation by NMR analysis (*Figure 67, pg. 91*). Protonation of the epoxide **94** results in the epoxide opening to the alcohol and a carbocation. This carbocation quickly rearranges two times through two Wagner-Meerwein shifts. The alcohol then reacts with the carbocation and close to the oxo-norbornane unit contained in oxacage **99**.

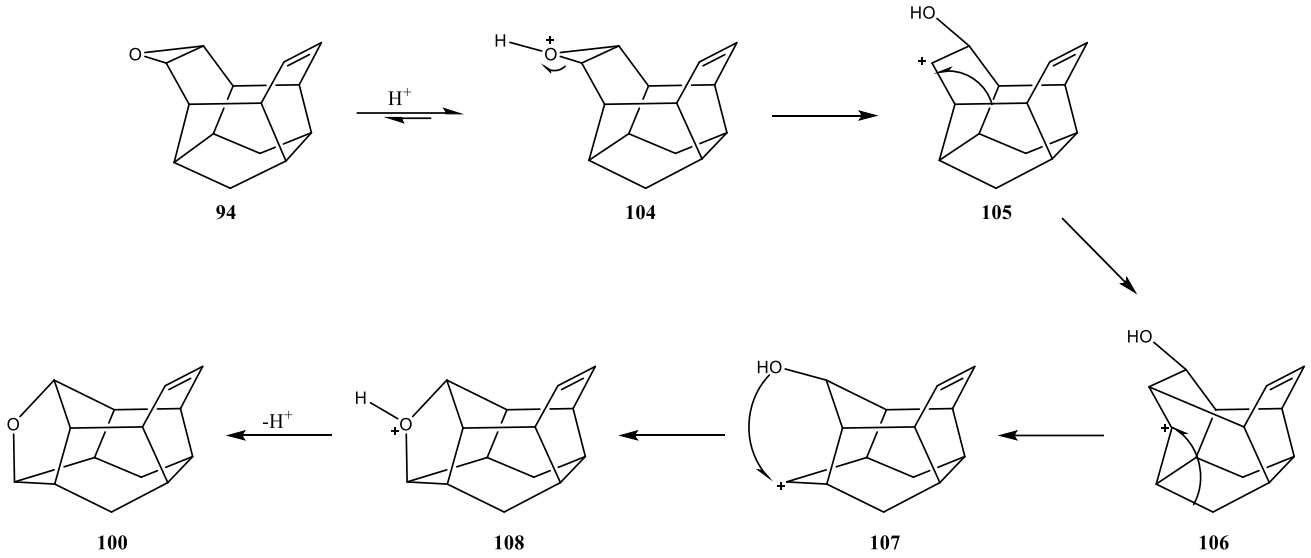

*Figure 67: Proposed mechanism for the first step of the isomerization of **94**. Mechanism **R-1** acts as the first rearrangement for all three epoxides as well as the second step for the bis-epoxide **95**.*

As no hydroxylation due to the presence of water (*Figure 63, pg. 85*) was observed, we can determine that these carbocation intermediates are likely short lived in the reaction. The rearrangement of **99** to **100** seems to be much more complex and likely relies on a similar mechanism to the last steps of the formation of 1,16-dimethyldodecahedrane (*Figure 68, pg. 92*).[62]

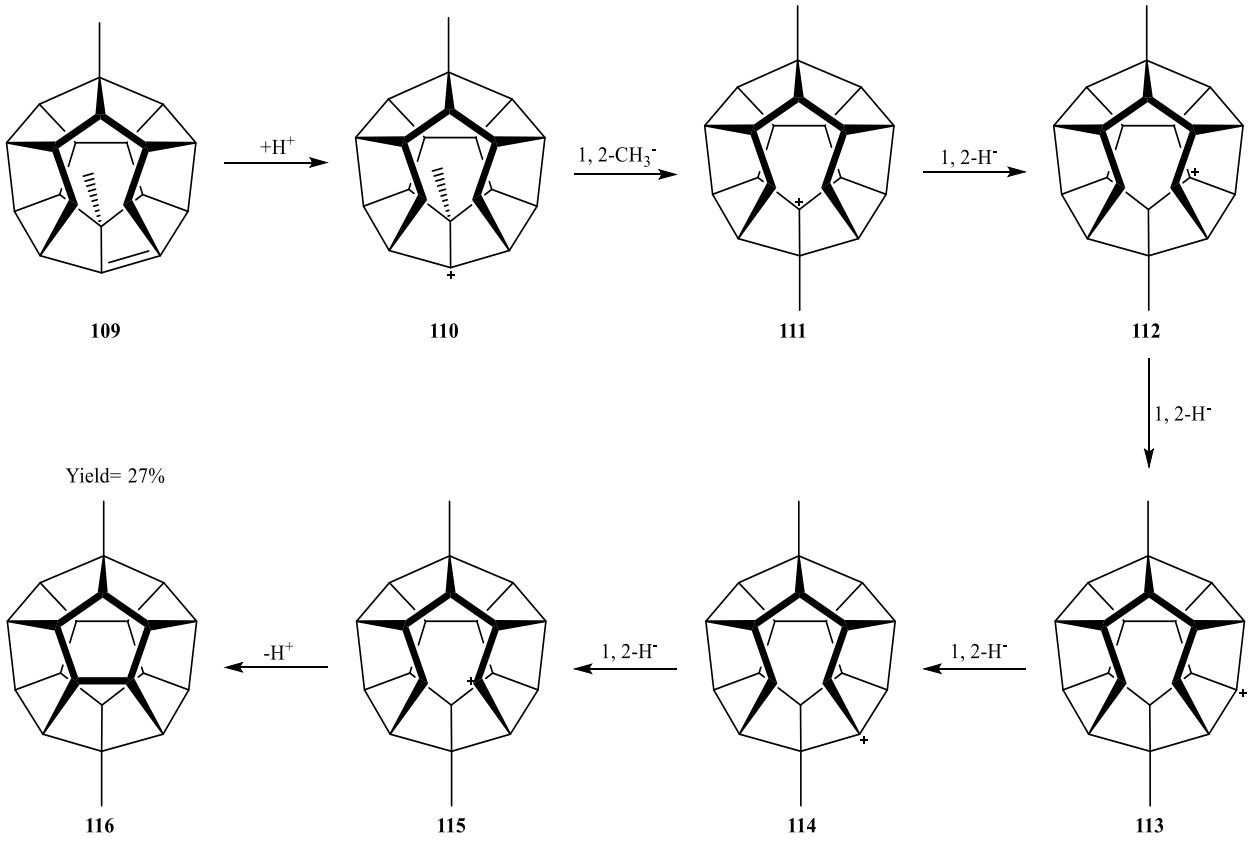

*Figure 68: Proposed mechanism for the acid catalyzed isomerization of **109** to **116**.*[62]

In the synthesis of 1,16-dimethyldodecahedrane **116**, the alkene **109** was converted to **116** using the powerful trifluoromethanesulfonic acid. This reaction was proposed to proceed rapidly through a series of carbocation rearrangements followed by the elimination of hydronium and ring closure to the final scaffold **116 (***Figure 68, pg. 92*).[62] In the final step of this rearrangement the carbocation of **114** migrates from a tertiary to a secondary position to the carbocation **115**. It was proposed that due to the perhydrotriquinacene substructure of the carbocations these tertiary carbocations were unstable.[62-64] This argument was based on the rate of solvolysis of perhydrotriquinacene and the high stability of a tertiary perchlorate derived from a related structure.[65, 66] The high stability of the perchlorate despite it being a good leaving group displays the instability of the analogous carbocation.[66] This instability of the tertiary carbocation drives the

formation of the secondary carbocation of **114**. While oxacages **99** and **100** do not share this same substructure as 1,16-dimethyldodecahedrane **116**, the final ring formation may undergo an analogous mechanism for the formation of **100** (*Figure 69, pg. 93)*. No hydrolysis of the carbocation intermediates was observed, implying that these are short-lived intermediates.

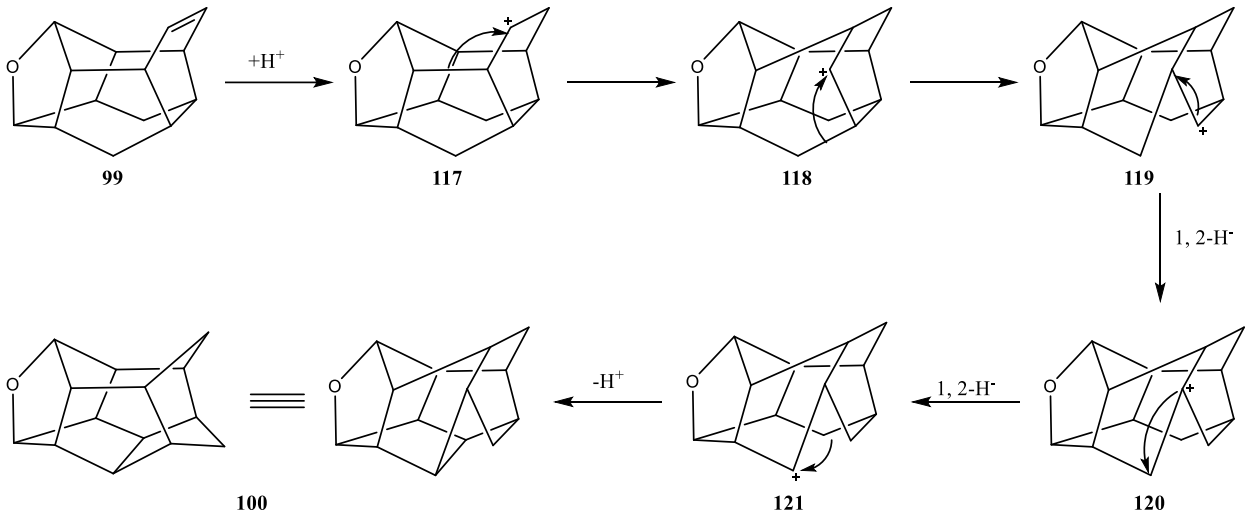

*Figure 69: Proposed mechanism **R-2** for the rearrangement of **99** to **100**.*

Mechanism **R-2** is unique in the series of epoxide rearrangements as no protonation of the oxygen is proposed. Upon protonation of the olefin, two Wagner-Meerwein shifts lead to the carbocation **119**. The system then undergoes two 1,2-hydride shifts. The ring formation in the last step and elimination of a hydronium yields **100**. The overall trend for the rearrangement of **94** to **100** is energetically downhill (*Table 10, pg. 94*) much like the rearrangement of **1** to **92** (*Figure 57, pg. 78*).

*Table 10: Change in enthalpy (H°) and heat of formation (E) in the rearrangement of **94** to **100**. Overall change in strain energy was ΔE_{strain} =-174.9904 kJ/mol Calculated by DFT using the B3-LPY 6-31J* basis set.*

	94	**99**	**100**
H° (E_h)	-617.988204	-618.0249	-618.05307
E (E_h)	-618.27206	-618.31035	-618.33872
ΔE_{strain} (kJ/mol)	0	100.5086	74.48175

3.3.3.1.1 NMR analysis of **99** and **100**

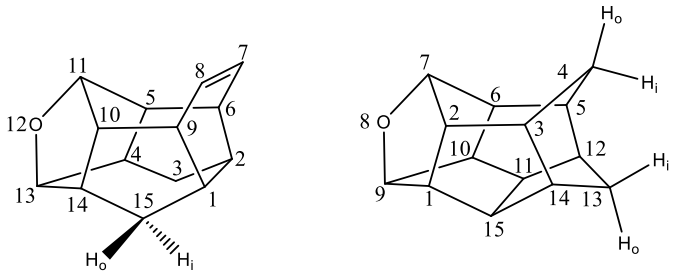

*Figure 70: Compounds **99** and **100** with IPAC numbering.*

The ^{1}H-NMR of oxacage **99** displays nine signals consistent with the compounds C_s symmetry. Two of the signals are shown with integration equal to one proton and seven signals with integration equal to two protons. Two of the signals integrating to two protons show significant overlap but are not isochronic and can be easily assigned using 2-D NMR experiments. In the olefinic region, a multiplet of higher order centered at 6.10 ppm was observed for protons H-7, -8. The two signals observed at chemical shifts of 4.25 ppm and 3.97, displayed as triplets ($^3J_{\text{H-11, H-5, -10}}$= $^3J_{\text{H-13, H-4, -14}}$ = 5.7 Hz), were assigned as H-13 and H-11, respectively. These chemical shifts were within the typical range of protons α to a C-O bond. The lower field signal

associated with H-13 likely has a higher chemical shift due to the steric environment being more crowded than H-11.

Within the structure of **99** is an oxo-norbornane subunit. The protons H-4, -14 and H-5, -10, those that are bound to this subunit displayed overlapping signals at a chemical shift of 2.70 ppm. These protons are proximate to the ether oxygen and carbons of **99** resulting in a higher chemical shift versus the protons proximate to the olefin. The allylic protons H-6, -9 were observed as an apparent singlet at a chemical shift of 2.52 ppm, while the lower bridgehead protons H-1, -2 were observed at a chemical shift of 2.10 ppm. The protons H-1, -2 were also observed as an apparent singlet. The signals associated with the methylene positions H-3 and H-15 were delineated as H-3_i, -15_i and H-3_o, -3_o due to the mirror plane of the compound. These signals are characteristic due to the large geminal coupling observed; $^2J_{\text{H-3i, -3o}} = {}^2J_{\text{H-15i, -15o}} = 13.7$ Hz. The signal associated with the interior methylene protons, H-3_i, -15_i, were observed at a higher chemical shift, 1.99 ppm, versus the outer position at 1.34 ppm. This is consistent considering the rigid structure of the cage and the effect of steric environments on chemical shift.

The ^{13}C-NMR of oxacage **103** displayed eight signals, consistent with the C_s symmetry of the compound. The lowest field signal observed in the olefin region is indicative of the carbons C-7, -8. At chemical shifts of 80.2 and 79.6 ppm, in the ethereal carbon region, the carbons C-13 and C-11 were observed. The bridgehead positions proximate to the ether unit of **99** were observed in a tight chemical shift range with C-4, -14 having a slightly higher chemical shift. This was also observed for the allylic carbons and the lower bridgeheads C-1, -2. The methylene carbons C-3, -13 were observed at highest field with a chemical shift of 28.2 ppm.

All signals were unequivocally assigned using common 2-D homonuclear and heteronuclear correlation experiments. The COSY spectrum displayed clear coupling between the

olefinic protons H-7, -8 and the bridgehead protons H-6, -9 with an intense crosspeak. H-7, -8 showed no other couplings within the scaffold. The protons H-6, -9 displayed a strong coupling to bridgehead H-1, -2 and H-5, -10. The lower bridgehead H-1, -2 shows coupling to the outer methylene protons H-3_o, -15_o which can be easily identified due to the doublet signal structure mentioned above. The methylene protons H-3_o, -15_o can also be observed coupling to the lower bridgehead protons H-4, -14. Methylene protons H-3_o, -15_o and H-3_i, -15_i show the typical intense crosspeak expected of geminal protons, however, due to the dihedral angel between the inner methylene protons H-3_i, -15_i and all four lower bridgehead positions little to no coupling was observed. The lower bridgehead protons H-4, -14 displayed a strong coupling to the upper bridgehead protons H-5, -10. Protons H-4, -14 displayed a strong coupling to the ethereal proton H-13 while the upper bridgehead protons H-5, -10 displayed strong coupling to the ethereal proton H-11.

HMQC data clearly supports these assignments with H-7, -8 showing correlation to the carbon signal in the olefinic region. Protons H-13 and H-11 showed correlations to the carbons in the ethereal region of the spectrum. Correlations between respective bridgehead positions is clear allowing for unequivocal distinction. The methylene protons H-3, -15 showed correlation to the highest field signal consistent with the above-mentioned observations.

The ^{1}H-NMR of oxacage **100** displays eleven signals consistent with the compounds C_s symmetry. Six of the signals are shown with integration equal to one proton and five signals with integration equal to two protons. The two signals observed at chemical shifts of 4.93 ppm and 4.12, displayed as triplets ($^3J_{\text{H-9, H-1, -10}} = {}^3J_{\text{H-7, H-2, -6}} = 5.4$ Hz), were assigned as H-9 and H-7, respectively. These chemical shifts were within the typical range of protons α to a C-O ether bond. The lower field signal associated with H-9 likely has a higher chemical shift due to the steric

environment being more crowded than H-7. Within the structure of **99** is an oxo-norbornane subunit. The protons H-2, -6 of this subunit were observed as a broad multiplet of higher order centered at 2.87 ppm. Other protons of the oxo-norbornane subunit H-1, -10 were observed at significantly higher field with a chemical shift of 2.67 ppm; this signal was also a broad multiplet of higher order. Observed between the protons proximate to the oxygen at a chemical shift of 2.77 ppm, the lower bridgehead protons H-12, -14 were displayed as a sharp multiplet of higher order. The protons of the zero bridge, H-11, -15 were observed as a sharp multiplet of higher order at a chemical shift of 2.55 ppm. The upper bridgehead position H-3, -5, shown at a chemical shift of 2.36, has the lowest chemical shift of the bridgehead protons. This signal also displays as a multiplet of higher order. The signals associated with the methylene positions H-4, -13 were all observed as individual signals. Protons H-4_i, H-4_o, and H-13_o were all displayed as doublet of triplets while H-13_i was displayed as a doublet. Both pairs of protons showed the characteristic large geminal coupling; $^2J_{\text{H-13i,H-13o}}$ = 12.2, $^2J_{\text{H-4i, H-4o}}$ = 13.4. The signal associated with H-13 were observed at higher chemical shift than H-4. Protons H-13_i and H-13_o were observed at 1.68 and 1.30 ppm, respectively, while the protons H-4_i and H-4_o were observed at 1.21 and 1.00 ppm.

The ^{13}C-NMR of oxacage **100** displayed nine signals, consistent with the C_s symmetry of the compound. At chemical shifts of 80.2 and 79.6 ppm, in the ethereal carbon region, the carbons C-9 and C-7 were observed. The bridgehead positions proximate to the ether unit of **100** were observed in a tight chemical shift range with C-2, -6 having a slightly higher chemical shift versus C-1, -10. The zero bridge carbons C-11, -15 had a higher chemical shift that the bridgehead carbons C-3, -5 and C-12, -14 consistent with the more strained positions being closer to the ether moiety. Carbons C-3, -5 and C-12, -14 displayed a wide chemical shift range, unlike C-2, -6 and C-1, -10, with C-3, -5 being significantly up field. The methylene positions C-13 and C-4 also displayed a

wide chemical shift range with C-13 having a chemical shift of 31.1 versus C-4 with a chemical shift of 20.4 ppm.

All signals were unequivocally assigned using common and advanced 2-D homonuclear and heteronuclear correlation experiments. The COSY spectrum displayed clear coupling the ethereal proton H-9 and bridgeheads H-1, -10. Coupling between the upper ethereal proton H-7 and H-2, -6 can also be clearly seen in the spectrum. Both correlations showed intense crosspeak indicative of a dihedral angle of less than 45°. The dihedral angle between H-1, -10 and H-2, -6 was estimated to be close to 0° supporting the very strong coupling and intense crosspeak observed in the COSY. Both bridgeheads of the oxo-norbornane unit H-1, -10 and H-2, -6 displayed strong couplings to the adjacent bridgeheads H-11, -15 and H-3, -5, respectively. H-11, -15 showed strong coupling to the bridgeheads H-12, -14, supporting the connectivity of the determined structure. Protons H-12, -14 and H-3, -5 showed an intense crosspeak, suggesting a strong coupling between the positions. The upper bridgehead H-3, -5 showed strong coupling to the methylene H-4 while the lower bridgehead H-12, 14 showed strong coupling to the methylene H-13. Both methylene positions can be easily identified due to the dt and d signal structure mentioned above and the intense crosspeak indicative of geminal coupling. Due to the dihedral angel between the inner methylene protons $H\text{-}4_i$ and $H\text{-}13_i$ and the adjacent bridgehead positions little to no coupling was observed. The advanced 2-D method tROSEY was used to confirm these correlations and displayed the through-space interactions needed to elucidate the structure.

HMQC data clearly supports these assignments. Protons H-9 and H-7 showed correlations to the carbons in the ethereal region of the spectrum. Correlations between respective bridgehead positions is clear allowing for unequivocal distinction. The methylene protons of H-13 showed

correlation to the high field signal at 31.3 ppm. The methylene protons H-4 of showed correlation to the highest field signal consistent with the above-mentioned observations.

3.3.3.2 Attempted Cleavage of the Ether Moiety in **100**

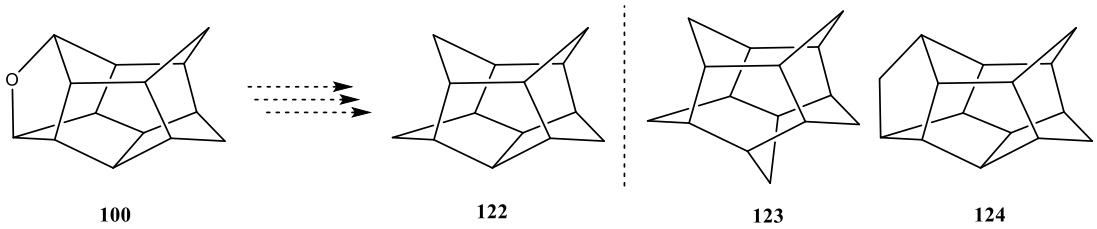

*Figure 71: Oxacage **100** may be a possible precursor to the elusive norpentaasterane **122**, a model compound for the unknown pentaasterane **123**.*

The substructure of norpentaasterane **122** is visible in the structure of oxacage **100** (*Figure 71, pg. 99*). Utilizing ether cleavage reactions, we intended to access this interesting framework. To date, only hydrocarbon **124** has displayed **122** as a substructure. In addition, hydrocarbon **124** does not appear to be an appropriate precursor to norpentaasterane **122**.[67] Previous attempts to obtain this scaffold *via* the pyrolysis of **125** failed to deliver the targeted hydrocarbon and instead furnished hydrocarbon **128** as the result of a possible hydrogen migration (*Figure 72, pg. 100*).[68]

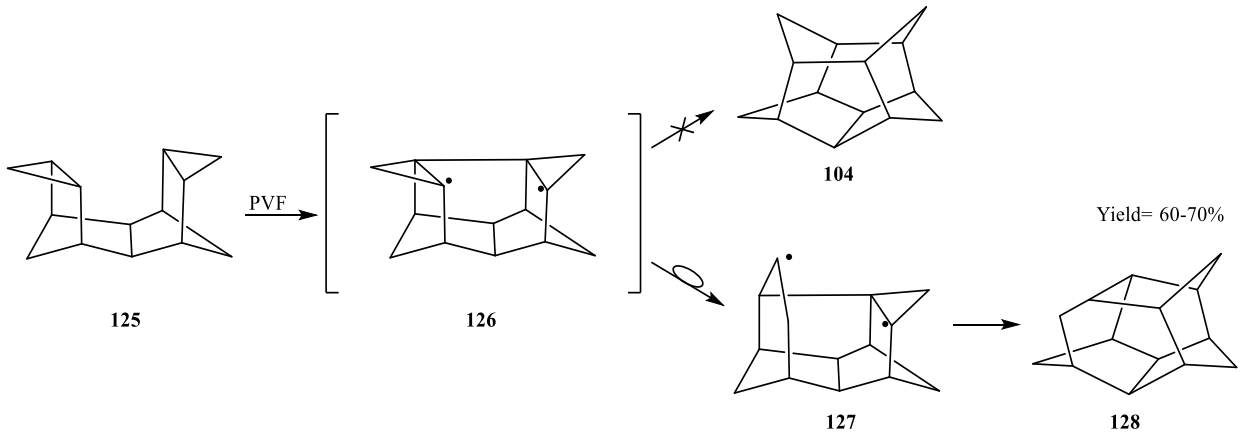

*Figure 72: Flash vacuum pyrolysis (PVF) of **125** was used in an attempt to synthesize **122** but resulted in the hydrocarbon **128**. The proposed mechanism involves a hydrogen migration.*[68]

We considered several methods of cleaving the ether moiety in **100**. Initially, we attempted to cleave the ether by reacting **100** with lithium bromide (LiBr) and benzyl bromide (BzBr) to generate the benzyl ether **131** (*Figure 73, pg. 101*). Lithium bromide was intended to cleave the ether bond of **100** and then trap the resulting reactive species with benzyl bromide. This could then be converted to the halide cage using HX with subsequent dehalogenation furnishing the norpentaasterane **122**. Unfortunately, this ultimately failed to deliver the benzyl ether **131,** as no conversion was observed.

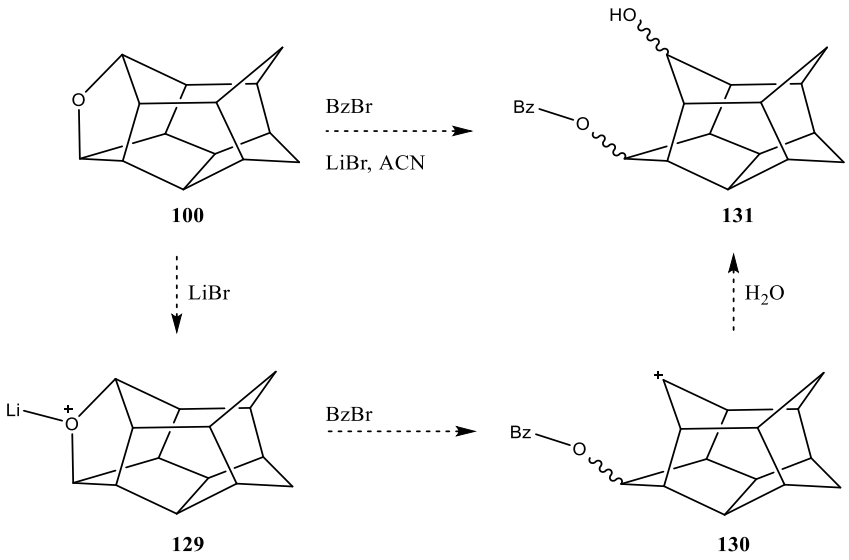

*Figure 73: Attempted ether cleavage to the benzyl ether **131**. No conversion was observed.*

Next, we attempted to adapt a literature protocol utilizing TMSI developed using belt-shaped systems such as **132** (*Figure 74, pg. 101*).[69, 70] When preformed on the belt-shaped system **132**, ether cleavage to **134** was observed and proceed through the tetraiodo intermediate **133**.[69]

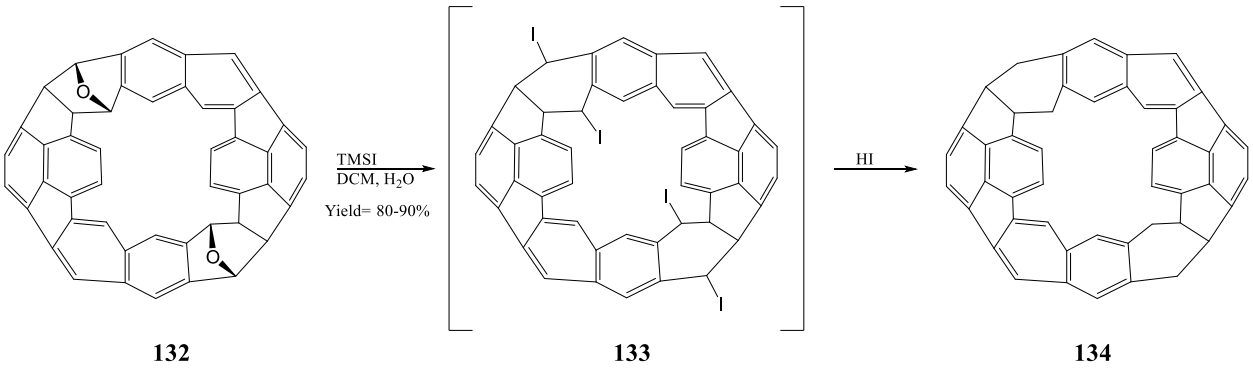

*Figure 74: Compound **132** reacted with TMSI to form a tetraiodo intermediate **133**. Intermediate **133** reacted with HI (generated from TMSI and water) to form a diiodo system and subsequently the hydrocarbon **134**.*

This reaction preformed on **100** was intended to furnish the iodo-cage **136** (*Figure 75, pg. 102*). Subsequent dehalogenation of **136** was intended to yield norpentaasterane **122**. TMSI has been utilized to form silyl ethers *via* ether cleavage. Silyl ethers may form in the cases of both **132** and **100** but was not described for the belt-shaped system **132**; tetraiodo **133** was not isolated and may have been derived from a silyl ether. Hydrolysis of silyl ethers under acidic conditions deliver the corresponding alcohol; some hydrolysis of the intermediates to **136** were observed but attempts to selectively reproduce the hydrolysis were not successful. The alcohol intermediates formed in this reaction should undergo protonation and substitution to the corresponding iodo species (e.g., *Figure 75, pg. 102*).

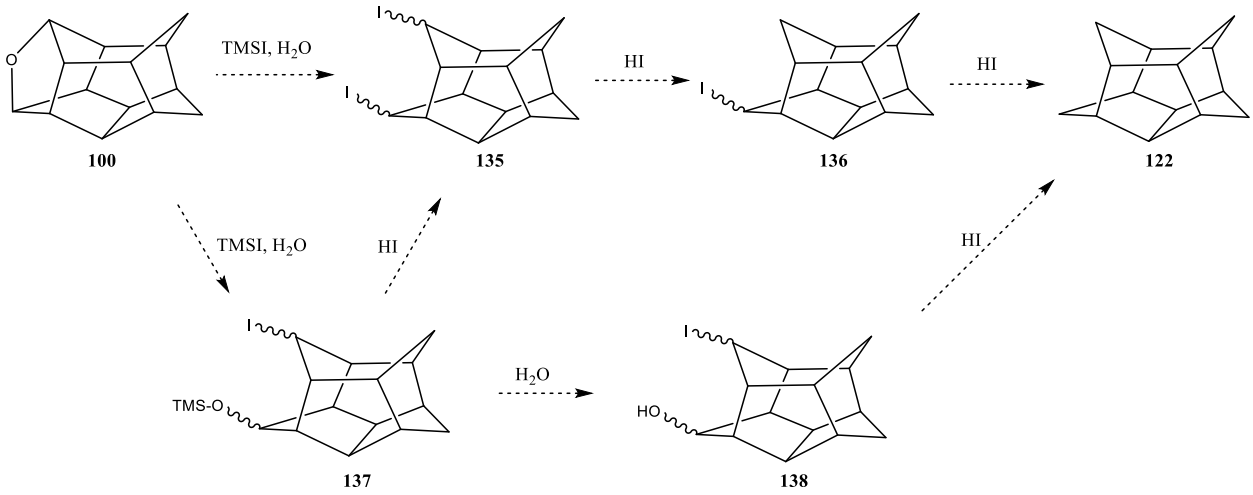

*Figure 75: Oxacage **100** was treated with TMSI and water. The proposed mechanism follows the formation of the diiodide **135**, which will dehalogenate in the presence of HI. An alternative pathway is the formation and hydrolysis of silyl ether **137** to the iodo-alcohol **138**.*

When **100** was treated with TMSI in DCM or chloroform and small amounts of water the targeted hydrocarbon **122** was not observed. Instead, the major products of the reaction were three distinct compounds with an observed mass of *m/z*= 311 ($C_{14}H_{16}I$) in the GC/MS with a 2:1:1 ratio

by ^{1}H-NMR. Upon standing in 2:1 hexanes/EtOAc over three days crystals formed and the remaining oil was removed by trituration with *n*-pentane and crystalline material identified as **149** (*Figure 76, pg. 103*). The true mass of **149** was likely not observed in the GC/MS due to decomposition facilitated by the weak C-I bond. The products removed by trituration were likely isomers of this cage but did not crystalize due to concentration and differing physical properties. The identity of the compounds comprising the oil was determined to be a mixture of stereoisomers of **149** as the mixture yielded the same product, hydrocarbon **151**, as the pure crystalline material when subjected to dehalogenation; this was also supported by similar signal patterns in the ^{1}H-NMR and identical mass observed by GC/MS. Multiple degenerate pathways were elucidated to explain the formation of diiodide **149** from oxacage **100** (*Figure 76, pg. 103; Figure 77, pg. 104*).

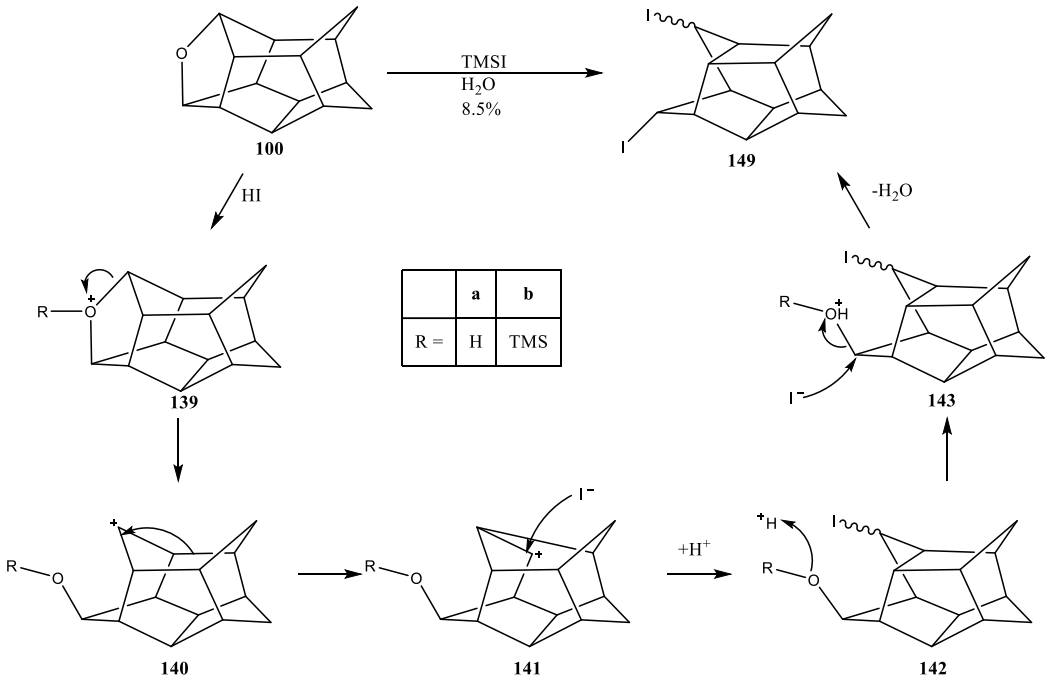

*Figure 76: Two of the possible degenerate mechanisms **EC-1a** and **EC-1b** for the attempted ether cleavage and rearrangement of **100**. (A) TMSI generates the strong acid HI when exposed to water. (B) TMSI can react with ethers to form the TMS ether.*

When TMSI reacts with water, the strong hydroiodic acid (HI) forms. This acid reacts with the ether resulting in the protonation and opening of the ether bridge to **142a**. The carbocation undergoes a Wagner-Meerwein shift before the carbocation is trapped by residual I^- anions. The alcohol is then protonated, and a substitution reaction occurs to deliver the diiodo cage **149**. The stereochemistry of **149** was ambiguous and requires further investigation. Alternatively, TMSI can react with the ether opening to the TNS ether carbocation **143b**. Under a degenerate mechanism this can form **149**

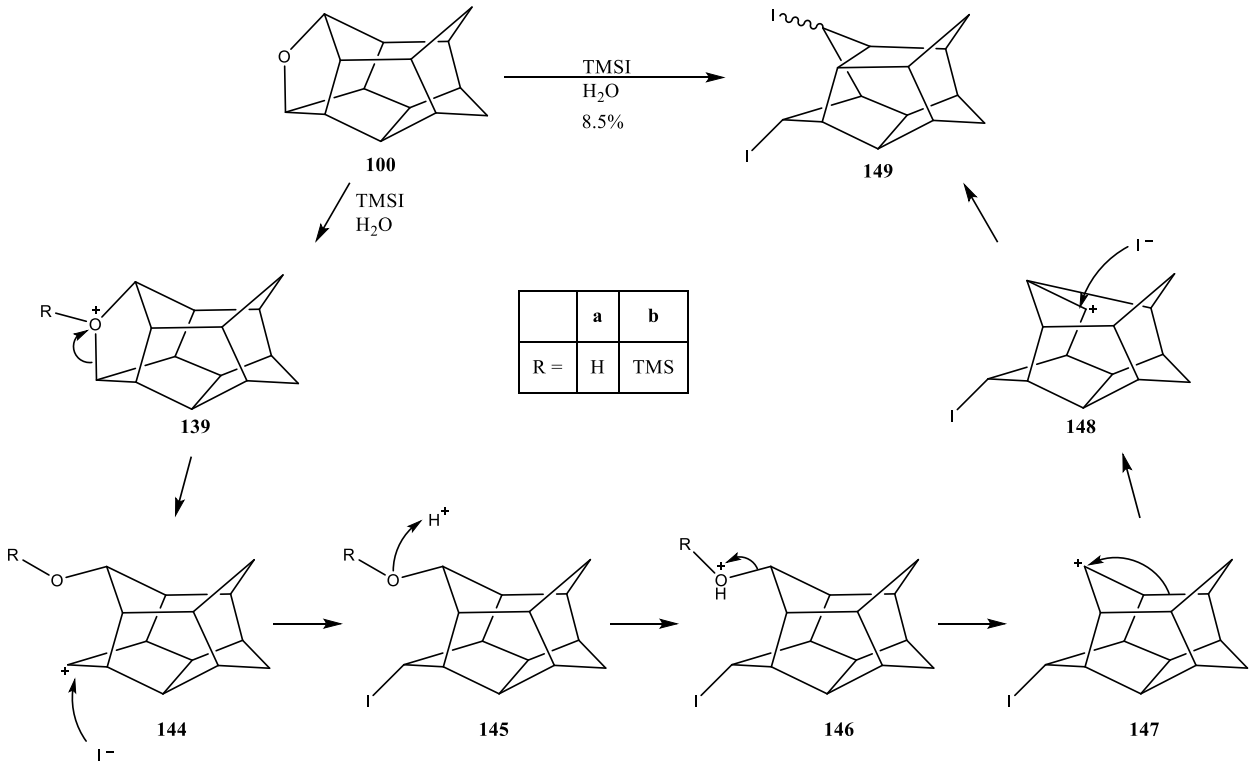

*Figure 77: Alternative degenerate mechanisms **EC-2a** and **EC-2b** for the formation of diiodocage **149**.*

The diiodo cage **149** may also be formed from other mechanisms where the rearrangement occurs at a different step (*Figure 77, pg. 104*). TMSI reacts with water to generate HI or with the ether moiety of **100** to give the carbocation **139**. Unlike mechanism **EC-1** (*Figure 76, pg. 103*) the

carbocation does not rearrange and instead reacts with a nucleophile (in this case I^-) to form **145**. This then undergoes similar hydrolysis to mechanism **EC-1** to give the carbocation **147** which undergoes rearrangement by Wagner-Meerwein shift before reacting with another I^- equivalent furnishing **149**.

When subjecting a mixture of the iodocage **149** and its isomers to various dehalogenation methods, only one product, hydrocarbon **151**, was observed. Three methods for dehalogenation were attempted: Birch-type, tributyl tin hydride, and lithium aluminum hydride (*Figure 78, pg. 105*). Only the product of the birch type dehalogenation was isolated (31%), however, conversion of 90% or greater was observed for the other methods and was confirmed to be identical based on GC/MS and NMR.

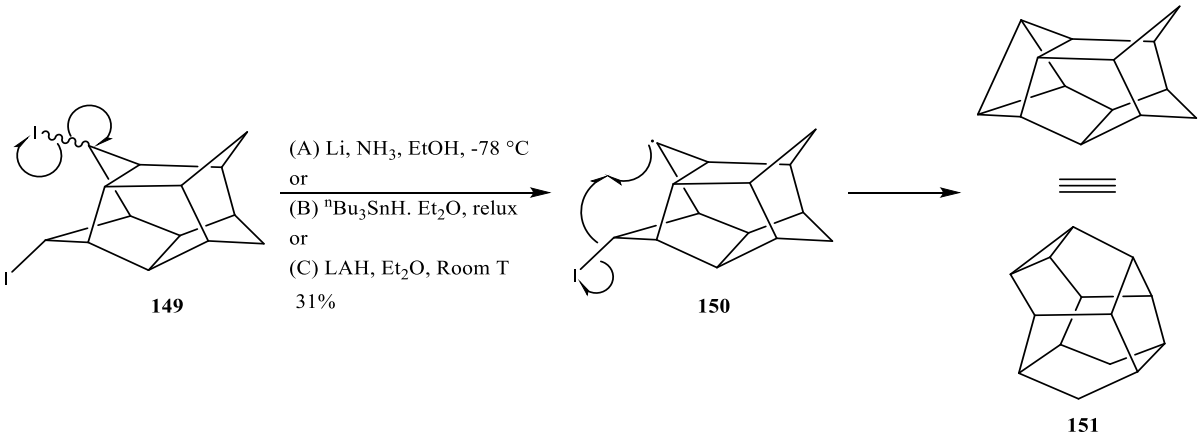

*Figure 78: Proposed mechanism of the dehalogenation of **149** to give the hydrocarbon **151**. All reaction conditions yielded the same product.*

This, along with identifying **149** as the major product from reactions with TMSI, imply rearrangement of the ether cage occurs during the ether cleavage step. Consequently, other methods will be required to synthesize norpentaasterane **122** from the oxacage **100**.

3.3.3.1.2 NMR Analysis of **149** and **151**

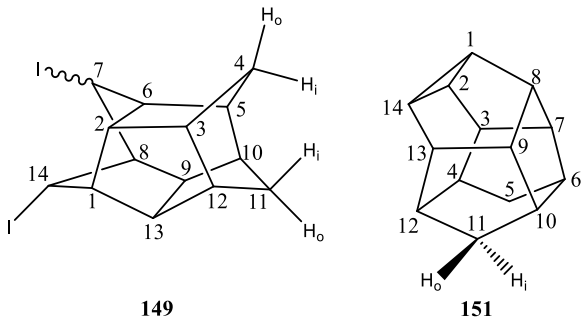

*Figure 79: Compounds **147** and **149** with IUPAC numbering.*

The ^{1}H-NMR of diiodocage **149** displays fourteen signals, inconsistent with the compounds low C_i symmetry. Integration and 2-D NMR techniques revealed significant overlap of two sets of two signals and were determined to not be isochronic. Twelve signals were observed integrating to one proton and the two sets of overlapping signals were observed integrating to two protons. The two signals observed at chemical shifts of 4.73 and 4.48 ppm are indicative of H-C-I moieties within the scaffold. The signal observed at 4.73 ppm with a doublet signal structure was assigned as H-14 and integrated to one proton. The signal observed at 4.48 ppm with a singlet signal structure was assigned as H-7 and integrated to one proton. The various bridgehead protons were observed over a large chemical shift range and no specific trends in signal patterns could be determined. The signals associated with the methylene positions H-4, -11 were all observed as individual signals. Protons H-4$_i$, H-4$_o$, and H-11$_i$, -11$_o$ were all displayed as doublets. Both pairs of protons showed the characteristic large geminal coupling; $^{2}J_{\text{H-4i, H-4o}} = {}^{2}J_{\text{H-11i, H-11o}} = 12.1$ Hz. Protons H-11$_i$ and H-11$_o$ were observed at 1.54 and 0.86 ppm, respectively, while the protons H-1$_i$ and H-1$_o$ were observed at 1.80 and 1.16 ppm.

The ^{13}C-NMR of diiodocage **149** displayed sixteen signals, consistent with the C_i symmetry of the compound. Chemical shifts were observed over a large range (between 58.2 -27.4

ppm), but each signal was within in a small range the next with the average difference in chemical shift being less than 5.0 ppm. At chemical shifts of 41.1 and 37.3 ppm the halogenated carbons C-7 and C-14 were observed. The methylene positions C-4 and C-11 were observed at 31.7 and 27.4 ppm, respectively.

All signals were unequivocally assigned using common and advanced 2-D homonuclear and heteronuclear correlation experiments. The COSY spectrum displayed the H-14 signal at 4.73 ppm showing strong correlation with the H-8 signal at 2.14 ppm and a weak correlation to the H-1 signal at 3.05 ppm. H-8 showed only one other coupling to one of the signals in the group at 2.51 ppm assigned as H-9 and H-10. This pair of signals also displayed coupling to the methylene proton H-11o at 0.86 ppm. The signal at 2.51 ppm also showed a weak coupling to the signal at 2.54 ppm assigned as H-5. The methylene H-11o showed a strong coupling to the H-12 signal at 2.90 ppm. H-12 displayed a strong coupling to the signal at 2.64 ppm which is comprised of the H-6 and H-13 signals. The signal associated with H-13 can be observed correlating to H-1. The signal associated with H-6 showed a very weak coupling to the H-7 signal at 4.48 ppm and a strong coupling to H-5. H-5 was observed coupling to the other methylene H-4 which in turn displayed a strong coupling to the H-3 signal at 2.38 ppm. The H-2 signal at 3.32 ppm displayed a strong coupling to the H-3 signal as well as the H-6 signal. Only a very weak coupling between H-2 and H-1 was observed likely due to the dihedral angle. The H-7 and H-14 protons displayed some weak coupling implying some through space coupling, suggesting that both hydrogens point inwards. This would be consistent with the steric considerations for the molecule as well as mechanistic reasoning.

HMQC data clearly supports these assignments as correlations between respective bridgehead positions is clear allowing for unequivocal distinction. The H-7 and H-14 protons

correlate to carbons in the region typically observed with C-I moieties. The methylene protons of H-4 showed correlation to the high field signal at 31.7 ppm. The methylene proton H-11 showed correlation to the highest field signal consistent with the above-mentioned observations.

The ^{1}H-NMR of hydrocarbon **151** displays nine signals, two signals integrating to one proton and seven signals integrating to two protons, consistent with the compounds C_s symmetry. At a chemical shift of 3.06 ppm, the middle bridgehead protons H-7, -9 were observed as a multiplet of higher order and integration equal to two protons. The middle bridgeheads H-3, -13 and upper bridgehead atom H-8 were observed overlapping forming a broad multiplet centered at 2.43 ppm integrating to three (two + one) protons. The lower bridgehead positions H-6, -10 were observed as a multiplet of higher order at 2.17 ppm. The second signal observed with an integration of one proton was observed as a multiplet of higher order at a chemical shift of 1.99 ppm. This signal corresponds to H-1 of the cyclopropane subunit of **151**. The lower bridgeheads H-4, -12 were observed at slightly lower chemical shift versus lower bridgeheads H-6, -10 at 1.85 ppm. The signals associated with the methylene positions H-5 and H-11 were delineated as H-5$_i$, -11$_i$ and H-5$_o$, -11$_o$ due to the mirror plane of the compound. These signals are characteristic due to the doublet signal structure and large geminal coupling; $^{2}J_{\text{H-5o, -5i}} = {}^{2}J_{\text{H-11o, -11i}} = 11.3$ Hz. The signal associated with the interior methylene protons, H-5$_i$, -11$_i$, were observed at a higher chemical shift, 1.76 ppm, versus the outer position at 0.90 ppm. This is consistent considering the rigid structure of the cage and the effect of steric environments on chemical shift. Observed between the inner and outer methylene signals, at a chemical shift of 1.28 ppm, were the upper bridgeheads H-2, -14. These protons are likely higher up field than other bridgehead protons due to the cyclopropane subunit.

The ^{13}C-NMR of hydrocarbon **151** displayed eight signals, consistent with the C_s symmetry of the compound. At a chemical shift of 49.5 ppm, C-8 was observed. At chemical shifts of 37.2

and 23.6 ppm the carbons C-1 and C-2, -14 of the cyclopropane subunit were observed. Carbons C-2, -14 were observed at highest field. The methylene carbons C-5, 11 were observed at a chemical shift of 32.3 ppm.

All signals were unequivocally assigned using common 2-D homonuclear and heteronuclear correlation experiments. The COSY spectrum displayed clear coupling between H-1 and H-2, 14. The cyclopropane proton H-1 also shows a strong coupling to H-8. While H-8 shows overlap with H-3, -13 the connectivity can still be clearly determined. Cyclopropane protons H-2, -14 displayed a strong coupling to middle bridgeheads H-3, -13 but no other coupling other than to H-1 was observed. The middle bridgehead protons H-3, -13 displayed strong couplings to the middle bridgehead protons H-7, -9 and the lower bridgeheads H-4, -12. The middle bridgehead protons H-7, -9 also showed coupling to the lower bridgehead protons H-6, -10. The lower bridgeheads H-4, -12 and H-6, -10 displayed coupling to the middle bridgeheads and to the outer methylene protons H-5_o, -11_o which can be easily identified due to the doublet signal structure mentioned above. Methylene protons H-5_o, -11_o and H-5_i, -11_i show the typical intense crosspeak expected of geminal protons, however, for the lower bridgehead positions little to no coupling was observed.

HMQC data clearly supports these assignments with clear correlations between respective bridgehead positions allowing for unequivocal distinction. The methylene protons H-8, -12 showed correlation to the high field signal consistent with the above-mentioned observations. The cyclopropane protons H-2, -14 displayed correlation to the highest field signal consistent with the above observations.

3.3.3.3 Rearrangement Reactions of the Bis-epoxide Cage **95**

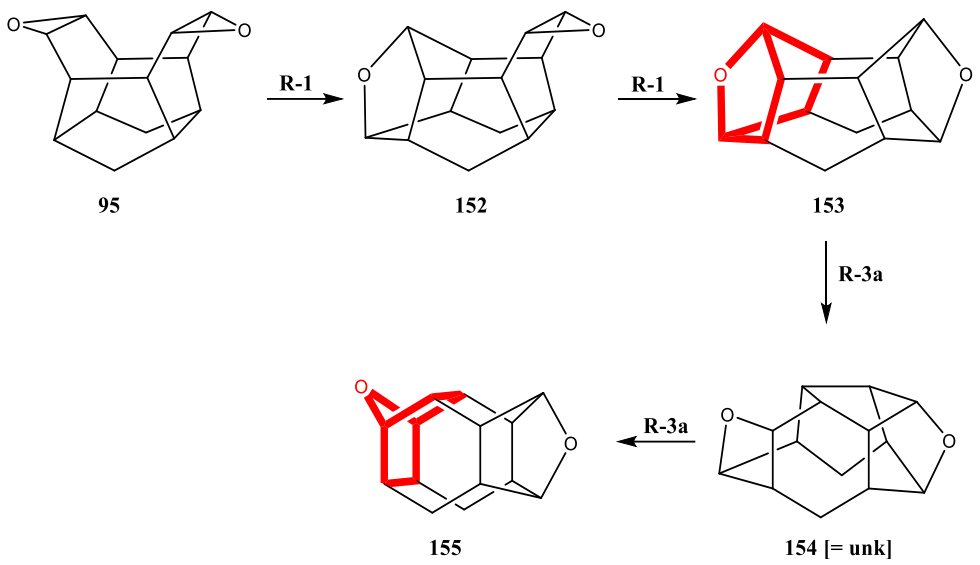

*Figure 80: Isomerization of the bis-epoxide **95**. Rearrangements one and two adhere to Mechanism **R-1** (Figure 67, pg. 91). Highlighted in red is the formal 90° rotation of the oxo-norbornane unit observed in the subsequent rearrangement steps following Mechanism **R-3a**.*

Bis-epoxide **95** was also subjected to isomerization using protocol **R-B** (*Figure 66, pg. 90*). When bis-epoxide **95** was treated with periodic acid (protocol **R-A**, *Figure 63, pg. 85*) no reaction took place. This was surprising as periodic acid treatment of **94** resulted in oxacages **99** and **100** following treatment with Amberlyst-15. However, when only exposed to Amberlyst-15 (2.0 eq), bis-epoxide **95** did undergo rearrangement resulting in four distinct products observed by GC/MS (bis-epoxide **95** required longer reaction times than the mono-epoxide **94** and saturated mono-epoxide **96**).

These four stable rearrangement products were separated using column chromatography (SiO_2, hexanes/EtOAc gradient; 10:1, 5:1, 2:1 followed by 5:5:1 hexanes/DCM/MeOH) in up to 94% purity for two of the four products, oxacages **153** and **155**, and were characterized from

enriched samples. Oxacage **152** was first identified from enriched samples but was later prepared by the epoxidation of **99** (*Figure 63, pg. 85*). Compound **154** could not be identified unequivocally due to low concentrations of enriched fractions and significant overlap of ^{1}H-NMR signals but is hypothesized to be an oxetane; further study will be needed to confirm this structure including isolation of clean material and possible XRD analysis. Compound **154** was determined to be an intermediate in the formation of **155** using timed intervals obtain by GC/MS. These time points also revealed the order in which these rearrangements occur by determining the ratio of products over time.

The initial steps of the rearrangement of **95** are identical to those observed in the rearrangement of **94** and **96** (*Figure 67, pg.91; Figure 80, pg. 110*). The first two rearrangements that occurred in this sequence were the same on both sides of the molecule following Mechanism **R-1**. The third and fourth rearrangements are proposed to go through an oxetane intermediate. Protonation of an oxygen results in opening of the ether bridge to a carbocation. Carbocation rearrangement by Wagner-Meerwein shift results in another carbocation in close proximity to the hydroxyl group. This then closes to the oxetane. The oxetane intermediate, while stable, reacts quickly due to the strain of the four-membered ring opening again and undergoing another carbocation rearrangement. This carbocation reacts with the hydroxyl functionality to deliver the final product, oxacage **155**. This mechanism is analogous to that observed in rearrangement of **96** (Mechanism **R-3a**, *Figure 85, pg. 118*). Both the saturated mono-epoxide **96** and bis-epoxide **95** see a formal 90° rotation of the oxo-norbornane unit, supporting analogous mechanisms (*Figure 80, pg. 110*, highlighted in red).

As **100** is a potential precursor to the norpentaasterane **122** (*Figure 71, pg. 99*), **153** may be a possible precursor to the secopentaasterane **156** (*Figure 81, pg. 112*). This compound could

also prove useful in modeling the properties of the elusive pentaasterane **123** when investigated in tandem with the norpentaasterane **122** as they all share a similar scaffold (*Figure 71, pg. 99*). While the geometry of **156** is likely to be quite different compared to **122**, hydrocarbon **156** may reveal important information on the strain energy and conformation of the lower rings of **123**. Norpentaasterane **122** has a zero-bridge between the lower carbons, while pentaasterane **123** has a one-bridge. The lack of bridge between the lower carbons of secopentaasterane **156** places it analogous to compounds like secohexaprismane, compounds that have been used to model properties of hexaprismane **11** (*Figure 3, pg. 3*).[5, 6]

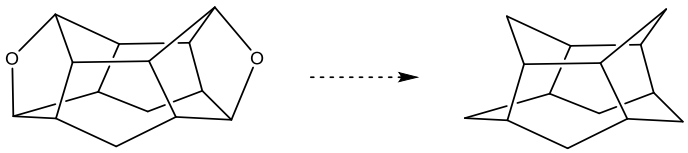

153 **156**

*Figure 81: The oxacage **153** may be a possible precursor to the hydrocarbon **156**.*

3.3.3.3.1 NMR Analysis of **152**, **153**, **154**, and **155**

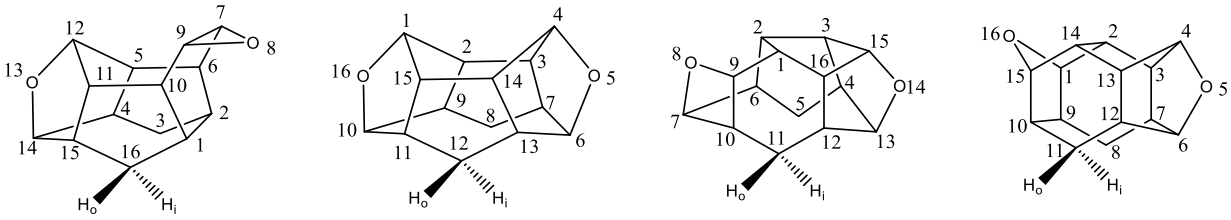

152 **153** **154** **155**

*Figure 82: Compounds **152**, **153**, **154** and **155** with IUPAC numbering.*

The NMR spectra of compound **152** shows many of the same signal patterns observed in **99** and **157**. The major differences observed is the lack of olefinic at low field or the ethano protons at high field. These positions correspond to oxirane protons H-7, -9 at 3.32 ppm. Other evidence

that supports the first rearrangement step comes from the epoxidation of **99**. When reacted with MCPBA compound **99** is epoxidized to **152**. The same ^{1}H-NMR spectrum can be observed in the isolated material from the rearrangement of **99** and the epoxidation.

The ^{1}H-NMR of oxacage **153** displays six signals consistent with the compounds C_{2v} symmetry. Two of the signals are shown with integration equal to four protons and four signals with integration equal to two protons. The two signals, both integrating to two protons, observed at chemical shifts of 4.29 ppm and 4.21 were assigned as H-1, -4 and H-6, -10, respectively. These chemical shifts were within the typical range of protons α to a C-O ether bond. The lower field signal associated with H-1, -4 was displayed as an apparent singlet and likely has a higher chemical shift due to the steric environment being more crowded than H-6, -10. The lower bridgehead protons H-7, -9, -11, -13 were observed as an apparent doublet with a large coupling constant; $^{3}J_{\text{H-8, -12,H-7, -9, -11, -13}}$ = 12.6 Hz. These protons were observed at a higher chemical shift of 3.20 ppm when compared to the upper bridgehead protons H-2, -3, -14, -15. The upper bridgehead protons were also observed as an apparent doublet with the same coupling constant. The signals associated with the methylene positions H-8 and H-12 were delineated as H-8$_i$, -12$_i$ and H-8$_o$, -12$_o$ due to the mirror plane of the compound. These signals are characteristic due to the large geminal coupling observed; $^{2}J_{\text{H-12i, -12o}} = {}^{2}J_{\text{H-8i, -8o}}$ = 15.5 Hz. The signal associated with the interior methylene protons, H-8$_i$, -12$_i$, were observed at a higher chemical shift, 2.15 ppm, versus the outer position at 1.75 ppm. This is consistent considering the rigid structure of the cage and the effect of steric environments on chemical shift. The interior methylene protons were observed a doublet, similar to the interior protons of many other scaffolds discuss, while the outer methylene protons displayed as a quintet.

The ^{13}C-NMR of oxacage **153** displayed five signals, consistent with the C_{2v} symmetry of the compound. At chemical shifts of 80.4 and 77.9 ppm, in the ethereal carbon region, the carbons C-9 and C-7 were observed. Similar to the signals observed in the ^{1}H-NMR spectrum, the lower bridgeheads C-7, -9, -11, -13 were observed at a higher chemical shift than the lower bridgehead signals of C-2, 3, -14, -15. At highest field, the methylene carbons C-8, -12 were observed.

All signals were unequivocally assigned using common 2-D homonuclear and heteronuclear correlation experiments. The COSY spectrum displayed clear coupling between the ethereal protons H-1, -4 and the upper bridgehead positions H-2, -3, -14, -15. The other pair of ethereal protons, H-6, -10 displayed strong coupling to the lower bridgehead positions H-7, -9, -11, -13. An intense crosspeak can be observed between the upper and lower bridgehead signals. The lower bridgeheads H-7, -9, -11, -13 shows correlation to the outer methylene protons H-8_o, -12_o which can be easily identified due to the doublet signal structure mentioned above. The methylene protons H-8_o, -12_o can also be observed coupling to the lower bridgehead protons H-3, -8. Methylene protons H-8_o, -12_o and H-8_i, -12_i show the typical intense crosspeak expected of geminal protons, however, due to the dihedral angel of nearly between the inner methylene protons H-8_i, -12_i and the lower bridgehead positions little to no coupling was observed.

HMQC data clearly supports these assignments with H-6, -10 and C-1, -4 showing correlations to the ethereal carbons. Correlations between respective bridgehead positions is clear allowing for unequivocal distinction. The methylene protons H-8, -12 showed correlation to the highest field signal consistent with the above-mentioned observations.

Absolute assignment for **154** was not possible due to low concentrations and overlapping signals. Some of the crucial evidence for the structure of **154** comes from the possible mechanisms for the rearrangement of **153** to **155**. Despite showing roughly equal concentration by GC/MS

between **153** and **154** the lack of any symmetry in **154** leads to severely diminished intensity of NMR signals. The ^{13}C-NMR gives the most evidence to support a nonsymmetrical system with thirteen of the possible fourteen signals recognizable; the low intensity likely results in the final signal being indistinguishable from noise. Due to overlap, the 2-D NMR techniques used were not helpful in determining the structure.

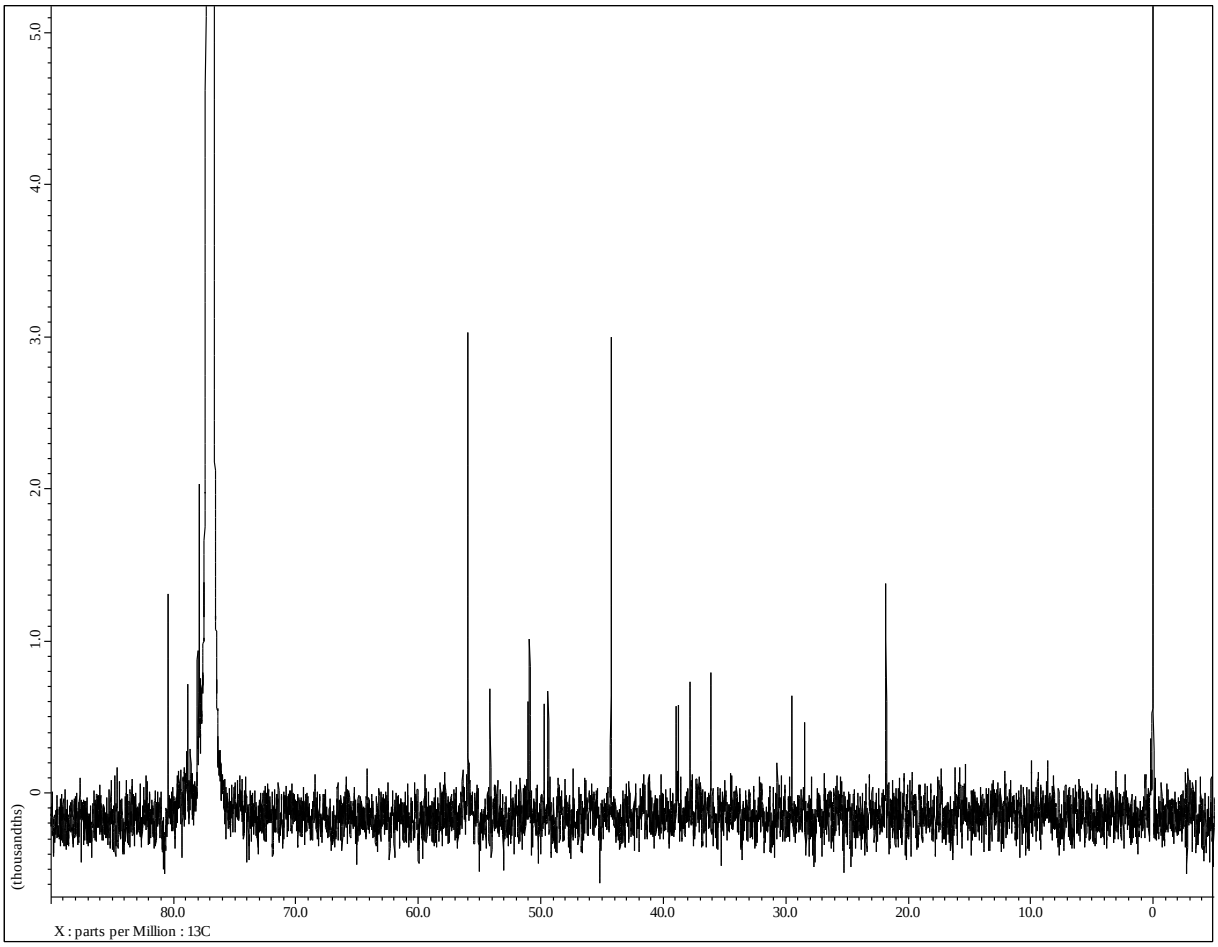

*Figure 83: ^{13}C-NMR spectrum of a mixture of **153** and **154**. This shows the thirteen signals that were used as supporting evidence for the determination of the structure of **154**.*

The ^{1}H-NMR of oxacage **155** displays nine signals consistent with the compounds C_s symmetry. Two of the signals observed are shown with integration equal to one proton and seven

signals with integration equal to two protons. In the C-O region of the ^{1}H-NMR spectrum three signals were observed; two signals integrating to one proton, assigned to H-4 and H-6, and one signal integrating to two protons, H-1, -15, consistent with the mirror plane of **155**. The two signals associated with H-4 at 5.08 ppm and H-6 at 4.02 ppm appeared as triplets in the spectrum while the signal associated with H-1, -15 at a chemical shift of 4.23 ppm appeared as a singlet. The upper bridgehead protons H-2, -14 were displayed as a singlet at 2.57 ppm and integration equal to two protons. The middle bridgeheads proximate to the ether carbon, H-3, -13 were observed at a chemical shift of 2.27 ppm as a singlet. This signal appeared within a small chemical shift range of the lower bridgehead protons H-9, -10 and H-7, -12. Protons H-9, -10 are displayed as a singlet at a chemical shift of 2.22 ppm and protons H-7, -12 are displayed as a multiplet of higher order at a chemical shift of 2.10 ppm. The signals associated with the methylene positions H-8 and H-11 were delineated as H-8$_i$, -11$_i$ and H-8$_o$, -11$_o$ due to the mirror plane of the compound. These signals are characteristic due to the large geminal coupling observed; $^{2}J_{\text{H-11i, -11o}} = {}^{2}J_{\text{H-8i, -8o}} = 15.3$ Hz. The signal associated with the interior methylene protons, H-8$_i$, -11$_i$, were observed at a slightly higher chemical shift, 1.92 ppm, versus the outer position at 1.80 ppm. This is consistent considering the rigid structure of the cage and the effect of steric environments on chemical shift. The interior methylene protons were observed a doublet, similar to the interior protons of many other scaffolds discuss, while the outer methylene protons displayed as a doublet of doublets.

The ^{13}C-NMR of oxacage **155** displayed eight signals, consistent with the C_s symmetry of the compound. At chemical shifts of 95.2, 81.7, and 79.1 ppm, in the ethereal carbon region, the carbons C-4, C-6, and C-1, -15 were observed, respectively. The various bridgehead atoms have a small range of chemical shifts between 38.3 and 35.6 ppm. At highest field, the methylene carbons C-8, -11 were observed at a chemical shift of 20.5 ppm.

All signals were unequivocally assigned using common 2-D homonuclear and heteronuclear correlation experiments. The COSY spectrum displayed clear coupling between the ethereal protons H-1, -15 and the upper bridgehead positions H-2, -14 and lower bridgehead positions H-9, -10. The H-2, -14 protons couple to the middle bridgehead protons H-3, -13. Middle bridgehead protons H-3, -13 showed strong coupling to the ethereal proton H-4 and the lower bridgeheads H-7, -12. H-4 displayed no other couplings. The lower bridgeheads H-7, -12 showed strong coupling to the ethereal proton H-6. Proton H-6 displayed no other couplings. The lower bridgeheads H-7, -12 and H-9, -10 showed coupling to the outer methylene protons H-8_o, -11_o which can be easily identified due to the dd signal structure mentioned above. Methylene protons H-8_o, -11_o and H-8_i, -11_i show the typical intense crosspeak expected of geminal protons, however, due to the dihedral angel between the inner methylene protons H-8_i, -11_i and the lower bridgehead positions little to no coupling was observed.

HMQC data clearly supports these assignments with H-1, 15, H-4, and H-6 showing correlations to the ethereal carbons. Correlations between respective bridgehead positions is clear allowing for unequivocal distinction. The methylene protons H-8, -11 showed correlation to the highest field signal consistent with the above-mentioned observations.

3.3.3.4 Rearrangement Reactions of the Saturated Mono-epoxide Cage **96**

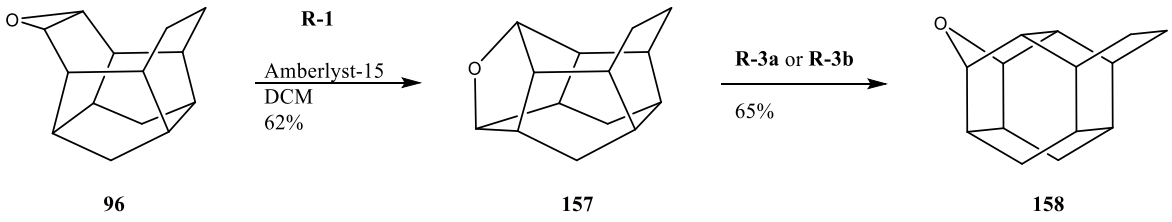

*Figure 84: Synthesis of the rearrangement products **157** and **158** from saturated epoxide **96**.*

A small sample of the saturated mono-epoxide **96** was left with trace amounts of MCPBA for one year. When reevaluated for purity, rearrangement to **158** was observed. When **96** was treated with Amberlyst-15 in DCM it quickly underwent rearrangement to **157**. Compound **157** was extremely labile, undergoing rapid rearrangement with trace amounts of acid to **158** (*Figure 84, pg. 117*). Compound **158** did not undergo further rearrangement when exposed to higher concentrations of acid and/or longer reaction times.

The rearrangement of **96** to **157** proceeds through Mechanism **R-1** (*Figure 67, pg. 91*). This is identical to the first rearrangements observed in **94** and **95**. We propose two possible mechanisms for the formation of **157**; mechanism **R-3a** or **R-3b**. Further studies including theoretical support is needed to confirm which mechanism is more favorable.

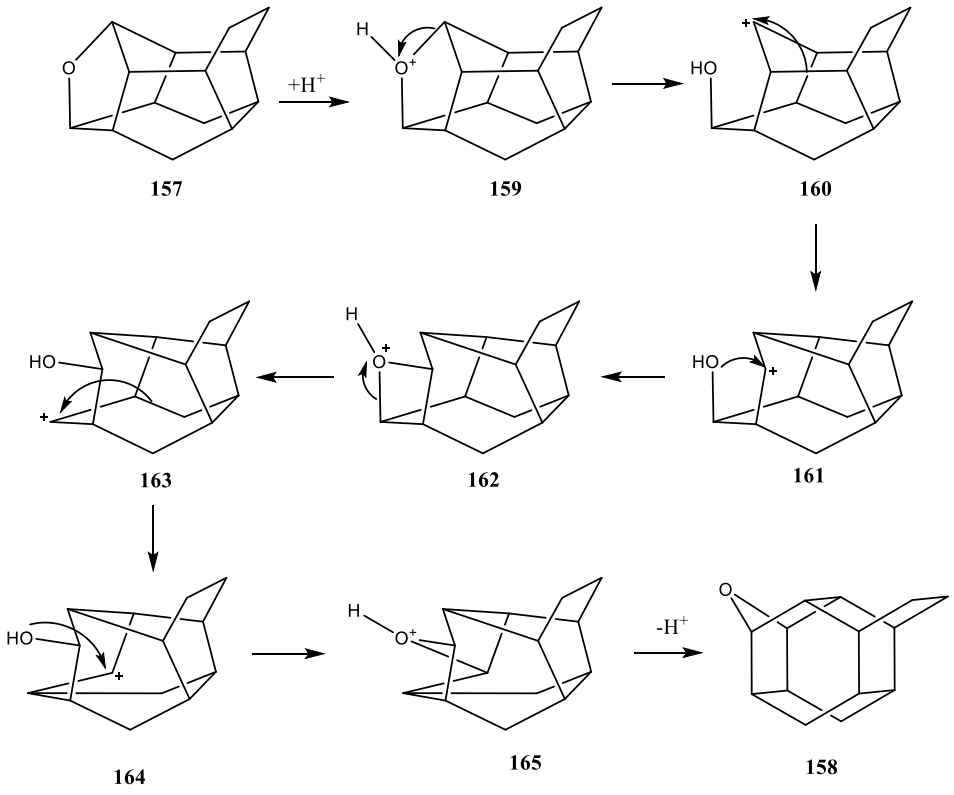

*Figure 85: First proposed mechanism for the formation of **158**, Mechanism **R-3a**.*

The first pathway begins with the protonation of the ether and opening to the carbocation cage followed by a Wagner-Meerwein shift. The carbocation of **161** is now proximate to the alcohol and in a nucleophilic attack forms a short lived protonated oxetane intermediate **162**. This is not stable due to the strain and presence of acid, opening to another carbocation. Two more Wagner-Meerwein shifts occur, followed by the alcohol again reacting with the carbocation of **164** yielding oxacage **158**.

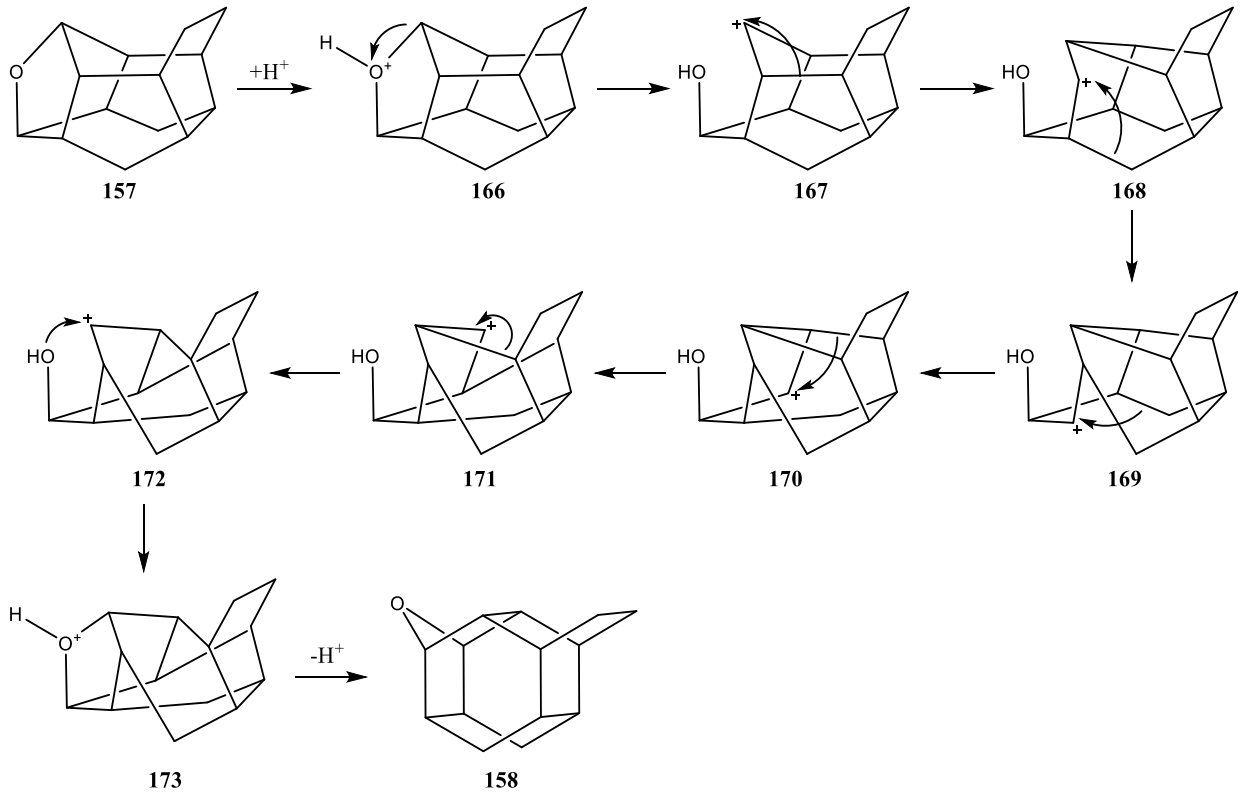

*Figure 86: Second proposed mechanism for the formation of **158**, Mechanism **R-3b**.*

The second possible pathway is more complex as it involves a higher number of individual steps but does not rely on the more strained oxetane intermediate making it potentially more favorable. Like the first proposed pathway, the ether is opened by protonation of the oxygen to the corresponding carbocation **167**. This is then followed by five sequential Wagner-Meerwein shifts

before the ether bridge is closed in a transannular nucleophilic attack to reform the ether bridge. This represents a formal 90° rotation of the oxo-norbornane subunit. Compound **158** is more stable than the previous cage due to the decrease in ring strain (*Table 11, pg. 120*); **157** contains a seven-membered ring while **158** is composed entirely of six-membered rings.

*Table 11: Change in enthalpy (H°) and heat of formation (E) in the rearrangement of **96** to **158**. Overall change in strain energy was ΔE_{strain} =-158.2665 kJ/mol Calculated by DFT using the B3-LPY 6-31J* basis set.*

	96	**157**	**158**
H° (E_h)	-619.18866	-619.22782	-619.24728
E (E_h)	-619.49689	-619.53781	-619.55718
ΔE_{strain} (kJ/mol)	0	107.4255	50.841

3.3.3.4.1 NMR Analysis of **157** and **158**

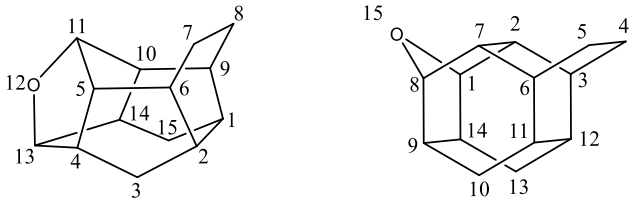

157 **158**

*Figure 87: Compounds **157** and **158** with IUPAC numbering.*

The ^{1}H-NMR of oxacage **157** displays nine signals; two showed integrations to one proton, five signals showed integration to two protons, and one signal showed integration to six protons. This is inconsistent with the ten signals suggested by compounds C_s symmetry. However, integration of the ^{1}H-NMR spectrum and 2-D NMR methods revealed the presence of a pair of isochronic signals. The ethano protons H-7 and H-8 should display two signals delineated as H-7_i,

-8_i and H-7_o, -8_o, however, these signals appear as a broad multiplet of higher order. In the C-O region of the ^{1}H-NMR spectrum two triplet signals integrating to one proton at chemical shift of 4.31 and 4.20 ppm were observed and assigned to H-11 and H-13, respectively. The lower bridgehead protons proximate to the ether moiety, H-4, -14, were displayed as a multiplet of higher order at 2.70 ppm and integration equal to two protons. The upper bridgeheads proximate to the ether moiety, H-3, -13, were also observed as a multiple at a slightly lower chemical shift of 2.66 ppm. The lower bridgehead protons H-1, -2 were observed as an apparent singlet at a chemical shift of 2.07 ppm. The signals associated with the methylene positions H-3 and H-15 were delineated as H-3_i, -15_i and H-3_o, -15_o due to the mirror plane of the compound. These signals are characteristic due to the large geminal coupling observed; $^2J_{\text{H-3i, H-3o}} = {}^2J_{\text{H-15i, H-15o}} = 13.6$. The signal associated with the interior methylene protons, H-3_i, -15_i, were observed at a higher chemical shift, 2.00 ppm, versus the outer position at 1.25 ppm. This is consistent considering the rigid structure of the cage and the effect of steric environments on chemical shift. The interior methylene protons were observed a doublet, similar to the interior protons of many other scaffolds discuss, while the outer methylene protons displayed as uniquely structured multiplet of higher order resembling a doublet. Between the signals assigned to the methylene units and centered at a chemical shift of 1.82 ppm a broad multiplet integrating to six protons was observed. This signal was determined to be comprised of the ethano protons H-7, -8 and the upper bridgehead position H-6, -9. It was possible to distinguish these signals using 2-D NMR experiments.

The ^{13}C-NMR of oxacage **157** displayed eight signals, consistent with the C_s symmetry of the compound. At chemical shifts of 79.2 and 78.8 ppm, in the ethereal carbon region, the carbons C-11 and C-13 were observed, respectively. The bridgehead atoms proximate to the oxygen displayed within a small range of chemical shift at 52.7 and 49.4 ppm for C-5, -10 and C-4, -14,

respectively. This trend was also observed for the other bridgehead positions C-1, -2 and C-6, -9 at chemical shifts of 37.9 and 36.5 ppm. The methylene carbons C-3, -15 were observed at a chemical shift of 29.1 ppm. At highest field the ethano carbons C-7, -8 were observed at a chemical shift of 20.1 ppm.

All signals were unequivocally assigned using common 2-D homonuclear and heteronuclear correlation experiments. The COSY spectrum displayed clear coupling between the ethereal proton H-11 and the upper bridgehead positions H-5, -10. The lower ethereal proton H-13 displayed clear coupling to the lower bridgehead positions H-4, -14. The bridgehead positions proximate to the oxygen displayed a strong coupling with an intense crosspeak. Upper bridgehead protons H-5, -10 are also shown to couple with H-6, -9. Protons H-6, -9 are the only signals to show coupling to the ethano protons H-7, -8, but also show a strong coupling to the lower bridgeheads H-1, -2. The lower bridgeheads H-1, -2 and H-4, -14 showed coupling to the outer methylene protons H-3_o, -15_o which can be easily identified due to the unique signal structure mentioned above. Methylene protons H-3_o, -15_o and H-3_i, -15_i show the typical intense crosspeak expected of geminal protons, however, due to the dihedral angel between the inner methylene protons H-3_i, -15_i and the lower bridgehead positions little to no coupling was observed.

HMQC data clearly supports these assignments with H-11 and H-13 showing correlations to the ethereal carbons. Correlations between respective bridgehead positions is clear allowing for unequivocal distinction. The methylene protons H-3, -15 showed correlation to the high field signal at 29.1 ppm. The ethano protons show correlation to the highest field signal of 20.1 ppm in the ^{13}C-NMR, consistent with the above-mentioned observations.

The ^{1}H-NMR of oxacage **158** displays nine signals, all with equivalent integration, consistent with the compounds C_s symmetry. Interestingly, the ethano protons H-4 and H-5 are not

isochronic, unlike the ethano protons of **157**. This may be due to the difference in bicyclo[3.2.2]nonane substructure seen in **157** versus the bicyclo[2.2.2]octane substructure of **158**.

At a chemical shift of 4.24 ppm, the ethereal protons H-1, -8 were observed as a singlet. This signal is within the expected range of an ethereal proton. The lower bridgehead positions H-9, -14 were observed as an apparent singlet at a chemical shift of 2.22. This was significantly higher than the chemical shift of the other bridgehead proximate to the oxygen, H-2, -7, observed at 2.03 ppm. Unlike many of the other scaffolds derived from diene **1**, the other bridgehead positions within the scaffold of **158** were observed between the chemical shifts of the inner and outer protons of methylene positions H-10 and H-13. The lower bridgeheads H-11, -12 were observed as an apparent singlet at 1.75 ppm. At chemical shifts of 1.61 and 1.42 the ethano protons H-4, -5 were observed. The lower field signal was assigned to the *exo* protons of H-4 and H-5, delineating this signal as H-4_{exo}, -5_{exo}. The higher field was assigned to the *endo* protons of H-4 and H-5, delineating this signal as H-4_{endo}, -5_{endo}. Upper bridgeheads H-3, -6 were observed as an apparent singlet at 1.30 ppm. The signals associated with the methylene positions H-10 and H-13 were delineated as H-10_i, -13_i and H-10_o, -13_o due to the mirror plane of the compound. These signals are characteristic due to the double signal structure and large geminal coupling; $^2J_{\text{H-10i, H-10o}} = {}^2J_{\text{H-13i, H-13o}}$ = 13.7 Hz. The signal associated with the interior methylene protons, H-10_i, -13_i, were observed at a higher chemical shift, 1.82 ppm, versus the outer position at 1.11 ppm. This is consistent considering the rigid structure of the cage and the effect of steric environments on chemical shift.

The ^{13}C-NMR of oxacage **158** displayed seven signals, consistent with the C_s symmetry of the compound. At a chemical shift of 79.8 in the ethereal carbon region, the carbons C-1, -8 were observed. The bridgehead carbons proximate to the oxygen were observed at lower field when

compared to the bridgeheads multiple bonds away. The ethano carbons C-4, -5 were observed at a chemical shift of 25.7 ppm. At highest field the ethano carbons C-10, -13 were observed at a chemical shift of 24.2 ppm.

All signals were unequivocally assigned using common 2-D homonuclear and heteronuclear correlation experiments. The COSY spectrum displayed clear coupling between the ethereal protons H-1, -8 with upper bridgehead positions H-2, -7 and H-1, -8 with the lower bridgehead positions H-9, -14. The bridgehead positions proximate to the oxygen displayed a strong coupling with an intense crosspeak. Upper bridgehead protons H-5, -10 are also shown to couple with H-3, -6. Protons H-3, -6 are the only signals to show coupling to the ethano protons H-4, -5, but also show a strong coupling to the lower bridgeheads H-11, -12. The lower bridgeheads H-11, -12 and H-9, -14 showed coupling to the outer methylene protons H-10_o, -13_o which can be easily identified due to the doublet signal structure mentioned above. Methylene protons H-10_o, -13_o and H-10_i, -13_i show the typical intense crosspeak expected of geminal protons, however, due to the dihedral angel between the inner methylene protons H-10_i, -13_i and the lower bridgehead positions little to no coupling was observed.

HMQC data clearly supports these assignments with H-1, -8 showing correlations to the ethereal carbon. Correlations between respective bridgehead positions is clear allowing for unequivocal distinction. The ethano protons H-10, -13 showed correlation to the high field signal at 25.7 ppm. The methylene protons show correlation to the highest field signal of 24.2 ppm in the ^{13}C-NMR, consistent with the above-mentioned observations.

3.3.4 Other Rearrangement reactions

A control experiment to probe the rearrangement of diol **174** was carried out (*Figure 88, pg. 125*). The hypothesis behind this reaction was that **174** would be protonated and lose water to

generate the same carbocation observed in the other reactions. This would then undergo the same set of rearrangements to the compounds **99** and **100**.

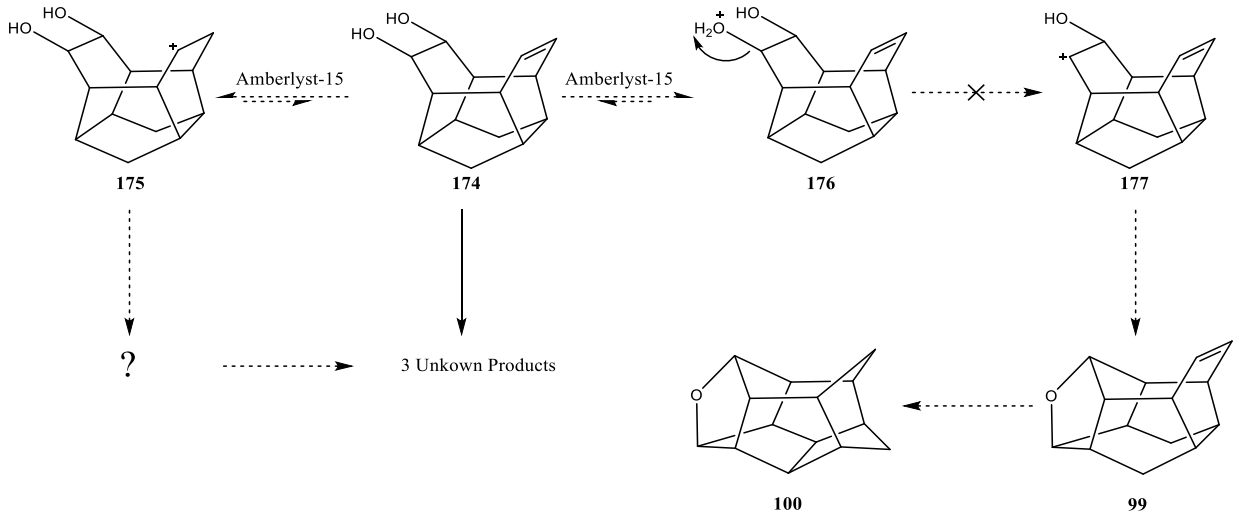

*Figure 88: Attempted dehydration and rearrangement of **174**.*

However, this was not the case. When **174** was treated with Amberlyst-15 under identical conditions as mono-epoxide **94**, neither **99** nor **100** was observed forming. Acid treatment of **174** was intended to protonate and dehydrate one of the alcohol moieties with the resulting carbocation expected to undergo rearrangement following mechanism **R-1**. Alternatively, protonation of the olefin would result in drastically different results. The material obtained from this reaction showed the same solubility pattern as **174** (discussed in *3.4.2 cis-Dihydroxylation of **1** & **24***).

When inspected by ^{1}H-NMR and ^{13}C-NMR it was clear that the crude material contained three different products. The ^{1}H-NMR shows a variety of signals. Noteworthy signals are the possibly three olefinic signals (two overlapping) at lower field and the higher order signal at approximately 4.0 ppm (*Figure 89, pg. 126*). This may be indicative of an ether bridge as observed in the rearrangements of the epoxides. The ^{13}C-NMR is also complex with six potential olefinic signals at lower field and the five signals in the ether and alcohol C-O range (*Figure 90, pg. 127*).

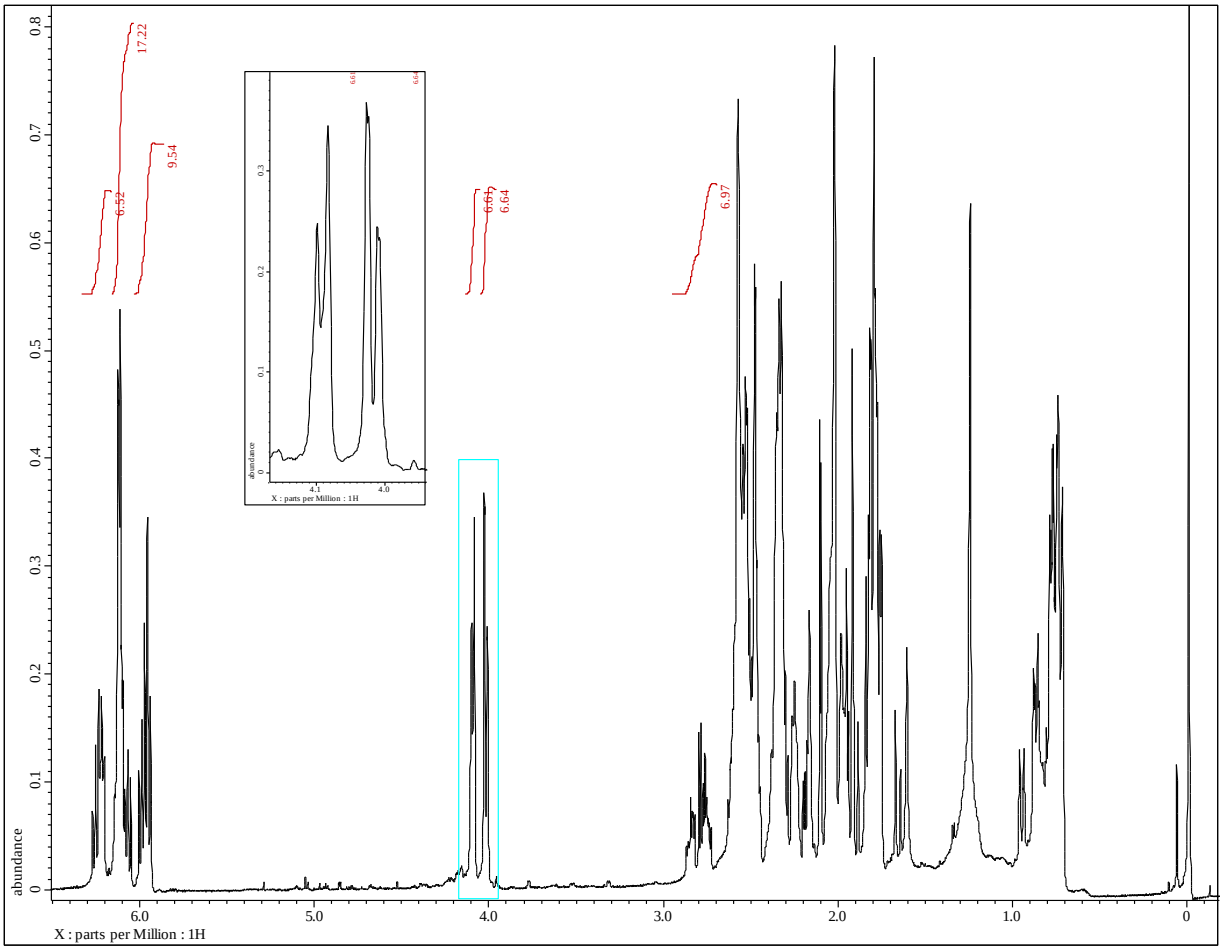

*Figure 89: The ^{1}H-NMR of the rearrangement of **174**.*

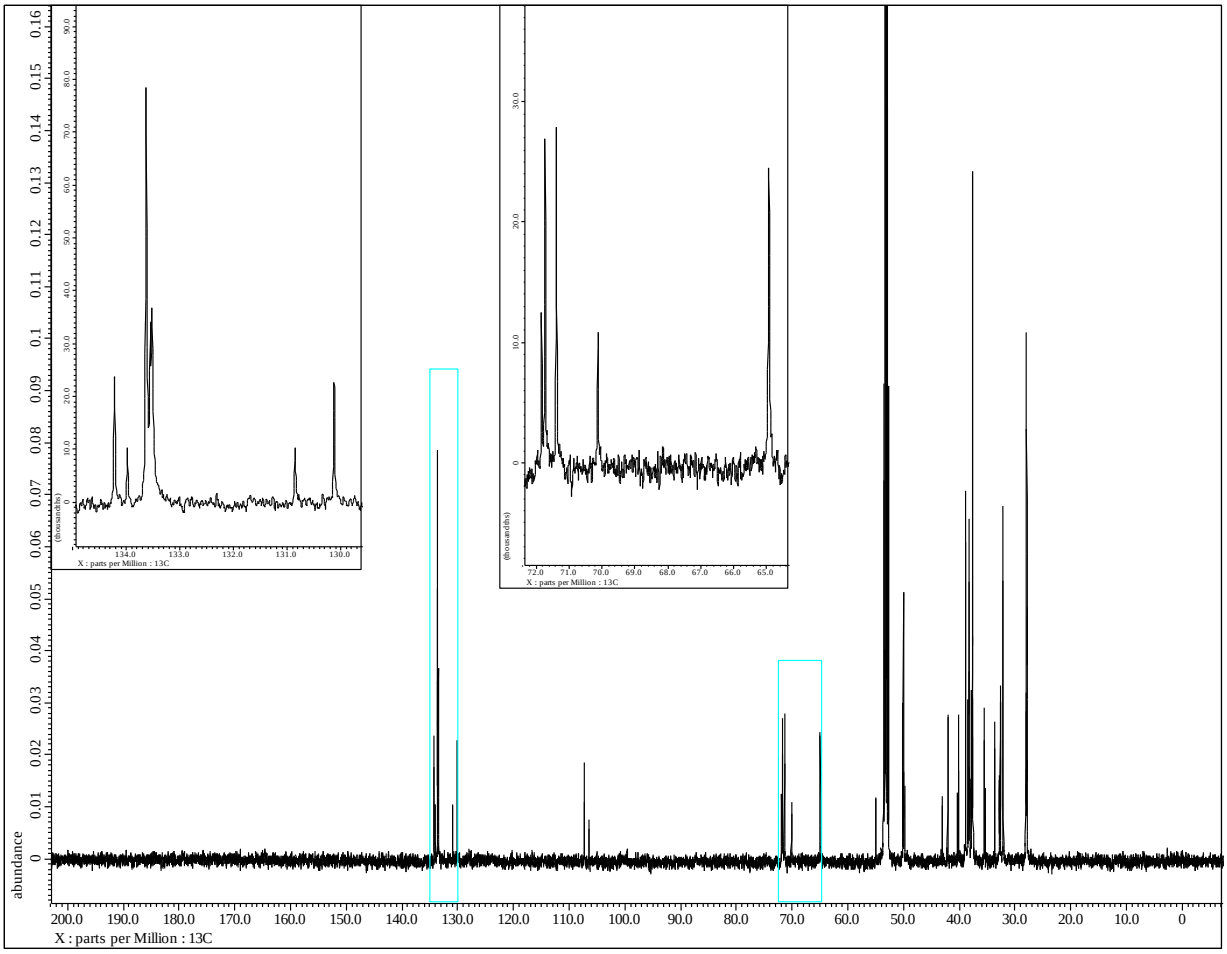

*Figure 90: The ^{13}C-NMR of the rearrangement of **174**.*

Interestingly, the GC/MS of this mixture showed only one trace with a $M^{\cdot+}$ peak of *m/z* = 200 ($C_{14}H_{16}O$), implying that these three compounds share comparable structure and polarity. Attempts to isolate these compounds by column chromatography (SiO_2, chloroform/MeOH 40:1) failed as all three products eluted together and did not separate. Ultimately characterization was not achieved, and further investigation is needed including separation of the components and full characterization.

3.3.5 Physical Data

*Table 12: Table of the epoxidation and rearrangement products detailing if compounds were fully assigned and if X-ray diffraction data was collected. The solvent used for crystal growth is specified and the melting point for each compound is given. Compound **100** decomposed at 249.9 °C. Compound **149** gave a large melting point range with the melt beginning at 88.5 °C.*

Product	I.D.	Assignment	XRD	Solvent	Melting Point, C°
Hydrocarbon Cage 1	**92**				
Hydrocarbon Cage 2	**92**	Yes			
Mono-epoxide	**94**	Yes	Yes	$CHCl_3$	261.4-261.9
Bis-epoxide	**95**	Yes	Yes	$CHCl_3$	309.3-311.5
Sat. Mono-epoxide	**96**	Yes			260.6-261.3
Oxacage 1	**99**	Yes			
Oxacage 2	**100**	Yes			263.2-263.4
Carbonyl Cage	**103**				
Iodo-Cage	**149**	Yes			88.5-98.6
Hydrocarbon Cage 3	**151**	Yes			
Oxacage 3	**152**	Yes	Yes	2:1 cyclohexane/EtOAc	305.7-305.9
Oxacage 4	**153**	Yes			
Oxacage 5	**154**				
Oxacage 6	**155**	Yes			
Oxacage 7	**157**	Yes			176.4-177.7
Oxacage 8	**158**	Yes			159.5-162.0

Many of the rearrangement products were isolated as waxy material that did not form single crystals in our hands (yet), however, XRD data was obtained oxacage **152**. The other rearrangement products of the bis-epoxide **95** were also crystalline but did not give in adequate crystallographic data. This was likely due to weathering of the crystals over time.

There is a clear trend in the change in melting points between the various scaffolds (*Table 12, pg. 128*). The bis-epoxide **95** and rearrangement product **152** both show high melting points relative to the other compounds. The mono-epoxide **94** and **174** both have higher melting points that the saturated system **96** and derived oxacages. This is due to the stronger intermolecular forces between the molecules of **95** versus **94** versus **96**. Bis-epoxide **95** and oxacage **152** both exhibit stronger polarization due to the presence of two oxygens, increasing the strength of dipole-dipole and dipole-induced dipole interactions. The two epoxide oxide oxygens may also participate in hydrogen bonding. The mono-epoxide **94**, saturated mono-epoxide **96**, and oxacages **100**, **157** and **158** also display dipole-dipole, dipole-induced dipole, and possible H-bonding interactions but are not as strong as **95** and **152** due to only containing one oxygen. Mono-epoxide **94** shows stronger dispersion forces versus **96**, **100**, **157**, and **158** due to the olefin while the decreasing trend in melting points (**100** > **96** > **157** > **158**) is likely due to the variations in configuration leading to varying polarity (display dipole-dipole and dipole-induced dipole forces).

3.3.6 X-Ray crystallography of Select Epoxide and Oxacage Scaffolds

*Table 13: X-ray crystallographic data obtained for compounds **94**, **95**, **152**.*

Parameter	Mono-epoxide	Bis-epoxide	Oxacage 3
Structure #	**94**	**95**	**152**
Empirical Formula	$C_{14}H_{16}O$	$C_{14}H_{16}O_2$	$C_{14}H_{16}O_2$
Formula Weight g/mol	200.27	216.27	216.27
Temperature, K	100	153(2)	55
Color	Colorless	Colorless	Colorless
Crystal size, mm^3	?×?×?	0.76×0.55×0.39	?×?×?
Crystal system, space group	Triclinic, P-1	Orthorhombic, $P2_12_12_1$	Monoclinic, $P2_1/c$
a, Å	6.8286 (2)	7.0800 (6)	11.5331 (6)
b, Å	11.7026 (4)	7.3565 (7)	7.0216 (4)
c, Å	12.3189 (3)	19.4820 (17)	12.1627 (6)
α, °	87.480 (2)	89	89
β, °	79.630 (3)	89	97.394 (4)
γ, °	87.292 (3)	89	89
Volume, $Å^3$	969.12 (5)	1014.75 (16)	976.75 (9)
Z	4	4	4
ρ_{calcd}, mg/m^3		1.416	
R_1[a] [$I > 2\sigma(I)$]		0.0317	
R_1[a] (all)		0.0320	
wR_2[b] [$I > 2\sigma(I)$]		0.0860	
wR_2[a] (all)		0.864	
Largest diff. peak/hole, e $Å^{-3}$		0.25/-0.19	

The epoxide **94** crystalizes in the triclinic space group P-1. Many of the bonds within this compound are longer than average. The C-C bonds found between C-1 and C-10 (1.573 Å), C-3 and C-8 (1.579 Å), C-3/8 and C-4/7 (1.559 Å), and C-4/7 and C-11/15 (1.588 Å) are all longer than average C_{sp3}-C_{sp3} bond length.

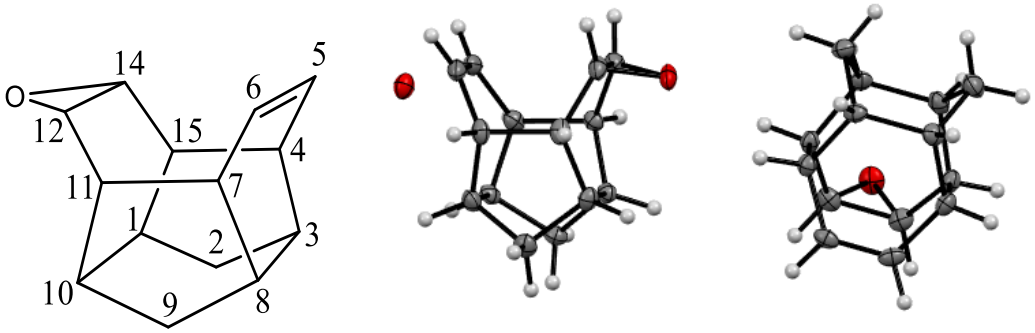

*Figure 91:Thermal ellipsoid plot of **94**. The crystal structure of **95** showed two cryptographically independent molecules, one of which also shows some disorder. Thermal ellipsoids are drawn at the 50 % probability level. Numbering is assigned through IUPAC conventions.*

Most of the carbon atoms in **94** do not show ideal geometry, however, C-1/10 and C-3/8 are the closest with at least one C-C-C bond angle close to the ideal 109°. Bond angles within the oxirane are close to ideal with only sight deviation for 60°. The deviations observed are likely due to the ring strain within the scaffold.

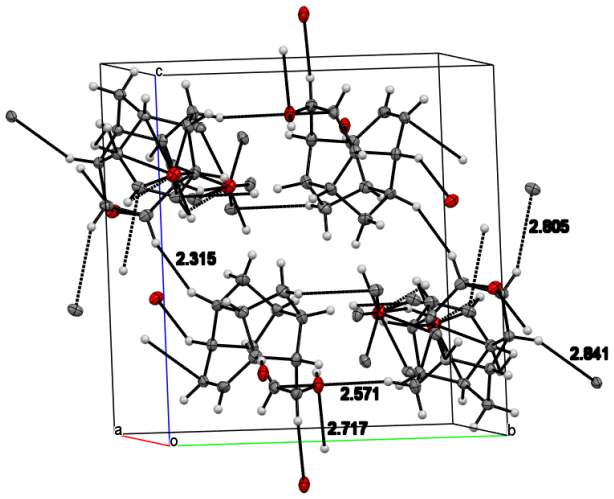

*Figure 92: Thermal ellipsoid plot of crystal packing within the monoclinic unit cell in the crystal structure of **94**. This plot shows the difference in packing and short contact between molecules in each discrete unit cell. Thermal ellipsoids are drawn at the 50% probability level*

The epoxide **94** crystalized in a centrosymmetric pattern with four molecules occupying each unit cell. It was observed that each unit cell of **94** contained two crystalographically independent molecules and that one of these showed some disorder in the position of the epoxide unit. This disorder may be caused by two competing molecule configurations that are near equal in energy. The crystal lattice has both configurations of the molecules in its occupancy giving the structure disorder. Within the unit cell short contacts between the molecules show two interactions. The $O^{\delta-}_{oxirane}\cdots H^{\delta+}_{methylene}$ and $H_{oxirane}\cdots H_{bridgehead}$ interactions show short contact distances of 2.571 and 2.315 Å. Interactions between each unit cell show three short contact distances. $C_{olefin}\cdots H_{bridgehead}$ and $C_{oxirane}\cdots H_{bridgehead}$ short contacts at 2.831 and 2.805 Å can be observed along with multiple $O^{\delta}\cdots H^{\delta+}_{bridgehead}$ interactions at 2.717 Å. This compound crystalized with some degree of disorder. Due to this, short contacts between the unit cells are more complex.

The epoxide **95** crystalizes in the orthorhombic space group $P2_12_12_1$ with most bonds being of typical length. The C-C bond distance between C-4/8 and C-12/16 are the longest bonds at 1.586 Å. This is significantly longer than the average C_{sp3}-C_{sp3} bond length. The next longest bond can be observed between C-1/3 and C-9/11. All other bonds are within normal deviation.

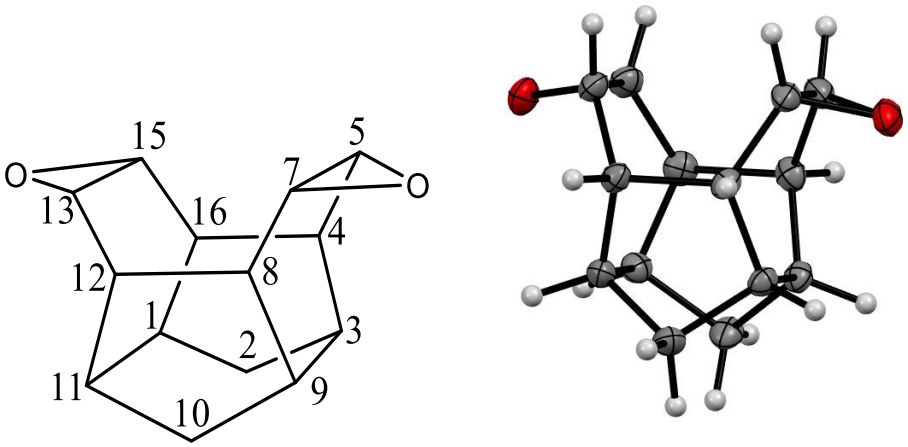

*Figure 93: Thermal ellipsoid plot of **95**. Thermal ellipsoids are drawn at the 50 % probability level. Numbering is assigned through IUPAC conventions.*

Carbons C-1/3/9/11 show the closest adherence to the ideal tetrahedral geometry. C-1/3/9/11 are the closest with at least one C-C-C bond angle close to the ideal 109°. The other sp3 carbon in the framework skew farther from the ideal tetrahedral geometry. Bond angles within the oxirane are close to ideal with only sight deviation for 60°.

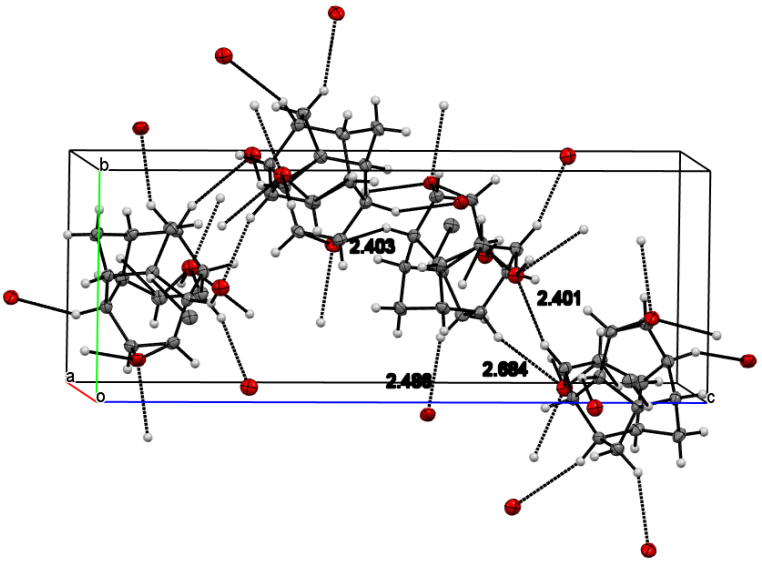

Figure 94 Thermal ellipsoid plot of crystal packing within the monoclinic unit cell in the crystal structure of ***95****. This plot shows the difference in packing and short contact between molecules in each discrete unit cell. Thermal ellipsoids are drawn at the 50% probability level.*

Compound **95** shares the orthorhombic crystal system with the bis-cyclopropane **41a**. In the solid state **95** crystalizes in an enantiomorphic pattern with four molecules occupying each $P2_12_12_1$ unit cell. This compound is also unique in that not all molecules within the unit cell show interactions. One of the four molecules is observed not having any short contact interactions within the unit cell. The other three molecules show the short contact interactions $O^{\delta}\cdots H^{\delta+}{}_{\text{bridgehead,}}$ $O^{\delta}\cdots H^{\delta+}{}_{\text{bridgehead,}}$ and $O^{\delta}\cdots H^{\delta+}{}_{\text{oxirane}}$ at 2.403, 2.683, and 2.401 Å. Interestingly, these are the same contacts that connect the molecules within the unit cell to the molecules of adjacent unit cells. The only new short contact observed between unit cells is along the a-o-c plane. The distance of the $O^{\delta}\cdots H^{\delta+}{}_{\text{methylene}}$ interaction is 2.485 Å.

The oxacage **152** crystalizes in the monoclinic space group $P2_1/c$ with most bonds being of typical length. The C-C bond of the oxirane is slightly shorter than the average at 1.454 Å.[38]

This also causes some distortion in the cyclohexane unit as the C-C bond distance of C-1 to C-2 is slightly longer than average at 1.558 Å; this is the longest bond in the scaffold.[38] There is also some distortion in the C-6/10 to C-7/9 bonds as they are significantly shorter than average at 1.502 Å. The shortest bonds are the C-O bonds of the oxo-norbornane unit at 1.453 Å but is within normal deviation of the C-O bonds of the THF subunit.[38]

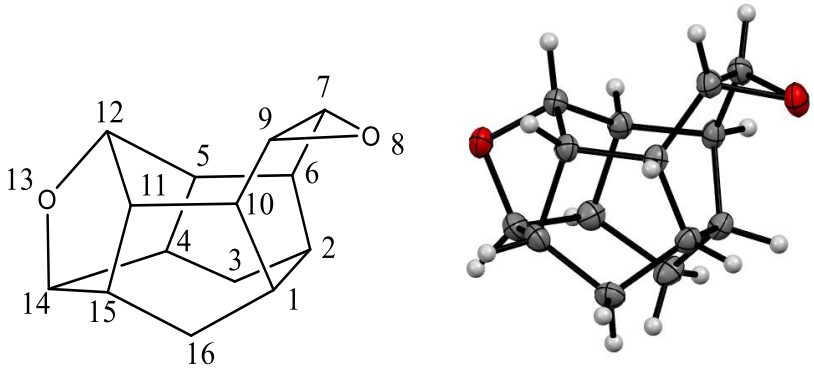

*Figure 95: Thermal ellipsoid plot of **152**. Thermal ellipsoids are drawn at the 50 % probability level. Numbering is assigned through IUPAC conventions.*

Bond angles within the oxirane are close to ideal with only sight deviation for 60°. The C-O-C angle is exactly 60° while the two C-C-O angles are at 60.05° and 59.94°. The C-O-C bond angle of the oxo-norbornane unit is 94.61° which is significantly smaller than the ideal bent angle of 120° and the 108° angles found in THF. This smaller angle may contribute to the strain energy than facilitates the rearrangement of this compound. All sp^3 carbons found in **152** deviates from the ideal tetrahedral geometry by some degree with larger deviations found at C-9/7 of the oxirane. The closest to ideal tetrahedral angles is found at the C-O carbons of the oxo-norbornane unit. The dihedral angles within the scaffold all measure significantly less than 90° except for the angle between the bridgehead positions H-1/2/4/15 and the interior methylene protons H-3i/16i. This is

consistent with the other scaffolds observed and gives explanation to the strong coupling observed in these compounds.

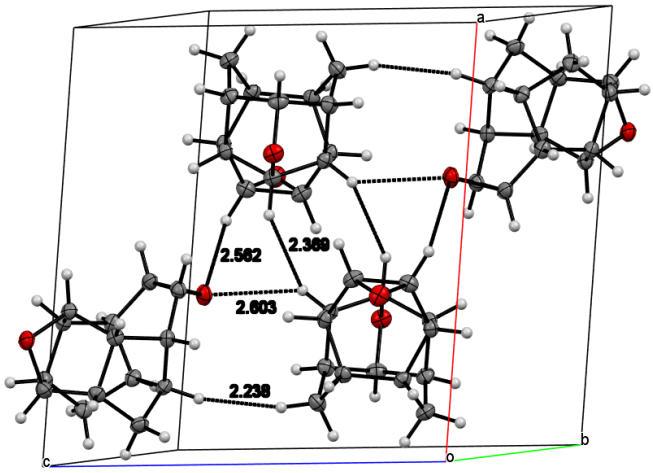

*Figure 96: Thermal ellipsoid plot of crystal packing within the monoclinic unit cell in the crystal structure of **152**. This plot shows the difference in packing and short contact between molecules in each discrete unit cell. Distances and short contacts between adjacent cells were omitted for clarity. Thermal ellipsoids are drawn at the 50% probability level.*

The epoxide **152** crystalized in a centrosymmetric pattern with four molecules occupying each unit cell. Short contact distances show interactions between molecules within the unit cell. Molecules on the outer edge of the unit cell display short contact distances to two molecules while the interior molecules show interactions with all other molecules within the unit cell. Interactions within the cell along the a-o-b plane show short contact distances of 2.603 and 2.238 Å for $O^{\delta-}_{oxirane}\cdots H^{\delta+}_{bridgehead}$ and $H_{bridgehead}\cdots H_{bridgehead}$ interactions, respectively. Along the b-o-c plane within the cell two sets of $O^{\delta-}_{oxirane}\cdots H^{\delta+}_{oxirane}$ and $H_{bridgehead}\cdots H_{bridgehead}$ are observed with short contact distances of 2.562 and 2.369 Å. Somewhat surprisingly there are no new intercell interactions along the b-o-c plane. The only observed interactions between unit cells along this

plane are identical to those already observed within the unit cell. Along the a-o-c plane three new interactions can be observed. One $H_{bridgehead}\cdots H_{bridgehead}$ short contact of 2.352 Å was observed as well as two $O^{\delta-}{}_{oxonorbornane}\cdots H^{\delta+}{}_{bridgehead}$ interactions with distances of 2.697 and 2.590 Å. Only one interaction along the a-o-b plane was observed with a short contact distance of 2.238 for a $H_{methylene}\cdots H_{bridgehead}$ interaction.

3.4 Multistep Synthetic Approach Towards the Preparation of a Novel Tetraoxacage

3.4.1 Introduction to Oxacage Chemistry

Oxacages, such as the epoxide rearrangement products discussed above, are a class of organic cage compounds that contain oxygen heteroatoms within the cage framework. A particular class of poly-oxacages, such as **178**-**181**, contain a hydrophobic hydrocarbon face and a hydrophilic face of alternating carbon-oxygen-carbon units (*Figure 97, pg. 138*). As such these scaffolds show a remarkable structural similarity to crown ethers and other cryptands, replacing the typical ethano spacer with a methyne spacer. This makes them particularly attractive substrates for metal complexation and molecular recognition as multidentate ligands. Additionally, while many of these oxacages are comprised of a series of cyclic acetals, they show remarkable acid stability once formed.[71] Currently, no concrete (limited) experimental data is available, however, it has been postulated that the unique conformations of the hydrophilic faces of some oxacages may lead to variations in binding affinity in select environments due to the rigid cage structure.[60, 71-75]

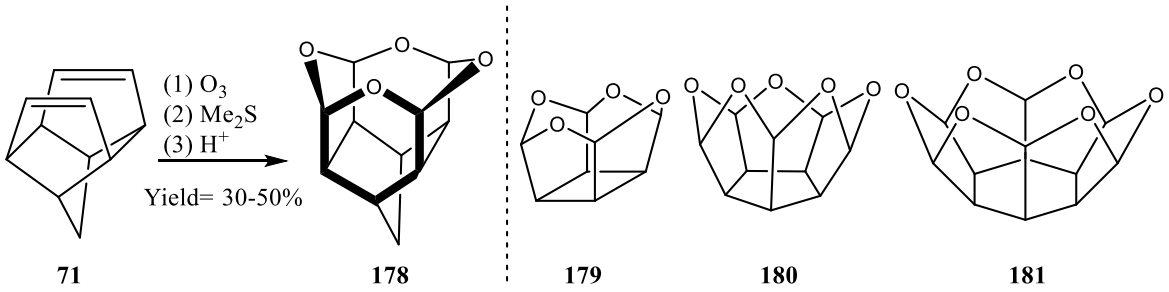

*Figure 97: Examples of four different oxacages. Oxacage **178** was derived from the cage diene homohypostrophene **71** by ozonolysis followed by acid treatment.*

Oxacages have been targeted from a variety of polycyclic compounds including non-cage substrates such as **184** (*Figure 99, pg. 139*) and cage dienes such as homohypostrophene **71** (*Figure 97, pg. 138*).[71] One of the most common strategies for oxacage synthesis has been the ozonolysis of olefin containing species, demonstrated by the preparation of tetraoxacage **178** and trioxacage **185** (*Figure 99, pg. 139*).[60, 71, 73, 74]

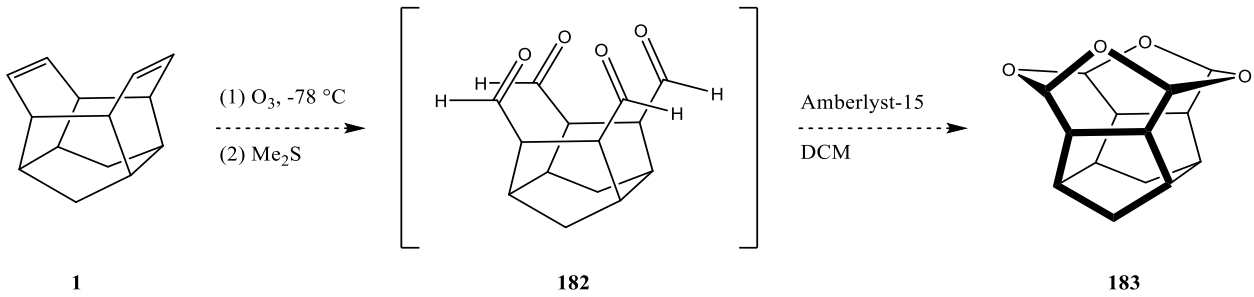

*Figure 98: Failed ozonolysis of **1**.[60]*

The tetraoxacage **183** was targeted *via* the ozonolysis of **1** but failed to deliver the targeted compound (*Figure 98, pg. 138*). No characterizable material other than nondescript polymer could be isolated after acid treatment.[60] Mehta cites the unfavorable strain of the seven-membered heterocycles as a major reason for this reaction not proceeding as expected. Mehta also notes that

the stereochemistry of the aldehyde intermediate plays an important role in promoting the intramolecular cyclization requiring the *all-cis*-tetraaldehyde **182**.[60]

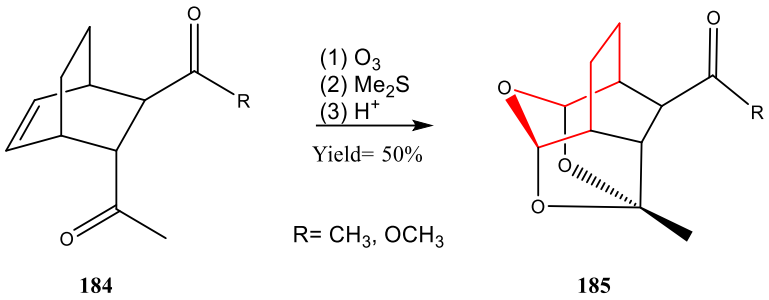

*Figure 99: Ozonolysis of **184** yielded oxacage **185**, containing a seven-membered cyclic acetal in moderate yields (highlighted in red).*[76]

While Mehta cites the formation of the seven-membered rings as to why the ozonolysis of **1** failed, there is literature precedent for the formation of seven-membered rings in oxacage scaffolds (*Figure 99, pg. 139*).[76] The ozonolysis of dione scaffold **184** resulted in the trioxacage **185** in moderate yields. This shows that the formation of the seven-membered ring is possible in an oxacage scaffold.

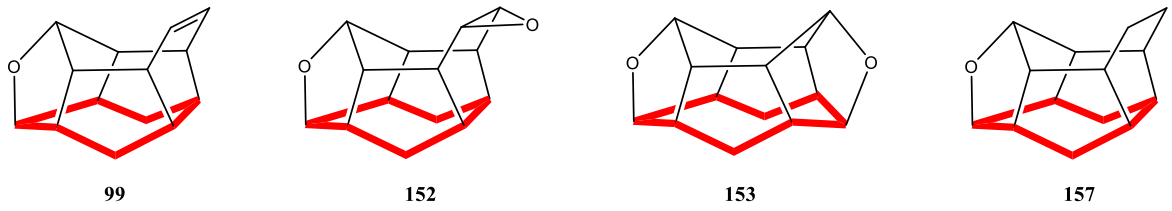

*Figure 100: The oxacages **99**, **152**, **153**, and **157** contain large ring subunits (highlighted in red).*

Additionally, the rearrangement of the epoxides **94**, **95**, and **96** (*3.3.3 Synthesis and Rearrangement of Epoxide Cages*) yielded a series of oxacages, some of which contained seven- or eight-membered ring subunits (*Figure 100, pg. 139*).

The preparation of **185** also shows that the stereochemistry of carbonyl groups that participate in the intramolecular cyclization is important. Therefore, the strain energy of the seven-membered ring formation may not have been as big of a factor as Mehta states and the relative stereochemistry of the aldehydes in tetraaldehyde intermediate **182** was the major contributing factor to why **183** was not obtained.[60, 76]

While the above sequence to oxacage **183** failed (*Figure 98, pg. 138*), the preparation of **183** may still be possible through a multi-step approach. This would avoid the various equilibrium driven reactions of the ozonolysis and allow for the targeted synthesis of several intermediates. A multi-step approach to **183** requires the introduction of oxygen functionality, which can be accomplished in a number of ways.

cis-Dihydroxylation is an effective tool to add oxygen functionality to olefins. The use of strong oxidizing agents such as potassium permanganate ($KMnO_4$) and osmium tetroxide (OsO_4) can be used in the *syn*-addition of two hydroxyl groups to olefin units.[77-79] Unfortunately, oxidation using $KMnO_4$ can lead to over-oxidation *via* the oxidative cleavage of double bonds to carboxylic acids (or ketones). Osmium tetroxide, although significantly more hazardous, has found extensive use in cage chemistry to synthesize diol and tetrol cages.[9, 80, 81]

The ene-diol **188** was synthesized using OsO_4 in benzene (*Figure 101, pg. 141*). The diene **186** was treated with 1.2 equivalents of OsO_4 in benzene resulting in a green powdery precipitate, identified as the mono osmate ester **187**. This osmate ester of **186** does not exist as the cyclic ester typically observed in *cis*-dihydroxylations, but instead as the half-ester. This is likely due to the steric requirements caused by the pagodane-like structure. Upon complete conversion of **186** the benzene was removed and the solid suspended in dry THF. The osmate ester was then reduced with LAH resulting in the diol **188**. Diol **188** was isolated in good yield (85%) by recrystallization

with DCM/ether. Interestingly, despite using equimolar amounts of the oxidizer, the tetrol **189** was not observed and could not be obtained using other oxidation methods (*e.g.*, $KMnO_4$).[80]

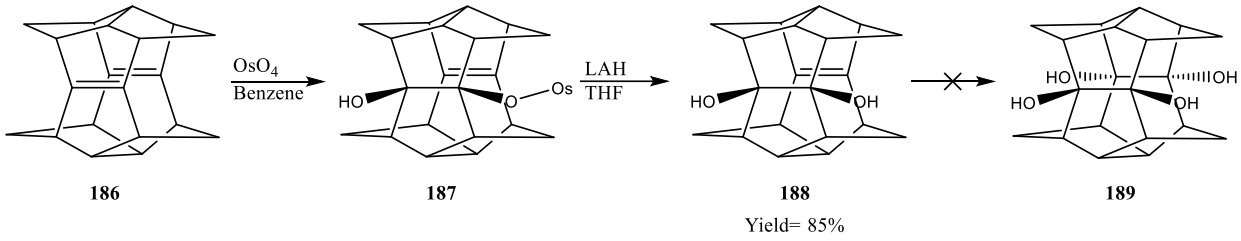

*Figure 101: Synthesis of diol **188** using osmium tetroxide in benzene (yield 85%). The diol was obtained by reduction of the osmate ester **187** with LAH. The tetrol **189** could not be prepared.*[80]

cis-Dihydroxylation reactions can be performed using stochiometric amounts of OsO_4 or in catalytic amounts in tandem with a secondary oxidizer to reform the osmium (VIII) species *in situ*. A variety of secondary oxidizers can be employed and mainly consist of tertiary amine oxides like *N*-methylmorpholine *N*-oxide (NMO) or trimethylamine *N*-oxide (Me_3NO).[9, 77-79, 82]. Catalytic *cis*-dihydroxylation also drastically improves the greenness of the reaction and reduces the cost of oxidations.[78] When applied to selected cage systems catalytic *cis*-dihydroxylation with OsO_4 has allowed access to tetrol systems without prohibitive amounts of reagent.

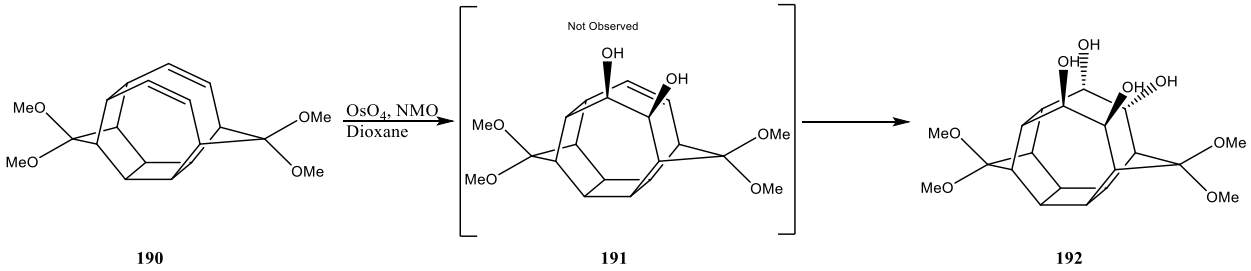

*Figure 102: Tetrol **192** obtained by cis-dihydroxylation of **190** in the presence of the secondary oxidizer NMO. No trace of the diol **190** was reported. No yield was reported.*[9]

The oxidation of **190** to the tetrol **192** was accomplished using small amounts of OsO_4 in 1,4-dioxane in the presence of 2.05 equivalents of NMO (*Figure 102, pg. 141*). Interestingly, the diol **191** was not observed forming in this reaction.[9] This suggests that the steric and conformational accessibility of the double bonds and/or the osmate ester play an important role in the second transformation. Proximity of the olefins and functionalized positions may play a role in accessibility and stability of the second transformation.[9, 80]

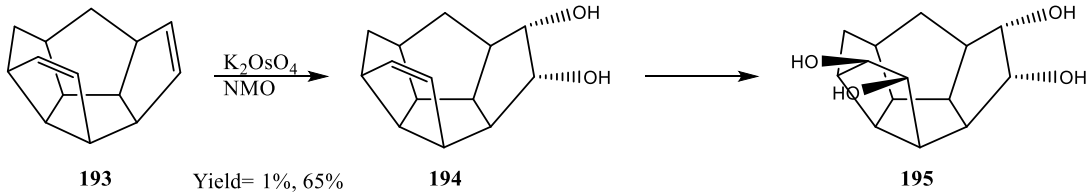

*Figure 103: Tetrol **195** was obtained by cis-dihydroxylation in the presence of NMO.*[81]

As an alternative to using OsO_4, water soluble salts such as potassium osmate (VI) (K_2OsO_4) can be used with secondary oxidizers to access hydroxylated cage systems. These salts are significantly less hazardous to handle as they are non-volatile, unlike crystalline OsO_4. Diene **193** was converted to diol **194** and tetrol **195** (*Figure 103, pg. 142*). The *cis*-dihydroxylation was performed with K_2OsO_4 (2 mol% in water) and NMO as the secondary oxidizer. Interestingly, the diol **194** was observed in only trace amounts (~1% yield) versus the tetrol (65% yield).[81] This is only slightly different from the synthesis of **192** where no diol was observed (*Figure 102, pg. 141).*[9]

While *cis*-dihydroxylation is a powerful tool for addition of oxygen functionality, it is not the only method for synthesizing hydroxylated cages. Hydroboration-oxidation has been used on a variety of cage systems to generate hydroxylated cages derived from monoene and diene cages.

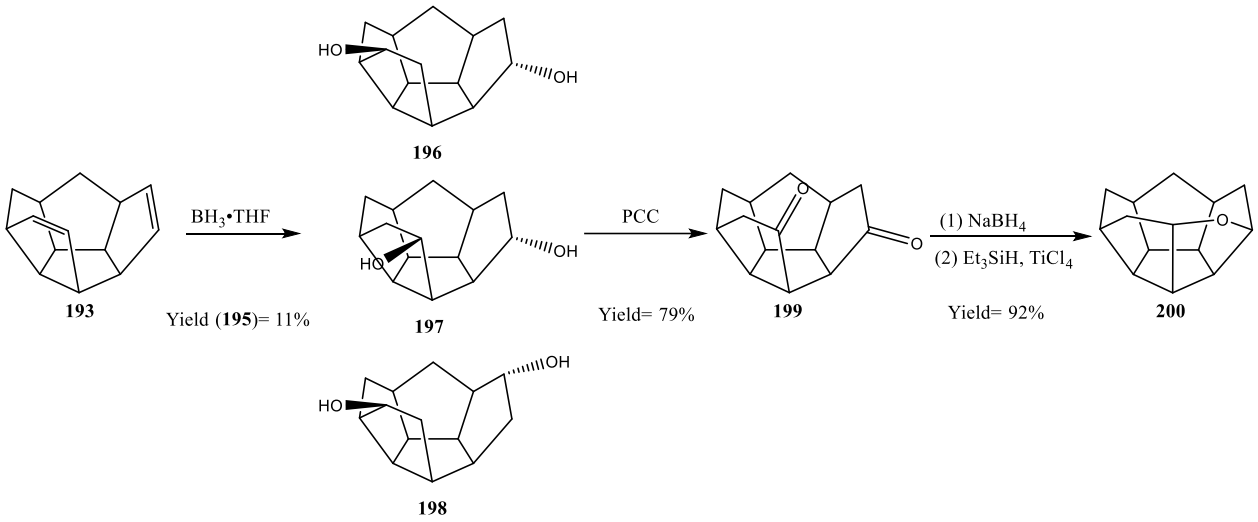

*Figure 104: The hydroboration-oxidation of **193** resulted in three isomers that were easily separated. Diol **197** was then subjected to further Jones oxidation to the dione **199**. Reduction and deoxygenation of **199** provided access to the mono-oxacage **200**.*[83]

Cage diene **193** was subjected to Brown hydroboration-oxidation to give the three different diol isomers **196**, **197**, and **198** (*Figure 104, pg. 143*). This reaction resulted in overall poor yield due to the three different possible products: 23%, 11%, and 12%, respectively. The diol **197** was then subjected to Jones oxidation to give the dione **199** in good yields (79% reported for oxidation of **196**). This dione could then be converted to an oxacage in two steps by reduction with sodium borohydride (85% yield) and deoxygenation with triethylsilane and titanium tetrachloride (92% yield).[83] The resulting oxacage **200** was an scaffold resembling the pentaoxa[5]peristylane **180** but with only one oxygen bridge(*Figure 97, pg. 138*; *Figure 104, pg. 143*).[73, 83]

While the oxacage **200** can be obtained through the hydroboration-oxidation of **193**, a shorter route *via* hydrobromination and reduction was also devised. The hydrobromination of **193** with NBS was used to target the bridged species **201**. However, **201** was not observed forming in this reaction and the bromo-cages **203**, **204**, and **206** were obtained (*Figure 105, pg. 144*).

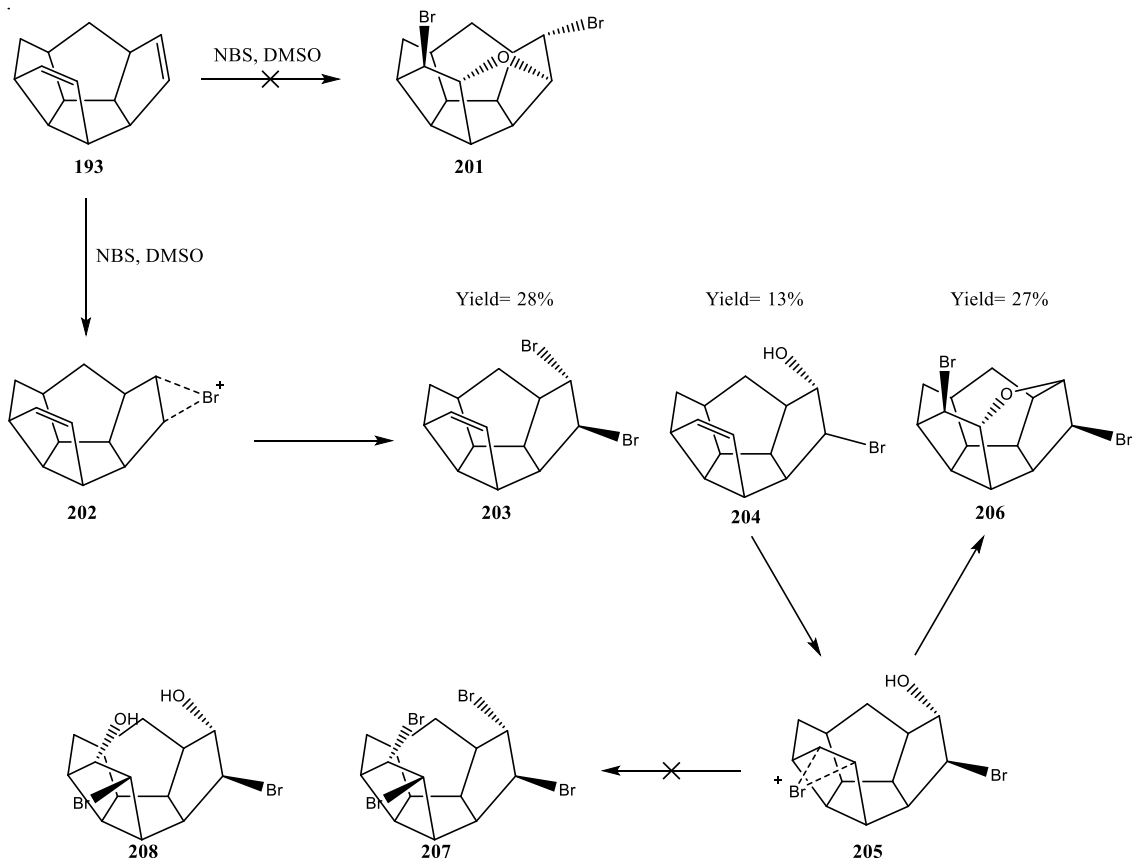

*Figure 105: Hydrobromination of **193** resulted in the bromo-cages **203**, **204** and **206**.*

Compounds **203** and **204** were derived from the bromonium ion **202**. Nucleophilic attack by water resulted in the bromohydrin **204** while attack by a bromide ion resulted in the dibromide **203**. The bridged system **206** was likely also derived from the bromohydrin **204** after a second bromonium ion **205** forms by hydrobromination of the remaining olefin. No trace of the tetrabromide **207** was reported nor the bis bromohydrin **208**.[83]

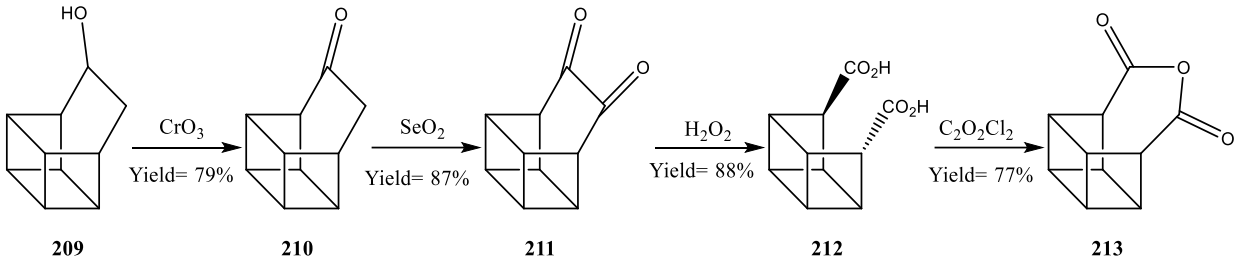

*Figure 106: Preparation of keto-cage **210** by Jones oxidation. Selenium dioxide (SeO_2) can then be used to obtain the dione **211**. Oxidation of **212** with oxalyl chloride ($C_2O_2Cl_2$) in the presence of pyridine yielded cage anhydride **213**.*

Diols are well known and often utilized as precursors to dione scaffolds, and a variety of different oxidation methods can be employed such as Jones (*Figure 104, pg. 143*) or Swern oxidation.[48, 83, 84] Jones oxidation has been used on cage compounds such as basketene derivative **209** to obtain keto-cages such as **210**. Swern oxidation has had only limited use in cage chemistry to obtain dione species. One reason that Swern oxidation may be preferable over Jones oxidation and chromium reagents is the typically lower yields observed in chromium-containing reactions due to adsorption of products on the reagent surface.

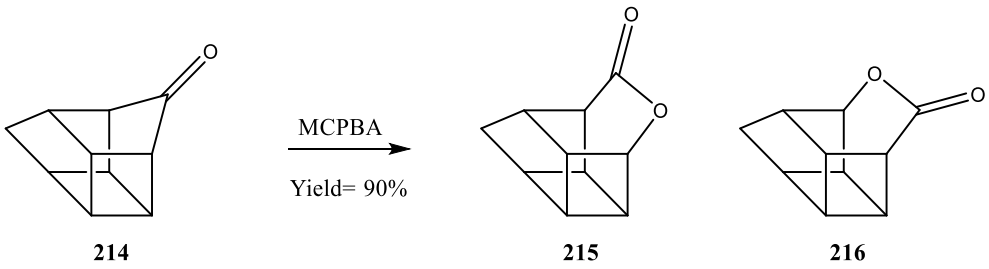

*Figure 107: The Baeyer-Villiger oxidation of the bishomocubanone **214** resulted in two lactones, the isomers **215** and **216**.*[85]

It has also been observed that keto-cage systems can be converted into the respective lactone cages *via* Baeyer-Villiger oxidation with MCPBA. The keto-cage **214** rapidly converts to

the lactones **215** and **216** (5:1 ratio by ^{1}H-NMR) when treated with MCPBA (*Figure 107, pg. 145*). The lactones can also be readily reduced to the lactols with LAH.[85, 86]

3.4.2 *cis*-Dihydroxylation of **1** & **24**

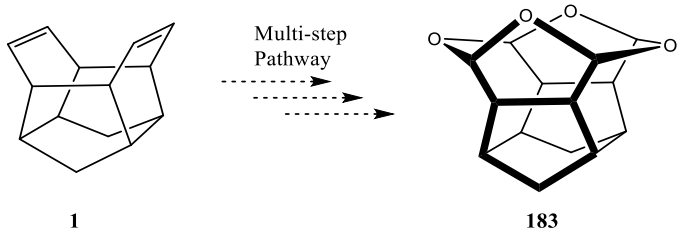

1 **183**

*Figure 108: In an attempt to circumvent the issues experienced with the ozonolysis of **1**, a multistep linear synthesis was devised. Some of the potential routes are detailed below.*

While attempting to prepare the oxacage **183** (*Figure 98, pg. 138*) we investigated several pathways to obtain the elusive molecule *via* a multistep synthetic pathway. The multistep pathway required the initial introduction of oxygen functionality. Several methods were explored to do so, including *cis*-dihydroxylation (*3.4.2 cis-Dihydroxylation of **1** & **24***), epoxidation (*3.3.3 Synthesis and Rearrangement of Epoxide Cages*), hydroboration, and hydrobromination (*3.4.6 Miscellaneous Attempts at Oxygen Introduction*). It was observed that *cis*-dihydroxylation and epoxidation were the most effective ways to introduce oxygen functionality, however, as mentioned above the epoxides proved to be more labile than expected resulting in rearrangement.

The diol **174** was synthesized *via* the *cis*-dihydroxylation of **1** under several different conditions (*Figure 109, pg. 147*), all of which resulted the same intermediate **217**. Reacting osmium tetroxide and a secondary oxidizer with **1** under various conditions led to mixtures of the osmate ester **217** and the diol **174**. Through either hydrolysis or reduction of the osmate ester the diol could be isolated in poor to moderate yield, depending on the method (*Table 14, pg. 148*).

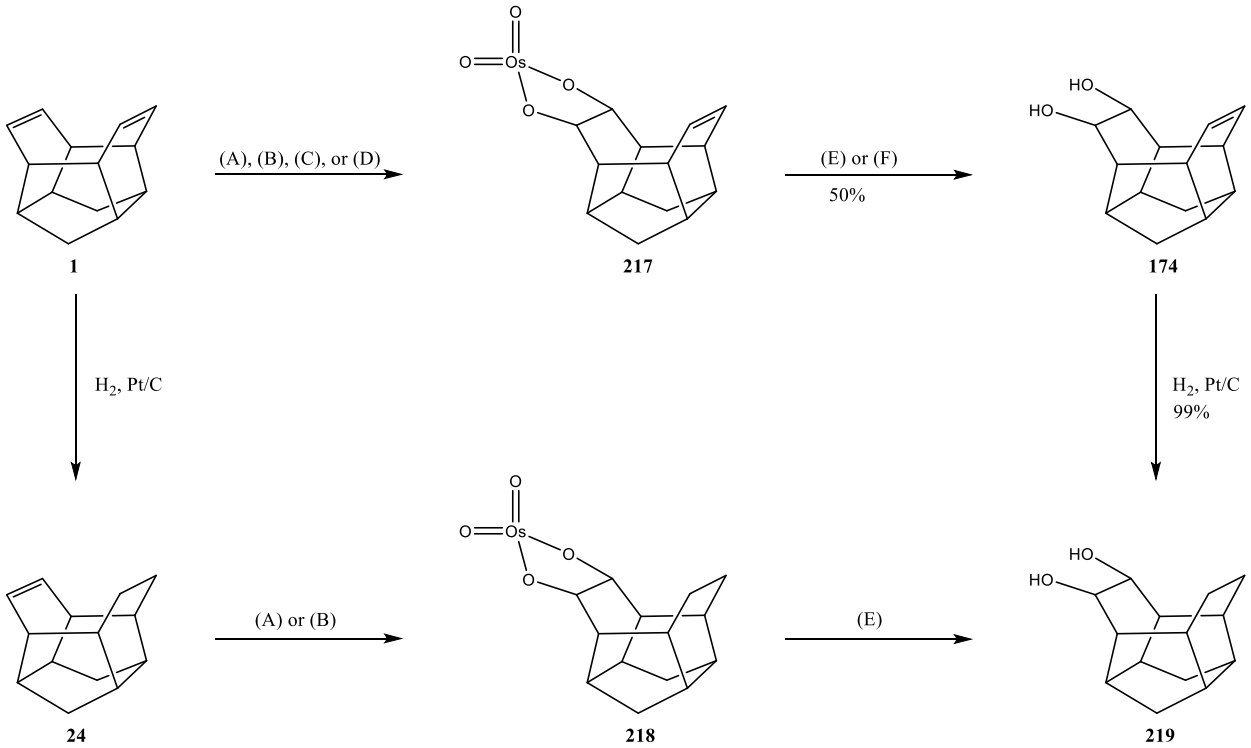

*Figure 109: The synthesis of **174** and **219** was carried out with a variety of protocols: (A) 2% OsO_4 solution, Me_3NO, AcOH, THF, Water;[82] (B) 2% OsO_4 solution, NMO, THF, Water;[78] (C) K_2OsO_4, NMO, acetone, water, ^tBuOH;[81] (D) OsO_4, benzene.[80] (E) K_2CO_3, sat. $NaHSO_3$; (F) LAH, THF.*

*Table 14: Table showing protocols and results of the different attempts at the synthesis of **174**. Product distributions based on ^{1}H-NMR data.*

Protocol	Work Up	Time (days)	Conversion	Product Distribution **1**:**217**:**174**	Isolated Yield of **174**
O-A	E	2	31%	3:1:0	0 %
O-B	E	7	75%	1:1:2	49 %
O-C	E	2	100%	0:1:0	0%
O-D	F	5	85%	2:10:1	50 %

The first protocol, Protocol **O-A**, did not result in any diol **174** in detectable amounts and only the osmate ester **217** was obtained. Diene **1** was dissolved in THF/water with trimethylamine N-oxide and acetic acid. To this a catalytic amount of 2% solution of OsO_4 in ^{t}BuOH was added and resulted in a green suspension after multiple days stirring. The hydrolysis with potassium carbonate and sodium bisulfite resulted in conversion to solely the osmate ester **217** (31%) isolated as a green crystalline material. When using stochiometric amounts of the OsO_4 solution minor conversion (<10%) to **174** was observed by ^{1}H-NMR using the same reaction time.

The second protocol, Protocol **O-B,** utilized similar reaction conditions (*i.e.*, catalytic amounts of OsO_4 solution) but eliminated the acetic acid and utilized NMO as the secondary oxidizer. Using the same molar equivalents as of secondary oxidizer as Protocol **O-A**, the reaction resulted in low conversion (>15%) to **174** and product could not be isolated. To optimize this reaction greater amounts of the secondary oxidizer, longer reaction time, and specific hydrolysis timing were used. When subjected to hydrolysis for extended periods of time decomposition of all

materials in the reaction were observed an no material could be recovered. Optimization of the hydrolysis gave significantly more conversion to diol **174**. Unreacted starting material **1** was removed from the crude reaction mixture by trituration with *n*-pentane. Subsequent trituration with chloroform was used to purify **174** separating the diol form osmate ester **217**. The diol **174** was observed to have limited solubility in chloroform while **217** completely dissolved. This allowed for simple separation of osmate easter **217** from diol **174**. Reactions using a stochiometric amount of OsO_4 and NMO resulted in similar ratios of product distribution (1:2 **217**/**174**) as catalytic reactions but with 90+% conversion of **1**.

The saturated diol **219** was target along protocol **O-B**, but product could not isolated. When reacting **24** (in a 4:1 mixture of **24** and **25**) with OsO_4 in the presence of NMO as the secondary oxidizer full conversion to the desired product was not observed (up to 50% conversion). The crude mixture contained unreacted monoene **24** and saturated cage **25** as well as the saturated osmate ester **218** and saturated diol **219** (**218**:**219** was approximately 1:1 based on ^{1}H-NMR). Efforts to separate **218** and **219** were unsuccessful as purification by trituration with chloroform was ineffective. The solubility of osmate ester **218** was more comparable to the diol **219** and both materials precipitated out of chloroform. This is contradictory to the solubility patterns of **217** and **174**. The saturated diol **219** was, however, readily available *via* the catalytic hydrogenation of **174** in nearly quantitative yield (99%) without the need for purification.

The third protocol, Protocol **O-C,** employed the use of the osmium salt K_2OsO_4 instead of OsO_4 solution. Utilizing the osmium salt and NMO in acetone/water/^{t}BuOH conversion was exceedingly slow. Only 10% conversion was observed after 48 hours and up to 15 days were needed till full conversion to **217** was observed. After work-up by vacuum distillation, no trace of product(s) was observed. A solid material with poor solubility was obtained but could not be

identified. Further work-up utilizing the hydrolysis optimized in Protocol **O-B** also did not yield any identifiable products.

Finally, we employed Protocol **O-D** resulting in the successful synthesis of **174**. This method did not utilize a secondary oxidizer and was carried out by adding approximately 1 equivalent of crystalline OsO_4 (exact amounts not recorded) to a solution of **1** in benzene. The reaction resulted in a green suspension after multiple days indicating that the OsO_4 was consumed. Thin-layer chromatography (TLC) was used to confirm full conversion of **1**. Removal of the benzene *via* pipette and vacuum distillation gave a green, powdery, solid. The solid was identified as a mixture of **1**, **217**, and trace amounts of **174** and trituration with *n*-pentane was used to remove unreacted starting material **1**. The resulting mixture of **217** and **174** was suspended in dry THF and treated with LAH. Reduction of the osmate ester to the diol resulted in better conversion to the desired product diol **174** and subsequently better isolated yields (50%) when the crude crystalline material was triturated with chloroform. Crystals of **174** grown from DCM/chloroform were colorless needles suitable for XRD but data still needs to be acquired.

When **1** was reacted with stochiometric amounts of OsO_4 following Protocol **O-D** neither the mono-osmate ester **217,** bis osmate ester **220**, diol **174**, nor the tetrol **221** were observed (*Figure 110, pg. 151*). A black flakey material was obtained after removal of the solvent and attempted LAH reduction resulted in a complex mixture of materials. None of these materials could be isolated or identified but are not presumed to be the tetrol based on current ^{1}H-NMR data. Further investigations are needed to synthesize the tetrol **221**.

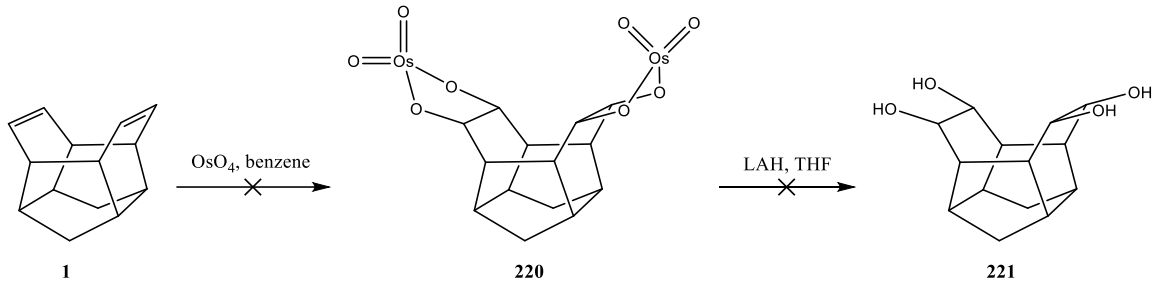

*Figure 110: The stochiometric reaction of **1** did not yield detectable amounts of the bis osmate ester **220**. No trace of the tetrol **221** could be identified after reduction.*

Care was required for the reduction with LAH as trace moisture in the THF caused H_2 gas evolution and reduction of the olefin of **174** giving the saturated diol **219**. It is possible that the osmium salts act as a metal catalyst for this hydrogenation reaction. Separation of the two diols **174** and **219** was challenging with only small amounts of **174** being separated.

The solubility phenomenon observed with osmate ester **217** versus diol **174** may be due to the acid content of the two solvents. Chloroform may contain trace amounts of HCl in significantly higher concentration versus DCM. This change in pH to may facilitate crystallization of **174** by protonation of an alcohol and providing a nucleation site for crystallization.

3.4.2.1 NMR Analysis of Osmate Ester **217**, Diol **174**, and Saturated Diol **219**

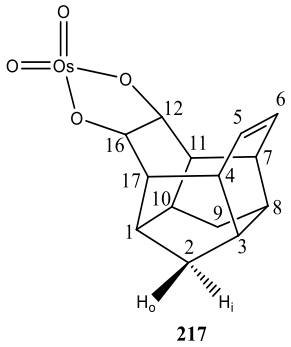

*Figure 111: Osmate ester **217**. Numbering is according to IUPAC conventions.*

The ^{1}H-NMR of osmate ester **217** displays seven signals, all with equivalent integration, consistent with the compounds C_s symmetry. In the olefinic region, a multiplet of higher order centered at 6.23 ppm was observed for protons H-5, -6. The protons at a chemical shift of 5.06 ppm, observed as an apparent singlet were assigned as H-12, -16. This chemical shift is outside the typical range of protons α to a C-O bond due to the osmate ester. The upper bridgehead protons H-11, -17 was observed as an apparent doublet at a chemical shift of 2.81 ppm and the other upper bridgehead positions, protons H-4, -7, were observed at slightly higher field. The H-4, -7 protons were observed as a broad multiplet of higher order centered at 2.77 ppm. The lower bridgehead positions H-3, -8 had a higher chemical shift, displayed at 2.34 ppm, when compared to the protons assigned to H-1, -10, displayed at 2.02 ppm; both lower bridgehead positions are displayed as apparent singlets. The signals associated with the methylene positions H-2 and H-9 were delineated as H-2_i, -9_i and H-2_o, -9_o due to the mirror plane of the compound. These signals are characteristic due to the large geminal coupling observed; $^{2}J_{\text{H-9i, -9o}} = {}^{2}J_{\text{H-2i, -2o}} = 11.7$ Hz. The signal associated with the interior methylene protons, H-2_i, -9_i, were observed at a higher chemical shift, 1.87 ppm, versus the outer position at 0.79 ppm. This is consistent considering the rigid structure of the cage and the effect of steric environments on chemical shift.

The ^{13}C-NMR of osmate ester **217** displayed seven signals, consistent with the C_s symmetry of the compound. The lowest field signal, observed in the olefinic region, was assigned as carbons C-5, -6 at a chemical shift of 134.1 ppm. At a chemical shift of 90.1 ppm, the carbons bound to the osmate ester, C-11, -17, were observed. This position has a significantly higher chemical shift due to the desheilding effects of the metal center. The most intense signals in the ^{13}C spectrum are observed at highest field and are associated with the methylene positions C-2, -

9. This higher intensity can be explained by the methylene carbons being secondary with a shorter relaxation time versus the tertiary bridgehead and oxygen-bound carbons, and the olefinic carbons.

All signals were unequivocally assigned using common 2-D heteronuclear correlation experiments. HMBC data clearly supports these assignments with H-5, -6 showing correlation to the C-4, -7 carbons. Protons H-11, -17 and H-3, -8 also displayed correlation to the C-4, -7 carbons. H-11, -17 show correlation to the C-12, -16 carbons. The methylene protons H-2, -9 showed correlation to both lower bridgehead positions C-1, -10 and C-3, -8. The HMQC supports these correlations allowing for clear assignments of protons to carbons utilized to interpret the HMBC. No COSY spectrum was obtained for this compound

The signals at 3.19 and 49.4 ppm in the ^{1}H-NMR and ^{13}C-NMR are unresolved impurities. These impurities did not carry over in subsequent reactions and do not appear in the NMR spectra of the diol **174**. The saturated osmate ester **216** could not be isolated from the saturated diol **219** as a clean material for characterization.

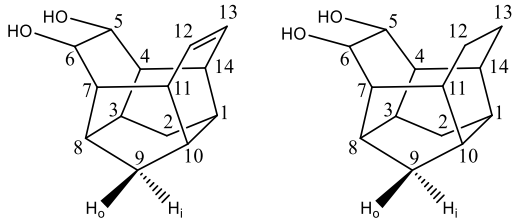

*Figure 112: Ene-diol **174** and saturated diol **219** with IUPAC numbering.*

The ^{1}H-NMR of diol **174** displays nine signals, all with equivalent integration, consistent with the compounds C_s symmetry. In the olefinic region, a multiplet of higher order centered at 6.14 ppm was observed for protons H-12, -13. The protons at a chemical shift of 3.83 ppm, observed as an apparent singlet were assigned as H-5, -6. This chemical shift is within the typical

range of protons α to a C-O bond. The upper bridgehead protons H-11, -14 were observed as a broad multiplet of higher order centered at 2.62 ppm and the other upper bridgehead positions, protons H-4, -7, were observed at slightly higher field. H-4, -7 was observed as an apparent doublet at a chemical shift of 2.46 ppm. These two positions can be distinguished as H-11, 14 displayed a slightly higher chemical shift due to the proximity to the olefin unit. The lower bridgehead positions H-3, -8 had a higher chemical shift, displayed at 2.38 ppm, when compared to the protons assigned to H-1, -10, displayed at 2.01 ppm; both lower bridgehead positions are displayed as apparent singlets. A broad singlet was observed at a chemical shift of 2.21 ppm, indicating the presence of exchangeable hydroxyl protons. The signal intensity was observed decreasing in the presence of D_2O, confirming that these protons were exchangeable. The signals associated with the methylene positions H-2 and H-9 were delineated as H-2_i, -9_i and H-2_o, -9_o due to the mirror plane of the compound. These signals are characteristic due to the large geminal coupling observed; $^2J_{\text{H-9i, -9o}} = {}^2J_{\text{H-2i, -2o}} = 11.7$ Hz. The signal associated with the interior methylene protons, H-2_i, -9_i, were observed at a higher chemical shift, 1.86 ppm, versus the outer position at 0.76 ppm. This is consistent considering the rigid structure of the cage and the effect of steric environments on chemical shift.

The ^{13}C-NMR of diol **174** displayed seven signals, consistent with the C_s symmetry of the compound. The lowest field signal observed in the olefin region is indicative of the carbons C-12, -13. At a chemical shift of 65.4 ppm, in the C-O-R (R= H, alk, ar) region, the carbons H-5, -6 were observed. The most intense signals in the ^{13}C spectrum are observed at highest field and are associated with the methylene positions C-2, -9. This higher intensity can be explained by the methylene carbons being secondary with a shorter relaxation time versus the tertiary bridgehead and hydroxyl-bound carbons, and the olefinic carbons.

All signals were unequivocally assigned using common 2-D homonuclear and heteronuclear correlation experiments. The COSY spectrum displayed clear correlations between the olefinic protons H-12, -13 and the bridgehead protons H-11, -14 with an intense crosspeak. H-12, -13 showed no other couplings within the scaffold. The protons H-11, -14 displayed a strong correlation to bridgehead H-4, -7 and H-1, -10. The dihedral angle between H-11, -14 and H-4, -7 is close to 0° and had the highest intensity crosspeak within the spectrum. The lower bridgehead H-1, -10 shows correlation to the outer methylene protons H-2_o, -9_o which can be easily identified due to the doublet signal structure mentioned above. The methylene protons H-2_o, -9_o can also be observed coupling to the lower bridgehead protons H-3, -8. Methylene protons H-2_o, -9_o and H-2_i, -9_i show the typical intense crosspeak expected of geminal protons, however, due to a dihedral angel of nearly 70° between the inner methylene protons H-2_i, -9_i and all four lower bridgehead positions little to no coupling was observed. The lower bridgehead protons H-3, -8 displayed a strong coupling to the upper bridgehead protons H-4, -7. The upper bridgehead protons H-4, -7 also display coupling with the low field singlet associated with the H-C-O protons, H-5, -6. Protons H-5, -6 show no other couplings. No coupling can be observed between the broad singlet associated with the hydroxy protons, implying separation.

HMQC data clearly supports these assignments with H-12, -13 showing correlation to the carbon signal in the olefinic region. Protons H-5, -6 displayed correlation to the carbon signal at 65.4 ppm. The methylene protons H-2, -9 showed correlation to the highest field signal consistent with the above-mentioned observations. In addition, correlations between respective bridgehead positions is clear allowing for unequivocal distinction.

The saturated diol **219** gives a nearly identical set of spectra. The major difference is the disappearance of the olefinic signal at 6.14 and the appearance of one ethano signal at 1.68 ppm

assigned to H-12, -13. The C-12, -13 signal at 134.0 ppm is also altered to the ethano carbons C-12, -13 at 19.1 ppm. Other signals show some slight changes in chemical shift but are not characteristic of the reduction of the olefin.

3.4.3 Attempted Periodate cleavage of **174**

The oxidative cleavage of **174** was attempted with sodium periodate but did not result in detectable formation of **101** (*Figure 113, pg. 156*). The reaction resulted in a crude mixture of multiple unidentified materials. ^{1}H-NMR data suggests some possible aldehyde compounds as well as some compounds with nonsymmetrical olefin signals.

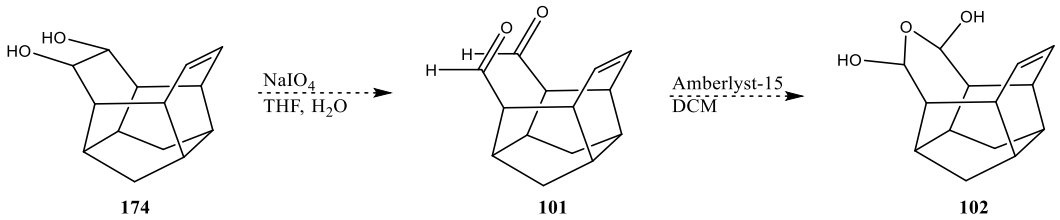

*Figure 113: Proposed pathway for the oxidative cleavage of **174** to the dialdehyde **101**. When treated with Amberlyst-15 **101** may undergo intramolecular ketal formation to the lactol **102.***

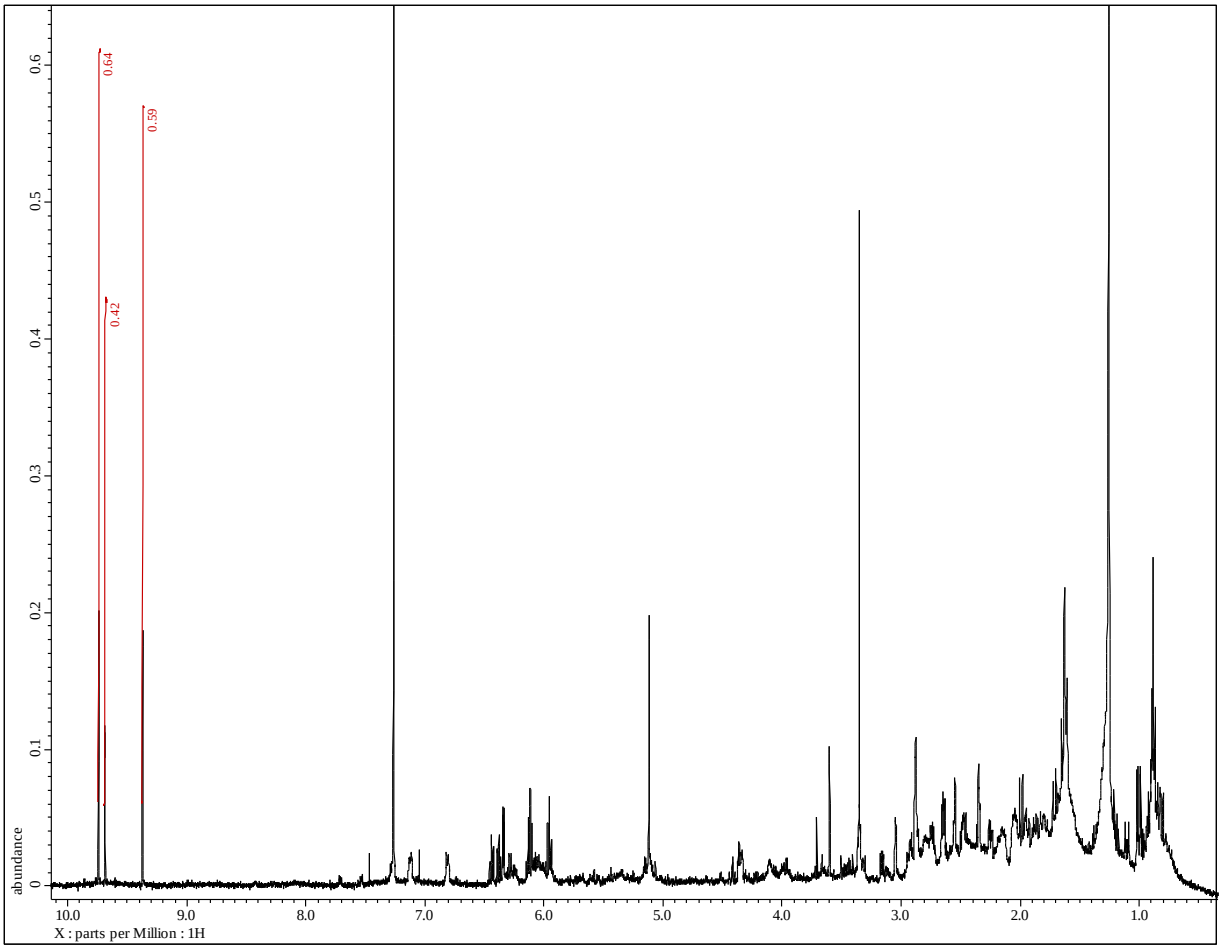

*Figure 114:[1]H-NMR of the crude material from the attempted oxidative cleavage of **174**.*

Analysis of the ^{1}H-NMR (*Figure 114, pg. 157*) shows no single major product with identifiable substructures. Three sharp signals at low field can be observed and may be related to an aldehyde product(s). The ^{13}C-NMR supports this as an intense carbonyl signal was observed. The crude mixture was treated with Amberlyst-15 in an attempt to propagate the formation of acetal **102**. While some unification of signals in the aliphatic region of the ^{1}H-NMR was observed no single product was identifiable. Interestingly, the potential aldehyde protons at lowest field were unaffected by Amberlyst-15. Further investigation into this reaction and the outcome is needed to determine the viability of this oxidative cleavage towards the oxacage **183** including isolation and

characterization of the obtained materials as well as repetition and optimization of reaction conditions.

3.4.4 Synthesis of Ene-Dione **222** and Saturated Dione **225** *via* Swern Oxidation

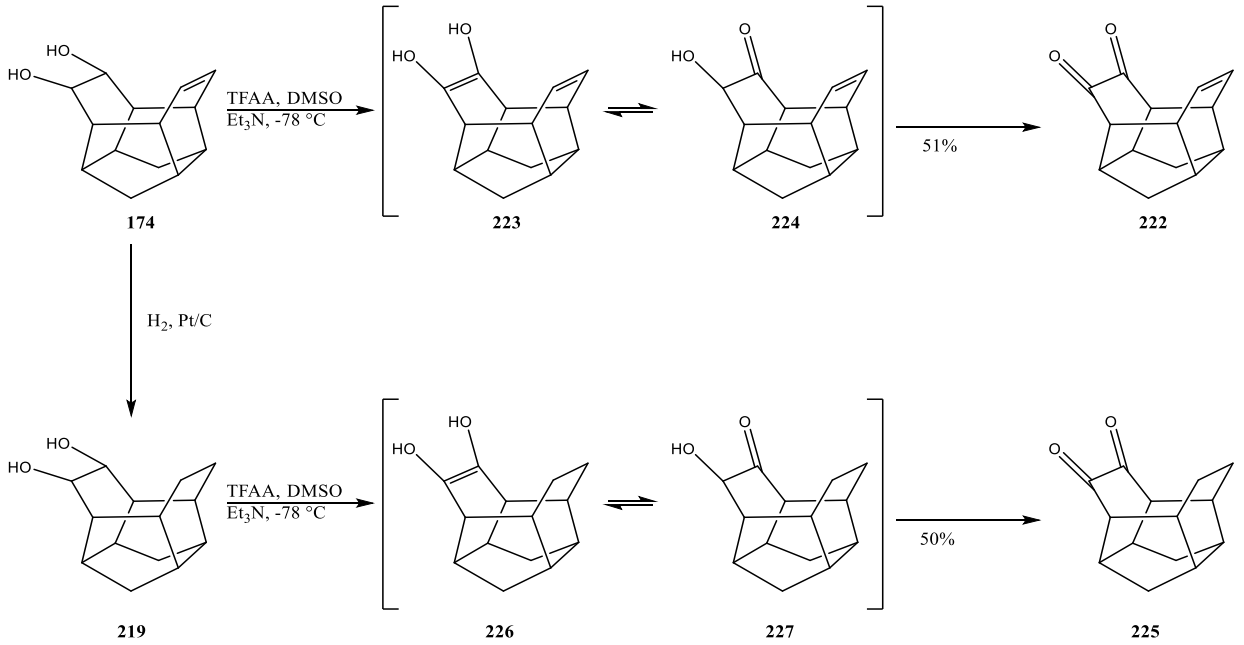

*Figure 115: Swern oxidation of **174** and **219** gave the diones **222** and **225**, respectively. The keto-enol tautomers of both species were also observed.*

While current approaches to **183** *via* oxidative cleave of **67** and **174** have yet to be successful, further oxidation of **174** may provide another avenue towards the tetraoxacage. Swern oxidation of diol **174** resulted in full conversion to a mixture of the diketone **222** and the keto-enol tautomers **223** and **224** (*Figure 115, pg. 158*). The dione and tautomers were separated by column chromatography (SiO_2, 5:1 hexanes/EtOAc). The dione **222** was isolated as a yellow crystalline solid in moderate yields (51%). This reaction was also observed to run to completion with excellent yield (100%) on smaller scale (16 mg). At larger scale (>100 mg) longer reaction times may eliminate partial oxidation products. The tautomers **223** and **224** could not be separated for

individual assignment, however, ^{1}H-NMR data of the crude material shows an approximate 1:1 ratio of the tautomers (*Figure 116, pg. 159*). This was determined using the olefinic signals at low field.

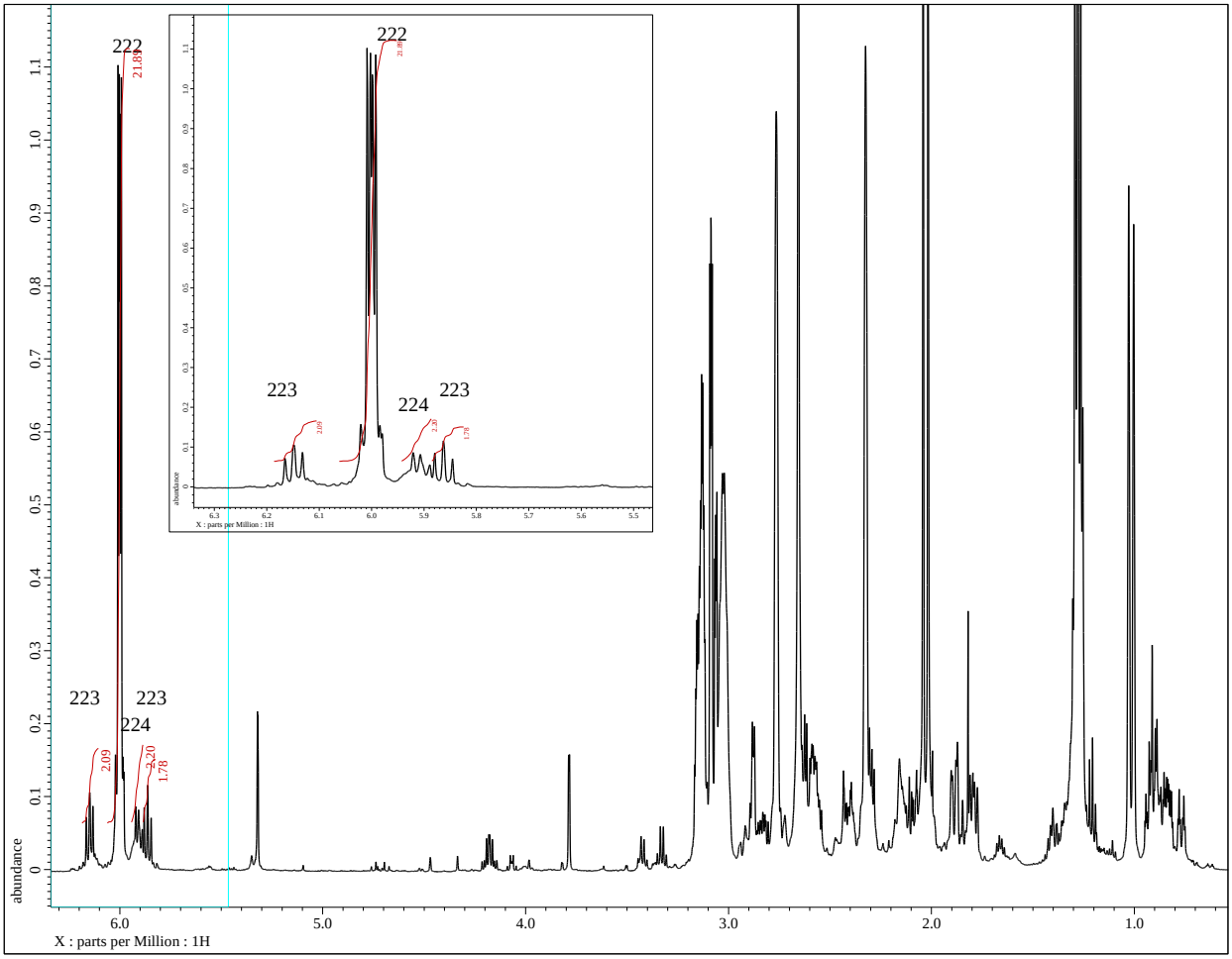

*Figure 116: ^{1}H-NMR of crude product mixture from the Swern oxidation of **174**. The two tautomers **223** and **224** are visible in an approximate 1:1 ratio.*

Swern oxidation of saturated diol **219** also resulted in full conversion to a mixture of the diketone **225** and the keto-enol tautomers **226** and **227** (*Figure 115, pg. 158*). Dione **225** was purified by column chromatography (SiO_2, 5:1 hexanes/EtOAc). The dione **225** was isolate as yellow crystalline solid in moderate yields (50%). The tautomers **226** and **227** could not be separated for

individual assignment. It is unknown which form of the tautomers **226** and **227** was as there was no defining signal observed in the crude ^{1}H-NMR or ^{13}C-NMR the distribution of the tautomers and the identity of the major tautomer could not be determined.

Neither dione **222** nor **225** showed the unusual solubility patterns observed of their precursors. The two diones were both soluble in chloroform and other common solvents.

3.4.5.1 NMR Analysis of Ene-Dione **222** and Saturated Dione **225**

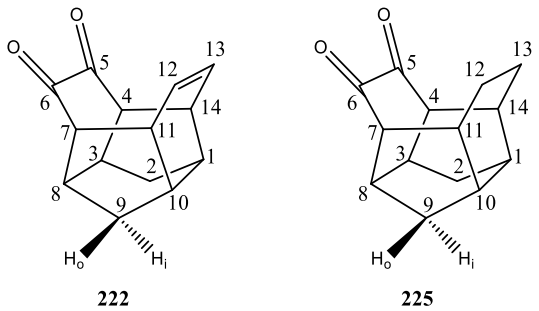

*Figure 117: Ene-dione **222** and saturated dione **225** with IUPAC numbering.*

The ^{1}H-NMR of dione **222** displays seven signals, all with equivalent integration, consistent with the compounds C_s symmetry. Two signals associated with the upper bridgehead positions H-4, -7 and H-11, -14 overlap but are not isochronic as clear assignments can be made using 2-D methods.

In the olefinic region, a multiplet of higher order centered at 6.24 ppm was observed for protons H-12, -13. The signal at a chemical shift of 3.14 ppm integrated to double the other signals due to the overlap of the upper bridgehead positions H-4, -7 and H-11, -14. The lower bridgehead positions H-3, -8 had a higher chemical shift, displayed at 2.79 ppm, when compared to the protons assigned to H-1, -10, displayed at 2.36 ppm; both lower bridgehead positions are displayed as

apparent singlets. The signals associated with the methylene positions H-2 and H-9 were delineated as H-2_i, -9_i and H-2_o, -9_o due to the mirror plane of the compound. These signals are characteristic due to the large geminal coupling observed; $^2J_{\text{H-9i, -9o}} = {}^2J_{\text{H-2i, -2o}} = 12.1$ Hz. The signal associated with the interior methylene protons, H-2_i, -9_i, were observed at a higher chemical shift, 2.05 ppm, versus the outer position at 1.04 ppm. This is consistent considering the rigid structure of the cage and the effect of steric environments on chemical shift.

The ^{13}C-NMR of dione **222** displayed seven signals, consistent with the C_s symmetry of the compound. The lowest field signal observed in the carbonyl region is indicative of the carbons C-5, -6. The chemical shift is also consistent with a ketone carbonyl, supporting the assigned structure. In the olefinic region at a chemical shift of 130.0 ppm the carbons H-12, -13 were observed. At a chemical shift of 56.6 ppm, the upper β-carbonyl bridgehead positions C-11, -15 were observed. This bridgehead positions has a significantly higher chemical shift that other bridgehead positions due to the desheilding effects of the carbonyl. The most intense signals in the ^{13}C spectrum are observed at highest field and are associated with the methylene positions C-2, -9. This higher intensity can be explained by the methylene carbons being secondary with a shorter relaxation time versus the tertiary bridgehead and hydroxyl-bound, and the olefinic carbons.

All signals were unequivocally assigned using common 2-D homonuclear and heteronuclear correlation experiments. The COSY spectrum displayed clear correlations between the assigned signals with all showing similar crosspeak intensity, except for the geminal coupling of the methylene positions. Clear coupling between the olefinic protons H-12, -13 and the bridgehead protons H-11, -14 was observed with H-12, -13 showing no other couplings within the scaffold. The protons H-11, -14 displayed coupling to bridgehead H-4, -7 and H-1, -10. The lower bridgehead H-1, -10 shows correlation to the outer methylene protons H-2_o, -9_o which can be easily

identified due to the doublet signal structure mentioned above. The methylene protons H-2_o, -9_o can also be observed coupling to the lower bridgehead protons H-3, -8. Methylene protons H-2_o, -9_o and H-2_i, -9_i show the typical intense crosspeak expected of geminal protons, however, due to a dihedral angel of nearly 70° between the inner methylene protons H-2_i, -9_i and all four lower bridgehead positions little to no coupling was observed. The lower bridgehead protons H-3, -8 displayed coupling to the upper bridgehead protons H-4, -7.

HMQC data clearly supports these assignments with H-12, -13 showing correlation to the carbon signal in the olefinic region. Protons H-4, -7 displayed correlation to the carbon signal at 56.6 ppm indicative of the β-carbonyl position. The methylene protons H-2, -9 showed correlation to the highest field signal consistent with the above-mentioned observations. Carbons C-5, -6 showed no correlation to a proton signal, supporting the observation of a carbonyl signal.

The saturated dione **225** gives a nearly identical set of spectra. The major difference is the disappearance of the olefin H-12, -13 signal at 6.24 and the appearance of two ethano signals at 1.83 and 1.48 ppm. The C-12, -13 signal at 130.1 ppm is also altered to the ethano carbons C-12, -13 at 18.9 ppm. Other signals show some slight changes in chemical shift but are not characteristic of the of the differences between **222** and **225** such as the difference in chemical shift of the carbonyl carbons at 198.0 and 200.4 ppm, respectively.

3.4.5 Synthesis of Ene-Anhydride **228** and Saturated Anhydride **229** *via* Baeyer-Villiger Oxidation

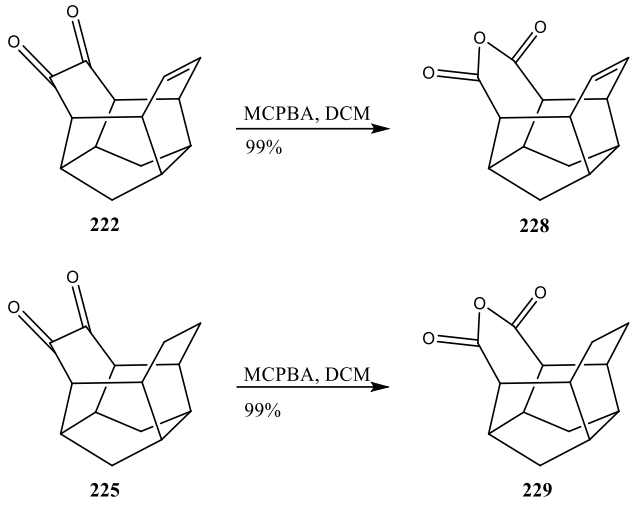

*Figure 118: The anhydrides **228** and **229** were obtained via the Baeyer-Villiger oxidation of the respective diones **222** and **225**. Both were obtained in excellent yields.*

The two diones **222** and **225** were both subjected Baeyer-Villiger oxidation with MCPBA in DCM (*Figure 118, pg. 163*). Dione **222** was fully converted to the corresponding anhydride **228** with 1.1 equivalents of MCPBA. The anhydride was isolated in excellent yields (99%) and no further purification was needed. The anhydride shared the same yellow coloration as the dione. Interestingly, no epoxidation was observed in this reaction. The saturated analog of **228** was prepared form the dione **225** under similar conditions. Dione **225** was converted to anhydride **229** with 1.5 equivalents of MCPBA. The product was isolated as a yellow crystalline solid by column chromatography (SiO_2, 5:1 hexanes/EtOAc) in excellent yield (99%).

3.4.6.1 NMR Analysis of Ene-Anhydride **228** and Saturated Anhydride **229**

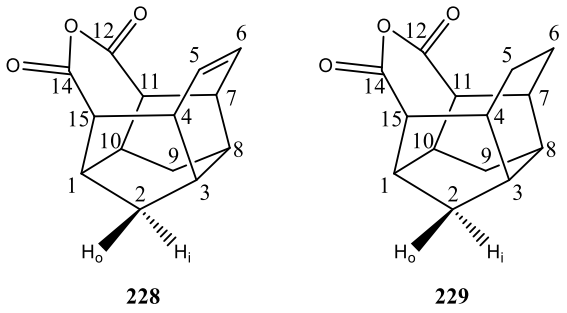

*Figure 119: Ene-anhydride **228** and saturated anhydride **229** with IUPAC numbering.*

The ^{1}H-NMR of anhydride **228** displays seven signals, all with equivalent integration, consistent with the compounds C_s symmetry. In the olefinic region, a multiplet of higher order centered at 6.23 ppm was observed for protons H-5, -6. The H-11,-15 signal at a chemical shift of 3.58 ppm was observed as a doublet of triplets and is in the range expected of β-carbonyl protons. The other pair of upper bridgehead protons, H-4, -7, were observed as a multiplet of higher order at a chemical shift of 3.23 ppm, consistent with allylic protons observed in other cage scaffolds discussed. The lower bridgehead positions H-1, -10 had a higher chemical shift, displayed at 2.81 ppm, when compared to the protons assigned to H-3, -8, displayed at 2.35 ppm due to the inductive effects of the anhydride moiety; both signals appeared as apparent singlets. The signals associated with the methylene positions H-2 and H-9 were delineated as H-2_i, -9_i and H-2_o, -9_o due to the mirror plane of the compound. These signals are characteristic due to the large geminal coupling observed; $^{2}J_{\text{H-9i, -9o}} = {}^{2}J_{\text{H-2i, -2o}} = 12.3$ Hz. The signal associated with the interior methylene protons, H-2_i, -9_i, were observed at a higher chemical shift, 2.01 ppm, versus the outer position at 0.93 ppm. This is consistent considering the rigid structure of the cage and the effect of steric environments on chemical shift.

The ^{13}C-NMR of dione **222** displayed seven signals, consistent with the C_s symmetry of the compound. The lowest field signal observed in the carbonyl region is indicative of the carbons C-12, -14. The chemical shift is also consistent with a carboxylic acid carbonyl at 167.9 ppm, supporting the assigned structure. In the olefinic region at a chemical shift of 131.9 ppm the carbons C-5, -6 were observed. At a chemical shift of 57.3 ppm, the upper β-carbonyl bridgehead positions C-11, -15 were observed. This bridgehead positions has a significantly higher chemical shift that other bridgehead positions due to the desheilding effects of the carbonyl. The most intense signals in the ^{13}C spectrum are observed at highest field and are associated with the methylene positions C-2, -9. This higher intensity can be explained by the methylene carbons being secondary with a shorter relaxation time versus the tertiary bridgehead and hydroxyl-bound, and the olefinic carbons.

All signals were unequivocally assigned using common 2-D homonuclear and heteronuclear correlation experiments. The COSY spectrum displayed clear coupling between the olefinic protons H-5, -6 and the bridgehead protons H-4, -7 was observed with H-5, -6 showing no other couplings within the scaffold. The protons H-4, -7 displayed strong coupling to upper bridgeheads H-11, -15 with an intense crosspeak. Protons H-4, -7 also show coupling to lower bridgeheads H-3, -8, but is not as strong of a correlation. The lower bridgehead H-3, -8 shows coupling to the outer methylene protons H-2_o, -9_o which can be easily identified due to the doublet signal structure mentioned above. The methylene protons H-2_o, -9_o can also be observed coupling to the lower bridgehead protons H-1, -10. Methylene protons H-2_o, -9_o and H-2_i, -9_i show the typical intense crosspeak expected of geminal protons, however, due to a dihedral angel of nearly 70° between the inner methylene protons H-2_i, -9_i and all four lower bridgehead positions little to no coupling was observed.

HMQC data clearly supports these assignments with H-5, -6 showing correlation to the carbon signal in the olefinic region. Protons H-11, -15 displayed correlation to the carbon signal at 57.3 ppm. The methylene protons H-2, -9 showed correlation to the highest field signal consistent with the above-mentioned observations. Carbons C-12, -14 showed no correlation to a proton signal, supporting the observation of a carbonyl signal.

The saturated dione **229** gives a nearly identical set of spectra. The major difference is the disappearance of the olefin H-5, -6 signal at 6.23 and the appearance of two ethano signals at 1.82 and 1.76 ppm. The C-5, -6 signal at 131.9 ppm is also altered to the ethano carbons C-5, -6 at 18.5 ppm. Other signals show some slight changes in chemical shift but are not characteristic of the differences between **228** and **229**.

3.4.6 Miscellaneous Attempts at Oxygen Introduction

Two other methods were investigated in attempts to introduce oxygen functionality. Hydroboration-oxidation and bromohydrin chemistry have been shown to be effective ways at introducing hydroxyl functional groups into cage scaffolds.[48, 83] When executed on our frameworks (diene **1** and monoene **24**) we obtained complex mixtures and no distinct products could be isolated, however, analytical data of these reactions show promising results that require further investigation.

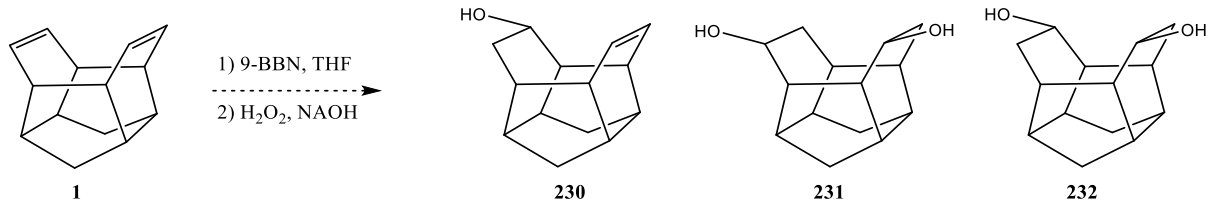

*Figure 120: Hydroboration of **1** did not result in identifiable alcohol **230** nor diols **231** or **232**. Despite this, some functionalization (likely hydroxylation) was observed.*

The hydroboration of **1** was attempted with 9-Borabicyclo[3.3.1]nonane (9-BBN) (*Figure 120, pg. 166*). 9-BBN was selected as it is a single borane equivalent and would potentially decrease the risk of borane-cage-borane polymer formation. The crude material obtained from this reaction was then subjected to oxidation along the standard protocol of hydrogen peroxide under basic conditions. While some reaction certainly occurred based on ^{1}H-NMR data (approximately 50% conversion), the hydroxylated cages **230** and/or **231**/**232** could not be identified from the mixture. Multiple olefinic signals were observed in the ^{1}H-NMR (*Figure 121, pg. 167*), implying that some mono functionalization occurred, possibly through multiple pathways.

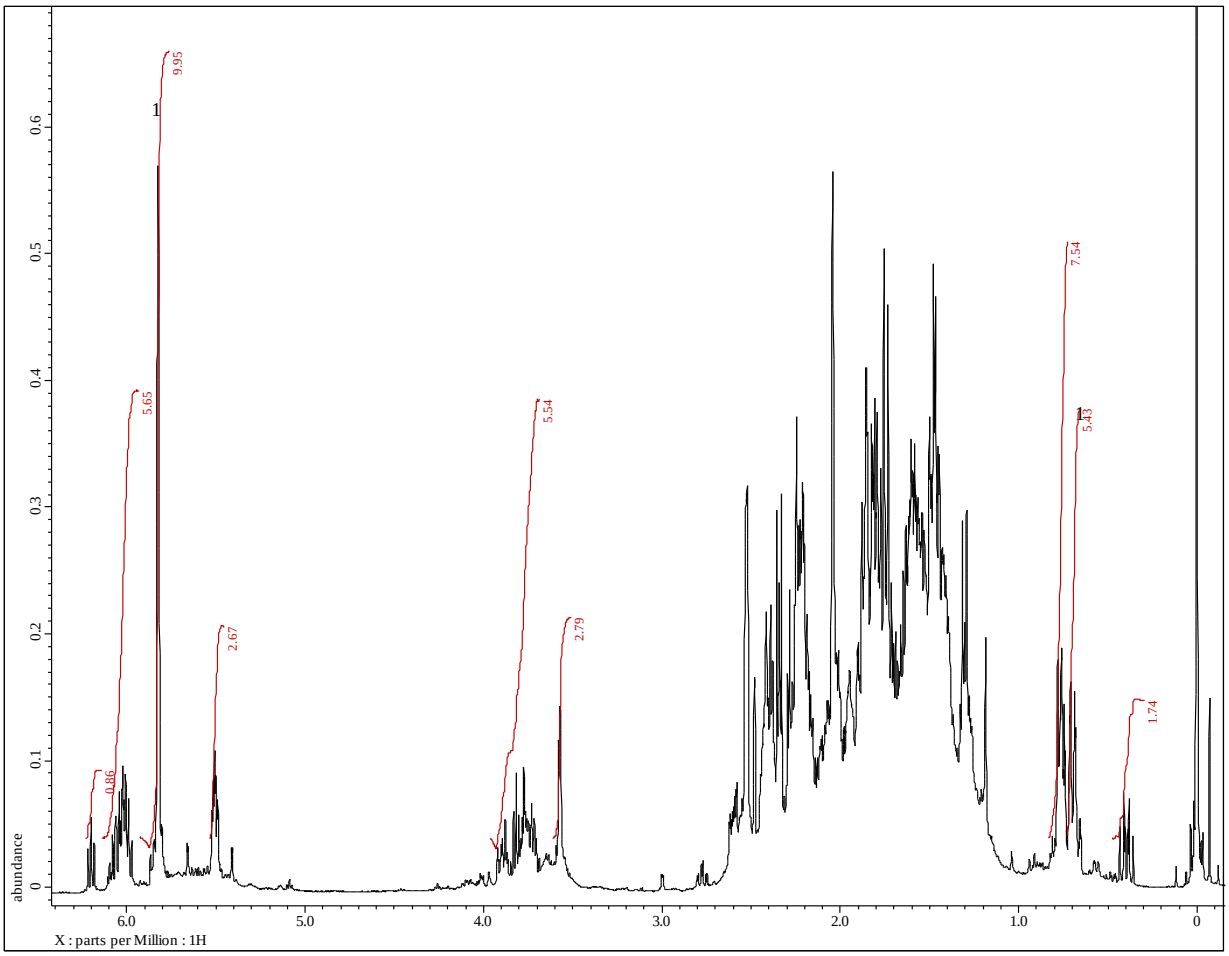

*Figure 121: ^{1}H-NMR of the hydroboration-oxidation of **1**.*

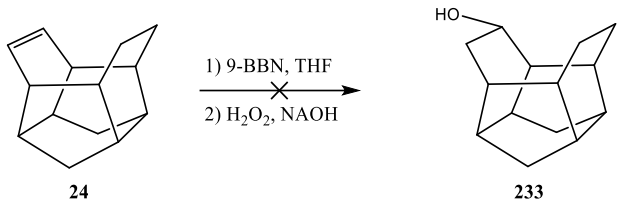

*Figure 122: : Hydroboration of **24** did not result in detectable amounts of the mono alcohol **233**.*

This same reaction was performed on the monoene **24** (*Figure 122, pg. 168*) and gave similar results with approximately 70% conversion of **24**. No identifiable formation of **233** was observed. ^{1}H-NMR shows multiple products (*Figure 123, pg. 169*), and this was also observed in TLC of the mixture (six spots observed). Purification by column chromatography (SiO_2, 3:1 hexanes/EtOAc) was ineffective as separating the products observed. Several low field signals can be observed that do not show a recognizable signal structure implying a loss of symmetry and the potential for multiple functionalization pathways

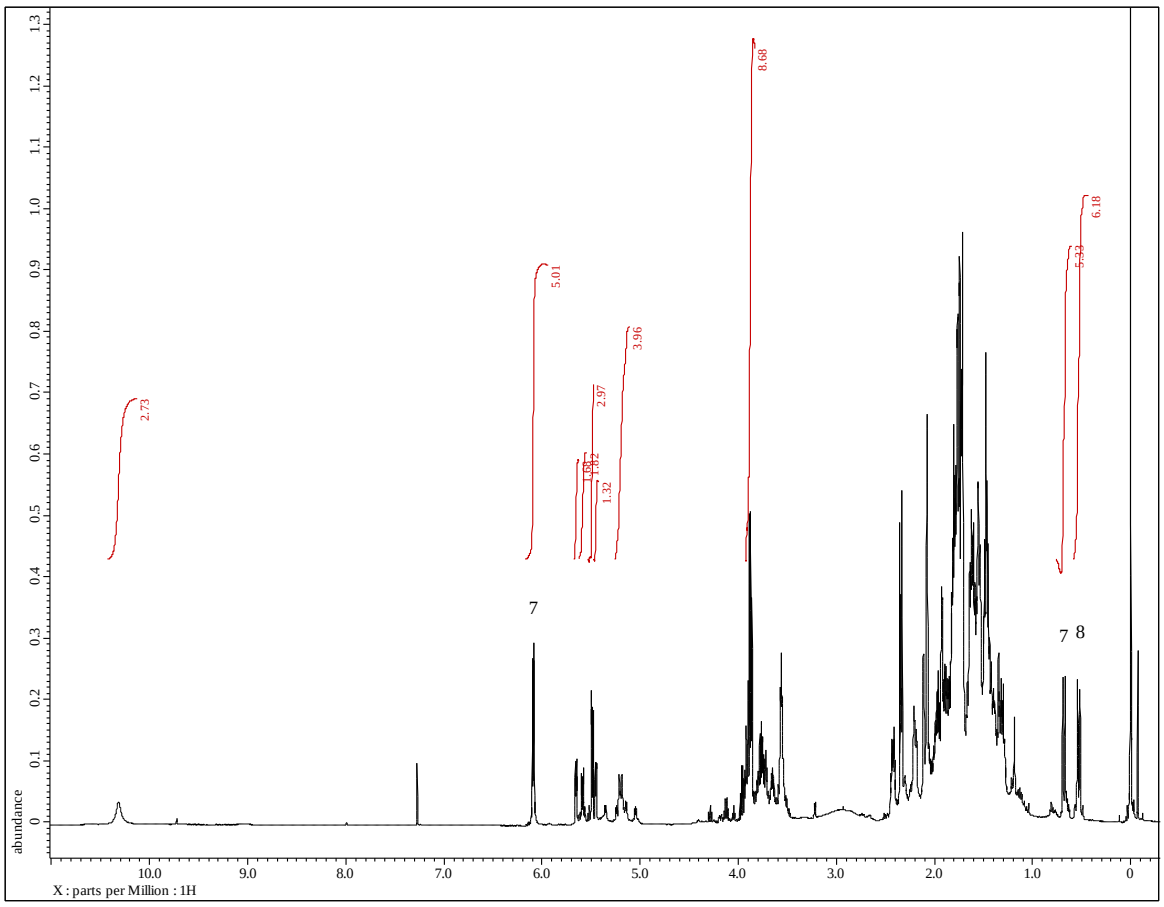

*Figure 123: ^{1}H-NMR of the hydroboration-oxidation of **24**.*

The hydrobromination of **1** with NBS in DMSO was attempted to access the bromohydrins **234** or **235** (*Figure 124, pg. 169*). This reaction gave a mixture of at least eight compounds based on GC/MS and NMR data. TLC of the crude mixture showed five spots of varying R_f value.

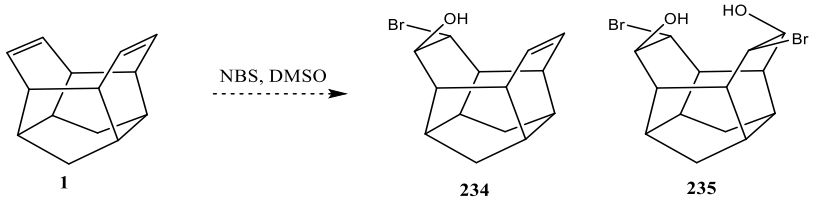

*Figure 124: Attempted hydrobromination to obtain the mono- and bis-bromohydrins **234** and **235**.*

Of the eight compounds observed by GC/MS, none could be isolated in sufficient purity by column chromatography (SiO_2, 5:1 hexanes/EtOAc) for full characterization.

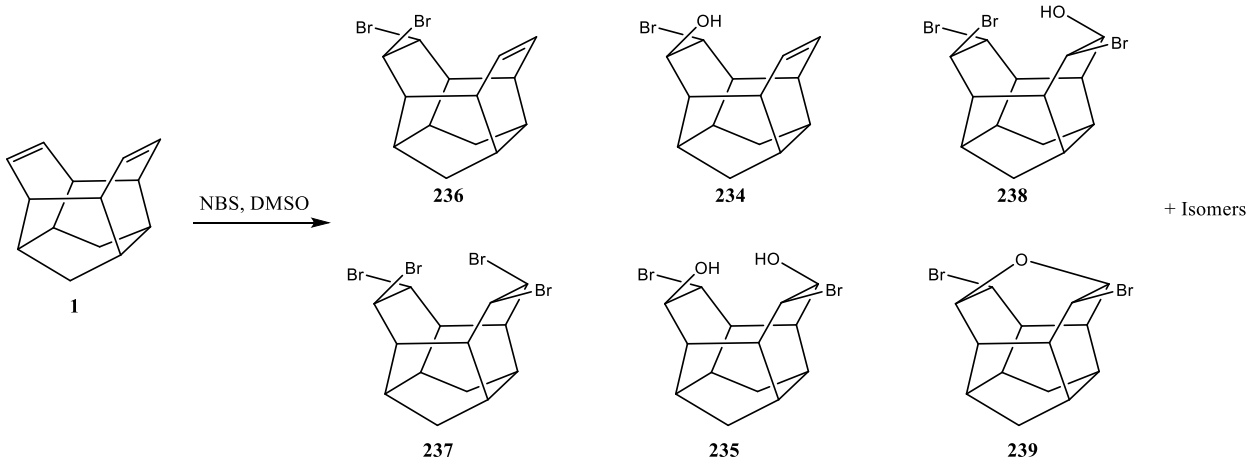

*Figure 125: Possible products obtained from the hydrobromination of **1**.*

Based on GC/MS and NMR data some of the possible compounds in the product mixture may include the dibromocage **236**, the tetrabromocage **237**, the mono- and bis-bromohydrins **234** and **235**, the tribromhydroxyocage **238**, and possible bridged systems like **239**. Isomers of all of these compounds may also exist, making an even more complex analysis of any compounds obtained (*Figure 125, pg. 170*).

4 CONCLUSIONS

4.1 Carbene Chemistry of Cage Compounds

The carbene addition reactions of diene **1**, monoene **24**, and saturated cage **25** granted some insight into the reactivity patterns of carbenes in cage systems. It was observed that in highly strained cage systems such as hydrocarbon **15** may result in ring-expansion reactions (*Figure 14, pg. 16*).[24] In the reactions of **1** and its derivatives no ring-expansion was observed. Multiple potential C-H carbene insertion products derived from **1**, **24**, and **25** were identified but not characterized. These carbene insertion adducts display the potential to exploit C-H bond activation in cage systems for different functionalization such the hydroxylation of hydrocarbon **25** (*Figure 61, pg. 84*). C-H bond activation is a valuable tool for building larger scaffold; adamantly groups have found application as bulky spacers in material science (*e.g.*, adamantly spacers in polymers and in carbon nanotubes).[87, 88] Select carbene adducts were also analyzed by XRD; it was observed that the presence and identity of halogen substituent greatly impacted interactions with the unit cell as well as the crystal packing. Conversely, the effects of the functionalization on the individual molecules was negligible and only minor variations in bond lengths, angles, and transannular distances were observed.

Future work on this chemistry will focus on obtaining missing crystallographic data, full characterization of the various insertion products, and preparing other mixed carbene adducts to improve the library of known compounds we established herein. We also would like to explore the reactivity patterns of other carbene equivalents and their potential impact on the scaffold. Examples of this may include variation of the PTC to target C-H insertion, observe rates of addition versus insertion using more reactive carbene equivalents, and using diazo compounds introduce other functional groups to the scaffold.

4.2 Preparation of Cage Hydrocarbons and Oxacages *Via* Rearrangement of Cage Scaffolds

The rearrangements of diene **1** and its epoxide derivatives **94**, **95**, and **96** were investigated utilizing the sulfonic acid catalyst, Amberlyst-15. These Brønsted acid catalyzed rearrangements lead to a variety of unique hydrocarbon and oxacage scaffolds, including oxacage **100**, a potential precursor to the elusive norpentaasterane **122** (*Figure 71, pg. 99*). The rearrangement of diene **1** resulted in the hydrocarbons **92** and **93**.

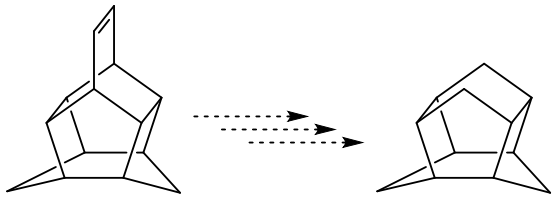

*Figure 126: Hydrocarbon **93** may provide access to hydrocarbon **240** by oxidative cleavage followed by decarbonylation.*

Hydrocarbon **93** poses a unique substructure that could provide access to elusive compounds like hydrocarbon **240**, a highly strained alicyclic cage containing no small rings (*Figure 126, pg. 172*).[89] This scaffold may be accessed *via* the oxidative cleavage and subsequent decarbonylation of **93**.

Investigations into the ether cleavage of **100** were also carried out and a series of conditions were screened, however, have yet to deliver norpentaasterane **122**. This endeavor did result in the isolation of two unusual cage compounds, diiodo-cage **149** and hydrocarbon **151**. Hydrocarbon **151** is proposed to form through a radical pathway from **149**. In addition, the mechanisms for some of the rearrangements was proposed including mechanism **R-1** which was found to be identical in the cases of epoxides **94**, **95**, and **96** as the first step in each rearrangement (*Figure 67, pg. 91*).

Future work includes the isolation and full characterization of the suspected oxetane intermediate **154**, investigations into the rearrangement of the cyclopropane-epoxide **98**, XRD analysis of all obtained rearrangement products, and identification of conditions to obtain the norpentaasterane **122** from oxacage **100**.

4.3 Multistep Synthetic Approach Towards the Preparation of a Novel Tetraoxacage

In the work described herein, we were able to prepare a series of oxygen-functionalized species using selected oxidative transformations on diene **1** and monoene **24**. These derivatives provide the foundation for a multi-step synthesis of tetraoxacage **183**. While many of the reactions investigated require further work to fully understand the viability of the chemistry employed the current progress has allowed for a diversification of approaches.

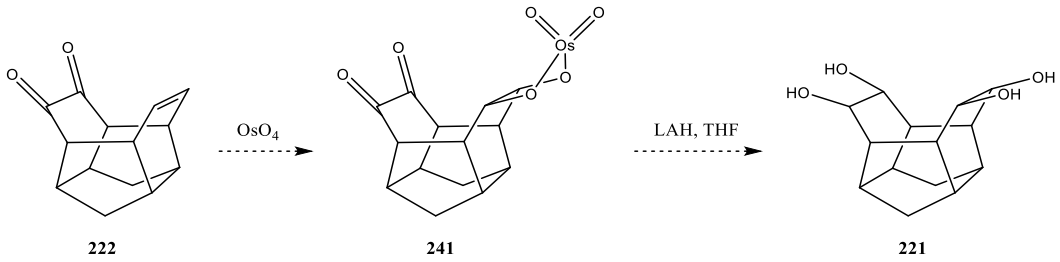

*Figure 127: Proposed alternative route to tetrol **221**.*

As the preparation of tetrol **221** was unsuccessful under the conditions investigated, other pathways must be explored to obtain this unique and interesting scaffold. Two-fold alkene functionalization of **1** seems to be quite challenging. As such, future attempts at synthesizing **183** will utilize asynchronous transformations to obtain the desired materials. For instance, *cis*-dihydroxylation of the dione **222** may provide access to the osmate ester **241**. Reduction of this species would then presumably yield the tetrol **221** (*Figure 127, pg. 173*).

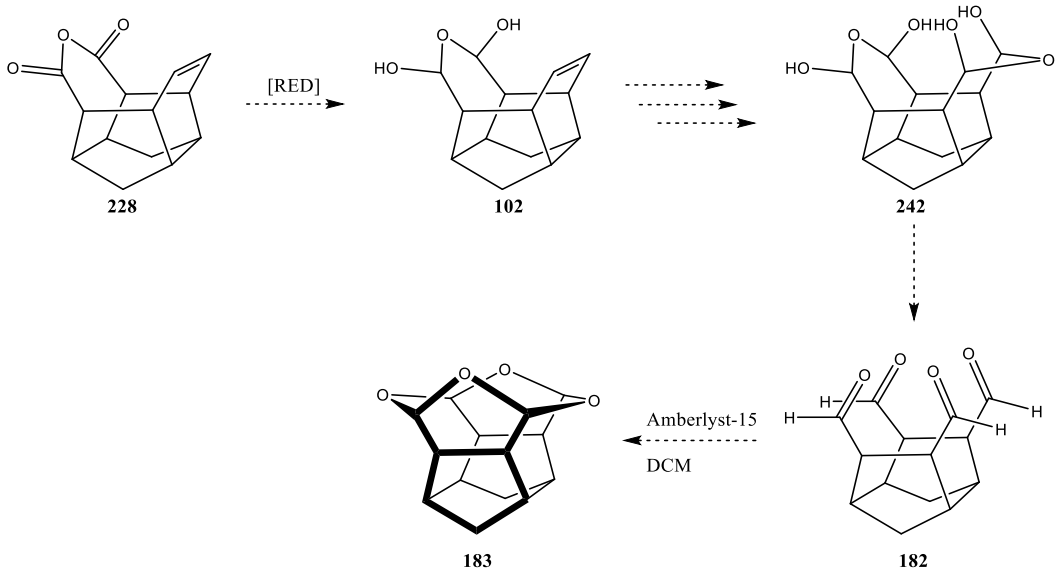

*Figure 128: Proposed alternative route to oxacage **183**.*

An alternative path to this may be the reduction of anhydride **228** (*Figure 128, pg. 174*). This would provide vital evidence for the proposed step-wise approach to **183** as it is equivalent to a seven-membered ring acetal (*Figure 128, pg. 174*). Repeated functionalization of the remaining olefin may provide access to the bis acetal **242**. Subsequent opening of the acetals and resubjecting to acidic conditions may lead to **183**.

In conclusion, the syntheses of diol **174**, dione **222**, and anhydride **228** represent significant milestones towards the eventual preparation of the proposed tetraoxacage **183**.

5 EXPERIMENTAL

5.1 General Comments

5.1.1 Nuclear Magnetic Resonance

^{1}H NMR 300 MHz JOEL ECX-300

500 MHz Joel As500

^{13}C NMR 300 MHz JOEL ECX-300

500 MHz Joel As500

^{19}F NMR 300 MHz JOEL ECX-300

500 MHz Joel As500

All spectra were recorded at 298 K unless otherwise specified. Delta NMR software v. 5.3.3 was used for data analysis. Chemical shifts in chloroform-*d* are reported in ppm, assigning tetramethylsilane (Acros Organics, NMR grade, 99.9% purity), [δ(TMS) = 0.00 ppm] as 1H and 13C reference and trichlorofluoromethane [δ($CFCl_3$) = 0.00 ppm] as 19F reference. Chemical shifts in other solvents are reported in ppm, assigning the respective solvent peak as 1H and 13C reference. Signal assignments were made based on homo- and heteronuclear 2D NMR experiments and on comparison with analogous compounds when applicable. Chemical shifts denoted with * were not conclusively assigned. The signal structure is indicated with the usual abbreviations for singlet (s), doublet (d), etc., and multiplets are quoted over the entire signal range. If a multiplet has an apparent singlet or doublet structure it is quoted as s_{app} or d_{app}, respectively.

5.1.2 Infrared Spectroscopy

AT-IR spectra were collected on a PerkinElmer SpectrumOne FT-IR Spectrometer with Spectrum software version 5.0.2.

5.1.3 Mass Spectroscopy

GC/MS measurements were taken using an Agilent Technologies 6850 Network GC System with Agilent MSD Chemstation and GC/MS Data Analysis Software.

5.1.4 X-ray Crystallographic Analysis

X-ray diffraction data were collected using a Bruker SMART APEX II diffractometer equipped with an APEX II 4 K charge-coupled device (CCD) area detector (by use of the program APEX)207 and a sealed-tube X-ray source (graphite-monochromated Mo-Kα radiation, λ = 0.71073 Å). A complete sphere of data was collected to better than 0.8 Å resolution. Processing was carried out by using the program SAINT,208 which applied Lorentz and polarization corrections to three-dimensionally integrated diffraction spots. The program, SADABS,209 was used for the scaling of diffraction data, the application of decay correction based on redundant reflections. All calculations were made using the SHELXTL Plus package210 for structure determination, refinement, and molecular graphics. Unit cell dimensions and crystal lattice are confirmed using the XPREP210 101 program. Unit cells, distance and angle measurements were found using Mercury 2020.3.0 software. A solution was obtained using direct methods. Successive difference Fourier syntheses revealed all atoms. The final refinement was obtained by introducing a weighting factor and anisotropic thermal parameters for all non-hydrogen atoms.

5.1.5 Chemicals and Materials

All chemicals were purchased commercially and used as received unless otherwise specified. For column chromatography silica gel was purchased from Silicycle Chemical Division. The

Amberlyst-15 (ACROS LOT# A0207724001) has a catalyst loading of 4.95 eq/kg (equivalent to 4.95 mol/kg).

5.2 Preparation of Monoene and Fully Saturated Cage

5.2.1 Preparation of Monoene and Fully Saturated Cage Mixture

*Hydrogenation of Diene **1**:* H_2 gas (approximately 3-4 balloons) was bubbled through a suspension of diene **1** (500 mg, 2.717 mmol) and Pt/C 5% in EtOAc (20 mL). The reaction was monitored by GC/MS until approximately 75% conversion was observed or relative concentration monoene **24** was at least 50%. The suspension was then filtered over a pad of silca gel using EtOAc as the eluting solvent and concentrated to afford a colorless crystalline solid (503 mg) containing **1** (25%), **24** (50%), and **25** (25%). The mixture was then subject to repeated column chromatography (SiO_2, *n*-pentane) to yield mixtures of **1**, **24**, and **25** (299 mg), a 4:1 mixture of **24** and **25** (184 mg), and clean **25** (20 mg, 10%).

Pentacyclo[8.4.0.$0^{3,8}$.$0^{4,15}$.$0^{7,11}$]tetradeca-5-ene (24)

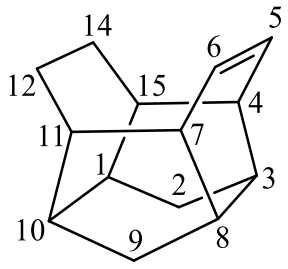

$C_{14}H_{18}$ (186), R_f = 0.95 by SiO_2-TLC; visualized by UV or vanillin stain

^{1}H-NMR ($CDCl_3$, 500 MHz): δ = 6.17† (m, 2H, H-5, -6), 2.50 (m, 2H), 2.27 (m, 2H), 2.19 (s_{app}, 2H), 2.00 (s_{app}, 2H), 1.83† (d, 2H, H-2_i, -9_i), 1.56† (m, 2H, H-12_i, -14_i), 1.41† (m, 2H, H-12_o, -14_o), 0.75† (d, 2H, H-2_o, 9_o) ppm;

$^{2}J_{\text{H-2o, -2i}} = {}^{2}J_{\text{H-9o, -9i}} = 11.3$ Hz.

^{13}C-NMR ($CDCl_3$, 100.7 MHz): δ = 134.4† (C-5, -6), 45.1, 40.7, 38.5, 37.5, 28.9† (C-2, -9), 19.8† (C-12, -14) ppm.

†: Assignments based on compounds of similar structure.

MS (EI, 70 eV): *m/z* (%) = 186 (29.9) [$M^{\cdot+}$], 143 (12.9), 141 (7.9), 132 (10.4), 131 (13.4), 130 (20.1), 129 (36.9), 128 (21.5), 119 (7.9), 118 (10.2), 117 (30.6), 116 (13.4), 115 (29.1), 108 (8.1), 106 (11.7), 105 (18.6), 104 (47.0), 103 (10.3), 95 (45.5), 94 (28.8), 93 (35.1), 92 (45.5), 91 (100.0), 81 (10.6), 80 (21.8), 79 (57.2), 78 (34.0), 77 (52.8), 67 (17.1), 66 (9.1), 65 (27.6), 63 (8.4), 53 (13.7), 52 (9.2), 51 (13.9).

Spectra:

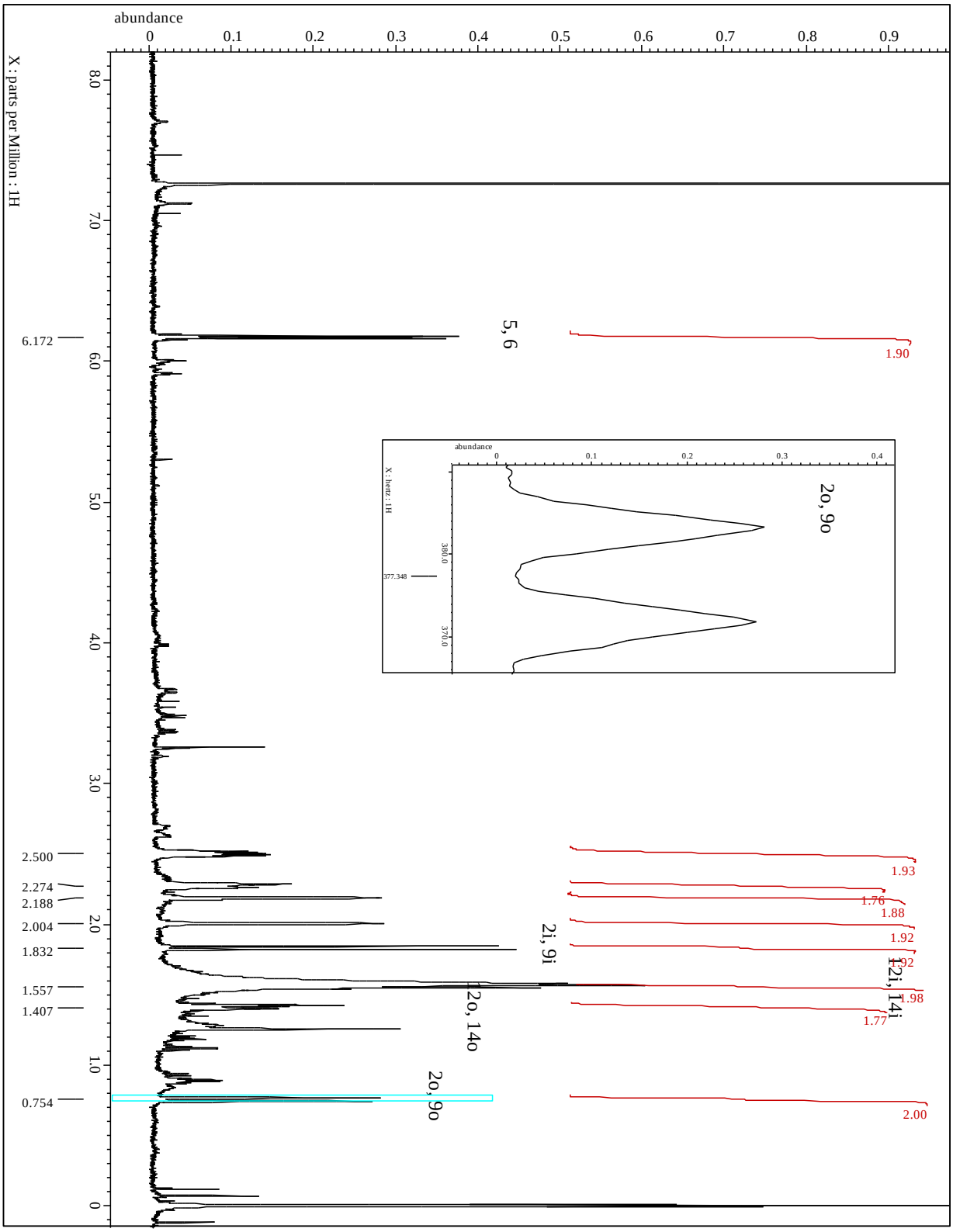
abundance
X : parts per Million : 1H
6.172
2.500
2.274
2.188
2.004
1.832
1.557
1.407
0.754
5, 6
1.90
2o, 9o
2i, 9i
1.93
1.76
1.88
1.92
1.92
12i, 14i
1.98
1.77
2o, 14o
2o, 9o
2.00
X : hertz : 1H
380.0
377.348
370.0

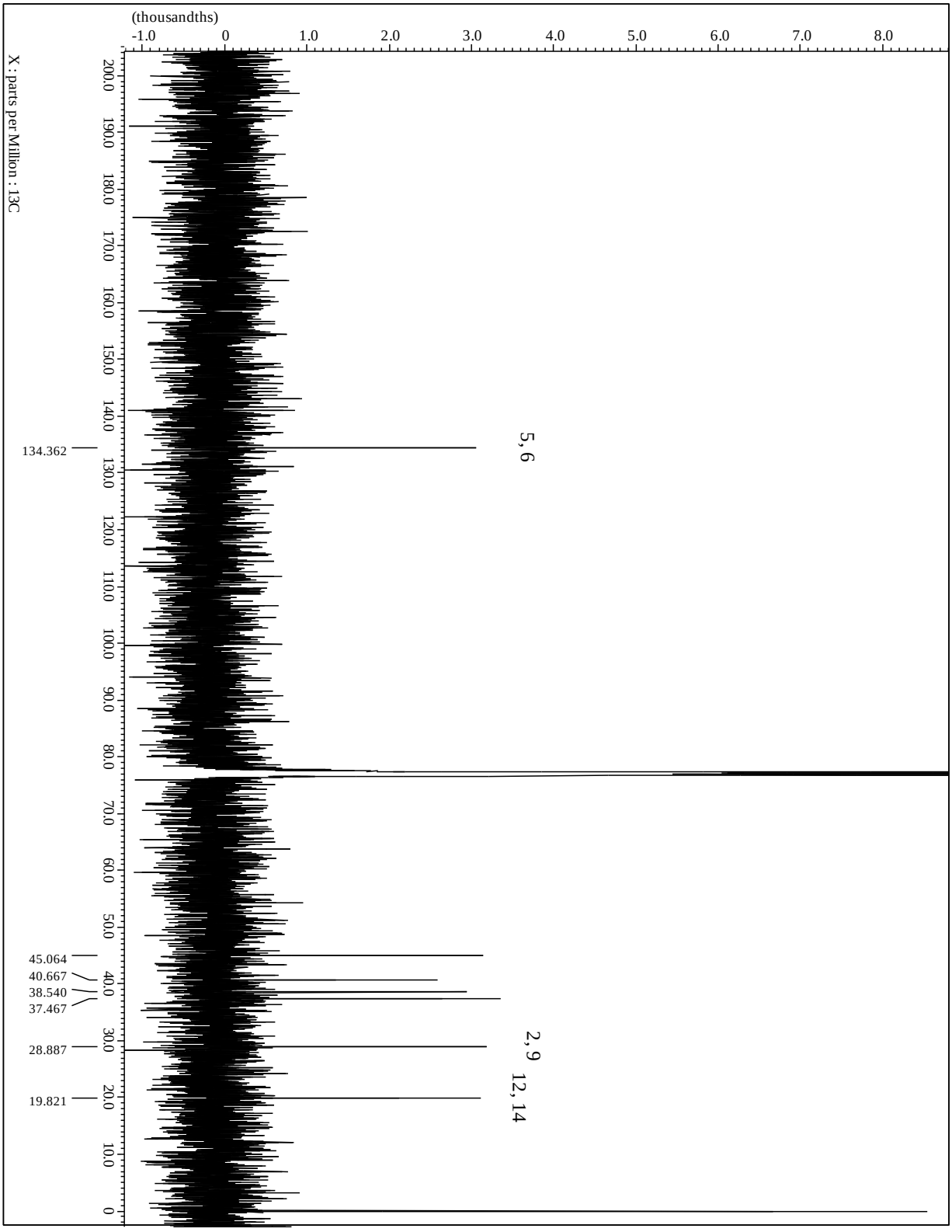
(thousandths)
-1.0
0
1.0
2.0
3.0
4.0
5.0
6.0
7.0
8.0
X : parts per Million : 13C
200.0
190.0
180.0
170.0
160.0
150.0
140.0
130.0
120.0
110.0
100.0
90.0
80.0
70.0
60.0
50.0
40.0
30.0
20.0
10.0
0
134.362
45.064
40.667
38.540
37.467
28.887
19.821
5, 6
2, 9
12, 14

Pentacyclo[8.4.0.0^{3,8}.0^{4,15}.0^{7,11}]tetradecane (25)

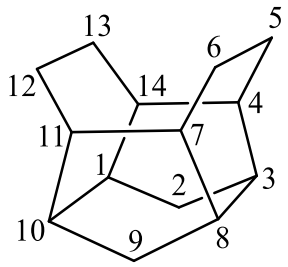

$C_{14}H_{20}$ (188), R_f = 0.99 by SiO_2-TLC; visualized by vanillin stain

MP = 185.6-187.2 °C (*n*-pentane)

IR (AT-IR): $\tilde{\nu}$ = 2906 (s, C-H), 1454 (m, C-C), 1132 (w), 819 (w) cm^{-1}.

^{1}H-NMR ($CDCl_3$, 500 MHz): δ = 2.15 (s_{app}, 4H, H-1, -3, -8, -10), 1.83 (d, 2H, H-2$_i$, -9$_i$), 1.79 (s_{app}, 8H, H-5$_i$, -6$_i$, -12$_i$, -13$_i$; H-4, -7, -11, -14), 1.62 (d, 4H, H-5$_o$, -6$_o$, -12$_o$, -13$_o$), 0.60 (d, 2H, H-2$_o$, -9$_o$) ppm;

$^2J_{H\text{-}2i,\,\text{-}2o} = {}^2J_{H\text{-}9i,\,\text{-}9o} = 11.1$; $^2J_{H\text{-}5i,\,\text{-}5o} = {}^2J_{H\text{-}6i,\,\text{-}6o} = {}^2J_{H\text{-}12i,\,\text{-}12o} = {}^2J_{H\text{-}13i,\,\text{-}13o} = 10.1$ Hz

^{13}C-NMR ($CDCl_3$, 100.7 MHz): δ = 37.3 (C-1, -3, -8, -10), 36.5 (C-4, -7, -11, -14), 28.4 (C-2, -9), 18.9 (C-5, -6, -12, -13) ppm.

MS (EI, 70 eV): *m/z* (%) = 189 (9.6) [M$^{\cdot+}$+1], 188 (65.0) [M$^{\cdot+}$], 173 (23.5), 160 (10.8), 159 (26.5), 147 (9.3), 146 (17.5), 145 (33.5), 134 (19.2), 133 (12.4), 132 (18.8), 131 (37.3), 129 (9.2), 128 (8.5), 120 (11.5), 119 (23.9), 118 (13.1), 117 (37.1), 115 (19.0), 110 (9.2), 106 (13.2), 105 (31.6), 104 (11.8), 103 (9.4), 95 (21.1), 94 (12.1), 93 (27.2), 92 (43.6), 91 (100.0), 81 (15.8), 80 (22.5), 79 (81.7), 78 (23.7), 77 (63.8), 67 (22.4), 66 (9.9), 65 (23.2), 55 (10.1), 54 (8.6), 53 (18.0), 51 (11.1).

Spectra:

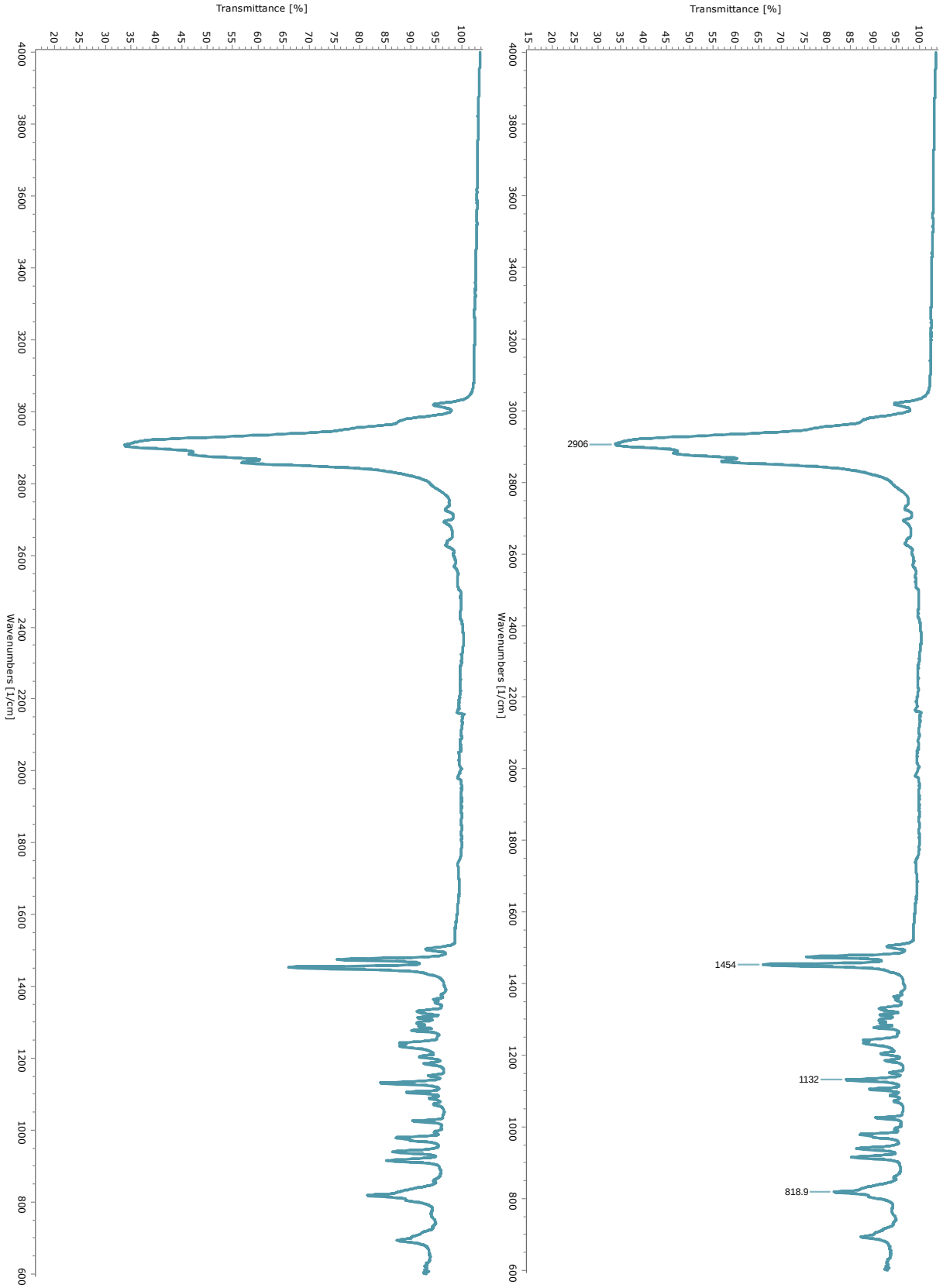
Transmittance [%]
Wavenumbers [1/cm]
2906
1454
1132
818.9

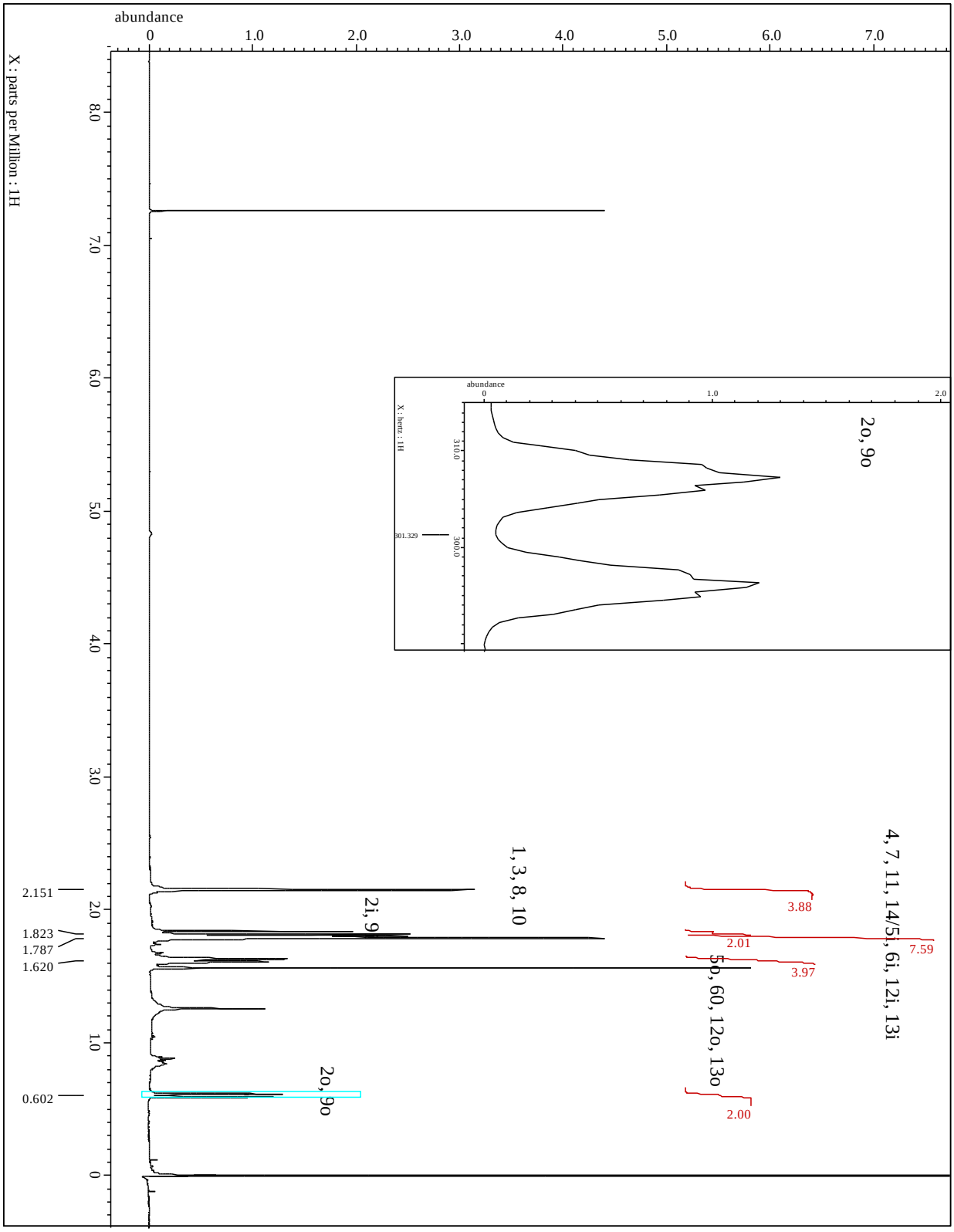
abundance
X : parts per Million : 1H
2.151
1.823
1.787
1.620
0.602
2i, 9
1, 3, 8, 10
2o, 9o
4, 7, 11, 14/5, 6i, 12i, 13i
5o, 6o, 12o, 13o
7.59
3.88
2.01
3.97
2.00
2o, 9o
X : hertz : 1H
310.0
301.329
300.0

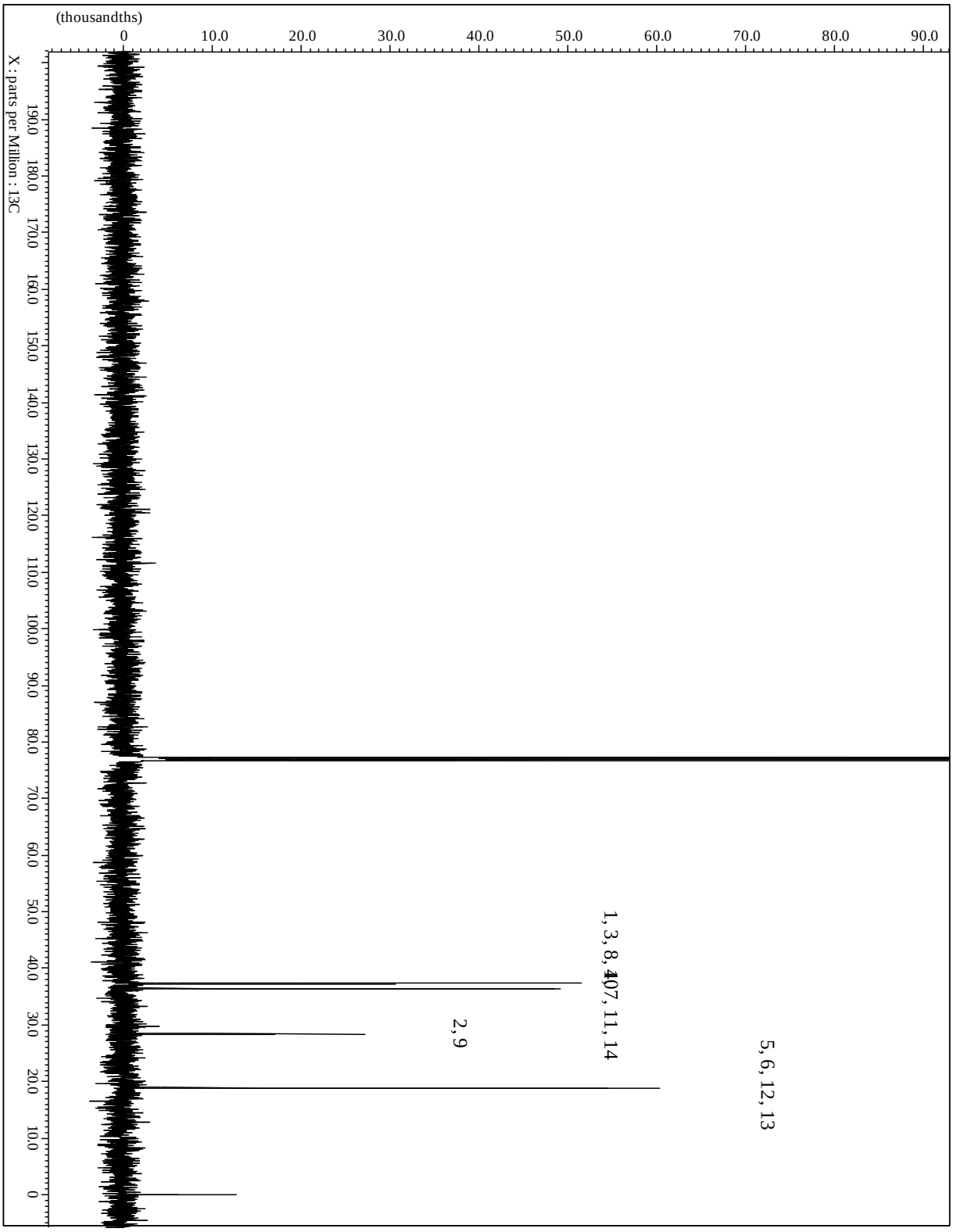
(thousandths)
0
10.0
20.0
30.0
40.0
50.0
60.0
70.0
80.0
90.0
X : parts per Million : 13C
190.0
180.0
170.0
160.0
150.0
140.0
130.0
120.0
110.0
100.0
90.0
80.0
70.0
60.0
50.0
40.0
30.0
20.0
10.0
0
5, 6, 12, 13
2, 9
1, 3, 8, 10, 7, 11, 14

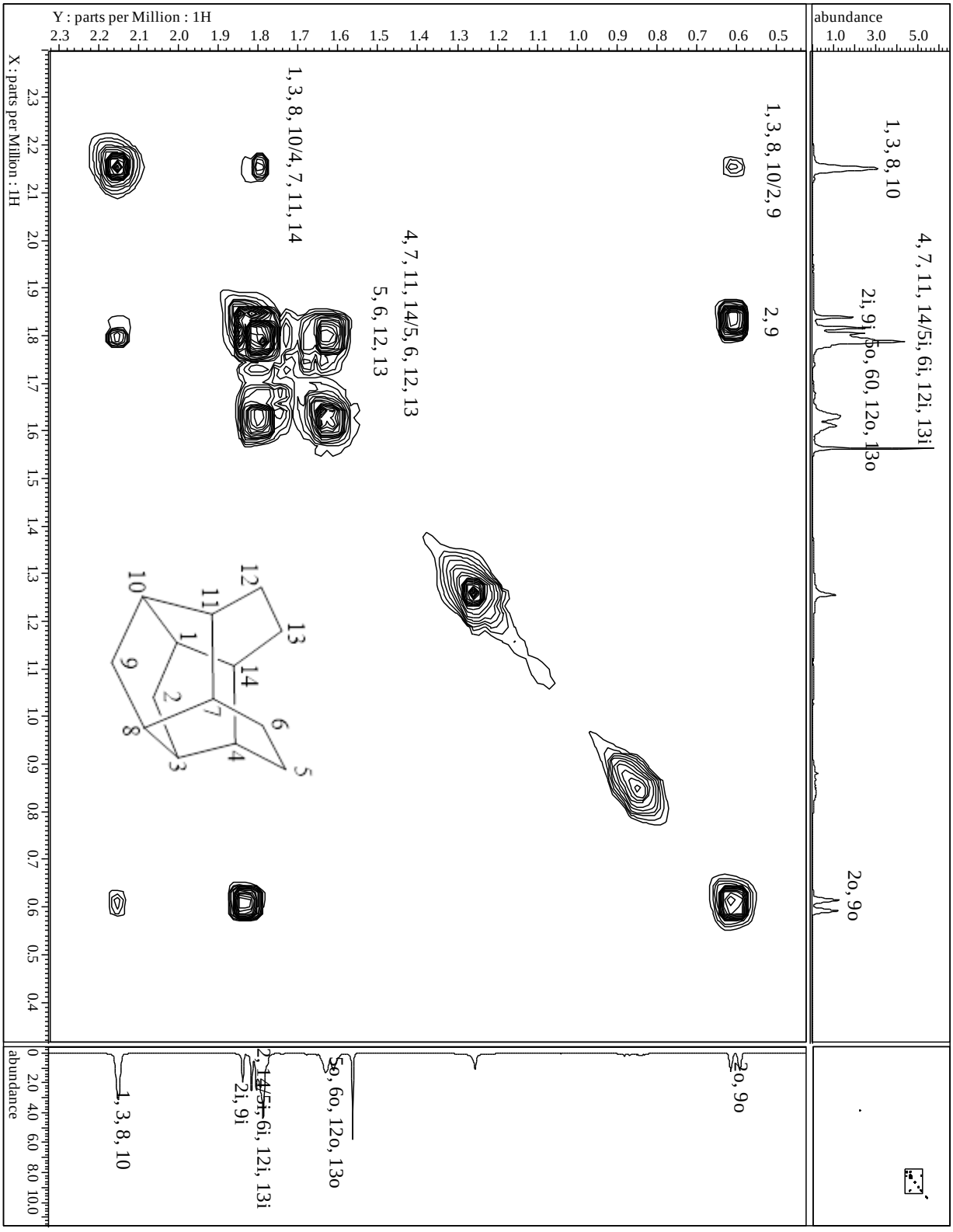
abundance
1.0 3.0 5.0
4, 7, 11, 14/5i, 6i, 12i, 13i
1, 3, 8, 10
2i, 9i
5o, 6o, 12o, 13o
2o, 9o
Y : parts per Million : 1H
2.3 2.2 2.1 2.0 1.9 1.8 1.7 1.6 1.5 1.4 1.3 1.2 1.1 1.0 0.9 0.8 0.7 0.6 0.5
1, 3, 8, 10/2, 9
2, 9
4, 7, 11, 14/5, 6, 12, 13
5, 6, 12, 13
1, 3, 8, 10/4, 7, 11, 14
X : parts per Million : 1H
2.3 2.2 2.1 2.0 1.9 1.8 1.7 1.6 1.5 1.4 1.3 1.2 1.1 1.0 0.9 0.8 0.7 0.6 0.5 0.4
1
2
3
4
5
6
7
8
9
10
11
12
13
14
2o, 9o
5o, 6o, 12o, 13o
2, 14/5i, 6i, 12i, 13i
2i, 9i
1, 3, 8, 10
0 2.0 4.0 6.0 8.0 10.0
abundance

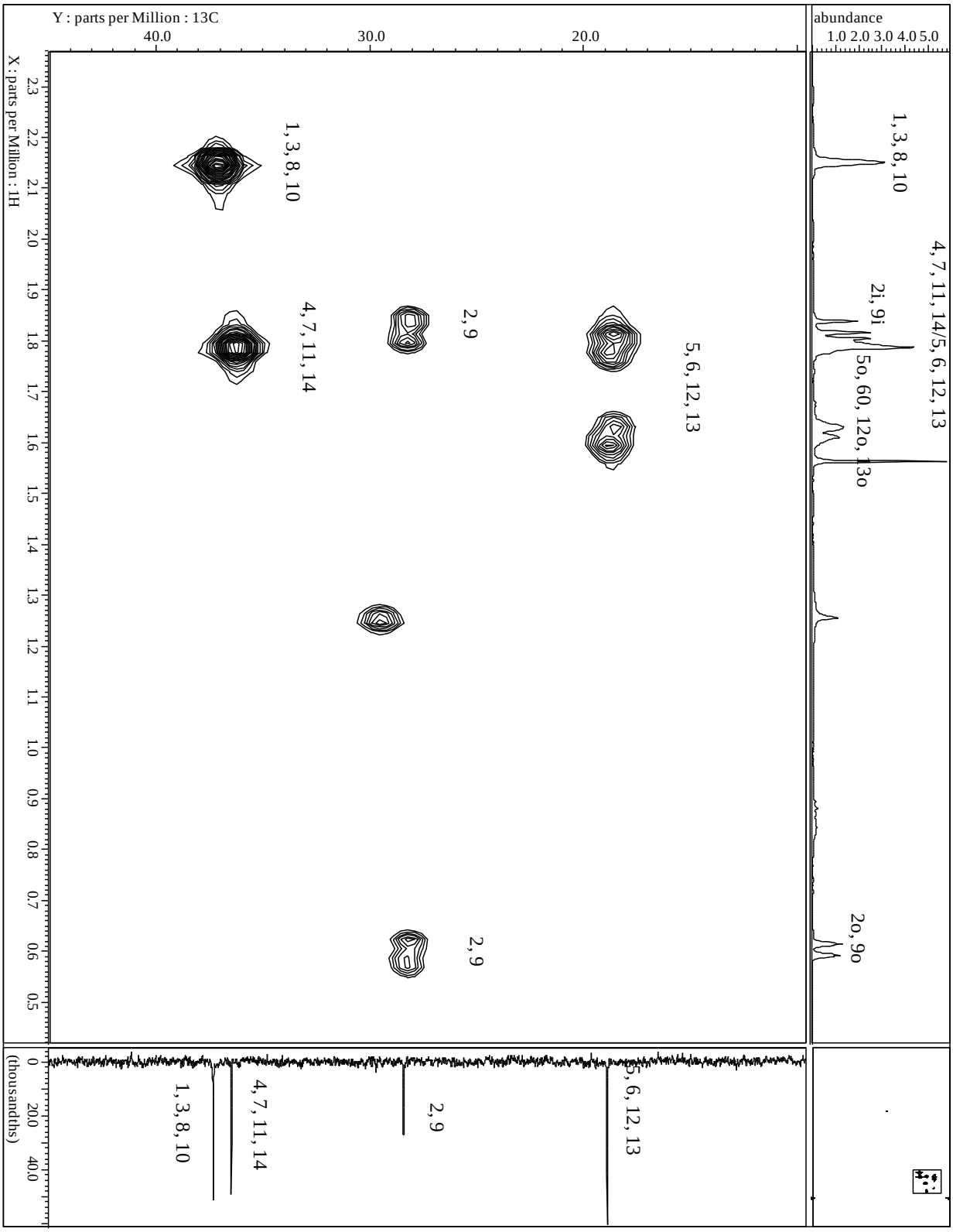
abundance
1.0 2.0 3.0 4.0 5.0
1, 3, 8, 10
4, 7, 11, 14/5, 6, 12, 13
2i, 9i
5o, 6o, 12o, 13o
2o, 9o
Y : parts per Million : 13C
40.0
30.0
20.0
5, 6, 12, 13
2, 9
2, 9
1, 3, 8, 10
4, 7, 11, 14
X : parts per Million : 1H
2.3 2.2 2.1 2.0 1.9 1.8 1.7 1.6 1.5 1.4 1.3 1.2 1.1 1.0 0.9 0.8 0.7 0.6 0.5
5, 6, 12, 13
2, 9
4, 7, 11, 14
1, 3, 8, 10
0
20.0
40.0
(thousandths)

5.3 Experimental: Carbene Chemistry of Cage Compounds

5.3.1 General Comments about Carbene Chemistry

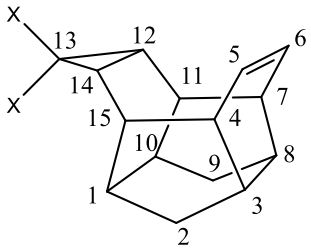

23a-d

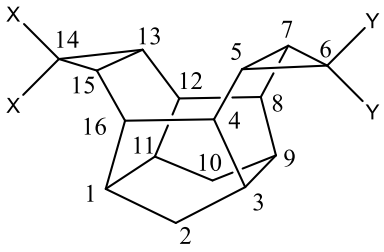

24a-g

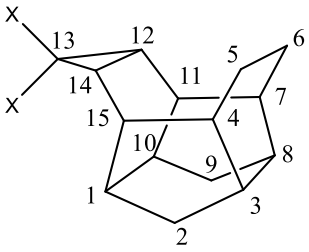

25a-d

	a	**b**	**c**	**d**	**e**	**f**	**g**
X=	H	F	Cl	Br	H	H	Cl
Y=	H	F	Cl	Br	Cl	Br	Br

Figure 129: IUPAC numbering for the mono, bis, mixed, and saturated carbene adducts.

The bis carbene adducts were synthesized in the same reaction as the monocarbene adducts as seen in the general procedures. The exception to this is the bis cyclopropane **41a** which was targeted individually *via* the dehalogenation of **41c**.

*Synthesis of Difluorocarbene Adducts***:** In pressure flask charged with N_2 and NaI (16.3 mg, 0.4 eq, 0.109 mmol), the diene **1** (50 mg, 0.272 mmol) was added and dissolved in dry THF (3 mL). $TMSCF_3$ (0.372 ml, 10 eq, 2.72 mmol) was added, and the flask sealed. The reaction was heated to 65 °C for 72 hours. The solution was cooled to room temperature then taken up in ether (15 mL) and concentrated under vacuum to remove the THF resulting in an orange oil. The crude oil was taken up in ether (15 mL) and water (15 mL) and extracted with ether (3x15 mL). The combined organic phase was washed with sat. Na_2SO_3 (15 mL), sat. $NaHCO_3$ (15mL), and water (15 mL) then dried ($MgSO_4$) and concentrated under vacuum to give an orange solid (224 mg). The mixture

was then purified by column chromatography (SiO_2, *n*-pentane). The two products **40b** (20 mg, 31%) and **41b** (34 mg, 44%) were obtained as colorless solids.

Synthesis of Dichlorocarbene Adducts: To the diene **1** (155 mg, 0.842 mmol), dissolved in chloroform (3 mL), a catalytic amount of TEBA-Cl (≈ 20 mg) was added followed by 50% NaOH (3 mL) added dropwise. The reaction was then stirred for 6 hours. Water (10 mL) was added, the phases separated, and extracted with DCM (3x20 mL). The combined organic phase was washed with water (2x10 mL) then dried ($MgSO_4$) and concentrated under vacuum to yield a colorless solid (208 mg). The mixture was then purified by column chromatography (SiO_2, *n*-pentane). The two products **40c** (91 mg, 40%) and **41c** (30 mg, 10%) were obtained as colorless solids. Mixtures of **1** and **40c** (51 mg, 7:1) and **40c** and **41c** (31 mg, 1:1) were also obtained. Crystals of both compounds for XRD were obtained from chloroform.

Monoene **24** (65 mg, 0.349 mmol) was reacted under the same conditions to give a colorless solid (169 mg). The mixture (233 mg from two batches of 65 mg) was then purified by column chromatography (SiO_2, *n*-pentane). The product **42c** (40 mg, 21%) was obtained as a colorless crystalline solid. The remaining material was recovered as mixed fractions of **24b, 25**, and **42c**. Crystals for XRD were obtained from chloroform.

The mono cyclopropane **40a** (43 mg, 0.217 mmol) was reacted under the same conditions to give a colorless solid (68 mg). The mixture was triturated with *n*-pentane to give product **41e** (30 mg, 49%) as a crystalline solid. The titrant (38 mg) contained a mixture of the insertion products **CI-4a**, **CI-5a**, and unreacted starting material. Single crystals of **40a** for XRD were obtained from chloroform.

Synthesis of Dibromocarbene Adducts: To diene **1** (112 mg, 0.609 mmol) dissolved in bromoform (3 mL), a catalytic amount of TEBA-Cl (≈ 20 mg) was added followed by the dropwise addition of 50% NaOH (3 mL). The reaction was stirred for 24 hours. Water (10 mL) was added, the phases separated, and extracted with DCM (3x10 mL). The combined organic phase was dried ($MgSO_4$) and concentrated under vacuum to yield an orange solid (217 mg). The mixture was purified by column chromatography (SiO_2, *n*-pentane) yielding **1** (16 mg), **40d** (78 mg, 35%), **41d** (10 mg, 3%) and a mixture of **40d** and **41d** (1:1). This mixture was crystalized in DCM and triturated with EtOAc to give pure **41d** (60 mg, 19%, overall 22%) and pure **40d** (52 mg, 25%, overall 60%). Single crystals for XRD of **40d** were obtained from EtOAc and single crystals for **41d** were obtained from DCM.

The monoene **2** (98 mg, 0.527 mmol) was reacted under the same conditions to give an orange solid (165 mg). The mixture was then purified by column chromatography (SiO_2, *n*-pentane). The product **42d** (38 mg, 20%) was obtained as a colorless crystalline solid. The remaining material was recovered in various mixtures of **1** and **42d** and **42d** and insertion products. Crystals for XRD were obtained from chloroform.

The mono cyclopropane **40a** (38 mg, 0.192 mmol) was reacted under the same conditions to give a colorless solid (80 mg). The mixture was purified by column chromatography (SiO_2, *n*-pentane). The product **41f** (14 mg, 20%) was obtained as a colorless crystalline solid. The remaining material was recovered as mixed fractions of **41f** and **CI-4b**, **CI-4b** and **CI-5b** and pure **CI-5b** in varying amounts.

The mono-dichlorocarbene adduct **40c** (32 mg, 0.192 mmol) was reacted under the same conditions to give a colorless solid (48 mg). The mixture was purified by column chromatography

(SiO_2, hexanes). The product **41g** (30mg, 57%) was obtained as a colorless crystalline solid and unreacted staring material **40c** (18 mg).

*Synthesis of Diiodocarbene Adducts***:** To diene **1** (50 mg, 0.272 mmol) and iodoform (535.5 mg, 1.36 mmol) dissolved in CCl_4 (3 mL), a catalytic amount of TEBA-Cl (≈ 20 mg) was added followed by the dropwise addition of 50% NaOH (3 mL). The reaction was stirred for 6 hours. Water (10 mL) was added, the phases separated, and extracted with DCM (3x20 mL). The combined organic phase was washed with water (3x10 mL), dried ($MgSO_4$), and concentrated under vacuum giving a dark brown solid (514 mg). Due to decomposition, no product was isolated from the mixture.

Dehalogenation of Dichlorocarbene Adducts: Dichlorocarbene adduct **41c** (100 mg, 0.287 mmol) dissolved in THF (25 mL) was added to liquid ammonia at -78 °C. To the cold suspension 200 proof EtOH (1.5 mL, 41.3 mmol) was added dropwise. Freshly cut strips of Li (17.4 mg) were added until the color persisted for 1 hour. The reaction was quenched with NH_4Cl and slowly warmed to room temperature and let stand till remaining ammonia had evaporated. The reside was taken up in water (30 mL) and DCM (30 mL) and the phases separated. The aqueous phase was extracted with DCM (3x30 mL). The combined organic phase was dried ($MgSO_4$) and concentrated under vacuum to give a colorless solid (48 mg). The solid was rinsed with *n*-pentane to give **41a** as a colorless crystalline solid (48 mg, 79%). Crystals for XRD were obtained from chloroform. The mono adduct **40c** (98 mg, 0.367 mmol) was reacted under the above conditions to give **40a** as a colorless waxy solid (61 mg, 84%).

*Hydrogenation of Various Carbene Adducts***:** To **40a** (16 mg, 0.08 mmol) dissolved in ethanol (1.0 mL), anhydrous hydrazine (0.013 mL, 8 eq., 0.646 mmol) was added brought to reflux for 48 hours. The EtOH was removed under vacuum and the residue is taken up in DCM (15 mL) and

water (15 mL). The phases were separated, and the aqueous phase extracted with DCM (3x15 mL). The combined organic phase was dried ($MgSO_4$) and concentrated under vacuum resulting in a colorless solid (30 mg). The solid was rinsed with *n*-pentane to give **42a** as a colorless waxy solid (10 mg, 62%).

The mono-difluorocarbene **40b** (15 mg, 0.064 mmol) was reacted under the same conditions to give a colorless solid (71 mg). The crude material was purified by column chromatography (SiO_2, *n*-pentane) yielding **42b** (14 mg, 93%) as a colorless crystalline solid.

The mono-dibromocarbene **40d** (152 mg, 0.427 mmol) was reacted under the same conditions to give a colorless solid (190 mg). The crude material was purified by column chromatography (SiO_2, hexanes) yielding **42d** (102 mg, 67%) as a colorless crystalline solid. Crystals for XRD were obtained from chloroform.

5.3.2 Mono Carbene adducts **40a-d**

Hexacyclo[8.5.0.0^{3,8}.0^{4,15}.0^{7,11}.0^{12,14}]pentadec-5-ene (40a)

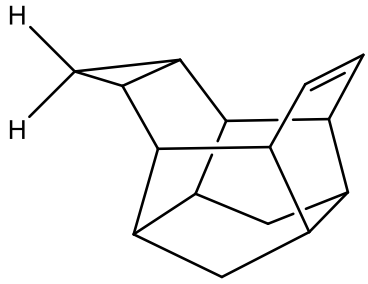

$C_{15}H_{18}$ (198), R_f = 0.90 by SiO_2-TLC; visualized by UV or vanillin stain

MP = 210.0-211.0 °C (*n*-pentane)

IR (AT-IR): $\tilde{\nu}$ = 3001 (m, C-H), 2927 (m, C-H), 1450 (w, C-C), 1016, 809 cm^{-1}.

^{1}H-NMR ($CDCl_3$, 500 MHz): δ= 6.17 (m, 2H, H-5, -6), 2.61-2.56 (m, 2H, H-4, -7), 2.45 (m, 2H, H-11, -15), 2.01 (s_{app}, 4H, H-1, -10; H-3, -8), 1.70 (d, 2H, H-2i, -9i), 0.78 (m, 2H, H-12, -14), 0.70 (d, 2H, H-2o, -9o), 0.24-0.19 (ddd, 1H, H-13), 0.07-0.03 (ddd, 1H, H-13) ppm;

$^{2}J_{\text{H-2i, -2o}} = {}^{2}J_{\text{H-9i, -9o}}$ =11.6, $^{2}J_{\text{H-5, H-13}}$ =4.77 Hz.

^{13}C-NMR ($CDCl_3$, 100.7 MHz): δ= 133.46 (C-5, -6), 45.44 (C-4, -7), 41.19 (C-11, -15), 38.46 (C-1, -10), 37.13 (C-3, -8), 28.43 (C-2, -9), 12.25 (C-12, -14), 4.89 (C-13) ppm.

MS(EI, 70 eV): *m/z* (%) = 198 ($M^{\cdot+}$, 14.0), 169 (8.7), 156 (9.1), 155 (10.9), 143 (11.0), 142 (16.9), 141 (14.6), 131 (13.7), 130 (18.1), 129 (33.8), 128 (19.3), 118 (12.9), 117 (22.7), 116 (15.5), 115 (23.0), 107 (25.1), 106 (17.1), 105 (31.2), 104 (14.2), 103 (9.0), 94 (10.8), 93 (16.1), 92 (35.7), 91 (100.0), 80 (7.6), 79 (46.0), 78 (24.7), 77 (34.1), 66 (8.2), 65 (17.9), 53 (8.1), 51 (10.0).

Spectra

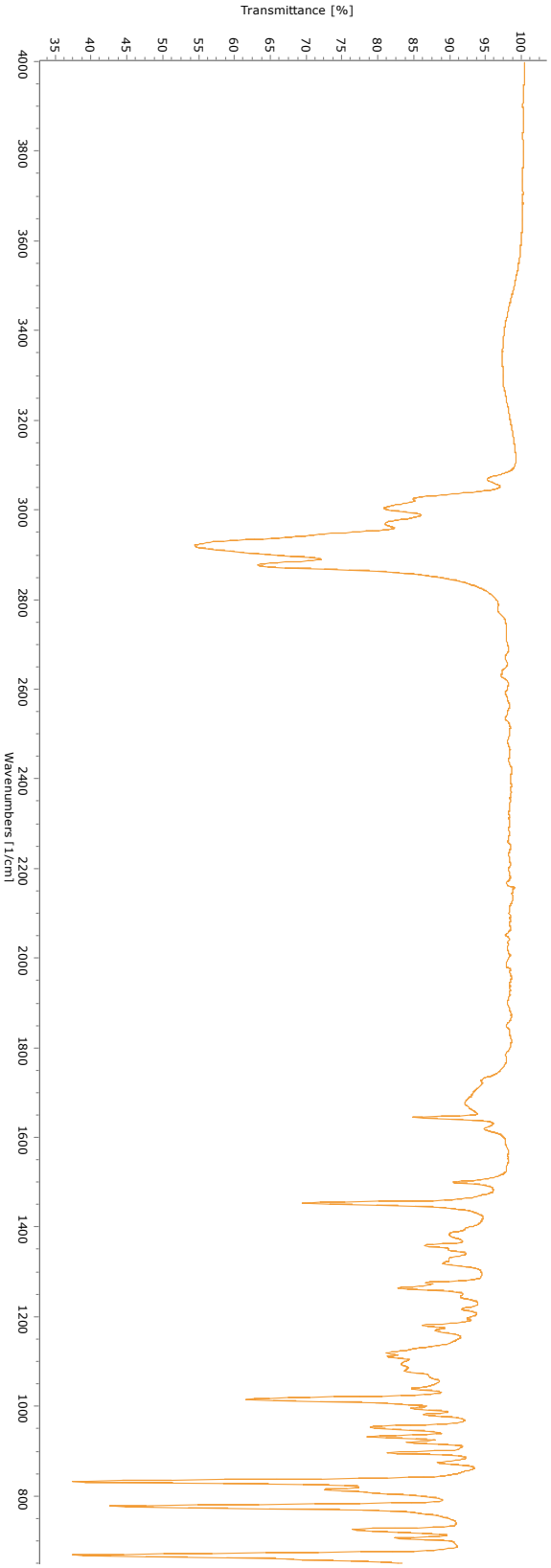
Transmittance [%]
Wavenumbers [1/cm]

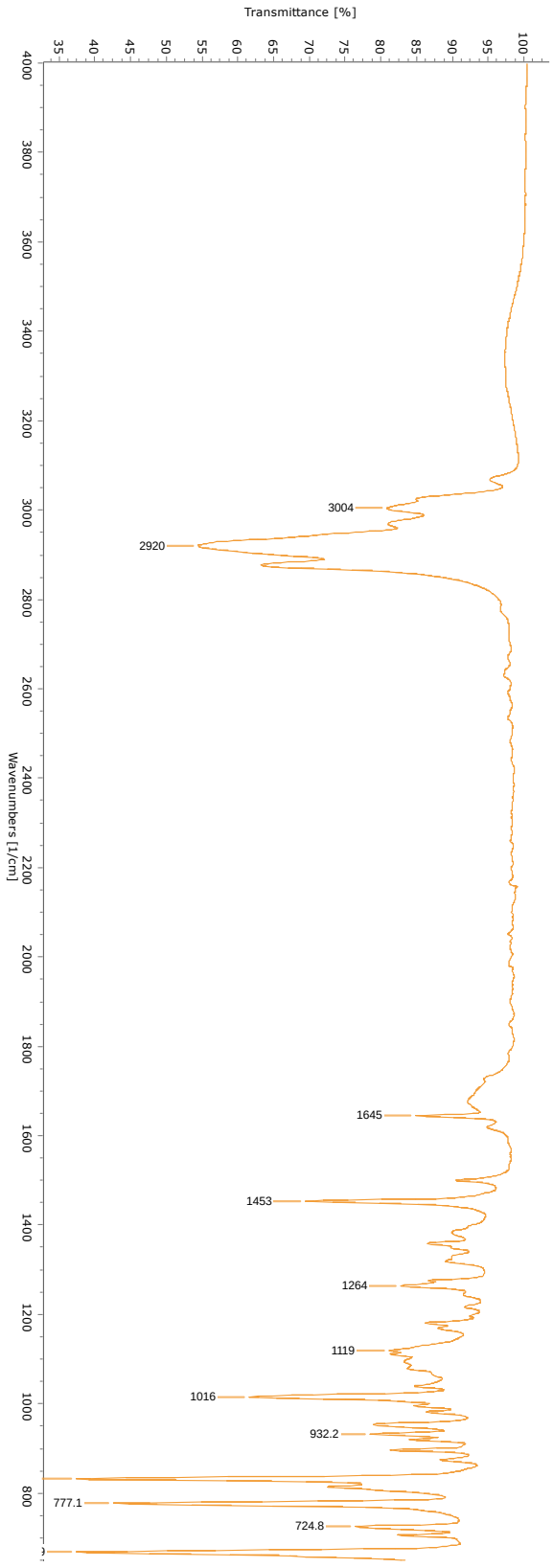
Transmittance [%]
Wavenumbers [1/cm]
3004
2920
1645
1453
1264
1119
1016
932.2
777.1
724.8

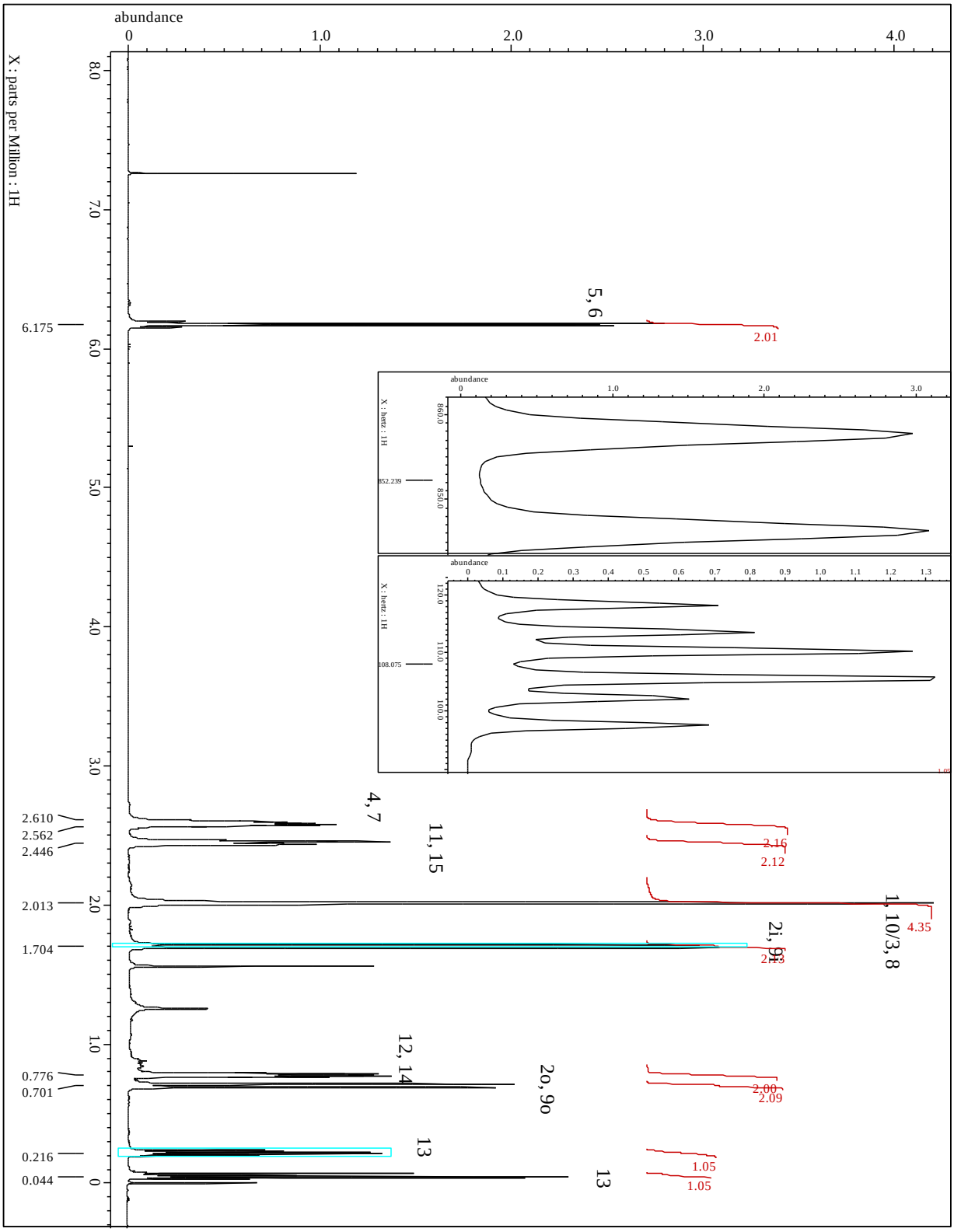
abundance
X : parts per Million : 1H
6.175
2.610
2.562
2.446
2.013
1.704
0.776
0.701
0.216
0.044
5, 6
2.01
4, 7
11, 15
2.16
2.12
1, 10/3, 8
4.35
2i, 9i
2.13
12, 14
2o, 9o
2.00
2.09
13
1.05
1.05
X : hertz : 1H
852.239
108.075

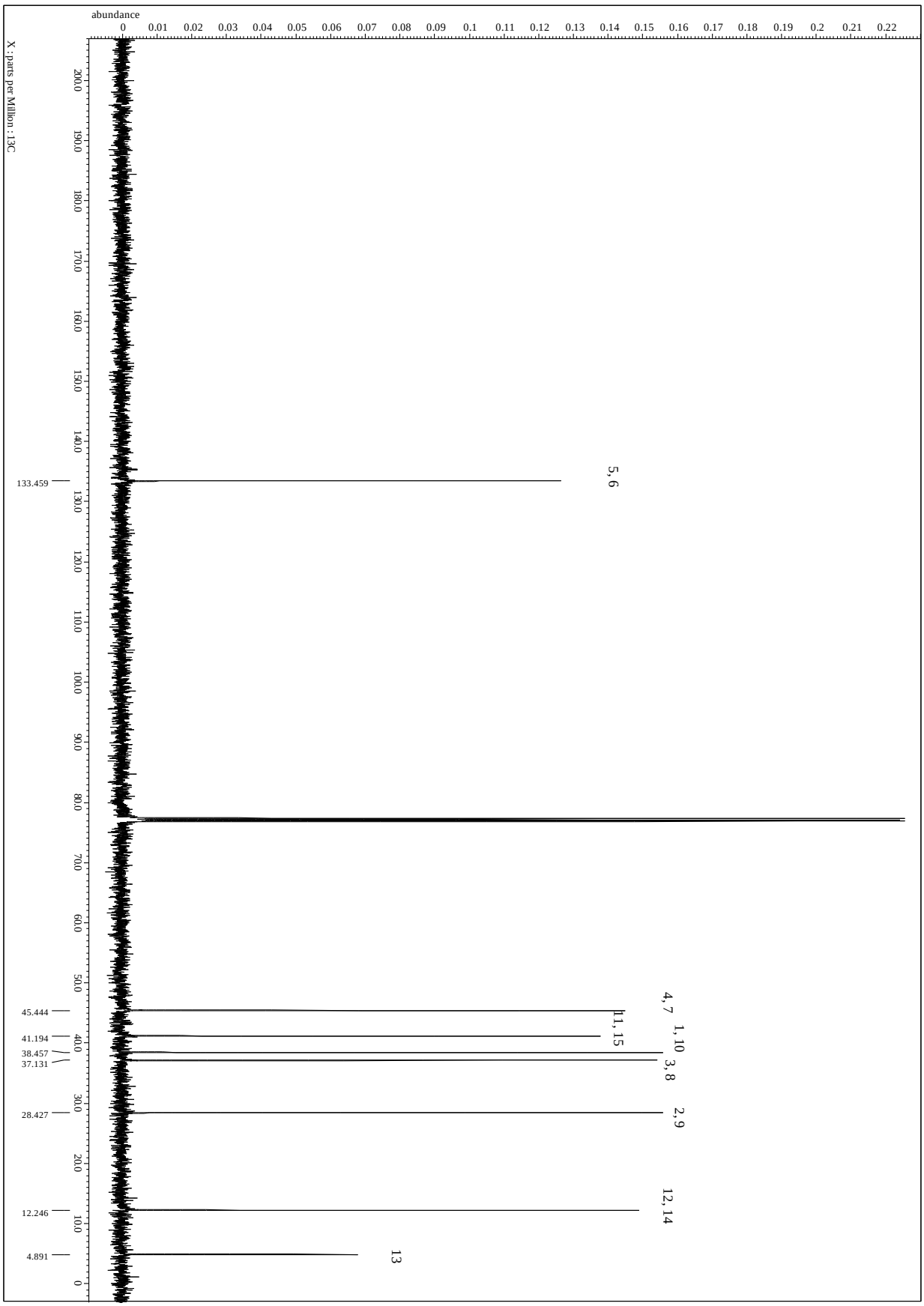
abundance
0 0.01 0.02 0.03 0.04 0.05 0.06 0.07 0.08 0.09 0.1 0.11 0.12 0.13 0.14 0.15 0.16 0.17 0.18 0.19 0.2 0.21 0.22
X : parts per Million : 13C
200.0 190.0 180.0 170.0 160.0 150.0 140.0 130.0 120.0 110.0 100.0 90.0 80.0 70.0 60.0 50.0 40.0 30.0 20.0 10.0 0
133.459
45.444
41.194
38.457
37.131
28.427
12.246
4.891
5, 6
4, 7
11, 15
1, 10
3, 8
2, 9
12, 14
13

13,13-difluorohexacyclo[8.5.0.0^{3,8}.0^{4,15}.0^{7,11}.0^{12,14}]pentadec-5-ene (40b)

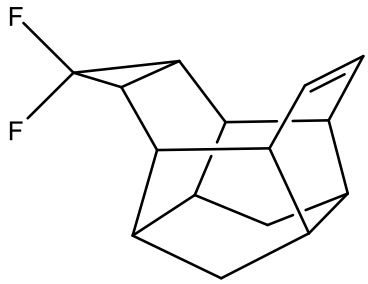

$C_{15}H_{16}F_2$ (234) , R_f = 0.75 by SiO_2-TLC; visualized by UV or vanillin stain

MP = 87.6-88.6 °C ($CDCl_3$)

IR(AT-IR): $\tilde{\nu}$ = 2962(s, C-H), 2925 (s, C-H), 1466 (m, C-C), 1131, 1090 775, 674 cm^{-1}.

^{1}H-NMR ($CDCl_3$, 500 MHz): δ= 6.18 (m, 2H, H-5, -6), 2.69 (m, 2H, H-4, -7), 2.48 (m, 2H, H-11, -15), 2.39 (s_{app}, 2H, H-1, 10), 2.04 (s_{app}, 2H, H-3, 8), 1.77 (d, 2H, H-2i, -9i), 1.43 (dt, 2H, H-12, -14), 0.71 (d, 2H, H-2o, -9o) ppm;

$^2J_{H\text{-}2i,\ -2o} = {}^2J_{H\text{-}9i,\ -9o}$ =11.4; $^3J_{H12,\ F}$ =16.5 Hz.

^{19}F-NMR ($CDCl_3$, 100.7 MHZ): δ= -120.05 (dt, 2F), -149.07 (d, 2F) ppm.

^{13}C-NMR ($CDCl_3$, 100.7 MHz): δ= 133 (C-5, 6), 116.0 (dd, C-13), 41.2 (C-11, 15), 41.1 (C-4, 7), 37.4 (C-1, 10), 37.1 (d, C-3, 8), 28.7 (C-2, 9), 22.7 (t, C-12, 14) ppm;

$^1J_{C\text{-}13,\ F}$ = 302.7 kHz.

MS(EI, 70 eV): *m/z* (%) = 234 ($M^{\cdot+}$, 4.6), 184.1 (1.9), 143 (9.4), 142.1 (13.7), 141 (19.3), 140 (8.5), 130 (8.0), 129.1 (27.2), 128 (15.5), 127 (21.0), 117 (15.8), 116 (13.8), 115 (21.5), 109 (8.7), 106 (7.9), 105.1 (15.3), 104 (13.1), 103 (9.1), 93.1 (18.7), 92 (30.8), 91.1 (100.0), 79 (21.5), 78 (25.2), 77 (35.3), 65 (16.3), 51 (15.2).

Spectra

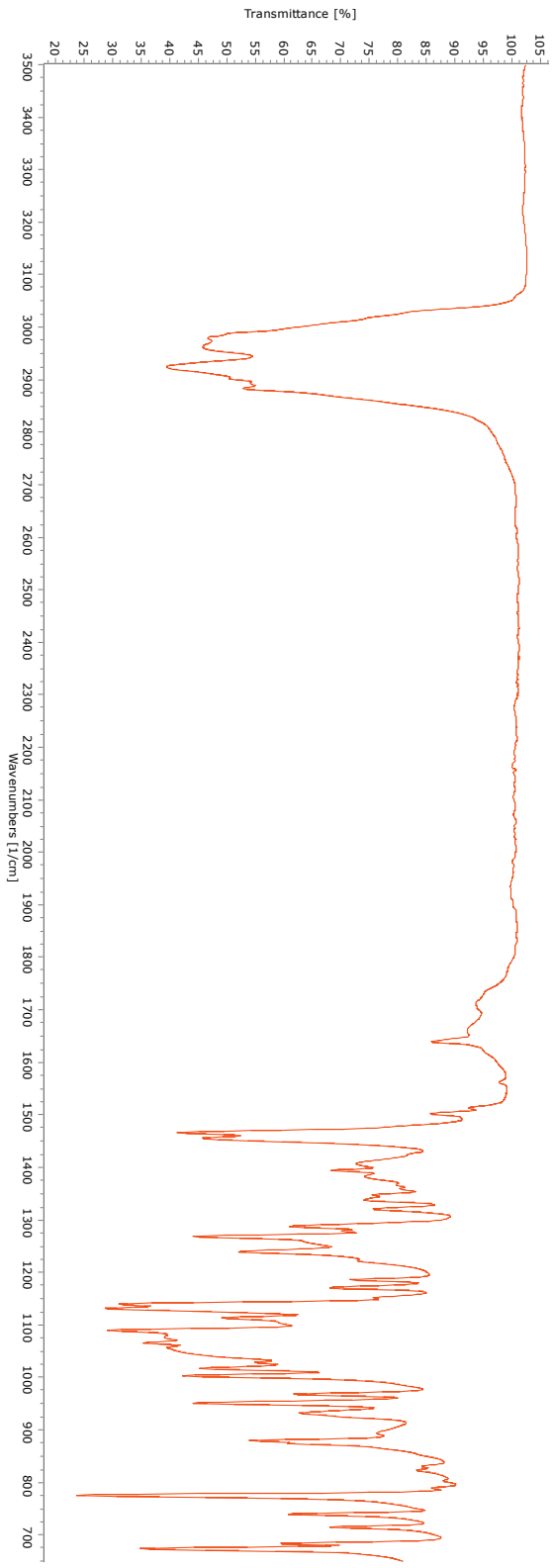
Transmittance [%]
Wavenumbers [1/cm]

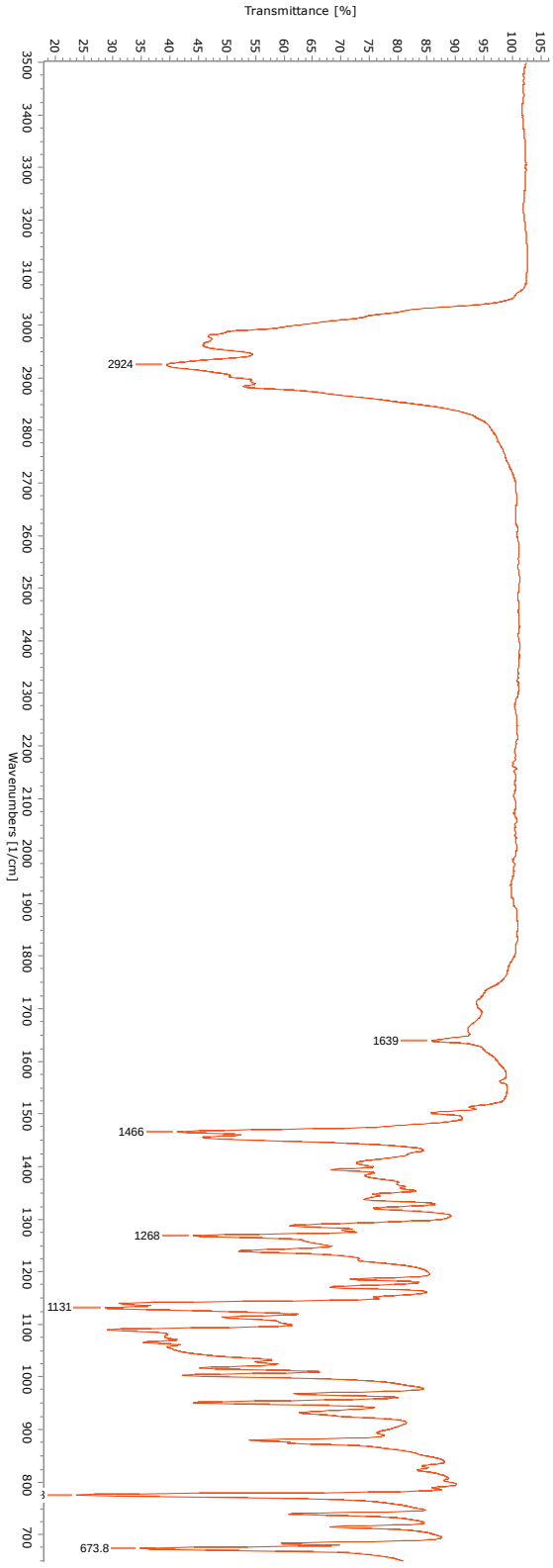
Transmittance [%]
Wavenumbers [1/cm]
2924
1639
1466
1268
1131
673.8

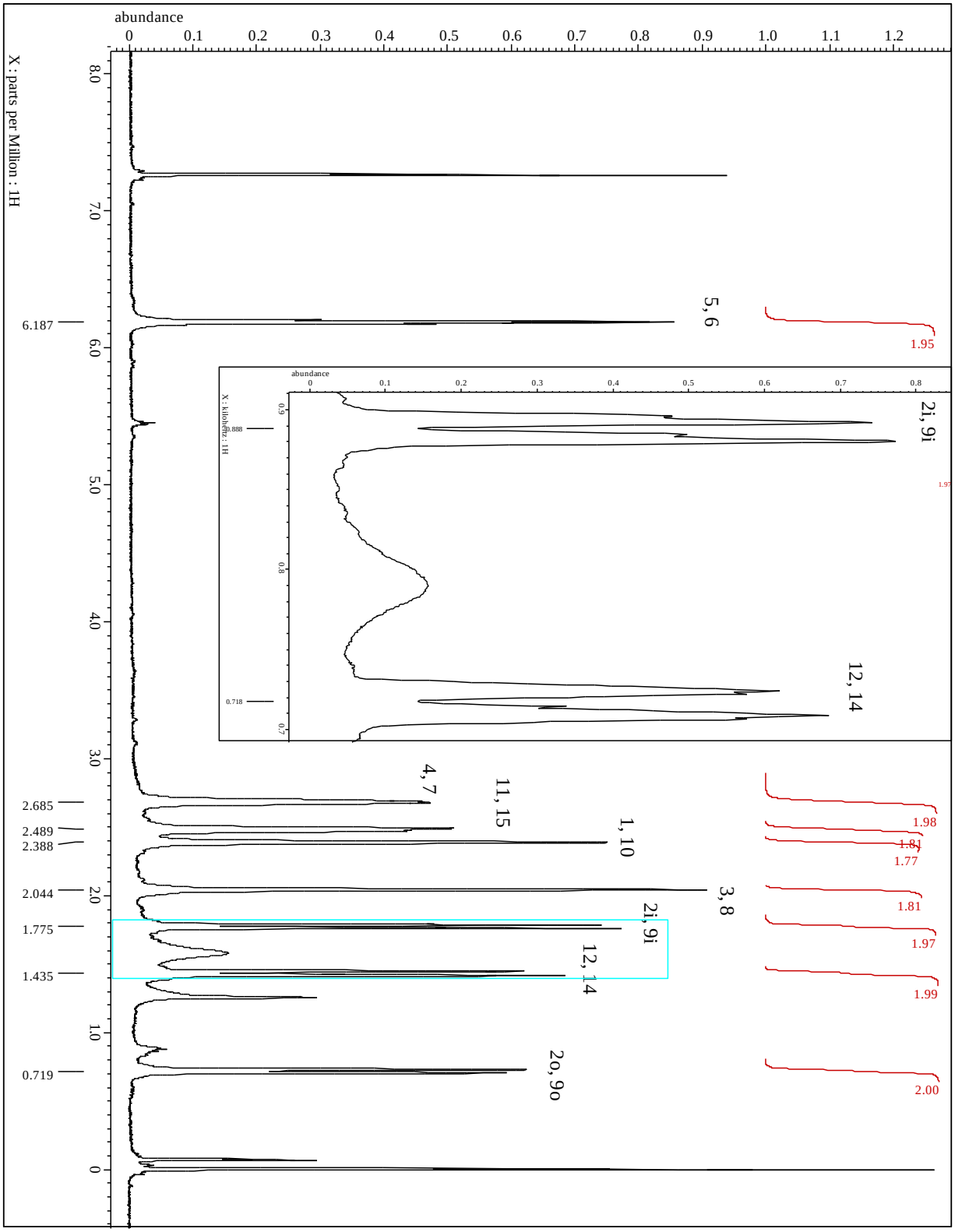
abundance
X : parts per Million : 1H
6.187
2.685
2.489
2.388
2.044
1.775
1.435
0.719
5, 6
4, 7
11, 15
1, 10
3, 8
2i, 9i
12, 14
2o, 9o
1.95
1.98
1.81
1.77
1.81
1.97
1.99
2.00
X : kilohertz : 1H
0.888
0.718
2i, 9i
12, 14
1.97

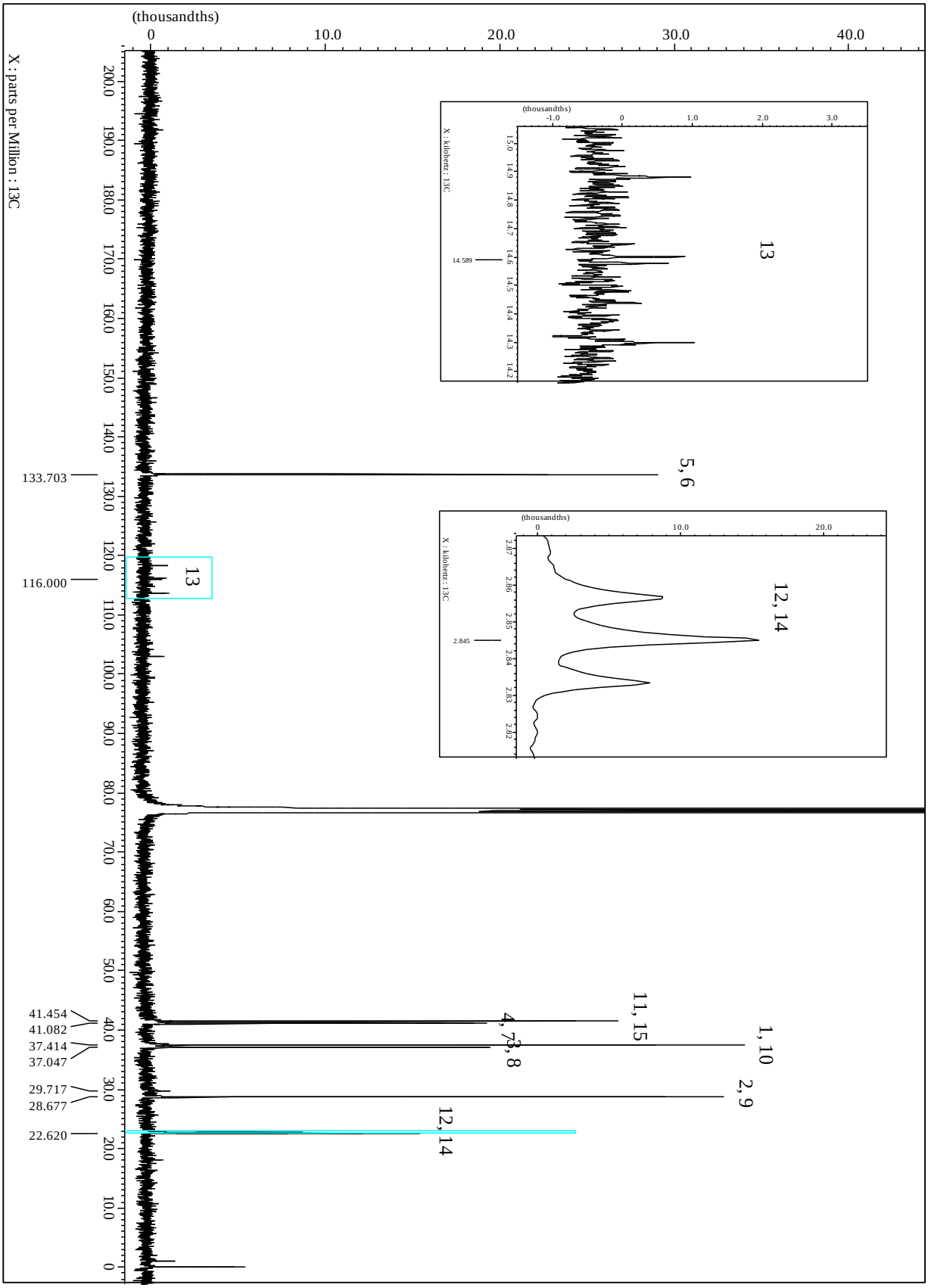
(thousandths)
0
10.0
20.0
30.0
40.0
X : parts per Million : 13C
200.0
190.0
180.0
170.0
160.0
150.0
140.0
130.0
120.0
110.0
100.0
90.0
80.0
70.0
60.0
50.0
40.0
30.0
20.0
10.0
0
133.703
116.000
41.454
41.082
37.414
37.047
29.717
28.677
22.620
5, 6
13
12, 14
11, 15
4, 7
3, 8
1, 10
2, 9
12, 14
(thousandths)
-1.0
0
1.0
2.0
3.0
X : kilohertz : 13C
15.0
14.9
14.8
14.7
14.6
14.5
14.4
14.3
14.2
14.589
13
(thousandths)
0
10.0
20.0
X : kilohertz : 13C
2.87
2.86
2.85
2.84
2.83
2.82
2.845
12, 14

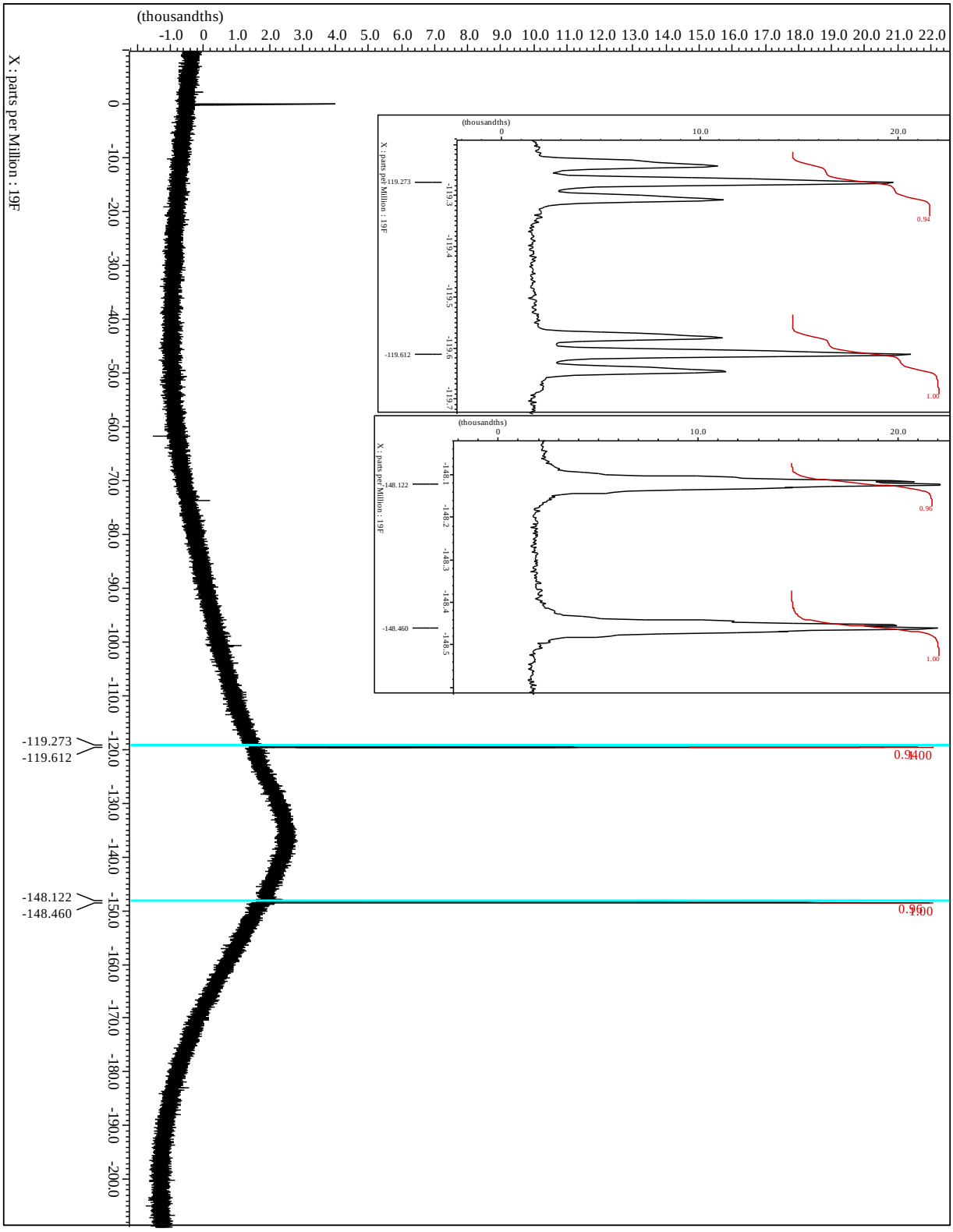
(thousandths)
X : parts per Million : 19F
-119.273
-119.612
-148.122
-148.460
0.94
1.00
0.96
1.00

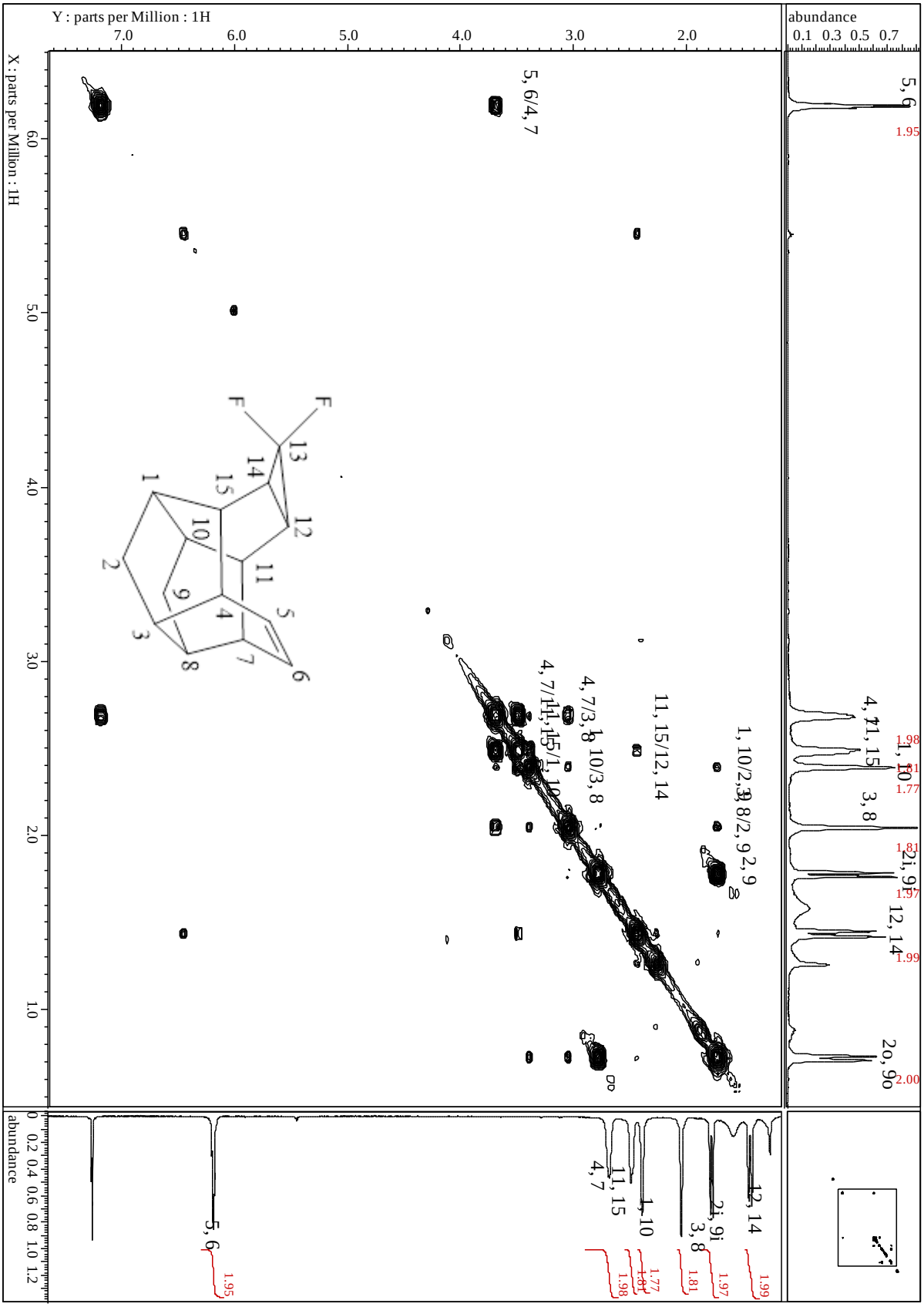
Y : parts per Million : 1H
X : parts per Million : 1H
abundance
5, 6
4, 7
11, 15
12, 14
1, 10
3, 8
2i, 9i
2o, 9o
1.95
1.98
1.81
1.77
1.97
1.99
2.00
F
F
1
2
3
4
5
6
7
8
9
10
11
12
13
14
15

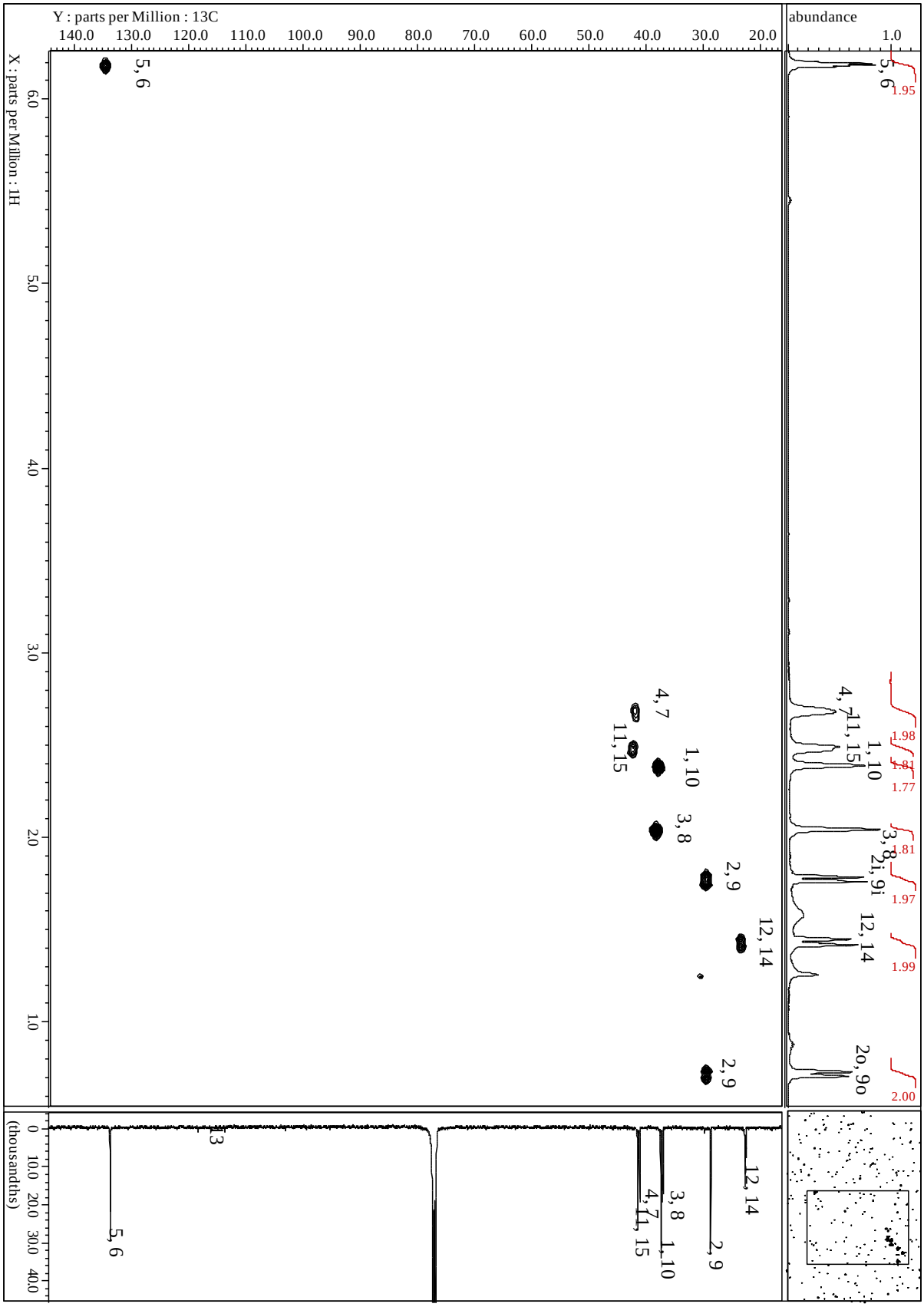
Y : parts per Million : 13C
X : parts per Million : 1H
abundance
(thousandths)
5, 6
4, 7
11, 15
1, 10
3, 8
2i, 9i
12, 14
2o, 9o
1.95
1.98
1.81
1.77
1.81
1.97
1.99
2.00
13

13,13-dichlorohexacyclo[8.5.0.0^{3,8}.0^{4,15}.0^{7,11}.0^{12,14}]pentadec-5-ene (40c)

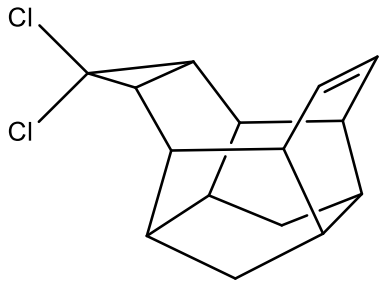

$C_{15}H_{16}Cl_2$ (266) , R_f = 0.60 by SiO_2-TLC; visualized by UV or vanillin stain

MP = 153.8-154.2 °C ($CHCl_3$)

IR(AT-IR): $\tilde{\nu}$ = 3036 (w, C-H), 2936 (s, C-H), 753 cm^{-1}.

^{1}H-NMR ($CDCl_3$, 500 MHz): δ= 6.17 (m,2H, H-5, -6), 2.72 (s_{app}, 4H, H-4, -7; H-11, -15), 2.56 (s_{app}, 2H, H-1, -10), 2.01 (s_{app}, 2H, H-3, -8), 1.78 (d, 2H, H-2i, -10i), 0.73 (d, 2H, H-2o, -10o) ppm; $^2J_{H\text{-}2i,\ -2o} = {}^2J_{H\text{-}9i,\ -9o}$ = 11.9 Hz.

^{13}C-NMR ($CDCl_3$, 100.7 MHz): δ= 134.0 (C-5, 6), 66.2 (C-13), 44.0(C-11, -15), 42.0 (C-4, -7), 37.1 (C-3, -8), 35.5 (C-1, -10), 31.7 (C-12, -14), 28.9 (C-2, 9) ppm.

MS(EI, 70 eV): *m/z* (%) = 270 ($M^{\cdot+}$+4, 0.8), 269 ($M^{\cdot+}$+3, 13.9), 268 ($M^{\cdot+}$+2, 21.1), 267 ($M^{\cdot+}$+1, 8.1), 266 ($M^{\cdot+}$, 46.2), 233 (25.7), 231 (32.0), 195 (16.8), 177 (100.0), 175 (34.7), 174 (21.7), 172 (9.8), 167 (22.6), 165 (11.6), 163 (20.2), 153 (46.8), 152 (18.8), 151 (48.6), 142 (14.9), 141 (23.1), 139 (21.1), 131 (24.6), 130 (39.7), 129 (9.9), 128 (8.2), 127 (23.5), 125 (25.1), 118 (10.6), 117 (11.9), 116 (15.6), 115 (16.4), 105 (18.0), 104 (22.8), 103 (10.6), 102 (14.8), 93 (13.4), 92 (12.9), 91 (9.2), 89 (21.5), 79 (30.0), 78 (10.0), 77 (4.2), 75 (3.4), 65 (21.1), 63 (13.9), 51 (16.1).

Spectra

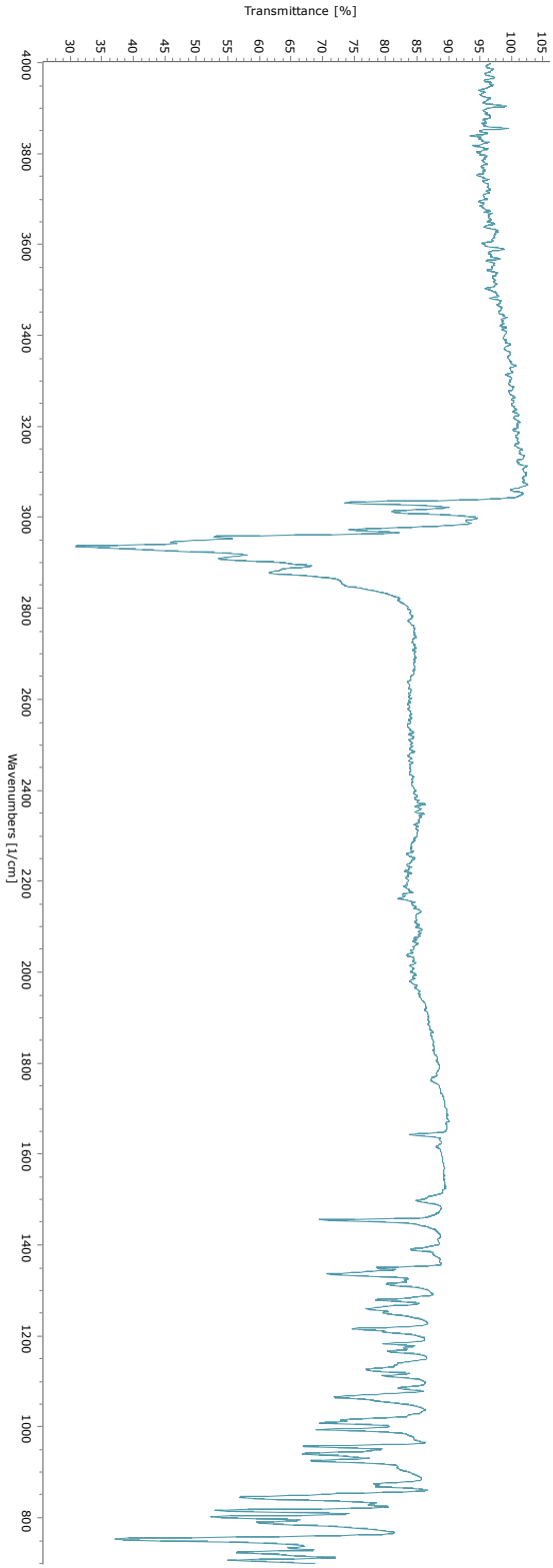
Transmittance [%]
Wavenumbers [1/cm]

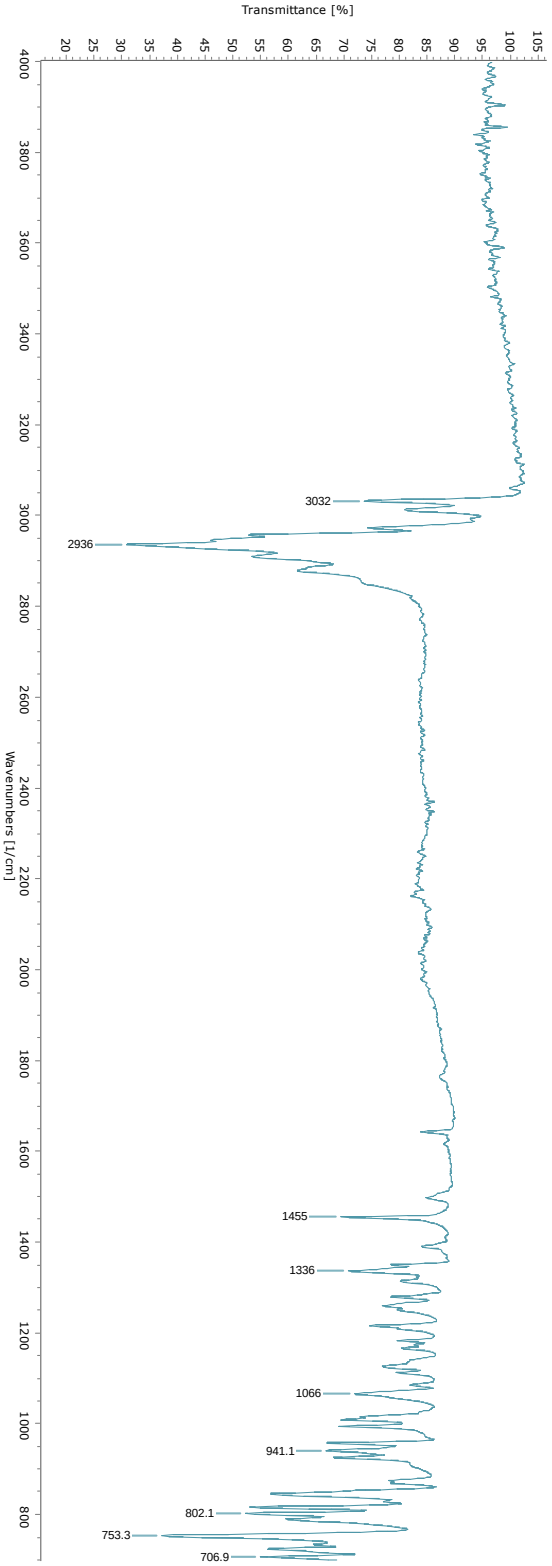
Transmittance [%]
Wavenumbers [1/cm]
3032
2936
1455
1336
1066
941.1
802.1
753.3
706.9

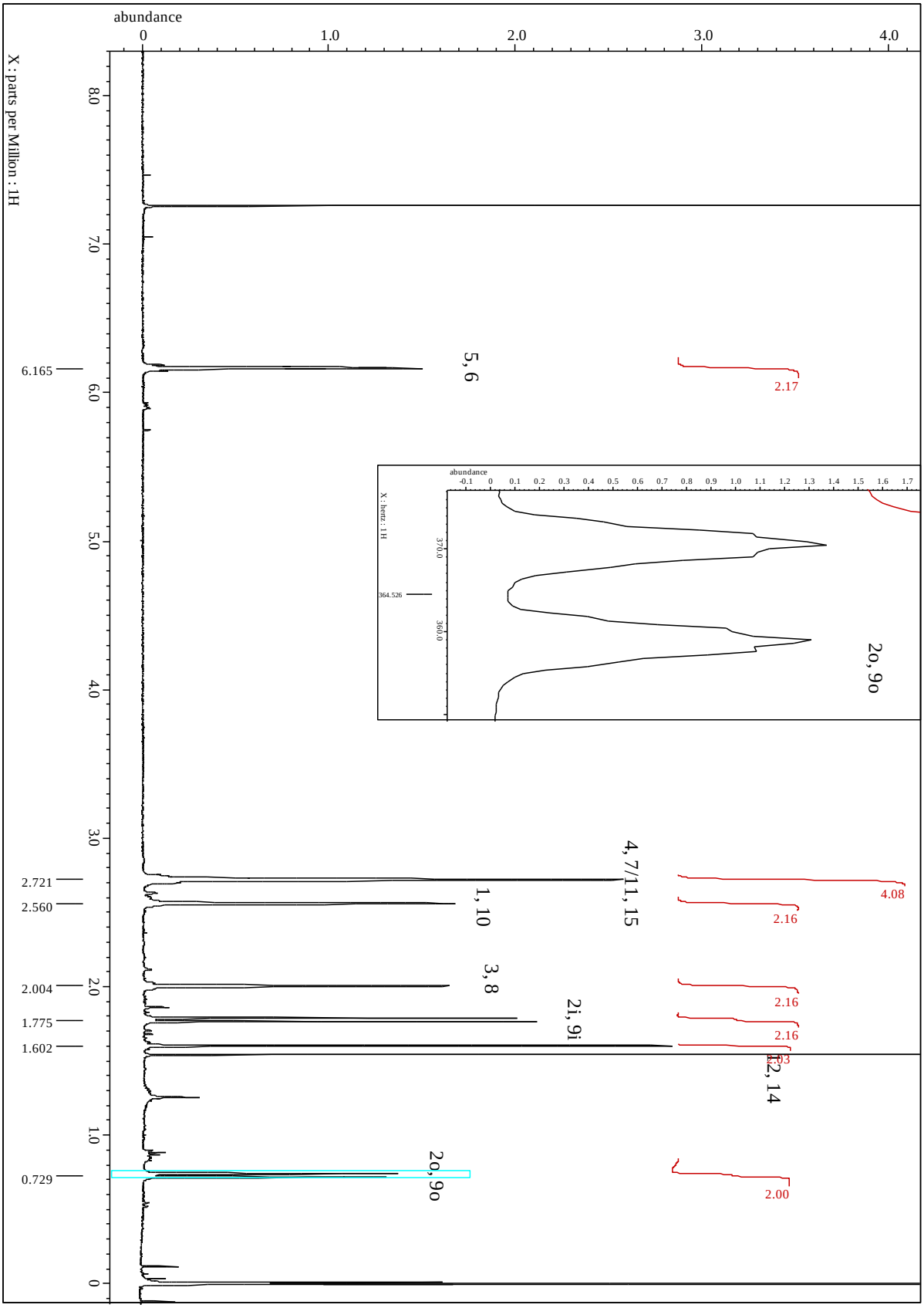
abundance
0
1.0
2.0
3.0
4.0
X : parts per Million : 1H
8.0
7.0
6.0
5.0
4.0
3.0
2.0
1.0
0
6.165
2.721
2.560
2.004
1.775
1.602
0.729
5, 6
4, 7/11, 15
1, 10
3, 8
2i, 9i
12, 13, 14
2o, 9o
2.17
4.08
2.16
2.16
2.16
2.16
2.00
abundance
X : hertz : 1H
370.0
364.526
360.0
2o, 9o

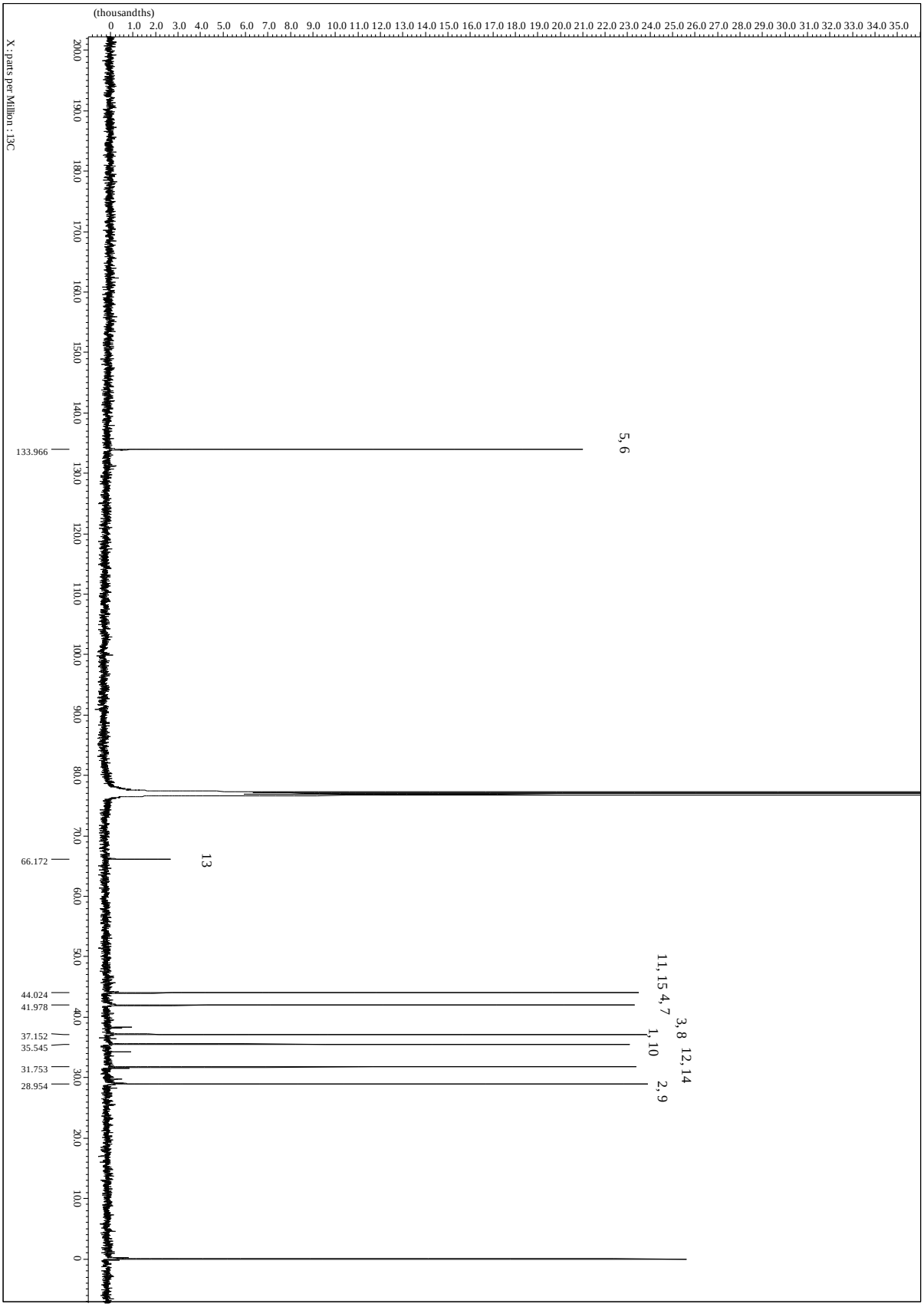
(thousandths)
X : parts per Million : 13C
133.966
66.172
44.024
41.978
37.152
35.545
31.753
28.954
5, 6
13
11, 15
4, 7
3, 8
1, 10
12, 14
2, 9

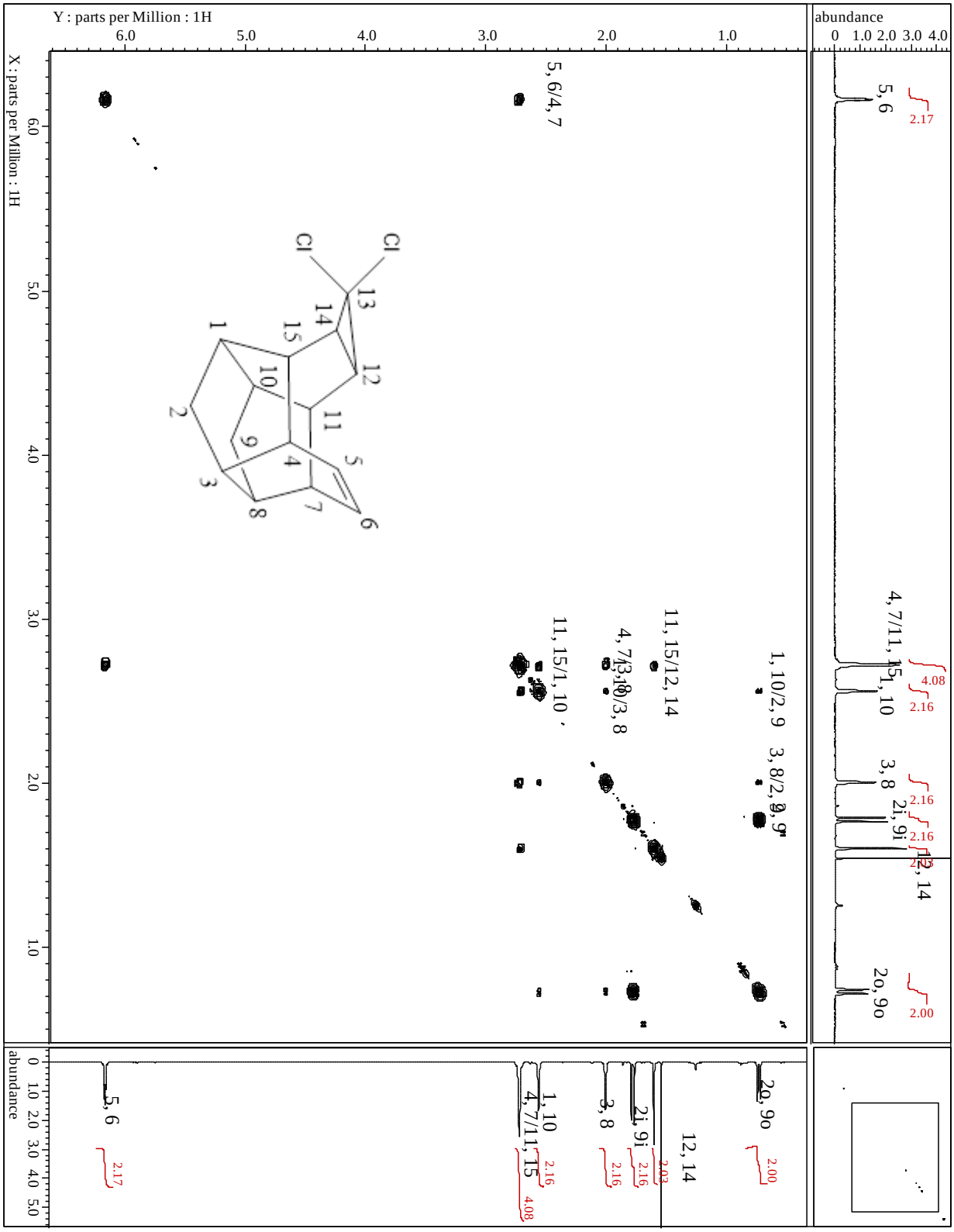
abundance
0 1.0 2.0 3.0 4.0
5, 6
2.17
4, 7/11, 15
1, 10
4.08
2.16
3, 8
2.16
2i, 9i
2.16
12, 14
2.16
2o, 9o
2.00
Y : parts per Million : 1H
6.0 5.0 4.0 3.0 2.0 1.0
X : parts per Million : 1H
Cl
Cl
1
2
3
4
5
6
7
8
9
10
11
12
13
14
15
1, 10/2, 9
3, 8/2i, 9i
2o, 9o
11, 15/12, 14
4, 7/3, 8
11, 15/1, 10
5, 6/4, 7
2o, 9o
2.00
12, 14
2.03
2i, 9i
2.16
3, 8
2.16
1, 10
2.16
4, 7/11, 15
4.08
5, 6
2.17
abundance
0 1.0 2.0 3.0 4.0 5.0

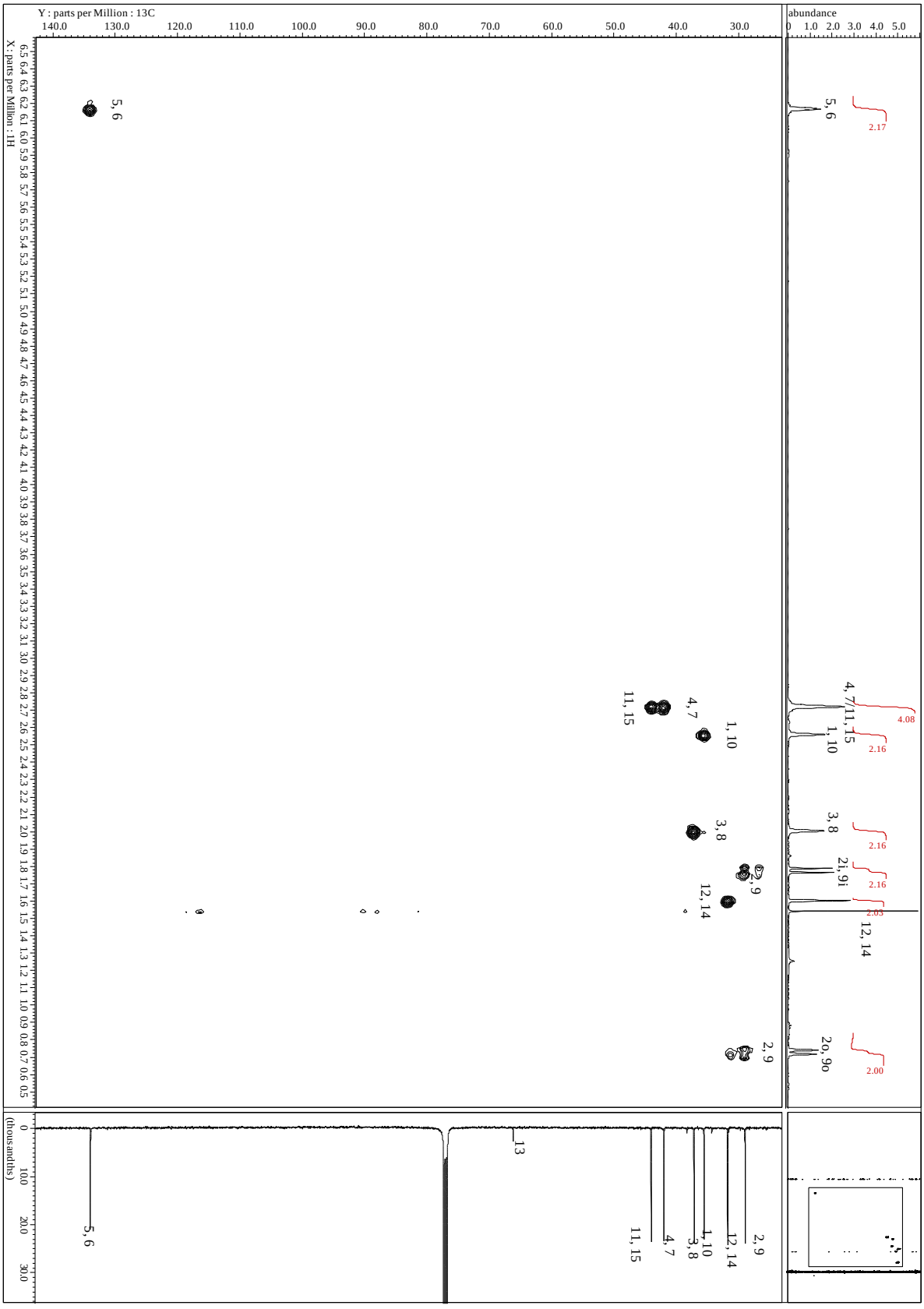
Y : parts per Million : 13C
X : parts per Million : 1H
abundance
(thousandths)
5, 6
2.17
4, 7/11, 15
1, 10
4.08
2.16
3, 8
2.16
21, 9i
2.16
2.03
12, 14
2o, 9o
2.00
2, 9
13

13,13-dibromohexacyclo[8.5.0.0^{3,8}.0^{4,15}.0^{7,11}.0^{12,14}]pentadec-5-ene (40d)

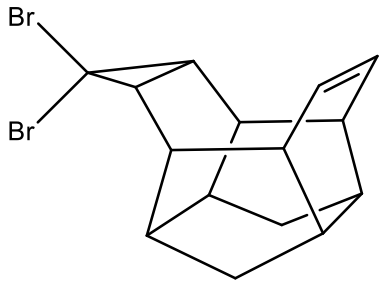

$C_{15}H_{16}Br_2$ (356) , R_f = 0.50 by SiO_2-TLC; visualized by UV or vanillin stain

MP = 164.6-164.8 °C (EtOAc)

IR(AT-IR): $\tilde{\nu}$ = 2962 (s, C-H), 2925 (s, C-H), 1466 (m, C-C), 1131, 1090 775, 674 cm^{-1}.

^{1}H-NMR ($CDCl_3$, 500 MHz): δ= 6.16 (m, 2H, H-5, -6), 2.80-2.76 (m, 2H, H-11, -15), 2.75-2.70 (m, 2H, H-4, -7), 2.63 (s_{app}, 2H, H-1, -10), 1.97 (s_{app}, 2H, H-3, -8), 1.77 (d, 2H, H-2i, -9i), 1.74 (dd, 2H, H-12, -14), 0.73 (d, 2H, H-2o, -9o) ppm;

$^2J_{H\text{-}2i,\ -2o} = {}^2J_{H\text{-}9i,\ -9o}$ =11.8 Hz.

^{13}C-NMR ($CDCl_3$, 100.7 MHz): δ = 134.1 (C-5, -6), 45.1 (C-11, -15), 42.1 (C-4, -7), 37.2 (C-3, -8), 36.0 (C-13), 35.1 (C-1, -10), 33.2 (C-12, -14), 28.9 (C-2, -9) ppm.

MS (EI, 70 eV): *m/z* (%) = 358 (0.2) [$M^{\cdot+}$+2], 356 (1.8) [$M^{\cdot+}$], 354 (0.3), 277 (9.2), 275 (8.8), 196 (19.5), 195 (64.1), 171 (17.1), 169 (14.7), 167 (9.1), 167 (16.9), 165 (13.2), 165 (13.7), 153 (12.1), 152 (14.0), 141 (13.3), 129 (49.3), 128 (10.1), 128 (23.7), 117 (11.5), 117 (40.8), 116 (16.8), 115 (64.7), 105 (12.0), 104 (19.6), 103 (16.6), 102 (7.6), 92 (13.2), 91 (100.0), 89 (12.1), 79 (19.6), 79 (8.1), 78 (35.4), 77 (14.5), 77 (22.8), 65 (14.2), 63 (9.2), 51 (15.8).

Spectra

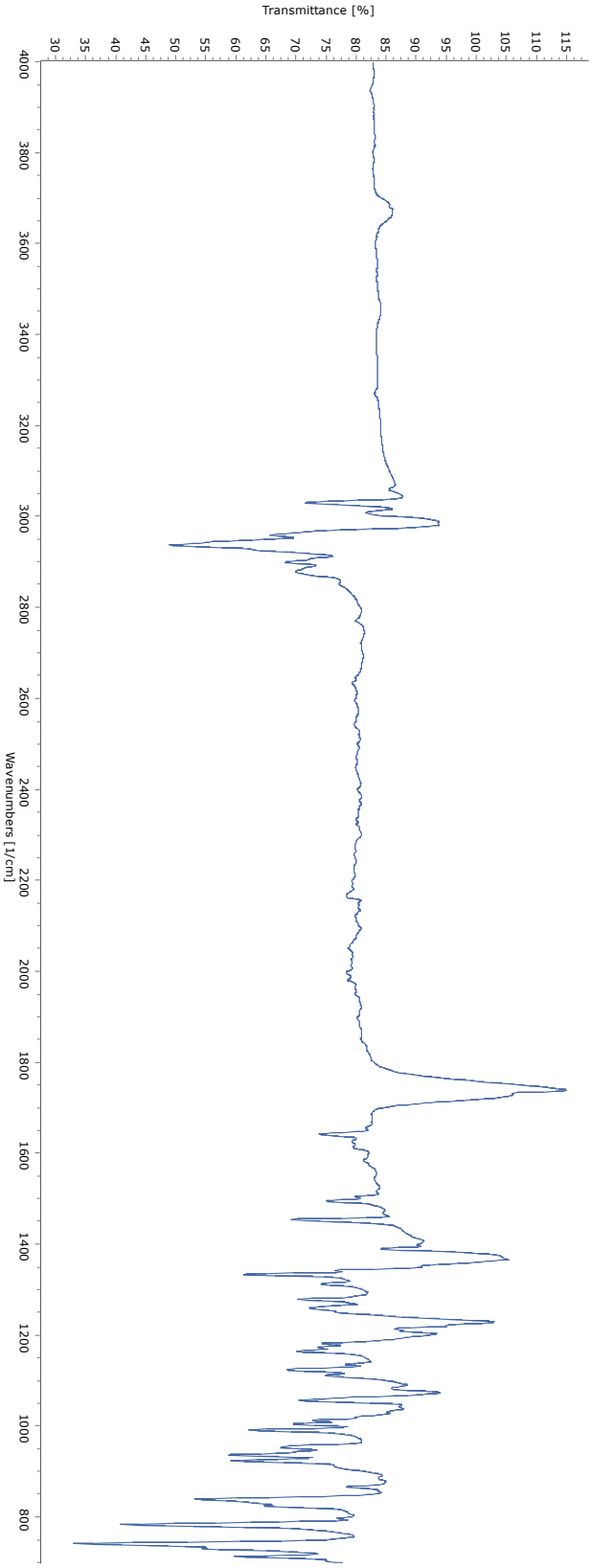
Transmittance [%]
Wavenumbers [1/cm]

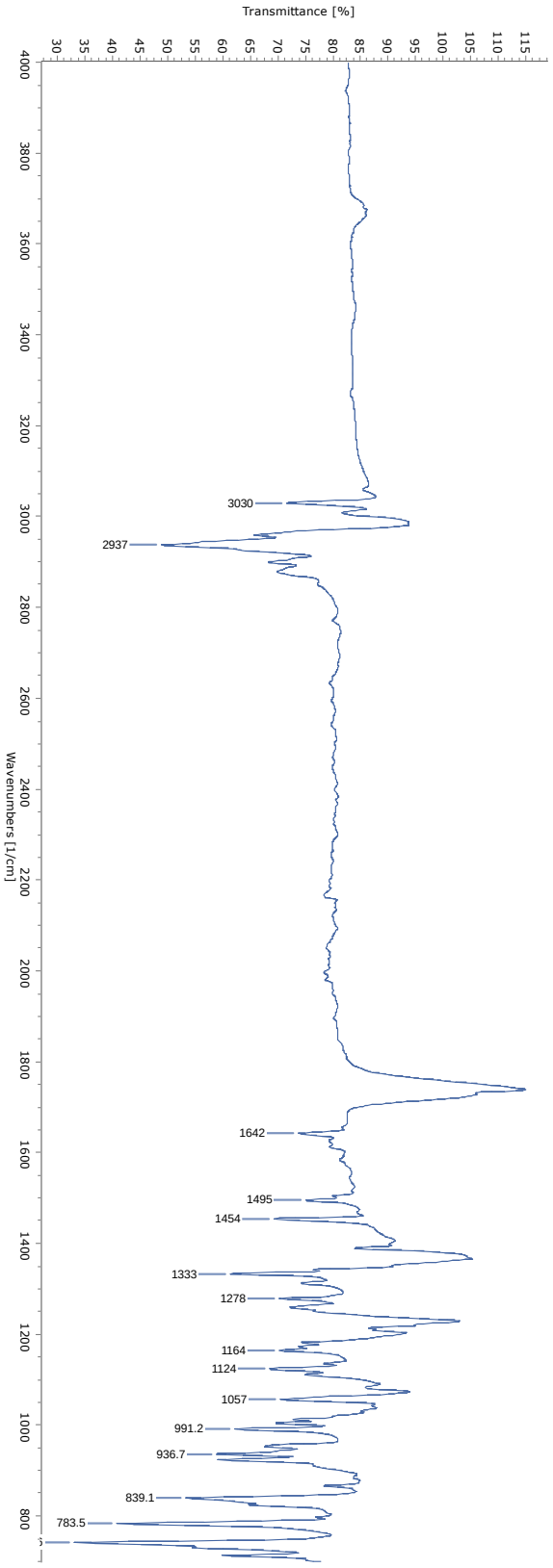
Transmittance [%]
Wavenumbers [1/cm]
3030
2937
1642
1495
1454
1333
1278
1164
1124
1057
991.2
936.7
839.1
783.5

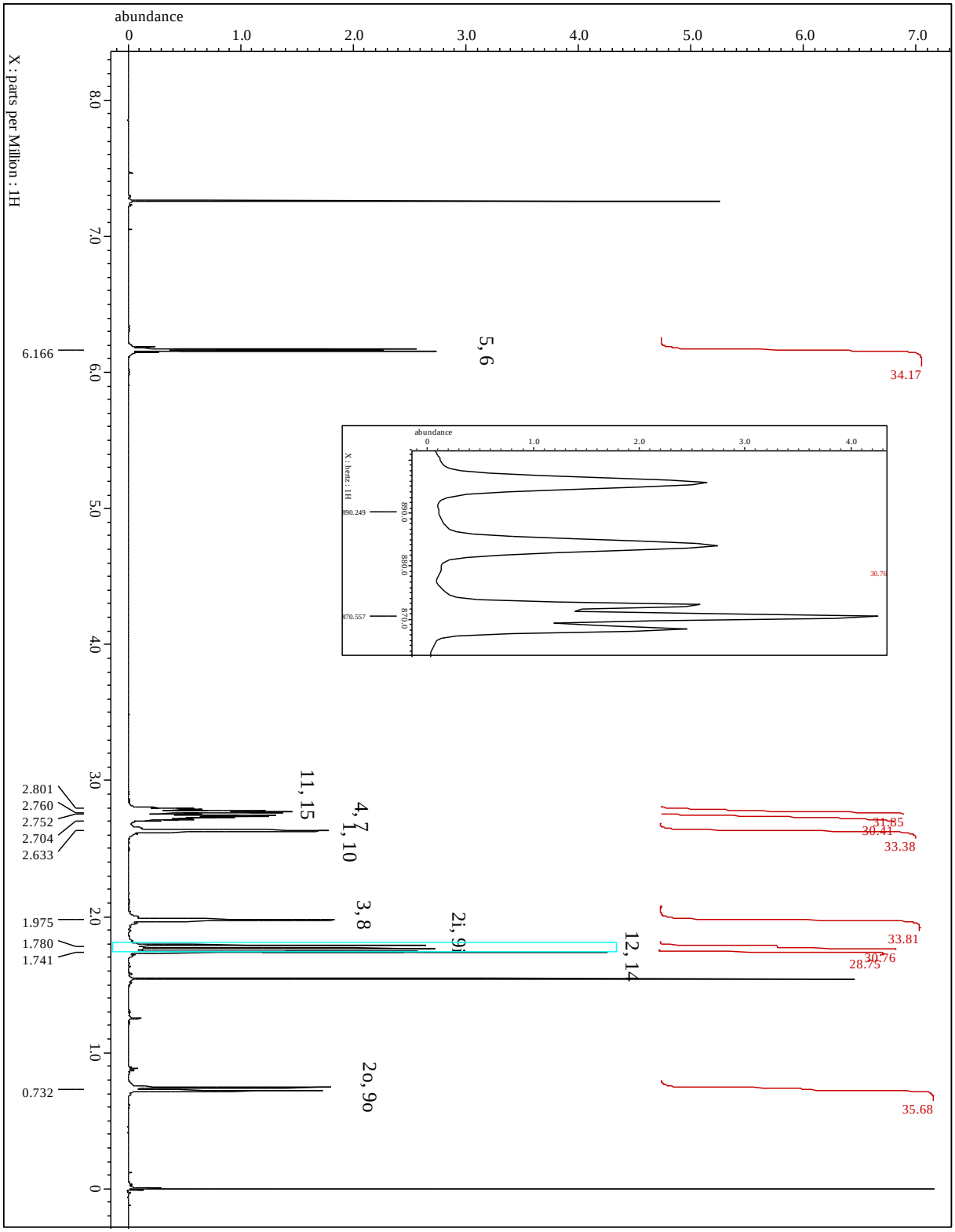
abundance
X : parts per Million : 1H
6.166
5, 6
34.17
2.801
2.760
2.752
2.704
2.633
11, 15
4, 7
1, 10
31.85
30.41
33.38
1.975
1.780
1.741
3, 8
2i, 9i
12, 14
33.81
30.76
28.75
0.732
2o, 9o
35.68
abundance
X : hertz : 1H
890.249
870.557
30.76

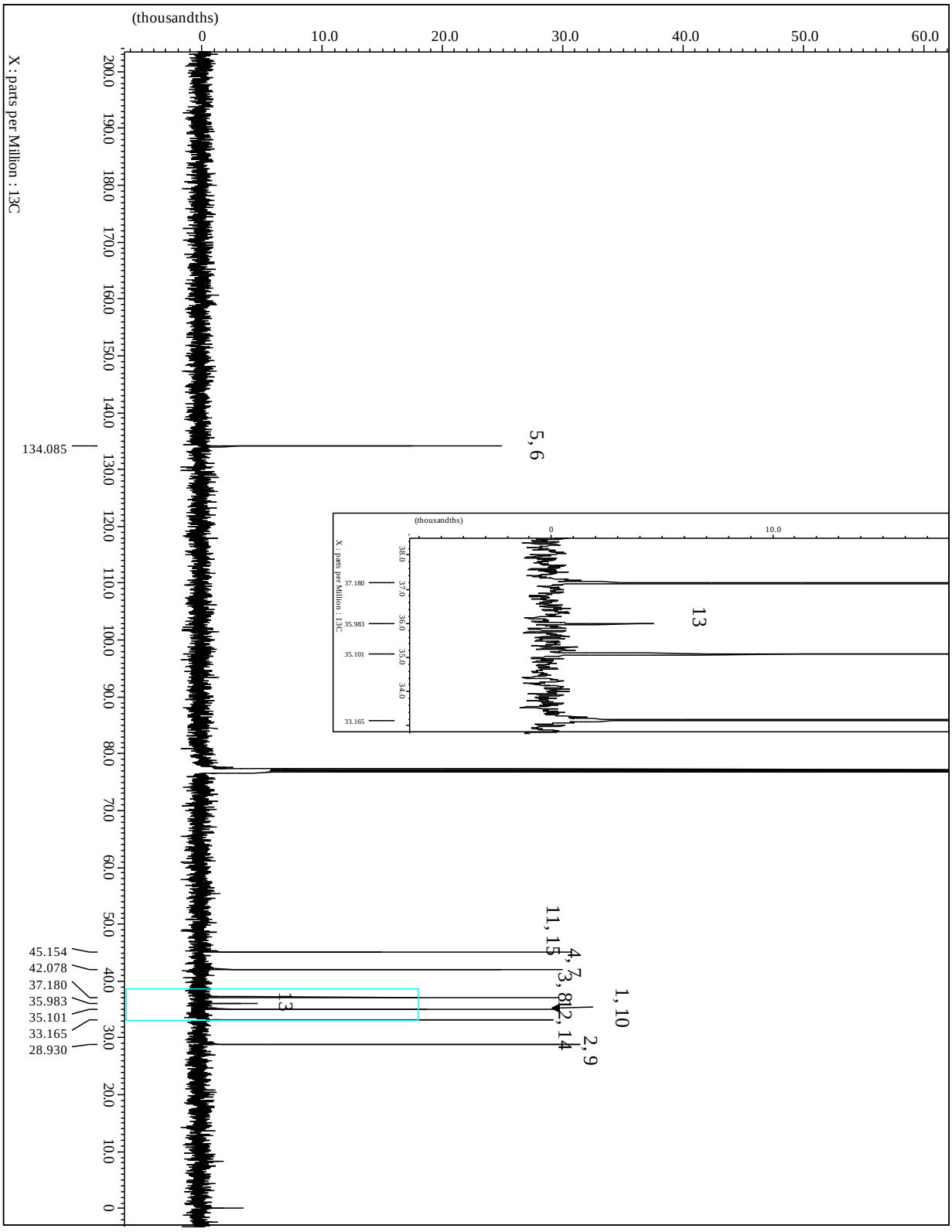
(thousandths)
0
10.0
20.0
30.0
40.0
50.0
60.0
X : parts per Million : 13C
200.0
190.0
180.0
170.0
160.0
150.0
140.0
130.0
120.0
110.0
100.0
90.0
80.0
70.0
60.0
50.0
40.0
30.0
20.0
10.0
0
134.085
45.154
42.078
37.180
35.983
35.101
33.165
28.930
5, 6
11, 15
4, 7
3, 8
12, 14
2, 9
1, 10
13
(thousandths)
0
10.0
X : parts per Million : 13C
38.0
37.0
36.0
35.0
34.0
37.180
35.983
35.101
33.165
13

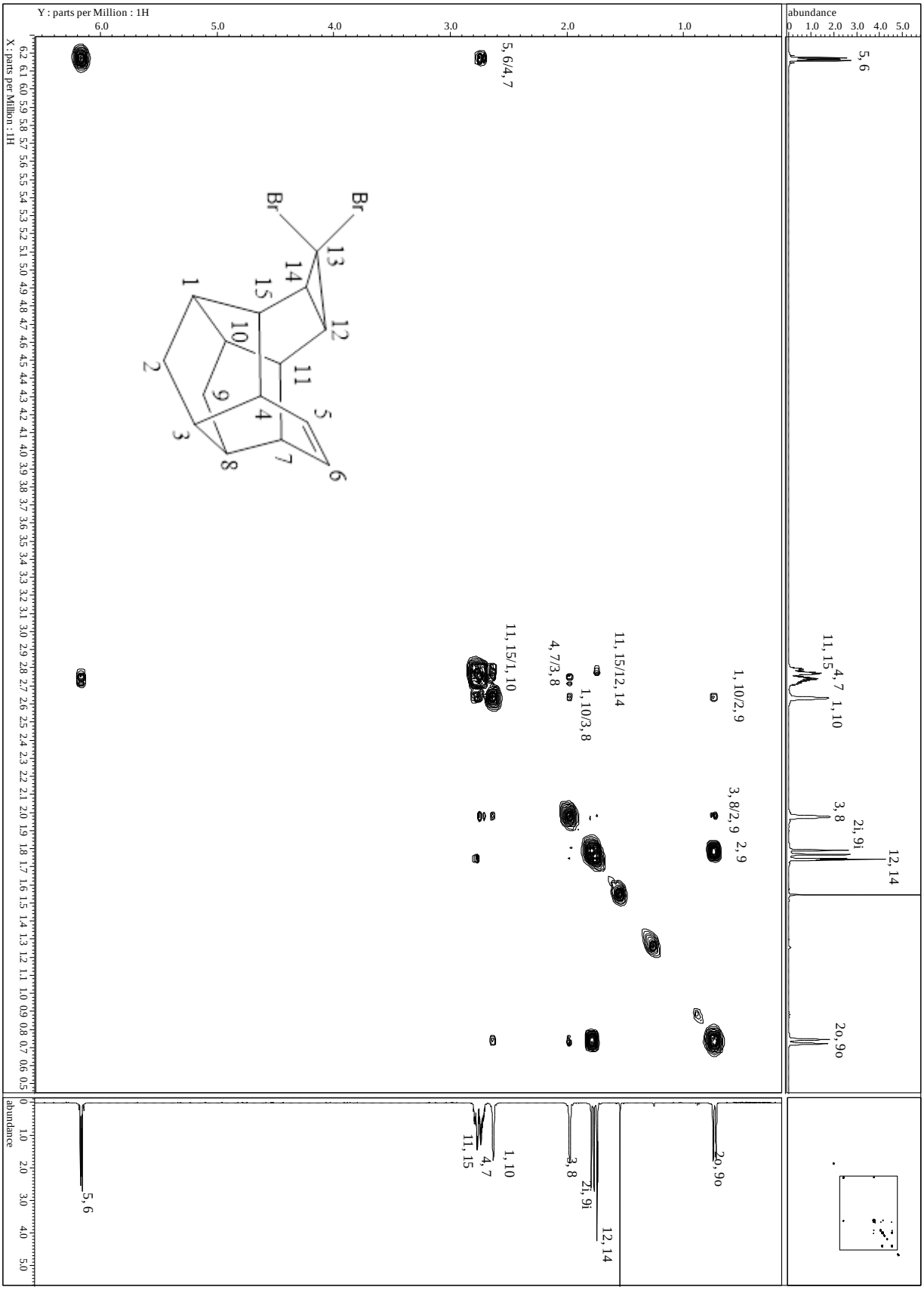
Y : parts per Million : 1H
X : parts per Million : 1H
abundance
5, 6
11, 15
4, 7
1, 10
3, 8
2i, 9i
12, 14
2o, 9o
1, 10/2, 9
3, 8/2, 9
2, 9
11, 15/12, 14
1, 10/3, 8
4, 7/3, 8
11, 15/1, 10
5, 6/4, 7
Br
Br
1
2
3
4
5
6
7
8
9
10
11
12
13
14
15

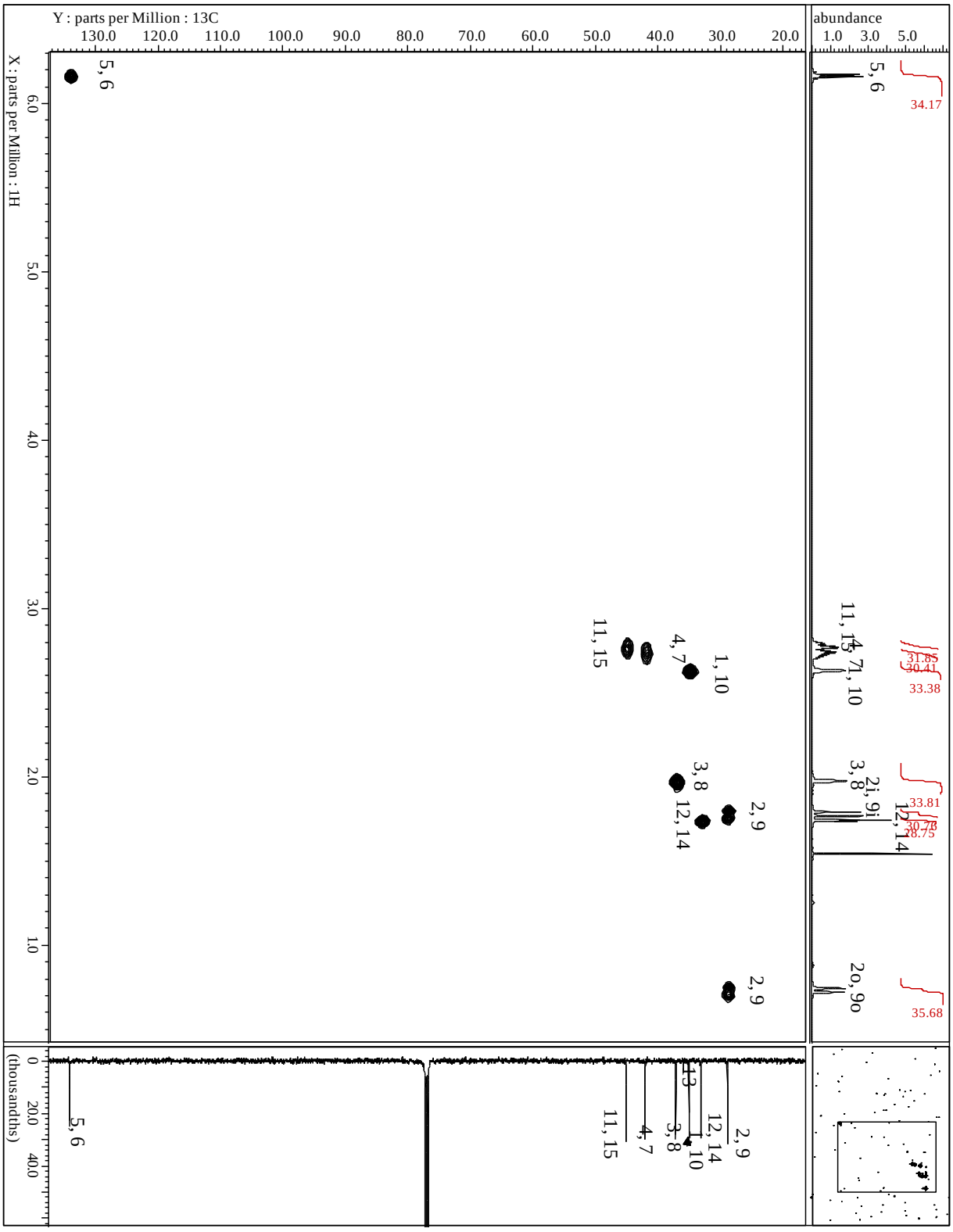
Y : parts per Million : 13C
X : parts per Million : 1H
abundance
(thousandths)
5, 6
34.17
11, 15
4, 7
1, 10
31.85
30.41
33.38
3, 8
2i, 9i
12, 14
33.81
30.78
28.75
2, 9
2o, 9o
35.68
13

5.3.3 Bis Carbene adducts **41a-d**

(5R,7S)-Heptacyclo[9.5.0.0^{3,9}.0^{4,16}.0^{5,7}.0^{8,12}.0^{13,15}]hexadecane (41a)

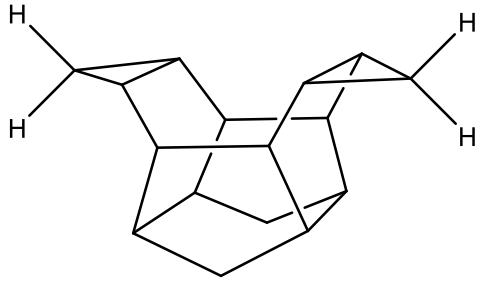

$C_{16}H_{20}$ (212) , R_f = 0.85 by SiO_2-TLC; visualized by vanillin stain

MP = 178.3 – 179.6 °C ($CDCl_3$)

IR(AT-IR): $\tilde{\nu}$ = 3068 (w, C-H), 3001 (m, C-H), 2947 (s, C-H), 2874 (m, C-H), 1450 (m, C-C), 1227, 1103, 1043, 1016, 809 cm^{-1}.

^{1}H-NMR ($CDCl_3$, 500 MHz): δ= 2.25 (4H, s, H-4, 8, 12, 16), 2.00 (4H, s, H-1, 3, 9, 11), 1.55 (2H, d, H-2i, 10i), 1.05 (4H, s, H-5, 7, 13, 15), 0.48 (2H, d, H-2o, 10o), 0.41-0.36 (1H, m, H-6, 14), 0.32-0.29 (1H, m, H-6, 14) ppm;

$^2J_{\text{H-2i, -2o}} = {}^2J_{\text{H-10i, -10o}}$ =11.6 $^2J_{\text{H6u-6d}}$ =4.6 Hz.

^{13}C-NMR ($CDCl_3$, 100.7 MHz): δ= 39.50 (C-4, 8, 12, 16), 36.72 (C-1, 3, 9, 11), 27.27 (C-2, 10), 12.07 (C-5, 7, 13, 15), 5.49 (C-6, 14) ppm.

MS(EI, 70 eV): *m/z* (%) = 212 ($M^{\cdot+}$, 10.5), 197 (8.6), 183 (9.4), 171 (7.9), 169 (13.3), 157 (7.8), 156 (10.0), 155 (14.5), 145 (10.9), 144 (10.7), 143 (21.5), 142 (13.9), 141 (18.5), 132 (18.0), 131 (29.0), 130 (29.3), 129 (43.1), 128 (26.9), 119 (11.1), 118 (15.5), 117 (40.8), 116 (15.5), 115 (31.6), 107 (9.3), 106 (12.0), 105 (31.1), 104 (19.5), 103 (11.6), 93 (16.0), 92 (24.4), 91 (100.0), 80 (8.3), 79 (39.5), 78 (21.9), 77 (40.8), 67 (12.4), 66 (7.9), 65 (20.4), 53 (9.7), 51 (9.9).

Spectra

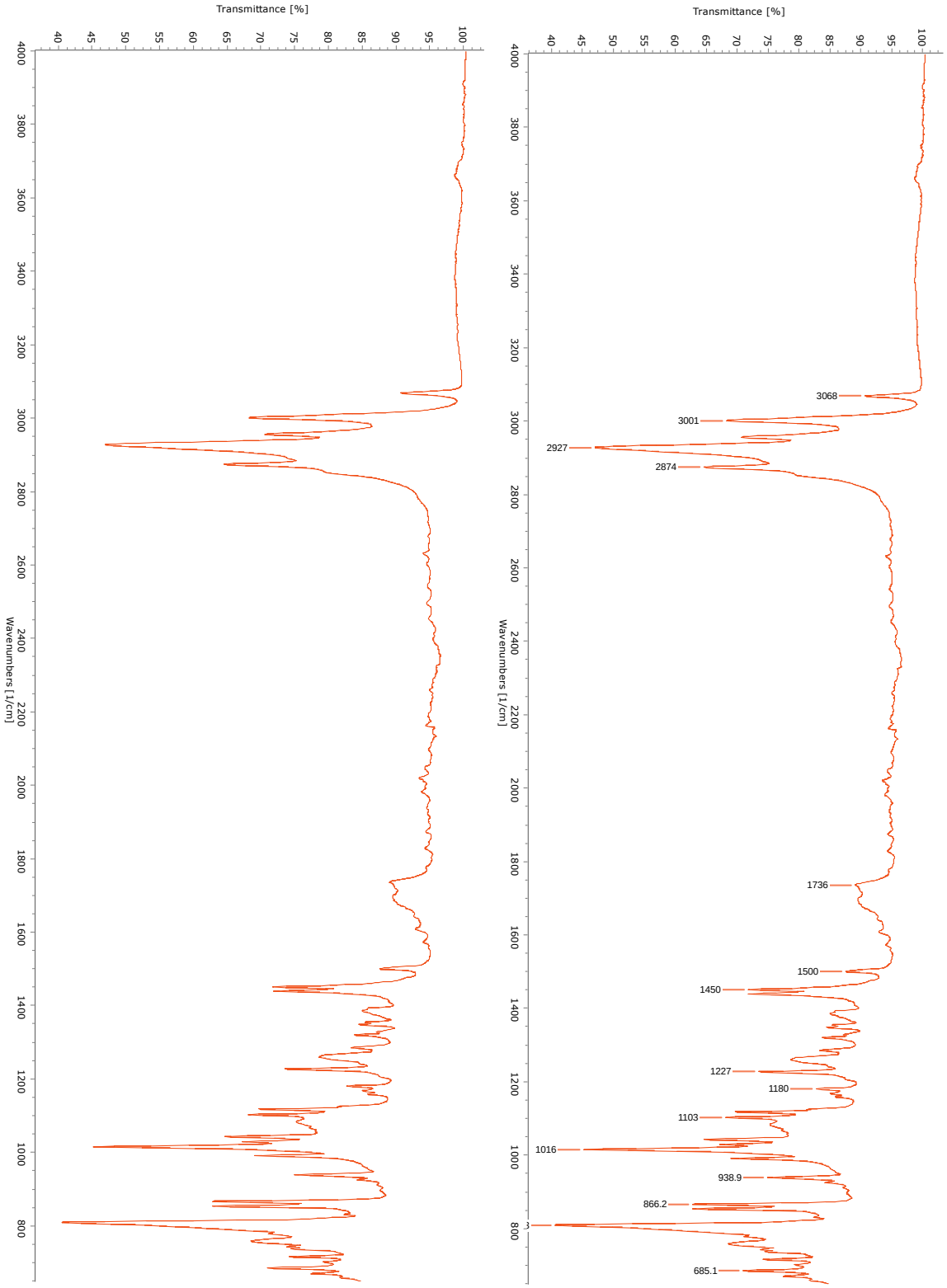
Transmittance [%]
Wavenumbers [1/cm]
3068
3001
2927
2874
1736
1500
1450
1227
1180
1103
1016
938.9
866.2
685.1

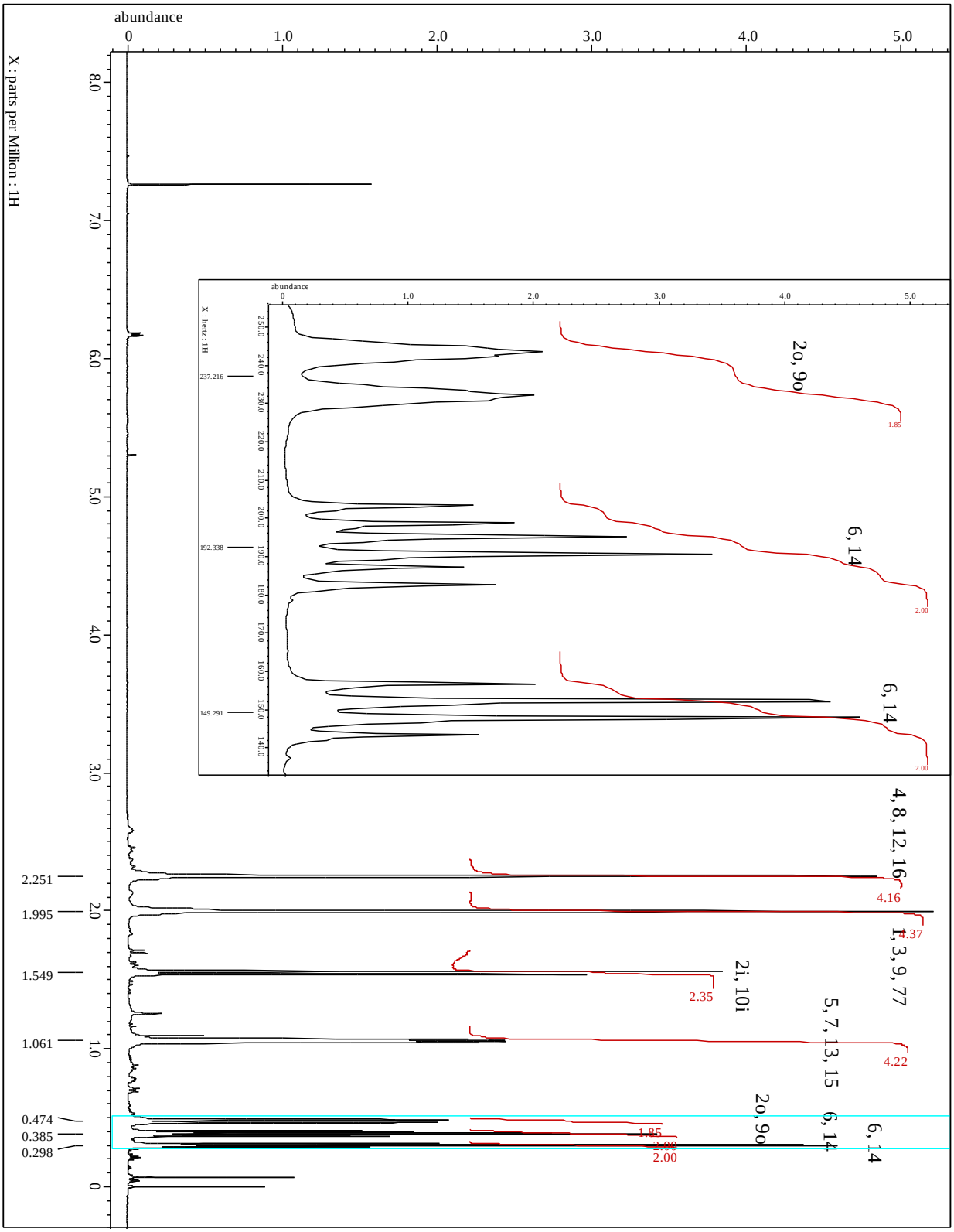
abundance
X : parts per Million : 1H
2.251
1.995
1.549
1.061
0.474
0.385
0.298
4, 8, 12, 16
4.16
1, 3, 9, 77
4.37
2i, 10i
2.35
5, 7, 13, 15
4.22
2o, 9o
1.85
6, 14
2.00
6, 14
2.00
abundance
X : hertz : 1H
237.216
192.338
149.291
2o, 9o
1.85
6, 14
2.00
6, 14
2.00

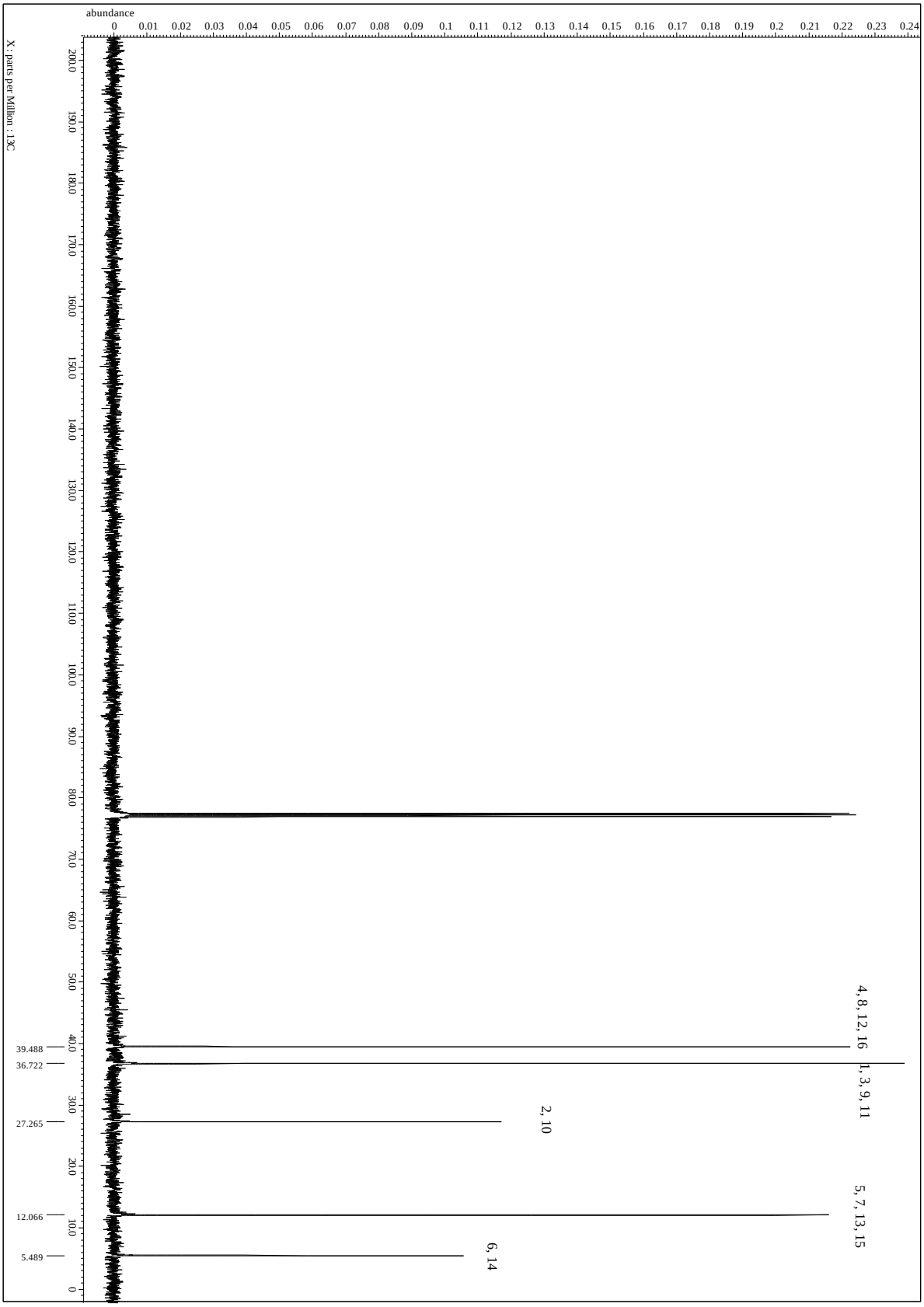
abundance
0 0.01 0.02 0.03 0.04 0.05 0.06 0.07 0.08 0.09 0.1 0.11 0.12 0.13 0.14 0.15 0.16 0.17 0.18 0.19 0.2 0.21 0.22 0.23 0.24
X : parts per Million : 13C
200.0 190.0 180.0 170.0 160.0 150.0 140.0 130.0 120.0 110.0 100.0 90.0 80.0 70.0 60.0 50.0 40.0 30.0 20.0 10.0 0
39.488
36.722
27.265
12.066
5.489
4, 8, 12, 16
1, 3, 9, 11
2, 10
5, 7, 13, 15
6, 14

(5R,7S)-6,6,14,14-tetrafluoroheptacyclo[9.5.0.0^{3,9}.0^{4,16}.0^{5,7}.0^{8,12}.0^{13,15}]hexadecane (41b)

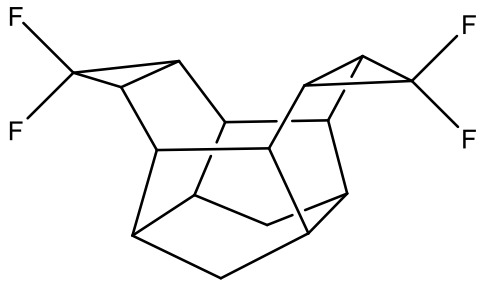

$C_{16}H_{16}F_4$ (284) , R_f = 0.55 by SiO_2-TLC; visualized by UV or vanillin stain

MP = 137.4-137.8 °C ($CDCl_3$)

IR (AT-IR): $\tilde{\nu}$ = 3685, 2988 (m, C-H), 2936 (m, C-H), 2903 (m, C-H), 1466, 1130, 1055, 775 cm^{-1}.

^{1}H-NMR ($CDCl_3$, 500 MHz): δ= 2.37 (8H, s, H-1, -3, -4, -8, -9, -11, -12, -16), 1.71-1.69 (2H, d, H-2i, -10i), 1.71-1.68 (4H, d, H-5, -7, -13, -15), 0.53 (2H, d, H-2o, -10o) ppm;

$^2J_{\text{H-2i, -2o}} = {}^2J_{\text{H-10i, -10o}}$; $^2J_{\text{H5, F}}$ = 16.5 Hz.

^{19}F-NMR ($CDCl_3$, 100.7 MHZ): ($CDCl_3$, 100.7 MHz): δ= -119.3 (2F, dt), -149.3 (2F, d) ppm.

^{13}C-NMR ($CDCl_3$, 100.7 MHz): δ= 116.0 (t, C-6, -14), 36.0 (d, C-4, -8, -12, -16), 35.0 (d, C-1, -3, -9, -11), 28.1 (C-2, -10), 22.4 (dd, C-5, 7, 13, 15) ppm.

$^1J_{\text{C-6, F}}$ = 288.5 kHz

MS(EI, 70 eV): *m/z* (%) = 284 ($M^{\cdot+}$, 5.0), 283 (2.4), 269 (11.6), 207 (7.8), 205 (9.8), 193 (11.9), 191 (9.3), 185 (8.6), 183 (12.4), 181 (9.8), 180 (8.1), 179 (15.3), 178 (8.2), 177 (12.1), 173 (8.5), 168 (20.1), 167 (21.0), 166 (15.4), 165 (27.8), 164 (11.5), 161 (9.6), 160 (8.5), 159 (22.5), 155 (13.2), 154 (15.7), 153 (27.9), 152 (8.8), 151 (9.9), 148 (13.7), 147 (38.8), 146 (27.1), 143 (15.1),

142 (22.8), 141 (51.6), 140 (32.0), 135 (22.1), 134 (11.8), 133 (28.6), 130 (7.9), 129 (27.1), 128 (34.2), 127 (99.0), 123 (19.9), 122 (14.9), 117 (21.5), 116 (20.0), 115 (49.7), 114 (9.8), 110 (8.9), 109 (49.5), 105 (16.3), 104 (13.2), 103 (31.1), 101 (19.5), 97 (14.8), 96 (11.6), 95 (10.0), 93 (7.6), 92 (17.5), 91 (100.0), 90 (7.5), 89 (10.9), 83 (14.9), 79 (35.4), 78 (29.8), 77 (75.5), 75 (11.1), 67 (8.4), 66 (11.0), 65 (21.5), 63 (10.8), 53 (9.0), 52 (7.7), 51 (28.8).

Spectra

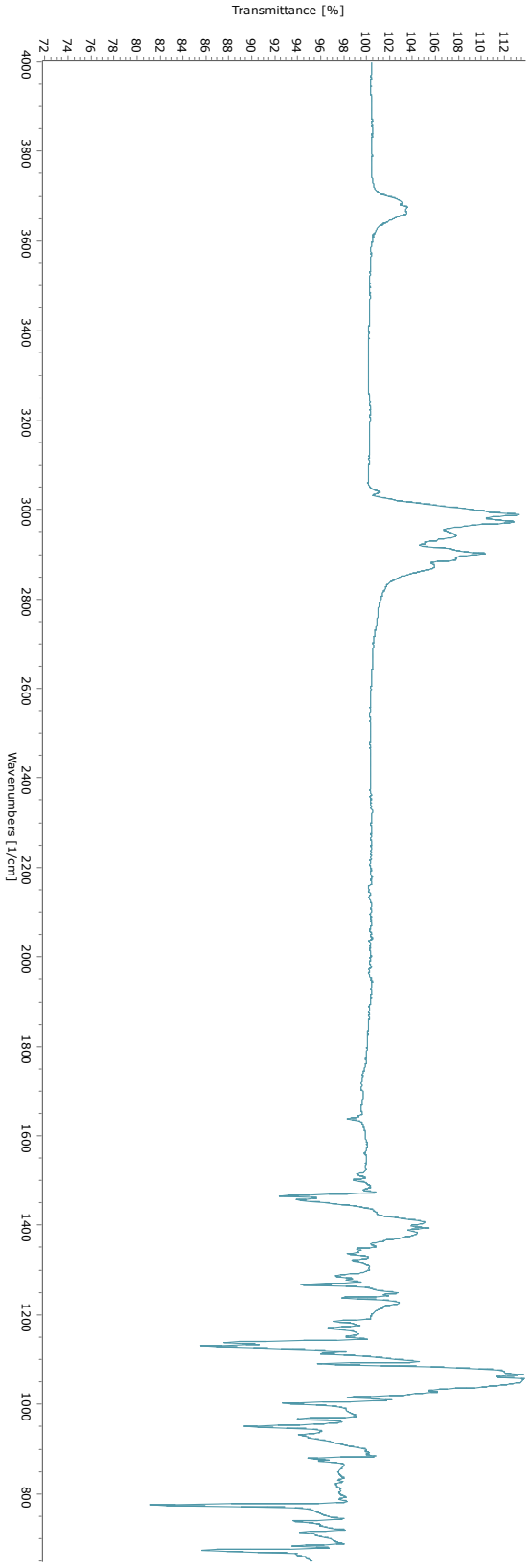
Transmittance [%]
Wavenumbers [1/cm]

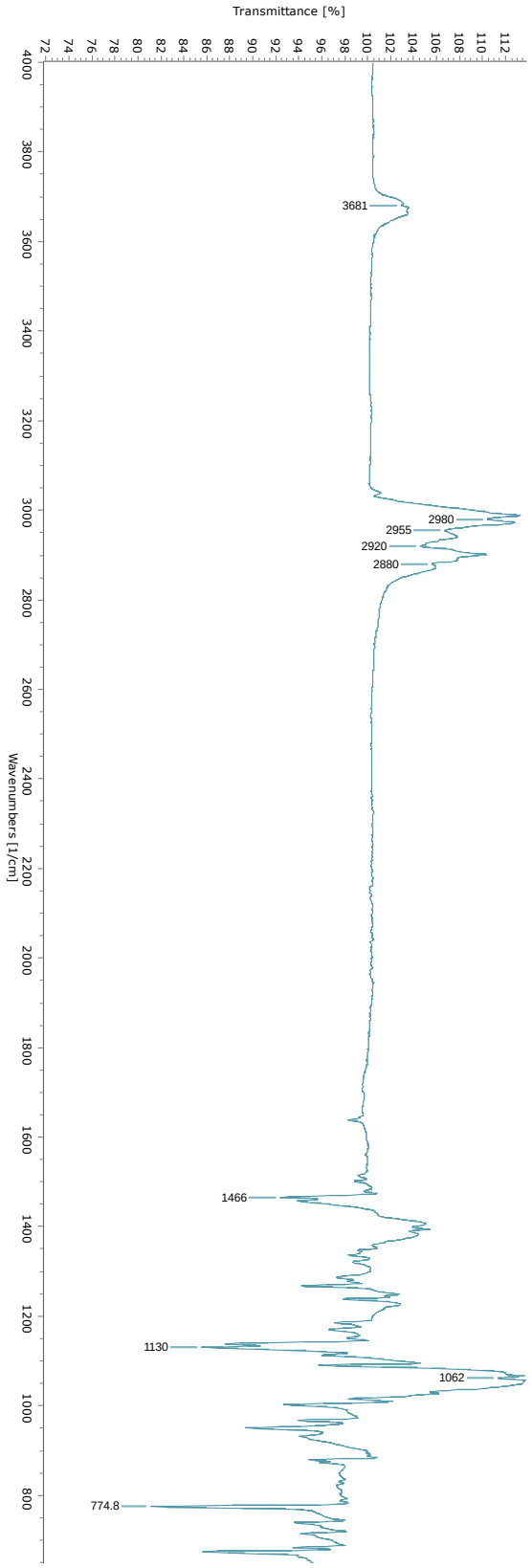
Transmittance [%]
Wavenumbers [1/cm]
3681
2980
2955
2920
2880
1466
1130
1062
774.8

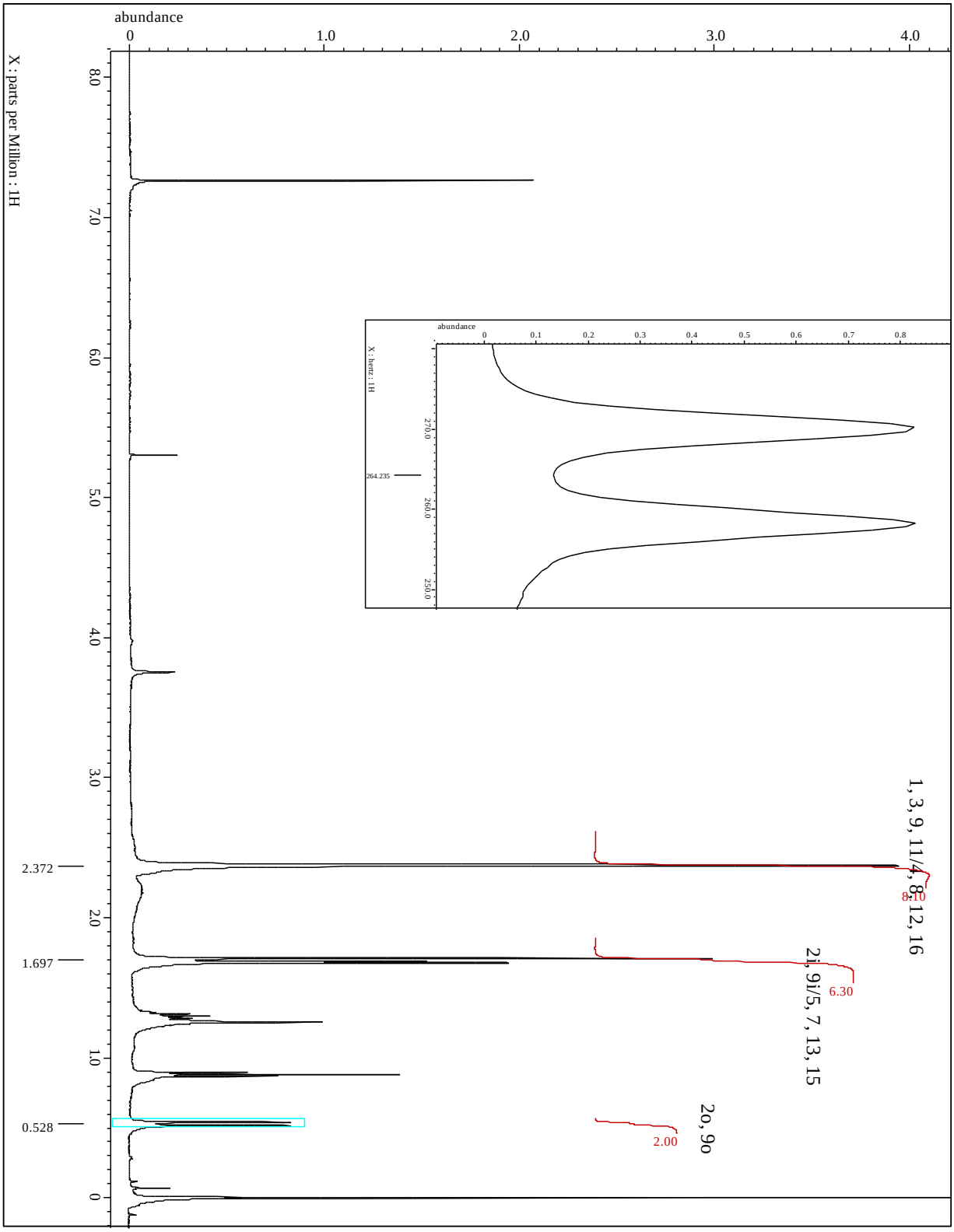
abundance
0
1.0
2.0
3.0
4.0
X : parts per Million : 1H
8.0
7.0
6.0
5.0
4.0
3.0
2.0
1.0
0
2.372
1.697
0.528
abundance
X : hertz : 1H
264.235
1, 3, 9, 11/4, 8, 12, 16
8.10
2i, 9i/5, 7, 13, 15
6.30
20, 9o
2.00

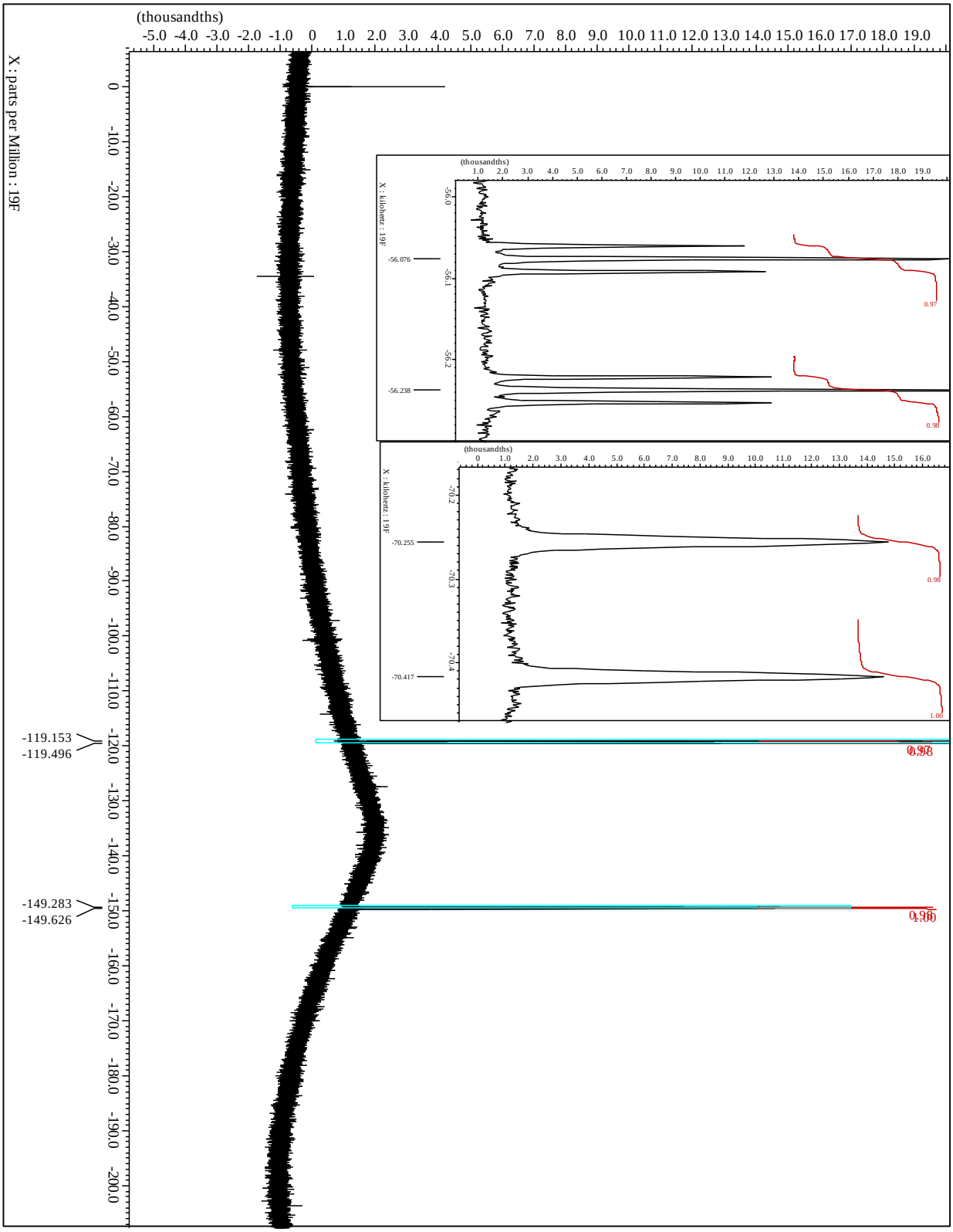
(thousandths)
X : parts per Million : 19F
-119.153
-119.496
-149.283
-149.626
X : kilohertz : 19F
-56.076
-56.238
0.97
0.98
-70.255
-70.417
0.98
1.00

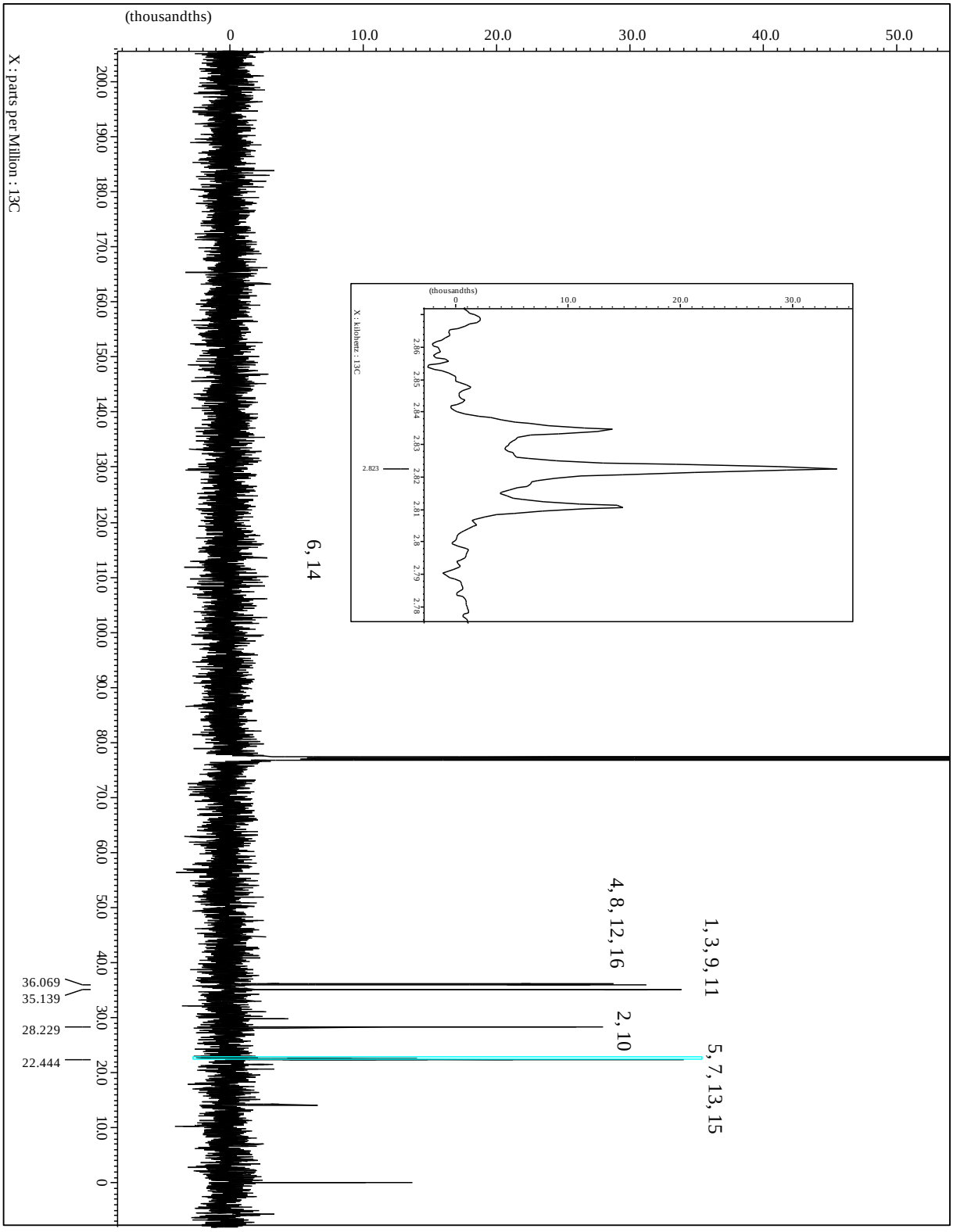
(thousandths)
0
10.0
20.0
30.0
40.0
50.0
X : parts per Million : 13C
200.0
190.0
180.0
170.0
160.0
150.0
140.0
130.0
120.0
110.0
100.0
90.0
80.0
70.0
60.0
50.0
40.0
30.0
20.0
10.0
0
36.069
35.139
28.229
22.444
6, 14
4, 8, 12, 16
1, 3, 9, 11
2, 10
5, 7, 13, 15
(thousandths)
0
10.0
20.0
30.0
X : kilohertz : 13C
2.86
2.85
2.84
2.83
2.823
2.82
2.81
2.8
2.79
2.78

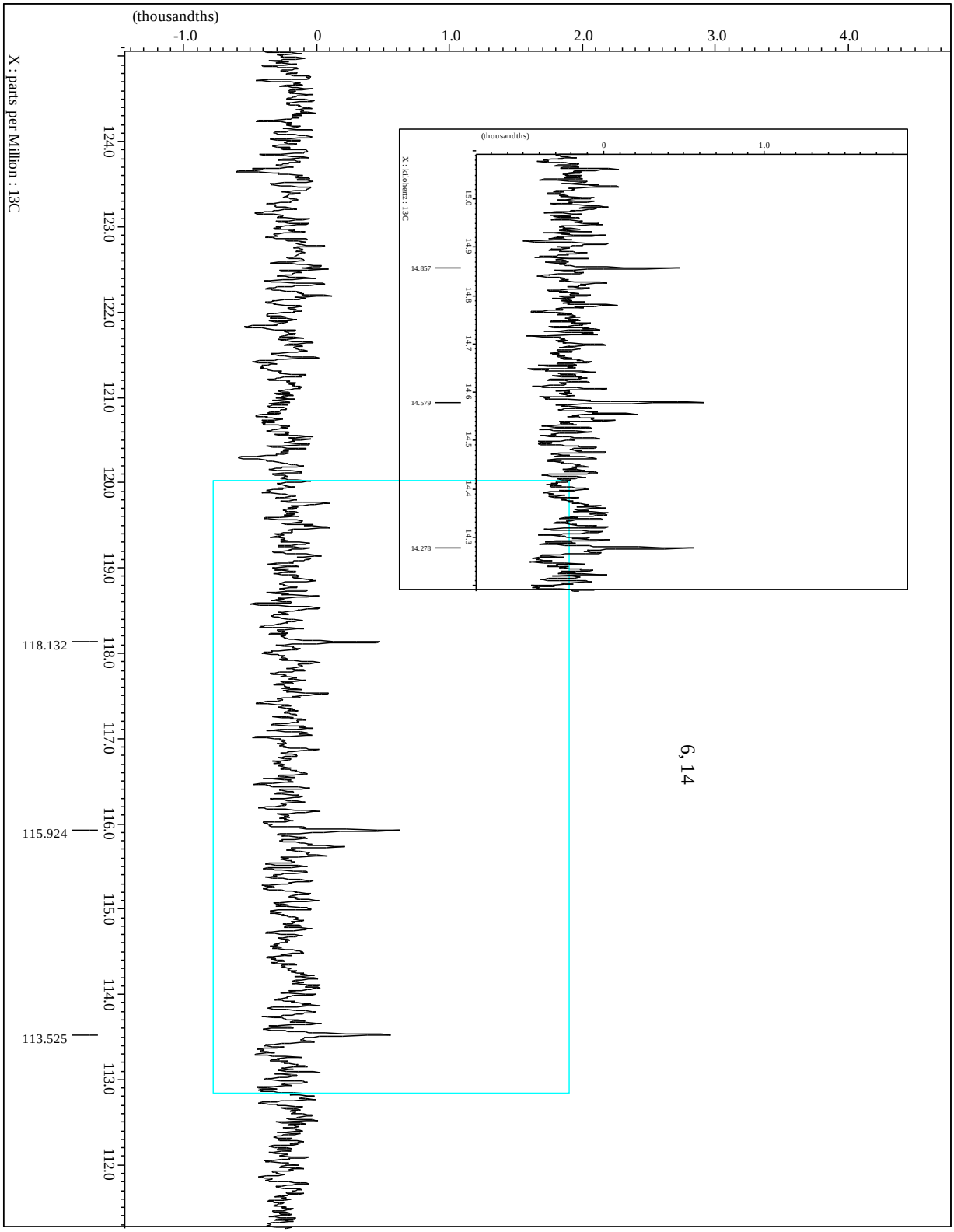
(thousandths)
-1.0
0
1.0
2.0
3.0
4.0
X : parts per Million : 13C
124.0
123.0
122.0
121.0
120.0
119.0
118.0
117.0
116.0
115.0
114.0
113.0
112.0
118.132
115.924
113.525
(thousandths)
0
1.0
X : kilohertz : 13C
15.0
14.9
14.8
14.7
14.6
14.5
14.4
14.3
14.857
14.579
14.278
6, 14

(5R,7S)-6,6,14,14-tetrachloroheptacyclo[9.5.0.0^{3,9}.0^{4,16}.0^{5,7}.0^{8,12}.0^{13,15}]hexadecane (41c)

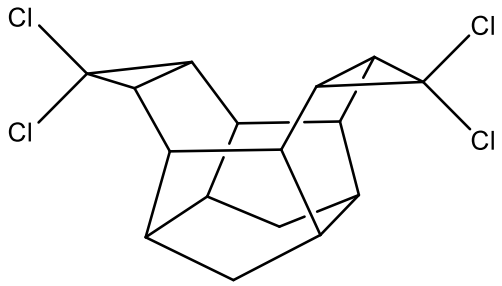

$C_{16}H_{16}Cl_4$ (348) , R_f = 0.40 by SiO_2-TLC; visualized by UV or vanillin stain

MP = 237.1-239.5 °C ($CHCl_3$)

IR (AT-IR): $\tilde{\nu}$ = 2961 (m, C-H), 1454 (w, C-C), 1261, 1140, 933, 874, 785, 717 cm^{-1}.

^{1}H-NMR ($CDCl_3$, 500 MHz): δ= 2.63 (s_{app}, 4H, H-4, -8, -12, -16), 2.56 (s_{app}, 4H, H-1, -3, -9, -11), 1.86 (s_{app}, 4H, H-5, -7, -13, -15), 1.69 (d, 2H, H-2i, -10i), 0.53 (d, 2H, H-2o, -10o) ppm;

$^2J_{\text{H-2i, H-2o}} = {}^2J_{\text{H10i, H10o}}$ = 12.0 Hz.

^{13}C-NMR ($CDCl_3$, 100.7 MHz): δ= 66.2 (C-6, -14), 38.3 (C-4, -8, -12, -16), 34.3 (C-1, -3, -9, -11), 31.6 (C-5, -7, -13, -15), 28.3 (C-2, -10) ppm.

MS(EI, 70 eV): *m/z* (%) = 355 ($M^{\cdot+}$+7, 0.4), 352 ($M^{\cdot+}$+4, 0.5), 351 ($M^{\cdot+}$+3, 0.2), 350 ($M^{\cdot+}$+2, 2.5), 348 ($M^{\cdot+}$, 3.2), 317 (10.0), 315 (33.0), 314 (10.5), 313 (34.1), 281 (18.7), 279 (27.7), 278 (10.1), 277 (45.0), 249 (7.7), 243 (10.0), 241 (26.8), 235 (8.4), 227 (10.2), 225 (16.9), 223 (9.8), 215 (8.4), 213 (17.4), 212 (10.7), 211 (17.0), 207 (31.5), 206 (10.3), 205 (18.2), 203 (19.1), 202 (14.8), 201 (22.2), 200 (11.1), 199 (26.4), 197 (15.6), 193 (10.3), 191 (18.7), 190 (11.7), 189 (25.7), 188 (8.1), 187 (19.6), 186 (12.5), 185 (10.4), 179 (18.3), 178 (26.3), 177 (36.3), 176 (30.6), 175 (57.8), 174 (46.7), 173 (35.8), 172 (41.5), 167 (20.3), 166 (16.0), 165 (68.9), 164 (18.0), 163 (51.3), 162 (24.0), 161 (35.3), 160 (11.0), 159 (34.1), 155 (11.9), 154 (10.8), 153 (38.3), 152 (30.3), 151 (41.1), 150

(11.3), 149 (24.4), 147 (10.8), 143 (7.8), 142 (12.1), 141 (52.2), 140 (18.2), 139 (79.5), 138 (32.0), 137 (16.9), 135 (8.2), 131 (8.0), 130 (16.1), 129 (60.8), 128 (65.1), 127 (71.2), 126 (20.9), 125 (91.7), 118 (8.3), 117 (43.4), 116 (24.2), 115 (90.5), 114 (10.0), 113 (29.9), 111 (19.5), 109 (17.2), 105 (25.7), 104 (15.6), 103 (57.5), 102 (31.4), 101 (36.4), 100 (9.2), 99 (28.6), 93 (9.5), 92 (14.2), 91 (100.0), 90 (8.0), 89 (42.7), 88 (8.3), 87 (11.5), 85 (9.6), 83 (9.5), 79 (41.0), 78 (25.6), 77 (88.9), 76 (13.6), 75 (28.6), 73 (20.1), 67 (13.5), 66 (8.3), 65 (31.7), 63 (26.6), 53 (11.7), 52 (7.7), 51 (30.2).

Spectra

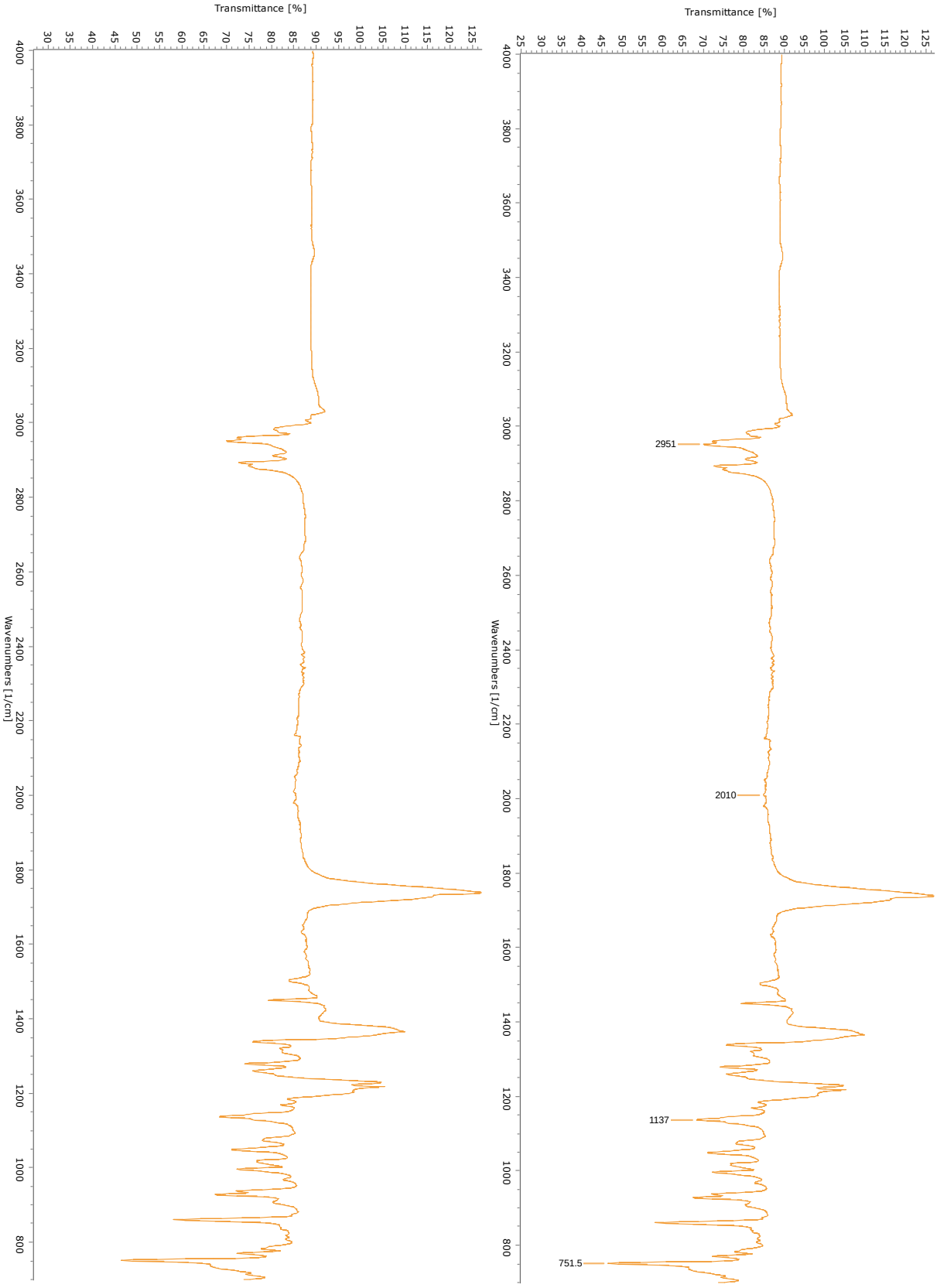
Transmittance [%]
Wavenumbers [1/cm]
2951
2010
1137
751.5

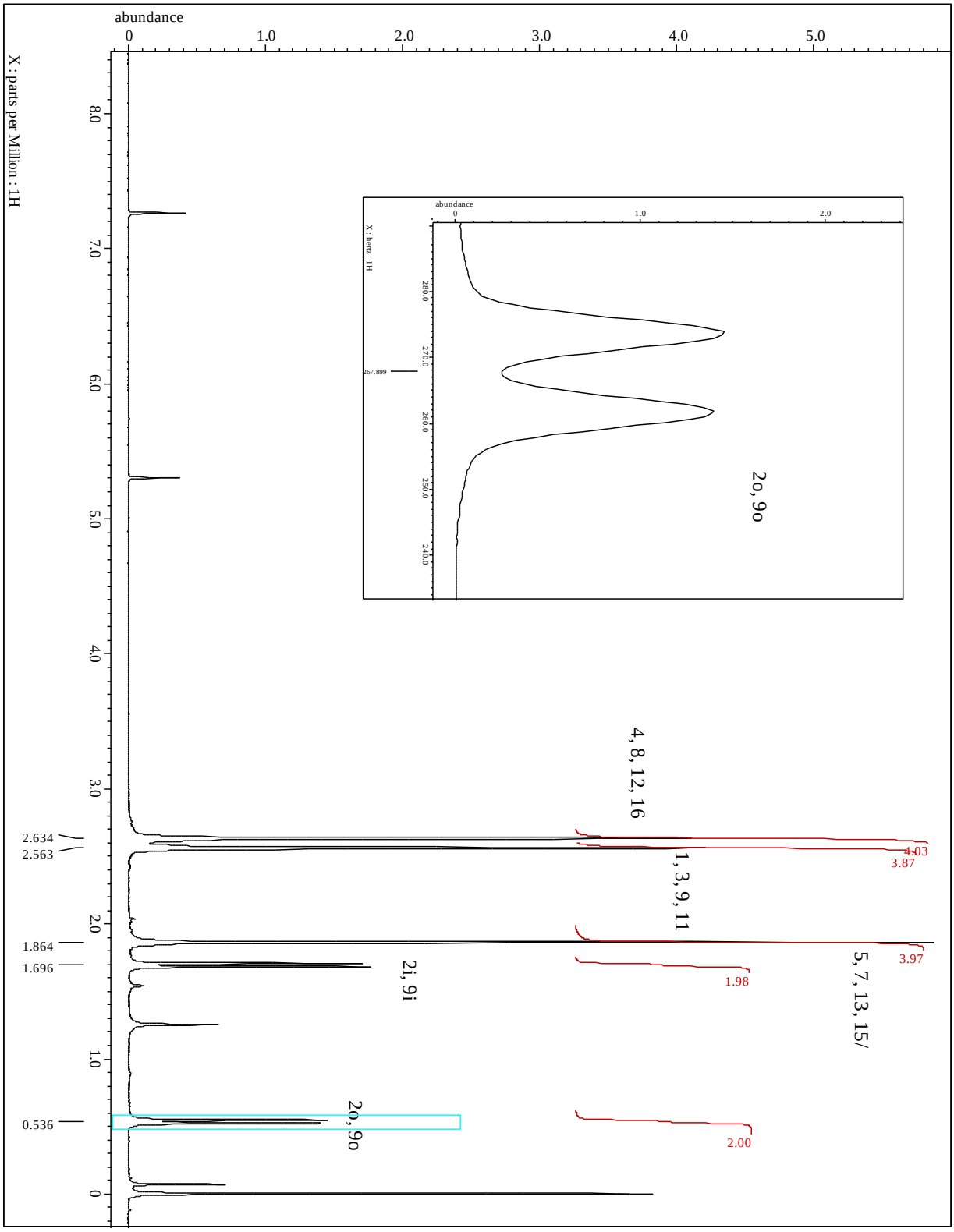
abundance
0
1.0
2.0
3.0
4.0
5.0
X : parts per Million : 1H
8.0
7.0
6.0
5.0
4.0
3.0
2.0
1.0
0
2.634
2.563
1.864
1.696
0.536
4, 8, 12, 16
1, 3, 9, 11
5, 7, 13, 15/
2i, 9i
2o, 9o
4.03
3.87
3.97
1.98
2.00
abundance
X : hertz : 1H
267.899
2o, 9o

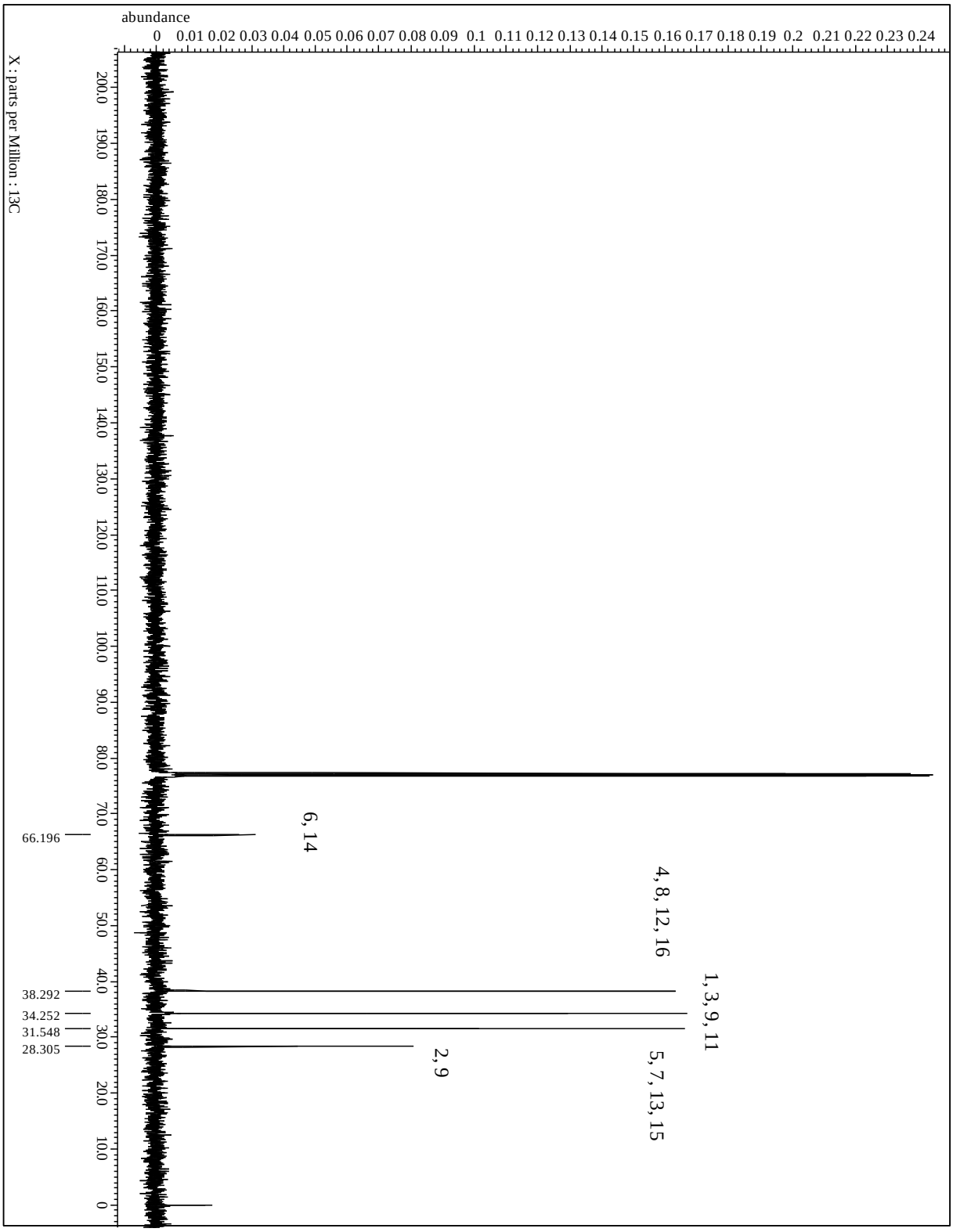
abundance
0 0.01 0.02 0.03 0.04 0.05 0.06 0.07 0.08 0.09 0.1 0.11 0.12 0.13 0.14 0.15 0.16 0.17 0.18 0.19 0.2 0.21 0.22 0.23 0.24
X : parts per Million : 13C
200.0 190.0 180.0 170.0 160.0 150.0 140.0 130.0 120.0 110.0 100.0 90.0 80.0 70.0 60.0 50.0 40.0 30.0 20.0 10.0 0
66.196
38.292
34.252
31.548
28.305
6, 14
4, 8, 12, 16
1, 3, 9, 11
2, 9
5, 7, 13, 15

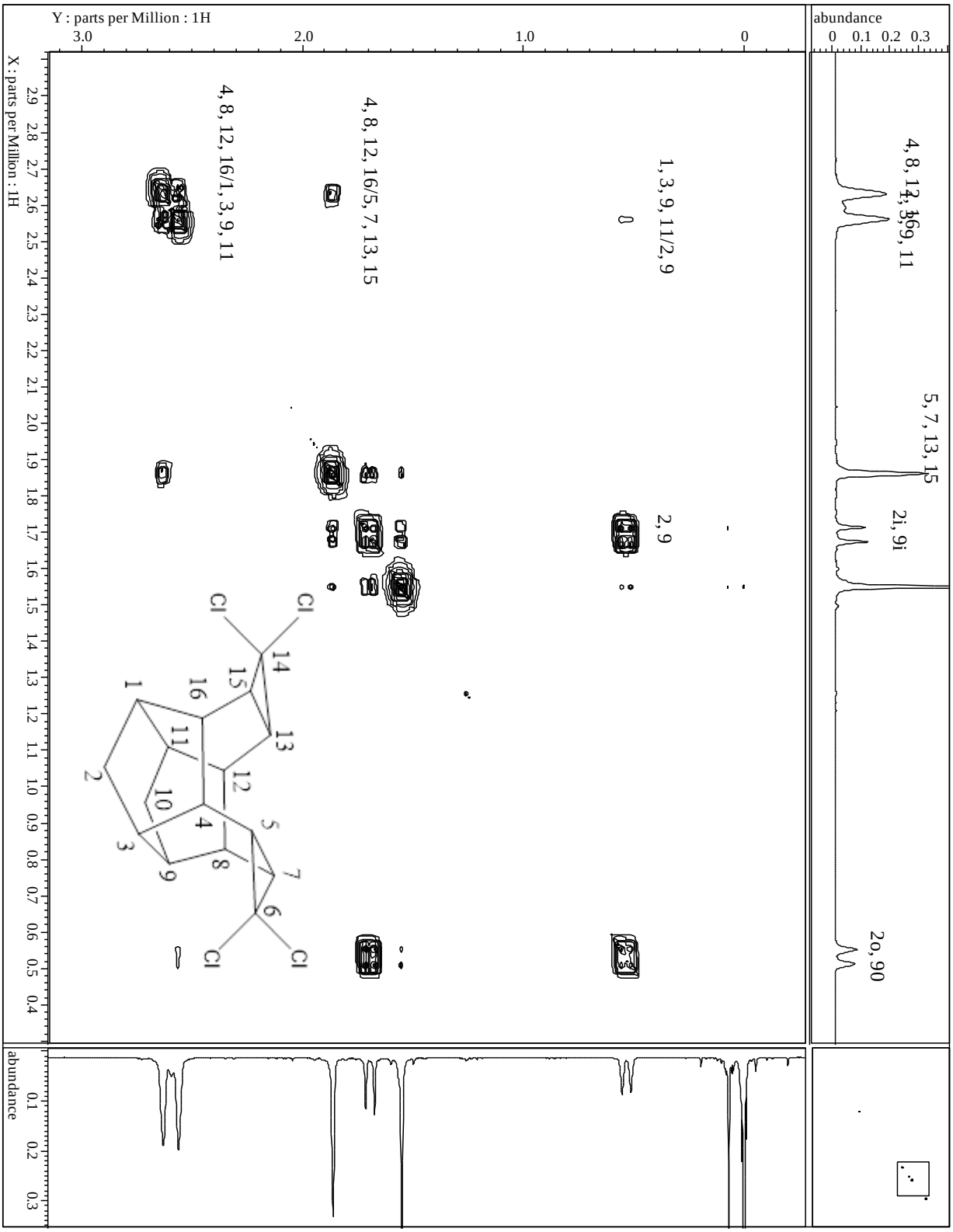
abundance
0 0.1 0.2 0.3
4, 8, 12, 16/5, 7, 13, 15
1, 3, 9, 11/2, 9
4, 8, 12, 16/1, 3, 9, 11
5, 7, 13, 15
2i, 9i
2o, 90
Y : parts per Million : 1H
3.0
2.0
1.0
0
X : parts per Million : 1H
2.9 2.8 2.7 2.6 2.5 2.4 2.3 2.2 2.1 2.0 1.9 1.8 1.7 1.6 1.5 1.4 1.3 1.2 1.1 1.0 0.9 0.8 0.7 0.6 0.5 0.4
Cl
Cl
Cl
Cl
1
2
3
4
5
6
7
8
9
10
11
12
13
14
15
16
abundance
0.1 0.2 0.3

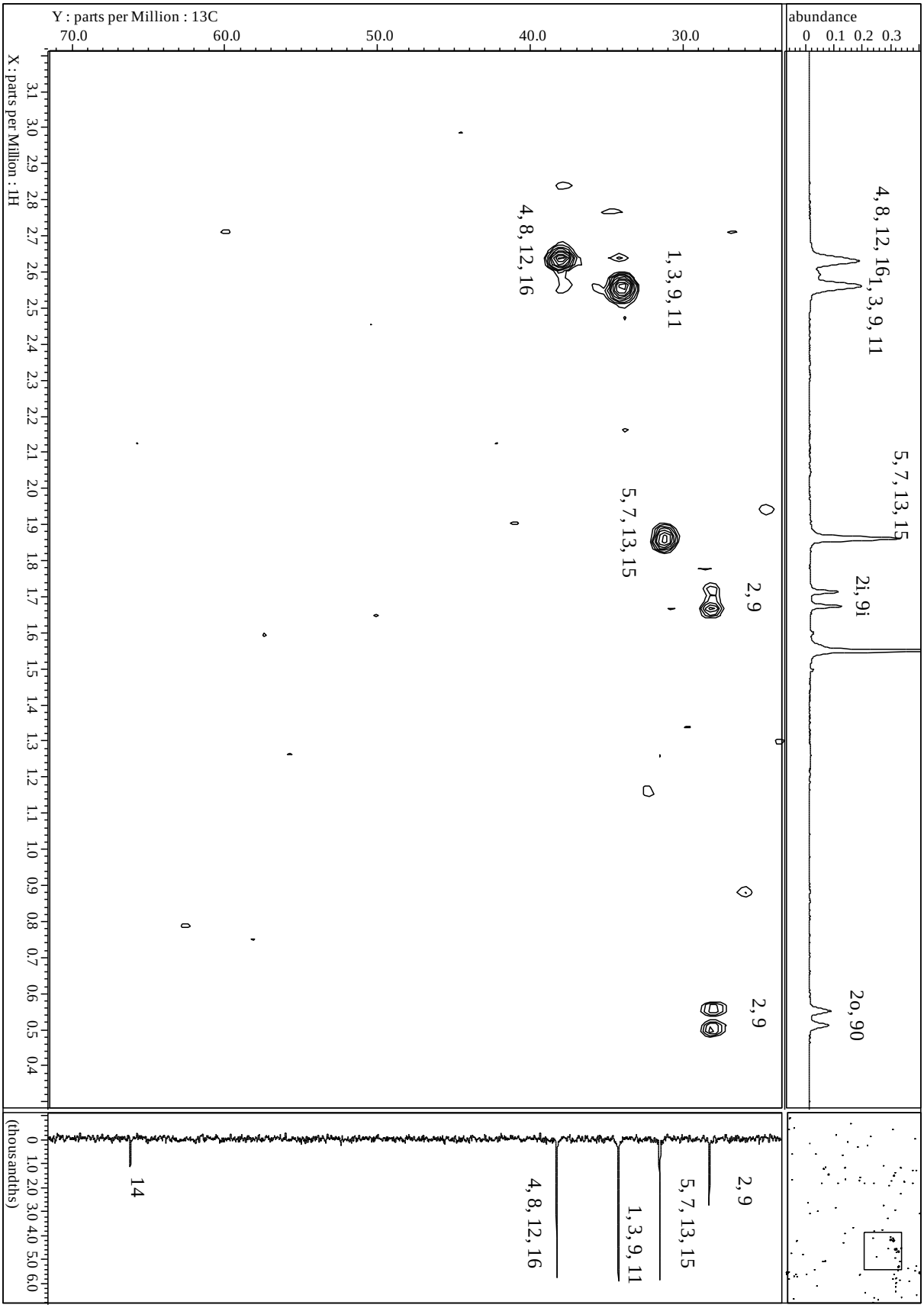
abundance
0 0.1 0.2 0.3
4, 8, 12, 16
1, 3, 9, 11
5, 7, 13, 15
2i, 9i
2o, 90
Y : parts per Million : 13C
70.0 60.0 50.0 40.0 30.0
X : parts per Million : 1H
3.1 3.0 2.9 2.8 2.7 2.6 2.5 2.4 2.3 2.2 2.1 2.0 1.9 1.8 1.7 1.6 1.5 1.4 1.3 1.2 1.1 1.0 0.9 0.8 0.7 0.6 0.5 0.4
1, 3, 9, 11
5, 7, 13, 15
2, 9
4, 8, 12, 16
2, 9
5, 7, 13, 15
1, 3, 9, 11
4, 8, 12, 16
14
0 1.0 2.0 3.0 4.0 5.0 6.0
(thousandths)

(5R,7S)-6,6,14,14-tetrabromoheptacyclo[9.5.0.0^{3,9}.0^{4,16}.0^{5,7}.0^{8,12}.0^{13,15}]hexadecane (41d)

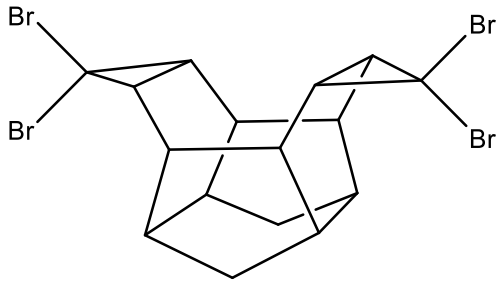

$C_{16}H_{16}Br_4$ (528) , R_f = 0.30 by SiO_2-TLC; visualized by UV or vanillin stain

MP = 189.7-190.6 °C (DCM)

IR (AT-IR): $\tilde{\nu}$ = 2951 (m, C-H), 2889 (m, C-H), 1136, 751 cm^{-1}.

^{1}H-NMR ($CDCl_3$, 500 MHz): δ= 2.69 (4H, s, H-4, -8, -12, -16), 2.63 (4H, s, H-1, -3, -9, -11), 1.99 (4H, s, H-5, -7, -13, -15), 1.69 (2H, d, H-2i, -10i), 0.53 (2H, d, H-2o, -10o) ppm;

$^2J_{H2i,\ H2o} = {}^2J_{H10i,\ H10o}$ = 11.9 Hz.

^{13}C-NMR ($CDCl_3$, 100.7 MHz): δ = 39.75 (C-4, -8, -12, -16), 34.94 (C-6, -14), 33.87 (C-1, -3, -9, -11), 32.96 (C-5, -7, -13, -15), 28.23 (C-2, -10) ppm.

MS: Decomposition under GC conditions.

Spectra

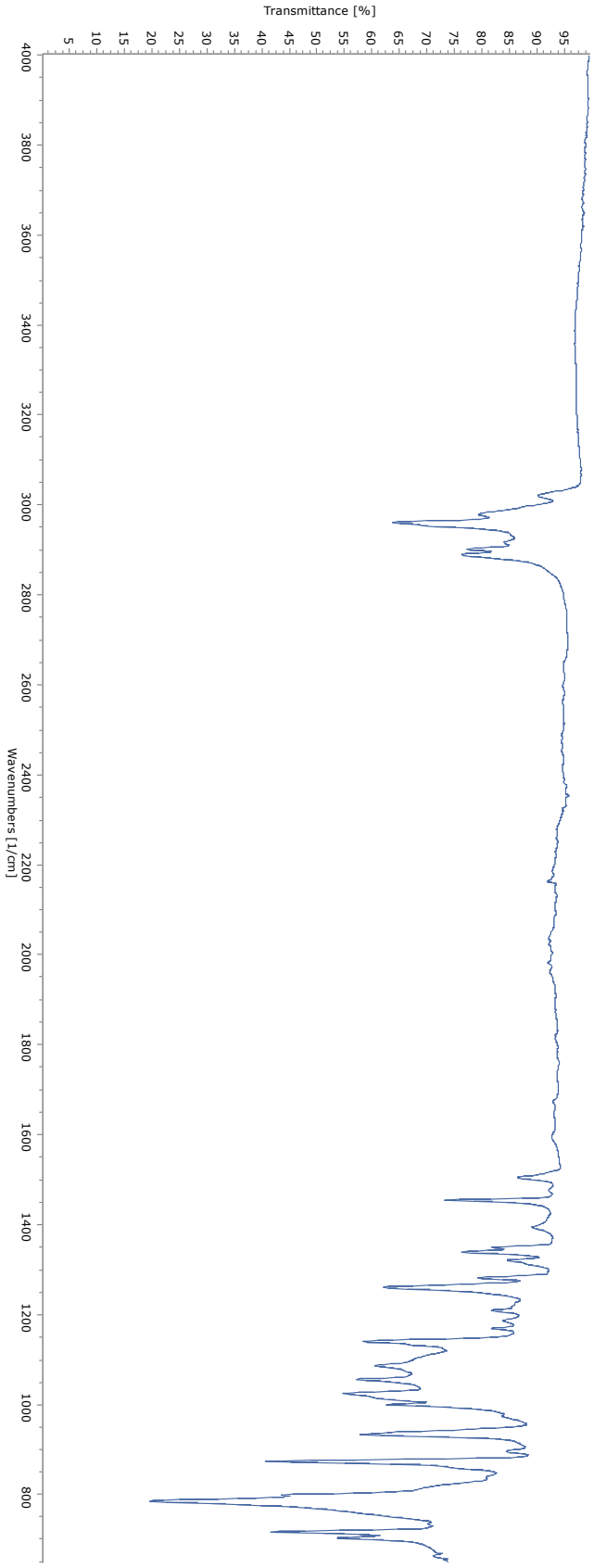
Transmittance [%]
Wavenumbers [1/cm]

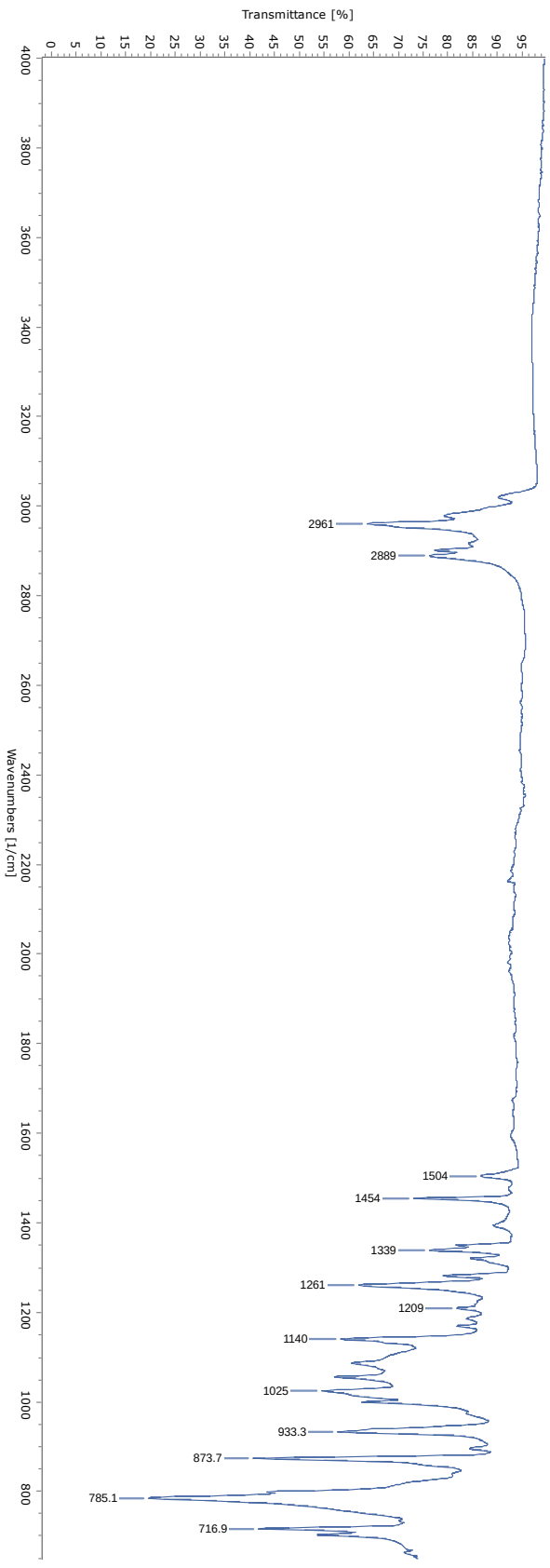
Transmittance [%]
Wavenumbers [1/cm]
2961
2889
1504
1454
1339
1261
1209
1140
1025
933.3
873.7
785.1
716.9

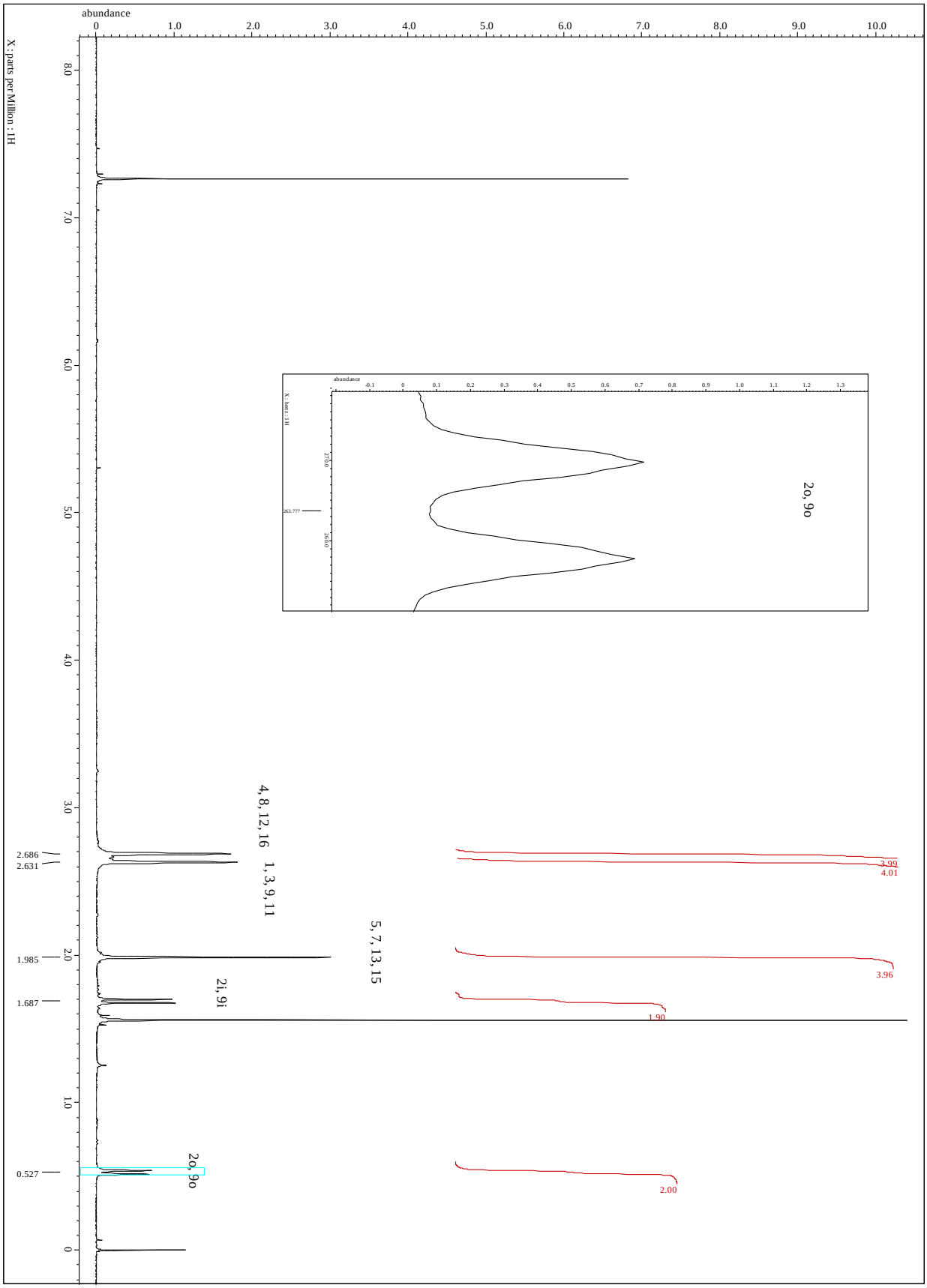
abundance
X : parts per Million : 1H
2.686
2.631
1.985
1.687
0.527
4, 8, 12, 16
1, 3, 9, 11
5, 7, 13, 15
2i, 9i
2o, 9o
2o, 9o
3.99
4.01
3.96
1.90
2.00

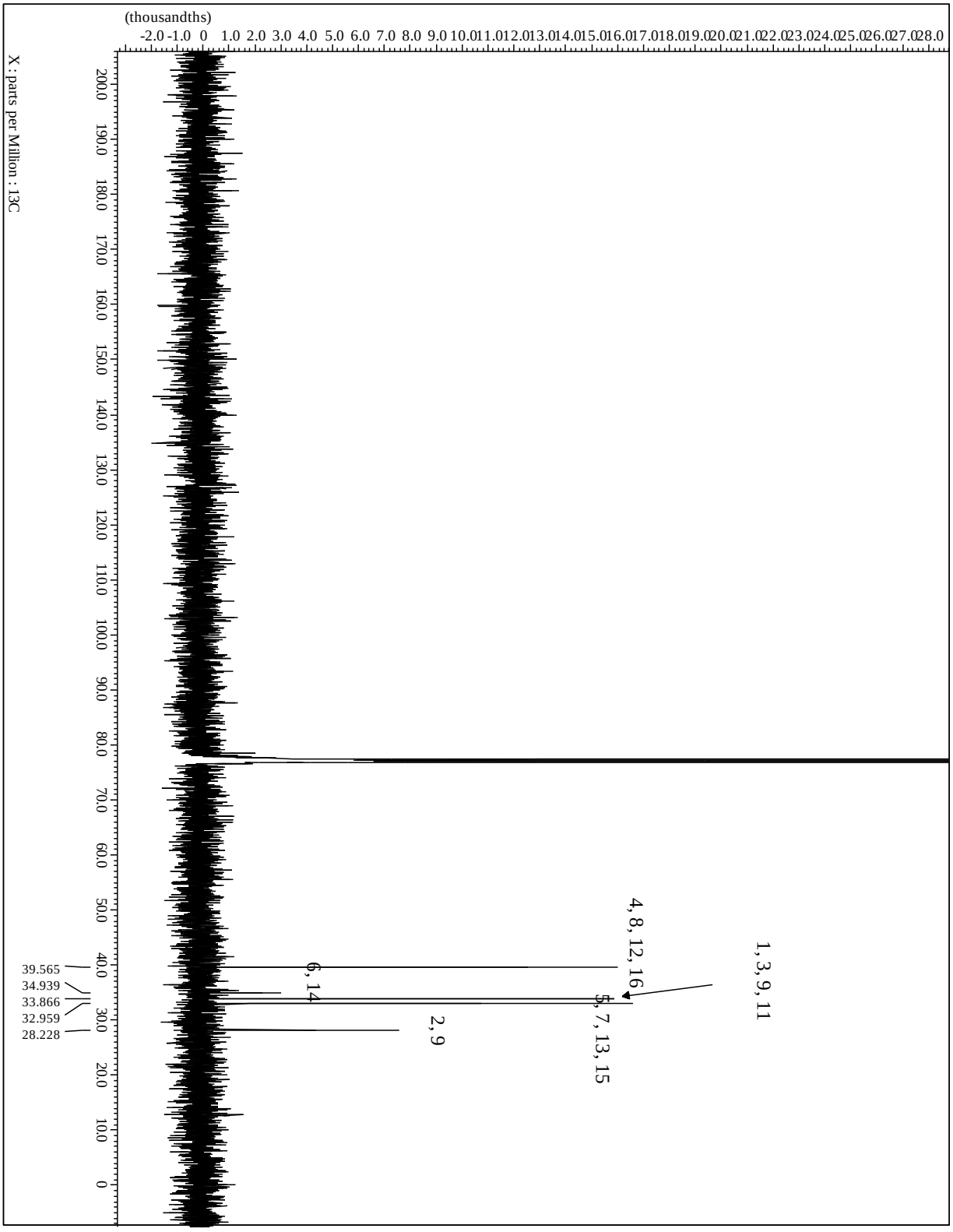
(thousandths)
-2.0 -1.0 0 1.0 2.0 3.0 4.0 5.0 6.0 7.0 8.0 9.0 10.0 11.0 12.0 13.0 14.0 15.0 16.0 17.0 18.0 19.0 20.0 21.0 22.0 23.0 24.0 25.0 26.0 27.0 28.0
X : parts per Million : 13C
200.0 190.0 180.0 170.0 160.0 150.0 140.0 130.0 120.0 110.0 100.0 90.0 80.0 70.0 60.0 50.0 40.0 30.0 20.0 10.0 0
39.565
34.939
33.866
32.959
28.228
1, 3, 9, 11
4, 8, 12, 16
5, 7, 13, 15
2, 9
6, 14

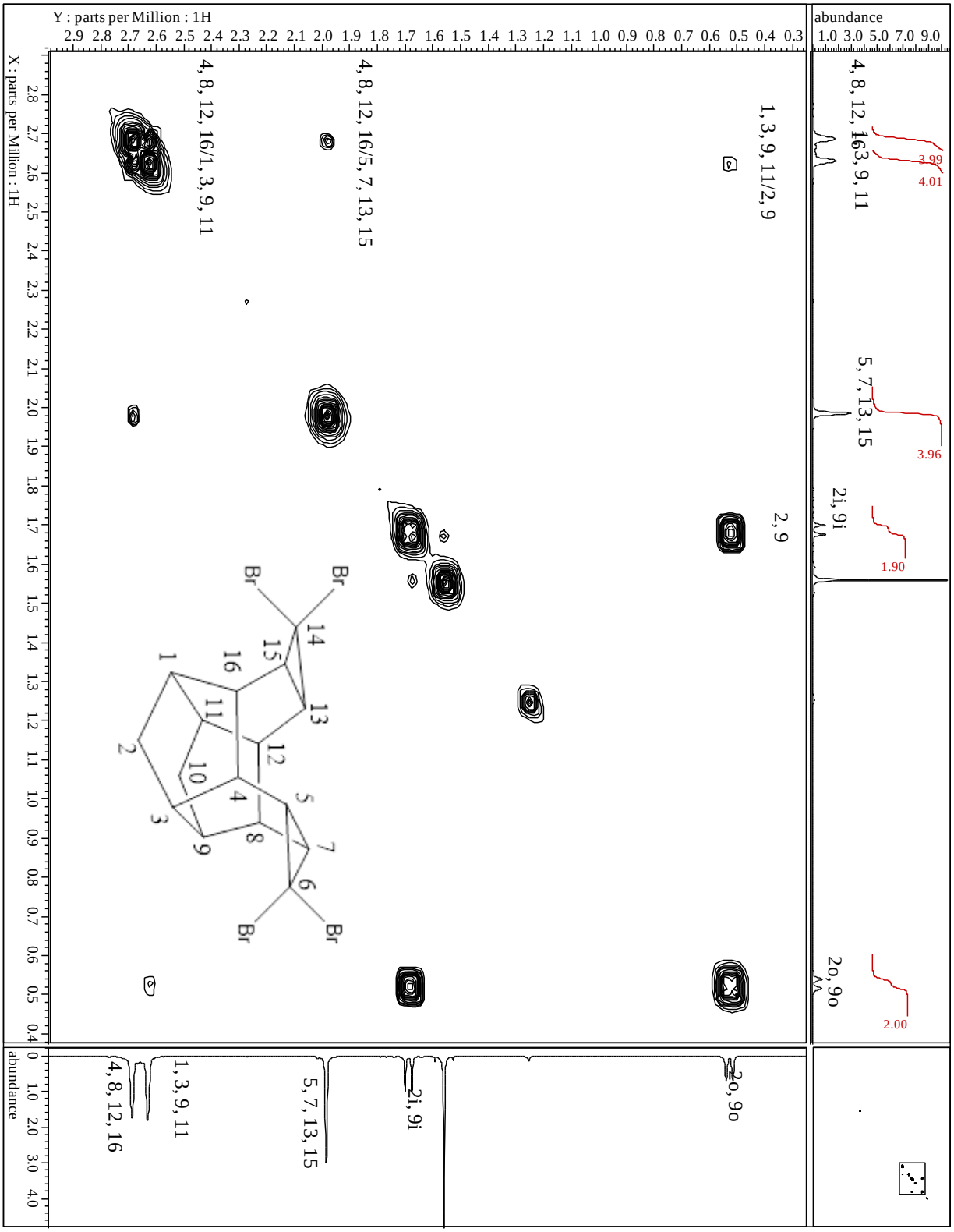
abundance
4, 8, 12, 16
3, 9, 11
3.99
4.01
5, 7, 13, 15
3.96
2i, 9i
1.90
2o, 9o
2.00
Y : parts per Million : 1H
1, 3, 9, 11
2, 9
4, 8, 12, 16
5, 7, 13, 15
X : parts per Million : 1H
Br
Br
Br
Br
1
2
3
4
5
6
7
8
9
10
11
12
13
14
15
16
2o, 9o
2i, 9i
5, 7, 13, 15
1, 3, 9, 11
4, 8, 12, 16
abundance

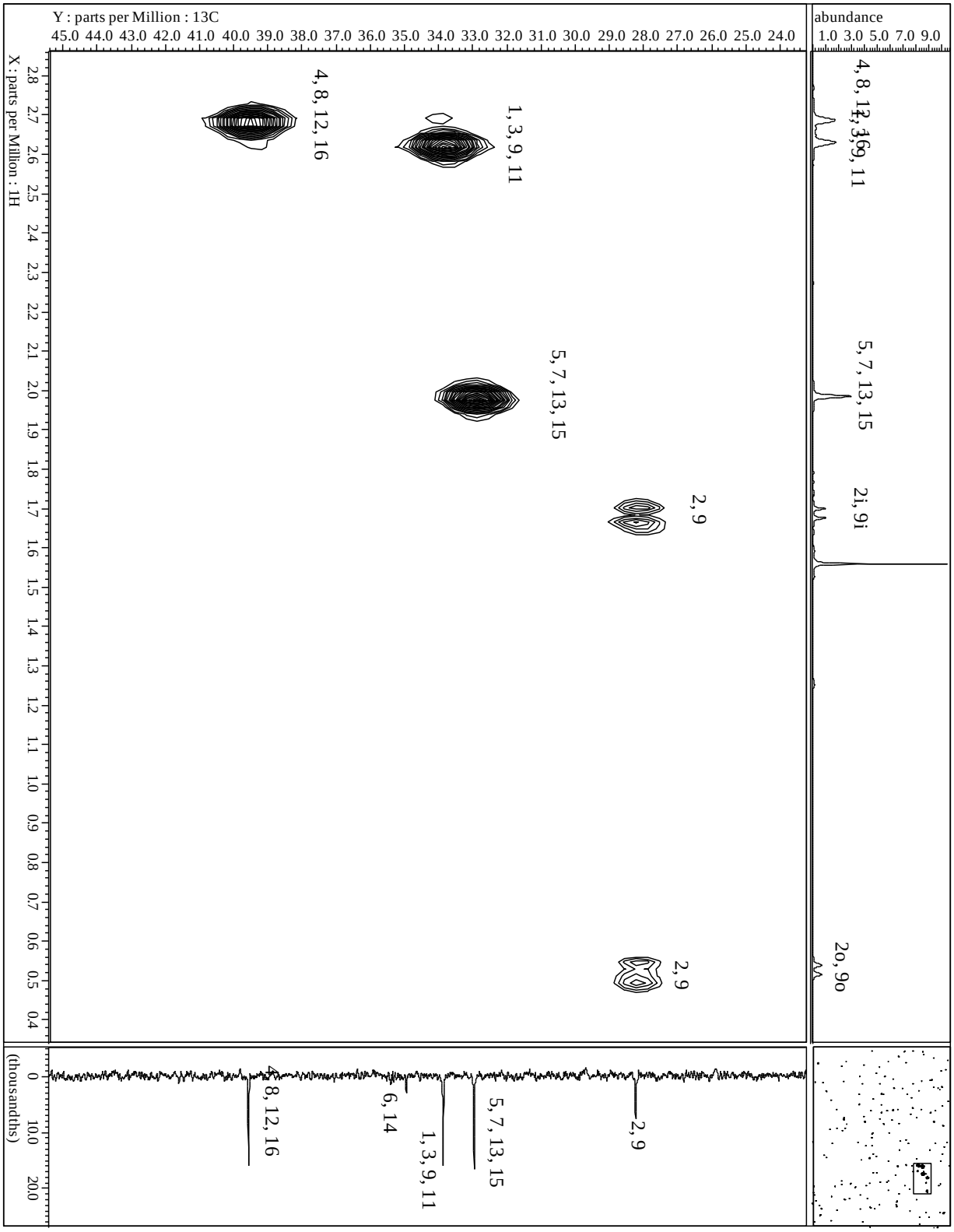
Y : parts per Million : 13C
X : parts per Million : 1H
abundance
(thousandths)
4, 8, 12, 16
1, 3, 9, 11
5, 7, 13, 15
2, 9
2i, 9i
2o, 9o
6, 14

5.3.4 Saturated Mono Carbene Adducts **42a-d**

Hexacyclo[8.5.0.0^{3,8}.0^{4,15}.0^{7,11}.0^{12,14}]pentadecane (42a)

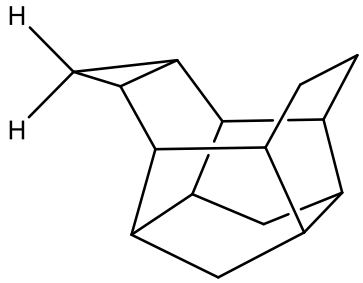

$C_{15}H_{20}$ (200) , R_f = 0.95 by SiO_2-TLC; visualized by vanillin stain

MP = 242.3-243.2 °C (*n*-pentane)

IR (AT-IR): $\tilde{\nu}$ = 2920 (s, C-H), 1454 (m), 1261 (w), 1013 (m), 831 (s) cm^{-1}.

^{1}H-NMR ($CDCl_3$, 500 MHz): δ= 2.14 (s_{app}, 2H, H-3, -8), 2.11 (m, 2H, H-11, -15), 2.02 (s_{app}, 2H, H-1, -10), 1.95-1.89 (m, 4H, H-5i, -6i; H-4, -7), 1.70 (d, 2H, H-2i, -9i), 1.64 (m, 2H, H-5o, -6o), 1.02 (m, 2H, H-12, -14), 0.53 (d, 2H, H-2o, -9o), 0.39 (sx, 1H, H-13), 0.34 (q, 1H, H-13) ppm;

$^2J_{\text{H-2i, -2o}} = {}^2J_{\text{H-9i, -9o}}$ = 11.3 Hz.

^{13}C-NMR ($CDCl_3$, 100.7 MHz): δ= 38.3 (C-11, -13), 37.2 (C-4, -7), 37.0 (C-3, -8), 36.8 (C-1, -10), 27.8 (C-2, -9), 19.2 (C-5, -6), 11.4 (C-12, -14), 6.0 (C-13) ppm.

MS(EI, 70 eV): *m/z* (%) = 200 ($M^{\cdot+}$, 30.3), 199 (7.9), 198 (8.8), 185 (10.9), 172 (12.1), 171 (15.7), 159 (7.8), 157 (17.3), 145 (9.6), 144 (13.2), 143 (25.1), 142 (8.3), 141 (11.6), 133 (7.7), 132 (11.7), 131 (26.8), 130 (21.1), 129 (40.2), 128 (23.4), 120 (24.5), 119 (18.0), 118 (24.8), 117 (44.9), 116 (14.2), 115 (30.5), 109 (8.3), 108 (8.0), 107 (12.6), 106 (22.1), 105 (32.9), 104 (28.5), 103 (11.1), 95 (12.8), 94 (11.3), 93 (23.9), 92 (32.0), 91 (100.0), 81 (12.7), 80 (18.7), 79 (51.8), 78 (22.1), 77 (46.4), 67 (17.9), 66 (8.5), 65 (22.3), 53 (12.9), 51 (10.5).

Spectra:

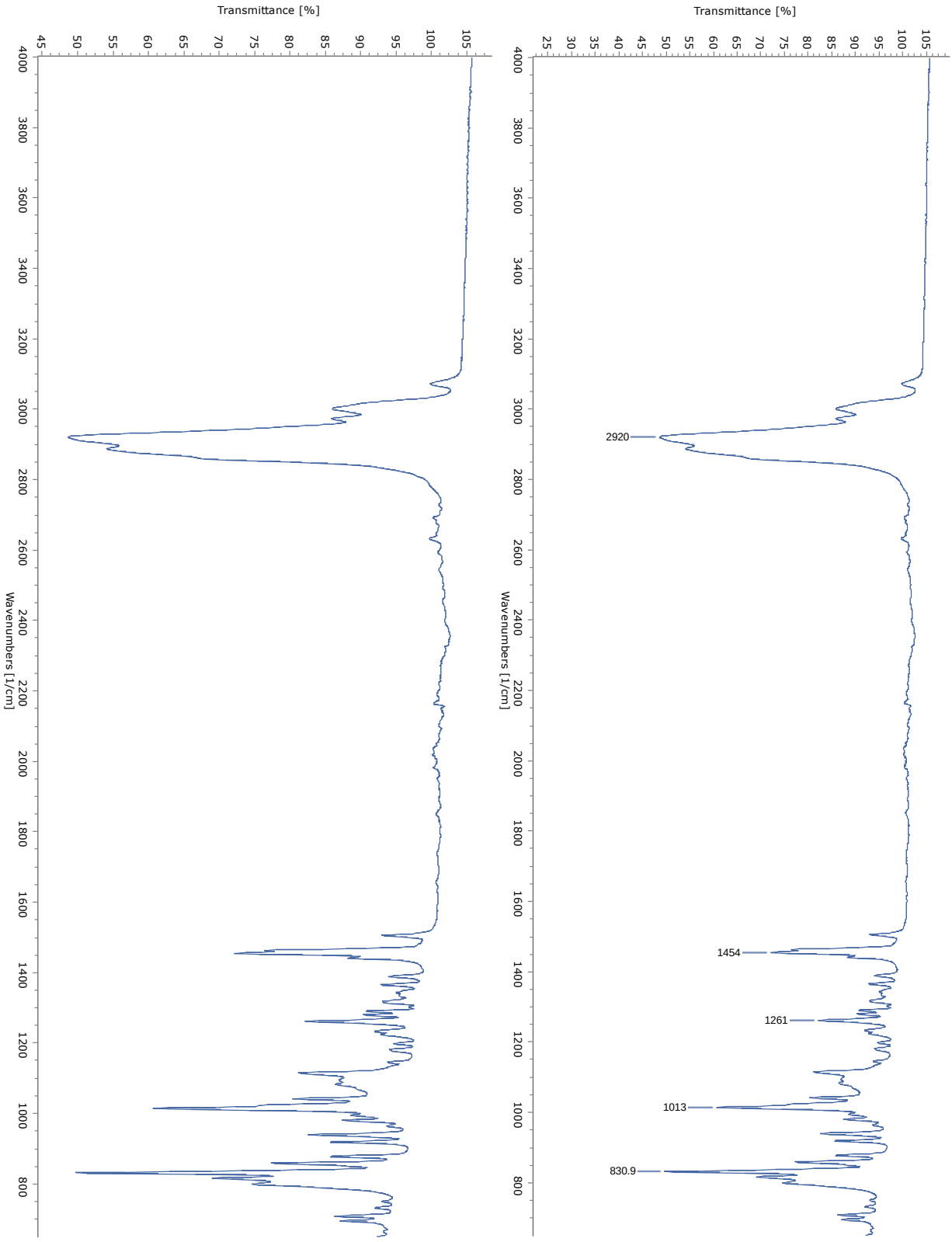

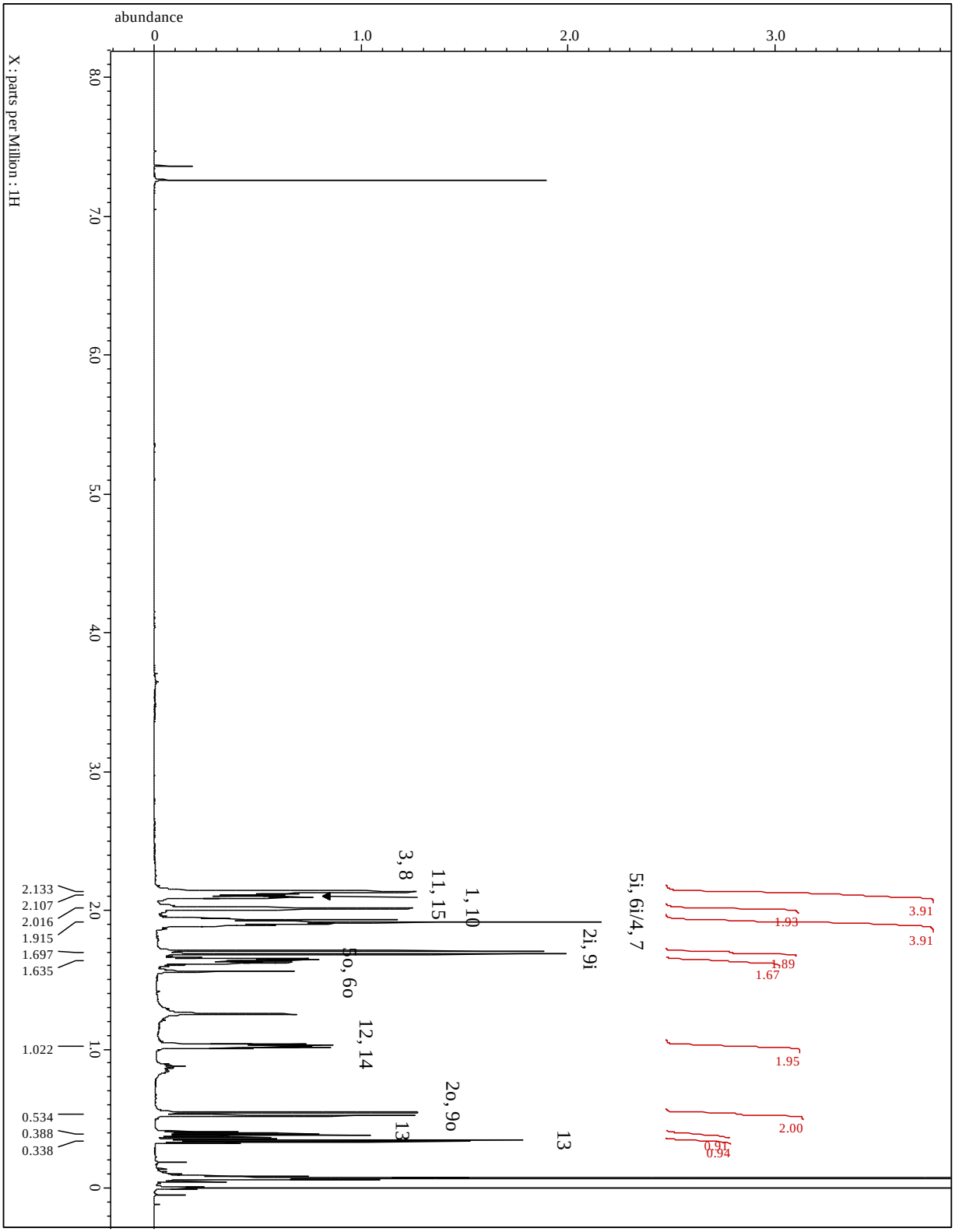
abundance
0
1.0
2.0
3.0
X : parts per Million : 1H
8.0
7.0
6.0
5.0
4.0
3.0
2.0
1.0
0
2.133
2.107
2.016
1.915
1.697
1.635
1.022
0.534
0.388
0.338
3, 8
11, 15
1, 10
2i, 9i
5o, 6o
12, 14
2o, 9o
13
13
5i, 6i/4, 7
3.91
1.93
3.91
1.89
1.67
1.95
2.00
0.91
0.94

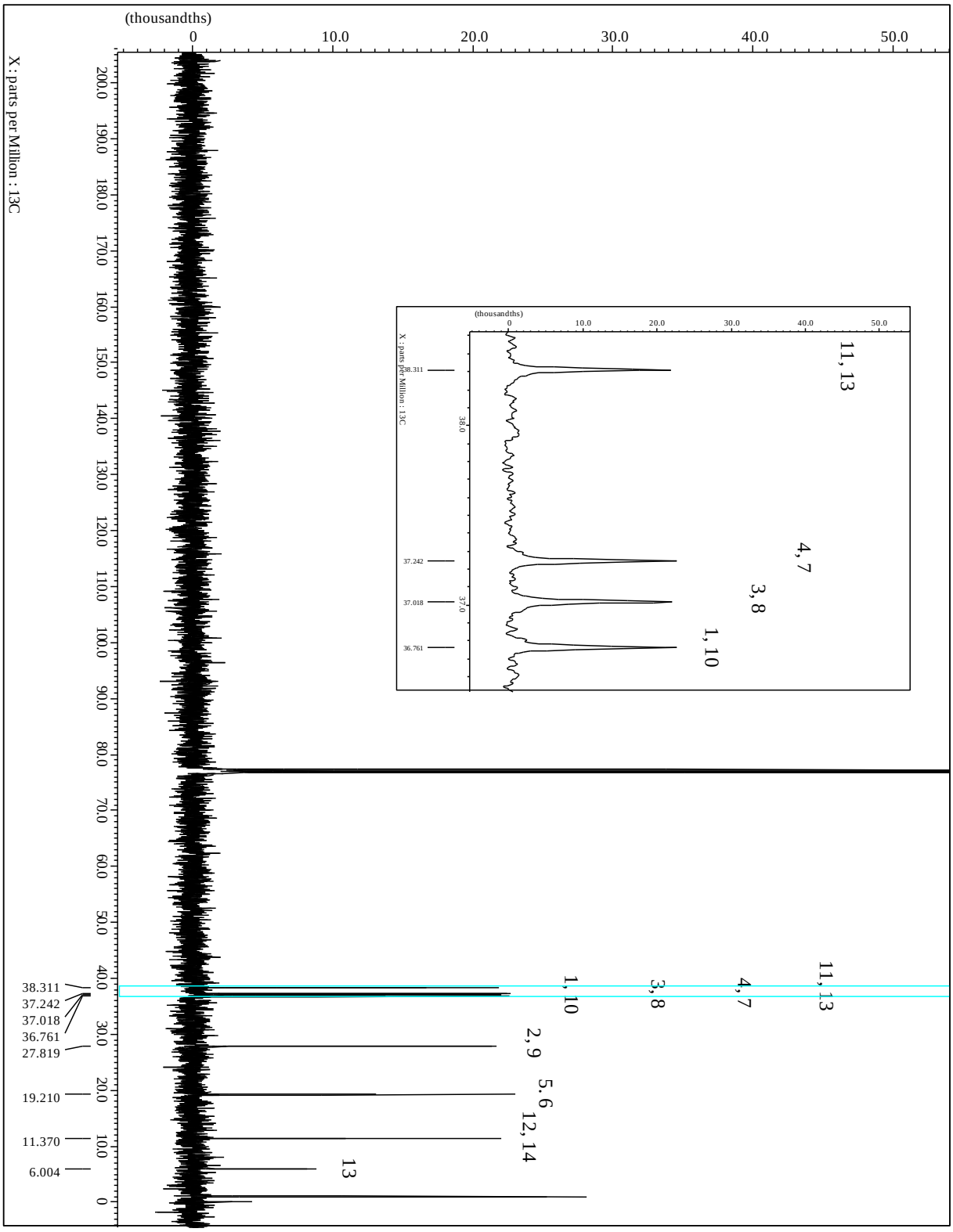
(thousandths)
0
10.0
20.0
30.0
40.0
50.0
X : parts per Million : 13C
200.0
190.0
180.0
170.0
160.0
150.0
140.0
130.0
120.0
110.0
100.0
90.0
80.0
70.0
60.0
50.0
40.0
30.0
20.0
10.0
0
38.311
37.242
37.018
36.761
27.819
19.210
11.370
6.004
11, 13
4, 7
3, 8
1, 10
2, 9
5, 6
12, 14
13

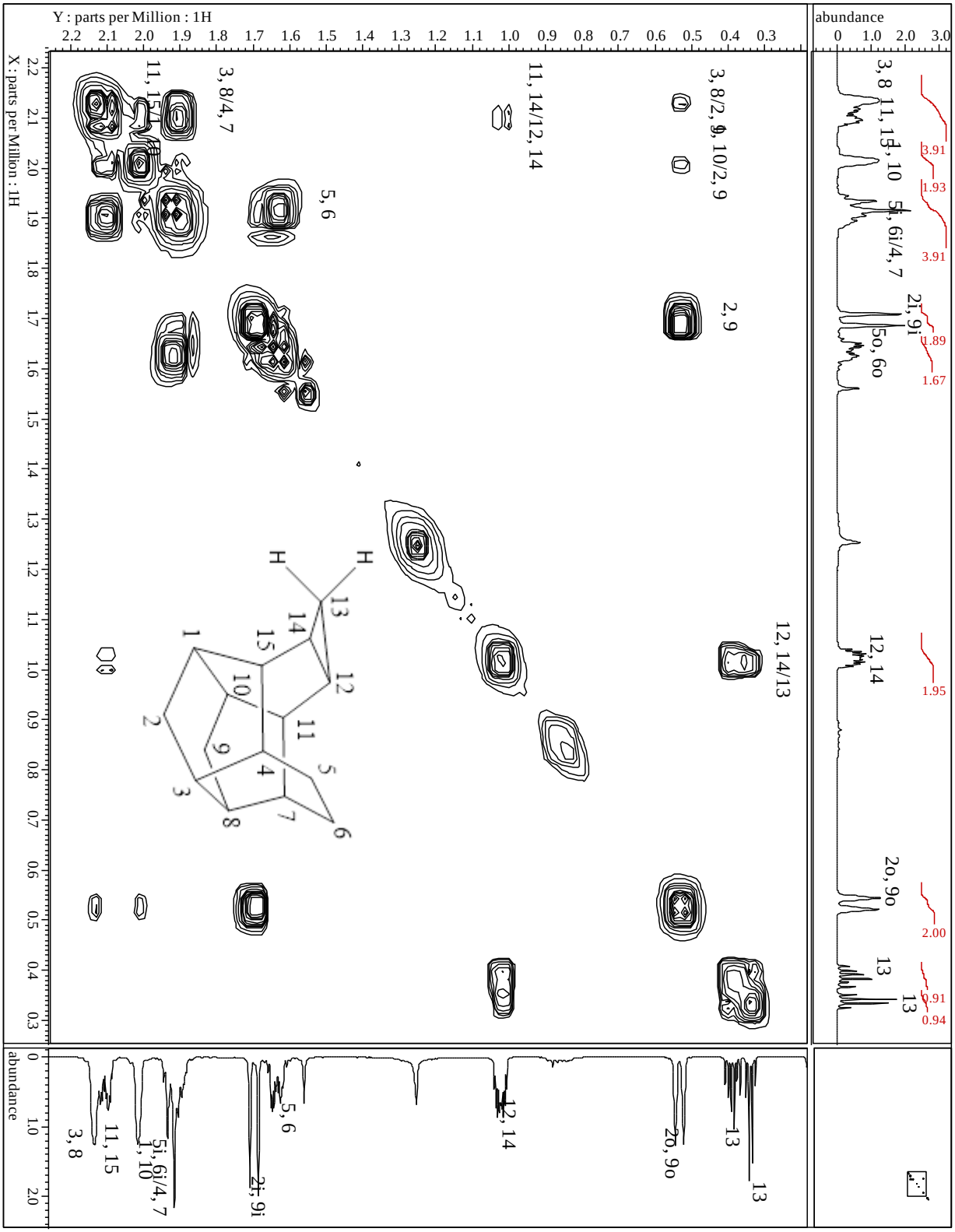
abundance
3, 8
11, 13
1, 10
5i, 6i/4, 7
2i, 9i
5o, 6o
2o, 9o
12, 14
13
3.91
1.93
3.91
1.89
1.67
1.95
2.00
0.91
0.94
Y : parts per Million : 1H
X : parts per Million : 1H
3, 8/2, 9
1, 10/2, 9
11, 14/12, 14
3, 8/4, 7
5, 6
12, 14/13
2, 9
11, 15
H
H
1
2
3
4
5
6
7
8
9
10
11
12
13
14
15
abundance

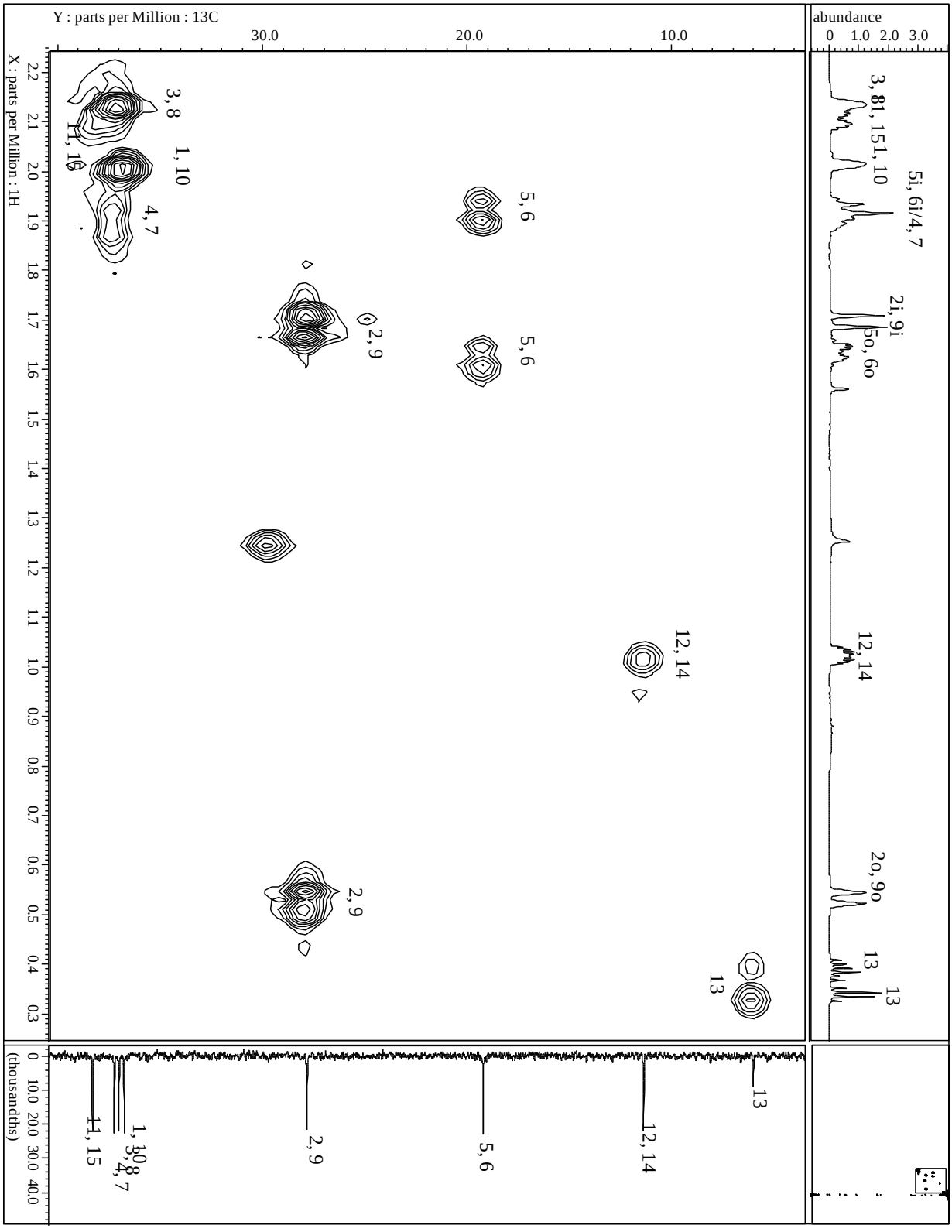
abundance
0 1.0 2.0 3.0
5i, 6i/4, 7
3, 8
1, 151, 10
2i, 9i
5o, 6o
12, 14
2o, 9o
13
13
Y : parts per Million : 13C
30.0
20.0
10.0
3, 8
1, 10
11, 15
4, 7
5, 6
5, 6
2, 9
12, 14
13
2, 9
X : parts per Million : 1H
2.2 2.1 2.0 1.9 1.8 1.7 1.6 1.5 1.4 1.3 1.2 1.1 1.0 0.9 0.8 0.7 0.6 0.5 0.4 0.3
13
12, 14
5, 6
2, 9
1, 10
3, 8
4, 7
11, 15
0 10.0 20.0 30.0 40.0
(thousandths)

13,13-difluorohexacyclo[8.5.0.0^{3,8}.0^{4,15}.0^{7,11}.0^{12,14}]pentadecane (42b)

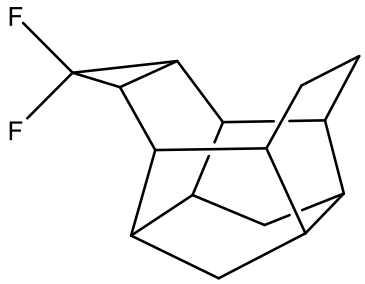

$C_{15}H_{18}F_2$ (236), R_f = 0.80 by SiO_2-TLC; visualized by UV or vanillin stain

MP = 104.5-106.3 °C (*n*-pentane)

IR (AT-IR): $\tilde{\nu}$ = 2925 (s, C-H), 2868 (m, C-H), 1455 (s), 1270 (m), 1233 (m), 1182 (m), 1151 (m), 1124 (s), 1090 (m), 1008 (m), 970 (m), 947 (m), 795 (w) cm^{-1}.

^{1}H-NMR ($CDCl_3$, 500 MHz): δ= 2.35 (s, 2H, H-1, -10), 2.17 (s, 2H, H-3, -8), 2.14 (m, 2H, H-11, -15), 2.00 (m, 2H, H-4, -7), 1.81 (m, 2H, H-5i, -6i), 1.77 (d, 2H, H-2i, -9i), 1.69 (m, 4H, H-5o, -6o; H-12, -14), 0.56 (d, 2H, H-2o, -9o) ppm;

$^2J_{H\text{-}2i,\ -2o} = {}^2J_{H\text{-}9i,\ -9o}$ = 11.5 Hz.

^{19}F-NMR ($CDCl_3$, 100.7 MHZ): δ= -119.6 (dt, 1F), -149.8 (d, 1F) ppm.

^{13}C-NMR ($CDCl_3$, 100.7 MHz): δ= 117.0 (dd, C-13), 37.3 (C-4, -7), 36.9 (C-1, -10), 36.3 (C-3, -8), 34.0 (C-11, -15), 28.3 (C-2, -9), 21.9 (t, C-12, -14), 19.3 (C-5, -6) ppm.

$^1J_{C6,\ F}$ = 276.7, $^2J_{C5,\ F}$ = 11.6 Hz

MS(EI, 70 eV): *m/z* (%) = 236 ($M^{\cdot+}$, 12.9), 221 (8.7), 208 (11.1), 207 (11.5), 194 (8.0), 193 (9.5), 187 (9.0), 179 (9.5), 171 (7.8), 169 (7.9), 167 (11.2), 166 (7.5), 165 (14.3), 160 (9.7), 159 (16.1), 157 (11.4), 156 (9.5), 155 (12.1), 154 (8.0), 153 (10.6), 152 (8.8), 147 (20.9), 146 (16.0), 145

(11.1), 143 (19.4), 142 (10.7), 141 (19.5), 140 (9.3), 138 (17.2), 135 (9.5), 133 (18.8), 132 (8.2), 131 (25.4), 130 (12.4), 129 (33.9), 128 (27.3), 127 (29.4), 123 (10.1), 121 (11.0), 120 (26.3), 119 (17.7), 118 (11.5), 117 (32.3), 116 (16.3), 115 (34.6), 109 (37.5), 107 (11.9), 106 (8.2), 105 (29.1), 104 (18.7), 103 (13.1), 97 (12.3), 96 (8.9), 95 (21.0), 94 (10.0), 93 (23.8), 92 (30.8), 91 (100.0), 83 (13.5), 81 (21.7), 80 (19.9), 79 (65.8), 78 (28.0), 77 (58.5), 69 (16.8), 67 (25.5), 66 (12.3), 65 (19.6), 57 (11.6), 55 (21.8), 53 (13.1), 51 (17.3).

Spectra

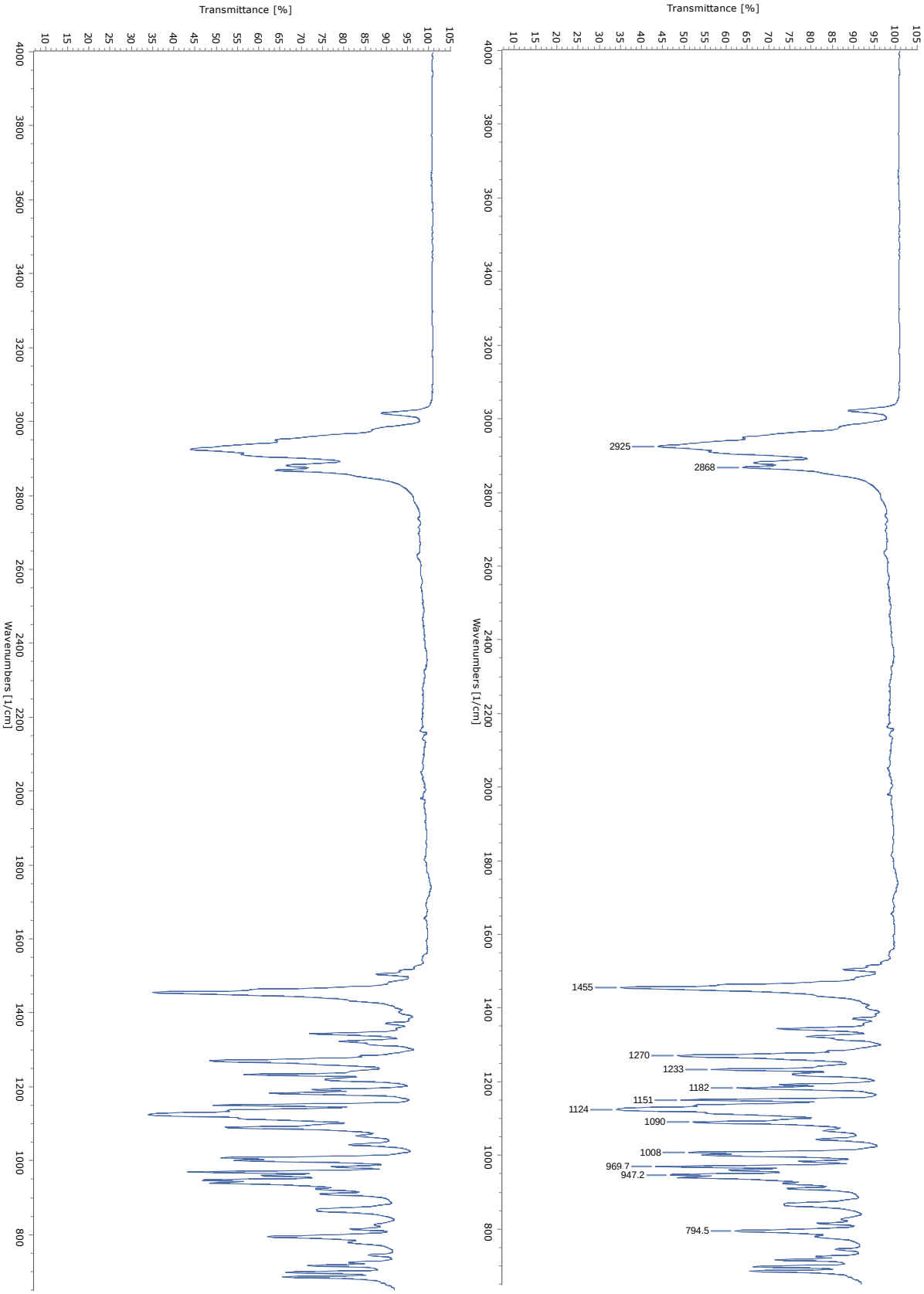
Transmittance [%]
Wavenumbers [1/cm]
2925
2868
1455
1270
1233
1182
1151
1124
1090
1008
969.7
947.2
794.5
Transmittance [%]
Wavenumbers [1/cm]

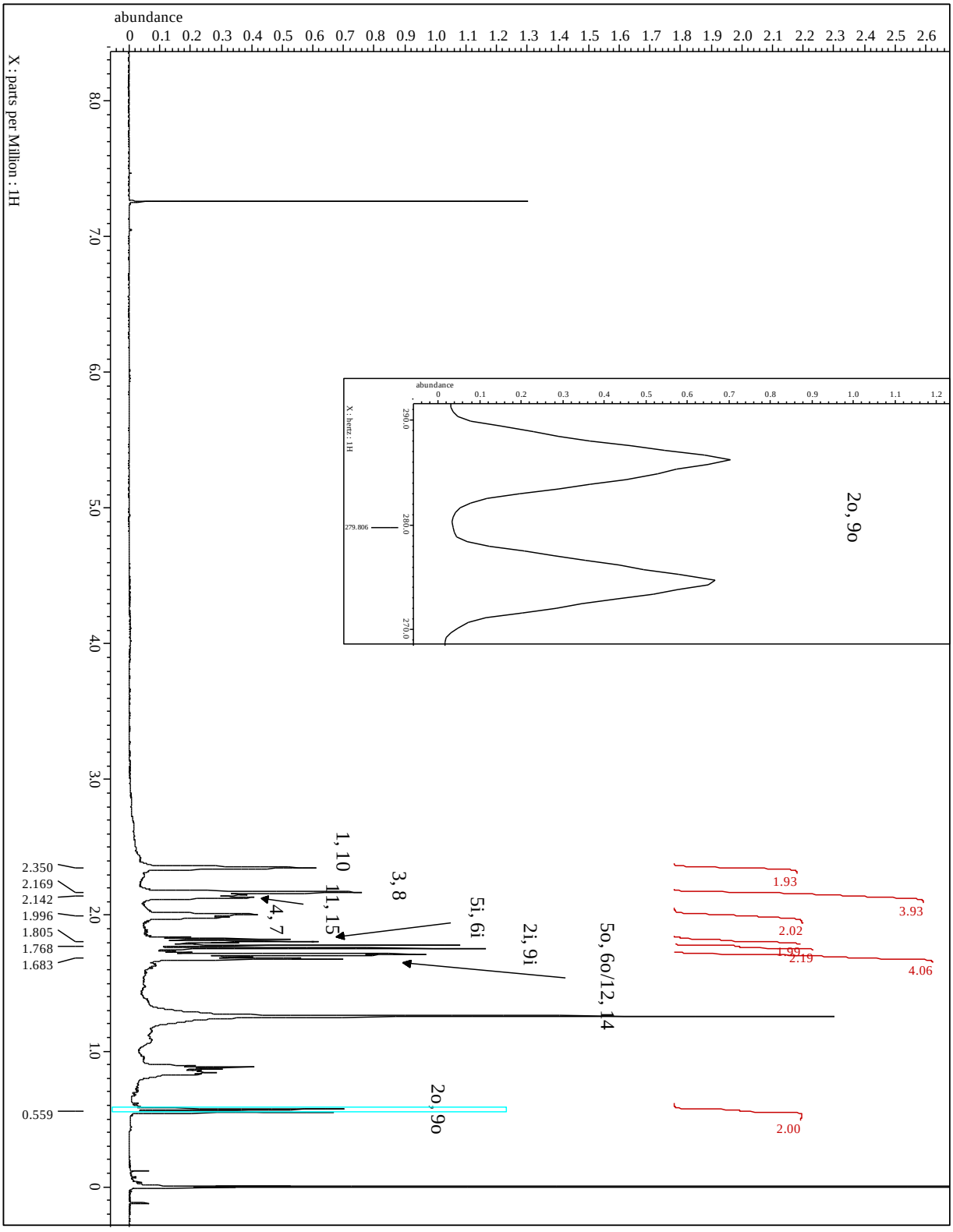
abundance
X : parts per Million : 1H
2.350
2.169
2.142
1.996
1.805
1.768
1.683
0.559
1, 10
11, 15
3, 8
4, 7
5i, 6i
2i, 9i
5o, 6o/12, 14
2o, 9o
1.93
3.93
2.02
1.99
2.19
4.06
2.00
X : hertz : 1H
279.806
2o, 9o

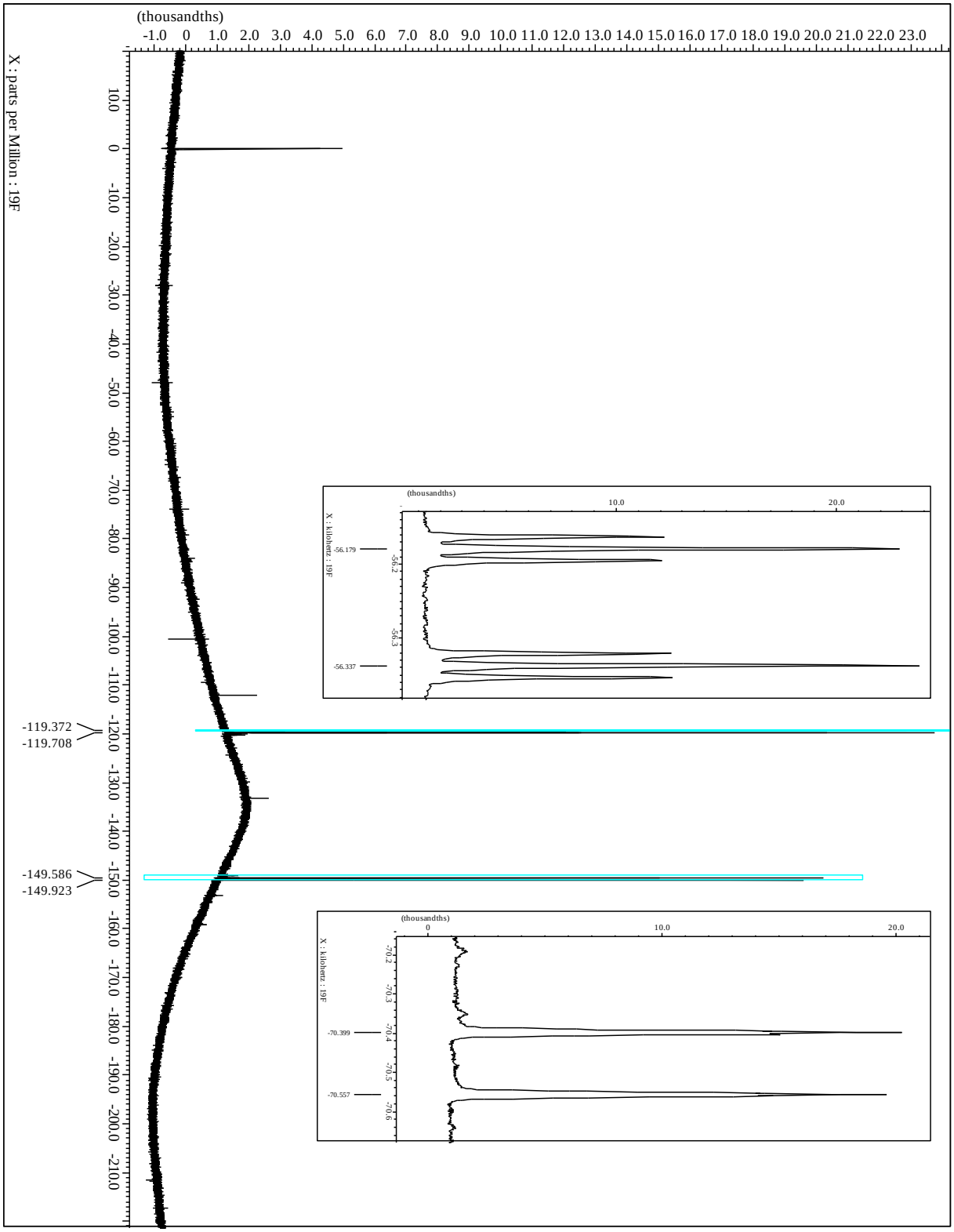
(thousandths)
-1.0 0 1.0 2.0 3.0 4.0 5.0 6.0 7.0 8.0 9.0 10.0 11.0 12.0 13.0 14.0 15.0 16.0 17.0 18.0 19.0 20.0 21.0 22.0 23.0
X : parts per Million : 19F
10.0 0 -10.0 -20.0 -30.0 -40.0 -50.0 -60.0 -70.0 -80.0 -90.0 -100.0 -110.0 -120.0 -130.0 -140.0 -150.0 -160.0 -170.0 -180.0 -190.0 -200.0 -210.0
-119.372
-119.708
-149.586
-149.923
(thousandths)
10.0
20.0
X : kilohertz : 19F
-56.179
-56.337
(thousandths)
0
10.0
20.0
X : kilohertz : 19F
-70.399
-70.557

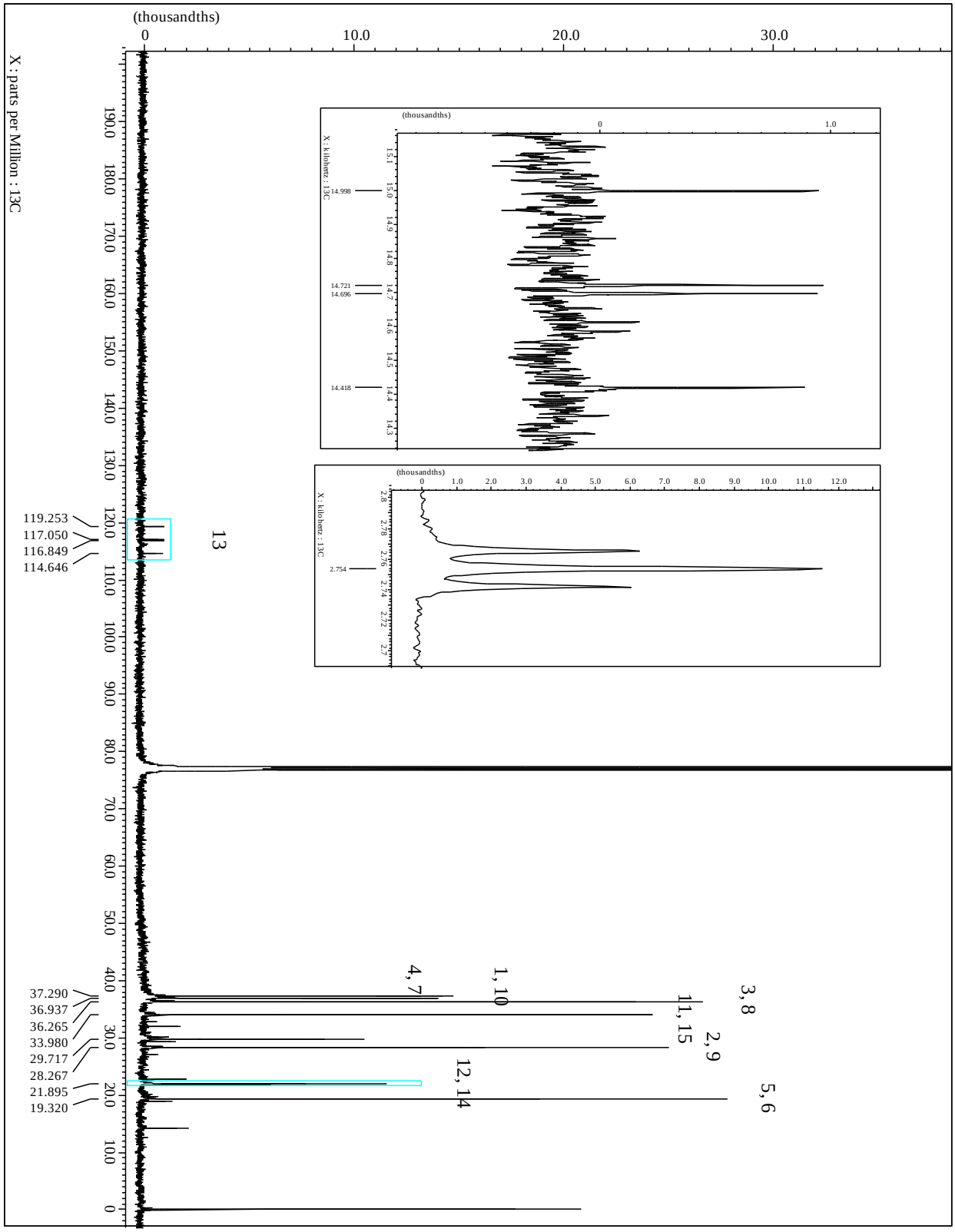
(thousandths)
0
10.0
20.0
30.0
X : parts per Million : 13C
190.0
180.0
170.0
160.0
150.0
140.0
130.0
120.0
110.0
100.0
90.0
80.0
70.0
60.0
50.0
40.0
30.0
20.0
10.0
0
119.253
117.050
116.849
114.646
13
37.290
36.937
36.265
33.980
29.717
28.267
21.895
19.320
4, 7
1, 10
11, 15
2, 9
3, 8
12, 14
5, 6
(thousandths)
0
1.0
X : kilohertz : 13C
14.998
14.721
14.696
14.418
(thousandths)
0
1.0
2.0
3.0
4.0
5.0
6.0
7.0
8.0
9.0
10.0
11.0
12.0
X : kilohertz : 13C
2.754

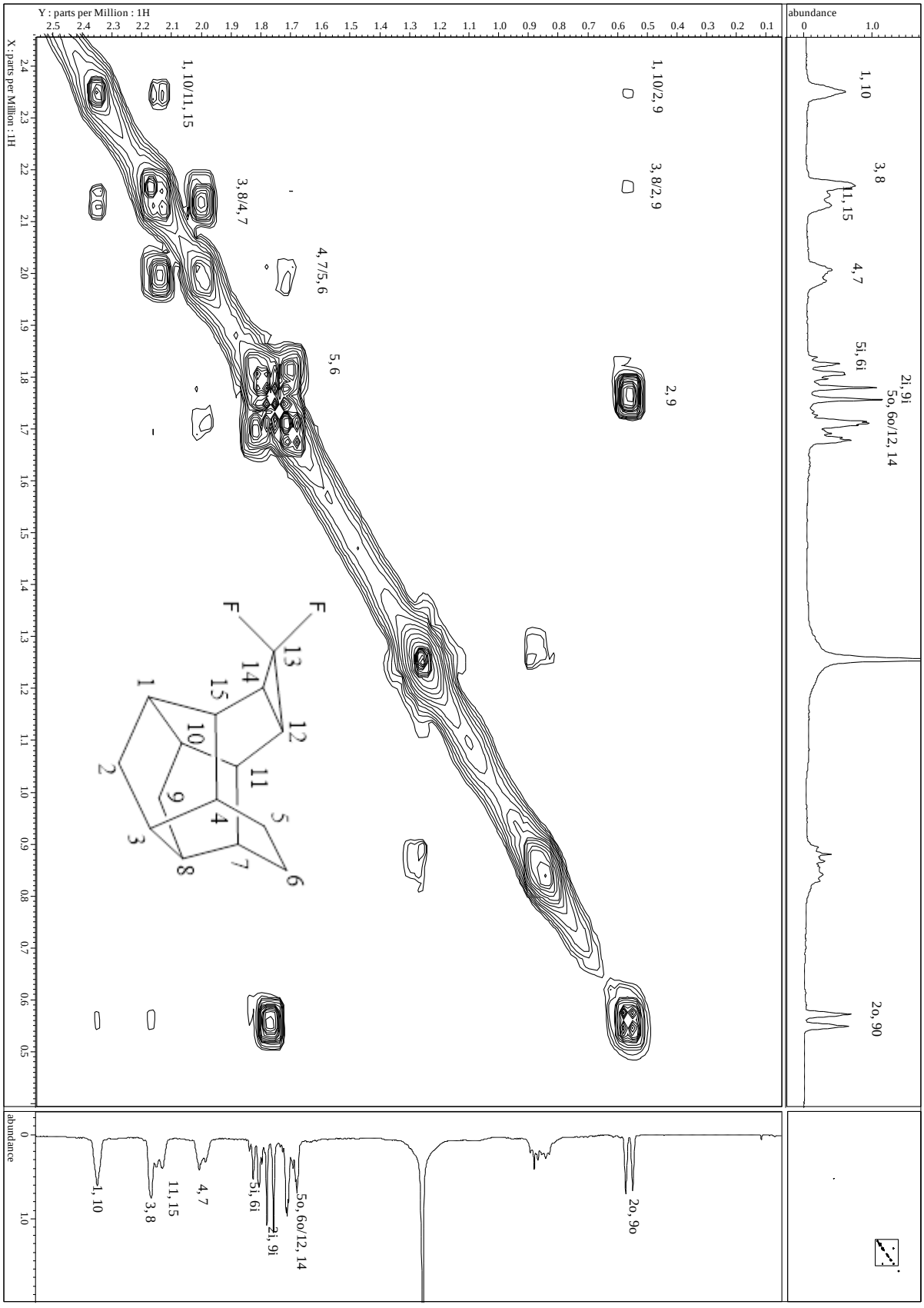
Y : parts per Million : 1H
X : parts per Million : 1H
abundance
1, 10
3, 8
11, 15
4, 7
5i, 6i
2i, 9i
5o, 6o/12, 14
2o, 9o
1, 10/2, 9
3, 8/2, 9
2, 9
4, 7/5, 6
5, 6
3, 8/4, 7
1, 10/11, 15
F
F
13
14
15
12
1
10
11
2
9
4
5
3
7
8
6
2o, 9o
5o, 6o/12, 14
2i, 9i
5i, 6i
4, 7
11, 15
3, 8
1, 10

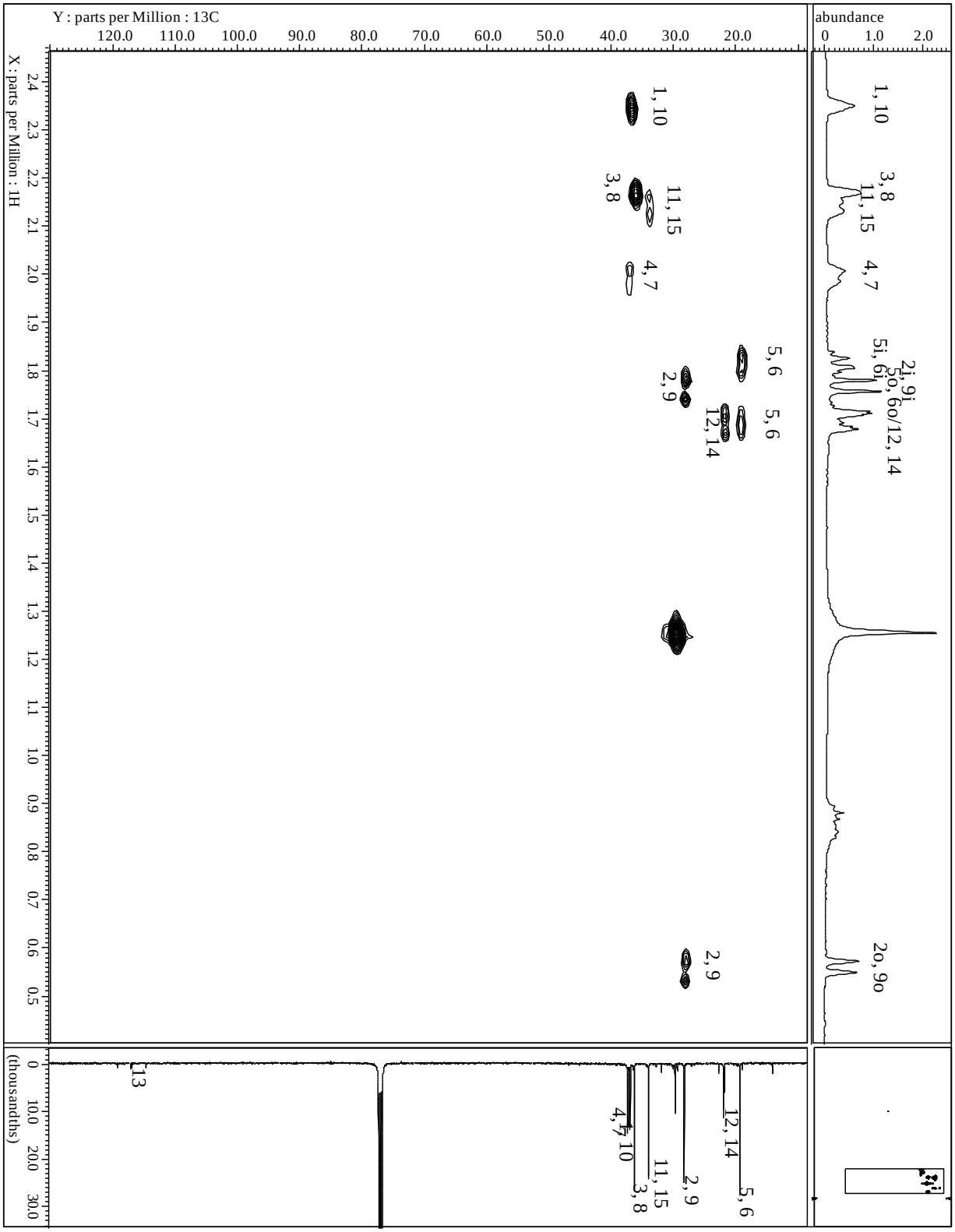
Y : parts per Million : 13C
X : parts per Million : 1H
abundance
(thousandths)
1, 10
3, 8
11, 15
4, 7
5i, 6i
2i, 9i
5o, 6o/12, 14
2o, 9o
5, 6
2, 9
12, 14
13

13,13-dichlorohexacyclo[8.5.0.0^{3,8}.0^{4,15}.0^{7,11}.0^{12,14}]pentadecane (42c)

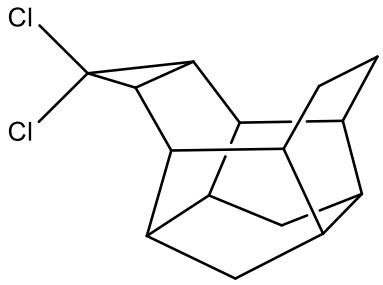

$C_{15}H_{18}Cl_2$ (268), R_f = 0.70 by SiO_2-TLC; visualized by UV or vanillin stain

MP = 184.1-184.9 °C ($CHCl_3$)

IR (AT-IR): $\tilde{\nu}$ = 2939 (s, C-H), 2916 (s, C-H), 2868 (m, C-H), 1462 (m), 1019 (m), 900 (m), 820 (s), 779 (s), 728 (s), 709 (m) cm^{-1}.

^{1}H-NMR ($CDCl_3$, 500 MHz): δ=2.54 (s_{app}, 2H, H-1, -10), 2.35 (d, 2H, H-11, -15), 2.15 (s_{app}, 2H, H-3, -8), 2.04 (m, 2H, H-4, -7), 1.89 (s_{app}, 2H, H-12, -14), 1.80 (d, 2H, H-5i, -6i), 1.77 (d, 2H, H-2i, -9i), 1.68 (m, 2H, H-5o, -6o), 0.57 (d, 2H, H2o, -9o) ppm;

$^2J_{H\text{-}2i,\,\text{-}2o} = {}^2J_{H\text{-}9i,\,\text{-}9o}$ = 12.0; $^2J_{H\text{-}5i,\,\text{-}5o} = {}^2J_{H\text{-}6i,\,\text{-}6o}$ = 9.4 Hz.

^{13}C-NMR ($CDCl_3$, 100.7 MHz): δ= 67.3 (C-13), 38.3 (C-4, -7), 36.1 (C-3, -8), 36.0 (C-11, -15), 35.4 (C-1, -10), 31.3 (C-12, -14), 28.3 (C-2, -9), 19.2 (C-5, -6) ppm.

MS(EI, 70 eV): *m/z* (%) = 270 ($M^{\cdot+}$+2, 2.8), 268 ($M^{\cdot+}$, 3.7), 235 (8.4), 234 (8.9), 233 (20.1), 232 (17.0), 197 (36.7), 177 (8.6), 176 (10.0), 175 (8.1), 174 (11.9), 172 (10.3), 169 (8.6), 167 (11.2), 165 (19.3), 164 (8.2), 163 (13.5), 162 (7.9), 155 (16.4), 154 (17.2), 153 (20.0), 152 (34.8), 151 (15.9), 143 (14.5), 142 (9.9), 141 (26.5), 139 (13.1), 138 (8.1), 133 (8.6), 131 (23.6), 130 (11.7), 129 (38.0), 128 (33.3), 127 (24.2), 125 (30.1), 120 (21.7), 119 (17.9), 118 (15.9), 117 (42.8), 116 (15.3), 115 (44.9), 113 (9.3), 109 (9.2), 107 (13.3), 106 (10.3), 105 (30.0), 104 (18.7), 103 (20.1),

102 (9.1), 95 (14.3), 94 (9.8), 93 (26.1), 92 (34.0), 91 (100.0), 89 (12.8), 83 (9.5), 81 (21.1), 80 (16.9), 79 (67.2), 78 (23.7), 77 (63.4), 75 (8.1), 67 (29.4), 66 (9.2), 65 (24.5), 63 (10.4), 55 (13.3), 53 (15.7), 51 (16.9).

Spectra

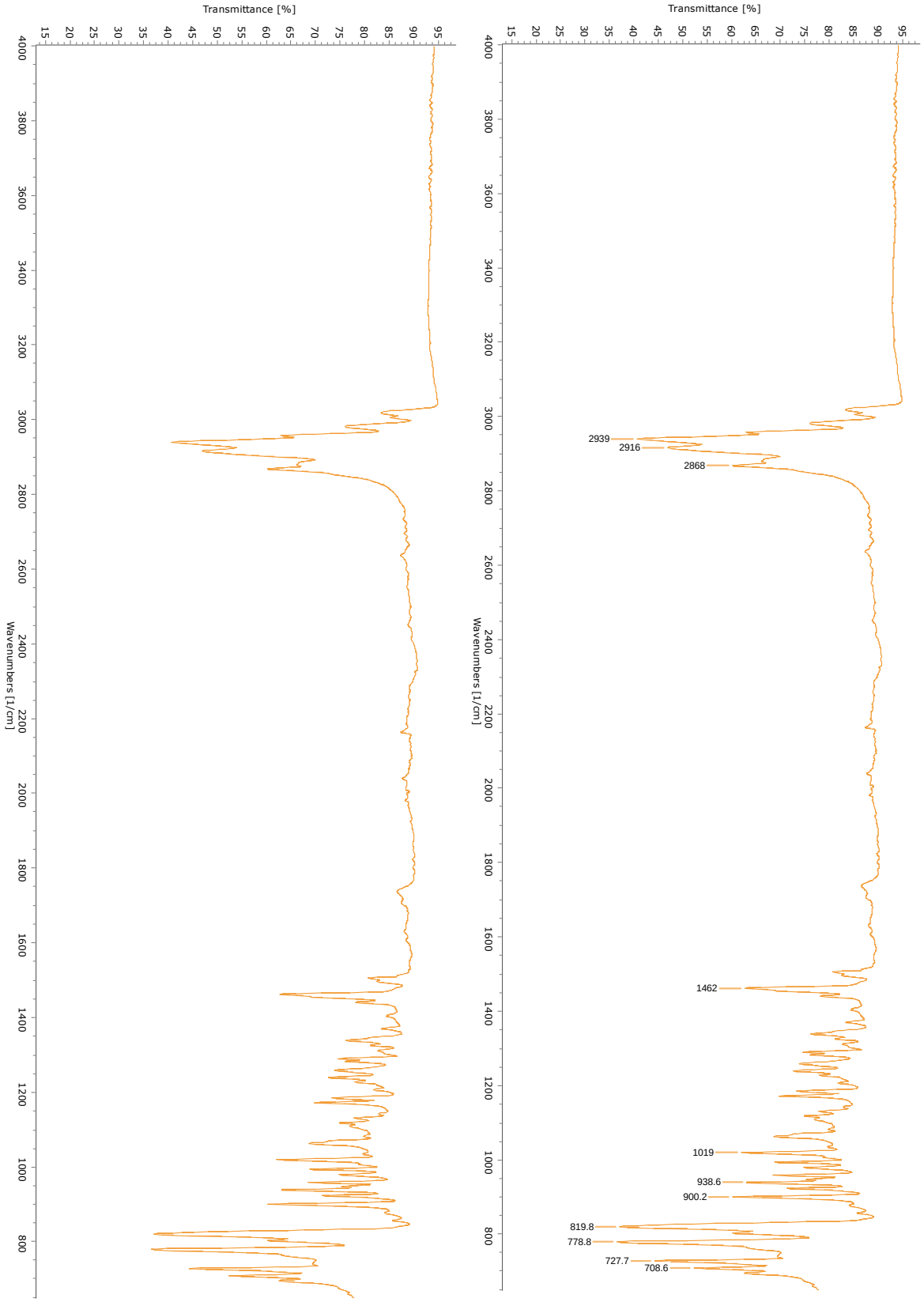
Transmittance [%]
Wavenumbers [1/cm]
2939
2916
2868
1462
1019
938.6
900.2
819.8
778.8
727.7
708.6

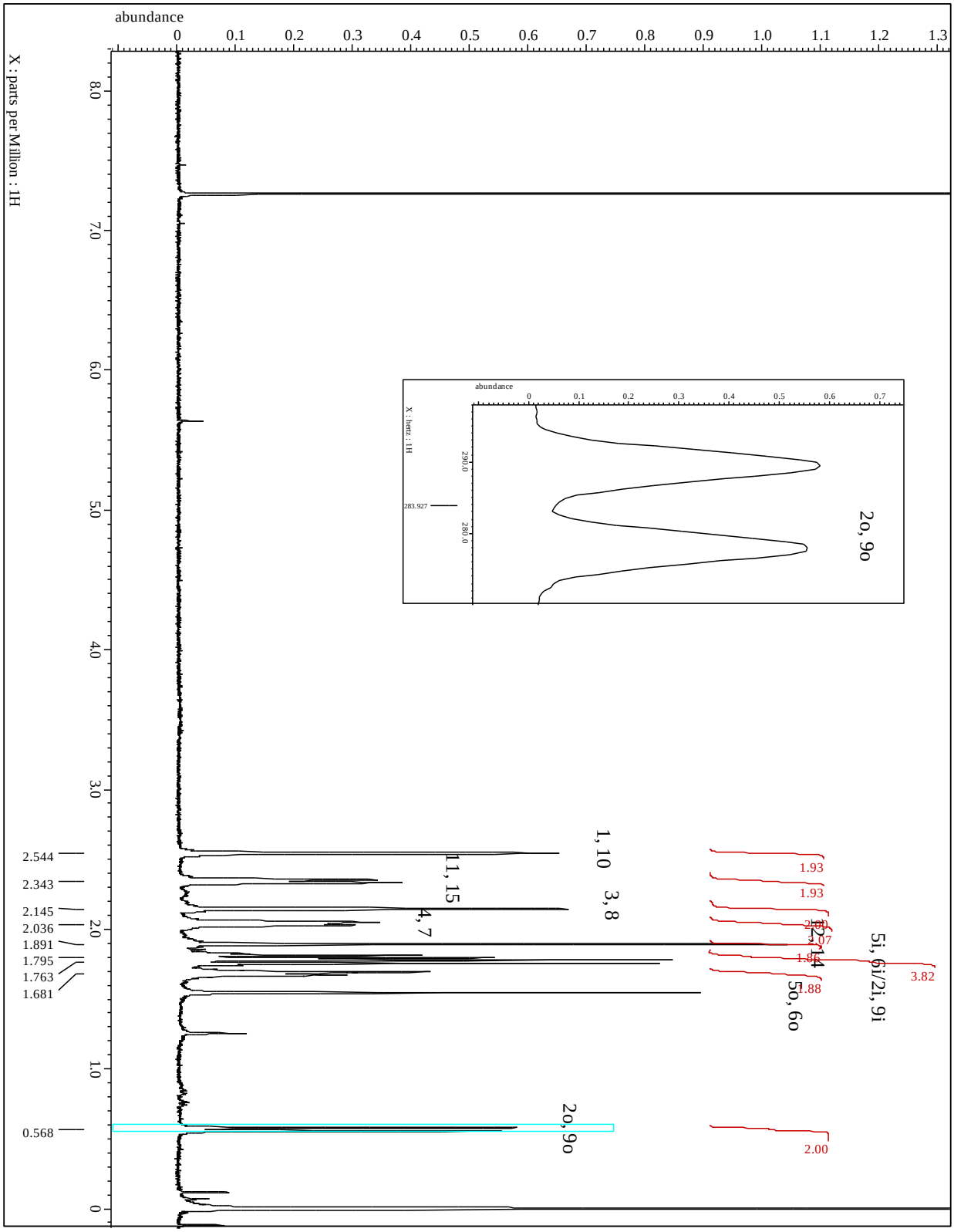
abundance
X : parts per Million : 1H
2.544
2.343
2.145
2.036
1.891
1.795
1.763
1.681
0.568
1, 10
3, 8
11, 15
4, 7
20, 9o
5o, 6o
5i, 6i/2i, 9i
1.93
1.93
3.82
1.88
2.00
2o, 9o
X : hertz : 1H
283.927

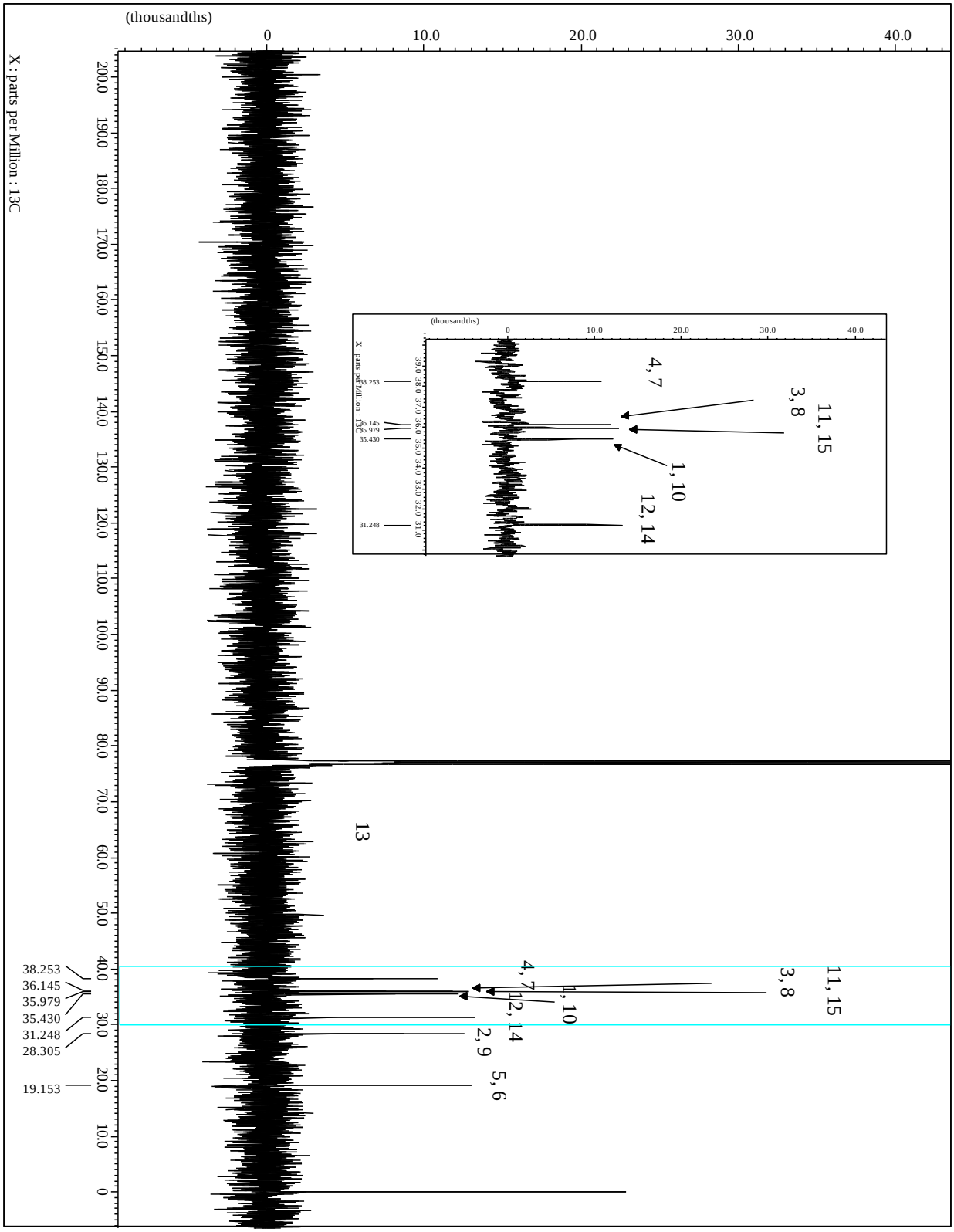
(thousandths)
0
10.0
20.0
30.0
40.0
X : parts per Million : 13C
200.0
190.0
180.0
170.0
160.0
150.0
140.0
130.0
120.0
110.0
100.0
90.0
80.0
70.0
60.0
50.0
40.0
30.0
20.0
10.0
0
38.253
36.145
35.979
35.430
31.248
28.305
19.153
13
11, 15
3, 8
4, 7
1, 10
12, 14
2, 9
5, 6

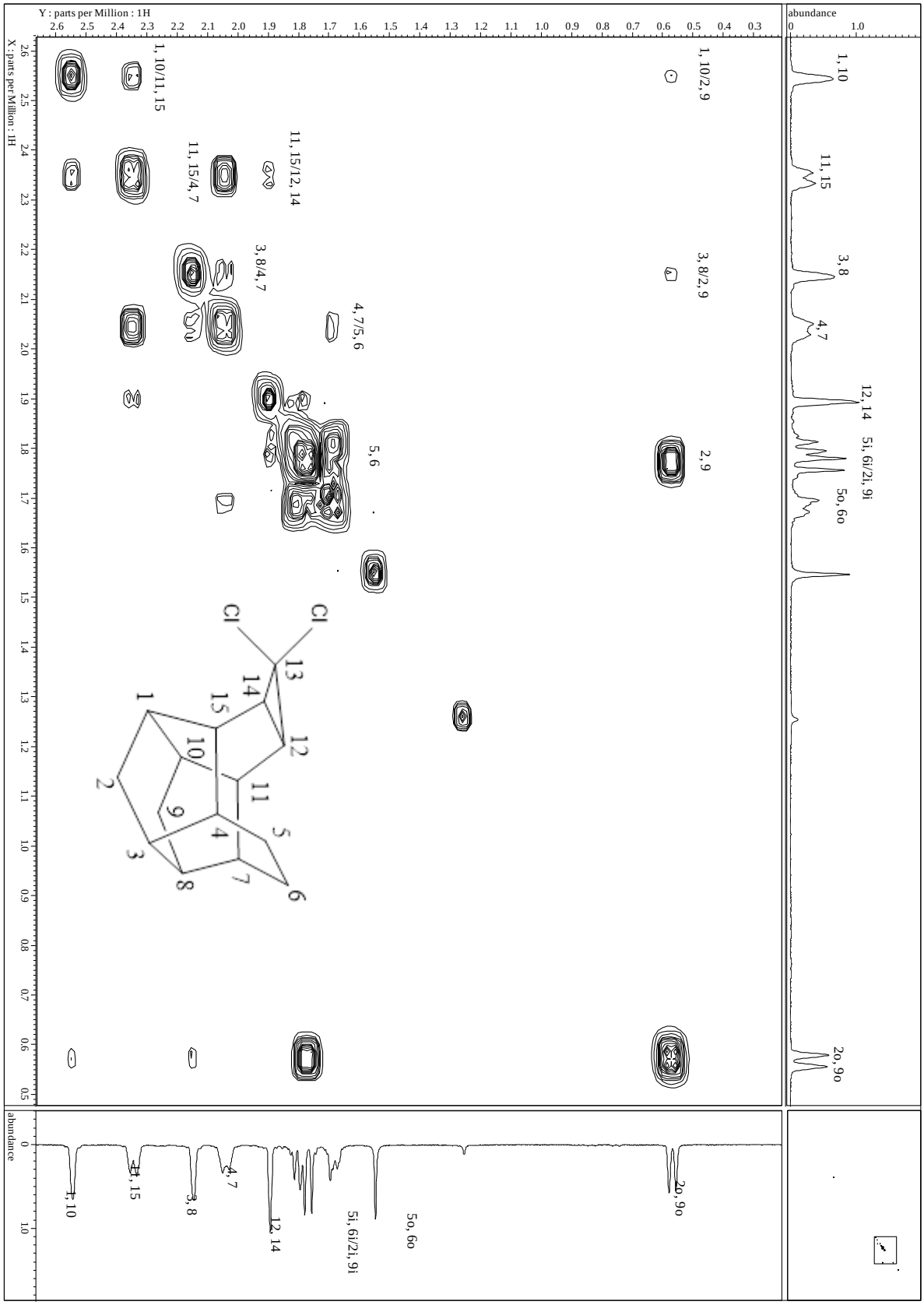
Y : parts per Million : 1H
X : parts per Million : 1H
abundance
1, 10
11, 15
3, 8
4, 7
12, 14
5i, 6i/2i, 9i
5o, 6o
2o, 9o
1, 10/2, 9
3, 8/2, 9
2, 9
4, 7/5, 6
5, 6
11, 15/12, 14
3, 8/4, 7
11, 15/4, 7
1, 10/11, 15
Cl
Cl
13
14
15
12
1
10
11
2
9
5
4
3
7
8
6
2o, 9o
5o, 6o
5i, 6i/2i, 9i
12, 14
4, 7
3, 8
11, 15
1, 10

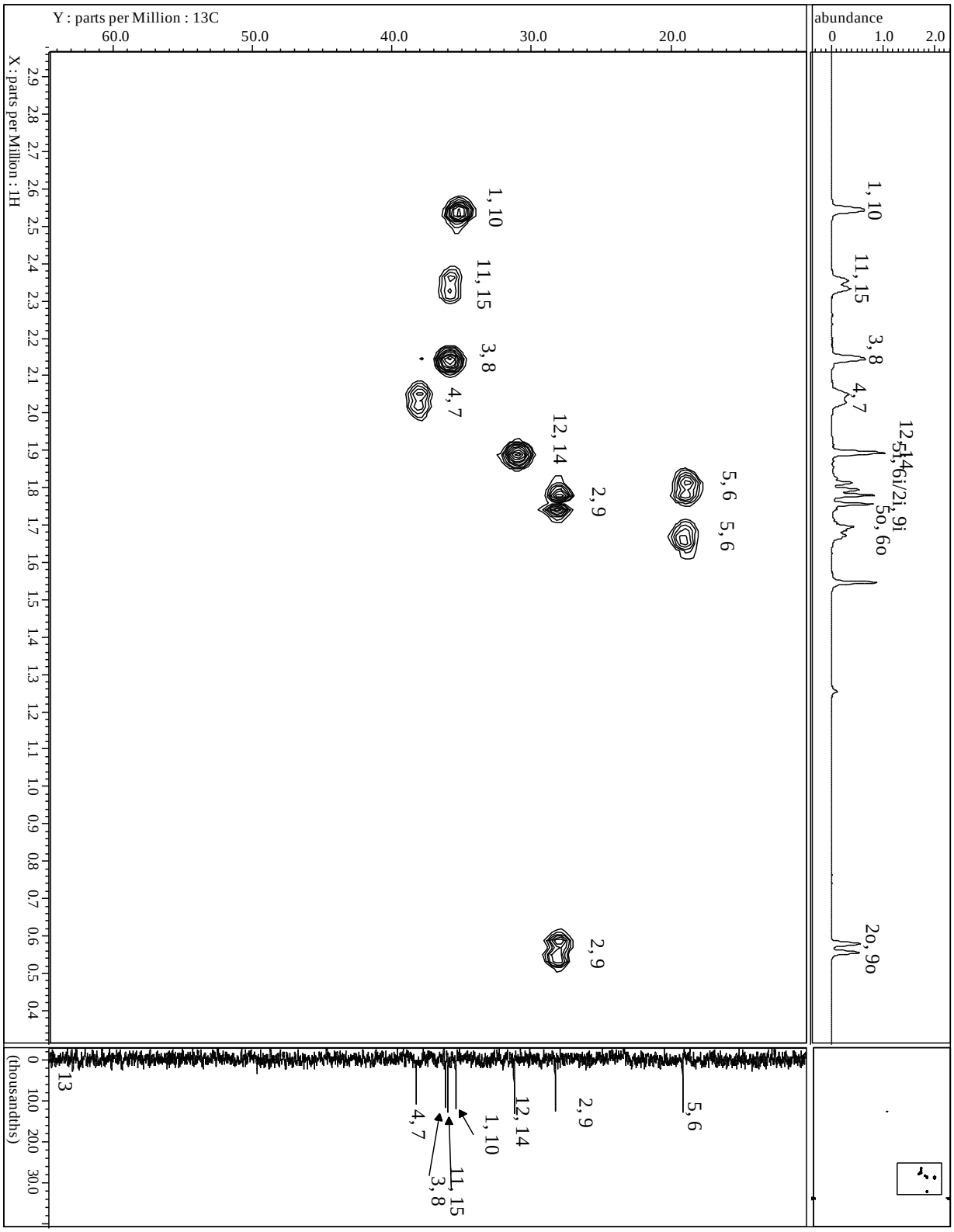
abundance
0
1.0
2.0
1, 10
11, 15
3, 8
4, 7
12, 5i, 14
6i/2i, 9i
5o, 6o
2o, 9o
Y : parts per Million : 13C
60.0
50.0
40.0
30.0
20.0
5, 6
5, 6
2, 9
12, 14
1, 10
11, 15
3, 8
4, 7
2, 9
X : parts per Million : 1H
2.9
2.8
2.7
2.6
2.5
2.4
2.3
2.2
2.1
2.0
1.9
1.8
1.7
1.6
1.5
1.4
1.3
1.2
1.1
1.0
0.9
0.8
0.7
0.6
0.5
0.4
13
5, 6
2, 9
12, 14
1, 10
11, 15
3, 8
4, 7
0
10.0
20.0
30.0
(thousandths)

13,13-dibromohexacyclo[8.5.0.0^{3,8}.0^{4,15}.0^{7,11}.0^{12,14}]pentadecane (42d)

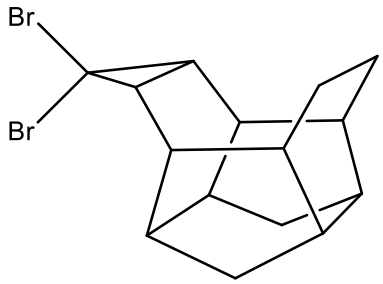

$C_{15}H_{18}Br_2$ (358) , R_f = 0.60 by SiO_2-TLC; visualized by UV or vanillin stain

MP = 191.9-192.5 (onset of browning at 186.4) °C ($CHCl_3$)

IR (AT-IR): $\tilde{\nu}$ = 2927 (s, C-H), 2863 (m, C-H), 1456 (m), 896 (m), 805 (m), 790 (m), 760 (s), 715 (m), 687 (s), 660 (m) cm^{-1}.

^{1}H-NMR ($CDCl_3$, 500 MHz): δ= 2.63 (s, 2H, H-1, -10), 2.49 (m, 2H, H-11, -15), 2.12 (s, 2H, H-3, -8), 2.03 (m, 2H, H-4, -7), 2.02 (t, 2H, H-12, -14), 1.80 (m, 2H, H-5i, -6i), 1.76 (d, 2H, H-2i, 10i), 1.67 (m, 2H, H-5o, -6o), 0.56 (d, 2H, H-2o, 10o) ppm;

$^2J_{\text{H-2i, -2o}} = {}^2J_{\text{H-9i, -9o}}$ = 11.5 Hz.

^{13}C-NMR ($CDCl_3$, 100.7 MHz): δ= 38.3 (C-4, -7), 37.0 (C-11, -15), 36.8(C-13), 36.1 (C-3, -8), 34.9 (C-1, -10), 32.6(C-12, -14), 28.2 (C-2, -9), 19.1 (C-5, -6) ppm.

MS(EI, 70 eV): *m/z* (%) = 358 ($M^{\cdot+}$, 0.7), 356 (0.3), 355 (0.1), 279 (13.1), 278 (9.5), 277 (13.3), 276 (7.5), 209 (8.7), 207 (7.7), 198 (20.5), 197 (94.1), 171 (24.8), 170 (8.8), 169 (45.6), 167 (11.6), 165 (14.2), 157 (8.6), 156 (9.0), 155 (34.7), 154 (11.5), 153 (18.9), 152 (15.3), 143 (19.4), 142 (19.3), 141 (58.6), 131 (27.9), 130 (16.0), 129 (68.6), 128 (68.1), 127 (18.3), 120 (9.9), 119 (22.6), 118 (9.6), 117 (61.2), 116 (26.6), 115 (71.3), 107 (9.6), 105 (26.4), 104 (22.1), 103 (22.7), 102 (11.4), 93 (14.4), 92 (19.7), 91 (100.0), 90 (11.9), 89 (17.8), 82 (17.5), 81 (23.7), 80 (23.3), 79

(70.1), 78 (29.8), 77 (66.9), 76 (8.5), 67 (30.1), 66 (9.7), 65 (29.0), 63 (15.3), 55 (8.3), 53 (15.5), 52 (9.2), 51 (12.0), 51 (8.6).

Spectra

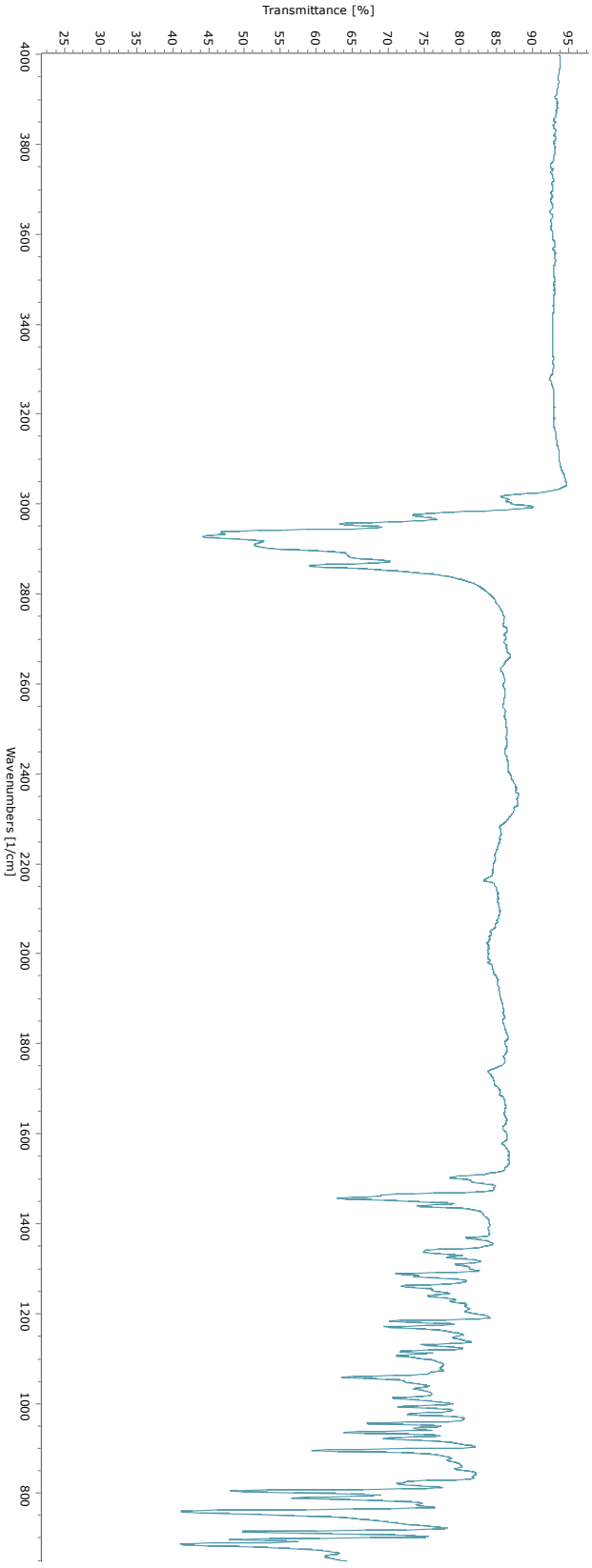
Transmittance [%]
Wavenumbers [1/cm]

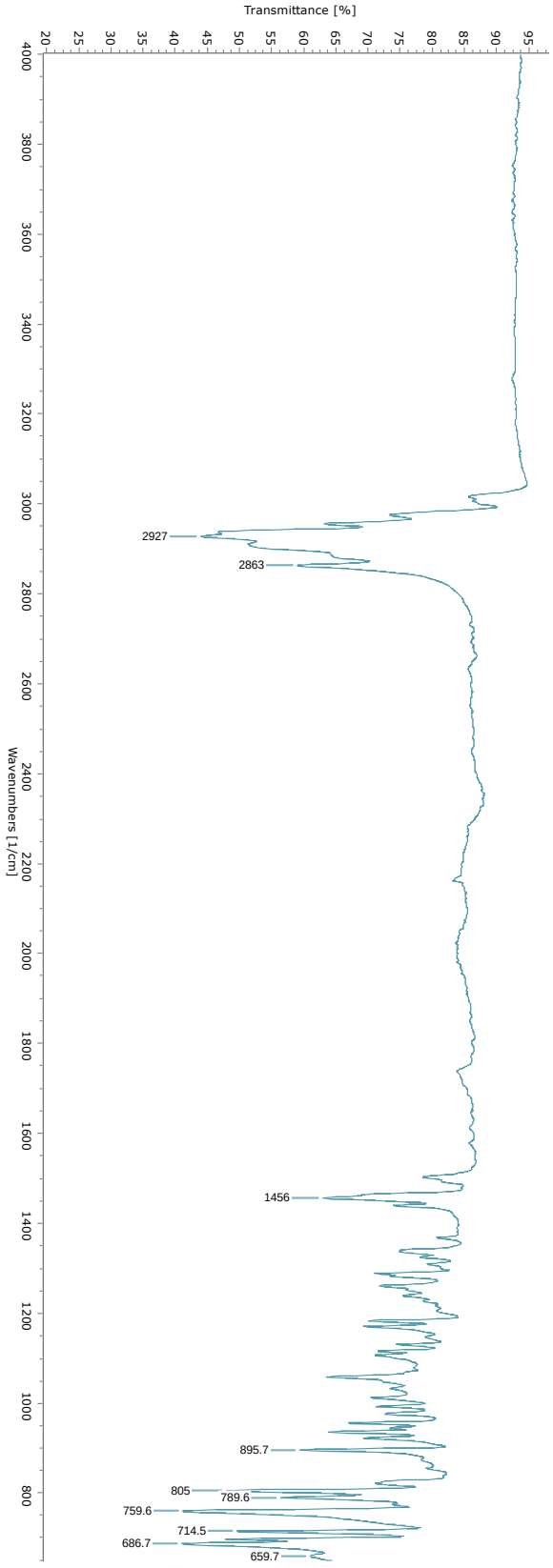
Transmittance [%]
Wavenumbers [1/cm]
2927
2863
1456
895.7
805
789.6
759.6
714.5
686.7
659.7

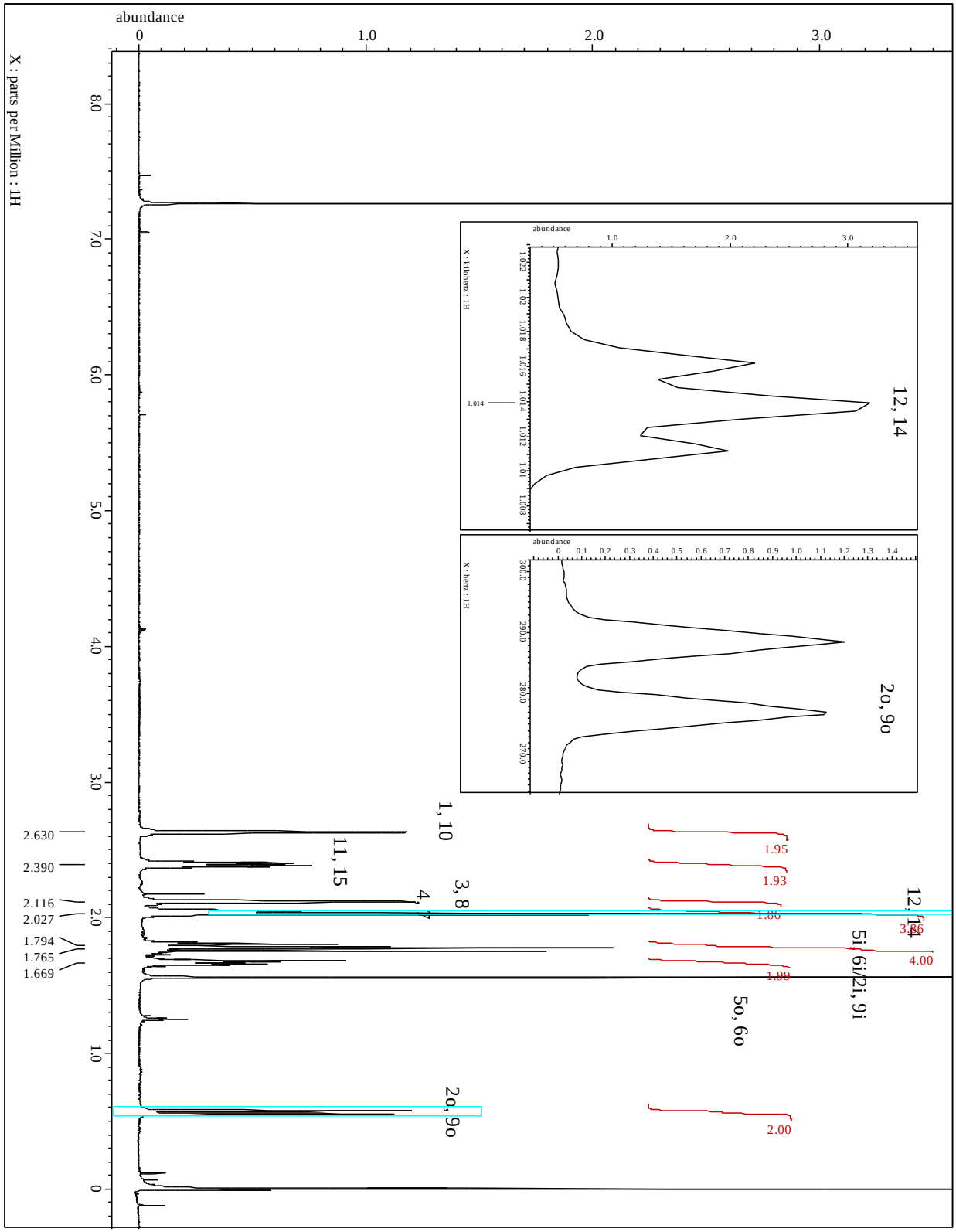
abundance
X : parts per Million : 1H
2.630
2.390
2.116
2.027
1.794
1.765
1.669
11, 15
1, 10
3, 8
4, 7
12, 14
5i, 6i/2i, 9i
5o, 6o
2o, 9o
1.95
1.93
1.86
3.86
4.00
1.99
2.00
abundance
X : kilohertz : 1H
1.014
12, 14
abundance
X : hertz : 1H
2o, 9o

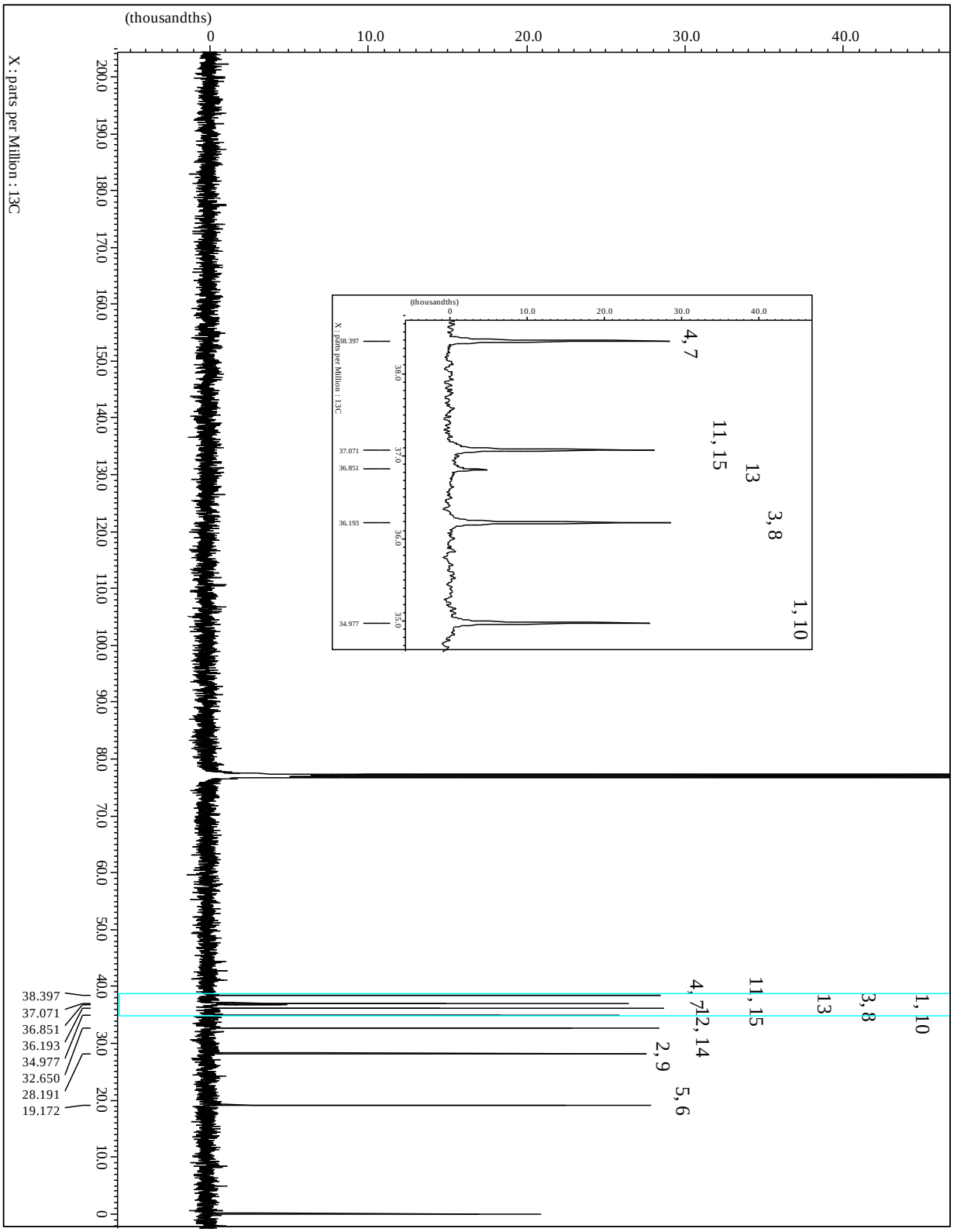
(thousandths)
0
10.0
20.0
30.0
40.0
X : parts per Million : 13C
200.0
190.0
180.0
170.0
160.0
150.0
140.0
130.0
120.0
110.0
100.0
90.0
80.0
70.0
60.0
50.0
40.0
30.0
20.0
10.0
0
38.397
37.071
36.851
36.193
34.977
32.650
28.191
19.172
1, 10
3, 8
13
11, 15
4, 7
12, 14
2, 9
5, 6
(thousandths)
0
10.0
20.0
30.0
40.0
X : parts per Million : 13C
38.397
37.071
36.851
36.193
34.977
38.0
37.0
36.0
35.0
4, 7
11, 15
13
3, 8
1, 10

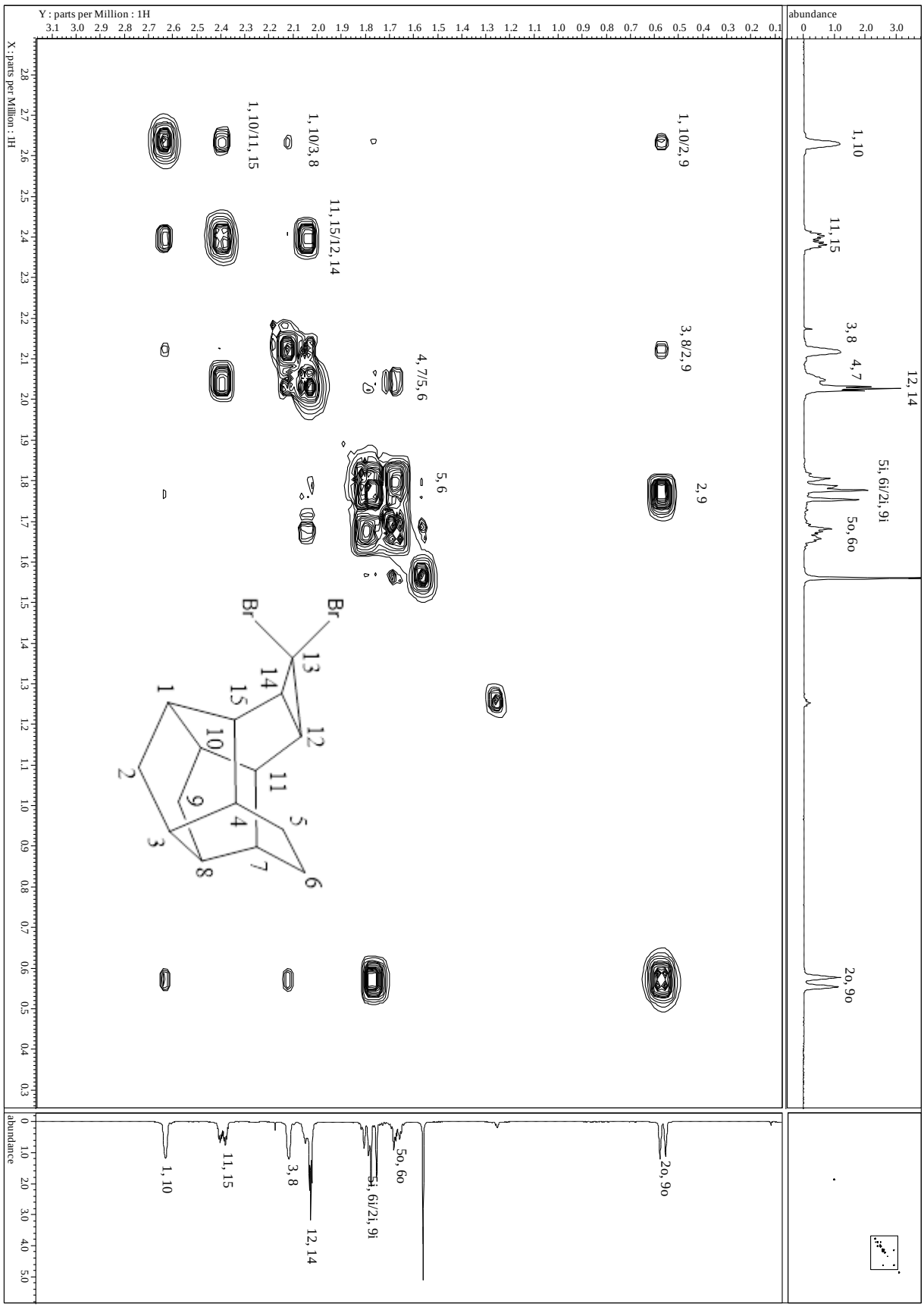
Y : parts per Million : 1H
X : parts per Million : 1H
abundance
1, 10
11, 15
3, 8
4, 7
12, 14
5i, 6i/2i, 9i
5o, 6o
2o, 9o
1, 10/2, 9
3, 8/2, 9
2, 9
4, 7/5, 6
5, 6
11, 15/12, 14
1, 10/3, 8
1, 10/11, 15
Br
Br
1
2
3
4
5
6
7
8
9
10
11
12
13
14
15

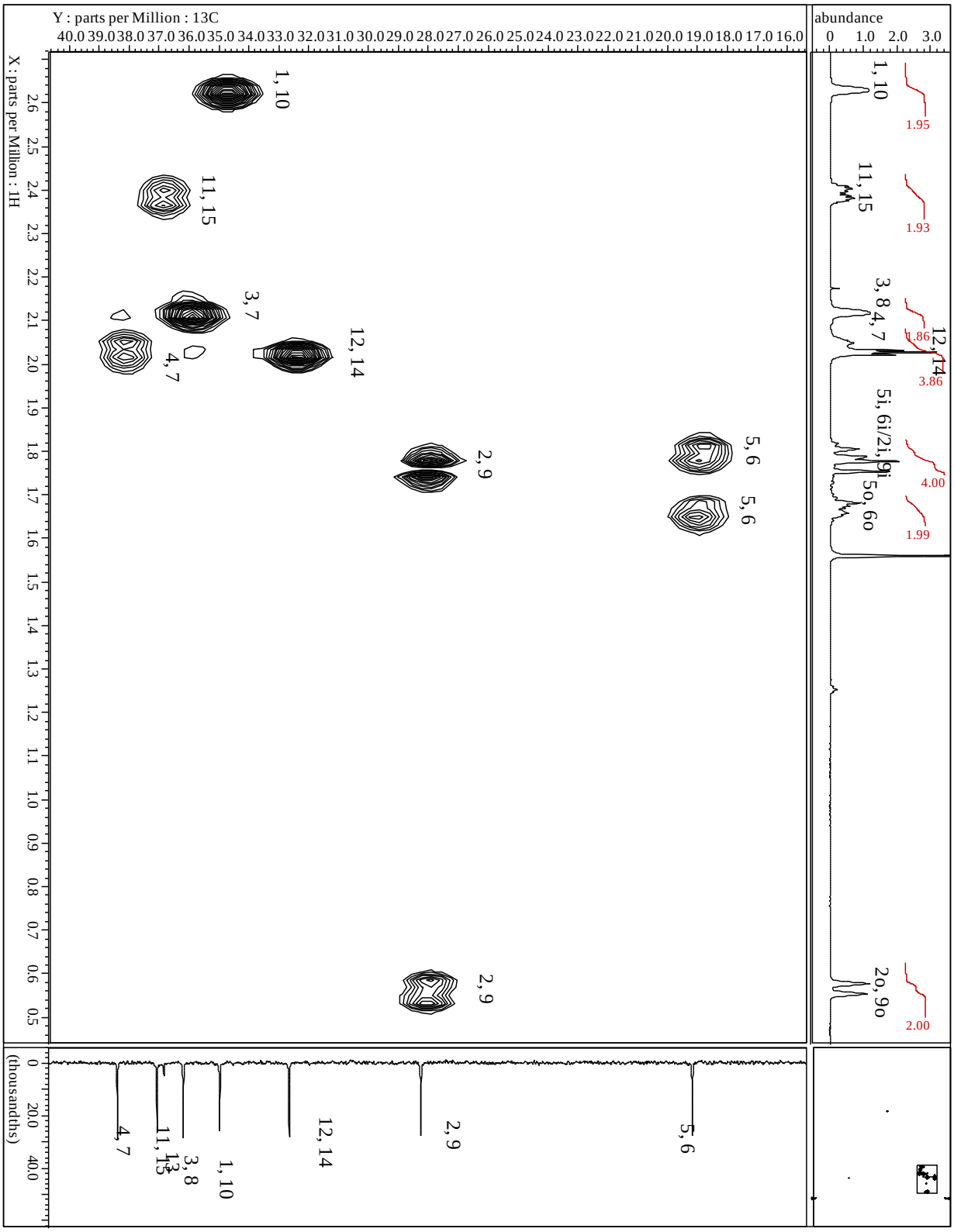
Y : parts per Million : 13C
X : parts per Million : 1H
abundance
(thousandths)
1, 10
11, 15
3, 8
4, 7
12, 14
5i, 6i/2i, 9i
5o, 6o
20, 9o
1.95
1.93
1.86
3.86
4.00
1.99
2.00
5, 6
2, 9
3, 7
11, 13

5.3.5 Mixed carbene Adducts **41e-g**

(5R,7S)-6,6-dichloroheptacyclo[9.5.0.0^{3,9}.0^{4,16}.0^{5,7}.0^{8,12}.0^{13,15}]hexadecane (41e)

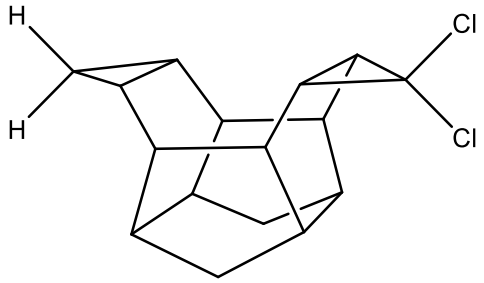

$C_{16}H_{18}Cl_2$ (280) , R_f = 0.70 by SiO_2-TLC; visualized by UV or vanillin stain

MP = 142.5-143.2 (full melt at 147.9) °C ($CHCl_3$)

IR (AT-IR): $\tilde{\nu}$ = 2939 (m, C-H), 1679 (m), 1260 (m), 1016 (s), 798 (s) cm^{-1}.

^{1}H-NMR ($CDCl_3$, 500 MHz): δ = 2.52 (s_{app}, 2H, H-3, -9), 2.49 (m, 2H, H-4, -8), 2.39 (m, 2H, H-12, -16), 2.01 (s_{app}, 2H, H-1, -11), 1.94 (s_{app}, 2H, H-5, -7), 1.62 (d, 2H, H-2i, -10i), 1.00 (m, 2H, H-13, -15), 0.50 (d, 2H, H-2o, -10o), 0.43 (sx, 1H, H-14), 0.37 (q, 1H, H-14) ppm;

$^2J_{H\text{-}2i,\ -2o} = {}^2J_{H\text{-}10i,\ -10o}$ =11.8 Hz.

^{13}C-NMR ($CDCl_3$, 100.7 MHz): δ= 67.1 (C-5), 40.4 (C-12, -16), 37.2 (C-4, -8), 35.6 (C-1, 11), 35.2 (C-3, -9), 31.9 (C-5, -7). 27.7 (C-2, -10), 11.8 (C-13, -15), 6.0 (C-14) ppm.

MS(EI, 70 eV): *m/z* (%) = 282 ($M^{\cdot+}$+2, 0.9), 280 ($M^{\cdot+}$, 1.5), 245 (18.2), 209 (23.9), 181 (8.8), 179 (10.8), 178 (10.4), 177 (10.9), 176 (8.4), 175 (9.5), 167 (16.9), 166 (9.4), 165 (24.0), 163 (12.4), 155 (11.5), 153 (17.2), 152 (15.3), 151 (11.0), 145 (7.7), 143 (18.5), 142 (12.9), 141 (28.9), 139 (13.7), 132 (22.2), 131 (27.7), 130 (14.2), 129 (41.9), 128 (37.4), 127 (24.8), 125 (26.8), 119 (10.6), 118 (10.2), 117 (47.5), 116 (16.1), 115 (52.9), 113 (8.5), 106 (9.5), 105 (26.9), 104 (21.3), 103

(25.6), 102 (9.9), 101 (8.1), 99 (9.8), 93 (14.7), 92 (18.6), 91 (100.0), 89 (16.7), 81 (10.3), 79 (43.4), 78 (29.7), 77 (63.3), 75 (8.5), 67 (17.7), 66 (11.0), 65 (25.4), 63 (13.2), 53 (13.3), 52 (8.4), 51 (17.9).

Spectra

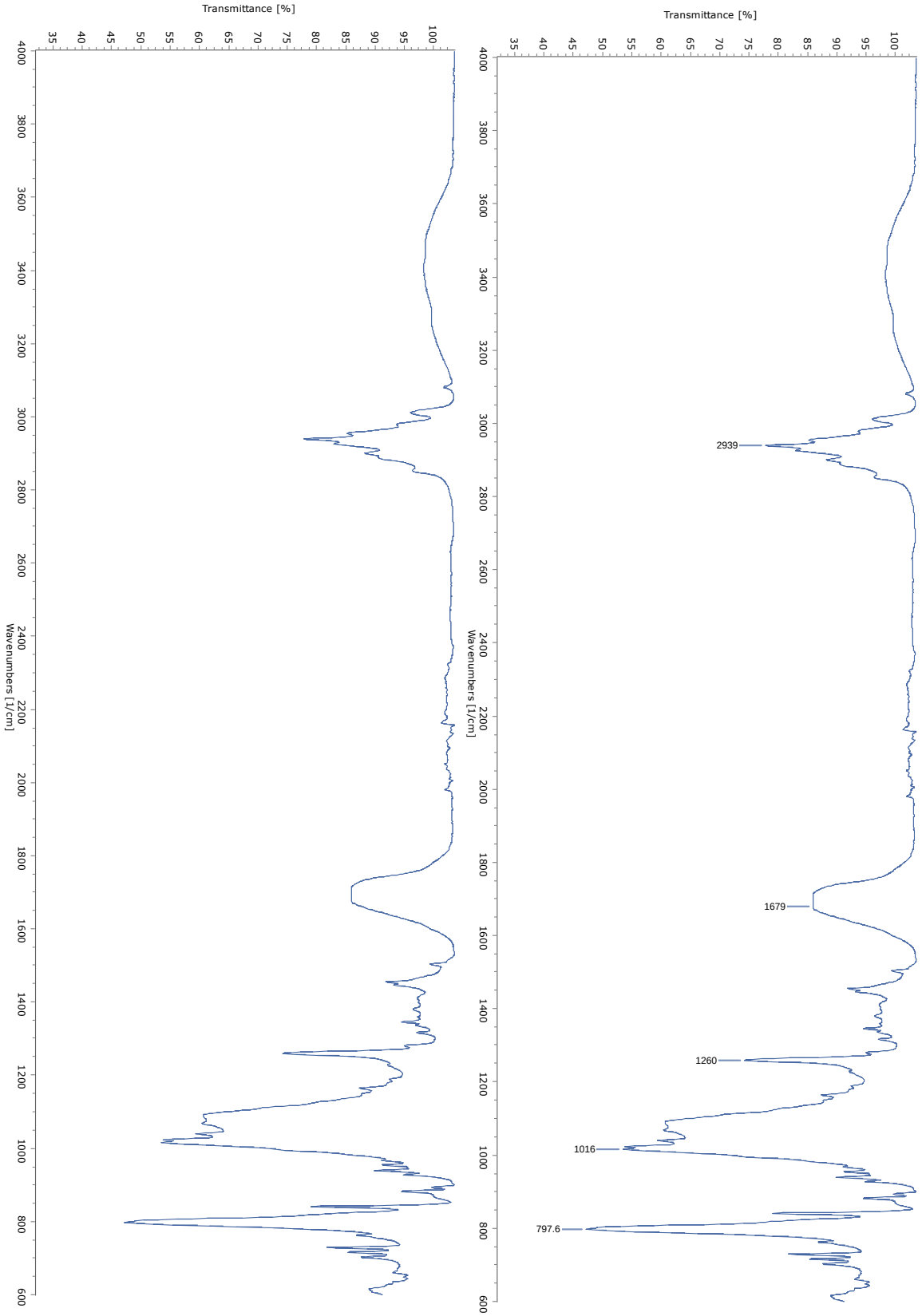
Transmittance [%]
Wavenumbers [1/cm]
2939
1679
1260
1016
797.6

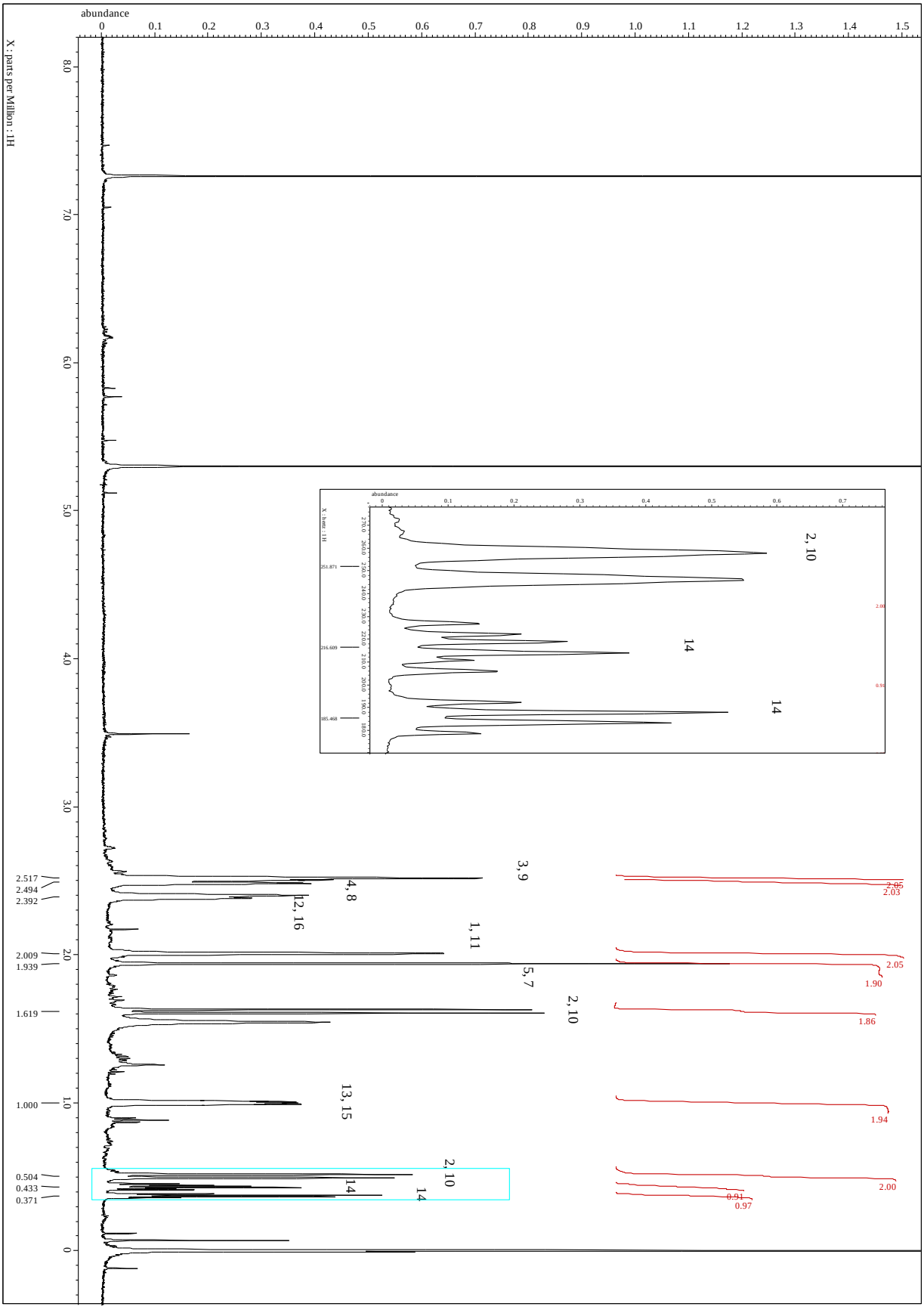
abundance
X : parts per Million : 1H
2.517
2.494
2.392
2.009
1.939
1.619
1.000
0.504
0.433
0.371
3, 9
4, 8
12, 16
1, 11
5, 7
2, 10
13, 15
14
2.05
2.03
2.05
1.90
1.86
1.94
2.00
0.91
0.97

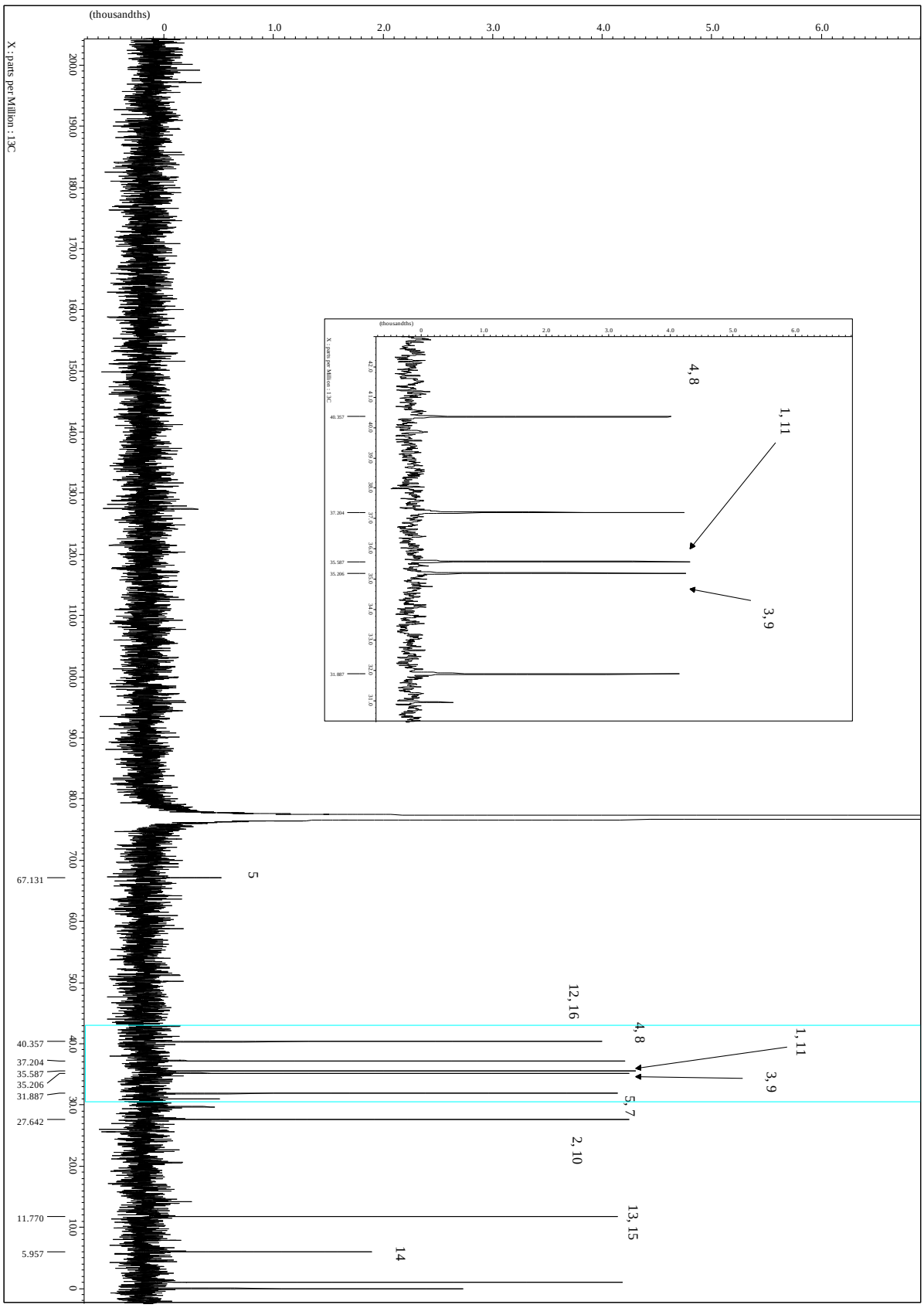
(thousandths)
X : parts per Million : 13C
67.131
40.357
37.204
35.587
35.206
31.887
27.642
11.770
5.957
5
12, 16
4, 8
1, 11
3, 9
5, 7
2, 10
13, 15
14

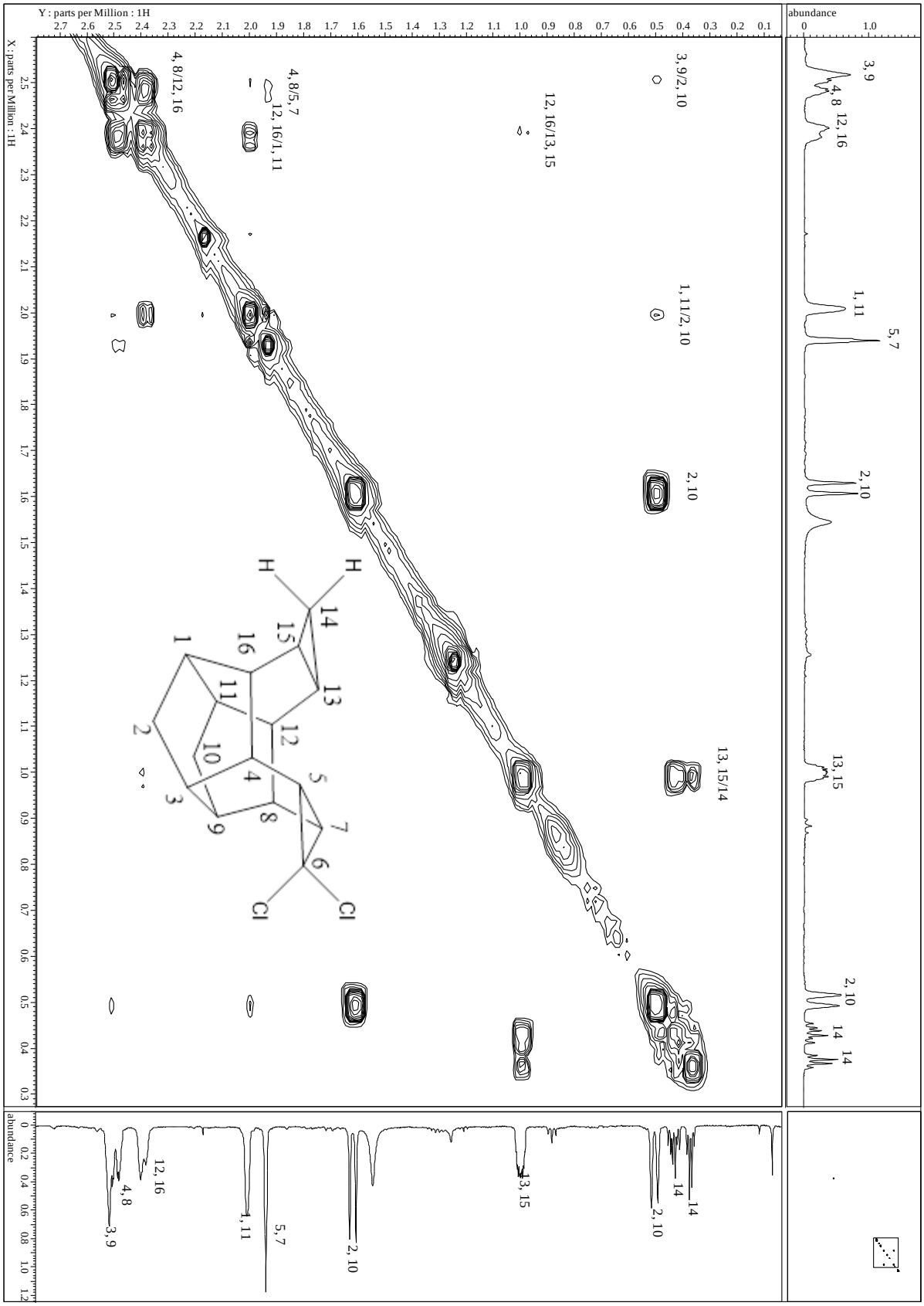
Y : parts per Million : 1H
X : parts per Million : 1H
abundance
3, 9
4, 8
12, 16
1, 11
5, 7
2, 10
13, 15
14
3, 9/2, 10
1, 11/2, 10
12, 16/13, 15
4, 8/5, 7
12, 16/1, 11
4, 8/12, 16
13, 15/14
H
Cl
Cl

(5R,7S)-6,6-dibromoheptacyclo[9.5.0.0^{3,9}.0^{4,16}.0^{5,7}.0^{8,12}.0^{13,15}]hexadecane (41f)

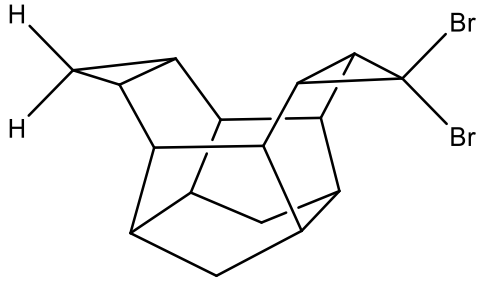

$C_{16}H_{18}Br_2$ (358) , R_f = 0.60 by SiO_2-TLC; visualized by UV or vanillin stain

MP = 144.5-146.2 °C ($CHCl_3$)

IR (AT-IR): $\tilde{\nu}$ = 2938 (s, C-H), 1731 (w), 1445 (w), 1280 (w), 1023 (m), 688 (s) cm^{-1}.

^{1}H-NMR ($CDCl_3$, 500 MHz): δ= 2.60 (s_{app}, 2H, H-3, -9), 2.55 (m, 2H, H-4, -8), 2.40 (m, 2H, H-12, -16), 2.08 (t, 2H, H-5, -7), 1.99 (s_{app}, 2H, H-1, -11), 1.62 (d, 2H, H-2i, -10i), 1.00 (m, 2H, H-13, -15), 0.50 (d, 2H, H-2o, -10o), 0.43 (sx, 1H, H-14), 0.39 (q, 1H, H-14) ppm;

$^2J_{H\text{-}2i,\ -2o} = {}^2J_{H\text{-}10i,\ -10o}$ =12.0 Hz.

^{13}C-NMR ($CDCl_3$, 100.7 MHz): δ= 40.5 (C-12, -16), 38.3 (C-4, -8), 36.9 (C-6), 35.6 (C-1, -11), 35.2 (C-3, -9), 34.8 (C-5, -7). 27.5 (C-2, -10), 11.8 (C-13, -15), 6.0 (C-14) ppm.

MS(EI, 70 eV): *m/z* (%) = 292 (3.2), 291 (13.8), 290 (3.7), 289 (14.5), 288 (2.1), 210 (14.7), 209 (43.9), 181 (10.4), 167 (18.1), 165 (12.4), 155 (12.4), 153 (12.4), 152 (8.7), 143 (19.1), 142 (9.1), 141 (27.2), 131 (19.8), 130 (11.2), 129 (51.1), 128 (30.2), 127 (7.6), 118 (9.3), 117 (44.1), 116 (16.0), 115 (47.7), 105 (18.6), 104 (17.8), 103 (10.9), 93 (12.9), 92 (13.3), 91 (100.0), 89 (9.4), 81 (13.4), 80 (11.1), 79 (32.4), 78 (24.9), 77 (35.3), 67 (11.2), 65 (18.5), 51 (13.8).

Spectra

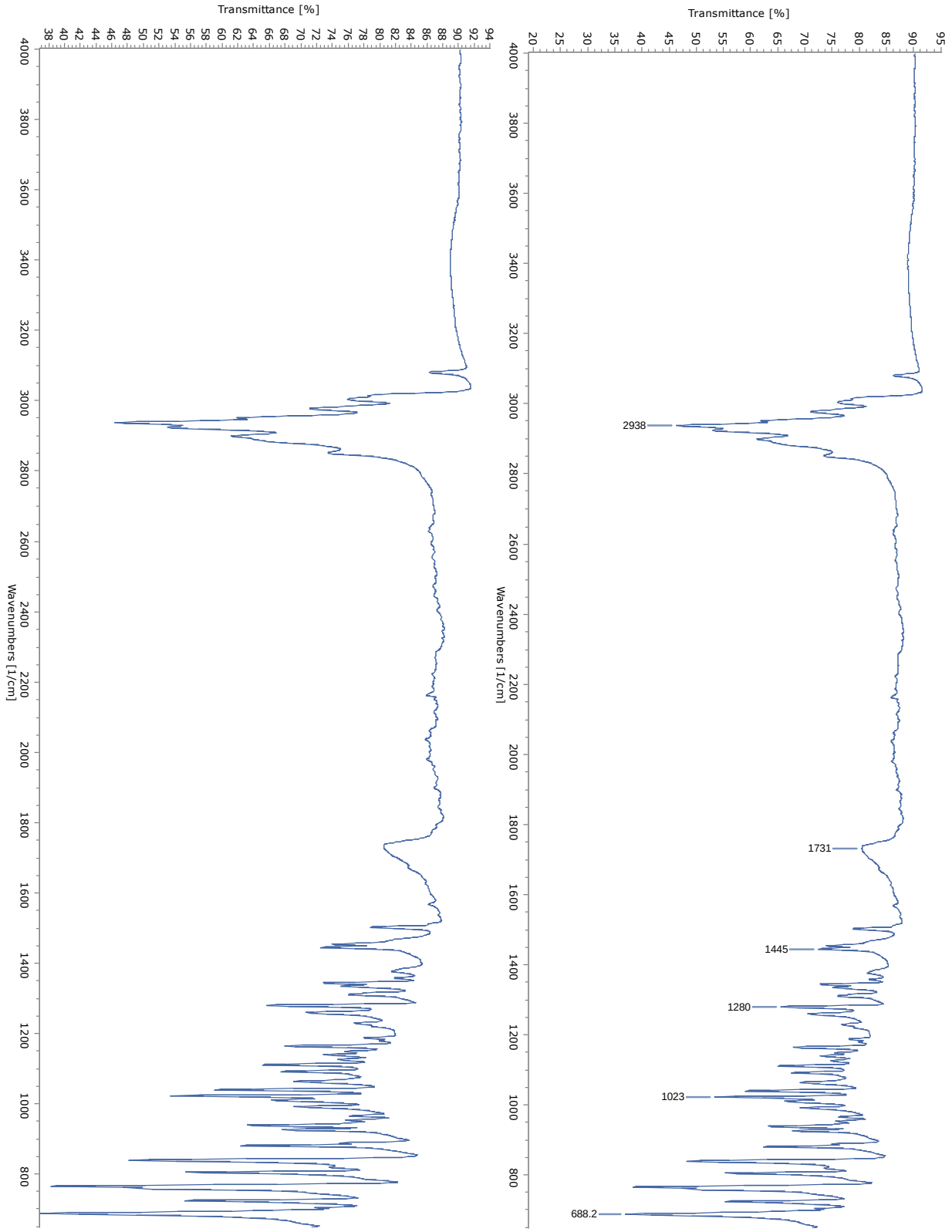
Transmittance [%]
Wavenumbers [1/cm]
2938
1731
1445
1280
1023
688.2

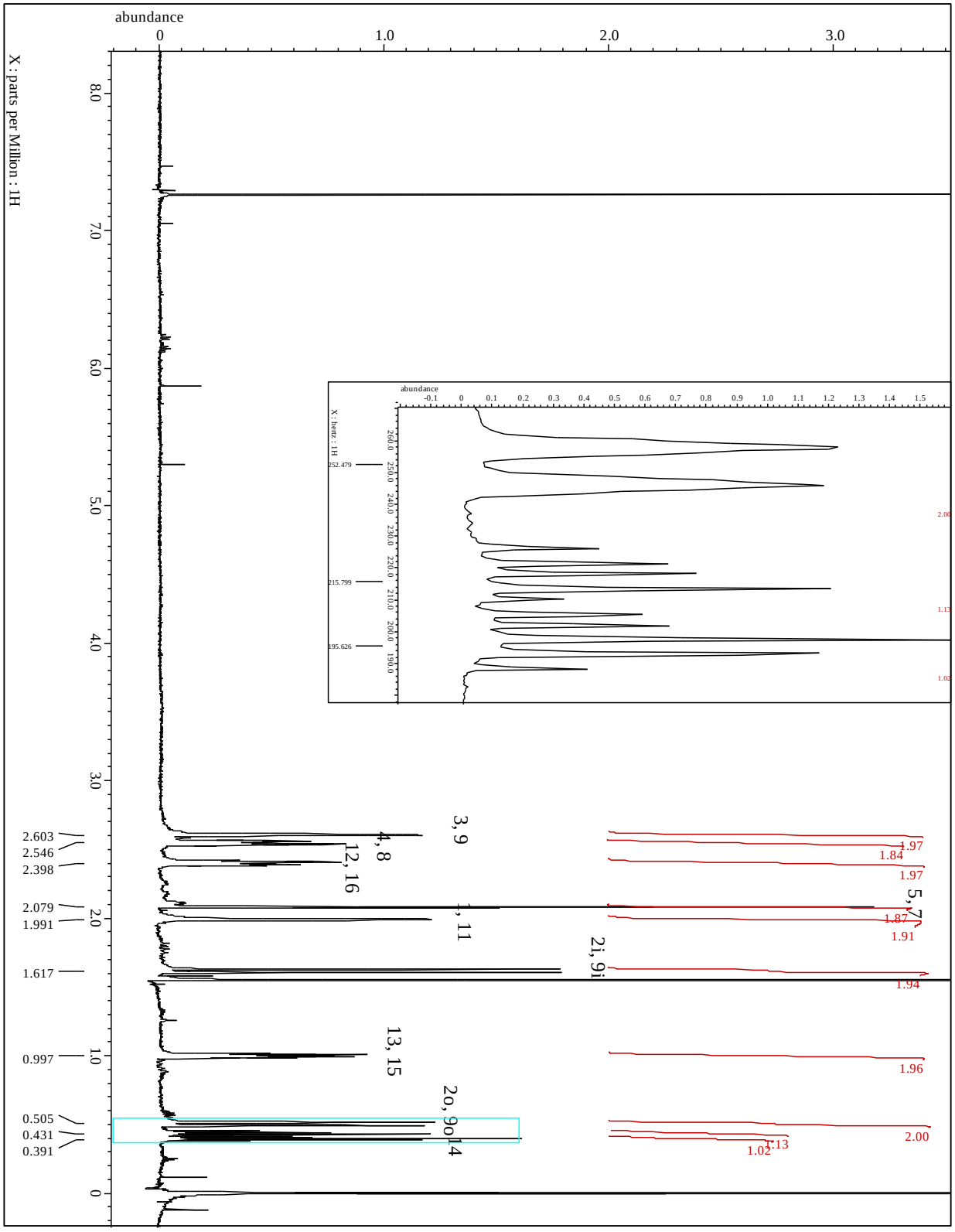
abundance
0
1.0
2.0
3.0
X : parts per Million : 1H
8.0
7.0
6.0
5.0
4.0
3.0
2.0
1.0
0
abundance
-0.1
0
0.1
0.2
0.3
0.4
0.5
0.6
0.7
0.8
0.9
1.0
1.1
1.2
1.3
1.4
1.5
X : hertz : 1H
252.479
215.799
195.626
260.0
250.0
240.0
230.0
220.0
210.0
200.0
190.0
2.00
1.13
1.02
2.603
2.546
2.398
2.079
1.991
1.617
0.997
0.505
0.431
0.391
4, 8
12, 16
3, 9
1, 11
2i, 9i
13, 15
2o, 9o
14
5, 7
1.97
1.84
1.97
1.87
1.91
1.94
1.96
2.00
1.13
1.02

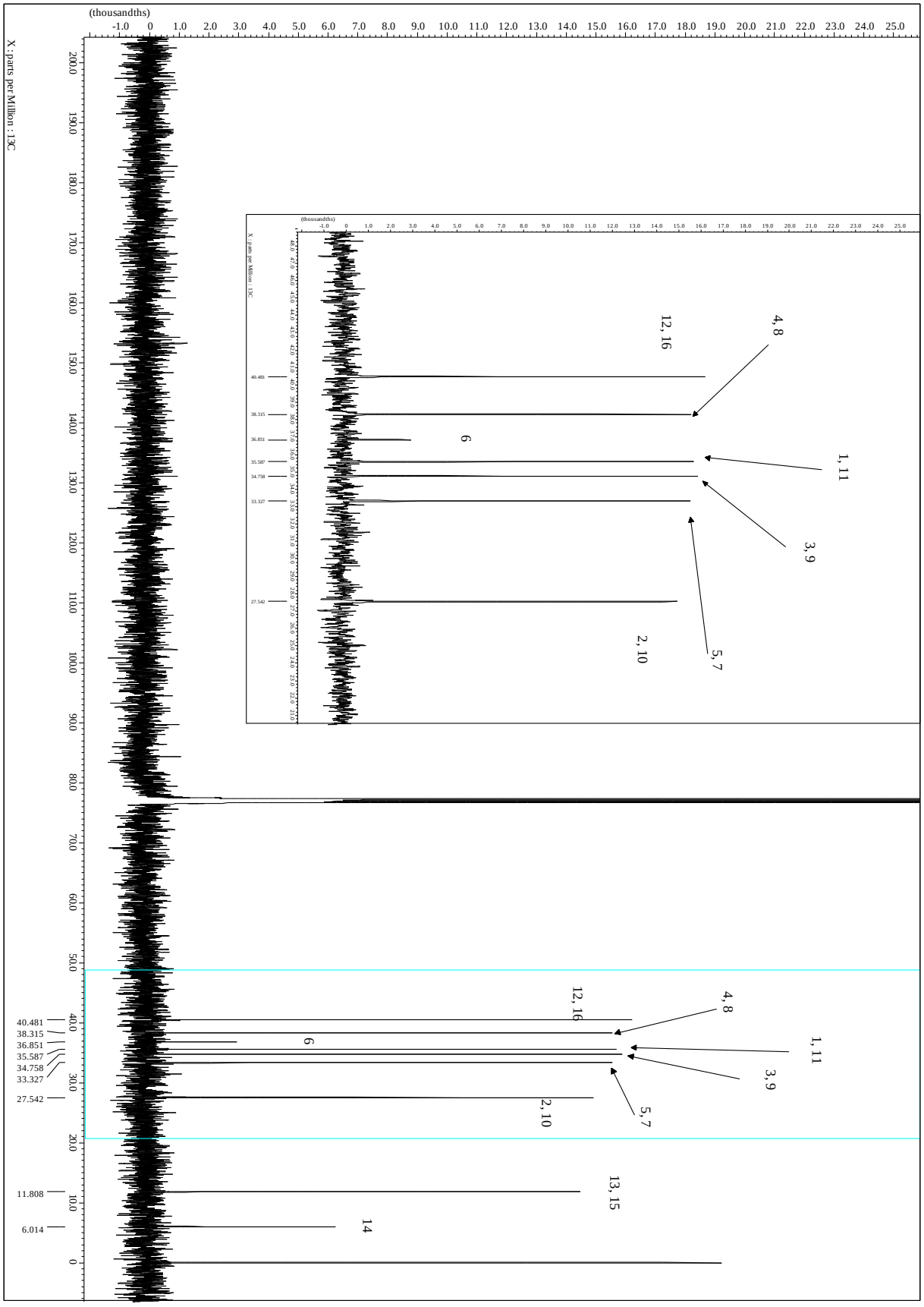
(thousandths)
X : parts per Million : 13C
40.481
38.315
36.851
35.587
34.758
33.327
27.542
11.808
6.014
12, 16
4, 8
6
1, 11
3, 9
5, 7
2, 10
13, 15
14

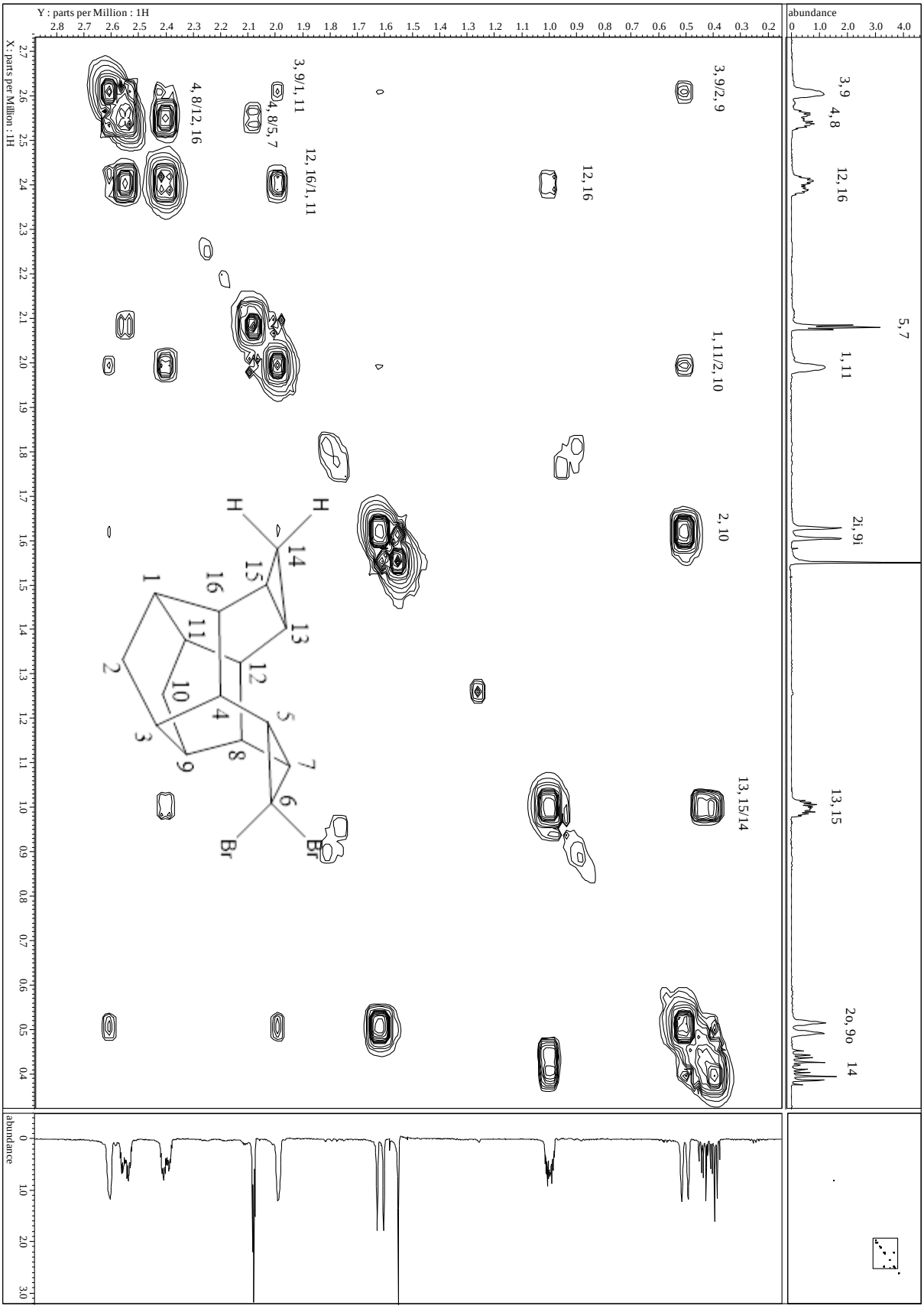
Y : parts per Million : 1H
X : parts per Million : 1H
abundance
3, 9
4, 8
12, 16
5, 7
1, 11
2i, 9i
13, 15
2o, 9o
14
3, 9/2, 9
12, 16
1, 11/2, 10
2, 10
13, 15/14
4, 8/5, 7
3, 9/1, 11
12, 16/1, 11
4, 8/12, 16
H
H
Br
Br
1
2
3
4
5
6
7
8
9
10
11
12
13
14
15
16

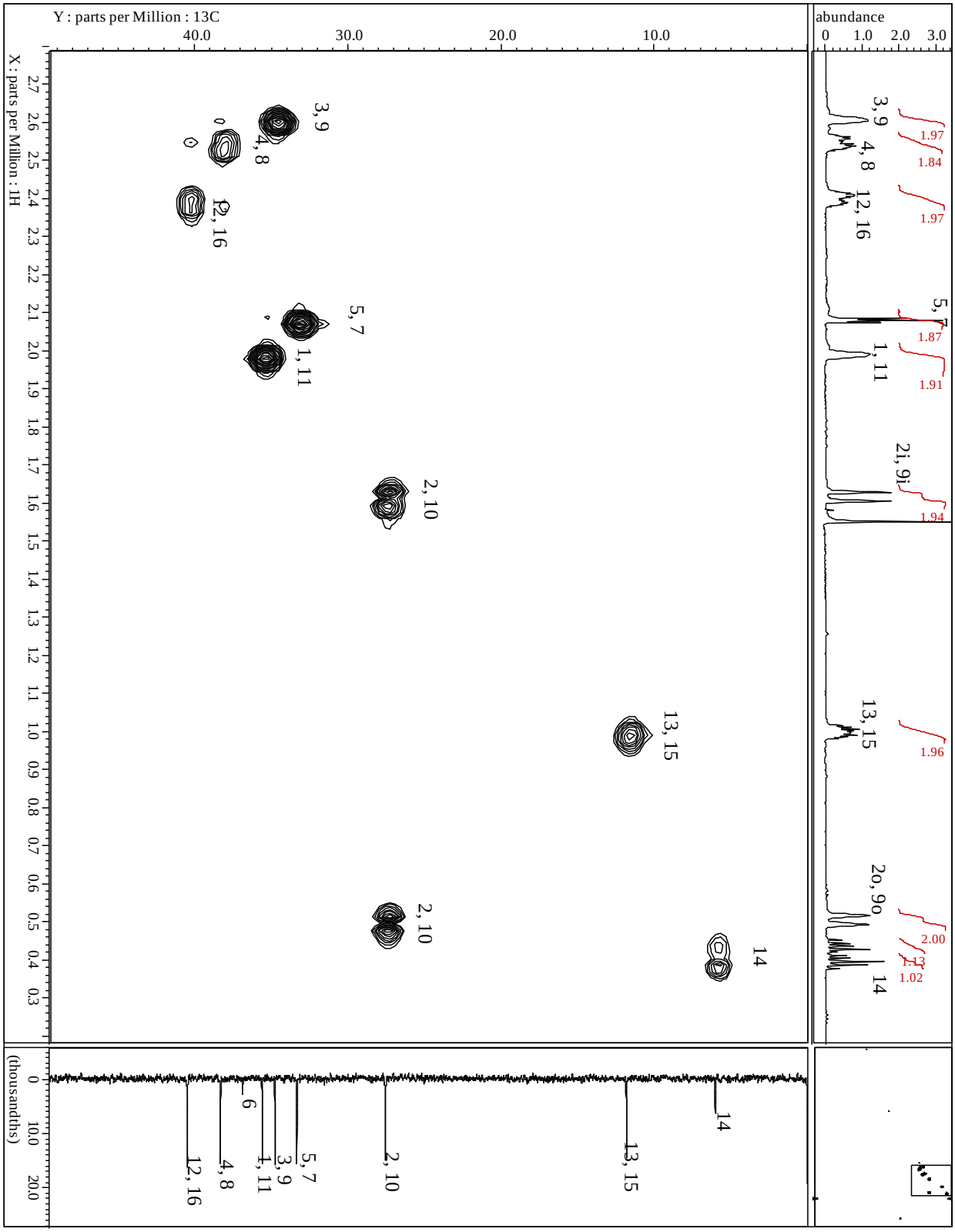
Y : parts per Million : 13C
X : parts per Million : 1H
abundance
(thousandths)
3, 9
4, 8
12, 16
5, 7
1, 11
2i, 9i
13, 15
20, 9o
14
2, 10
1.97
1.84
1.97
1.87
1.91
1.94
1.96
2.00
1.13
1.02

(5R,7S)-6,6-dibromo-14,14-dichloroheptacyclo[9.5.0.0^{3,9}.0^{4,16}.0^{5,7}.0^{8,12}.0^{13,15}]hexadecane (41g)

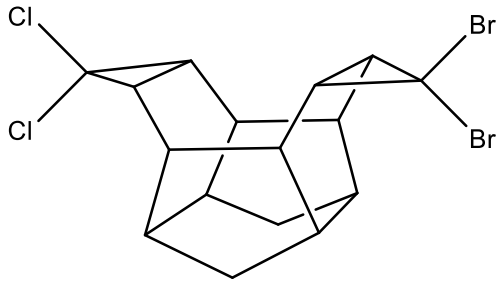

$C_{16}H_{16}Br_2Cl_2$ (439), R_f = 0.40 by SiO_2-TLC; visualized by UV or vanillin stain

MP = 193.6-195.0 °C ($CHCl_3$)

IR (AT-IR): $\tilde{\nu}$ = 2957 (m, C-H), 1455 (m), 1249 (m), 1075 (m), 1025 (m), 945 (m), 878 (s), 812 (s), 726 (s) cm^{-1}.

^{1}H-NMR ($CDCl_3$, 500 MHz): δ= 3.25 (s_{app}, 2H, H-5, -7), 2.65 (m, 2H, H-12, -16), 2.58 (s_{app}, 4H, H-1, -11; H-4, -8), 2.29 (s_{app}, 2H, H-3, -9), 1.86 (s_{app}, 2H, H-13, -15), 1.65 (d, 2H, H-2i, -10i), 0.54 (d, 2H, H-2o, -10o) ppm;

$^2J_{H\text{-}2i,\ -2o} = {}^2J_{H\text{-}10i,\ -10o}$ =12.0 Hz.

^{13}C-NMR ($CDCl_3$, 100.7 MHz): δ= 65.7 (C-14), 53.0 (C-5, -7), 40.8 (C-4, -8), 37.0 (C-12, -16), 35.9 (C-3, -9), 35.1 (C-1, -11), 30.9 (C-13, -15), 27.7 (C-2, -10), ** (C-6) ppm.

**: The CBr_2 ^{13}C-NMR signal was not observed.

MS(EI, 70 eV): *m/z* (%) = 284 (0.8), 283 (0.7), 282 (1.2), 281 (0.9), 247 (13.7), 219 (12.6), 211 (16.7), 193 (14.5), 189 (7.7), 183 (28.8), 181 (18.6), 179 (10.6), 178 (9.5), 177 (14.1), 175 (13.5), 173 (8.3), 172 (8.6), 169 (9.5), 168 (8.2), 167 (20.2), 166 (11.9), 165 (25.0), 164 (7.9), 163 (17.4), 162 (8.2), 161 (9.5), 159 (12.1), 155 (23.4), 154 (10.9), 153 (27.6), 152 (17.2), 151 (23.5), 149

(8.7), 145 (11.2), 143 (11.7), 142 (19.1), 141 (40.2), 139 (24.1), 138 (9.6), 133 (12.7), 131 (21.8), 130 (15.6), 129 (57.0), 128 (48.9), 127 (35.1), 126 (8.8), 125 (36.3), 121 (9.2), 119 (13.7), 118 (12.5), 117 (58.3), 116 (27.3), 115 (69.4), 113 (14.5), 111 (8.5), 109 (11.9), 107 (20.5), 106 (7.9), 105 (32.4), 104 (18.6), 103 (37.0), 102 (17.1), 101 (14.4), 99 (14.0), 95 (15.0), 94 (14.5), 93 (17.6), 92 (21.6), 91 (100.0), 89 (21.7), 83 (10.6), 82 (8.4), 81 (36.9), 80 (14.0), 79 (69.8), 78 (33.2), 77 (93.2), 76 (8.1), 75 (15.6), 73 (9.6), 67 (30.5), 66 (18.5), 65 (34.9), 63 (20.2), 55 (13.6), 53 (24.0), 52 (10.9), 51 (30.5).

Spectra

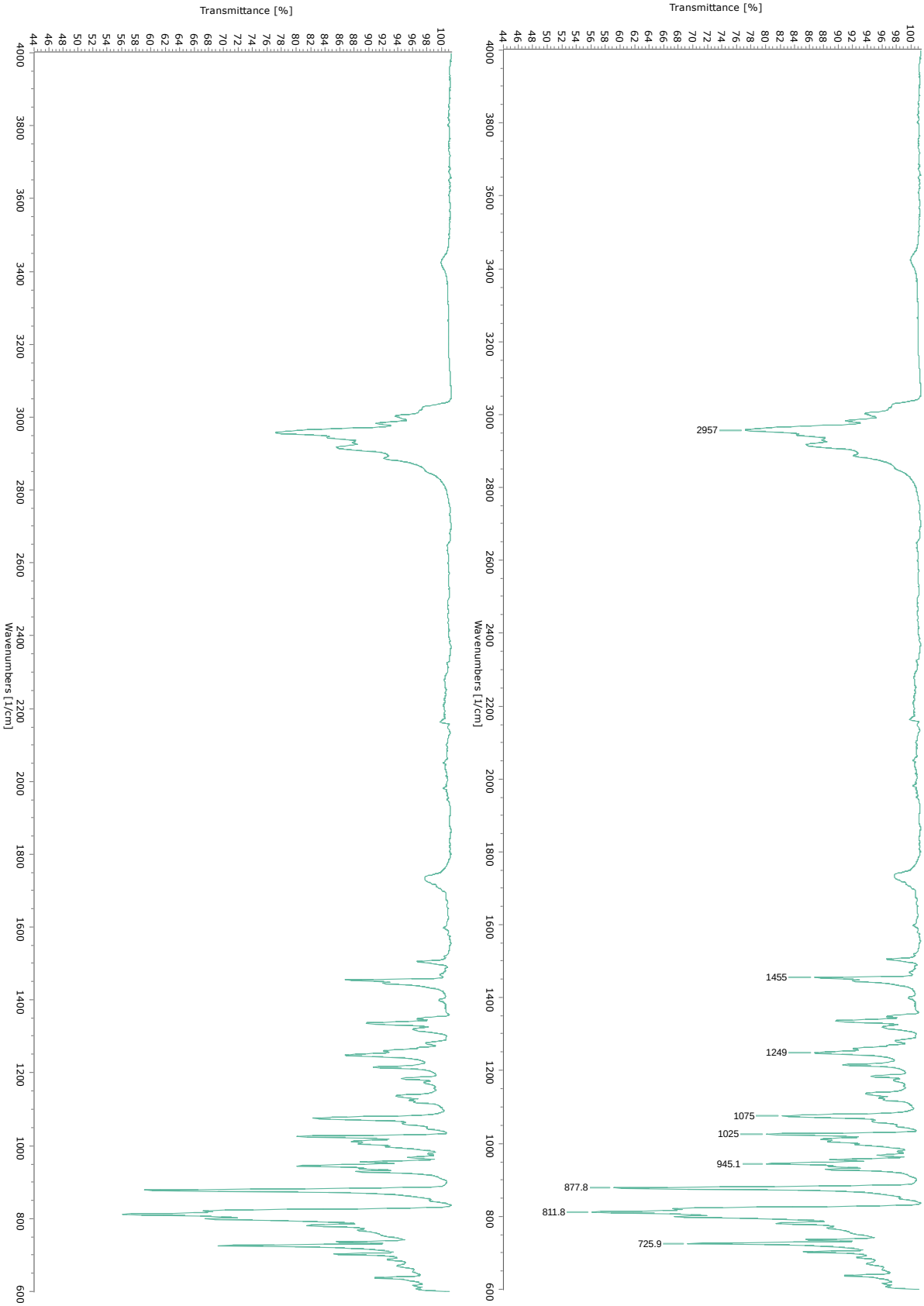
Transmittance [%]
Wavenumbers [1/cm]
2957
1455
1249
1075
1025
945.1
877.8
811.8
725.9
Transmittance [%]
Wavenumbers [1/cm]

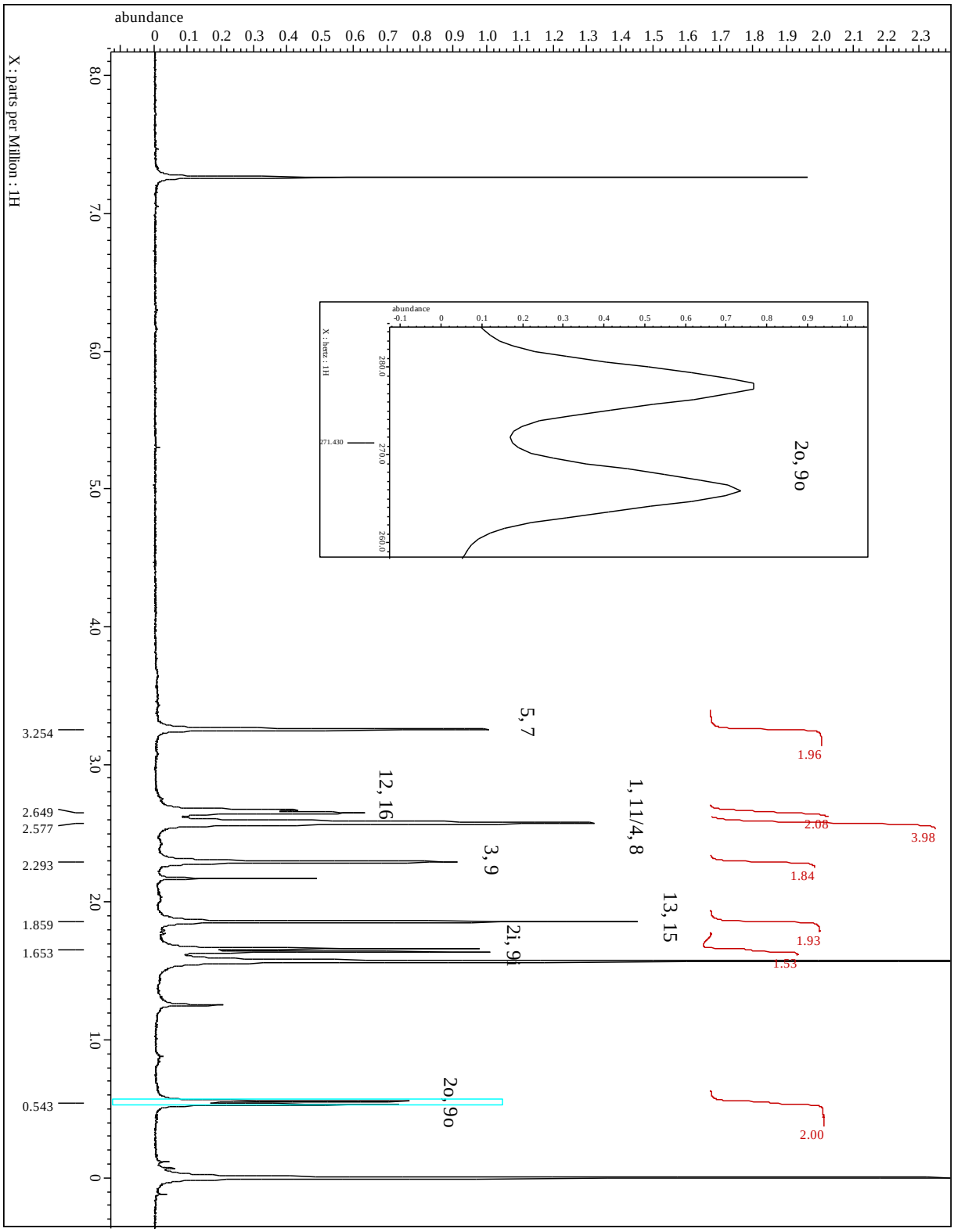
abundance
X : parts per Million : 1H
3.254
2.649
2.577
2.293
1.859
1.653
0.543
5, 7
12, 16
1, 11/4, 8
3, 9
13, 15
2i, 9i
2o, 9o
1.96
2.08
3.98
1.84
1.93
1.53
2.00
X : hertz : 1H
271.430

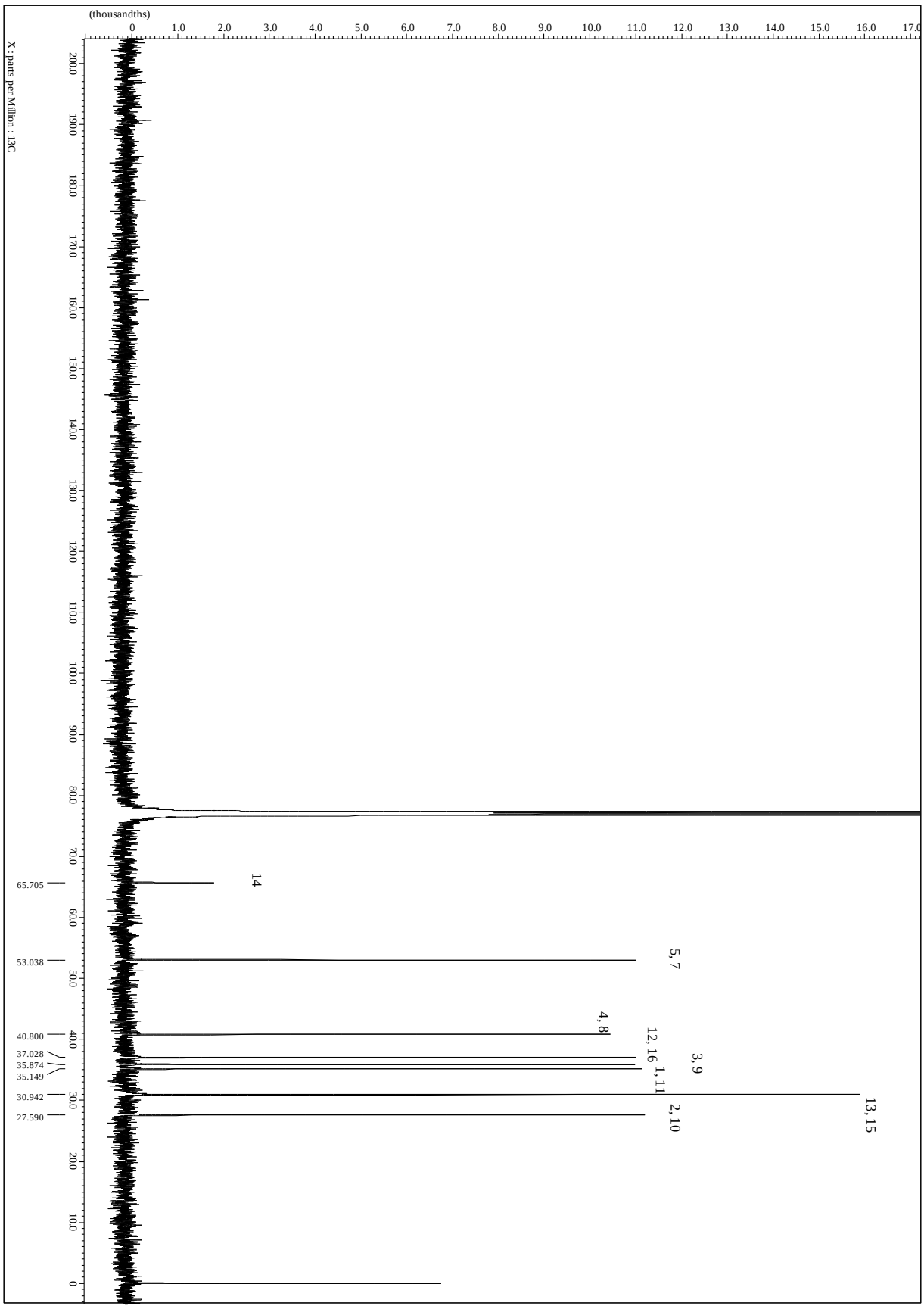
(thousandths)
X : parts per Million : 13C
65.705
53.038
40.800
37.028
35.874
35.149
30.942
27.590
14
5, 7
4, 8
12, 16
1, 11
3, 9
2, 10
13, 15

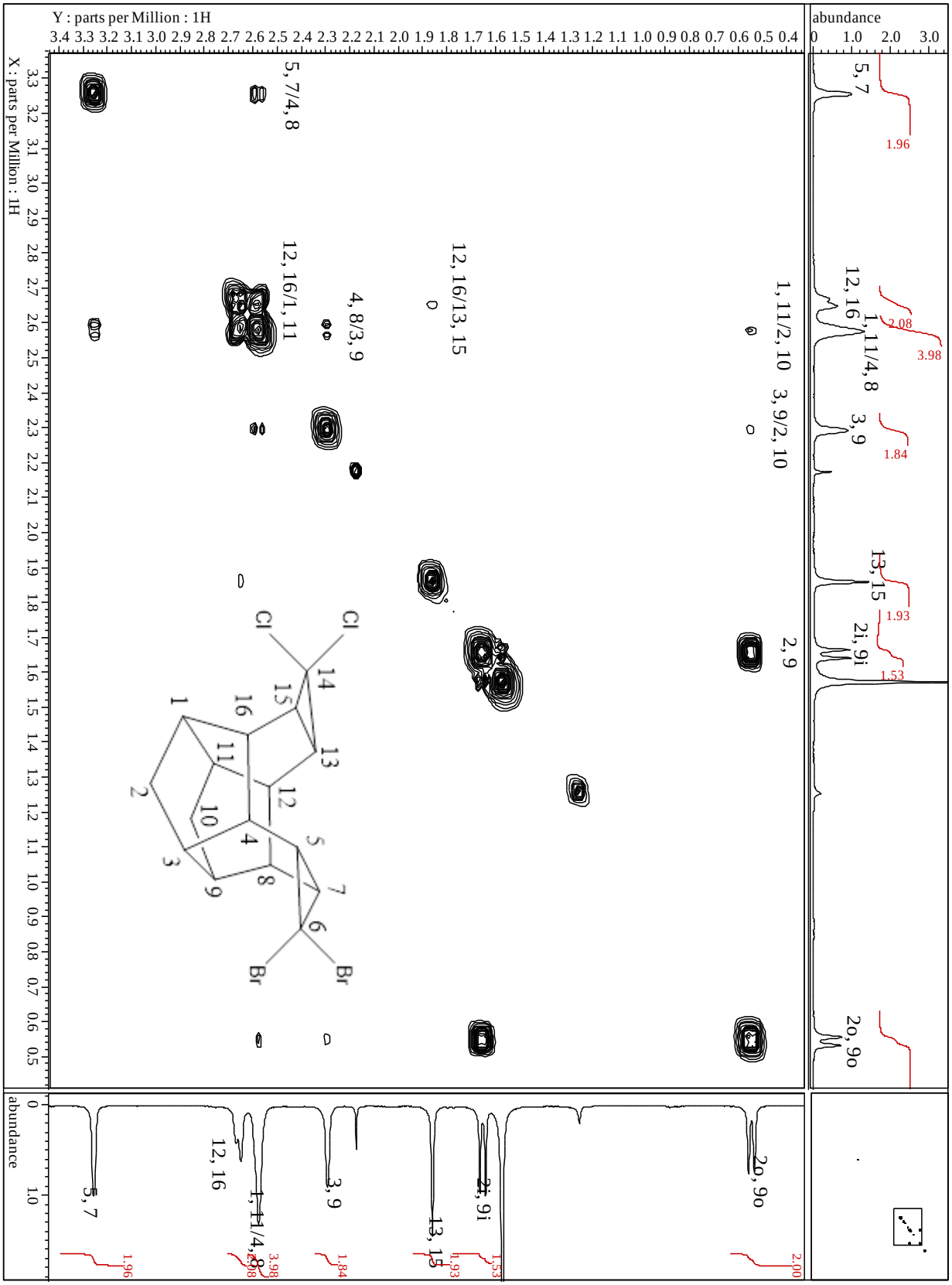
Y : parts per Million : 1H
X : parts per Million : 1H
abundance
5, 7
1.96
12, 16
1, 11/4, 8
2.08
3.98
3, 9
1.84
13, 15
1.93
2i, 9i
1.53
2o, 9o
2.00
1, 11/2, 10
3, 9/2, 10
2, 9
12, 16/13, 15
4, 8/3, 9
12, 16/1, 11
5, 7/4, 8
Cl
Cl
Br
Br
1
2
3
4
5
6
7
8
9
10
11
12
13
14
15
16

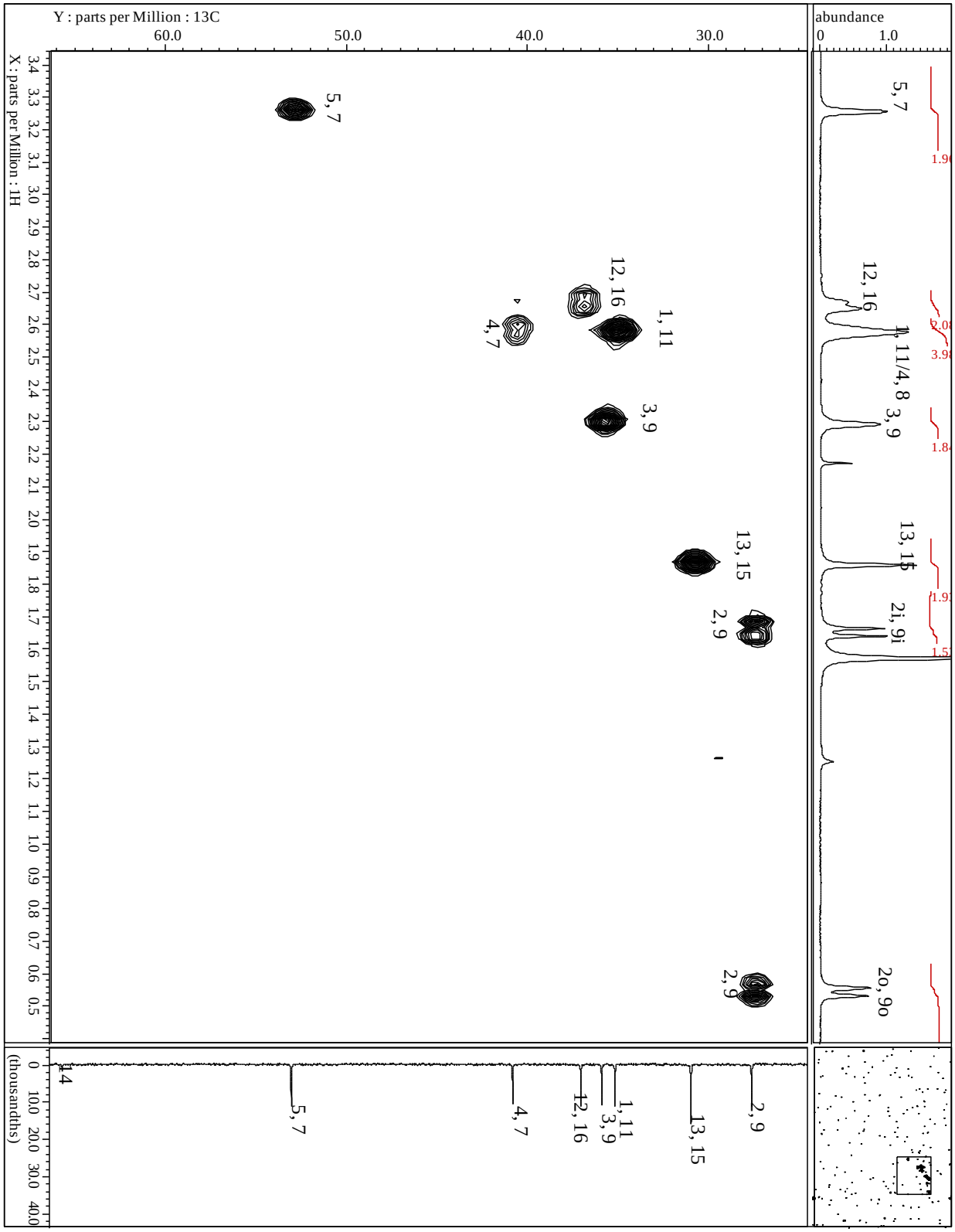
abundance
0
1.0
5, 7
12, 16
1, 11/4, 8
3, 9
13, 15
2i, 9i
2o, 9o
Y : parts per Million : 13C
60.0
50.0
40.0
30.0
X : parts per Million : 1H
3.4
3.3
3.2
3.1
3.0
2.9
2.8
2.7
2.6
2.5
2.4
2.3
2.2
2.1
2.0
1.9
1.8
1.7
1.6
1.5
1.4
1.3
1.2
1.1
1.0
0.9
0.8
0.7
0.6
0.5
5, 7
12, 16
1, 11
3, 9
4, 7
13, 15
2, 9
2, 9
13, 15
1, 11
3, 9
12, 16
4, 7
5, 7
0
10.0
20.0
30.0
40.0
(thousandths)

4.2 Experimental: Rearrangement Chemistry

5.4 Experimental: Preparation of Cage Hydrocarbons and Oxacages *Via* Rearrangement of Cage Scaffolds

5.4.1 General Comments

The epoxidation of diene **1** and monoene **24** can be performed in either DCM or chloroform with identical results. The DCM used in the rearrangement reactions was distilled under vacuum to separate from trace amounts of stabilizer. The DCM was not dried and may have contained trace amounts of moisture. When rearrangement reactions were performed with DCM dried and distilled over magnesium sulfate ($MgSO_4$), the rearrangement reactions failed to occur, implying that the trace amounts of moisture present may be necessary to activate the catalyst. Bis-epoxide **95** showed no reaction when subjected to periodic acid.

5.4.2 Rearrangement of the Diene **1**

Rearrangement with Silver Perchlorate: Silver perchlorate (28.1 mg, 0.136 mmol, 0.5 eq) was added to a solution of diene **1** (50 mg, 0.271 mmol) in benzene (5.0 mL) and stirred at room temperature for 48 hours. The solution was then stretched with ether and water then extracted with ether (3x20 mL). The combined organic phase was washed with water (2x 10 mL) before being dried ($MgSO_4$) and concentrated to afford a colorless solid (113 mg) identified as unreacted **1**.

Rearrangement with Silver Nitrate: Silver nitrate (125 mg, 0.736 mmol, 2.7 eq) was added to a solution of diene **1** (50 mg, 0.271 mmol) in MeOH/water (8.0 mL and 6.0 mL) and stirred at room temperature in the dark for 48 hours. The MeOH was then removed under vacuum and the aqueous solution extracted with ether (3x20 mL). The combined organic phase was then dried ($MgSO_4$) and concentrated to afford a colorless solid (118 mg) identified as unreacted **1**.

Rearrangement with Amberlyst-15: To a solution of diene **1** (100 mg, 0.543 mmol) in DCM (10 mL), Amberlyst-15 (200 mg, 0.990 mmol, 4.95 mol/kg) was added and the mixture stirred for 20 days. Additional DCM (5 mL) was added when needed (approximately every 48 hours) and additional Amberlyst-15 (1.0 eq) was added at 13 and 17 days to drive the reaction forwards. After **1** was consumed (based on GC/MS) the suspension was filtered and concentrated to afford a colorless solid (63 mg) comprised of **97** and unidentified hydroxylated compounds (determined by GC/MS). Purification by column chromatography (SiO_2, *n*-pentane) gave **97** as a colorless waxy solid in poor yield (14 mg, 14%).

Hexacyclo[6.5.1.$0^{3,11}$.$0^{4,14}$.$0^{5,10}$.$0^{9,13}$]tetradec-6-ene (93)

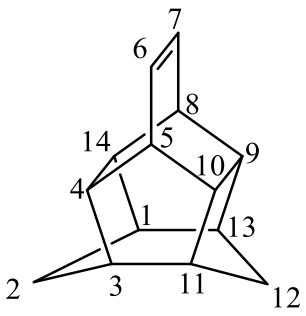

$C_{14}H_{16}$ (184), R_f = 0.80 by SiO_2-TLC; visualized by UV or vanillin stain

^{1}H-NMR ($CDCl_3$, 500 MHz): δ = 6.16 (m, 2H, H-6, -7), 2.49 (s_{app}, 2H, H-5, -8), 2.28 (s_{app}, 4H, H-1, -3, -11, -13), 1.98 (s_{app}, 4H, H-4, -9, -10, -14), 1.41 (d, 2H, H-2i, -12i), 1.11 (d, 2H, H-2o, -12o) ppm;

$^2J_{\text{H-2i, -2o}} = {}^2J_{\text{H-12i, -12o}} = 11.5$ Hz.

^{13}C-NMR ($CDCl_3$, 100.7 MHz): δ = 131.7 (C-6, -7), 50.3 (C-4, -9, -10, -14), 42.4 (C-1, -3, -11, -13), 37.9 (C-5, -8), 28.1 (C-2, -12) ppm.

MS (EI, 70 eV): *m/z* (%) = 185 (15.3) [$M^{\cdot+}$+1], 184 (48.0) [$M^{\cdot+}$], 184 (100.0), 169 (8.0), 155 (9.5), 143 (9.1), 142 (14.2), 141 (11.2), 130 (14.5), 129 (17.7), 128 (17.5), 118 (41.6), 117 (71.4), 116 (17.1), 115 (32.9), 106 (28.0), 105 (19.7), 104 (12.9), 103 (8.6), 93 (12.3), 92 (17.2), 91 (61.2), 80 (18.5), 79 (21.6), 78 (30.4), 77 (29.6), 65 (14.7), 51 (10.6).

Spectra:

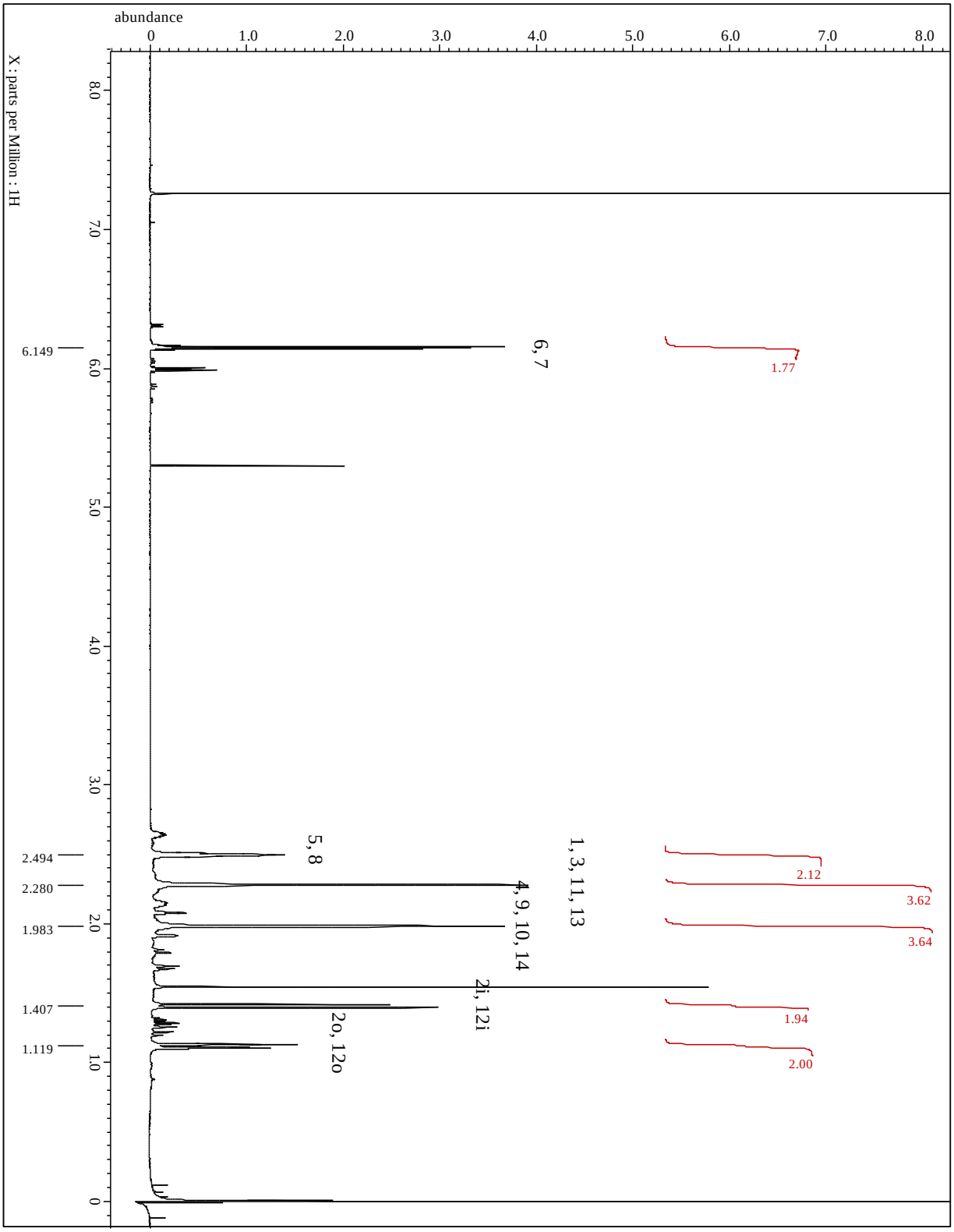
abundance
0
1.0
2.0
3.0
4.0
5.0
6.0
7.0
8.0
X : parts per Million : 1H
6.149
2.494
2.280
1.983
1.407
1.119
6, 7
5, 8
4, 9, 10, 14
1, 3, 11, 13
2i, 12i
2o, 12o
1.77
2.12
3.62
3.64
1.94
2.00

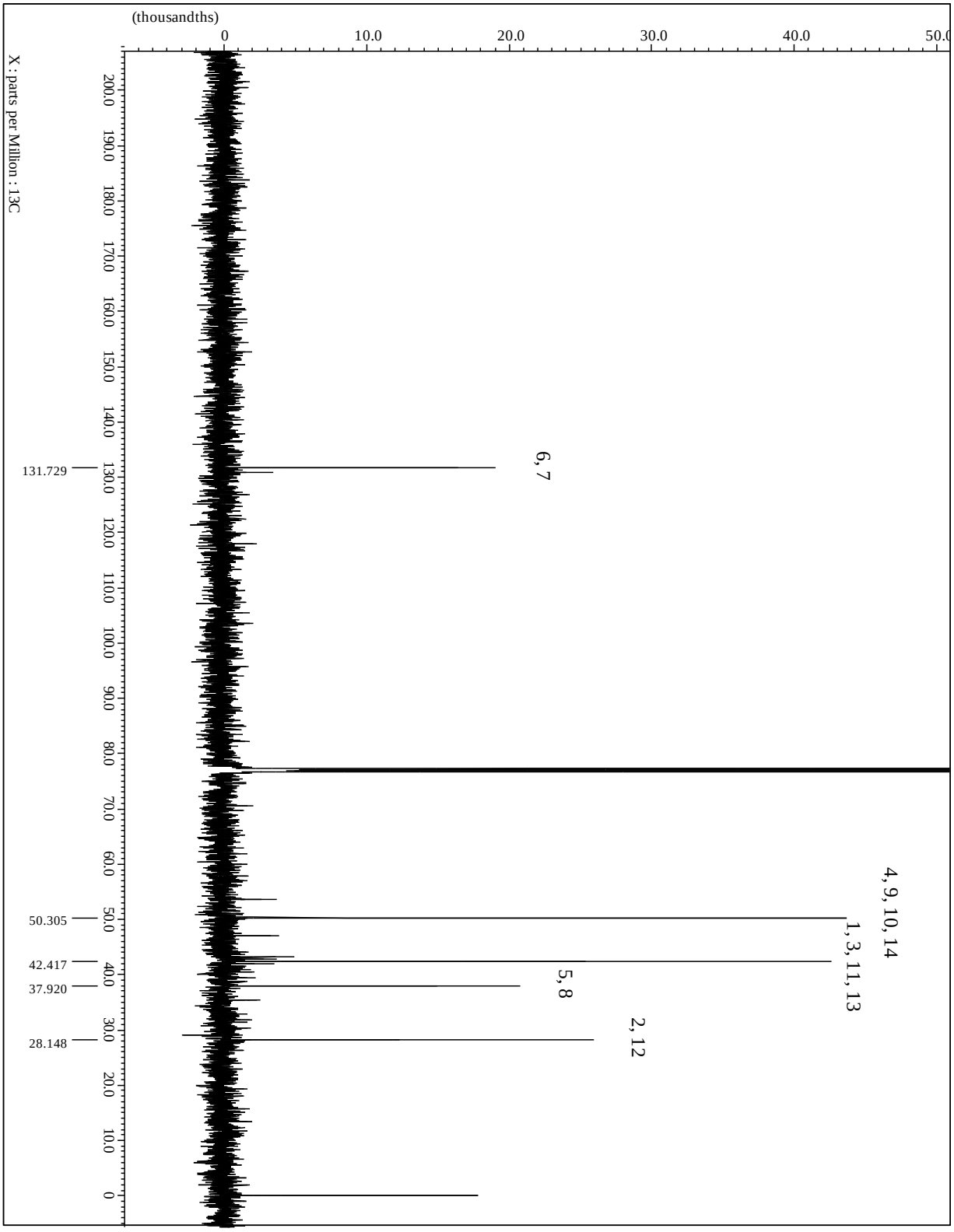
(thousandths)
0
10.0
20.0
30.0
40.0
50.0
X : parts per Million : 13C
200.0
190.0
180.0
170.0
160.0
150.0
140.0
130.0
120.0
110.0
100.0
90.0
80.0
70.0
60.0
50.0
40.0
30.0
20.0
10.0
0
131.729
50.305
42.417
37.920
28.148
6, 7
4, 9, 10, 14
1, 3, 11, 13
5, 8
2, 12

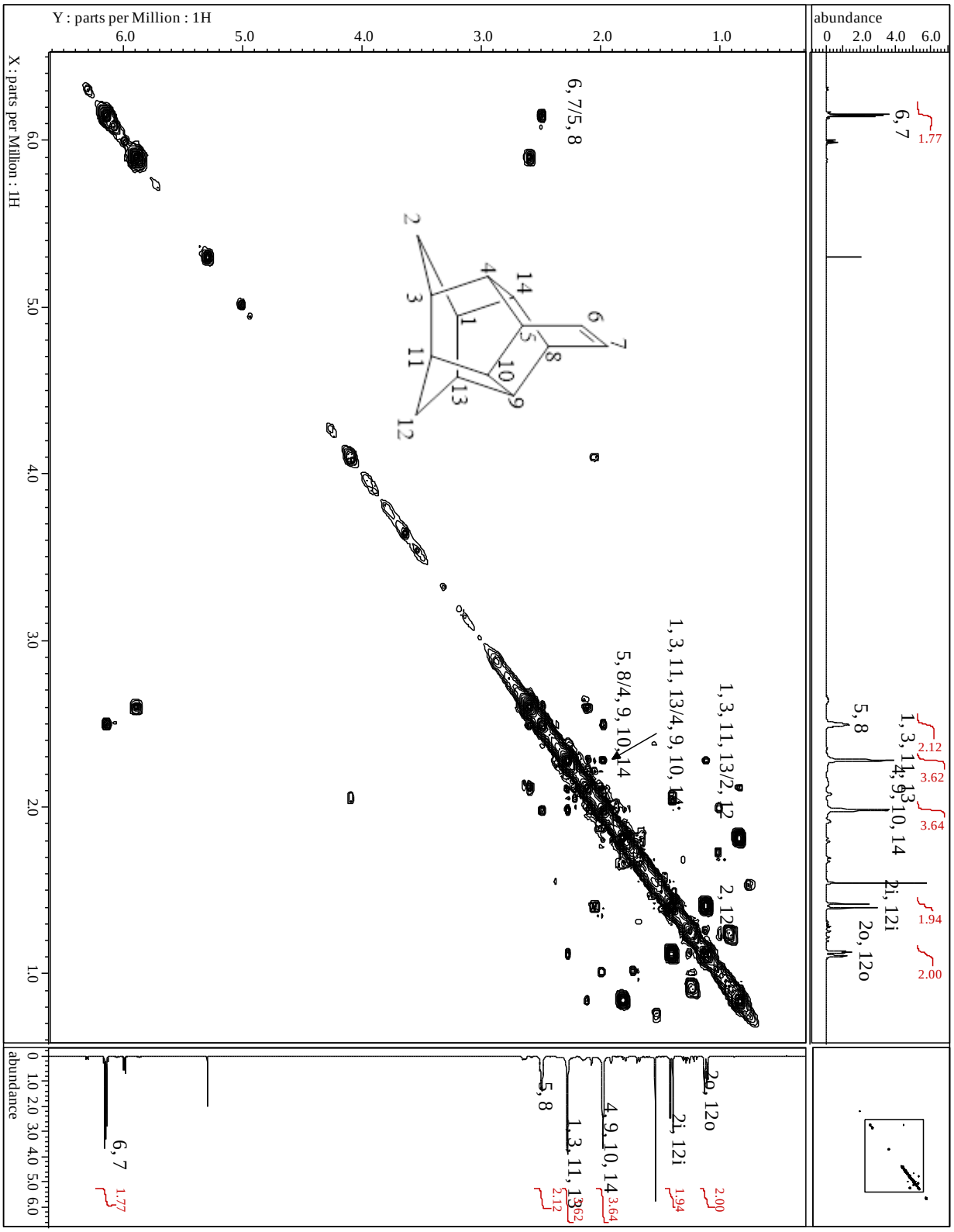
abundance
6, 7
1.77
1, 3, 11, 13/2, 12
2.12
4, 9, 10, 14
3.62
5, 8
3.64
2i, 12i
1.94
2o, 12o
2.00
Y : parts per Million : 1H
X : parts per Million : 1H
6, 7/5, 8
1, 3, 11, 13/4, 9, 10, 14
5, 8/4, 9, 10, 14
2, 12
2o, 12o
2.00
2i, 12i
1.94
4, 9, 10, 14
3.64
1, 3, 11, 13
3.62
5, 8
2.12
6, 7
1.77
abundance

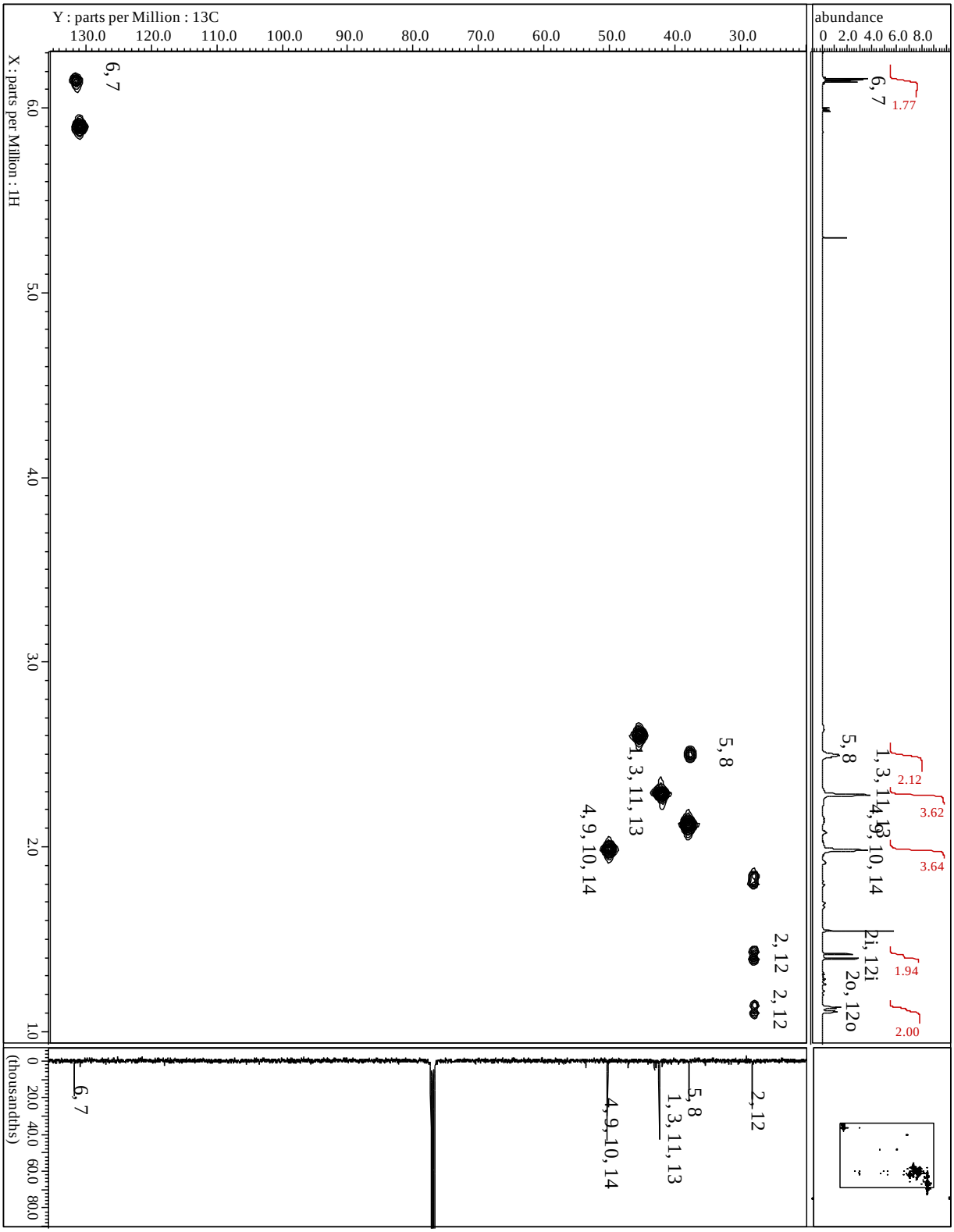
Y : parts per Million : 13C
130.0
120.0
110.0
100.0
90.0
80.0
70.0
60.0
50.0
40.0
30.0
X : parts per Million : 1H
6.0
5.0
4.0
3.0
2.0
1.0
abundance
0
2.0
4.0
6.0
8.0
6, 7
1.77
5, 8
1, 3, 11, 13
4, 9, 10, 14
2.12
3.62
3.64
2i, 12i
2o, 12o
1.94
2.00
2, 12
(thousandths)
0
20.0
40.0
60.0
80.0

5.4.3 Preparation of the Epoxide Cages

*Epoxidation of **1**:* MCPBA (321.0 mg, 1.304 mmol, 1.2 eq.) was added in small portions to a solution of diene **1** (150 mg, 0.815 mmol, 1 eq.) in DCM (8 mL) at 0 ^{o}C. The reaction mixture was stirred for 6 hours then quenched with water (30 mL). The solution was extracted with DCM (3x20 mL). The combined organic was washed with water (10 mL), sat. sodium thiosulfate solution (2x10 mL), sat. bicarbonate solution (2x10 mL) and again with water (10 mL). The organic phase was dried ($MgSO_4$) and concentrated under vacuum to yield the crude product as colorless crystals (200 mg). Column chromatography (SiO_2, 5:1 hexanes/EtOAc) furnished the products **94** (118 mg, 54%) and **95** (127 mg, 54%). Single crystals of both epoxides were obtained from $CHCl_3$.

*Epoxidation of **24**:* MCPBA (160 mg, 0.645 mmol, 1.2 eq.) was added in small portions to a solution of ene **24** and **25** (100 mg **24**, 0.538 mmol, 1 eq.) in DCM (5.5 mL) at 0 ^{o}C. The reaction mixture was stirred for 16 hours then quenched with water (30 mL). The solution was extracted with DCM (3x20 mL). The combined organic was washed with water (10 mL), sat. sodium thiosulfate solution (2x10 mL), sat. bicarbonate solution (2x10 mL) and again with water (10 mL). The organic phase was dried ($MgSO_4$) and concentrated under vacuum to yield the crude product as colorless crystals (119 mg). Column chromatography (SiO_2, 7:1 hexanes/EtOAc) furnished the product **96** (81 mg, 75%). When a large excess MCPBA (5 eq) is added, hydroxylation of **25** may be observed.

*Epoxidation of **40a***: MCPBA (34 mg, 0.145 mmol, 1.2 eq.) was added in small portions to a solution of mono-cyclopropane **40a** (24 mg, 0.121 mmol, 1 eq.) in chloroform (4 mL) at 0 ^{o}C. The reaction mixture was stirred for 4 hours then quenched with water (30 mL). The solution was extracted with DCM (3x20 mL). The combined organic was washed with water (10 mL), sat.

sodium thiosulfate solution (2x10 mL), sat. bicarbonate solution (2x10 mL) and again with water (10 mL). The organic phase was dried ($MgSO_4$) and concentrated under vacuum to yield the product **98** at colorless crystalline material (22 mg, 85%). No purification was necessary.

*Hydrogenation of **94**:* A catalytic amount of 5% Pt/C was suspended in a solution of mono-epoxide **94** (27.7 mg, 0.139 mmol) in EtOAc (6 mL). H_2 gas was bubbled through the suspension until the reaction reached 100% conversion (based on GC/MS). The catalyst was filtered off through a plug of silica gel and the filtrate concentrated under vacuum to give clean **96** as a colorless solid (26 mg, 93% yield).

13-Oxahexacyclo[8.5.0.0^{3,8}.0^{4,15}.0^{7,11}.0^{12,14}]pentadeca-5-ene (94)

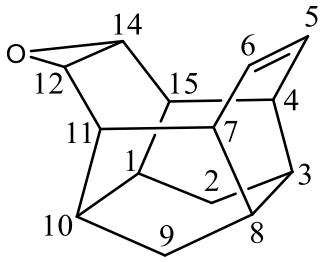

$C_{14}H_{16}O$ (200), R_f = 0.60 by SiO_2-TLC; visualized by UV or vanillin stain

MP = 261.4-261.9 ° C ($CHCl_3$)

IR (AT-IR): $\tilde{\nu}$ = 3017 (m, C-H), 2931 (s, C-H), 1642 (w, C=C), 1454 (m, C-C), 937 (s), 853 (s), 779 (s) cm^{-1}.

^{1}H-NMR ($CDCl_3$, 500 MHz): δ = 6.13 (m, 2H, H-5, -6), 3.06 (m, 2H, H-12, -14), 2.68 (m, 2H, H-4, -7), 2.54 (m, 2H, H-11, -15), 2.33 (s_{app}, 2H, H-1, -10), 2.08 (s_{app}, 2H, H-3, -8), 1.75 (d, 2H, H-2i, -9i), 0.73 (d, 2H, H-2o, -9o) ppm;

$^2J_{H\text{-}2i,\,\text{-}2o} = {}^2J_{H\text{-}9i,\,\text{-}9o}$ = 12.0 Hz.

^{13}C-NMR ($CDCl_3$, 75.6 MHz): δ = 132.2 (C-5, -6), 53.6 (C-12, -14), 43.9 (C-11, -15), 39.7 (C-4, -7), 38.2 (C-1, -10), 37.2 (C-3, -8), 28.2 (C-2, -9) ppm.

MS (EI, 70 eV): *m/z* (%) = 201 (10.7) [$M^{\cdot+}$+1], 200 (72.3) [$M^{\cdot+}$], 172 (14.9), 171 (9.9), 167 (7.9), 146 (8.9), 143 (14.2), 142 (8.2), 141 (13.2), 131 (13.4), 130 (21.4), 129 (38.9), 128 (26.1), 121 (9.3), 120 (13.3), 118 (11.9), 117 (28.3), 116 (15.4), 115 (30.2), 109 (18.8), 108 (7.9), 107 (12.4), 106 (12.6), 105 (21.5), 104 (19.4), 103 (10.7), 95 (8.9), 94 (15.1), 93 (20.2), 92 (40.4), 91 (100.0), 81 (27.0), 80 (20.4), 79 (49.5), 78 (26.4), 77 (48.8), 67 (10.5), 66 (13.5), 65 (22.3), 63 (8.1), 53 (12.3), 51 (15.0).

Spectra:

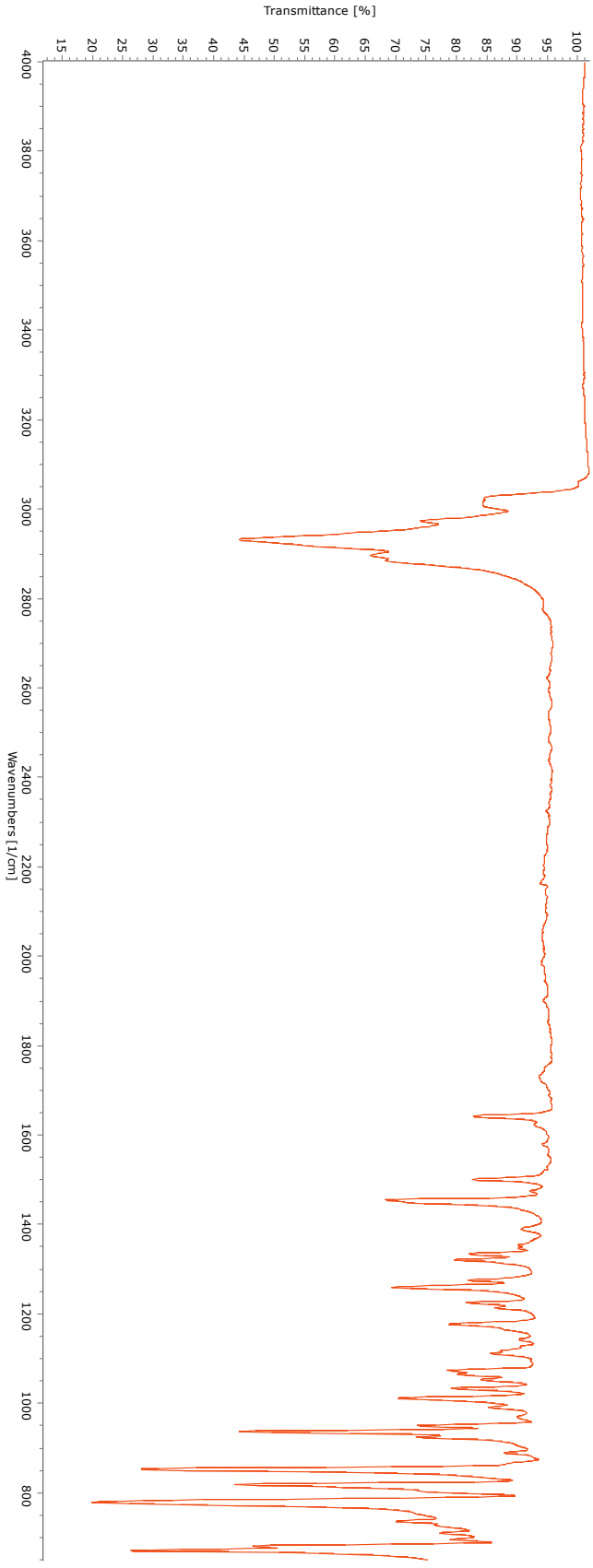
Transmittance [%]
Wavenumbers [1/cm]

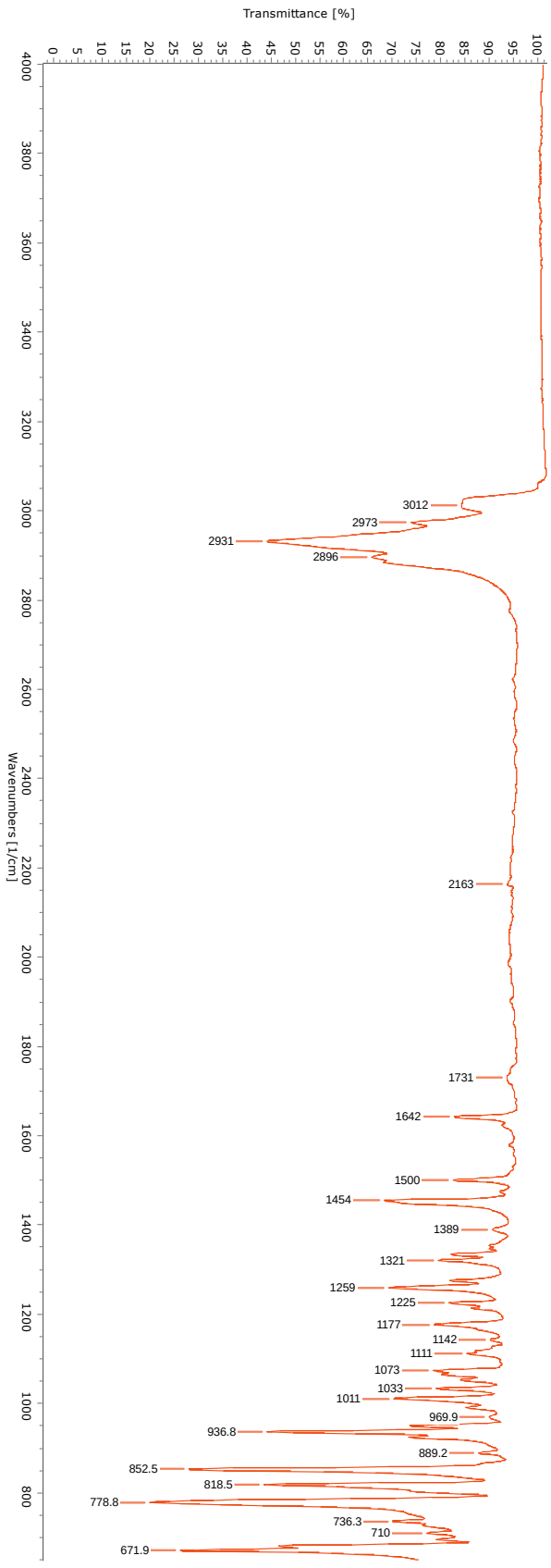
Transmittance [%]
Wavenumbers [1/cm]
3012
2973
2931
2896
2163
1731
1642
1500
1454
1389
1321
1259
1225
1177
1142
1111
1073
1033
1011
969.9
936.8
889.2
852.5
818.5
778.8
736.3
710
671.9

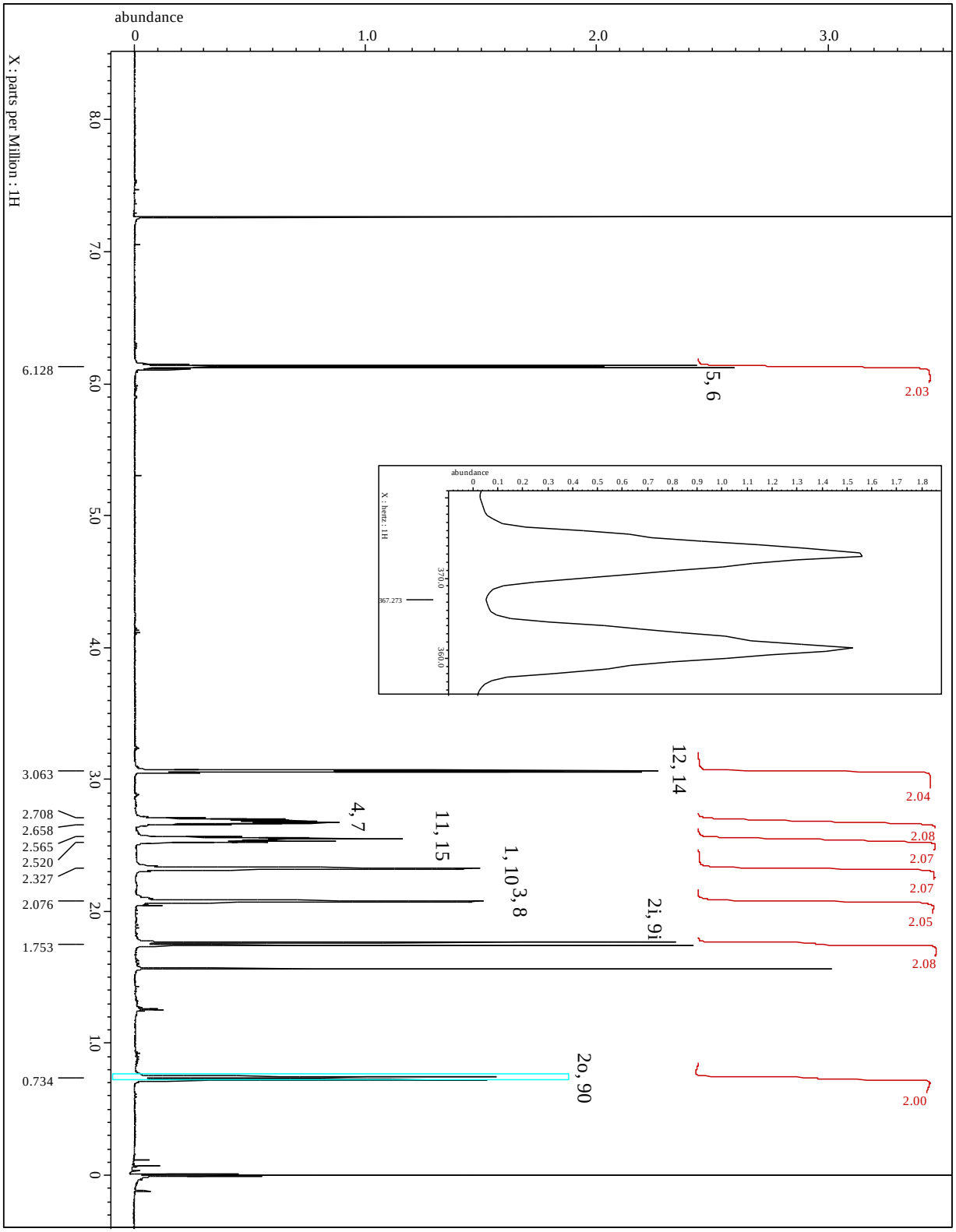
abundance
0
1.0
2.0
3.0
X : parts per Million : 1H
8.0
7.0
6.0
5.0
4.0
3.0
2.0
1.0
0
6.128
3.063
2.708
2.658
2.565
2.520
2.327
2.076
1.753
0.734
5, 6
2.03
12, 14
2.04
4, 7
2.08
11, 15
2.07
1, 10
3, 8
2.07
2i, 9i
2.05
2.08
2o, 90
2.00
abundance
X : hertz : 1H
370.0
367.273
360.0

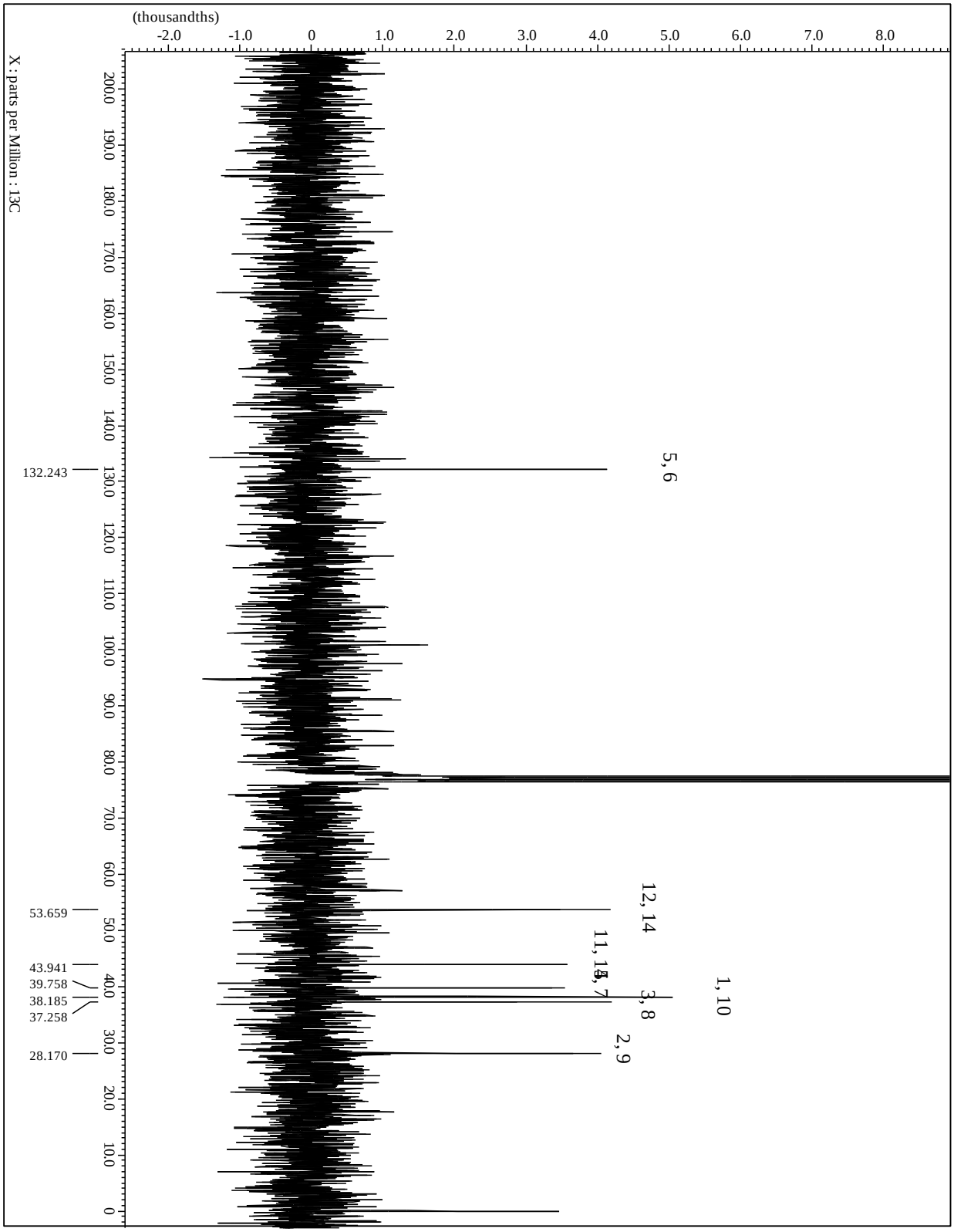
(thousandths)
-2.0
-1.0
0
1.0
2.0
3.0
4.0
5.0
6.0
7.0
8.0
X : parts per Million : 13C
200.0
190.0
180.0
170.0
160.0
150.0
140.0
130.0
120.0
110.0
100.0
90.0
80.0
70.0
60.0
50.0
40.0
30.0
20.0
10.0
0
132.243
53.659
43.941
39.758
38.185
37.258
28.170
5, 6
12, 14
11, 13
3, 8
2, 9
1, 10

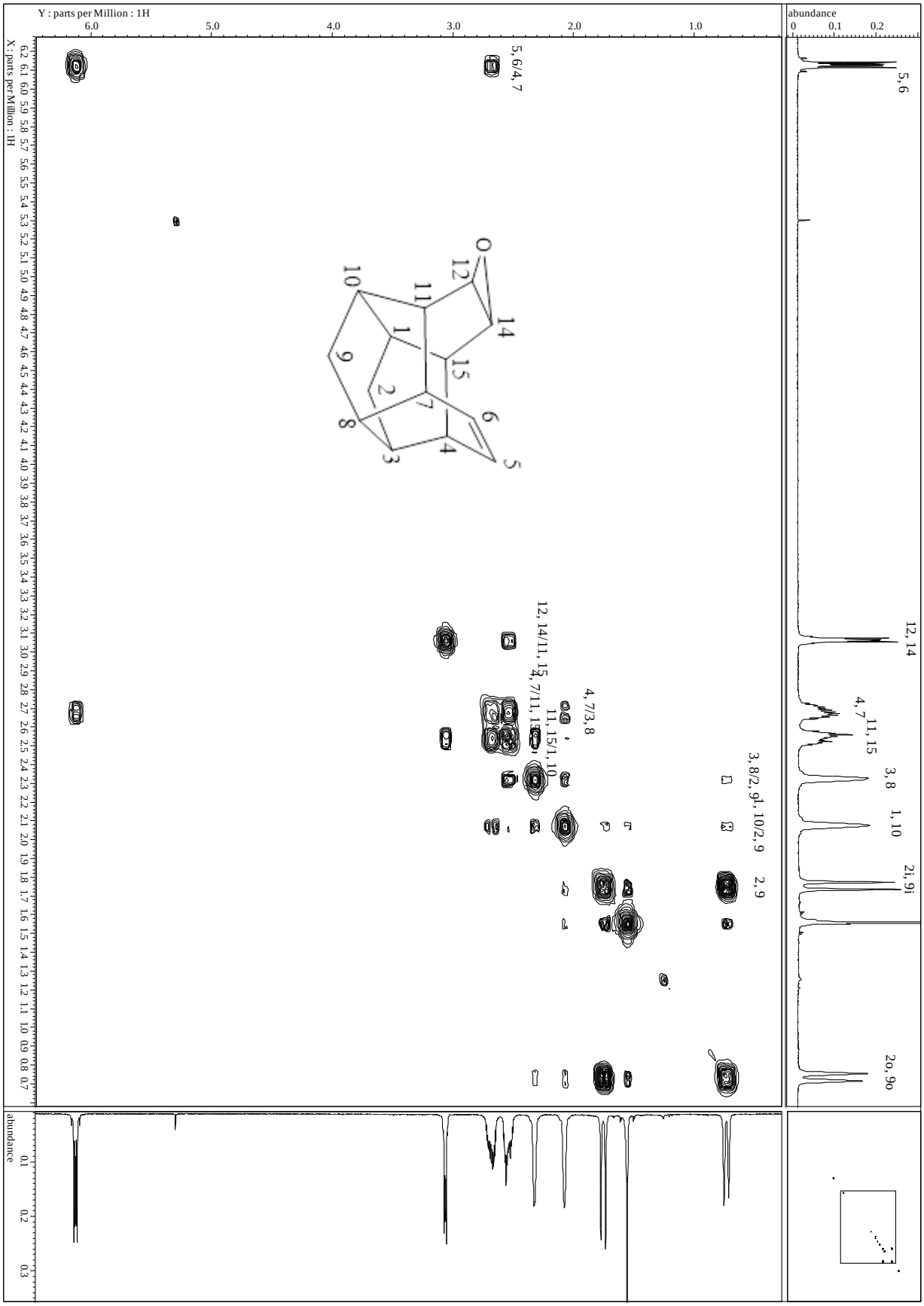
Y : parts per Million : 1H
X : parts per Million : 1H
abundance
5, 6
12, 14
4, 7
11, 15
3, 8
1, 10
2i, 9i
2o, 9o
5, 6/4, 7
4, 7/3, 8
11, 15/1, 10
12, 14/11, 15
4, 7/11, 15
3, 8/2, 9
1, 10/2, 9
2, 9
O
12
11
10
14
1
15
9
2
7
6
8
4
3
5

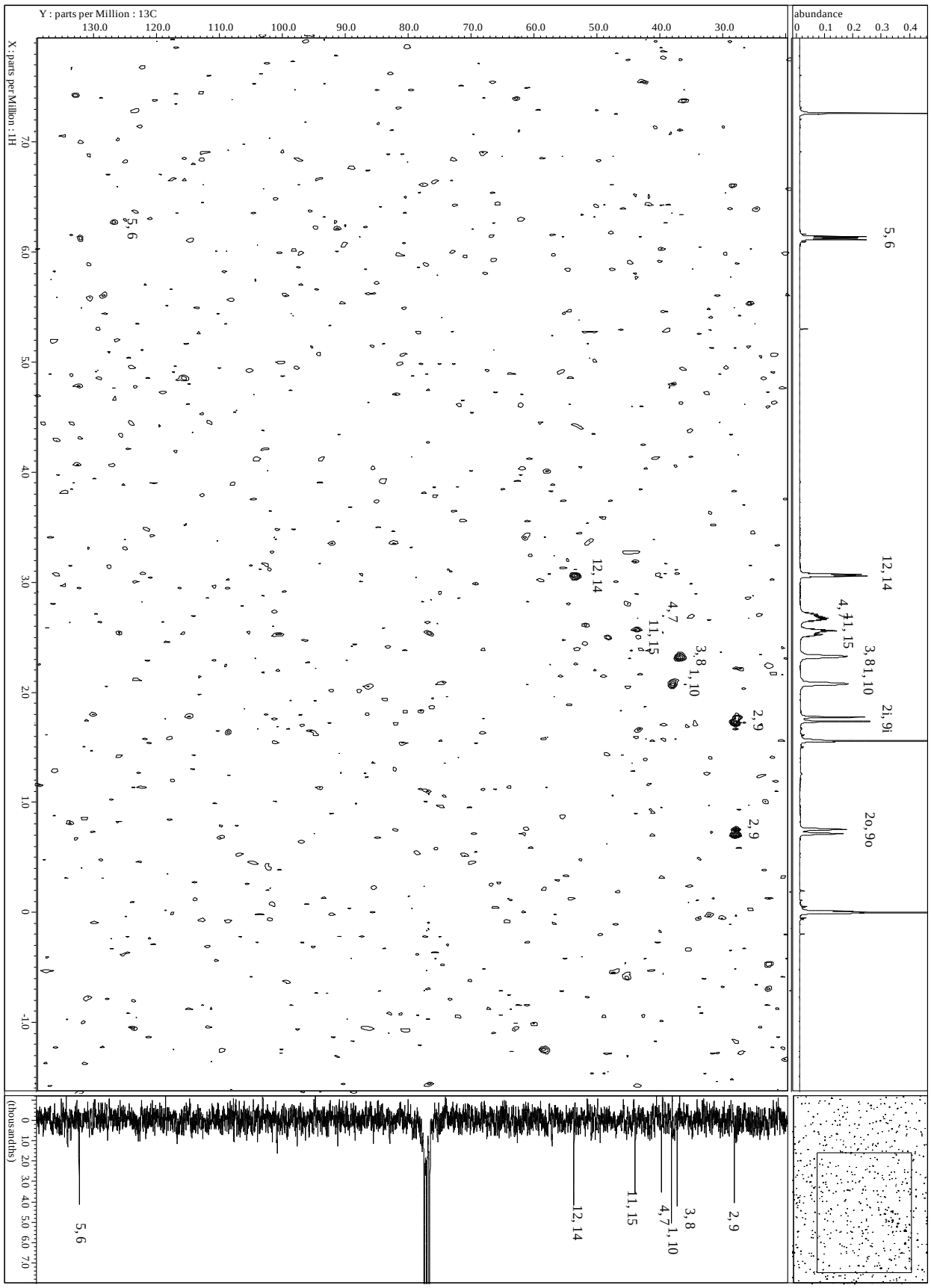
Y : parts per Million : 13C
X : parts per Million : 1H
abundance
5, 6
12, 14
4, 7
11, 15
3, 8
1, 10
2i, 9i
2o, 9o
2, 9
(thousandths)

6,14-Dioxaheptacyclo[9.5.0.0^{3,9}.0^{4,16}.0^{5,7}.0^{8,12}.0^{13,15}]hexadecane (95)

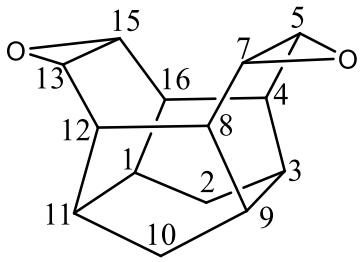

$C_{14}H_{16}O_2$ (216), R_f = 0.30 by SiO_2-TLC; visualized by UV or vanillin stain

MP = 309.3-311.5 °C ($CHCl_3$)

IR (AT-IR): $\tilde{\nu}$ = 2923 (s, C-H), 1718 (m, C-O-C), 1443 (m, C-C), 1259 (m), 1041 (m), 943 (m), 820 (s), 597 (s) cm^{-1}.

^{1}H-NMR ($CDCl_3$, 300 MHz): δ = 3.27 (s_{app}, 4H, H-5, -7, -13, -15), 2,58 (s_{app}, 4H, H-4, -8, -12, -16), 2.34 (s_{app}, 4H, H-1, -3, -9, -11), 1.62 (d, 2H, H-2i, -10), 0.55 (d, 2H, H-2o, -10o) ppm;

$^2J_{\text{H-2i, -2o}} = {}^2J_{\text{H-10i, -10o}}$ = 11.7 Hz.

^{13}C-NMR ($CDCl_3$, 75.6 MHz): δ = 52.4 (C-5, -7, -13, -15), 39.8 (C-4, -8, -12, -16), 36.8 (C-1, -3, -9, -11), 27.0 (C-2, -10) ppm.

MS (EI, 70 eV): *m/z* (%) = 216 (20.7) [$M^{\cdot+}$], 200 (7.9), 170 (7.5), 169 (9.9), 159 (16.6), 157 (8.3), 155 (11.7), 146 (9.8), 145 (13.9), 144 (9.9), 143 (14.9), 142 (15.4), 141 (20.9), 134 (11.4), 133 (23.5), 132 (9.9), 131 (35.4), 130 (19.5), 129 (41.1), 128 (28.6), 127 (8.4), 122 (8.2), 121 (10.3), 120 (15.4), 119 (17.6), 118 (18.0), 117 (45.0), 116 (22.5), 115 (33.6), 109 (12.2), 108 (16.4), 107 (29.0), 106 (9.3), 105 (30.1), 104 (17.2), 103 (13.7), 95 (18.6), 94 (26.8), 93 (21.3), 92 (31.1), 91 (100.0), 82 (12.1), 81 (60.2), 80 (16.4), 79 (70.7), 78 (29.8), 77 (59.6), 68 (10.4), 67 (21.0), 66 (19.3), 65 (27.9), 63 (10.4), 55 (14.8), 53 (24.3), 52 (8.7), 51 (21.0).

Spectra:

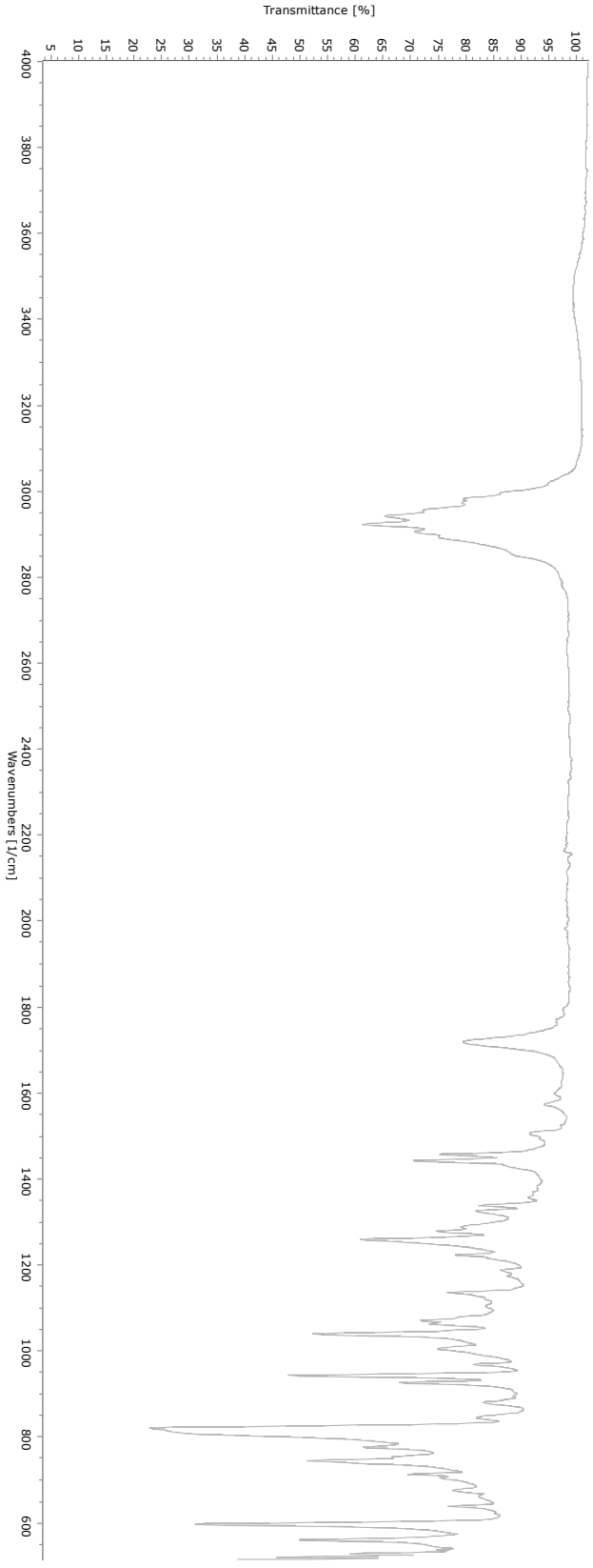
Transmittance [%]
Wavenumbers [1/cm]

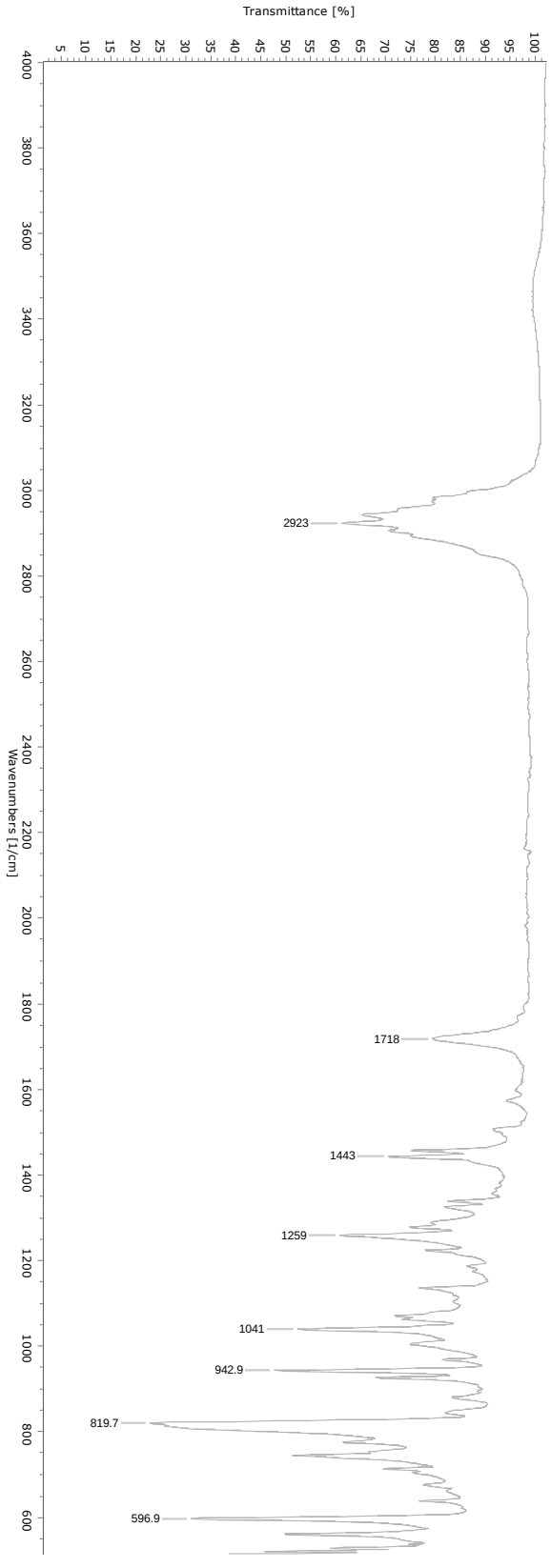
Transmittance [%]
Wavenumbers [1/cm]
2923
1718
1443
1259
1041
942.9
819.7
596.9

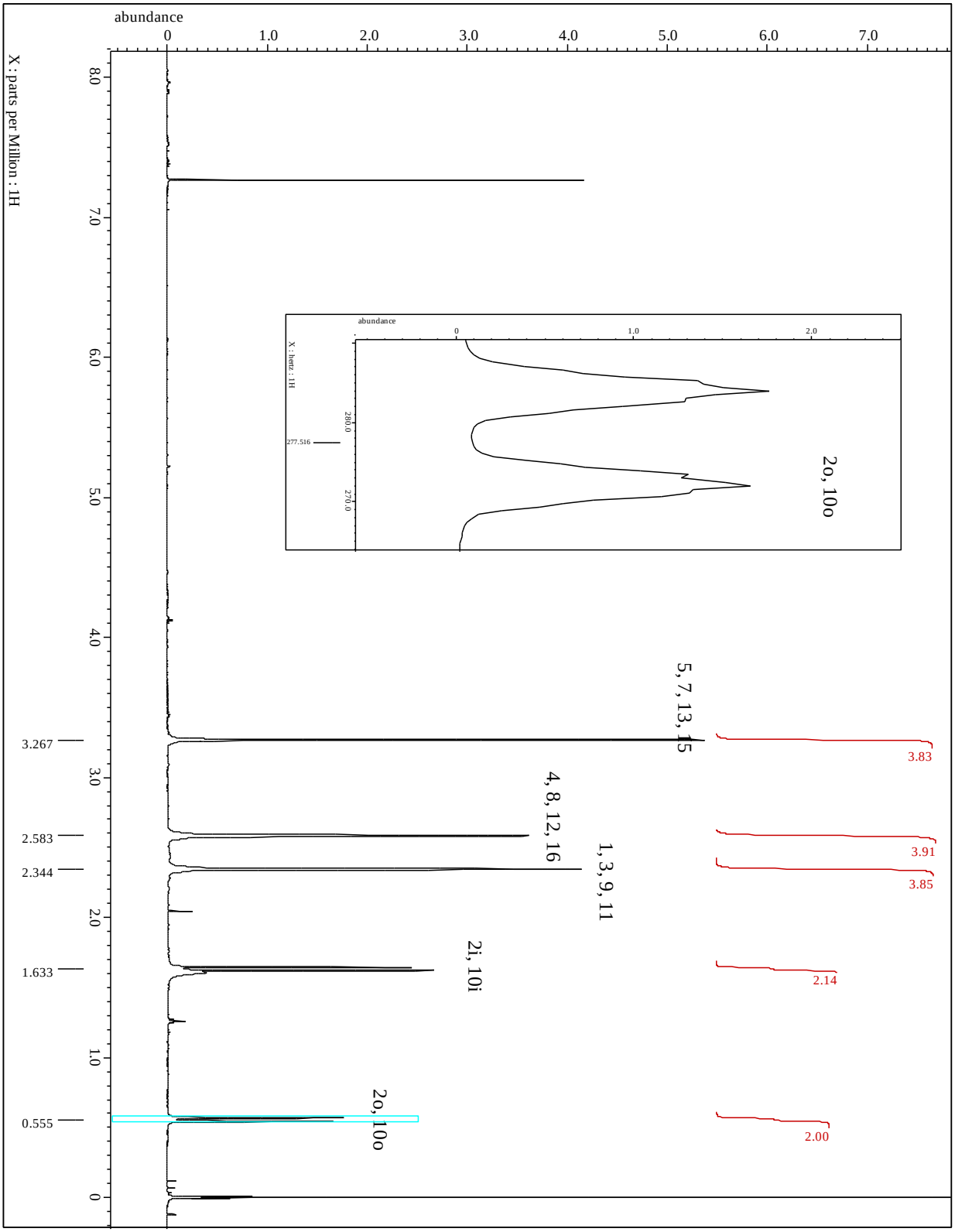
abundance
X : parts per Million : 1H
3.267
2.583
2.344
1.633
0.555
5, 7, 13, 15
4, 8, 12, 16
1, 3, 9, 11
2i, 10i
2o, 10o
3.83
3.91
3.85
2.14
2.00
abundance
X : hertz : 1H
277.516
2o, 10o

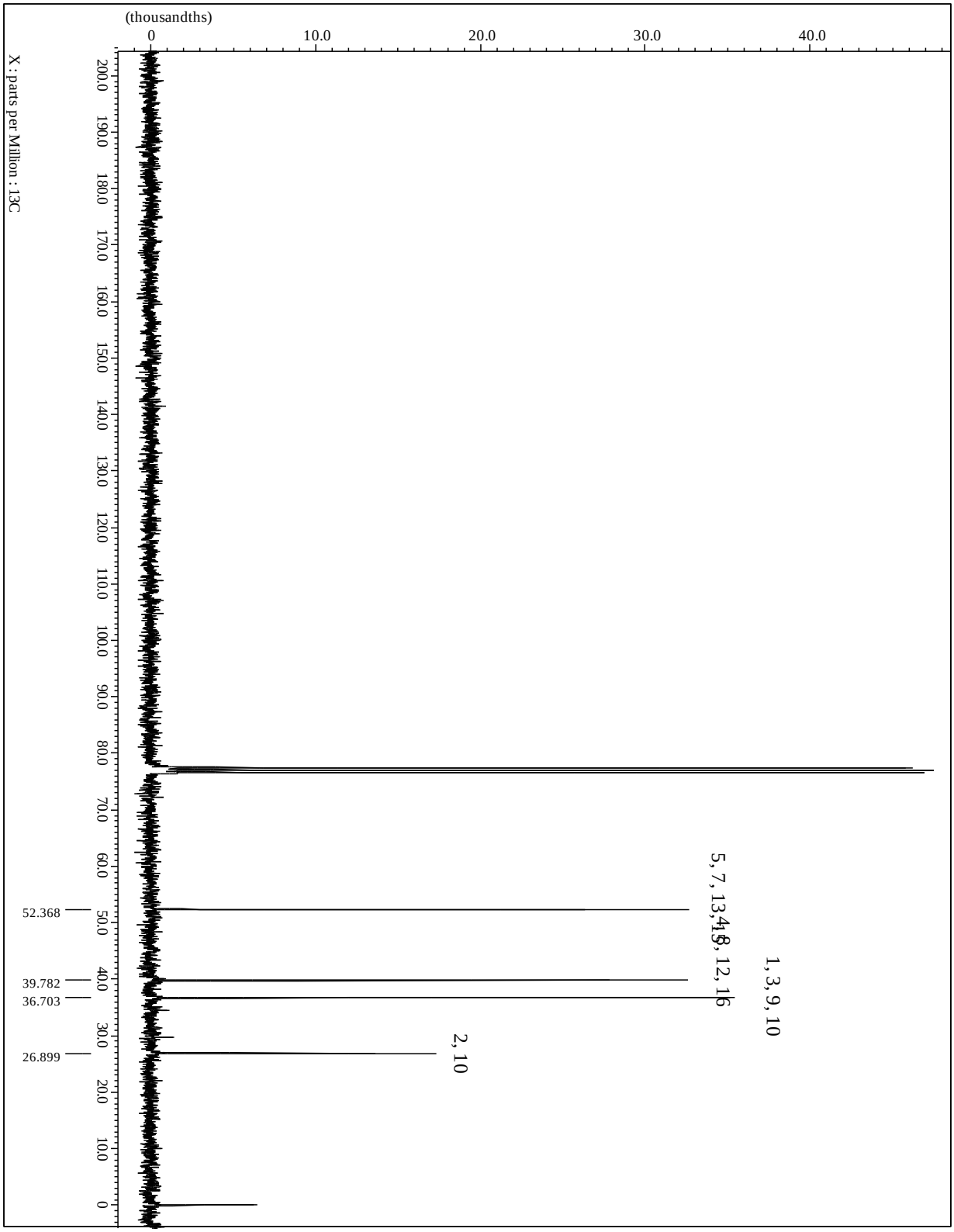
(thousandths)
0
10.0
20.0
30.0
40.0
X : parts per Million : 13C
200.0
190.0
180.0
170.0
160.0
150.0
140.0
130.0
120.0
110.0
100.0
90.0
80.0
70.0
60.0
50.0
40.0
30.0
20.0
10.0
0
52.368
39.782
36.703
26.899
5, 7, 13, 14, 15, 8, 12, 16
1, 3, 9, 10
2, 10

13-Oxahexacyclo[8.5.0.0^{3,8}.0^{4,15}.0^{7,11}.0^{12,14}]pentadecane (96)

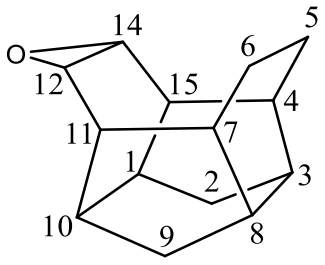

$C_{14}H_{18}O$ (202), R_f = 0.70 by SiO_2-TLC; visualized by UV or vanillin stain

MP = 260.6-261.3 °C ($CHCl_3$)

IR (AT-IR): $\tilde{\nu}$ = 2924 (s, C-H), 1454 (w, C-C), 1253, 836, 572 cm^{-1}.

^{1}H-NMR ($CDCl_3$, 500 MHz): δ = 3.28 (s_{app}, 2H, H-12, 14), 2.32 (m, 2H, H-11, 15), 2.29 (s_{app}, 2H, H-1, 10), 2.16 (s_{app}, 2H, H-3, 8), 2.09 (m, 2H, H-4, 7), 1.82-1.71 (m, 6H, H-2i, -9i; H-5i, -5o, -6i, -6o), 0.57 (d, 2H, H-2o, -9o) ppm;

$^2J_{\text{H-2i, -2o}} = {}^2J_{\text{H-9i, -9o}}$ = 12.0 Hz.

^{13}C-NMR ($CDCl_3$, 100.7 MHz): δ = 53.7 (C-5, -6), 38.6 (C-4, -7), 37.1 (C-3, -8), 36.9 (C-1, -10), 36.5 (C-11, -14), 27.8 (C-2, -9), 19.0 (C-12, -13) ppm.

MS (EI, 70 eV): *m/z* (%) = 203 (14.9) [$M^{\cdot+}$+1], 202 (100.0) [$M^{\cdot+}$], 184 (12.0), 174 (25.2), 173 (20.3), 171 (8.4), 169 (12.4), 159 (14.2), 158 (25.2), 156 (11.1), 155 (10.3), 146 (11.5), 145 (20.6), 143 (16.5), 142 (12.0), 141 (10.0), 133 (13.7), 132 (17.9), 131 (39.5), 130 (27.4), 129 (29.5), 128 (16.3), 121 (7.6), 120 (16.6), 119 (14.5), 118 (15.4), 117 (46.3), 116 (12.0), 115 (22.3), 108 (10.9), 107 (14.1), 106 (10.5), 105 (26.1), 104 (20.8), 103 (9.5), 95 (13.8), 94 (15.7), 93 (24.7), 92 (30.5), 91 (92.1), 81 (17.6), 80 (21.9), 79 (58.3), 78 (20.6), 77 (52.6), 67 (17.8), 66 (10.7), 65 (20.4), 55 (8.4), 53 (14.1), 51 (10.3).

Spectra:

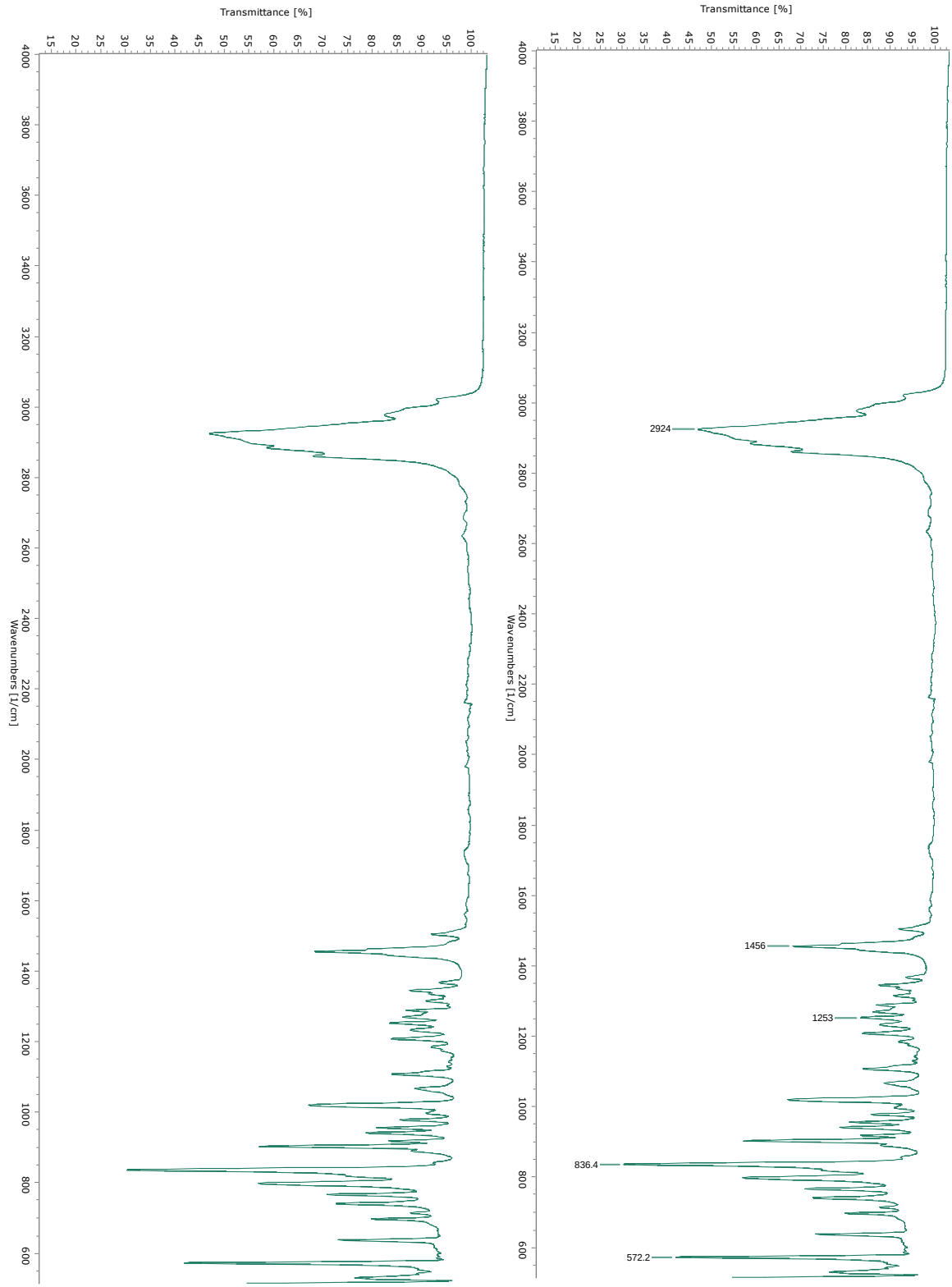

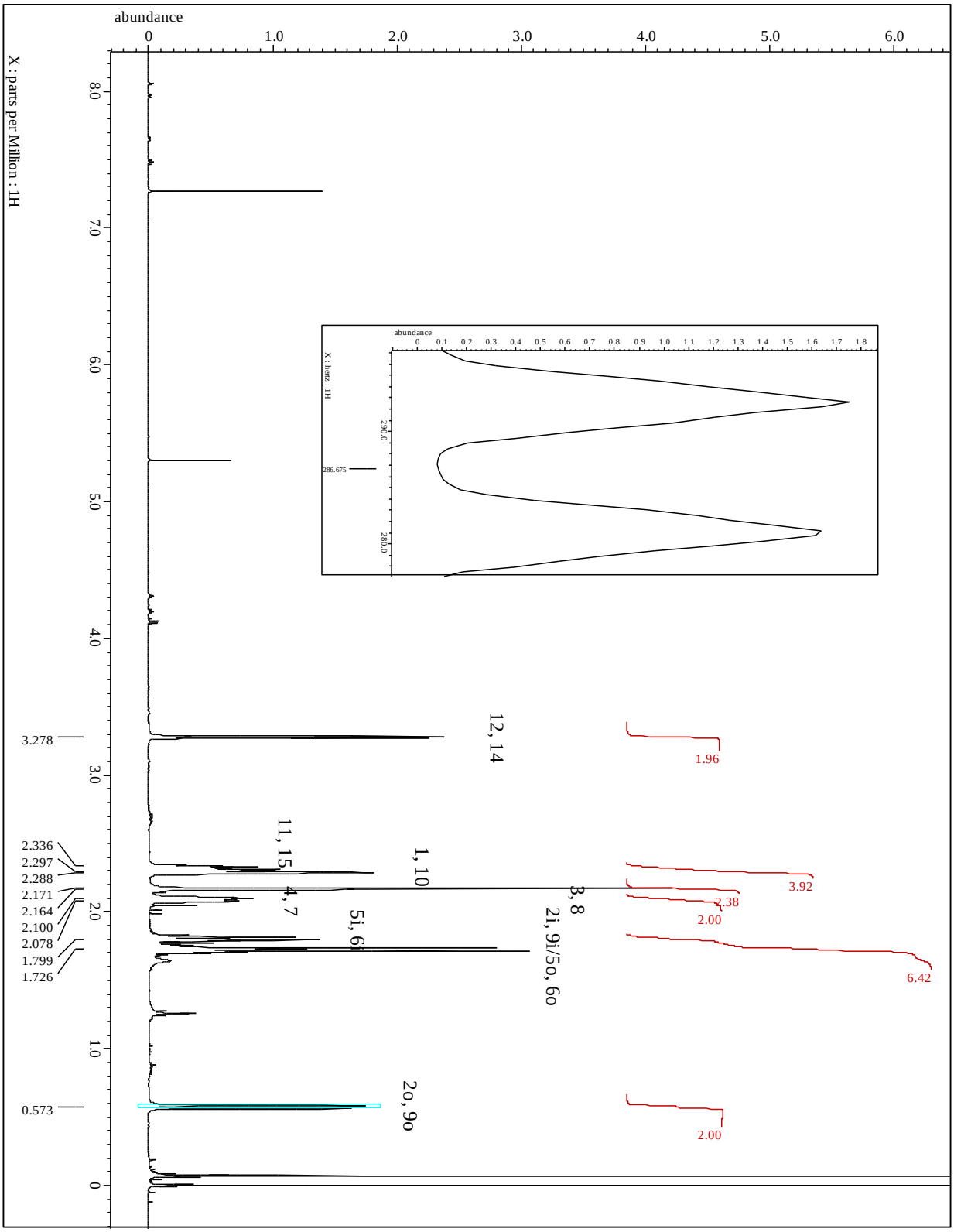
abundance
X : parts per Million : 1H
3.278
2.336
2.297
2.288
2.171
2.164
2.100
2.078
1.799
1.726
0.573
12, 14
11, 15
1, 10
4, 7
3, 8
5i, 6i
2i, 9i/5o, 6o
2o, 9o
1.96
3.92
2.38
2.00
6.42
2.00
X : hertz : 1H
286.675

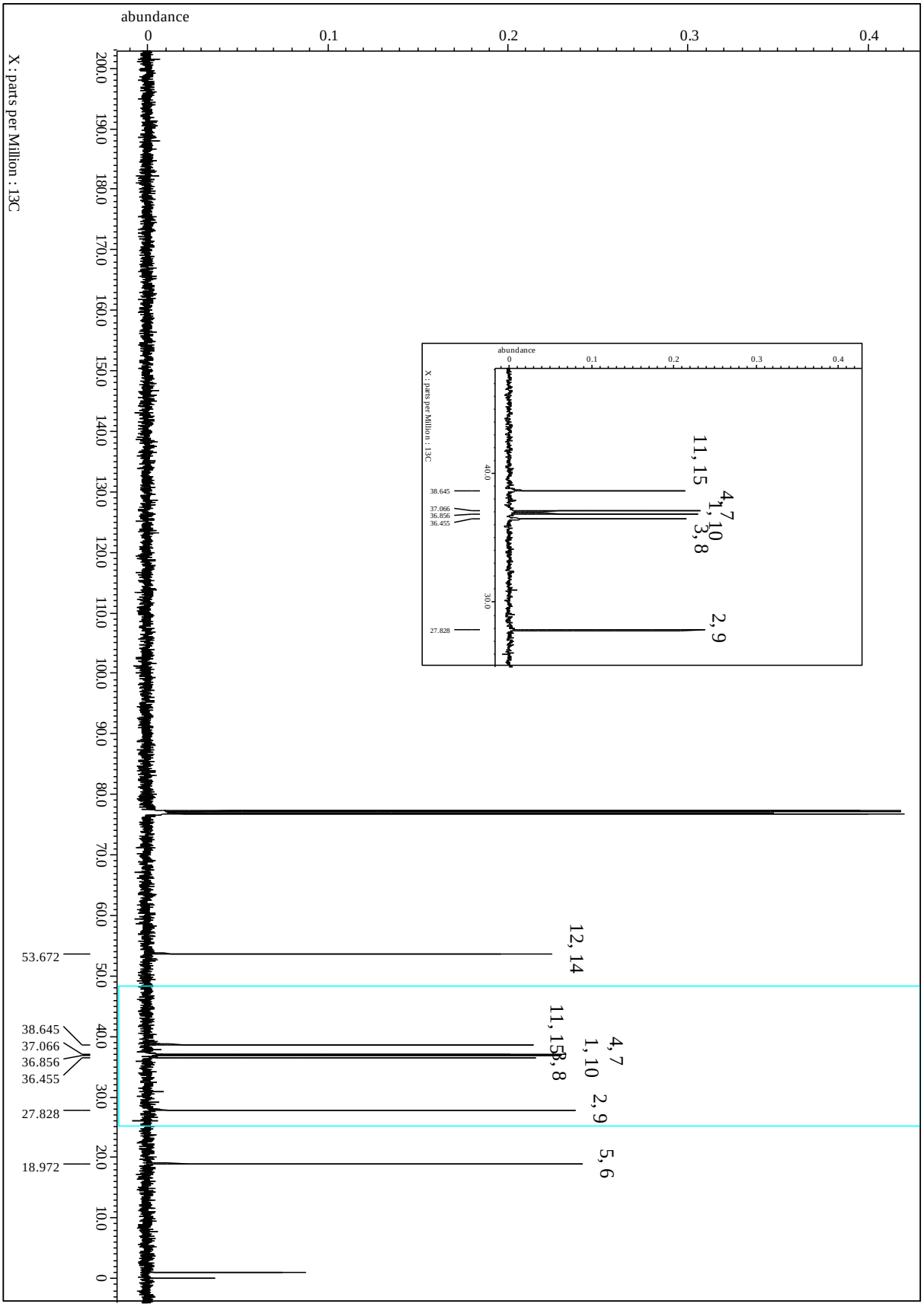
abundance
0
0.1
0.2
0.3
0.4
X : parts per Million : 13C
200.0
190.0
180.0
170.0
160.0
150.0
140.0
130.0
120.0
110.0
100.0
90.0
80.0
70.0
60.0
50.0
40.0
30.0
20.0
10.0
0
53.672
38.645
37.066
36.856
36.455
27.828
18.972
12, 14
11, 15
4, 7
1, 10
3, 8
2, 9
5, 6
40.0
30.0

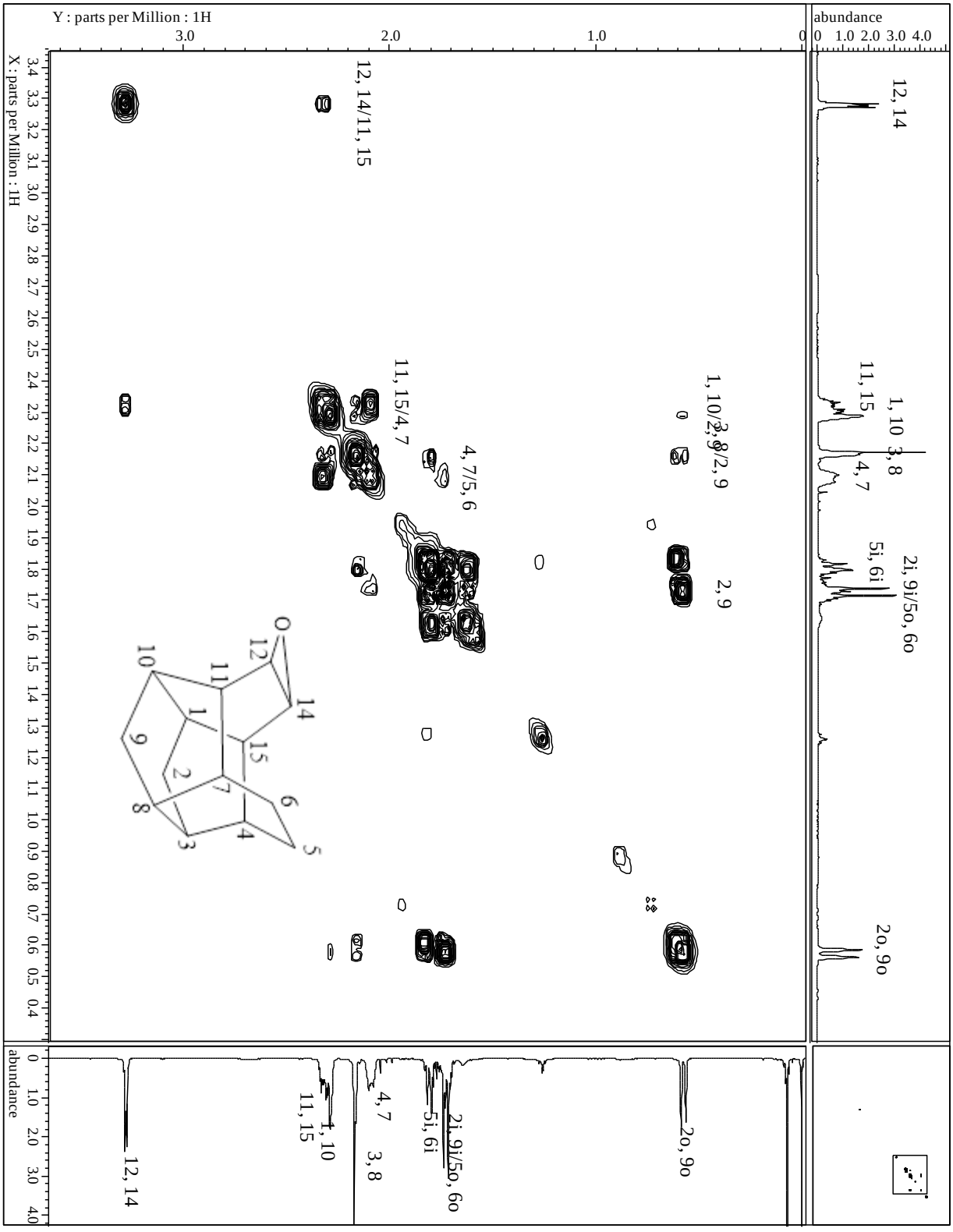
Y : parts per Million : 1H
X : parts per Million : 1H
abundance
12, 14
1, 10
11, 15
3, 8
4, 7
2i, 9i/5o, 6o
5i, 6i
2o, 9o
1, 10/2, 3, 8/2, 9
2, 9
4, 7/5, 6
11, 15/4, 7
12, 14/11, 15
O
12
14
10
11
1
15
9
2
7
6
8
4
5
3

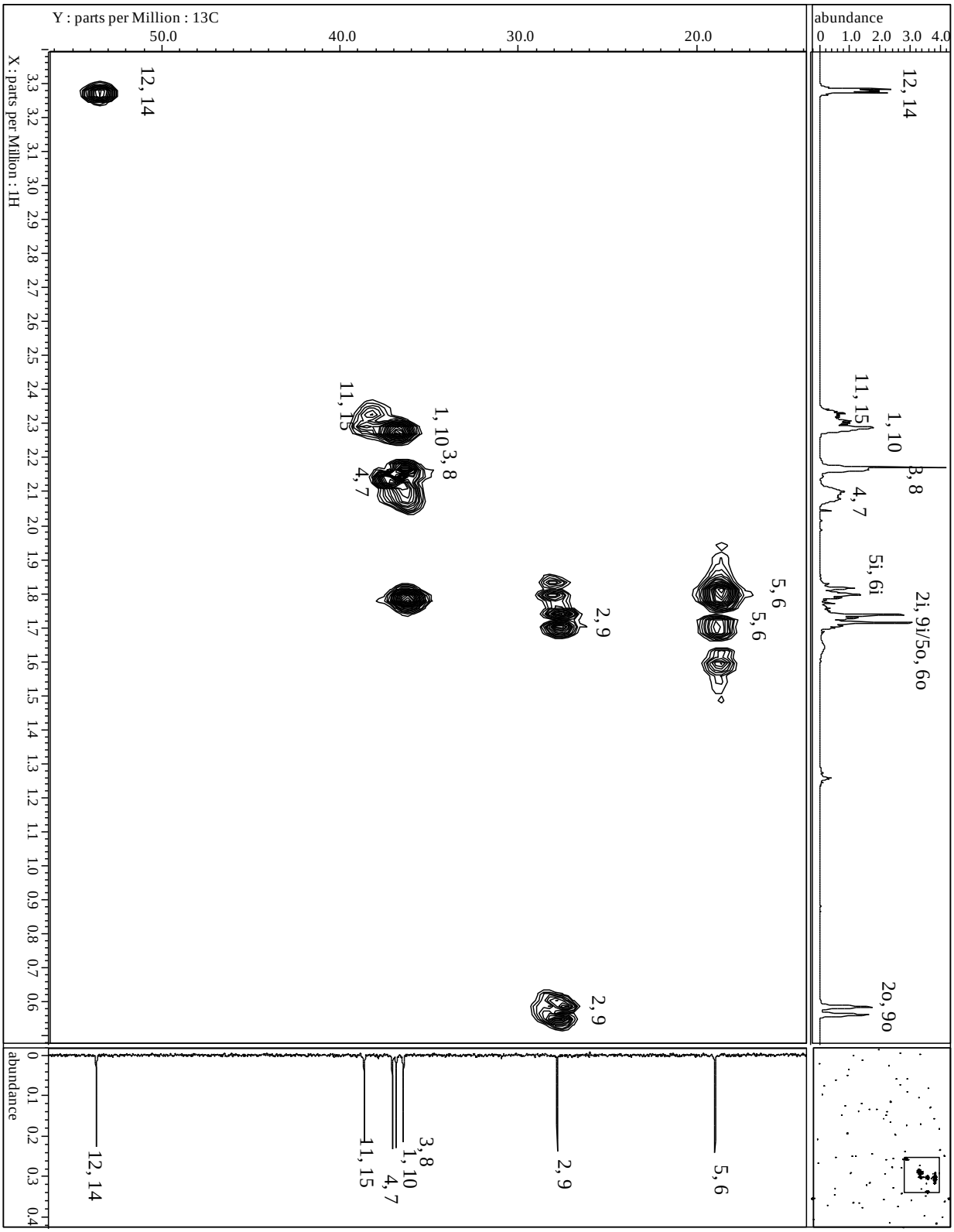
Y : parts per Million : 13C
X : parts per Million : 1H
abundance
12, 14
11, 15
1, 10
3, 8
4, 7
5i, 6i
2i, 9i/5o, 6o
2o, 9o
5, 6
2, 9
3, 8
1, 10
4, 7
11, 15
12, 14

(4S)-pentacyclo[8.4.0.0^{3,8}.0^{4,14}.0^{7,11}]tetradecan-4-ol (97a)

or

pentacyclo[8.4.0.0^{3,8}.0^{4,14}.0^{7,11}]tetradecan-1-ol (97b)

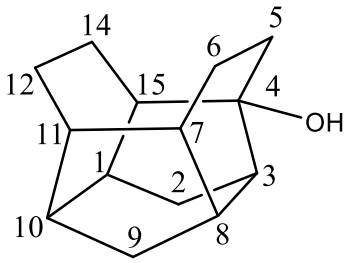

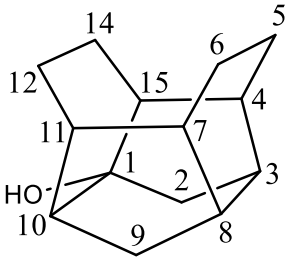

$C_{14}H_{18}O$ (202)

MP = Decomposition at 200 °C (decomposition product(s) melted at 248.3-249.9 ° C) ($CHCl_3$)

IR (AT-IR): $\tilde{\nu}$ = 3293 (br, m, O-H), 2923 (s, C-H), 1708 (w, C-O), 1505 (m), 1278 (s), 1133 (w), 1039 (s), 898 (m), 801 (m), 615 (w) cm^{-1}.

^{1}H-NMR ($CDCl_3$, 500 MHz): δ = 2.37 (m, 1H). 2.22 (m, 1H), 2.13 (m, 1H), 2.10-2.04 (m, 1H), 1.95-1.77 (m, 8H), 1.74-1.56 (m, 4H), 1.27 (ddd, 1H), 0.72 (ddd, 1H) ppm.

^{13}C-NMR ($CDCl_3$, 100.7 MHz): δ = 81.1, 47.7, 47.6, 39.0, 37.4, 37.1, 36.4, 36.1, 29.9, 29.3, 24.4, 19.8, 19.5, 18.3 ppm.

MS (EI, 70 eV): *m/z* (%) = 204 (2.1) [$M^{\cdot+}$], 203 (1.4), 202 (4.2), 187 (15.0), 186 (85.6), 171 (11.2), 158 (13.5), 157 (16.0), 145 (11.0), 144 (11.4), 143 (21.5), 141 (9.0), 132 (21.3), 131 (19.9), 130 (24.5), 129 (43.0), 128 (23.4), 120 (10.6), 119 (41.0), 118 (14.0), 117 (39.1), 116 (12.0), 115 (31.4), 109 (7.9), 108 (10.6), 107 (11.7), 106 (17.1), 105 (29.8), 104 (34.8), 103 (9.7), 96 (9.0), 95 (29.9),

94 (20.3), 93 (27.9), 92 (35.2), 91 (100.0), 81 (15.0), 80 (21.6), 79 (65.2), 78 (28.9), 77 (52.3), 67 (18.4), 66 (9.9), 65 (22.8), 55 (13.1), 54 (9.4), 53 (15.3), 51 (12.3).

Spectra:

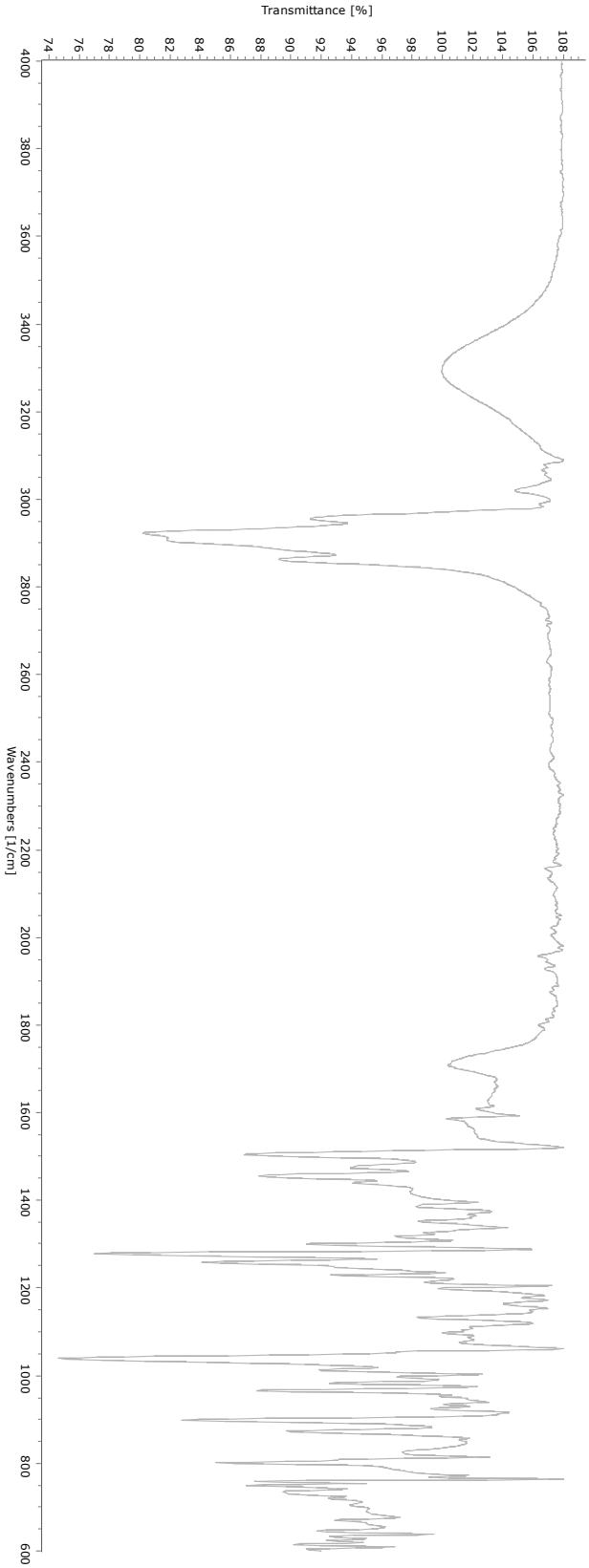
Transmittance [%]
Wavenumbers [1/cm]

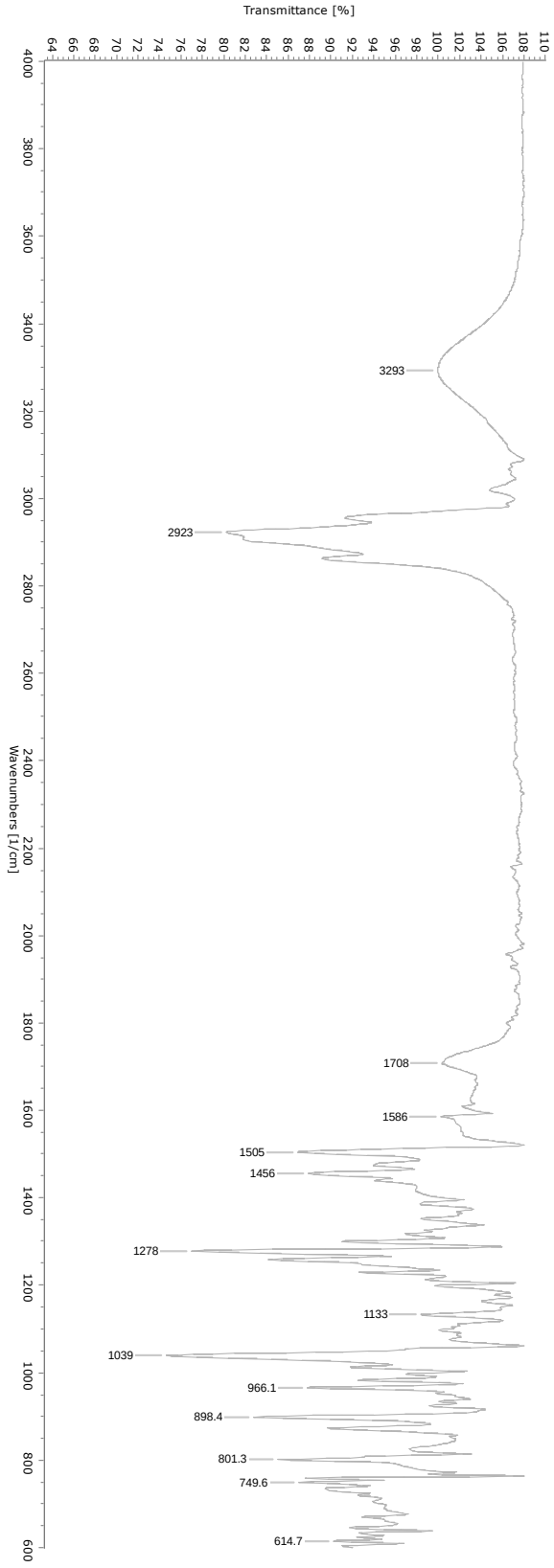
Transmittance [%]
Wavenumbers [1/cm]
3293
2923
1708
1586
1505
1456
1278
1133
1039
966.1
898.4
801.3
749.6
614.7

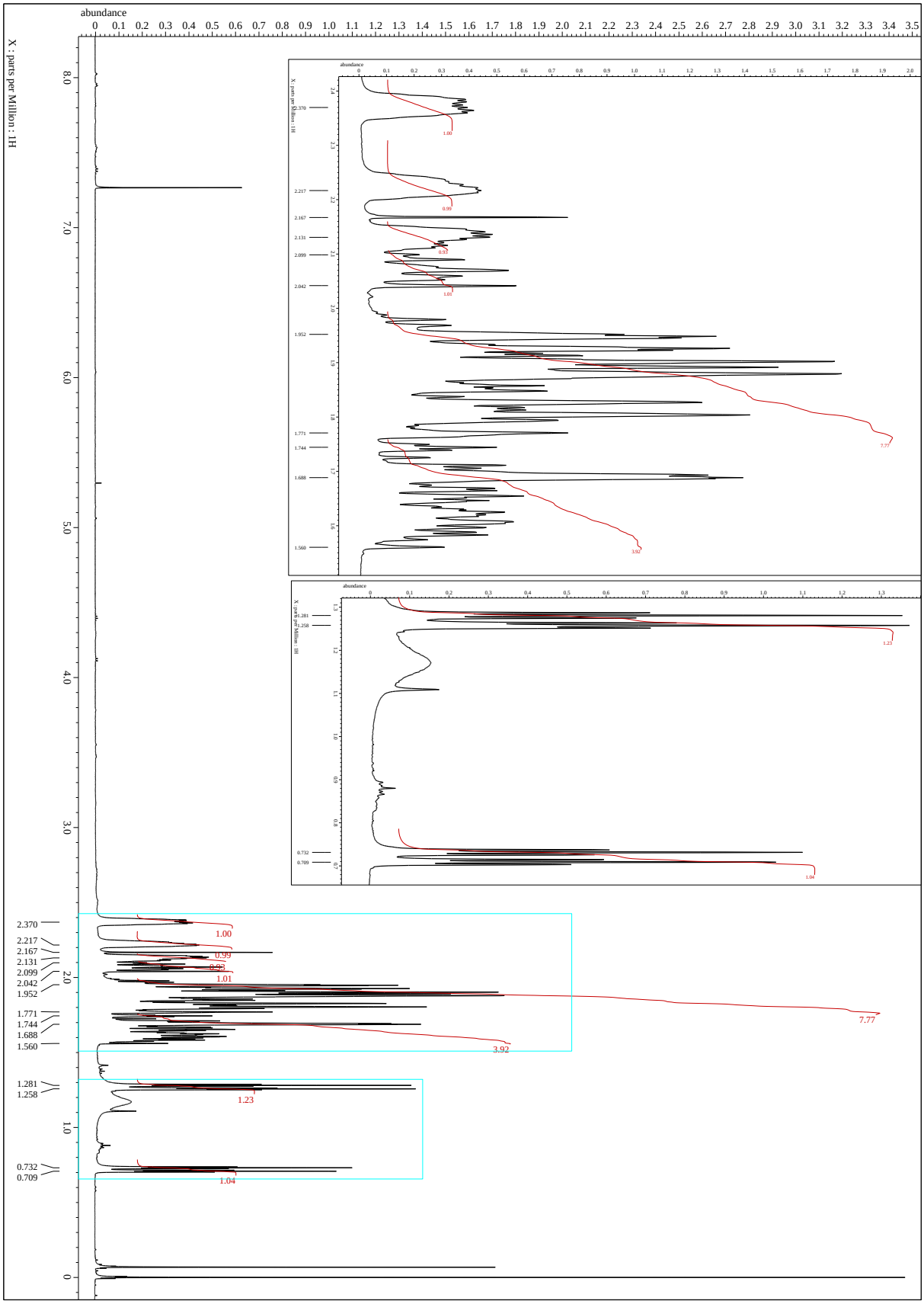
abundance
X : parts per Million : 1H
2.370
2.217
2.167
2.131
2.099
2.042
1.952
1.771
1.744
1.688
1.560
1.281
1.258
0.732
0.709
1.00
0.99
0.93
1.01
7.77
3.92
1.23
1.04

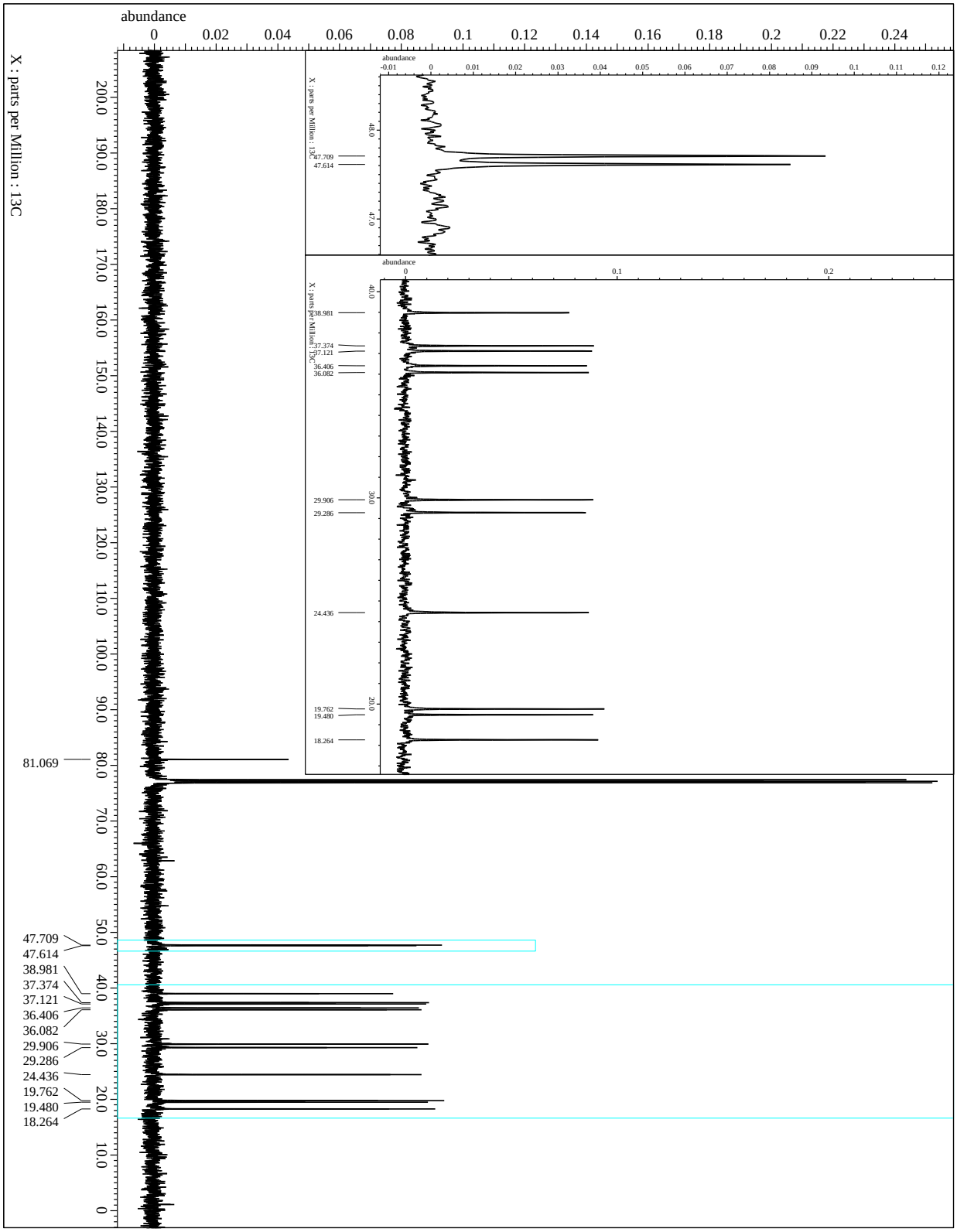
abundance
X : parts per Million : 13C
81.069
47.709
47.614
38.981
37.374
37.121
36.406
36.082
29.906
29.286
24.436
19.762
19.480
18.264

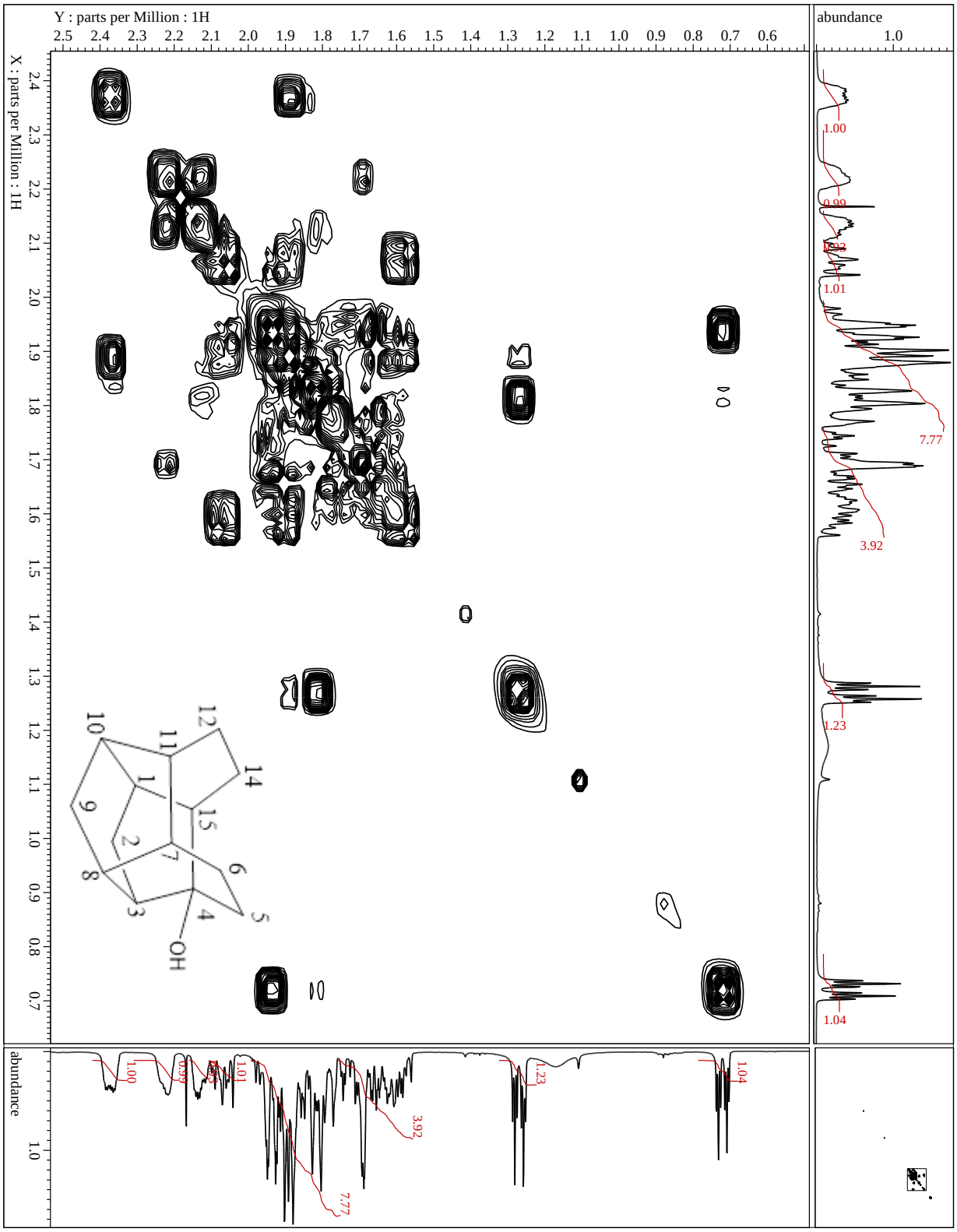
Y : parts per Million : 1H
X : parts per Million : 1H
abundance
1.00
0.99
1.01
7.77
3.92
1.23
1.04
OH

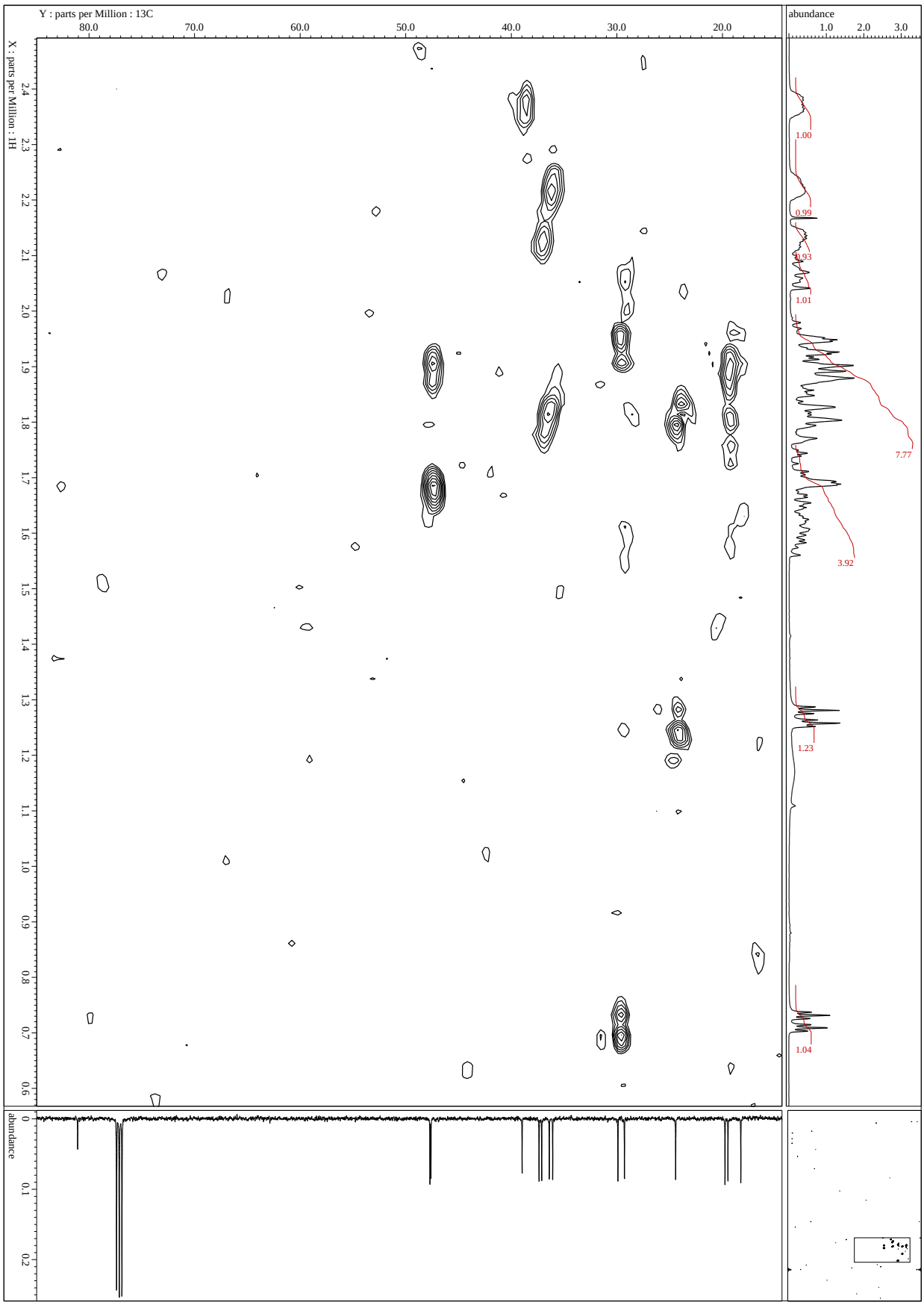
Y : parts per Million : 13C
80.0
70.0
60.0
50.0
40.0
30.0
20.0
X : parts per Million : 1H
2.4
2.3
2.2
2.1
2.0
1.9
1.8
1.7
1.6
1.5
1.4
1.3
1.2
1.1
1.0
0.9
0.8
0.7
0.6
abundance
1.0
2.0
3.0
1.00
0.99
0.93
1.01
7.77
3.92
1.23
1.04
abundance
0
0.1
0.2

(13R,15S)-6-oxaheptacyclo[9.5.0.0^{3,9}.0^{4,16}.0^{5,7}.0^{8,12}.0^{13,15}]hexadecane (98)

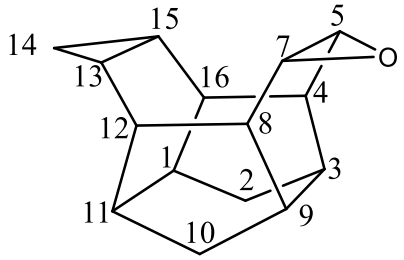

$C_{14}H_{18}O$ (214)

IR (AT-IR): $\tilde{\nu}$ = 2928 (s, C-H), 1710 (w, C-O), 1452 (m), 1261 (w), 1036 (m), 817 (s) cm^{-1}.

^{1}H-NMR ($CDCl_3$, 500 MHz): δ = 3.34 (s_{app}, 2H, H-5, -7), 2.44 (s_{app}, 4H, H-4, -8, -12, -16), 2.28 (s_{app}, 2H, H-3, -9), 2.05 (s_{app}, 2H, H-1, -11), 1.59 (d, 2H, H-2i, -10i), 1.00 (m, 2H, H-13, -15), 0.52 (d, 2H, H-2o, -10o), 0.43 (sx, 1H, H-14), 0.35 (q, 1H, H-14) ppm;

$^{2}J_{H\text{-}2i,\,\text{-}2o} = {}^{2}J_{H\text{-}10i,\,\text{-}10o}$ = 11.7 Hz.

^{13}C-NMR ($CDCl_3$, 100.7 MHz): δ = 54.0 (C-5, -7), 39.8, 37.1, 36.8, 36.4, 27.1 (C-2, -10), 11.4 (C-13, -15), 6.0 (C-14) ppm.

MS (EI, 70 eV): *m/z* (%) = 214 (16.8) [M$^{\cdot+}$], 207 (8.1), 185 (11.3), 167 (8.4), 158 (8.6), 157 (15.6), 155 (15.2), 145 (13.2), 144 (13.5), 143 (19.9), 142 (16.1), 141 (14.1), 134 (8.3), 133 (11.4), 132 (10.3), 131 (26.9), 130 (24.0), 129 (51.5), 128 (25.9), 127 (8.0), 121 (7.9), 120 (11.9), 119 (14.8), 118 (18.3), 117 (43.2), 116 (19.1), 115 (28.9), 108 (9.2), 107 (28.5), 106 (17.5), 105 (41.9), 104 (20.2), 103 (10.7), 95 (15.1), 94 (16.4), 93 (18.6), 92 (32.1), 91 (100.0), 81 (20.7), 80 (13.4), 79 (58.5), 78 (29.0), 77 (48.8), 67 (16.5), 66 (13.0), 65 (22.0), 55 (9.6), 53 (12.8), 51 (12.8).

Spectra:

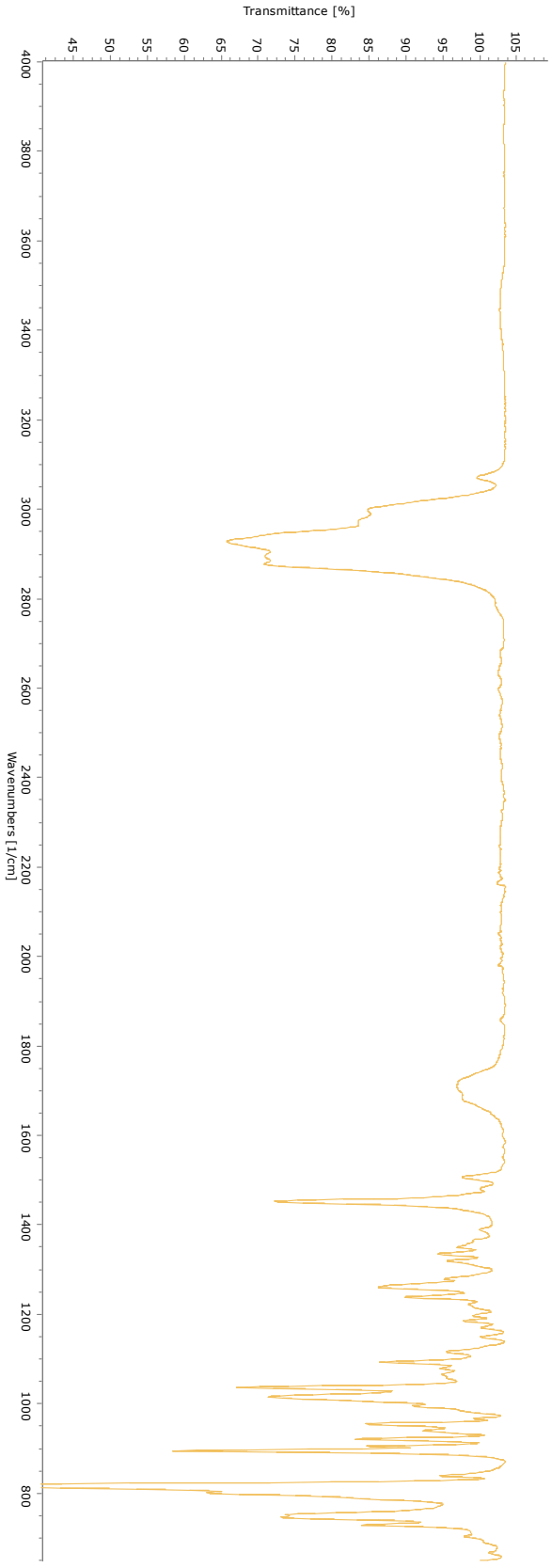
Transmittance [%]
Wavenumbers [1/cm]

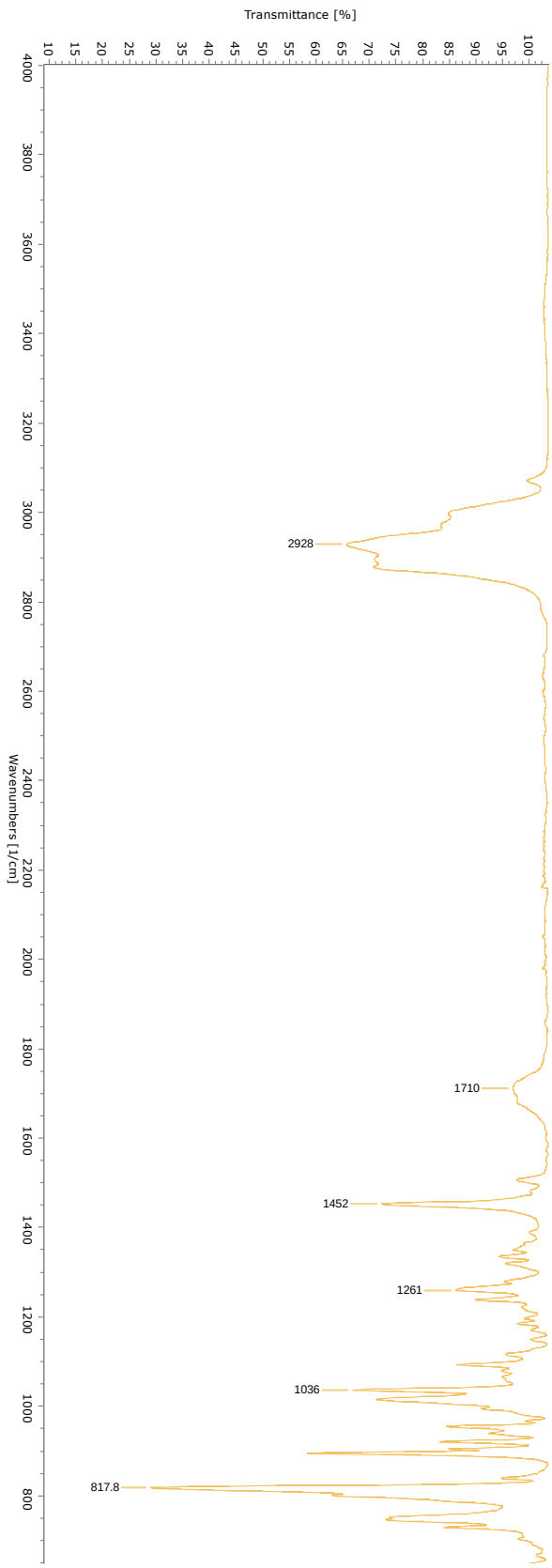
Transmittance [%]
Wavenumbers [1/cm]
2928
1710
1452
1261
1036
817.8

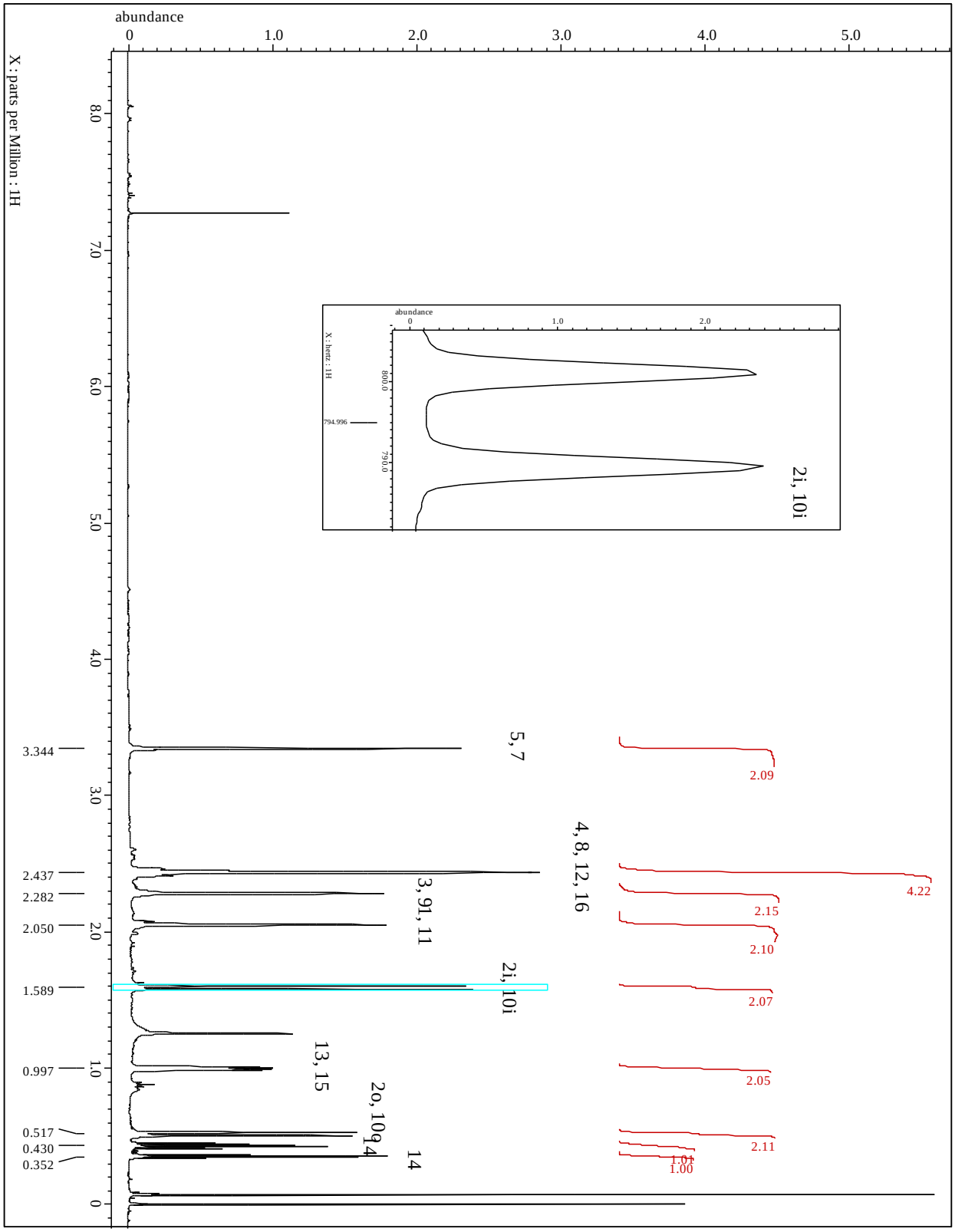
abundance
X : parts per Million : 1H
3.344
2.437
2.282
2.050
1.589
0.997
0.517
0.430
0.352
5, 7
4, 8, 12, 16
3, 9, 11
2i, 10i
13, 15
2o, 10q
14
14
2.09
4.22
2.15
2.10
2.07
2.05
2.11
1.01
1.00
abundance
X : hertz : 1H
794.996
2i, 10i

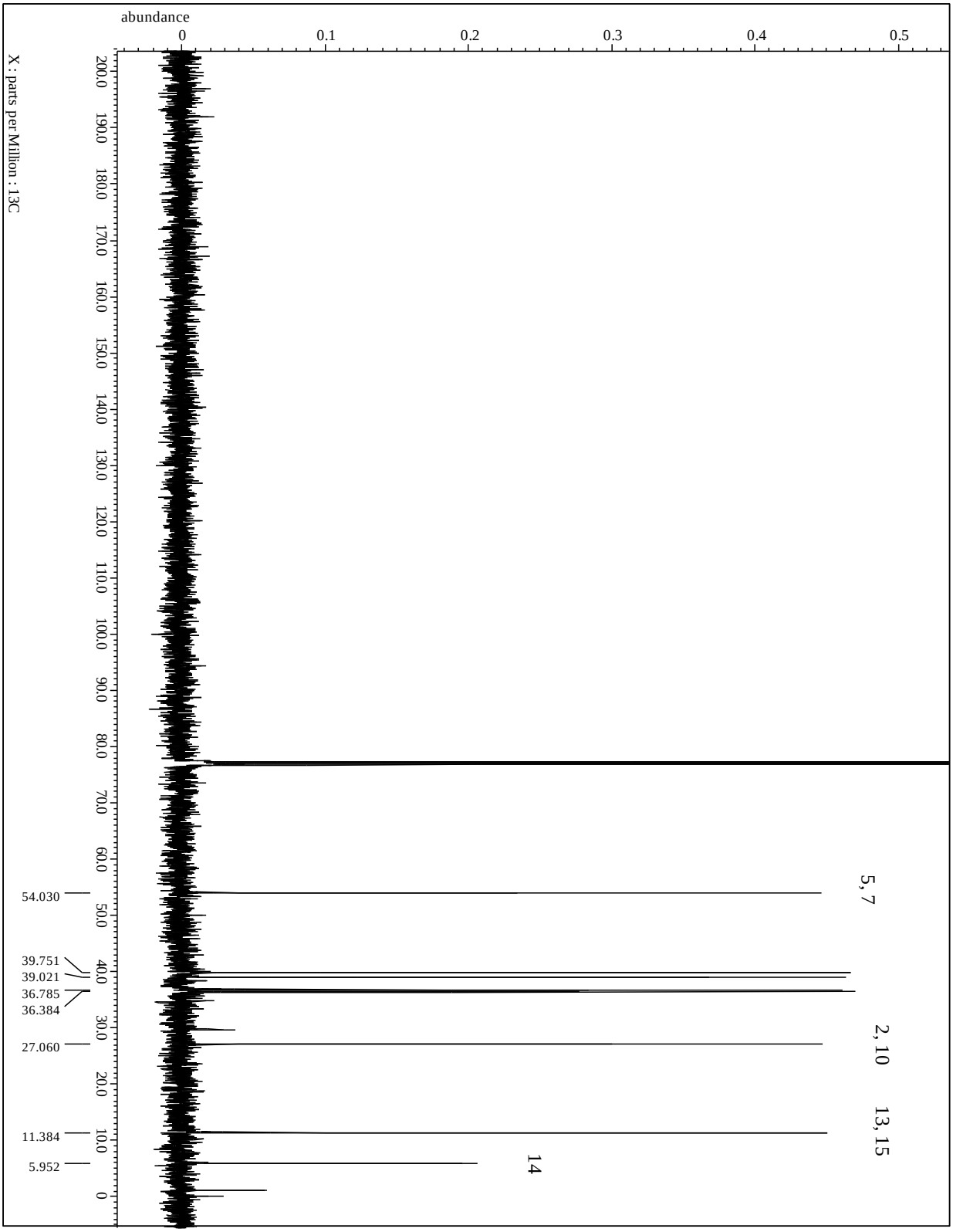
abundance
0
0.1
0.2
0.3
0.4
0.5
X : parts per Million : 13C
200.0
190.0
180.0
170.0
160.0
150.0
140.0
130.0
120.0
110.0
100.0
90.0
80.0
70.0
60.0
50.0
40.0
30.0
20.0
10.0
0
54.030
39.751
39.021
36.785
36.384
27.060
11.384
5.952
5, 7
2, 10
13, 15
14

5.4.4 Rearrangement of the Mono-epoxide Cage **94**

*Protocol #1 Rearrangement of Mono-epoxide **94**:* Step 1) To a solution of mono-epoxide **94** (510 mg, 2.55 mmol) in 1,4-dioxane/water (2:1, 7.1 mL) cooled to 0 °C, periodic acid (1.063 g, 4.66 mmol) was added in portions. The solution was stirred at 0 °C for 15 minutes, then warmed to room temperature and stirred an additional 2 hours. The solution was extracted with DCM (3x50 mL), dried ($MgSO_4$) and concentrated under vacuum resulting in poorly soluble crude material (400 mg). This material was taken as is for the subsequent reaction.

Step 2) To the poorly soluble material (400 mg, 2.0 mmol*) suspended in DCM (70 mL), Amberlyst-15 (816 mg, 4.0 mmol) was added. The suspension was then stirred for 16 hours. The Amberlyst-15 was filtered off and washed with DCM (3x25 mL). The filtrate and washings were combined and concentrated giving a colorless crystalline mixture of **99** and **100** (542 mg). Purification by column chromatography (SiO_2, 20:1 cyclohexane/EtOAc) gave two sets of mixed fractions containing 90% **100** (210 mg) and a 1:1 mixture of **99** and **100** (170 mg). Repeated column chromatographies gave small amounts of clean **100** (112 mg, 22%). Purification by epoxidation of **99** vastly improved isolated yields.

*Assumed same molar mass as the substrate

*Protocol #2 Rearrangement of Mono-epoxide **94**:* To a solution of mono-epoxide **94** (58.7 mg, 0.294 mmol) in DCM (6 mL), Amberlyst-15 (118.5 mg, 0.584 mmol, 4.95 mol/kg) was added and stirred for 16 hours. After **94** was consumed (based on GC/MS) the suspension was filtered and washed with DCM (3x25 mL). The filtrate and washings were combined and concentrated to afford a colorless solid (37 mg) comprised of a 2:1:1 mixture of **99**, **100**, and **103**. Purification by column chromatography (SiO_2, 13:1 cyclohexane: EtOAc) gave small amounts of clean **99** and **100** as well as **103** (10 mg, 15%).

*Epoxidation of **99/100** mixture:* To a solution of a mixture of **99** and **100** (60 mg, 3:1, 20 mg, 0.10 mmol of **99**) in DCM (5 mL), MCPBA (20.65 mg, 0.120 mmol, 1.2 eq) was added. The solution was then stirred at room temperature for 6 hours then quenched with water. The solution was extracted with DCM (3x50 mL). The combined organic was then washed with water (25 mL), aqueous sodium thiosulfate solution (2x25 mL), bicarbonate solution (2x25 mL) and again with water (25 mL). The organic phase was dried ($MgSO_4$) and concentrated under vacuum giving the crude product (107 mg) as colorless crystals. The crude material was purified by column chromatography (179 mg from two combined reactions, SiO_2, 10:1 Hexanes: EtOAc) yielding **152** (40 mg, 97%) and **100** (71 mg).

12-Oxahexacyclo[24.6.0.0^{2,6}.0^{4,13}.0^{5,11}.0^{10,14}]pentadic-24-ene (99)

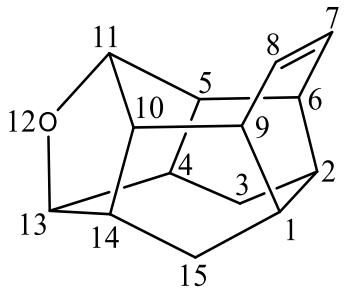

$C_{14}H_{16}O$ (200), R_f = 0.70 by SiO_2-TLC; visualized by UV or vanillin stain

^{1}H-NMR ($CDCl_3$, 500 MHz): δ = 6.10 (m, 2H, H-7, -8), 4.25 (t, 1H, H-13), 3.97 (t, 1H, H-11), 2.70 (m, 4H, H-4, -14; H-5, -10), 2.52 (s_{app}, 2H, H-6, -9). 2.10 (s_{app}, 2H, H-1, -2), 1.99 (d, 2H, H-3i, -15i), 1.34 (m, 2H, H-3o, -15o) ppm;

$^2J_{H\text{-}3i,\,\text{-}3o} = {}^2J_{H\text{-}15o,\,\text{-}15i}$ = 13.7; $^3J_{H\text{-}11,\,H\text{-}5,\,\text{-}10} = {}^3J_{H\text{-}13,\,H\text{-}4,\,\text{-}14}$ = 5.7 Hz

^{13}C-NMR ($CDCl_3$, 100.7 MHz): δ = 130.7 (C-7, -8), 80.2 (C-13), 79.6 (C-11), 49.1 (C-4, -14), 47.7 (C-5, -10), 41.0 (C-6, -9), 39.3 (C-1, -2), 28.2 (C-3, -15) ppm.

MS (EI, 70 eV): *m/z* (%) = 201 (13.6) [$M^{\cdot+}$+1], 200 (79.4) [$M^{\cdot+}$], 171 (9.1), 167 (9.8), 143 (11.0), 141 (14.1), 131 (11.1), 130 (15.9), 129 (35.9), 128 (36.1), 122 (15.7), 121 (8.3), 120 (7.5), 118 (11.6), 117 (29.5), 116 (18.2), 115 (37.6), 109 (13.6), 106 (8.9), 105 (14.7), 104 (18.5), 103 (12.0), 93 (13.1), 92 (29.6), 91 (100.0), 81 (14.0), 80 (11.3), 79 (37.5), 78 (32.4), 77 (43.1), 68 (14.1), 66 (12.2), 65 (22.1), 63 (9.7), 53 (10.9), 52 (7.5), 51 (15.4).

Spectra:

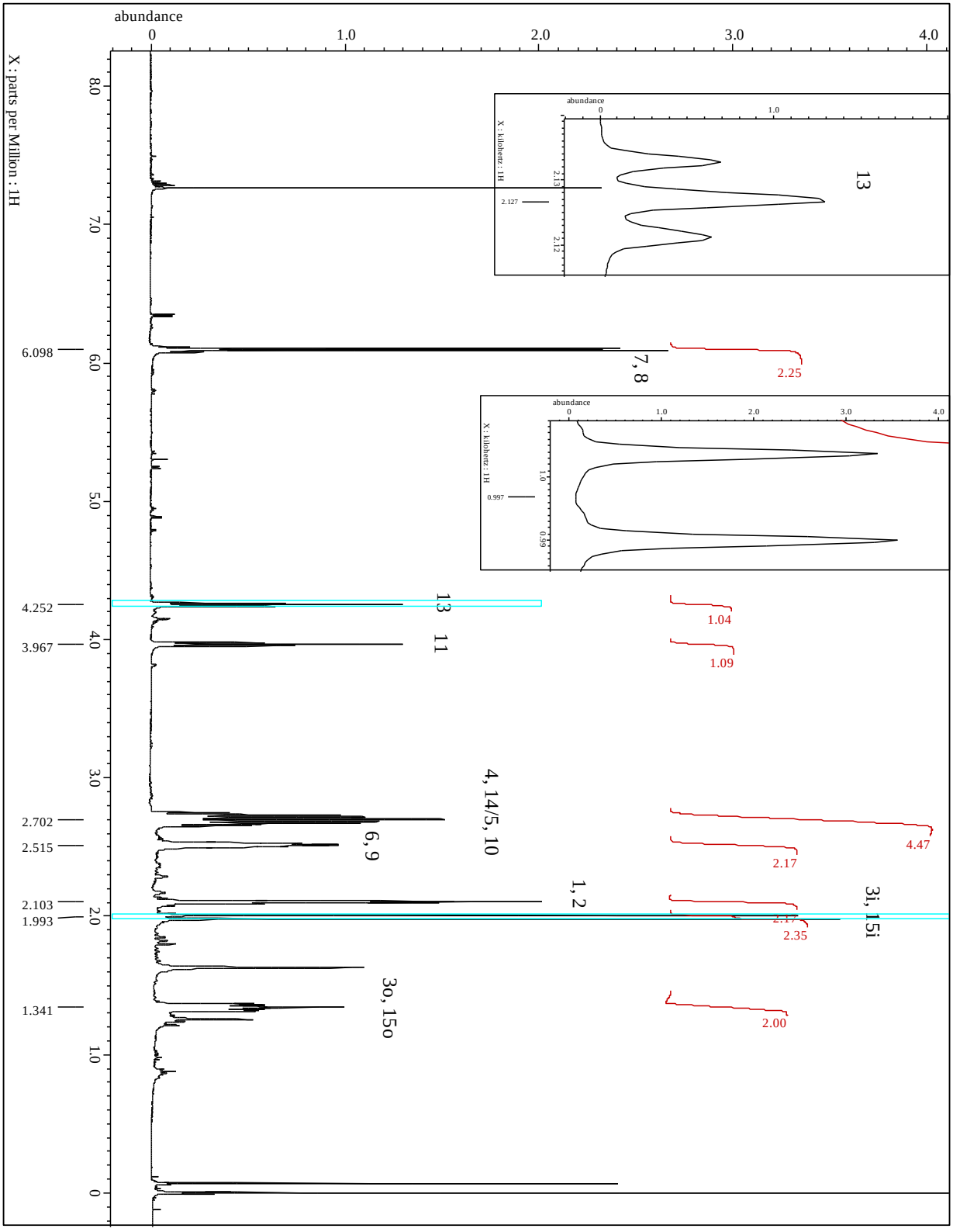
abundance
X : parts per Million : 1H
6.098
4.252
3.967
2.702
2.515
2.103
1.993
1.341
7, 8
13
11
6, 9
4, 14/5, 10
1, 2
3o, 15o
3i, 15i
2.25
1.04
1.09
4.47
2.17
2.35
2.00
X : kilohertz : 1H
2.127
0.997

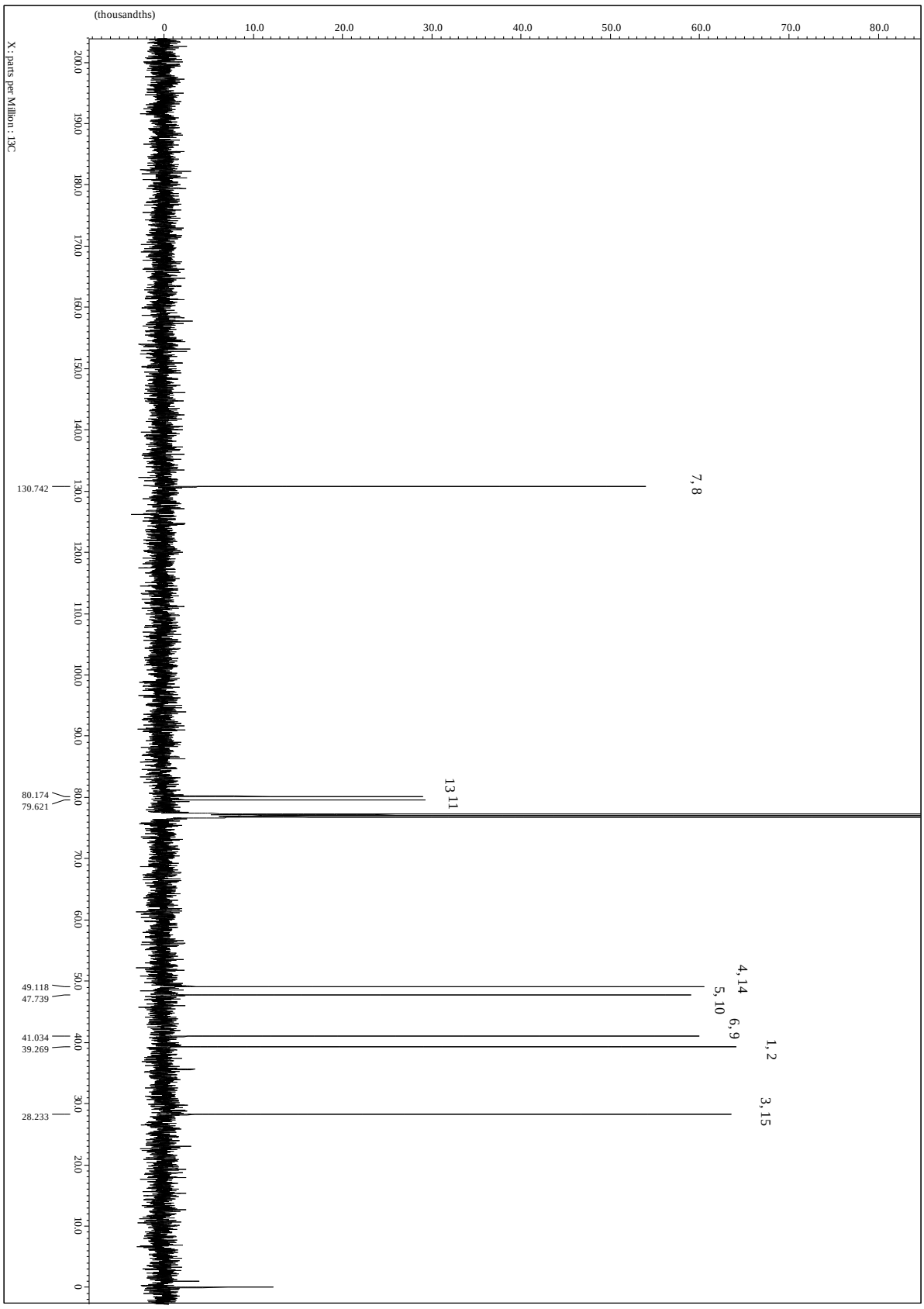
(thousandths)
0
10.0
20.0
30.0
40.0
50.0
60.0
70.0
80.0
X : parts per Million : 13C
200.0
190.0
180.0
170.0
160.0
150.0
140.0
130.0
120.0
110.0
100.0
90.0
80.0
70.0
60.0
50.0
40.0
30.0
20.0
10.0
0
130.742
80.174
79.621
49.118
47.739
41.034
39.269
28.233
7, 8
13
11
4, 14
5, 10
6, 9
1, 2
3, 15

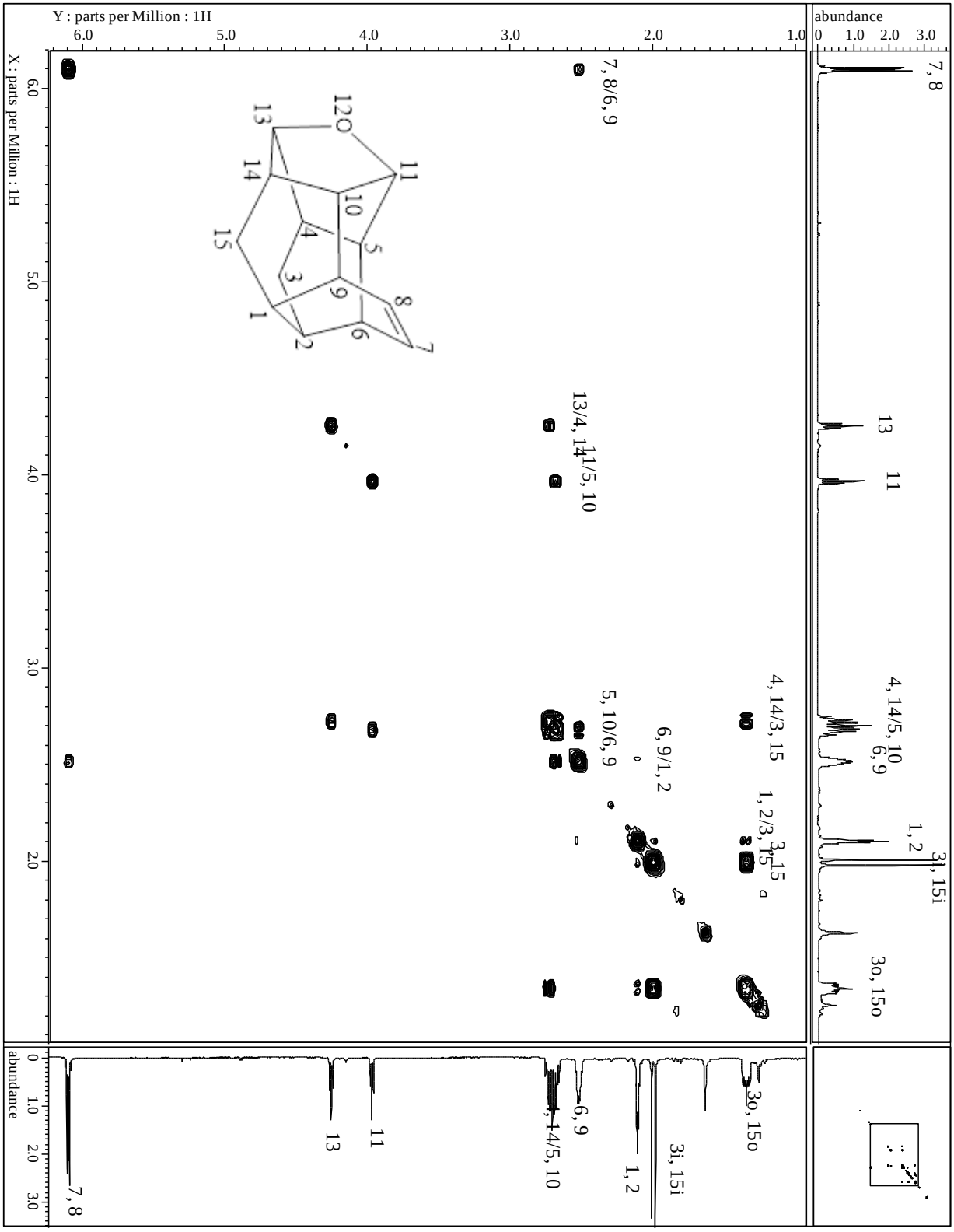
abundance
0 1.0 2.0 3.0
7, 8
13
11
4, 14/5, 10
6, 9
1, 2
3i, 15i
3o, 15o
Y : parts per Million : 1H
6.0 5.0 4.0 3.0 2.0 1.0
X : parts per Million : 1H
6.0 5.0 4.0 3.0 2.0
7, 8/6, 9
13/4, 14
11/5, 10
4, 14/3, 15
5, 10/6, 9
6, 9/1, 2
1, 2/3, 15
3i
3o
15
a
O
12
13
14
15
10
4
5
3
9
1
2
11
8
6
7
abundance
0 1.0 2.0 3.0
3o, 15o
3i, 15i
1, 2
6, 9
4, 14/5, 10
11
13
7, 8

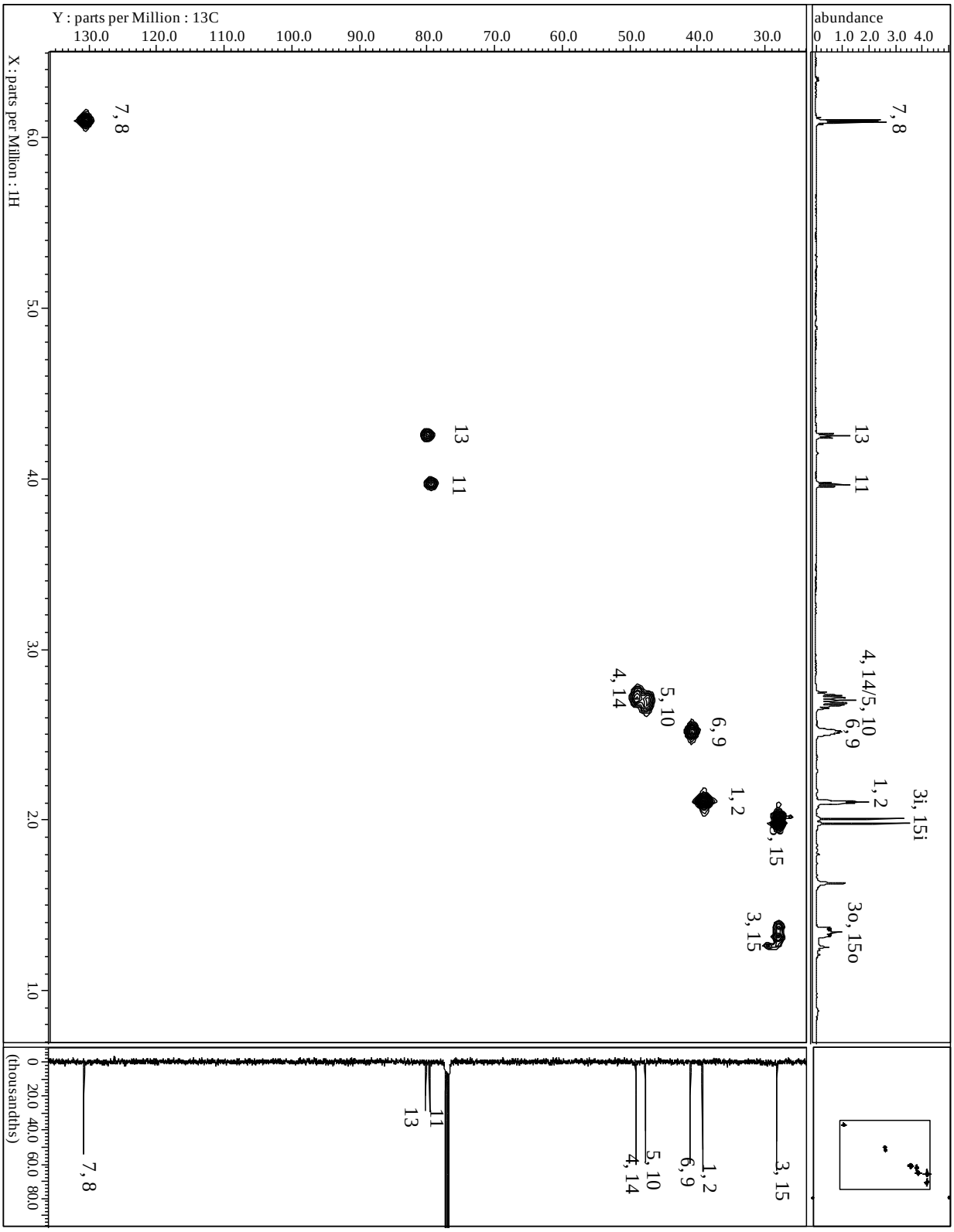
Y : parts per Million : 13C
X : parts per Million : 1H
abundance
(thousandths)
7, 8
13
11
4, 14/5, 10
6, 9
3i, 15i
1, 2
3, 15
3o, 15o
4, 14
5, 10
6, 9
1, 2
3, 15
13
11
7, 8

8-Oxaheptacyclo[7.6.0.0^{2,7}.0^{3,14}.0^{5,12}.0^{6,10}.0^{11,15}]pentadecane (100):

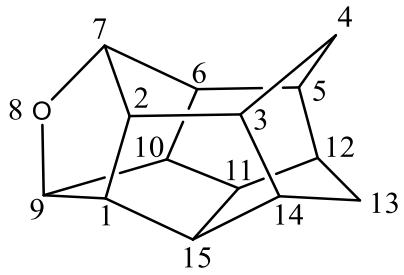

$C_{14}H_{16}O$ (200), R_f = 0.75 by SiO_2-TLC; visualized by vanillin stain

MP = 263.2-263.4 (slight burning at 249.9) °C ($CDCl_3$)

IR (AT-IR): $\tilde{\nu}$ = 2930 (s, C-H), 1722 (w, C-O-C), 1446 (w), 1342 (w), 1257 (w), 1021 (s), 931 (s), 820 (s) cm^{-1}.

^{1}H-NMR ($CDCl_3$, 500 MHz): δ = 4.93 (t, 1H, H-9), 4.12 (t, 1H, H-7), 2.89-2.84 (m, 2H, H-2, -6), 2.77 (m, 2H, H-12, -14), 2.70-2.65 (m, 2H, H-1, -10), 2.55 (m, 2H, H-11, -15), 2.36 (m, 2H, H-3, -5), 1.68 (d, 1H, H-13i), 1.30 (dt, 1H, H-13o), 1.21 (dt, 1H, H-4i), 1.00 (dt, 1H, H-4o) ppm;

$^2J_{H\text{-}13i,H\text{-}13o}$ = 12.2; $^2J_{H\text{-}4i,\ H\text{-}4o}$ = 13.4; $^3J_{H\text{-}9,\ H\text{-}1,\ -10}$ = $^3J_{H\text{-}7,\ H\text{-}2,\ -6}$ = 5.4 Hz

^{13}C-NMR ($CDCl_3$, 100.7 MHz): δ = 93.5 (C-9), 76.5 (C-7), 53.2 (C-2, -6), 52.5 (C-1, -10), 51.3 (C-11, -15), 50.7 (C-12, -14), 34.7 (C-3, -5), 31.3 (C-13), 20.4 (C-4) ppm.

^{1}H-NMR (C_6D_6, 500 MHz): δ = 4.86 (t, 1H, H-9), 4.02 (t, 1H, H-7), 2.77-2.72 (m, 2H, H-2, -6), 2.52 (m, 4H, H-1, -10; H-12, -14), 2.28 (m, 2H, H-11, -15), 2.06 (m, 2H, H-3, -5), 1.46 (d, 1H, H-13i), 1.1 (dt, 1H, H-13o), 0.93 (dt, 1H, H-4i), 0.7 (dt, 1H, H-4o) ppm

^{13}C-NMR (C_6D_6, 100.7 MHz): δ = 93.4 (C-9), 76.1 (C-7), 53.7(C-2, -6), 52.9 (C-12, -14), 51.5 (C-11, -15), 50.1 (C-1, -10), 34.8 (C-3, -5), 31.4 (C-13), 20.4 (C-4) ppm.

MS (EI, 70 eV): *m/z* (%) = 201 (14.3), 200 (95.9), 173 (8.0), 172 (65.6), 171 (27.3), 144 (10.4), 143 (13.6), 141 (11.0), 131 (10.9), 130 (22.1), 129 (49.3), 128 (24.9), 120 (7.9), 118 (15.0), 117 (32.3), 116 (17.2), 115 (39.5), 106 (11.4), 105 (20.9), 104 (20.7), 103 (14.5), 94 (19.2), 93 (16.4), 92 (37.3), 91 (100.0), 81 (24.7), 80 (33.7), 79 (62.3), 78 (38.0), 77 (64.2), 67 (12.1), 66 (21.6), 65 (30.6), 63 (10.4), 53 (12.9), 52 (8.3), 51 (14.7).

Spectra:

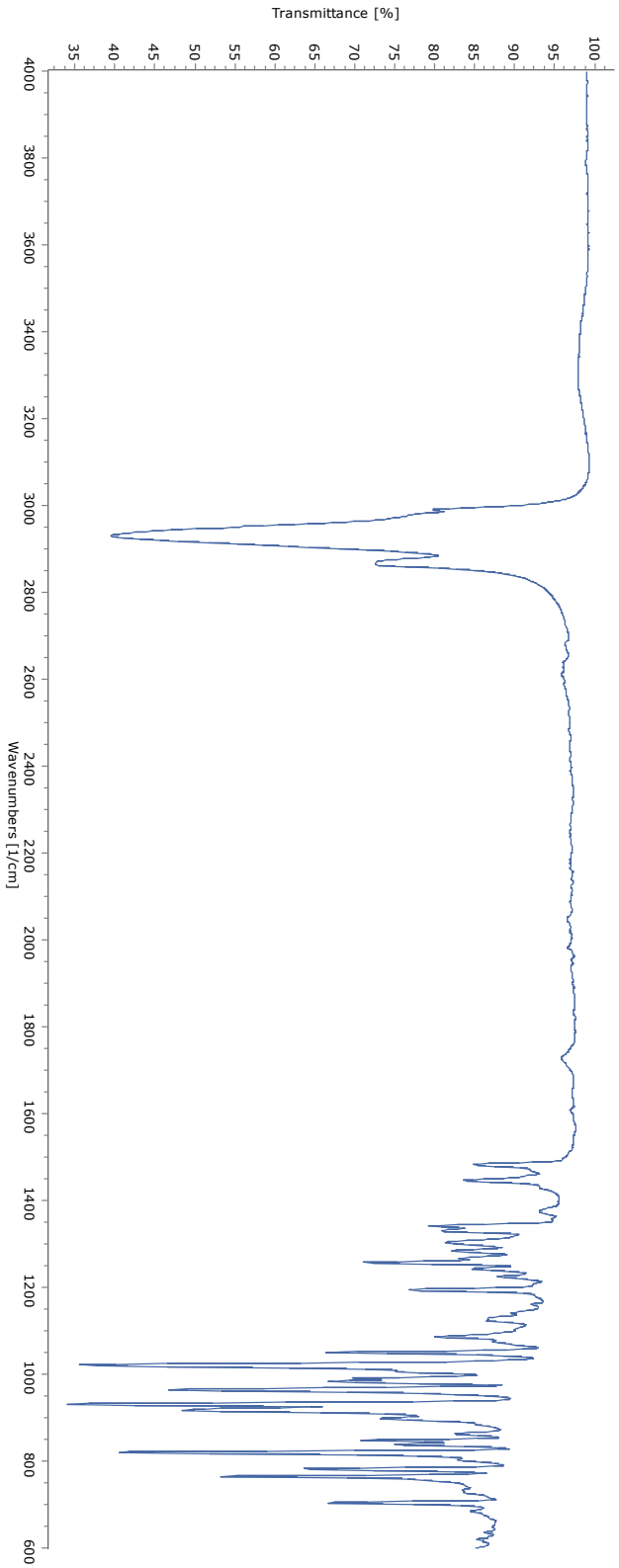
Transmittance [%]
Wavenumbers [1/cm]

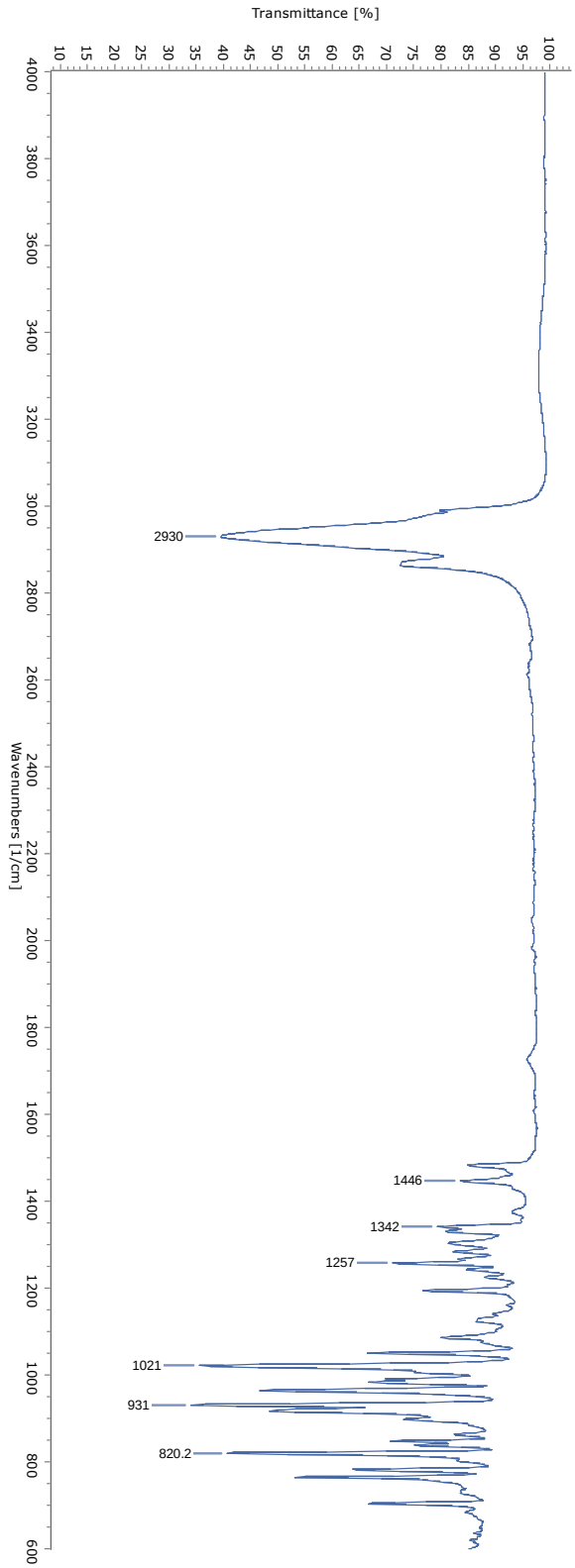
Transmittance [%]
Wavenumbers [1/cm]
2930
1446
1342
1257
1021
931
820.2

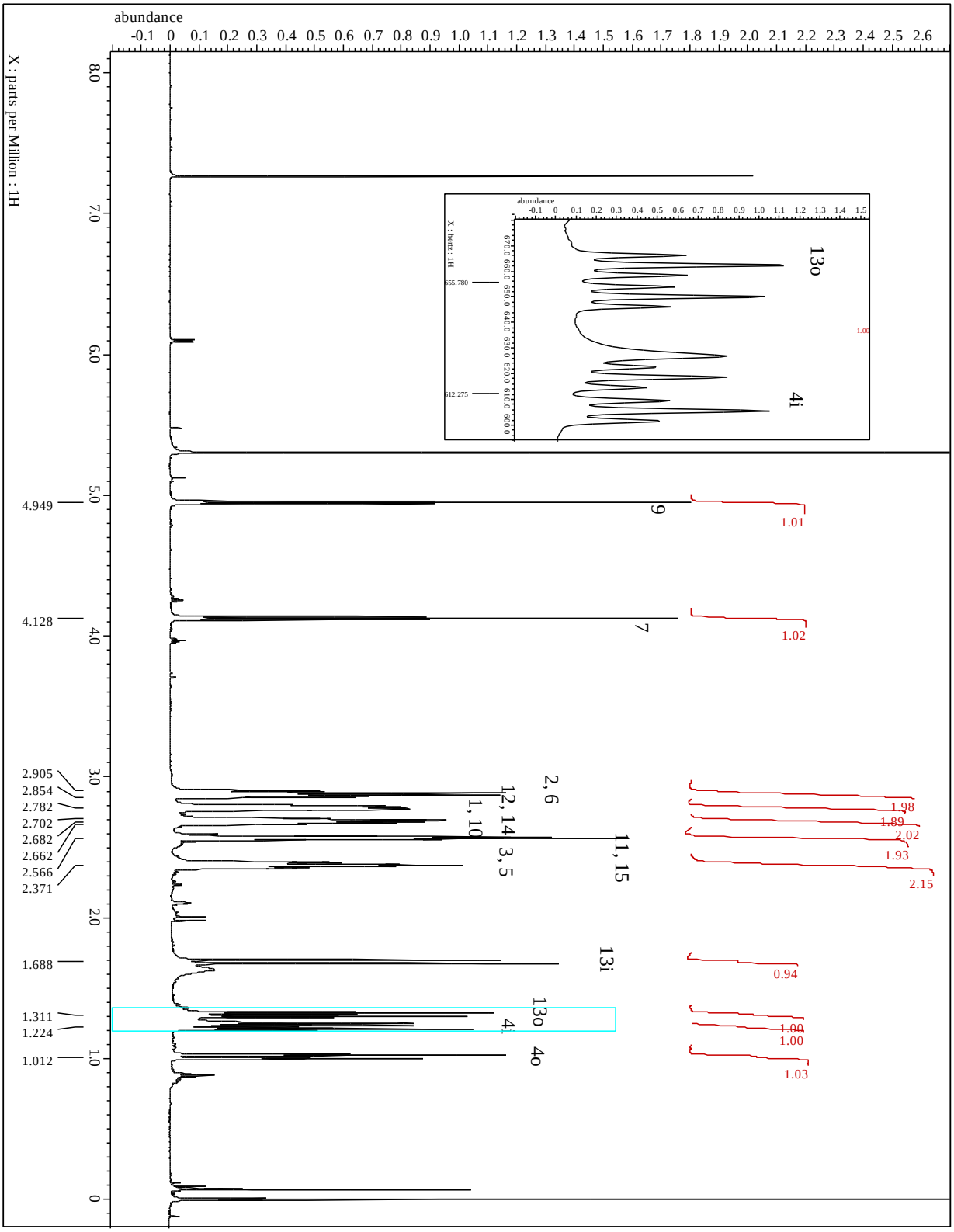
abundance
X : parts per Million : 1H
4.949
4.128
2.905
2.854
2.782
2.702
2.682
2.662
2.566
2.371
1.688
1.311
1.224
1.012
9
7
2, 6
12, 14
1, 10
3, 5
11, 15
13i
13o
4i
4o
1.01
1.02
1.98
1.89
2.02
1.93
2.15
0.94
1.00
1.00
1.03
X : hertz: 1H
555.780
612.275
1.00

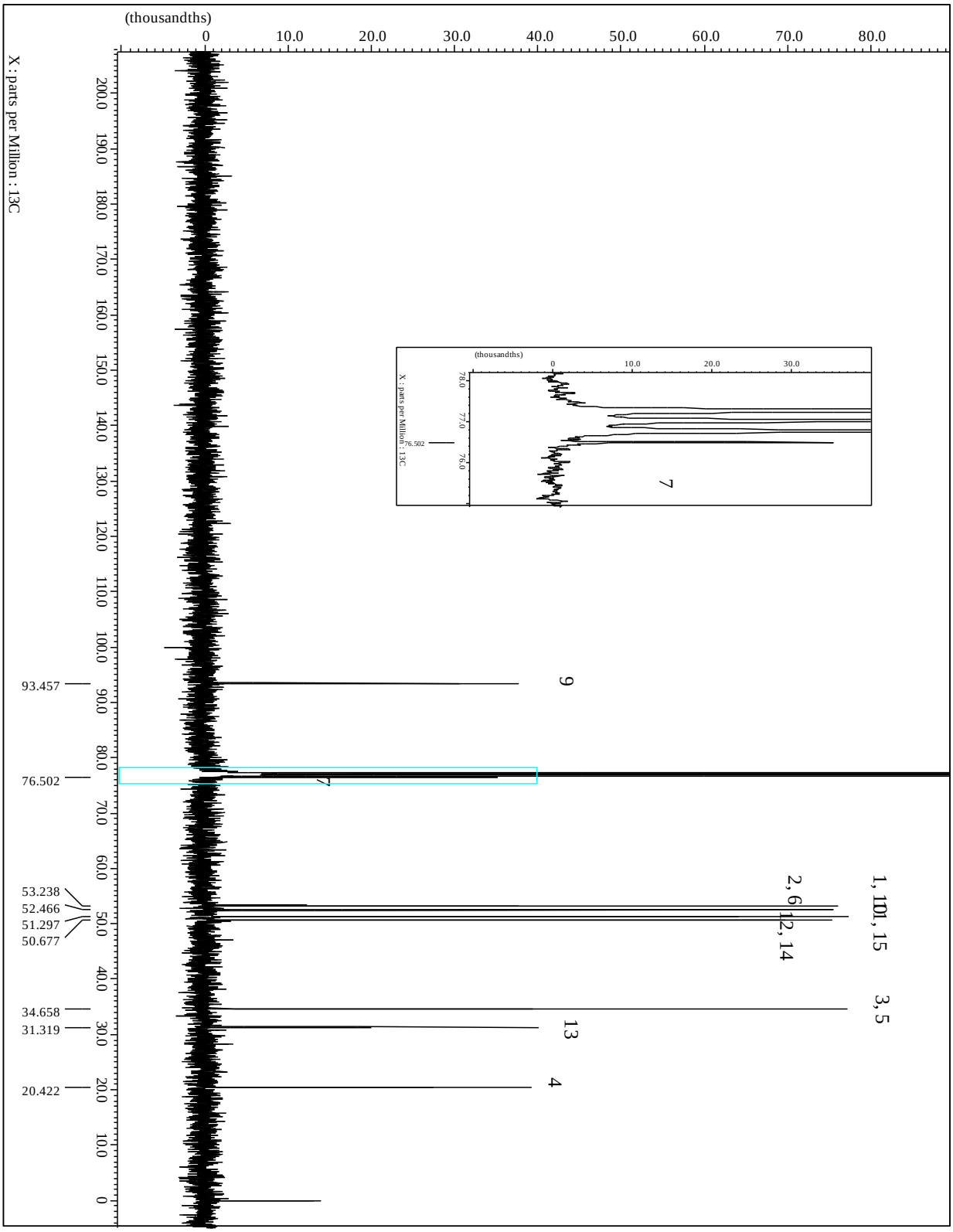
(thousandths)
0
10.0
20.0
30.0
40.0
50.0
60.0
70.0
80.0
X : parts per Million : 13C
200.0
190.0
180.0
170.0
160.0
150.0
140.0
130.0
120.0
110.0
100.0
90.0
80.0
70.0
60.0
50.0
40.0
30.0
20.0
10.0
0
93.457
76.502
53.238
52.466
51.297
50.677
34.658
31.319
20.422
9
7
1, 10, 11, 15
2, 6, 12, 14
3, 5
13
4
(thousandths)
0
10.0
20.0
30.0
X : parts per Million : 13C
78.0
77.0
76.0
76.502
7

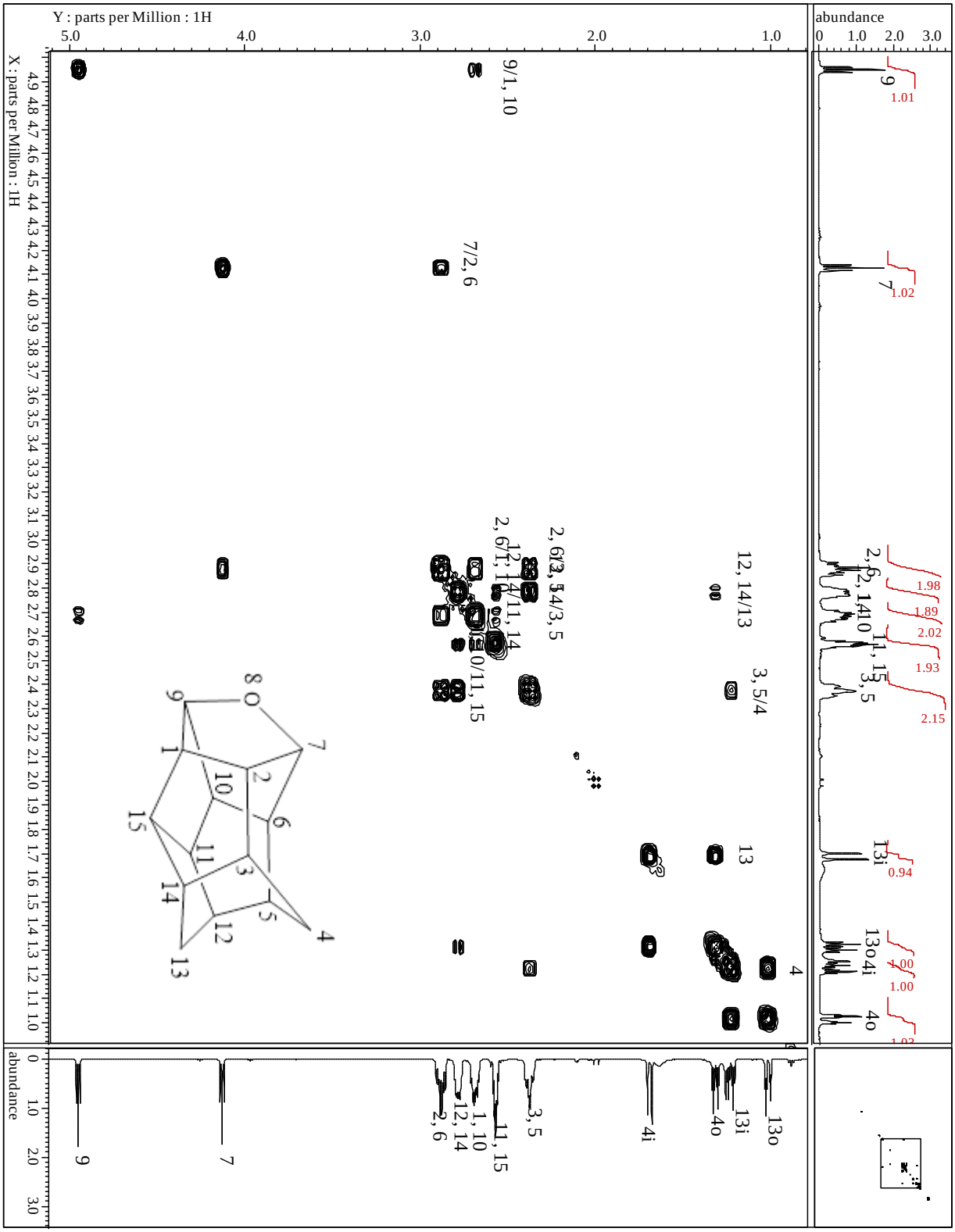
abundance
9
1.01
7
1.02
2, 6, 12, 14
10
11, 15
3, 5
1.98
1.89
2.02
1.93
2.15
13i
0.94
13o
4i
1.00
1.00
4o
Y : parts per Million : 1H
5.0
4.0
3.0
2.0
1.0
9/1, 10
7/2, 6
2, 6/12, 14/3, 5
2, 6/1, 12, 14/11, 14
10/11, 15
12, 14/13
3, 5/4
13
4
X : parts per Million : 1H
4.9 4.8 4.7 4.6 4.5 4.4 4.3 4.2 4.1 4.0 3.9 3.8 3.7 3.6 3.5 3.4 3.3 3.2 3.1 3.0 2.9 2.8 2.7 2.6 2.5 2.4 2.3 2.2 2.1 2.0 1.9 1.8 1.7 1.6 1.5 1.4 1.3 1.2 1.1 1.0
O
1
2
3
4
5
6
7
8
9
10
11
12
13
14
15
abundance
0
1.0
2.0
3.0
13o
13i
4o
4i
3, 5
11, 15
1, 10
12, 14
2, 6
7
9

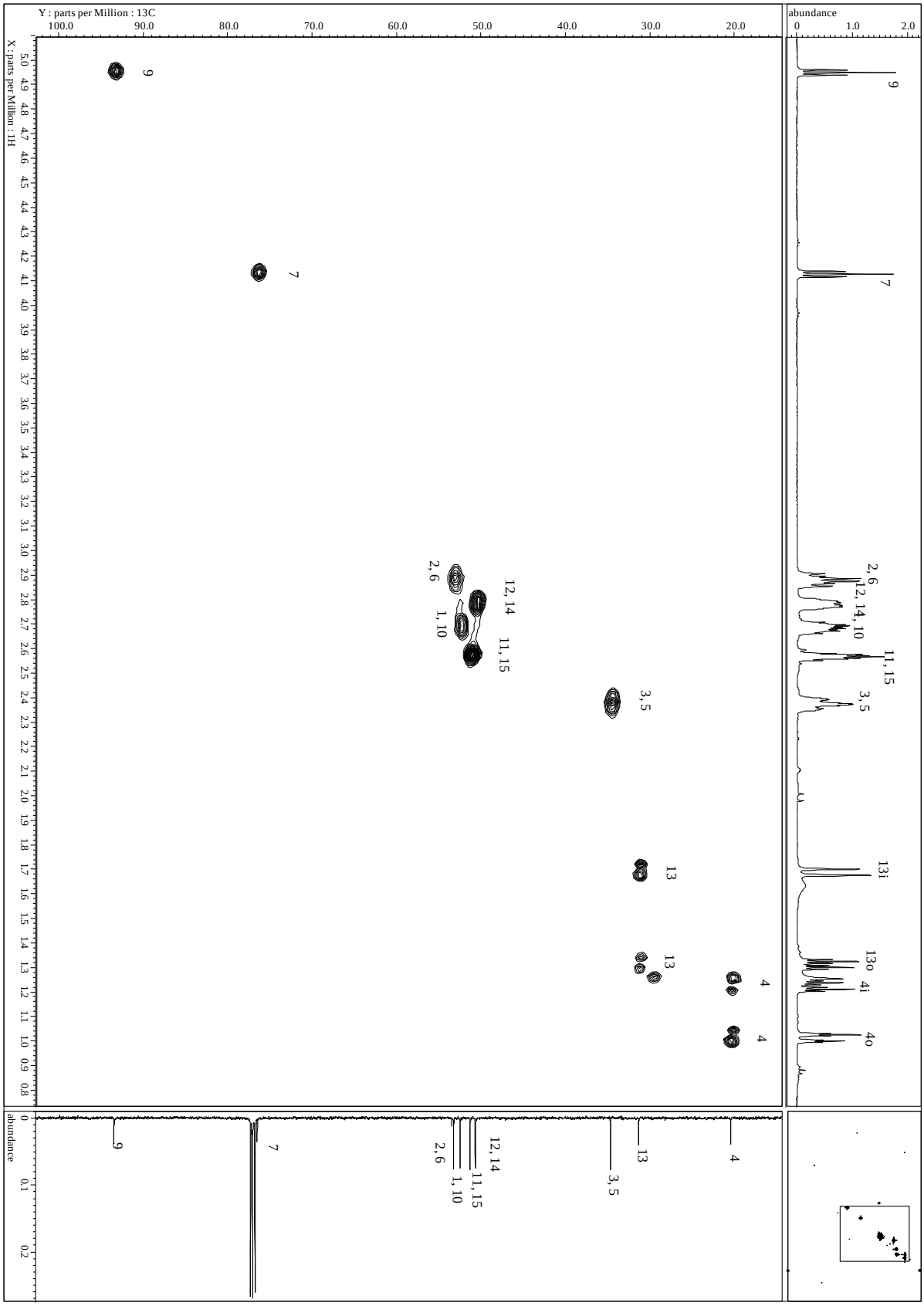
Y : parts per Million : 13C
X : parts per Million : 1H
abundance
9
7
2, 6
12, 14, 10
11, 15
3, 5
13i
13o
4i
4o
4
4
13
13
12, 14
11, 15
2, 6
1, 10

5.4.5 Ether Cleavage of **100** and Dehalogenation

Benzyl Bromide Ether Cleavage: Under Schlenk conditions, LiBr (19.54 mg, 0.225 mmol, 3 eq) was dried at 150 °C for 2 hours. To the dry LiBr, ether cage **100** (15 mg, 0.075 mmol) in ACN (0.5 mL) and benzyl bromide (15.39 g, 10.68 mL, 0.9 mmol, 1.2 eq) was added. The solution was stirred for 4 hours at room temperature then quenched with water. The solution was extracted with ether (3x20 mL) then dried ($MgSO_4$) and concentrated to afford an orange oil (28 mg). No reaction was detected by NMR or GC/MS.

TMSI Ether Cleavage: To **100** (75 mg, 0.375 mmol) in DCM (10 mL) and water (50 µL), TMSI (0.952 mL, 1.34 g, 6.69 mmol) was added and stirred at room temperature for 4 days until all **100** was consumed based on ^{1}H-NMR. The solution was then extracted with DCM (3x30 mL). The combined organic phase was then washed with $NaHSO_3$ (2x20 mL), dried ($MgSO_4$), and concentrated resulting in an orange crystalline and oil mixture of three isomers of **149** and **100** (161 mg). Column chromatography (SiO_2, 10:1 cyclohexane/EtOAc) was used to remove **100** from the product mixture. **149** (14 mg, 8.5%) was obtained through crystallization from 2:1 hexanes/EtOAc.

*Birch-type Dehalogenation of **149**:* To condensed liquid ammonia (100 mL) at -78 °C a mixture of isomers of **149** (65 mg, 0.148 mmol) in dry THF (10 mL) was added dropwise resulting in a white precipitate. Anhydrous EtOH (1.0 mL) was added to the suspension followed by freshly cut strips of Li metal (50 mg) until color persisted for 1 hour. The suspension was then quenched with NH_4Cl and the ammonia allowed to evaporate. The residue was taken up in water and extracted with DCM (3x20 mL). The combined organic phase was dried ($MgSO_4$) and concentrated affording colorless waxy material. Column chromatography (SiO_2, *n*-pentane) yielded **151** (12 mg, 31% yield).

*Tin Hydride Dehalogenation of **149**:* Diiodo cage **149** (159 mg, 0.363 mmol) in dry Et_2O (7.2 mL) under nitrogen was brough to reflux. To the refluxing solution, ^{n}BuSnH (0.363 mL) was added dropwise and refluxed for 3 hours. The solution was then washed with 5% NaOH (15 mL) and water (15 mL). The organic phase was then dried ($MgSO_4$) and concentrated crude oily material (582 mg). Upon standing 2 days a precipitate formed and the remaining oil containing **151** was removed with *n*-pentane. The product was not isolated but showed 90% conversion of **149** to **151** based on ^{1}H-NMR and GC/MS.

*LAH Dehalogenation of **149**:* To a solution of **149** (24 mg, 0.055 mmol) in dry EtO_2 (10 mL), LAH (30 mg) was added in portions. The suspension was then stirred for 3 hours at room temperature. The reaction was quenched according to the Fieser method (0.3 mL water, 0.9 mL 15% NaOH, 0.3 mL water). To the quenched suspension, a small portion of $MgSO_4$ was added and stirred an additional 15 minutes. The suspension was then filtered over Celite-545. The filtrate was concentrated to give **151** (20 mg). The product was not isolated but showed 90% conversion of **149** to **151** based on ^{1}H-NMR and GC/MS.

Diiodohexacyclo[6.5.1.$0^{2,6}$.$0^{3,12}$.$0^{5,10}$.$0^{9,13}$]tetradecane (149)

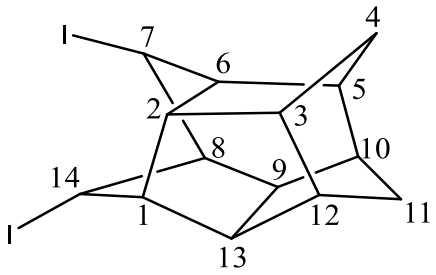

$C_{14}H_{16}I_2$ (438)

MP = 84.5-98.6 (90% melt at 86) °C ($CHCl_3$)

IR (AT-IR): $\tilde{\nu}$ = 2.934 (s, C-H), 2871 (m, C-H), 1449 (w), 1301 (m), 1252 (s), 1205 (m), 1164 (s), 993 (w) 924 (m), 880 (w), 797 (m), 696 (m) cm^{-1}.

^{1}H-NMR ($CDCl_3$, 500 MHz): δ = 4.73 (d. 1H, H-14), 4.48 (s_{app}. 1H, H-7), 3.32 (s_{app}. 1H, H-2), 3.05 (d. 1H, H-1), 2.90 (s_{app}. 1H, H-12), 2.64 (s_{app}. 2H, H-6; H-13), 2.54 (s_{app}. 1H, H-5), 2.51 (s_{app}. 2H, H-9; H-10), 2.38 (s_{app}. 1H, H-3), 2.14 (s_{app}. 1H, H-8), 1.80 (d. 1H, H-4i), 1.54 (d. 1H, H-11i), 1.16 (d. 1H, H-4o), 0.86 (d. 1H, H-11o) ppm;

$^{2}J_{\text{H-4i, H-4o}} = {}^{2}J_{\text{H-11i, H-11o}} = 12.1$ Hz.

^{13}C-NMR ($CDCl_3$, 100.7 MHz): δ = 58.2 (C-2), 54.5 (C-1), 51.8 (C-13), 50.9 (C-12), 49.2 (C-10), 45.2 (C-8), 43.3 (C-6), 41.6 (C-3), 41.5 (C-9), 41.1 (C-7), 37.3 (C-14), 31.7 (C-4), 31.2 (C-5), 27.4 (C-11) ppm.

MS (EI, 70 eV): *m/z* (%) = 311 (25.8), 184 (34.3), 183 (100.0), 155 (10.2), 141 (19.5), 129 (15.8), 128 (16.1), 127 (7.8), 118 (13.4), 117 (51.0), 115 (16.5), 105 (16.5), 104 (8.3), 93 (7.7), 92 (9.7), 91 (33.7), 79 (19.6), 78 (14.1), 77 (18.5), 67 (33.2).

Spectra:

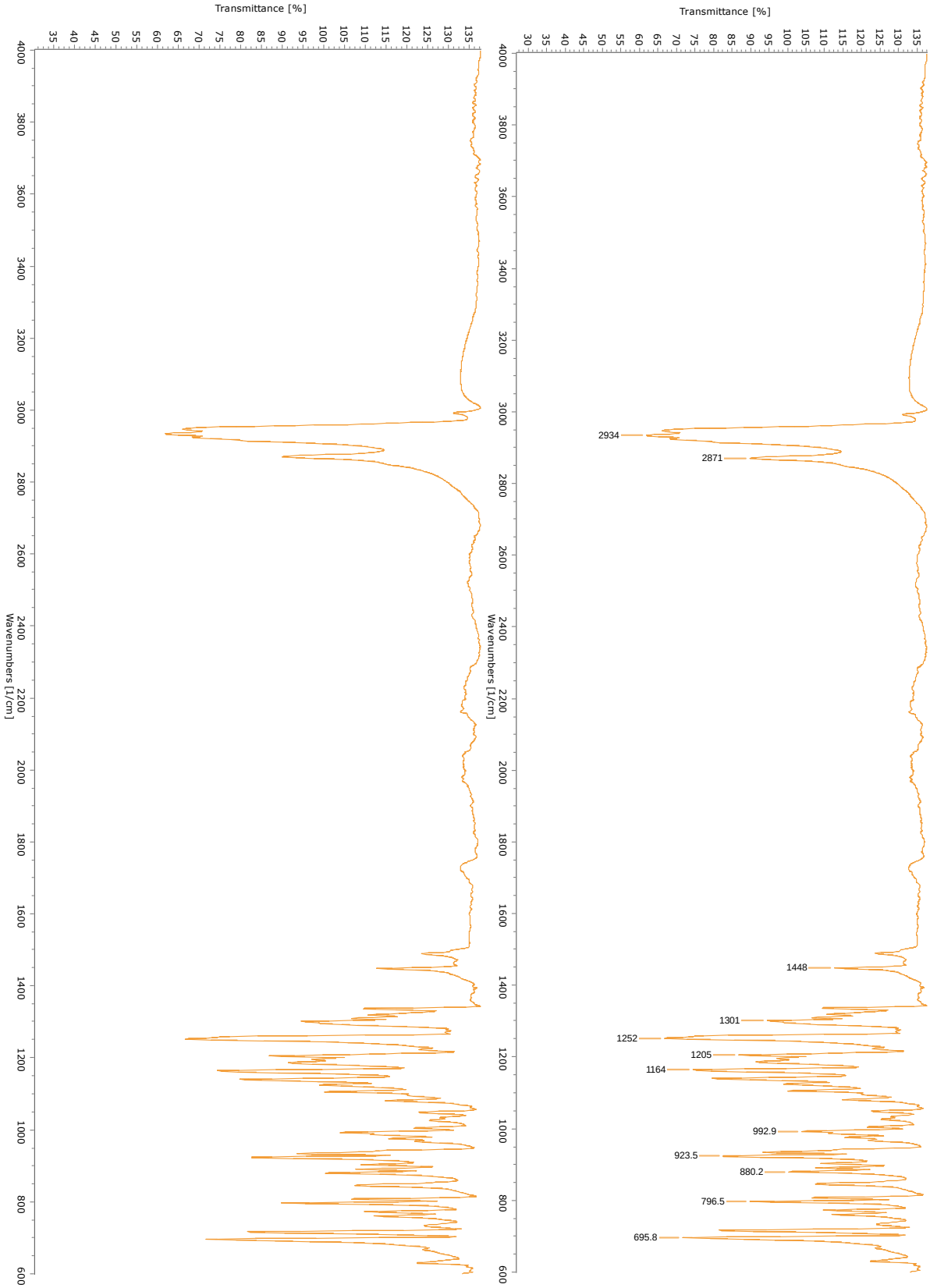
Transmittance [%]
Wavenumbers [1/cm]
2934
2871
1448
1301
1252
1205
1164
992.9
923.5
880.2
796.5
695.8

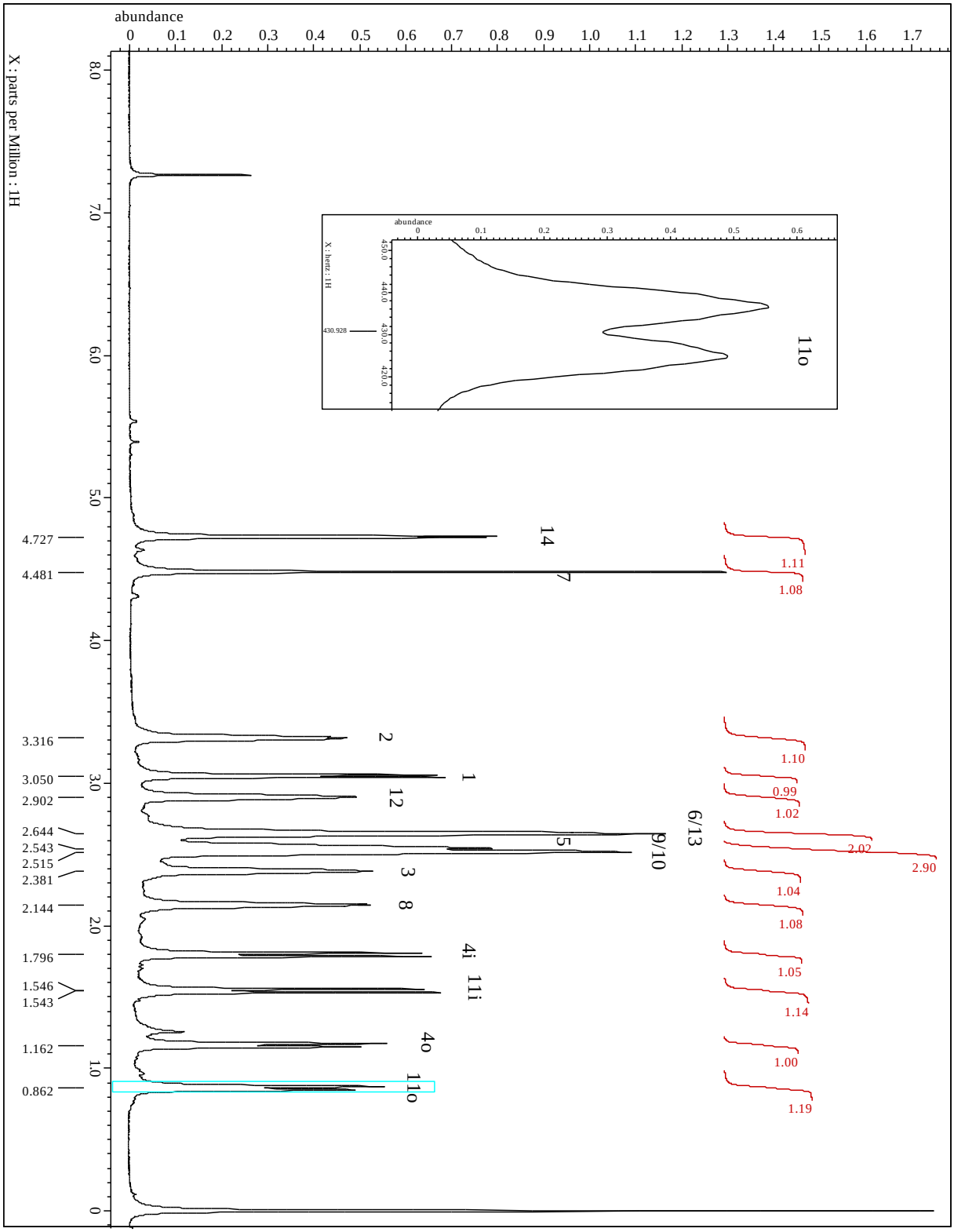
abundance
X : parts per Million : 1H
4.727
4.481
3.316
3.050
2.902
2.644
2.543
2.515
2.381
2.144
1.796
1.546
1.543
1.162
0.862
14
7
2
1
12
5
9/10
6/13
3
8
4i
11i
4o
11o
1.11
1.08
1.10
0.99
1.02
2.02
2.90
1.04
1.08
1.05
1.14
1.00
1.19
abundance
X : hertz : 1H
430.928
11o

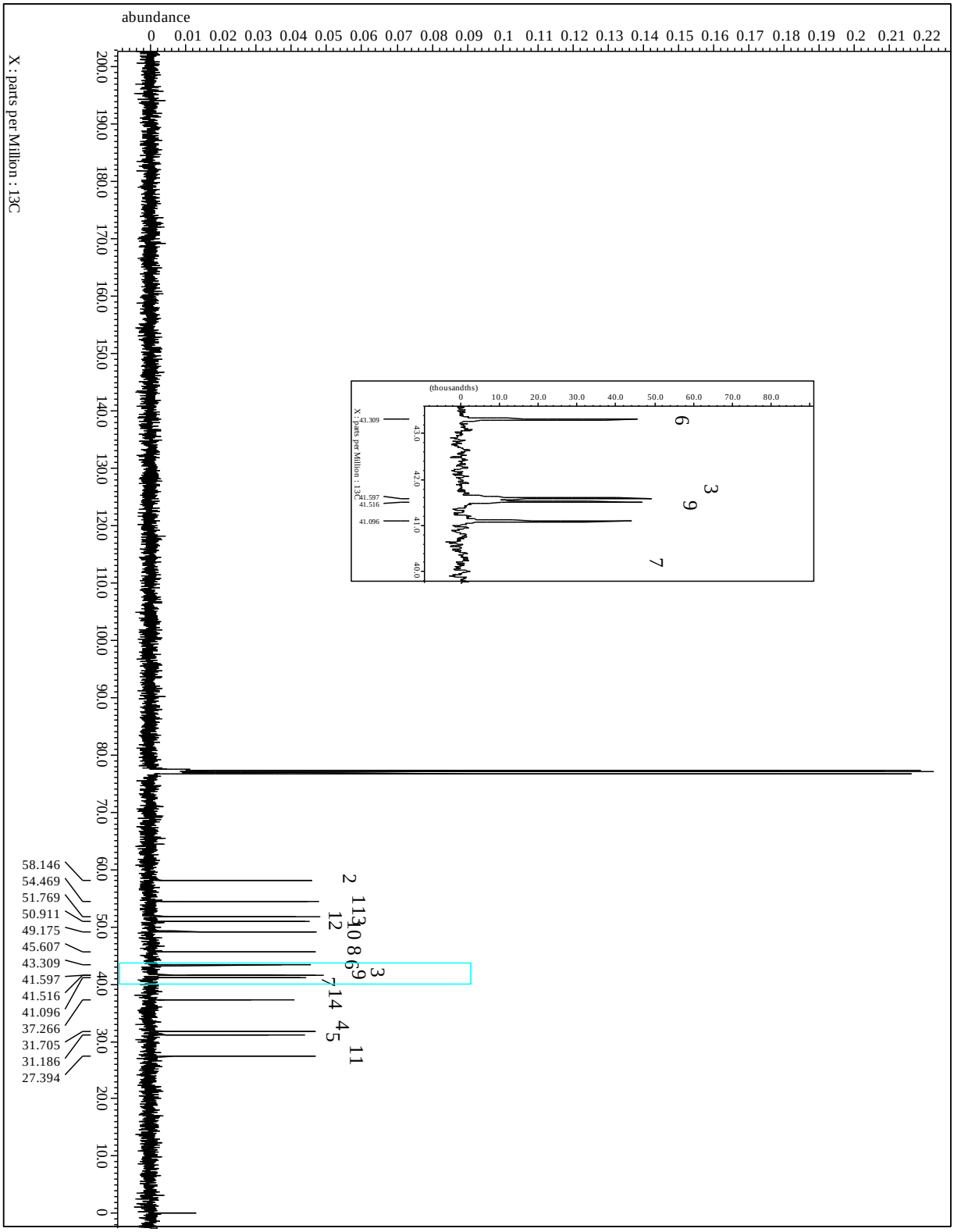
abundance
0 0.01 0.02 0.03 0.04 0.05 0.06 0.07 0.08 0.09 0.1 0.11 0.12 0.13 0.14 0.15 0.16 0.17 0.18 0.19 0.2 0.21 0.22
X : parts per Million : 13C
200.0 190.0 180.0 170.0 160.0 150.0 140.0 130.0 120.0 110.0 100.0 90.0 80.0 70.0 60.0 50.0 40.0 30.0 20.0 10.0 0
(thousandths)
0 10.0 20.0 30.0 40.0 50.0 60.0 70.0 80.0
43.309
41.597
41.516
41.096
58.146
54.469
51.769
50.911
49.175
45.607
43.309
41.597
41.516
41.096
37.266
31.705
31.186
27.394
2 11 13 10 12 8 6 9 3 7 14 4 5 11

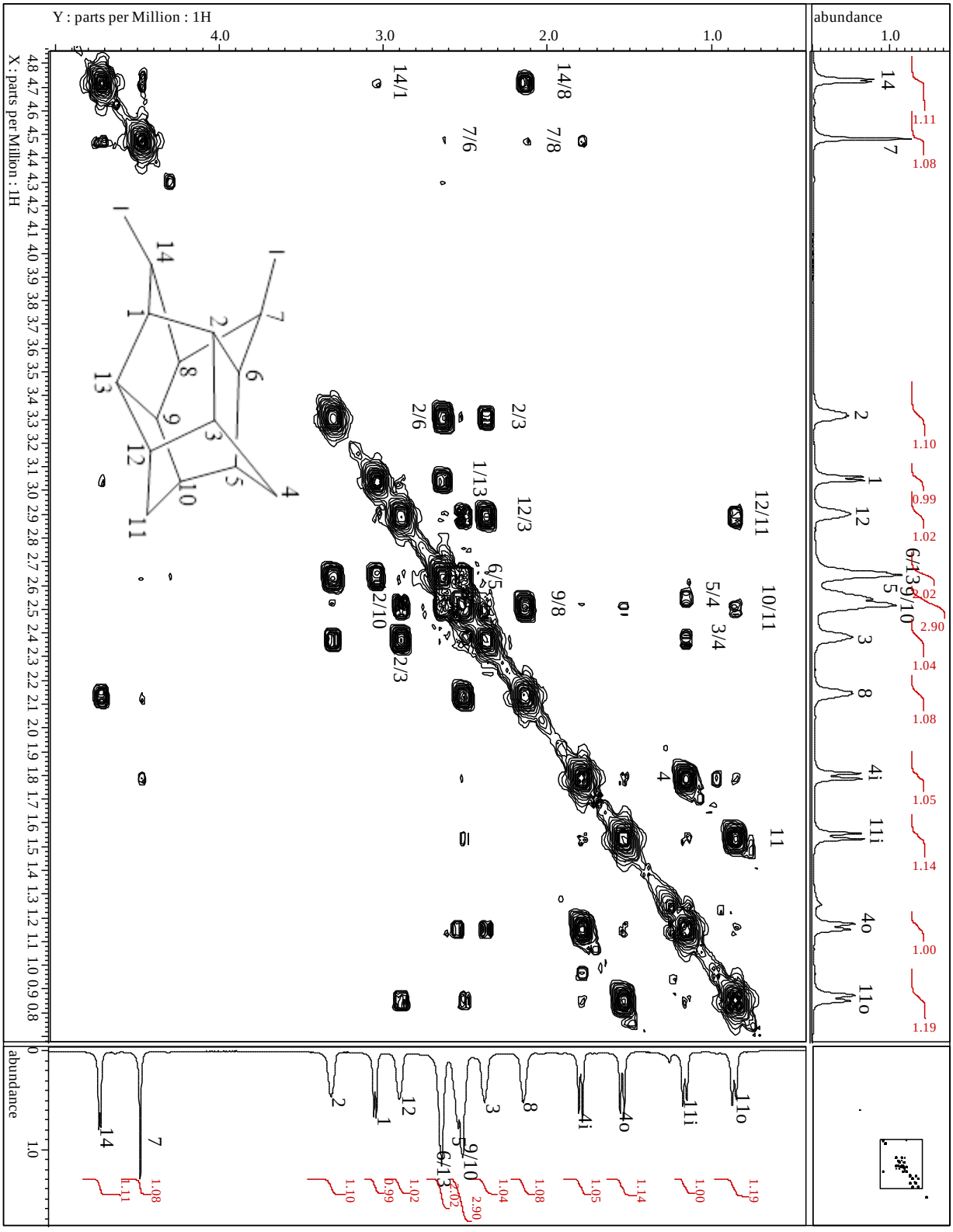
Y : parts per Million : 1H
X : parts per Million : 1H
abundance
abundance
14/8
7/8
7/6
14/1
2/3
2/6
12/11
10/11
12/3
9/8
1/13
6/5
2/10
2/3
5/4
3/4
11
11o
11i
4o
4i
8
3
9/10
6/13
5
12
1
2
14
7
1.19
1.00
1.14
1.05
1.08
1.04
2.90
1.02
6.99
1.10
1.08
1.11

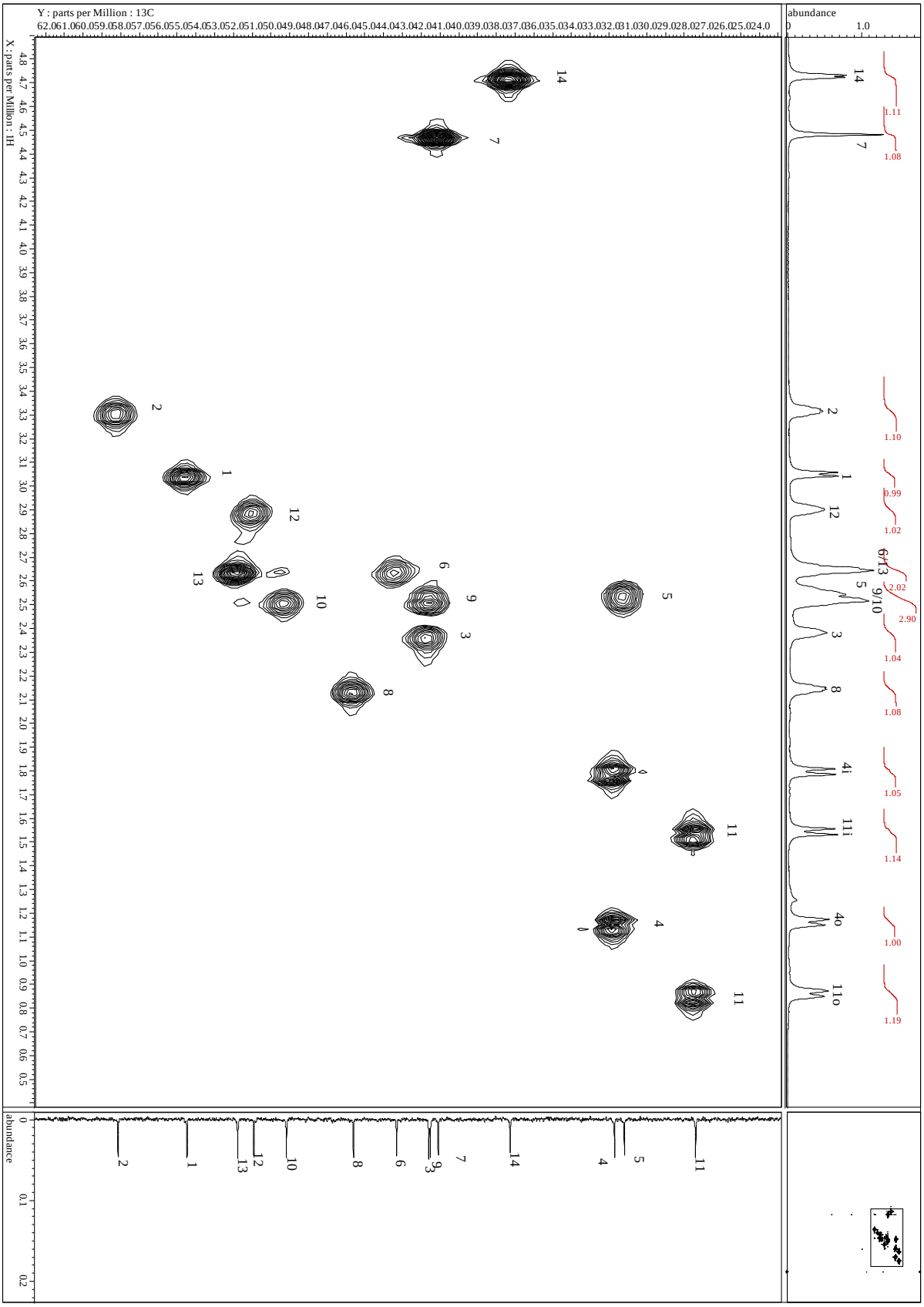
Y : parts per Million : 13C
X : parts per Million : 1H
abundance
1.11
1.08
1.10
0.99
1.02
2.02
2.90
1.04
1.08
1.05
1.14
1.00
1.19

Heptacyclo[6.6.0.0^{2,14}.0^{3,7}.0^{4,12}.0^{6,10}.0^{9,13}]tetradecane (151)

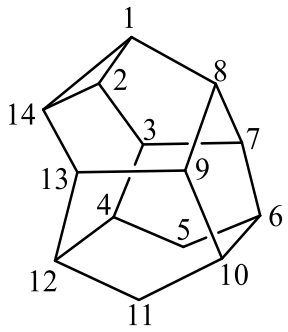

$C_{14}H_{16}$ (184)

^{1}H-NMR ($CDCl_3$, 500 MHz): δ = 3.06 (m, 2H, H-7, -9), 2.45-2.40 (m, 3H, H-3, -13; H-8), 2.17 (s_{app}, 2H, H-6, -10), 1.99 (m, 1H, H-1), 1.85 (s_{app}2H, H-4, -12), 1.76 (d, 2H, H-5i, -11i), 1.28 (m. 2H, H-2, -14), 0.90 (d, 2H, H-5o, -11o) ppm;

$^{2}J_{\text{H-5i, -5o}} = {}^{2}J_{\text{H-11i, -11o}} = 11.3$ Hz.

^{13}C-NMR ($CDCl_3$, 100.7 MHz): δ = 65.8 (C-7, -9), 49.5 (C-8), 44.8 (C-3, -13), 43.7 (C-6, -13), 37.2 (C-1), 32.3 (C-5, -11), 31.6 (C-4, -12), 23.6 (C-2, -14) ppm.

^{1}H-NMR (C_6D_6, 500 MHz): δ = 3.05 (m, 2H, H-7, -9), 2.44-2.38 (m, 3H, H-3, -13; H-8), 2.12 (s_{app}, 2H, H-6, -10), 2.02 (m, 1H, H-1), 1.84 (s_{app}2H, H-4, -12), 1.71 (d, 2H, H-5i, -11i), 1.27 (m. 2H, H-2, -14), 0.85 (d, 2H, H-5o, -11o) ppm;

$^{2}J_{\text{H-5i, -5o}} = {}^{2}J_{\text{H-11i, -11o}} = 11.5$ Hz.

^{13}C-NMR (C_6D_6, 100.7 MHz): δ = 66.1 (C-7, -9), 50.0 (C-8), 45.2 (C-3, -13), 44.0 (C-6, -10), 33.7 (C-1), 32.6 (C-5, -11), 32.0 (C-4, -12), 24.0 (C-2, -14) ppm.

MS (EI, 70 eV): *m/z* (%) = 185 (14.9) [$M^{\cdot+}$+1], 184 (100.0) [$M^{\cdot+}$], 169 (16.8), 156 (11.2), 155 (17.1), 143 (18.0), 142 (24.3), 141 (19.8), 130 (22.5), 129 (28.9), 128 (26.8), 127 (7.6), 119 (10.3),

118 (54.6), 117 (73.7), 116 (22.4), 115 (36.0), 106 (43.7), 105 (36.5), 104 (31.2), 103 (16.4), 93 (23.1), 92 (29.7), 91 (74.7), 80 (27.8), 79 (42.0), 78 (37.3), 77 (39.6), 65 (15.6), 63 (7.8), 51 (11.2).

Spectra:

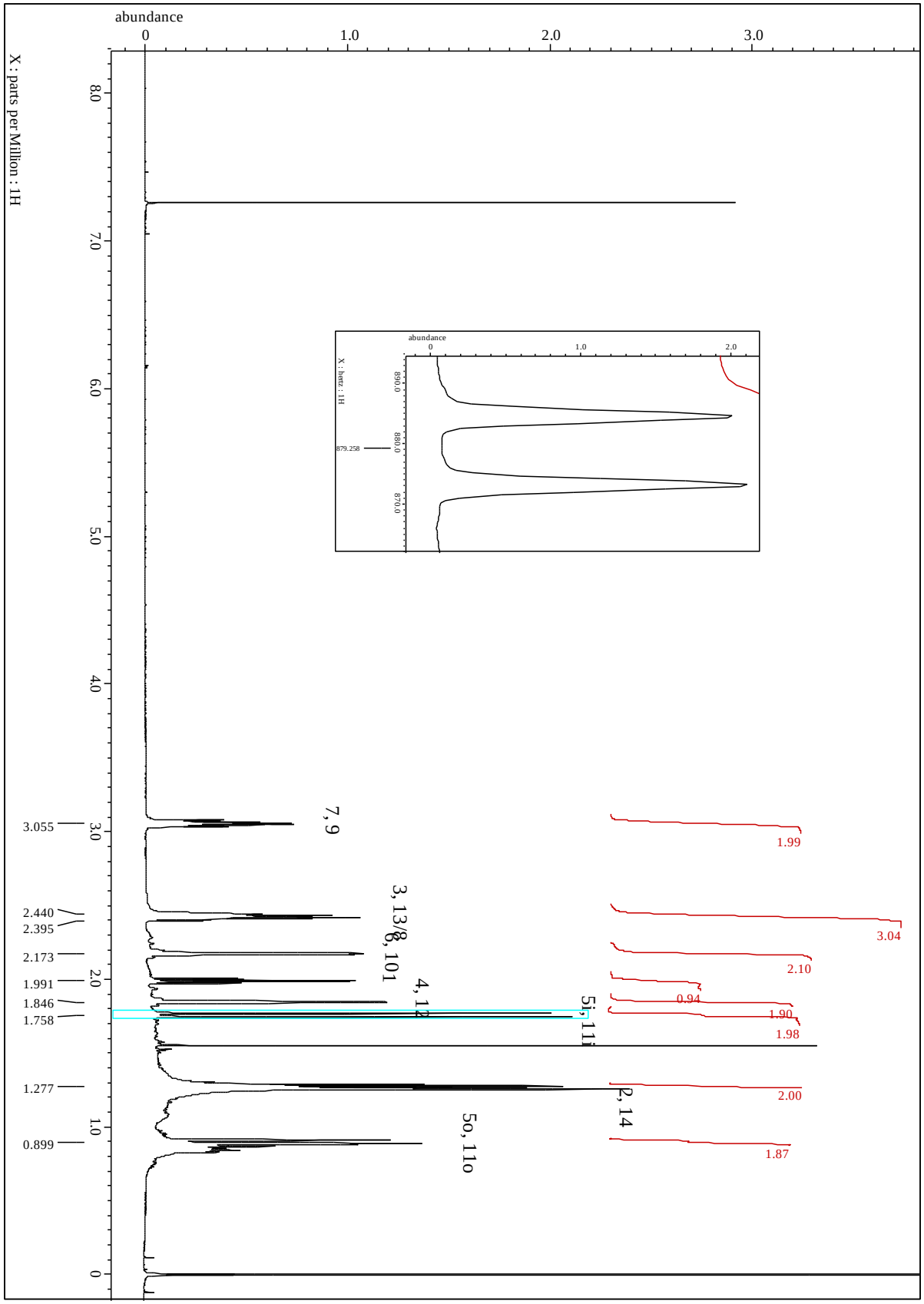
abundance
X : parts per Million : 1H
3.055
2.440
2.395
2.173
1.991
1.846
1.758
1.277
0.899
7, 9
3, 13/8, 101
4, 12
5i, 11i
5o, 11o
2, 14
1.99
3.04
2.10
0.94
1.90
1.98
2.00
1.87
X : hertz : 1H
879.258

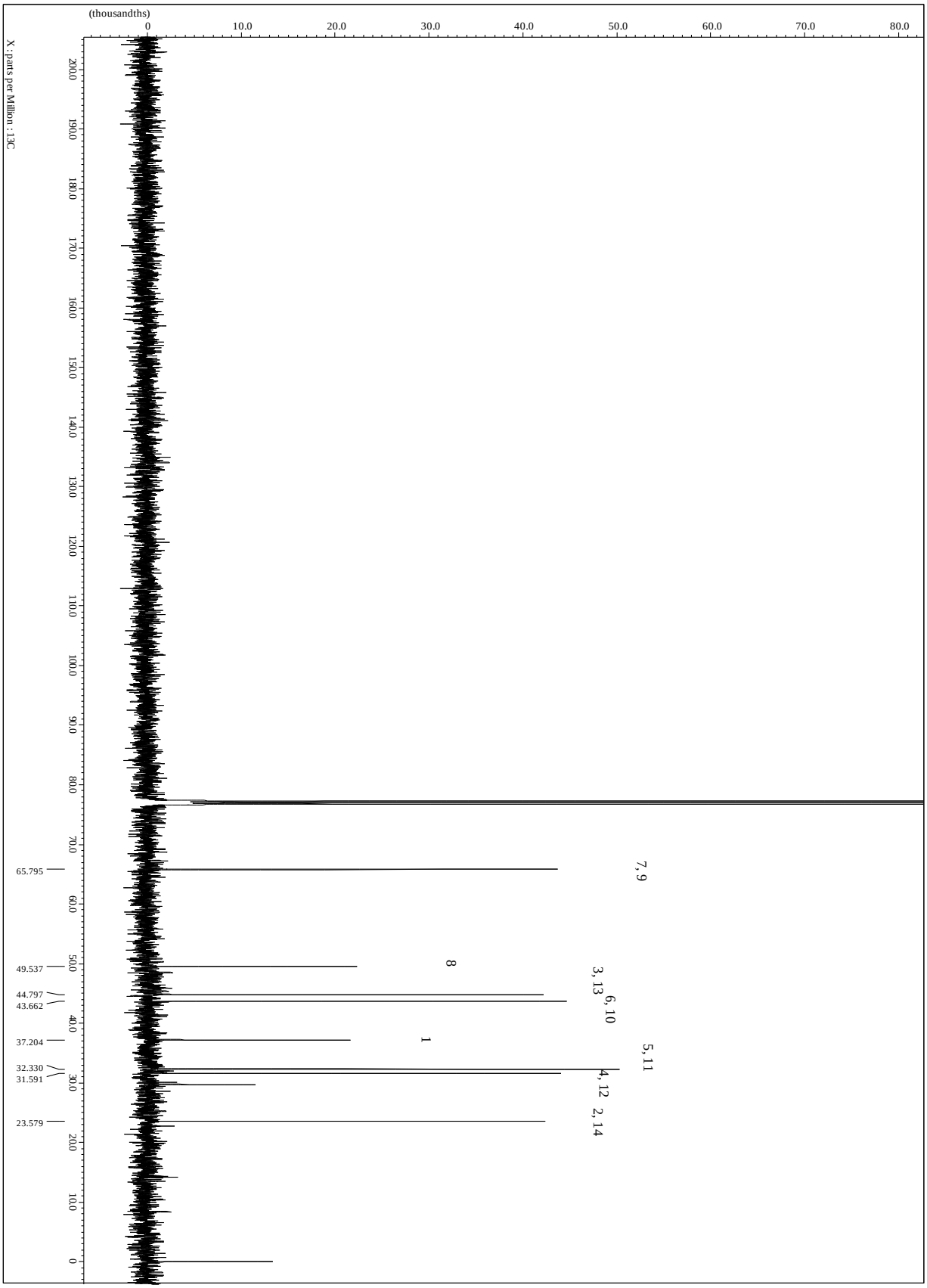
(thousandths)
0
10.0
20.0
30.0
40.0
50.0
60.0
70.0
80.0
X : parts per Million : 13C
200.0
190.0
180.0
170.0
160.0
150.0
140.0
130.0
120.0
110.0
100.0
90.0
80.0
70.0
60.0
50.0
40.0
30.0
20.0
10.0
0
65.795
49.537
44.797
43.662
37.204
32.330
31.591
23.579
7, 9
8
3, 13
6, 10
1
5, 11
4, 12
2, 14

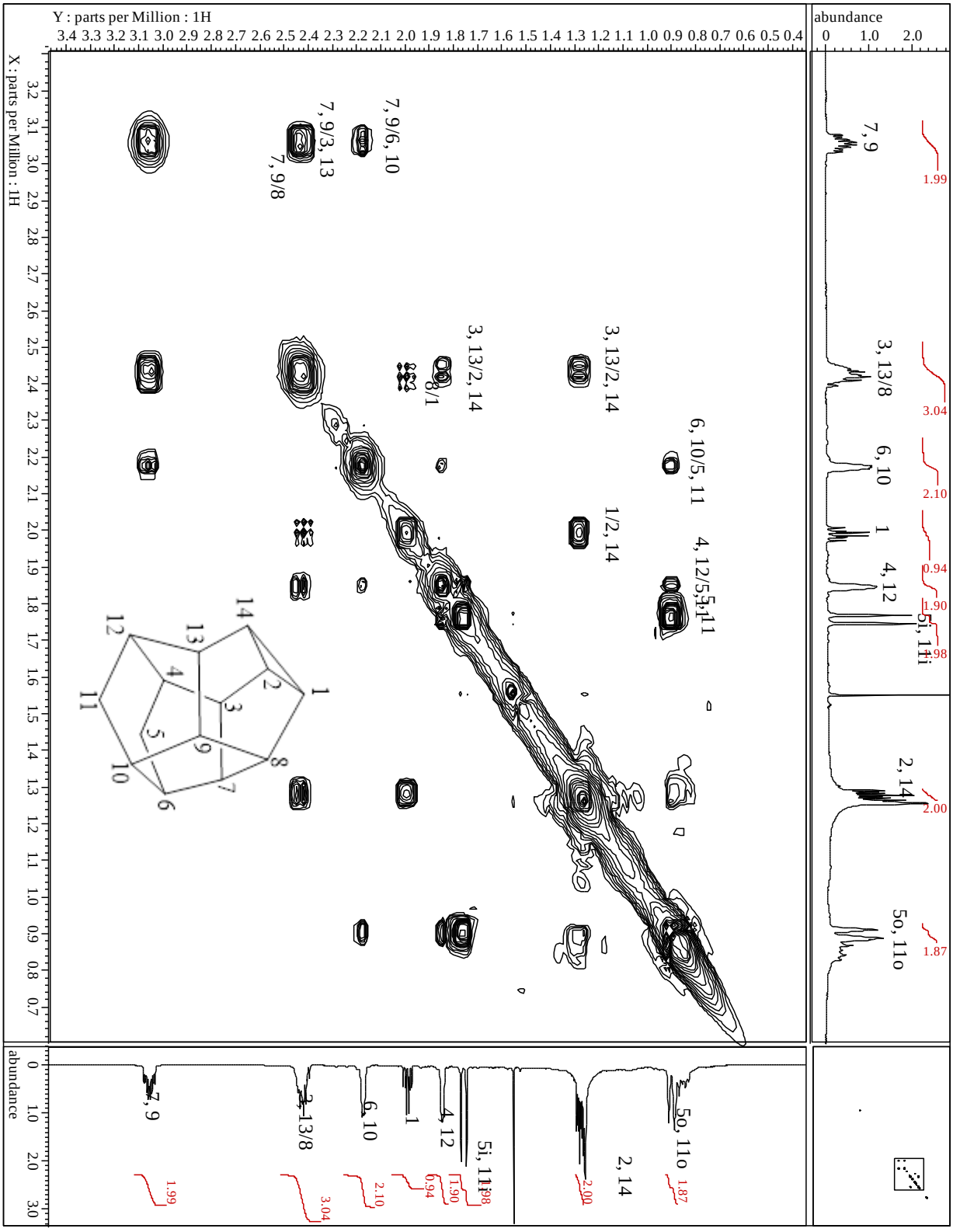
Y : parts per Million : 1H
X : parts per Million : 1H
abundance
7, 9
3, 13/8
6, 10
1
4, 12
5i, 11i
2, 14
5o, 11o
1.99
3.04
2.10
0.94
1.90
1.98
2.00
1.87
7, 9/8
7, 9/3, 13
7, 9/6, 10
3, 13/2, 14
8/1
1/2, 14
6, 10/5, 11
4, 12/5, 11
1
2
3
4
5
6
7
8
9
10
11
12
13
14

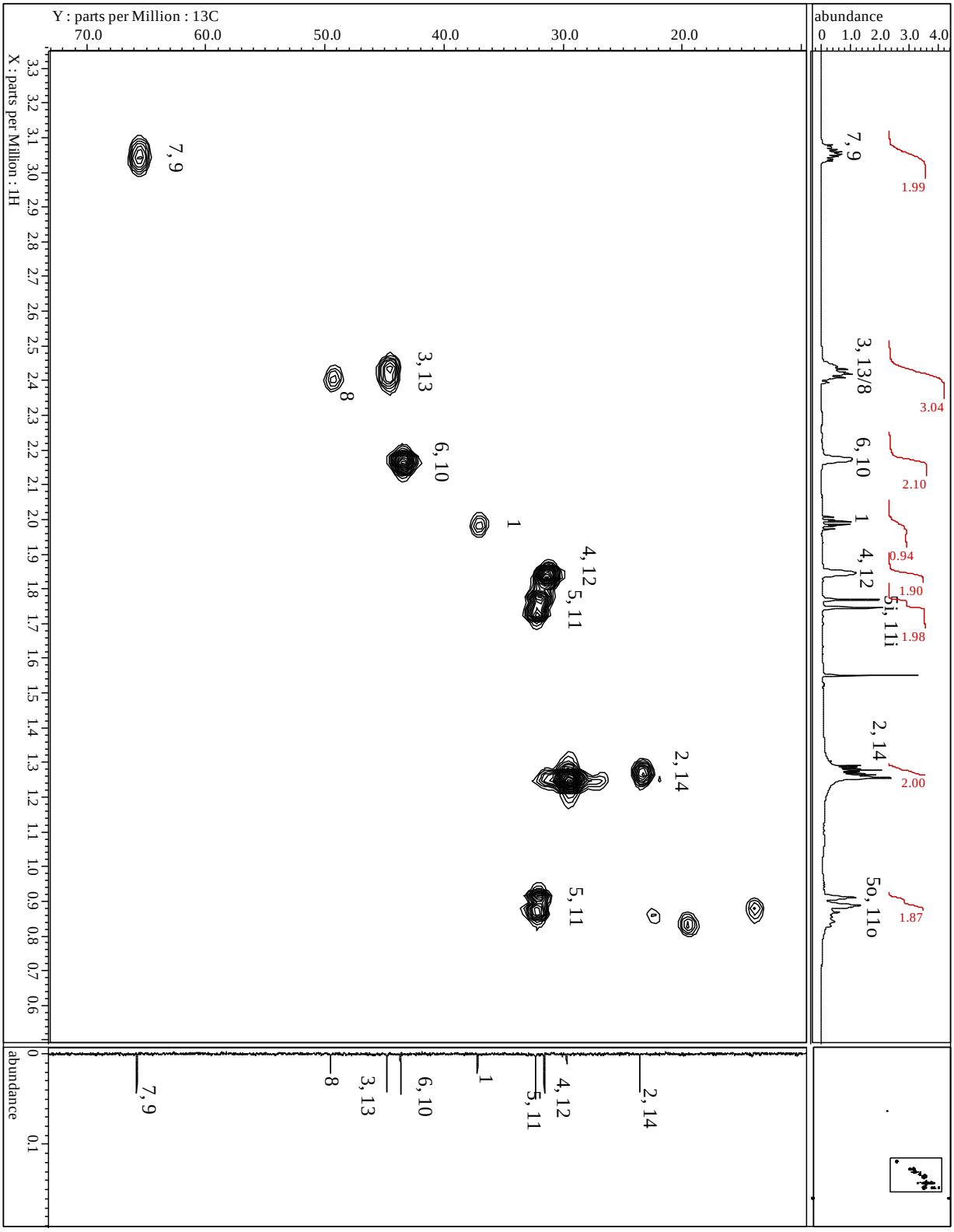
abundance
0 1.0 2.0 3.0 4.0
7, 9
1.99
3, 13/8
3.04
6, 10
2.10
1
0.94
4, 12
1.90
5i, 11i
1.98
2, 14
2.00
5o, 11o
1.87
Y : parts per Million : 13C
70.0 60.0 50.0 40.0 30.0 20.0
X : parts per Million : 1H
3.3 3.2 3.1 3.0 2.9 2.8 2.7 2.6 2.5 2.4 2.3 2.2 2.1 2.0 1.9 1.8 1.7 1.6 1.5 1.4 1.3 1.2 1.1 1.0 0.9 0.8 0.7 0.6
7, 9
3, 13
8
6, 10
1
4, 12
5, 11
2, 14
5, 11
abundance
0 0.1
2, 14
4, 12
5, 11
1
6, 10
3, 13
8
7, 9

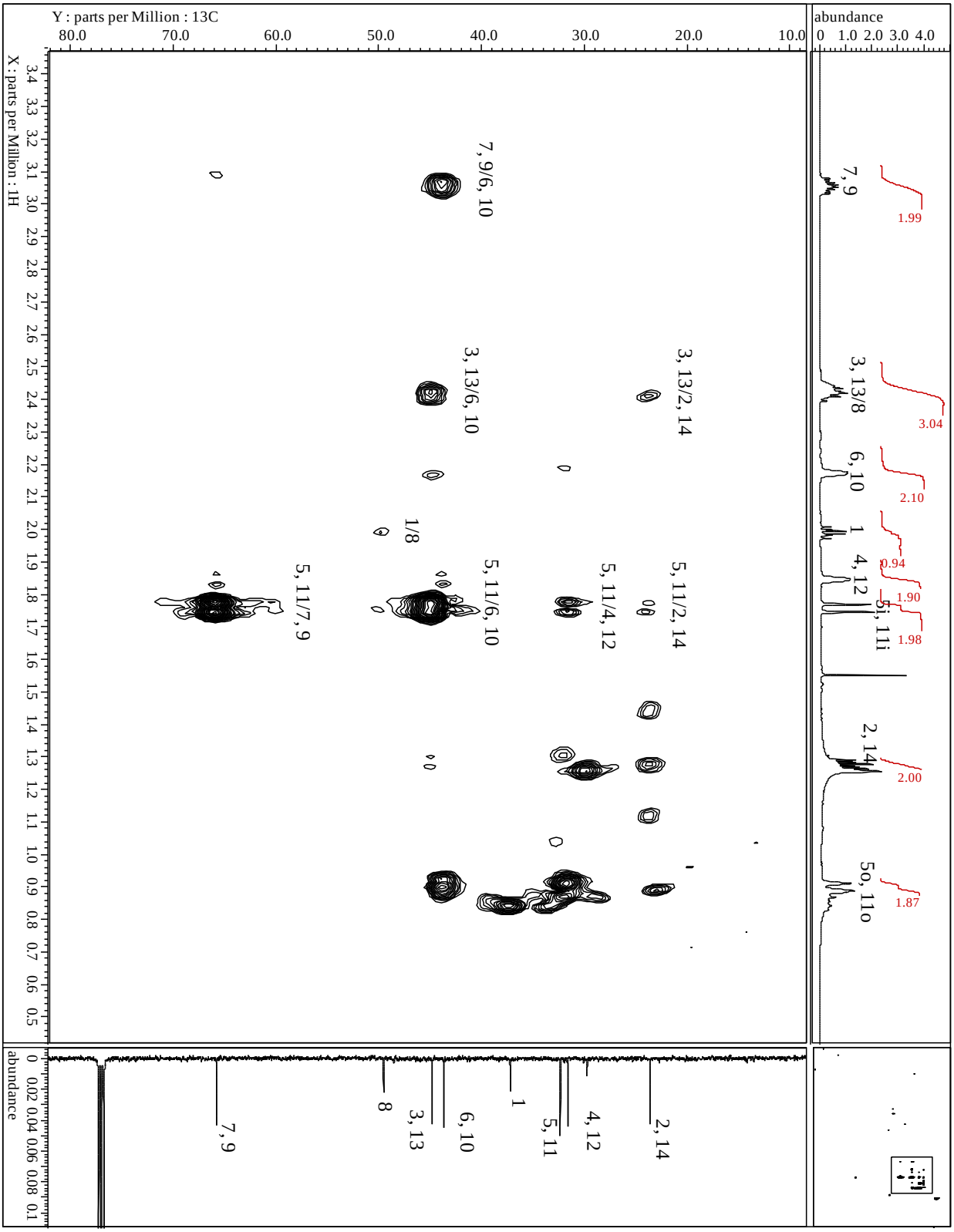
abundance
0 1.0 2.0 3.0 4.0
7, 9
1.99
3, 13/8
3.04
6, 10
2.10
1
0.94
4, 12
1.90
5i, 11i
1.98
2, 14
2.00
5o, 11o
1.87
Y : parts per Million : 13C
80.0 70.0 60.0 50.0 40.0 30.0 20.0 10.0
X : parts per Million : 1H
3.4 3.3 3.2 3.1 3.0 2.9 2.8 2.7 2.6 2.5 2.4 2.3 2.2 2.1 2.0 1.9 1.8 1.7 1.6 1.5 1.4 1.3 1.2 1.1 1.0 0.9 0.8 0.7 0.6 0.5
7, 9/6, 10
3, 13/6, 10
1/8
5, 11/6, 10
5, 11/7, 9
3, 13/2, 14
5, 11/2, 14
5, 11/4, 12
2, 14
4, 12
5, 11
1
6, 10
3, 13
8
7, 9
abundance
0 0.02 0.04 0.06 0.08 0.1

5.4.6 Rearrangement of Bis-epoxide Cage **95**

*Rearrangement of Bis-epoxide **95**:* To a solution of bis-epoxide **95** (363 mg, 1.68 mmol) in DCM (50 mL), Amberlyst-15 (679 mg, 3.36 mmol, 4.95 mol/kg) was added and stirred for 7 days until all **95** was consumed (based on GC/MS). Additional DCM (20 mL) and Amberlyst-15 (350 mg) was added after 4 days. The suspension was then filtered and washed with DCM (3x25 mL). The filtrate and washings were combined and concentrated to afford a colorless solid (247 mg). Purification by column chromatography (SiO_2, 10:1, 5:1, 2:1 hexanes/EtOAc gradient then 5:5:1 hexanes/DCM/MeOH) gave small amounts of enriched **152**, **153**, and **155**. **154** was not isolated in greater than an 80% enriched mixture with **155** (approximately 3 mg). The majority of the material obtained from the column was comprised of various mixtures of the four compounds.

8,13-Dioxaheptacyclo[8.6.0.0^{2,6}.0^{4,14}.0^{5,12}.0^{7,9}.0^{11,15}]hexadecane (152)

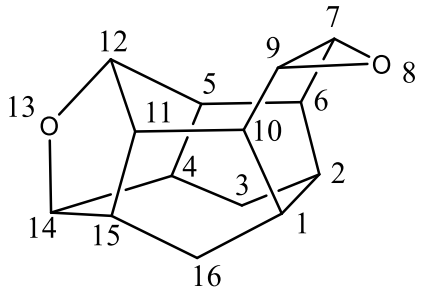

$C_{14}H_{16}O_2$ (216)

MP = 305.7-305.9 °C ($CHCl_3$)

IR (AT-IR): $\tilde{\nu}$ = 2984 (m, C-H), 2950 (s, C-H), 2929 (s, C-H), 2864 (m, C-H), 1448 (w, C-C), 982 (s), 917 (s), 819 (s) cm^{-1}.

^{1}H-NMR ($CDCl_3$, 500 MHz): δ = 4.47 (t, 1H, H-12), 4.28 (t, 1H, H-14), 3.32 (t, 2H, H-7, -9), 2.80 (m, 4H, H-4, -15; H-5, -11), 2.35 (s_{app}, 4H, H-1, -2; H-6, -10), 1.93 (d, 2H, H-3i, -16i), 1.19 (m, 2H, H-3o, -16o) ppm;

$^{2}J_{\text{H-3i, -3o}} = {}^{2}J_{\text{H-16i, -16o}} = 13.9$ Hz.

^{13}C-NMR ($CDCl_3$, 100.7 MHz): δ = 78.7 (C-12), 78.5 (C-14), 52.8 (C-7, -9), 49.3* 49.2* (C-4, 5, 11, 15), 41.2 (C-1, 2), 36.3 (C-6, 10), 27.5 (C-3, -16) ppm.

*: Carbons C-4, -15 and C-5, -11 are indistinguishable based on 2-D HMQC.

MS (EI, 70 eV): *m/z* (%) = 216 (32.9) [$M^{\cdot+}$], 171 (11.0), 170 (14.3), 169 (13.8), 159 (13.0), 157 (11.4), 156 (9.3), 155 (18.6), 154 (10.0), 145 (14.2), 144 (10.3), 143 (13.6), 142 (18.4), 141 (18.5), 133 (14.8), 132 (12.6), 131 (38.3), 130 (37.4), 129 (57.7), 128 (30.5), 121 (10.1), 120 (9.5), 119 (13.2), 118 (20.2), 117 (65.5), 116 (36.1), 115 (35.4), 109 (11.9), 108 (12.6), 107 (21.4), 106 (10.0), 105 (27.5), 104 (18.7), 103 (14.5), 95 (14.8), 94 (15.5), 93 (18.9), 92 (35.3), 91 (100.0), 82 (11.2), 81 (37.7), 80 (16.4), 79 (72.7), 78 (29.3), 77 (67.5), 69 (17.1), 68 (10.5), 67 (19.9), 66 (18.9), 65 (28.1), 63 (8.5), 55 (14.2), 53 (20.6), 52 (8.0), 51 (17.2).

Spectra:

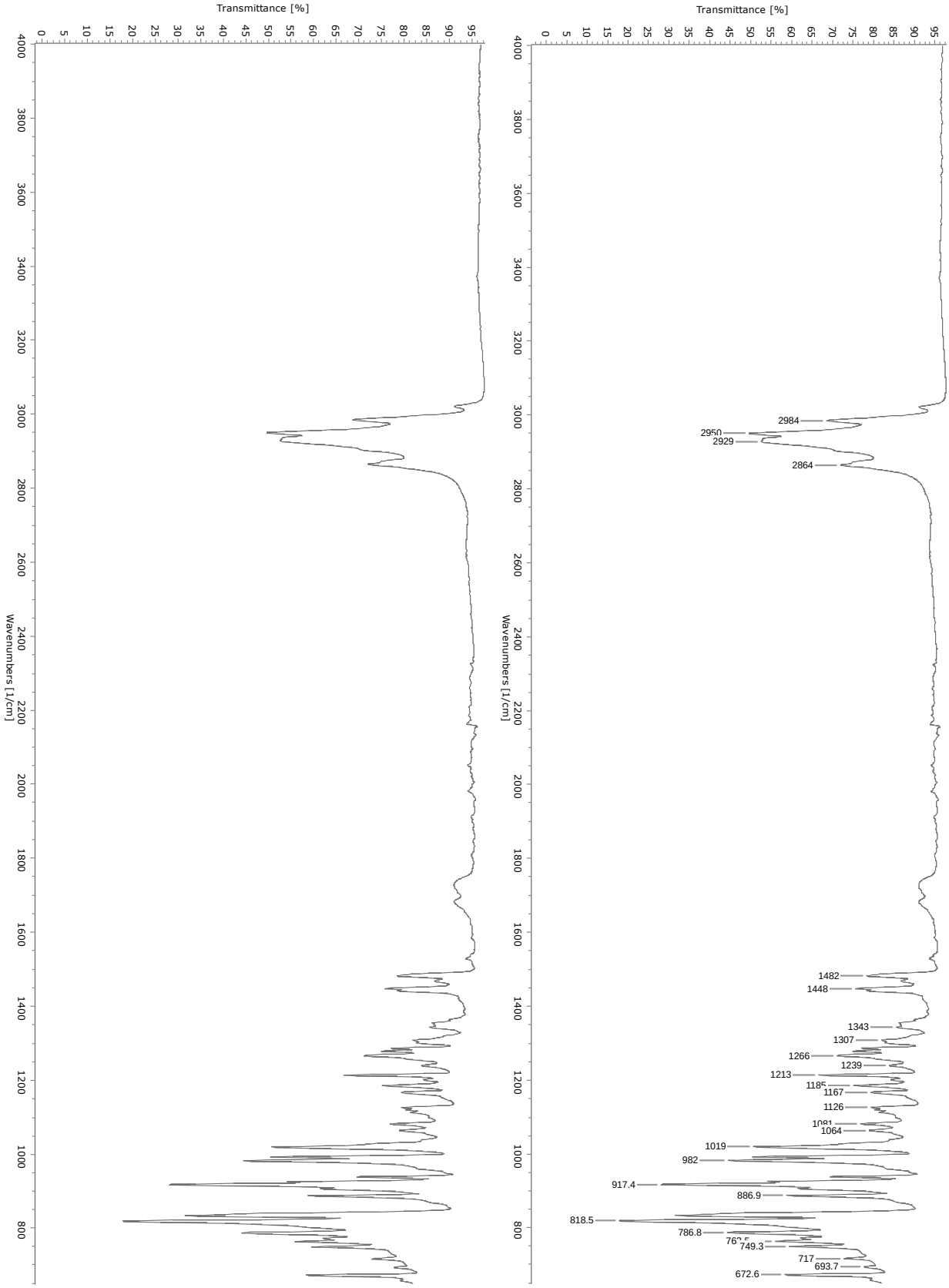
Transmittance [%]
Wavenumbers [1/cm]
2984
2950
2929
2864
1482
1448
1343
1307
1266
1239
1213
1185
1167
1126
1081
1064
1019
982
917.4
886.9
818.5
786.8
749.3
717
693.7
672.6

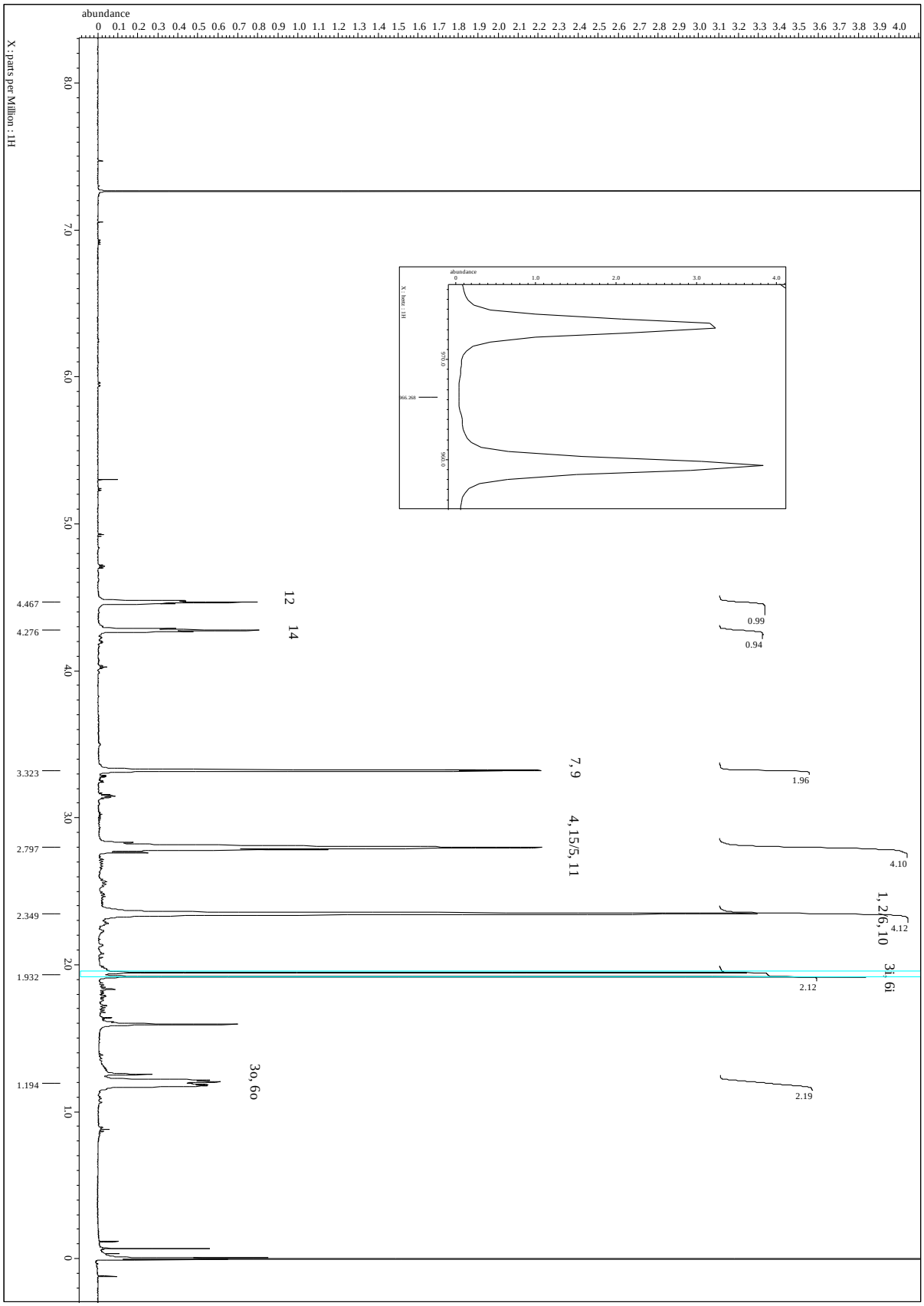
abundance
X : parts per Million : 1H
4.467
4.276
3.323
2.797
2.349
1.932
1.194
12
14
7, 9
4, 15/5, 11
1, 2/6, 10
3i, 6i
3o, 6o
0.99
0.94
1.96
4.10
4.12
2.12
2.19

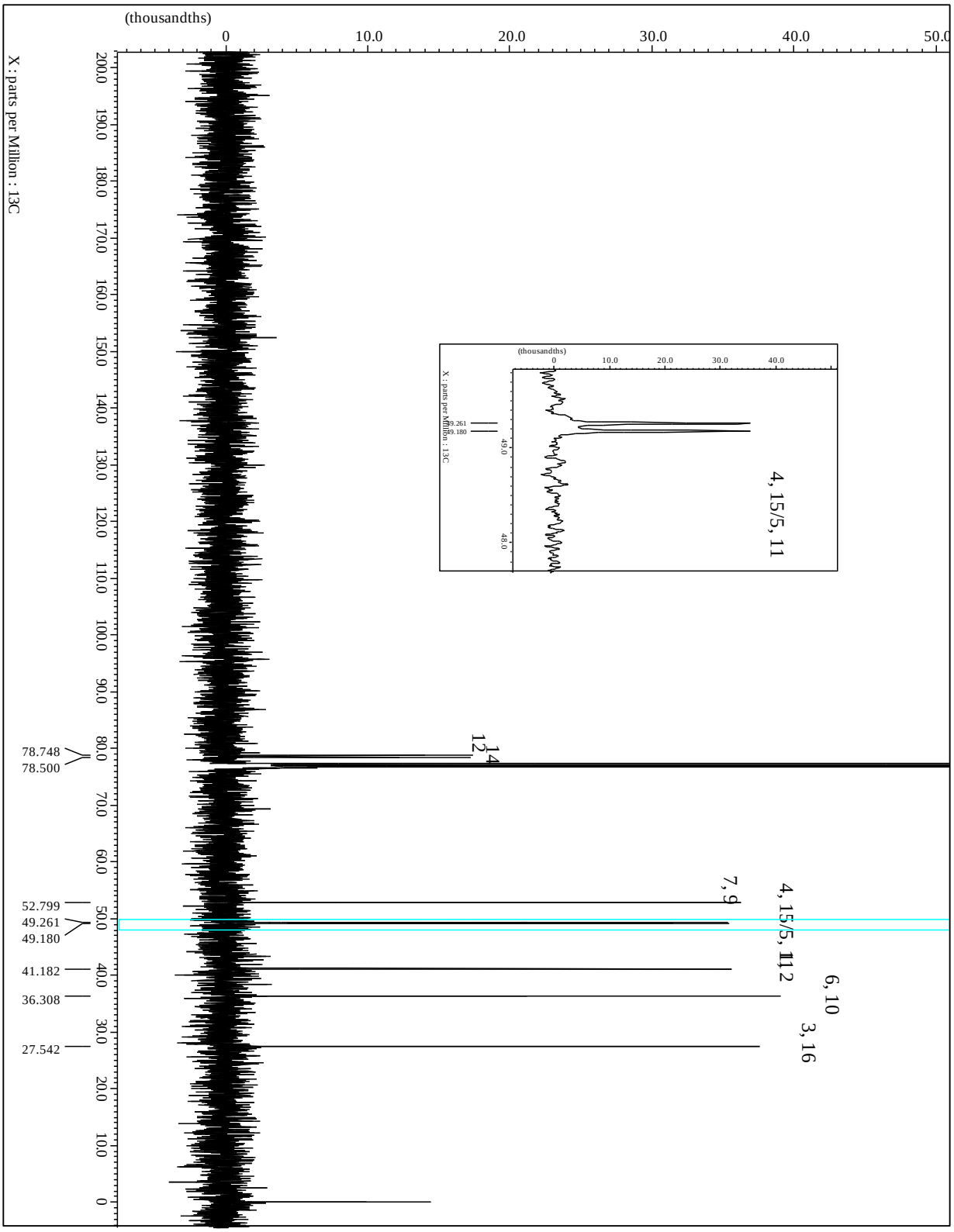
(thousandths)
0
10.0
20.0
30.0
40.0
50.0
X : parts per Million : 13C
200.0
190.0
180.0
170.0
160.0
150.0
140.0
130.0
120.0
110.0
100.0
90.0
80.0
70.0
60.0
50.0
40.0
30.0
20.0
10.0
0
78.748
78.500
52.799
49.261
49.180
41.182
36.308
27.542
12, 14
7, 9
4, 15/5, 11
2
6, 10
3, 16
(thousandths)
0
10.0
20.0
30.0
40.0
X : parts per Million : 13C
49.261
49.180
49.0
48.0
4, 15/5, 11

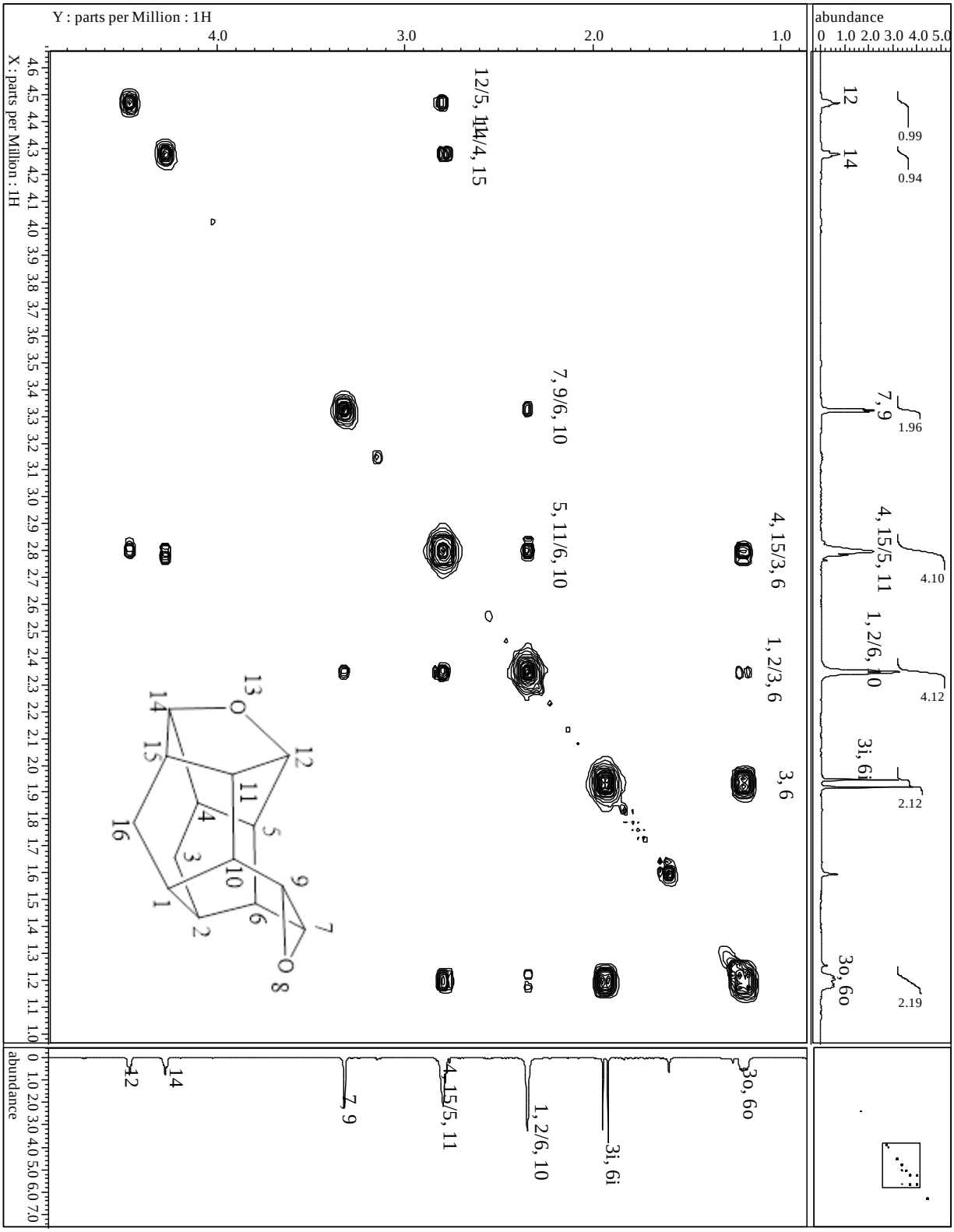
abundance
0 1.0 2.0 3.0 4.0 5.0
12
14
0.99
0.94
7, 9
1.96
4, 15/5, 11
4.10
1, 2/6, 10
4.12
3i, 6i
2.12
3o, 6o
2.19
Y : parts per Million : 1H
4.0
3.0
2.0
1.0
12/5, 11
14/4, 15
7, 9/6, 10
5, 11/6, 10
4, 15/3, 6
1, 2/3, 6
3, 6
X : parts per Million : 1H
4.6 4.5 4.4 4.3 4.2 4.1 4.0 3.9 3.8 3.7 3.6 3.5 3.4 3.3 3.2 3.1 3.0 2.9 2.8 2.7 2.6 2.5 2.4 2.3 2.2 2.1 2.0 1.9 1.8 1.7 1.6 1.5 1.4 1.3 1.2 1.1 1.0
13
14
15
16
12
11
4
3
5
10
1
2
6
9
7
8
O
O
3o, 6o
3i, 6i
1, 2/6, 10
4, 15/5, 11
7, 9
14
12
abundance
0 1.0 2.0 3.0 4.0 5.0 6.0 7.0

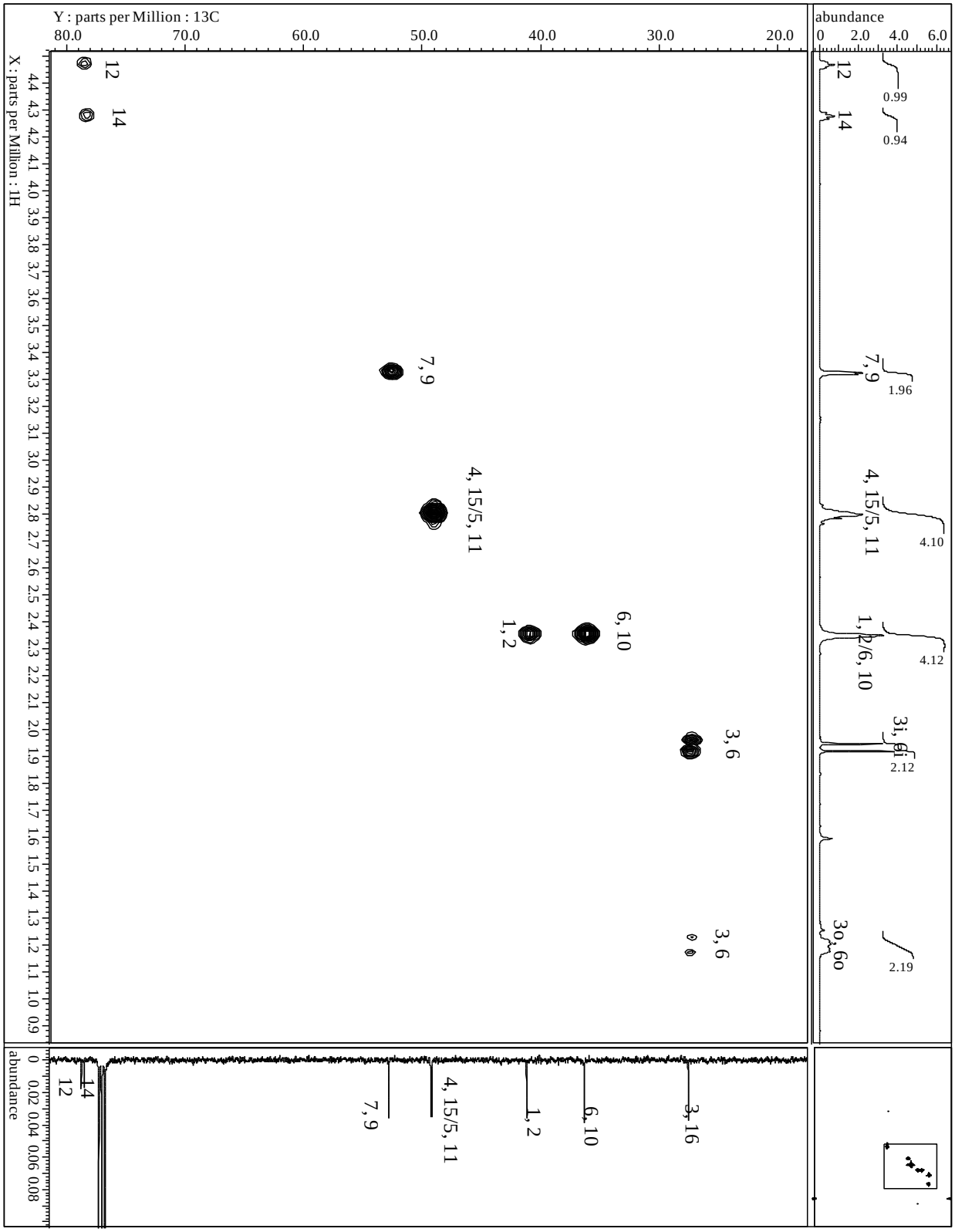
Y : parts per Million : 13C
X : parts per Million : 1H
abundance
0.99
0.94
1.96
4.10
4.12
2.12
2.19
12
14
7, 9
4, 15/5, 11
1, 2/6, 10
3i, 6i
3o, 6o
3, 6
6, 10
1, 2
4, 15/5, 11
7, 9
12
14
3, 16
6, 10
1, 2
4, 15/5, 11
7, 9
12
14
abundance

5,16-Dioxaheptacyclo[8.5.1.$0^{2,9}$.$0^{3,7}$.$0^{4,14}$.$0^{6,13}$.$0^{11,15}$]hexadecane (153)

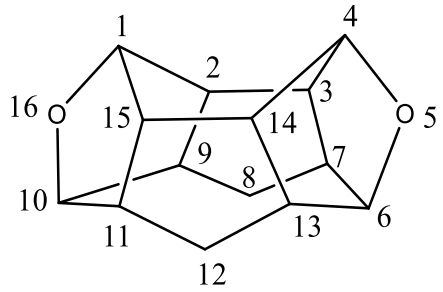

$C_{14}H_{16}O_2$ (216)

^{1}H-NMR ($CDCl_3$, 500 MHz): δ = 4.29 (s_{app}, 2H, H-1, -4), 4.21 (t, 2H, H-6, -10), 3.20 (d_{app}, 4H, H-7, -9, -11, -13), 2.81 (d_{app}, 4H, H-2, -3, -14, -15), 2.15 (d, 2H, H-8i, 12i), 1.75 (q, 2H, H-8o, 12o) ppm;

$^2J_{\text{H-8i, -8o}} = {}^2J_{\text{H-12i, -12o,}} = 15.5$; $^3J_{\text{H-8, -12,H-7, -9, -11, -13}} = 12.6$ Hz.

^{13}C-NMR ($CDCl_3$, 100.7 MHz): δ = 80.4 (C-6, -10), 77.9 (C-1, -4), 55.9 (C-7, -9, -11, -13), 44.26 (C-2, 3, -14, -15), 21.8 (C-8, -12) ppm.

MS (EI, 70 eV): *m/z* (%) = 216 (34.3) [$M^{\cdot+}$], 198 (9.9), 188 (12.3), 180 (21.7), 170 (17.2), 169 (23.7), 167 (15.9), 160 (9.0), 159 (21.9), 157 (15.9), 155 (20.0), 154 (26.0), 145 (12.2), 144 (9.4), 143 (17.0), 142 (45.8), 141 (20.7), 133 (11.0), 132 (10.2), 131 (35.7), 130 (20.1), 129 (60.7), 128 (37.7), 121 (9.1), 119 (10.5), 118 (18.7), 117 (68.7), 116 (70.6), 115 (40.4), 109 (23.3), 108 (11.6), 107 (11.6), 105 (20.2), 104 (14.4), 103 (13.3), 95 (12.6), 94 (12.3), 93 (18.4), 92 (31.0), 91 (100.0), 83 (7.9), 82 (11.7), 81 (31.3), 80 (18.3), 79 (69.2), 78 (25.4), 77 (64.5), 69 (13.2), 68 (8.9), 67 (19.8), 66 (22.9), 65 (28.4), 63 (8.4), 57 (8.2), 55 (15.1), 53 (19.8), 52 (8.2), 51 (17.7).

Spectra:

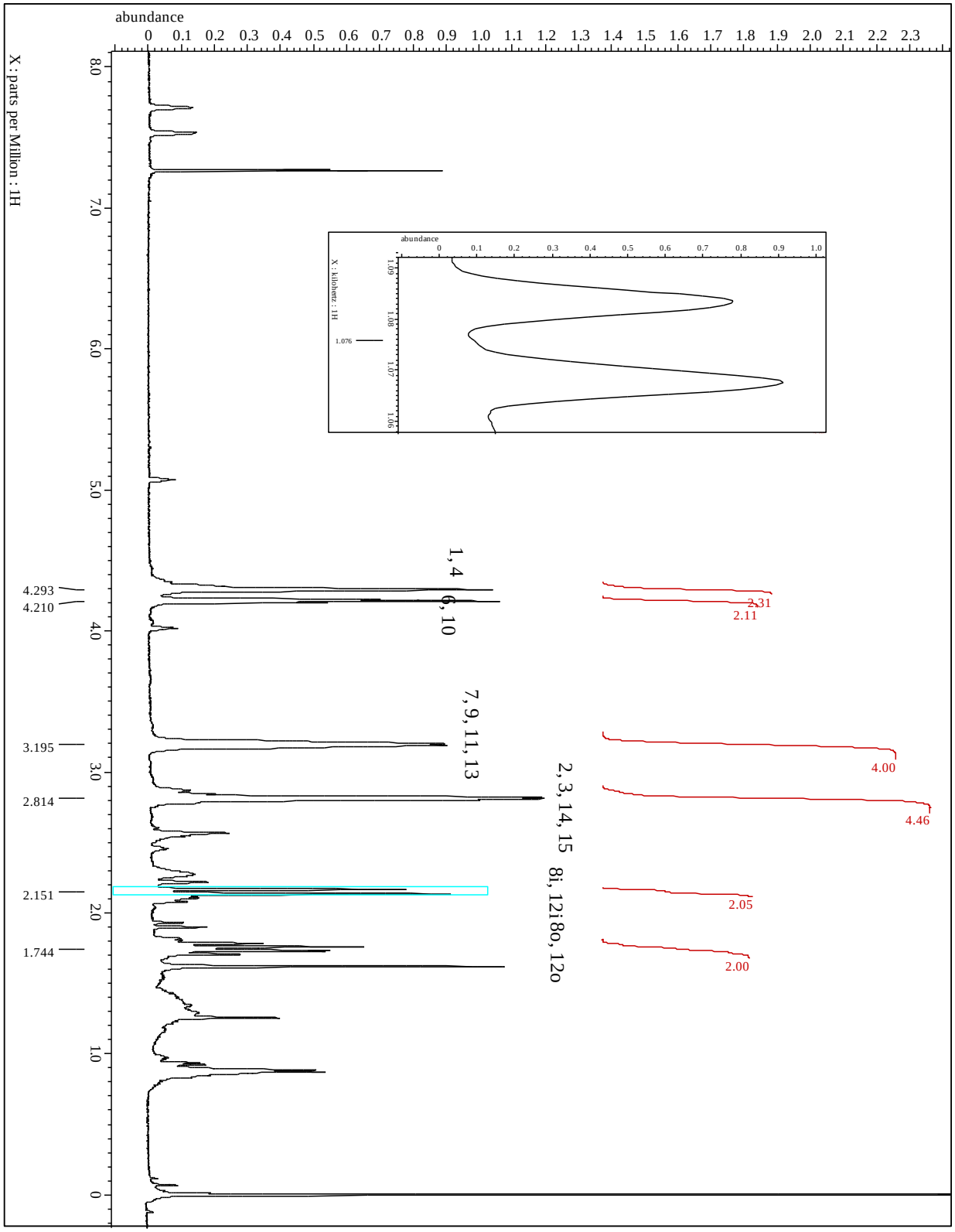
abundance
X : parts per Million : 1H
4.293
4.210
3.195
2.814
2.151
1.744
1, 4
6, 10
7, 9, 11, 13
2, 3, 14, 15
8i, 12i
8o, 12o
2.31
2.11
4.00
4.46
2.05
2.00
X : kilohertz : 1H
1.076

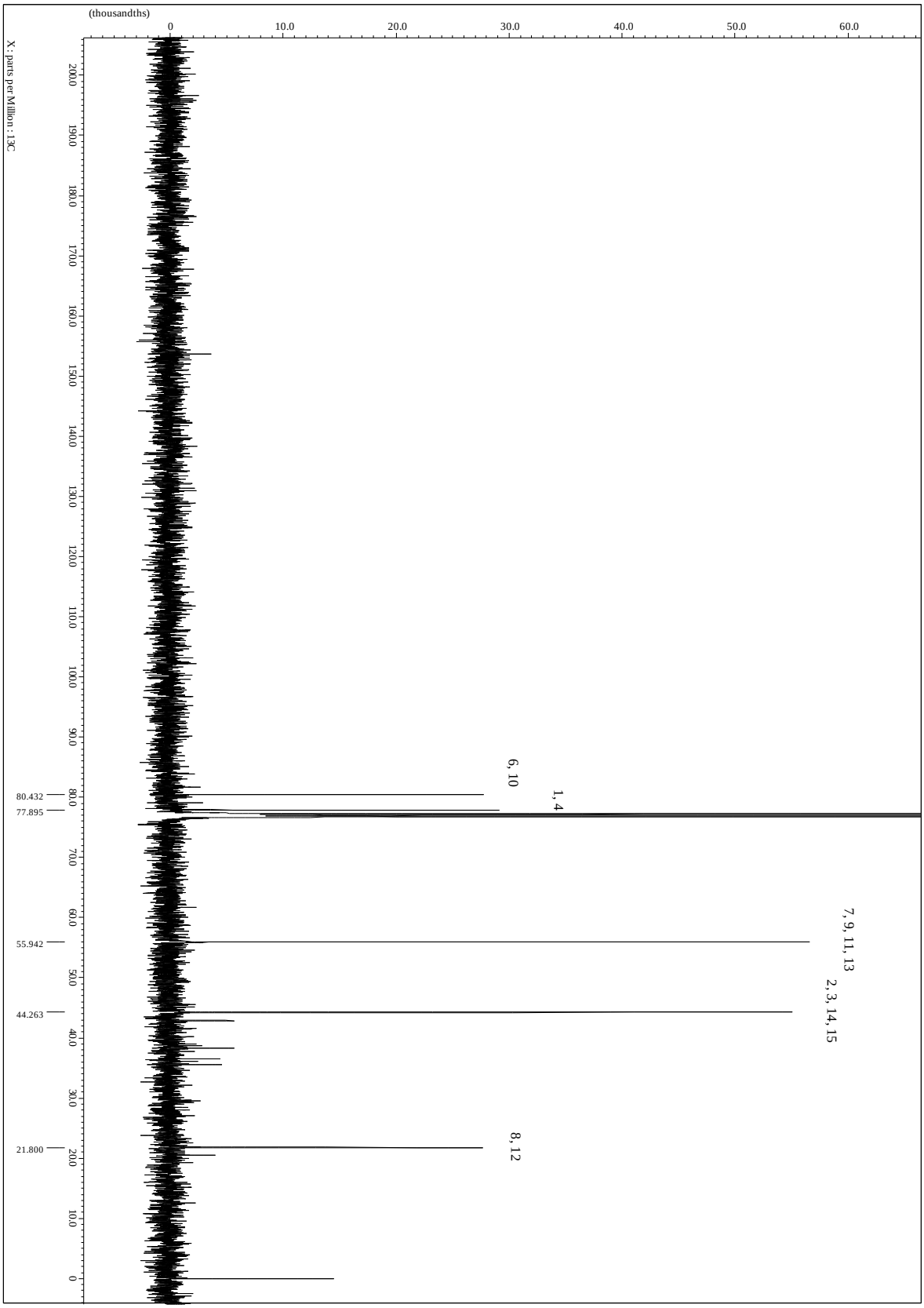
(thousandths)
0
10.0
20.0
30.0
40.0
50.0
60.0
X : parts per Million : 13C
200.0
190.0
180.0
170.0
160.0
150.0
140.0
130.0
120.0
110.0
100.0
90.0
80.0
70.0
60.0
50.0
40.0
30.0
20.0
10.0
0
80.432
77.895
55.942
44.263
21.800
6, 10
1, 4
7, 9, 11, 13
2, 3, 14, 15
8, 12

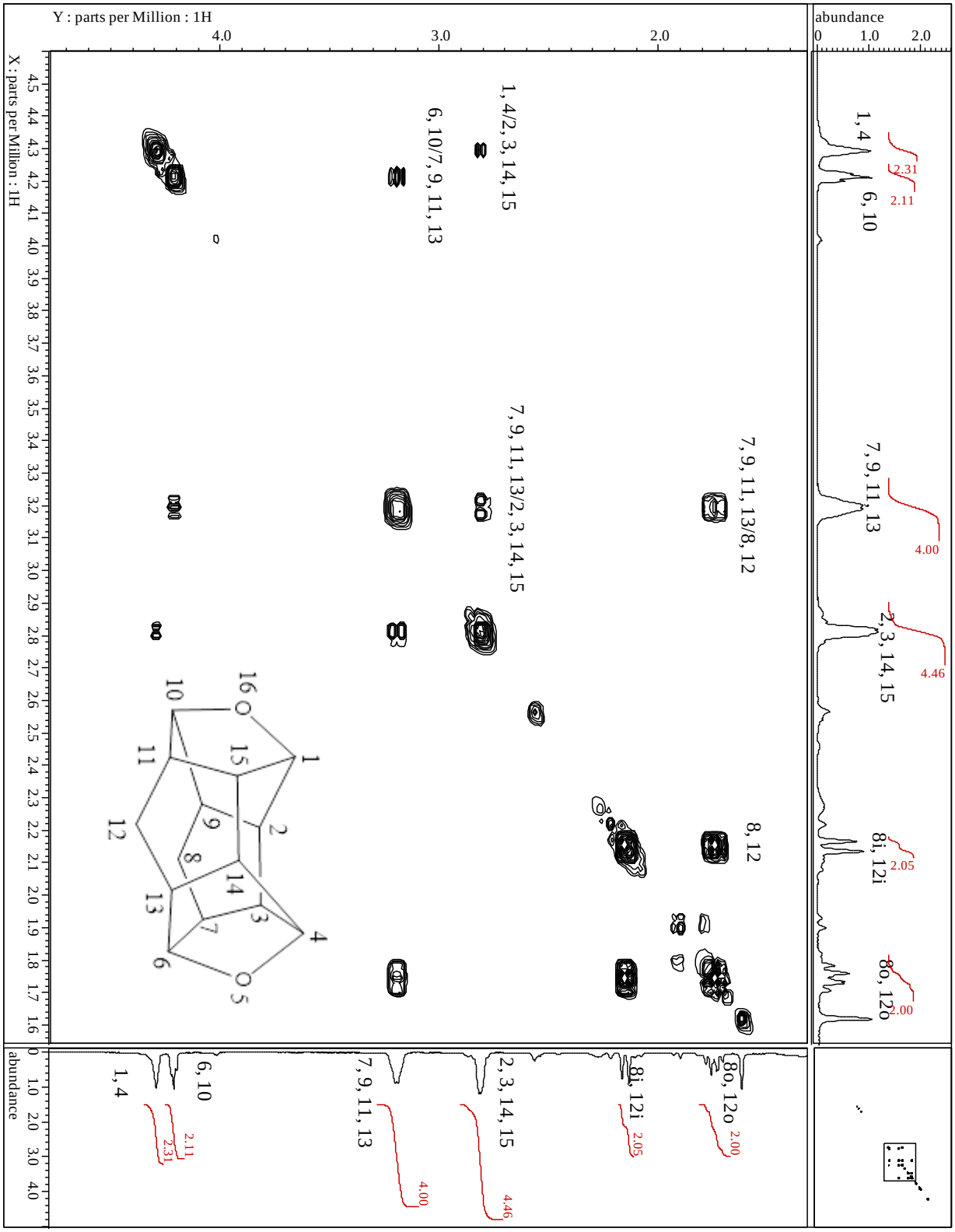
abundance
0
1.0
2.0
1, 4
2.31
2.11
6, 10
7, 9, 11, 13
4.00
2, 3, 14, 15
4.46
8i, 12i
2.05
8o, 12o
2.00
Y : parts per Million : 1H
4.0
3.0
2.0
1, 4/2, 3, 14, 15
6, 10/7, 9, 11, 13
7, 9, 11, 13/2, 3, 14, 15
7, 9, 11, 13/8, 12
8, 12
16
10
15
1
11
2
9
12
8
14
3
13
7
4
6
5
X : parts per Million : 1H
4.5
4.4
4.3
4.2
4.1
4.0
3.9
3.8
3.7
3.6
3.5
3.4
3.3
3.2
3.1
3.0
2.9
2.8
2.7
2.6
2.5
2.4
2.3
2.2
2.1
2.0
1.9
1.8
1.7
1.6
8o, 12o
2.00
8i, 12i
2.05
2, 3, 14, 15
4.46
7, 9, 11, 13
4.00
6, 10
2.11
2.31
1, 4
abundance
0
1.0
2.0
3.0
4.0

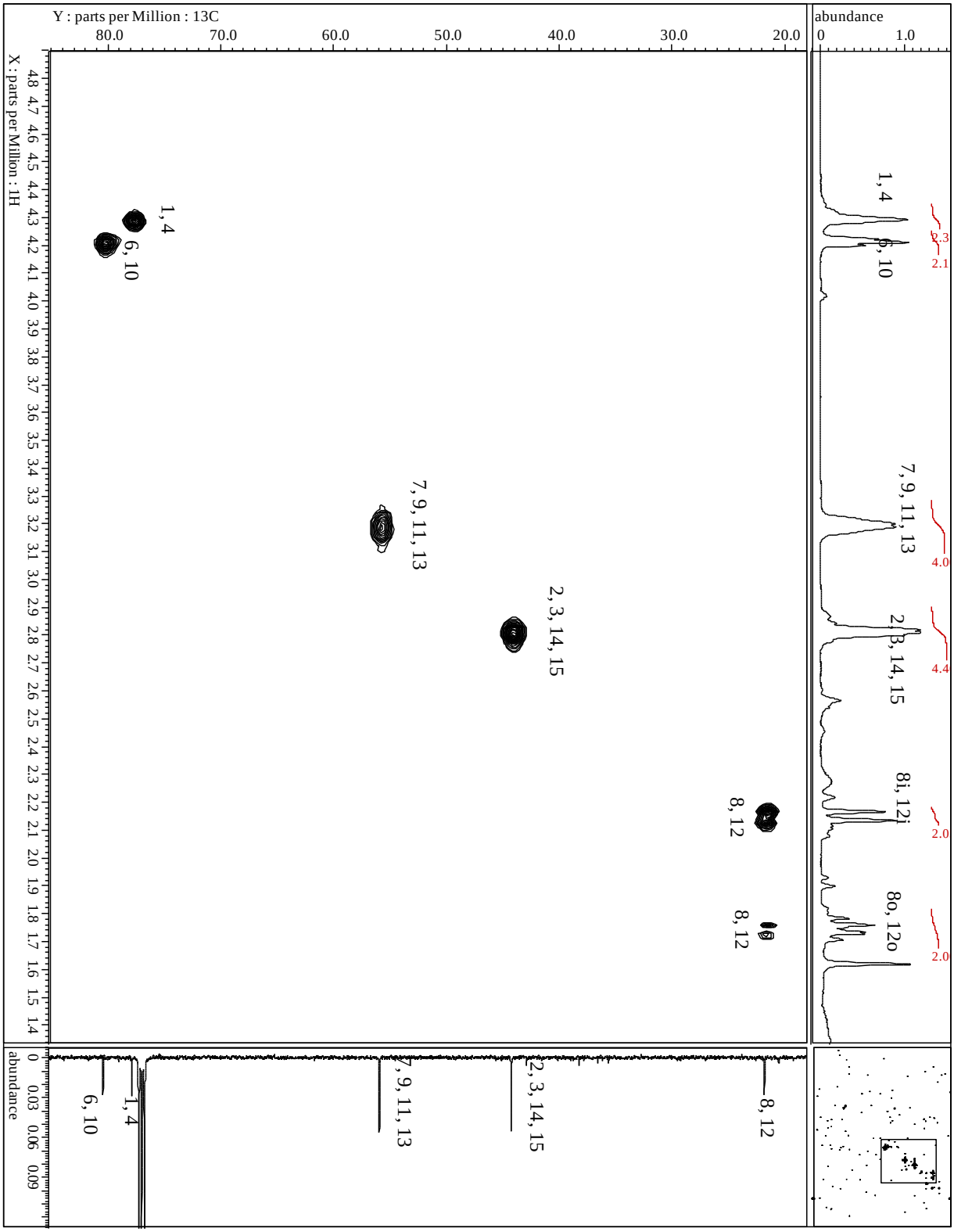
abundance
0
1.0
2.3
2.1
4.0
4.4
2.0
2.0
1, 4
6, 10
7, 9, 11, 13
2, 3, 14, 15
8i, 12i
8o, 12o
8, 12
8, 12
Y : parts per Million : 13C
80.0
70.0
60.0
50.0
40.0
30.0
20.0
X : parts per Million : 1H
1, 4
6, 10
7, 9, 11, 13
2, 3, 14, 15
8, 12
abundance
0
0.03
0.06
0.09
6, 10
1, 4
7, 9, 11, 13
2, 3, 14, 15
8, 12

5,16-Dioxaheptacyclo[7.7.0.0^{2,14}.0^{3,7}.0^{4,13}.0^{6,12}.0^{10,15}]hexadecane (155)

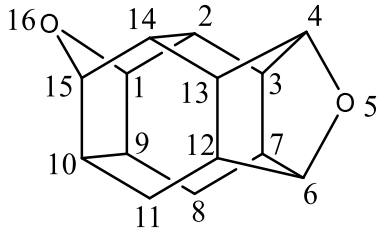

$C_{14}H_{16}O_2$ (216)

^{1}H-NMR ($CDCl_3$, 500 MHz): δ = 5.08 (t, 1H, H-4), 4.23 (s, 2H, H-1, -15), 4.02 (t, 1H, H-6), 2.57 (s, 2H, H-2, -14), 2.27 (s, 2H, H-3, -13), 2.22 (m, 2H, H-9, -10), 2.10 (m, 2H, H-7, -12), 1.92 (d, 2H, H-8i, -11i), 1.80 (dd, 2H, H-8o, -11o) ppm;

$^2J_{\text{H-8i, -8o}} = {}^2J_{\text{H-11i, -11o,}} = 15.3$; $^3J_{\text{H8, -11, H-7, -12}} = 7.7$ Hz.

^{13}C-NMR ($CDCl_3$, 100.7 MHz): δ = 95.2 (C-4), 81.7 (C-6), 79.1 (C-1, -15), 42.9 (C-2, -14), 38.3 (C-3, -13), 36.6 (C-7, -12), 35.6 (C-9, -10), 20.5 (C-8, -11) ppm.

MS (EI, 70 eV): *m/z* (%) = 217 (15.2) [$M^{\cdot+}$+1], 216 (100.0) [$M^{\cdot+}$], 188 (18.2), 187 (15.4), 172 (8.0), 170 (11.0), 169 (11.5), 160 (8.0), 159 (14.3), 157 (10.7), 155 (11.3), 154 (8.4), 146 (8.7), 145 (10.5), 144 (12.0), 143 (16.7), 142 (15.3), 141 (18.8), 133 (11.1), 132 (10.7), 131 (36.3), 130 (17.1), 129 (46.7), 128 (27.4), 122 (7.9), 120 (10.3), 119 (10.6), 118 (12.7), 117 (45.2), 116 (19.5), 115 (34.6), 109 (8.2), 108 (8.8), 107 (15.1), 106 (9.6), 105 (30.1), 104 (17.3), 103 (14.8), 96 (10.0), 95 (15.4), 94 (14.7), 93 (12.5), 92 (30.4), 91 (96.7), 83 (7.7), 82 (14.0), 81 (31.6), 80 (11.9), 79 (58.6), 78 (26.2), 77 (57.3), 68 (8.1), 67 (14.7), 66 (12.7), 65 (27.5), 63 (9.2), 55 (12.4), 53 (18.5), 52 (7.9), 51 (17.8).

Spectra:

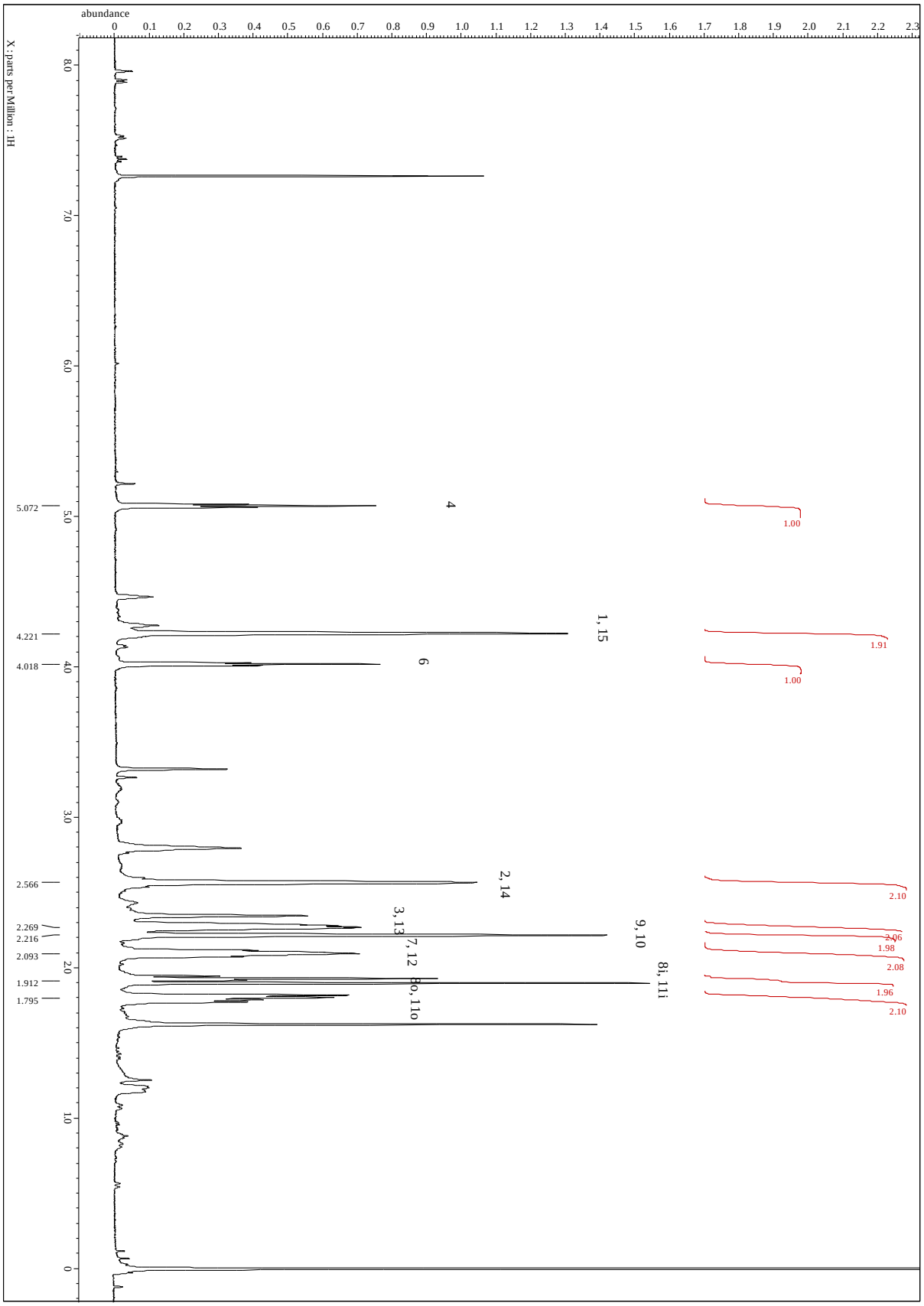
abundance
X : parts per Million : 1H
5.072
4.221
4.018
2.566
2.269
2.216
2.093
1.912
1.795
4
1, 15
6
2, 14
3, 13
7, 12
8o, 11o
9, 10
8i, 11i
1.00
1.91
1.00
2.10
2.06
1.98
2.08
1.96
2.10

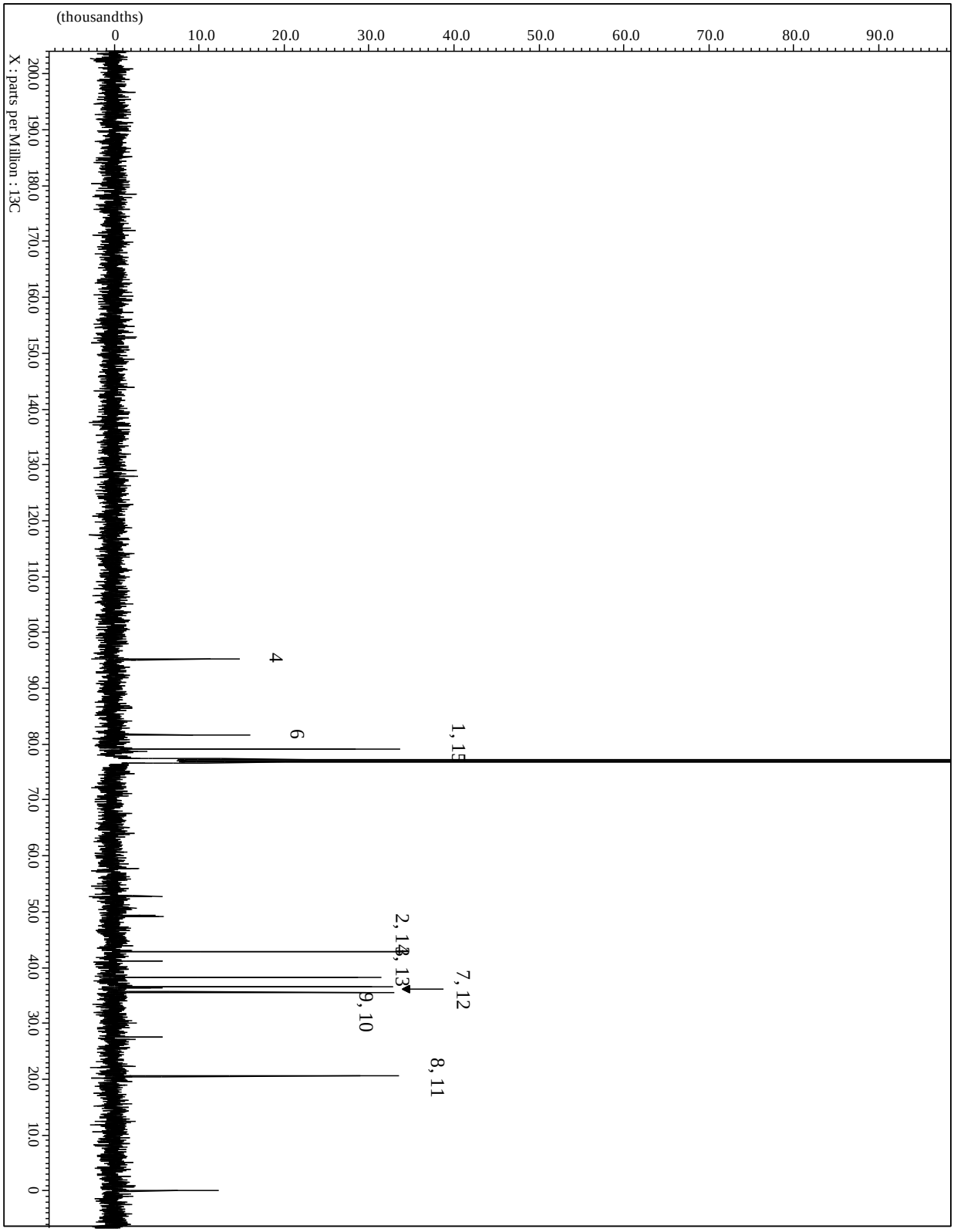
(thousandths)
0
10.0
20.0
30.0
40.0
50.0
60.0
70.0
80.0
90.0
X : parts per Million : 13C
200.0
190.0
180.0
170.0
160.0
150.0
140.0
130.0
120.0
110.0
100.0
90.0
80.0
70.0
60.0
50.0
40.0
30.0
20.0
10.0
0
4
6
1, 15
2, 14
3, 13
7, 12
9, 10
8, 11

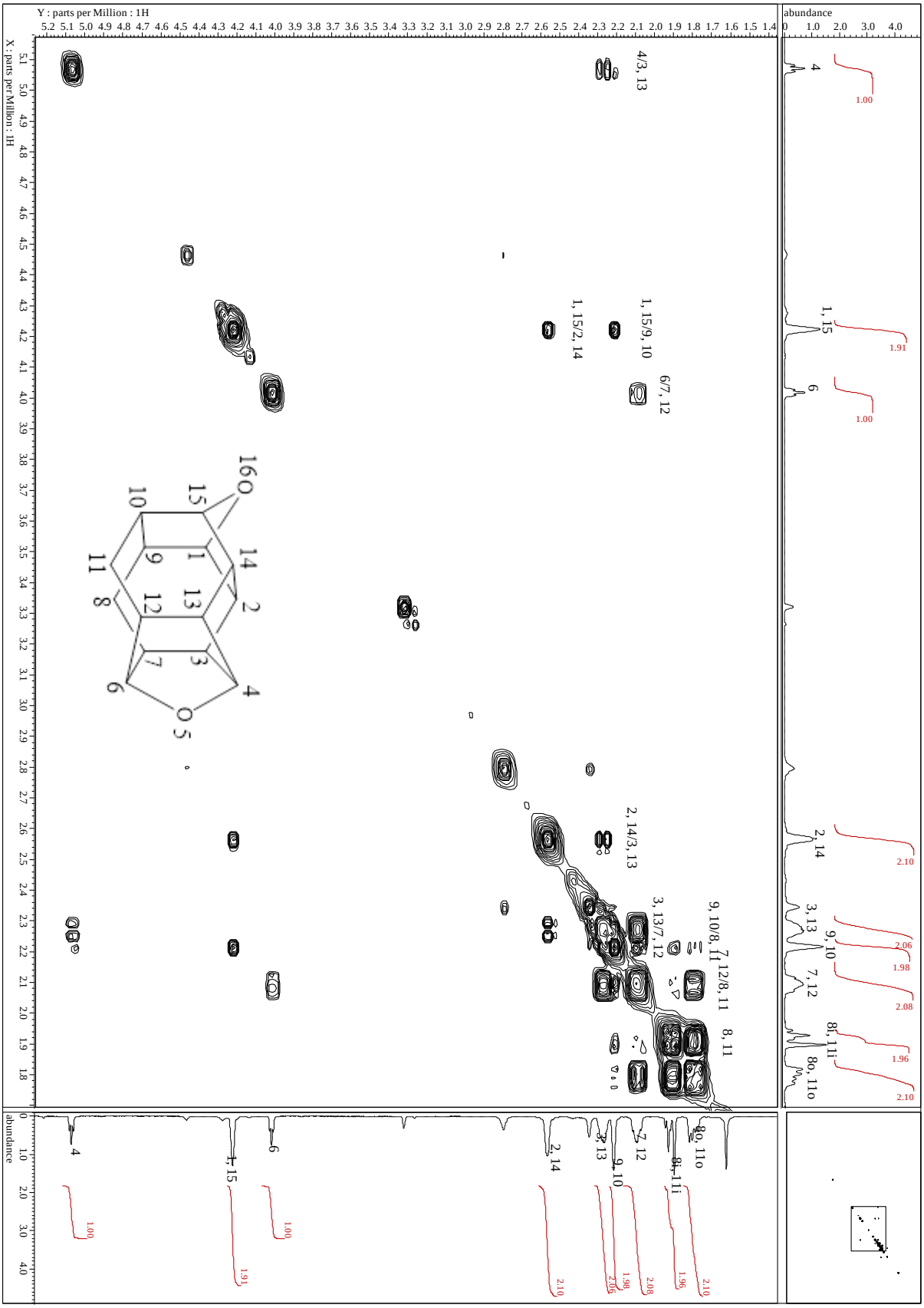
Y : parts per Million : 1H
X : parts per Million : 1H
abundance
4
1.00
1, 15
1.91
6
1.00
2, 14
2.10
3, 13
9, 10
2.06
1.98
7, 12
2.08
8, 11i
1.96
8o, 11o
2.10
4/3, 13
1, 15/9, 10
6/7, 12
1, 15/2, 14
2, 14/3, 13
3, 13/7, 12
9, 10/8, 11i
7, 12/8, 11
8, 11
16O
15
10
14
2
1
9
13
12
11
8
3
7
6
4
O
5

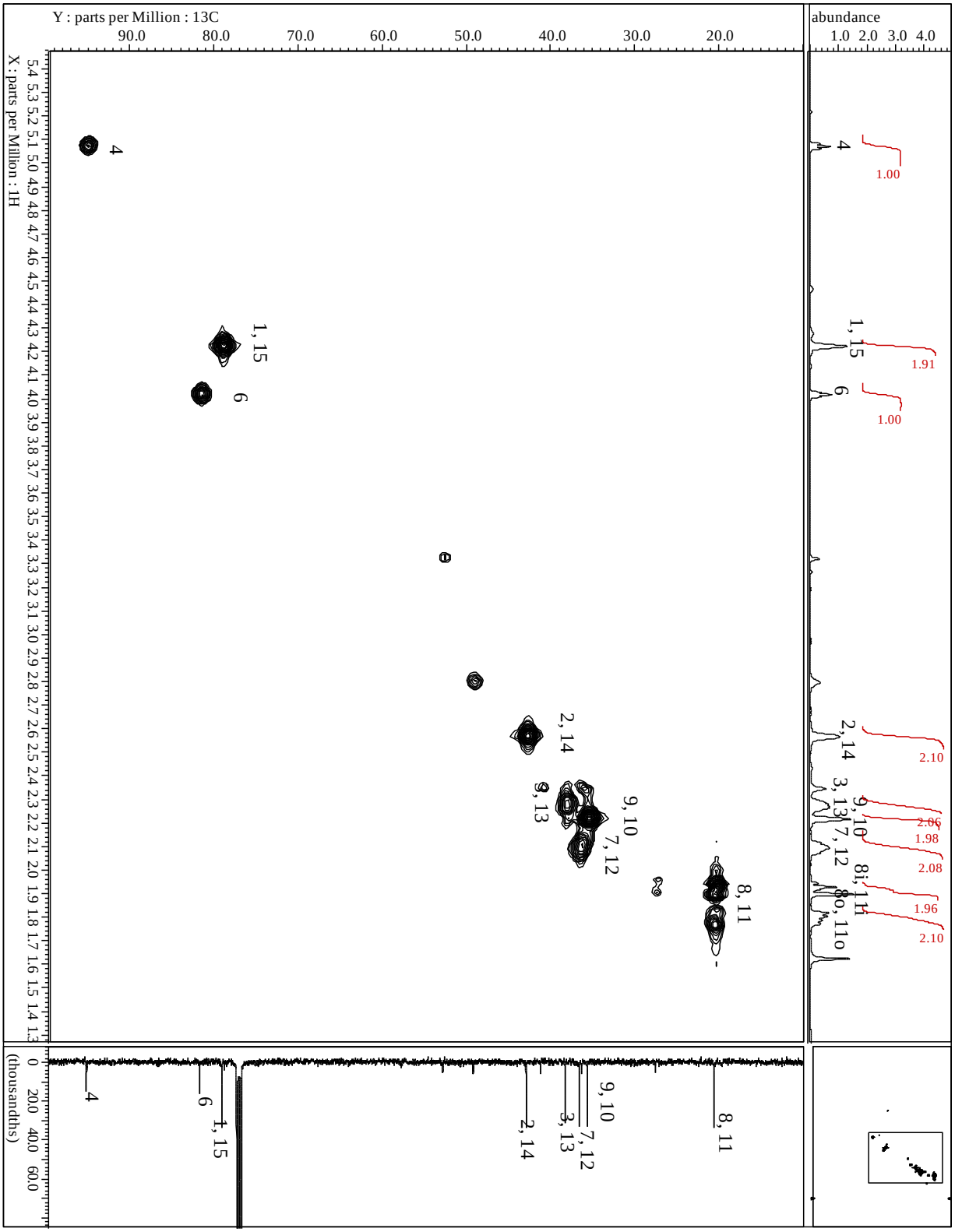
Y : parts per Million : 13C
X : parts per Million : 1H
abundance
(thousandths)
4
1, 15
6
2, 14
3, 13
9, 10
7, 12
8, 11
1.00
1.91
1.00
2.10
2.06
1.98
2.08
1.96
2.10

5.4.7 Rearrangement of Saturated Epoxide Cage **96**

*Rearrangement of Saturated Epoxide **96**:* To a solution of saturated mono-epoxide **96** (13 mg, 0.064 mmol) in DCM (4 mL), Amberlyst-15 (20 mg, 0.099 mmol, 4.95 mol/kg) was added and stirred for 4 hours until all **96** was consumed (based on GC/MS). The suspension was then filtered and washed with DCM (3x25 mL). The solution and washings were combined and concentrated to afford **157** (8 mg, 62%, 95% clean). No further purification was attempted.

*Rearrangement of **157**:* To a solution of oxacage **157** (20 mg, 0.099 mmol) in DCM (5 mL), Amberlyst-15 (40 mg, 0.197 mmol, 4.95 mol/kg) was added and stirred for 16 hours until all **157** was consumed (based on GC/MS). The suspension was then filtered and washed with DCM (3x25 mL). The solution and washings were combined and concentrated to afford colorless crystalline material (33 mg). Purification by column chromatography (SiO_2, 7:1 Hexanes/EtOAc) gave clean **158** (13 mg, 65%).

12-Oxahexacyclo[7.6.0.0^{2,6}.0^{4,13}.0^{5,11}.0^{10,14}]pentadecane (157)

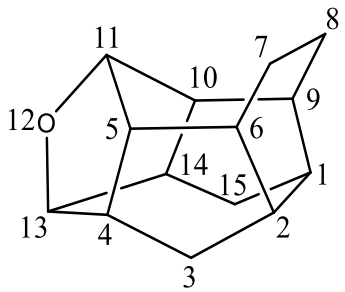

$C_{14}H_{18}O$ (202)

MP = 176.4-177.7 ° C ($CHCl_3$)

IR (AT-IR): $\tilde{\nu}$ = 2938 (s, C-H), 1735 (broad, w), 1280 (m), 688 (s) cm^{-1}.

^{1}H-NMR ($CDCl_3$, 500 MHz): δ = 4.31 (t, 1H, H-11), 4.20 (t, 1H, H-13), 2.70 (m, 2H, H-4, -14), 2.66 (m, 2H, H-5, -10), 2.07 (s_{app}, 2H, H-1, -2), 2.00 (d, 2H, H-3i, -15i), 1.85-1.79 (m, 6H, H-6, -9, H-7i, -7o, -8i, -8o), 1.25 (m, 2H, H-3o, -15o) ppm;

$^{2}J_{\text{H-3i, H-3o}} = {}^{2}J_{\text{H-15i, H-15o}} = 13.6$; $^{3}J_{\text{H-11, H-5, -10}} = {}^{3}J_{\text{H-13, H-4, -14}} = 6.0$ Hz

^{13}C-NMR ($CDCl_3$, 100.7 MHz): δ = 79.2 (C-11), 78.8 (C-13), 52.7 (C-5, -10), 49.4 (C-4, -14), 37.9 (C-6, -9), 36.5 (C-1, -2), 29.1 (C-3, -15), 20.1 (C-7, -8) ppm.

^{1}H-NMR (C_6D_6, 500 MHz): δ = 4.25 (t, 1H, H-11), 4.10 (t, 1H, H-13), 2.62 (m, 2H, H-4, -9), 2.58 (m, 2H, H-5, -10), 1.83 (m, 2H, H-1, -2), 1.75 (d, 2H, H-3i, -15i), 1.60 (m, 4H, H-7i, -7o, -8i, -8o), 1.58-1.54 (m, 2H, H-6, -9), 1.03-0.96 (m, 2H, H-3o, -15o) ppm;

$^{2}J_{\text{H-3i, H-3o}} = {}^{2}J_{\text{H-15i, H-15o}} = 13.9$; $^{3}J_{\text{H-11, H-4, -14}} = {}^{3}J_{\text{H-13, H-5, -10}} = 6.0$ Hz

^{13}C-NMR ($CDCl_3$, 100.7 MHz): δ = 78.7 (C-11), 78.4 (C-13), 53.2 (C-5, -10), 49.9 (C-4, -14), 38.1 (C-6, -9), 36.8 (C-1, -2), 29.3 (C-3, -15), 20.3 (C-7, -8) ppm.

MS (EI, 70 eV): *m/z* (%) = 202 (49.6) [$M^{\cdot+}$], 184 (8.4), 174 (19.7), 159 (8.4), 158 (17.0), 156 (7.9), 146 (7.7), 145 (14.0), 143 (10.9), 142 (8.5), 141 (7.8), 133 (9.6), 132 (11.4), 131 (25.7), 130 (19.3), 129 (24.7), 128 (18.9), 120 (8.7), 119 (10.5), 118 (11.9), 117 (39.5), 116 (13.3), 115 (30.9), 107 (8.4), 106 (8.7), 105 (24.9), 104 (15.2), 103 (12.5), 95 (8.5), 94 (8.9), 93 (18.5), 92 (26.8), 91 (100.0), 81 (16.6), 80 (23.5), 79 (70.1), 78 (30.4), 77 (70.6), 68 (17.9), 67 (20.8), 66 (16.5), 65 (30.6), 63 (9.0), 55 (12.1), 54 (11.7), 53 (21.3), 52 (9.8), 51 (17.7).

Spectra:

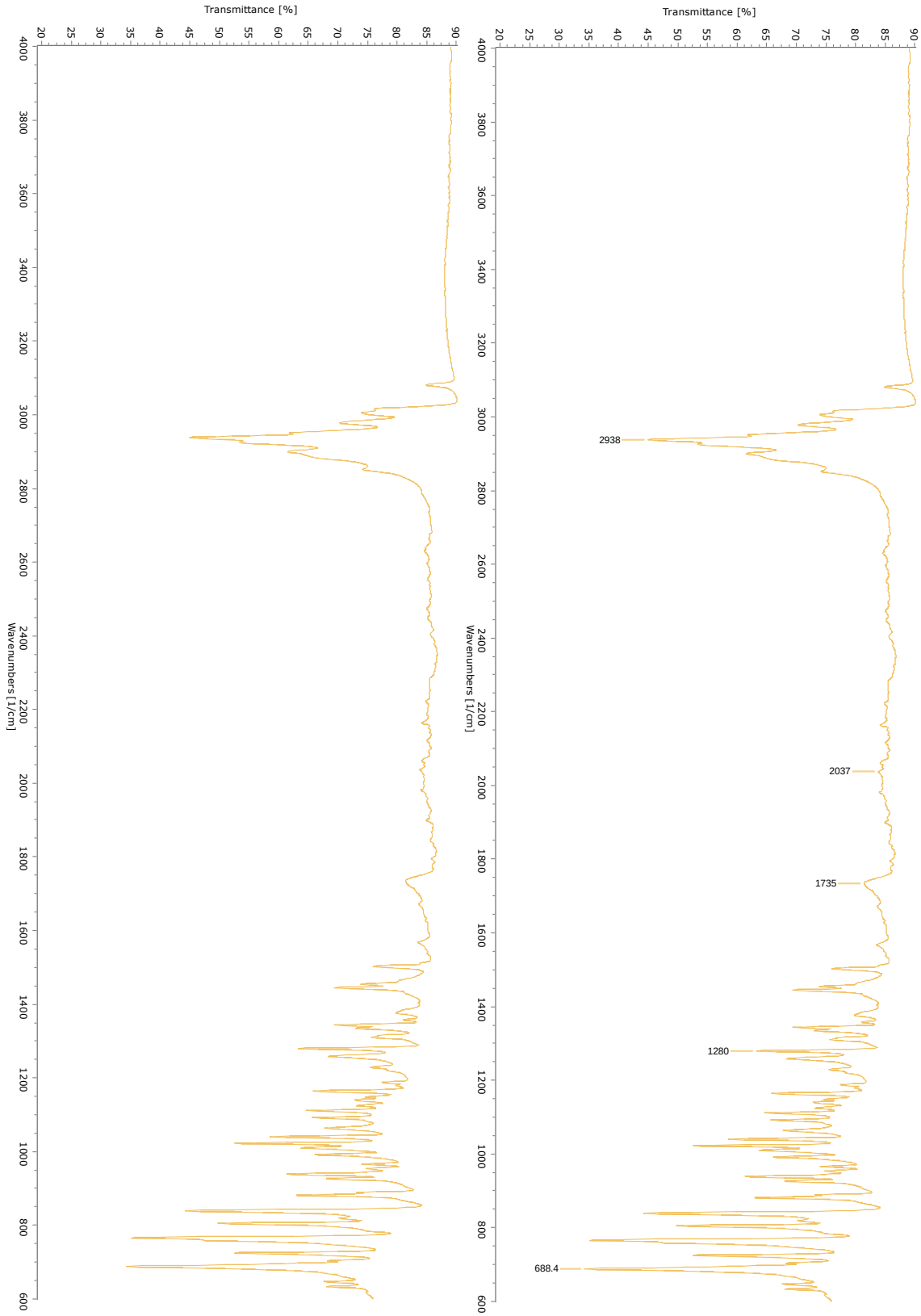
Transmittance [%]
Wavenumbers [1/cm]
2938
2037
1735
1280
688.4

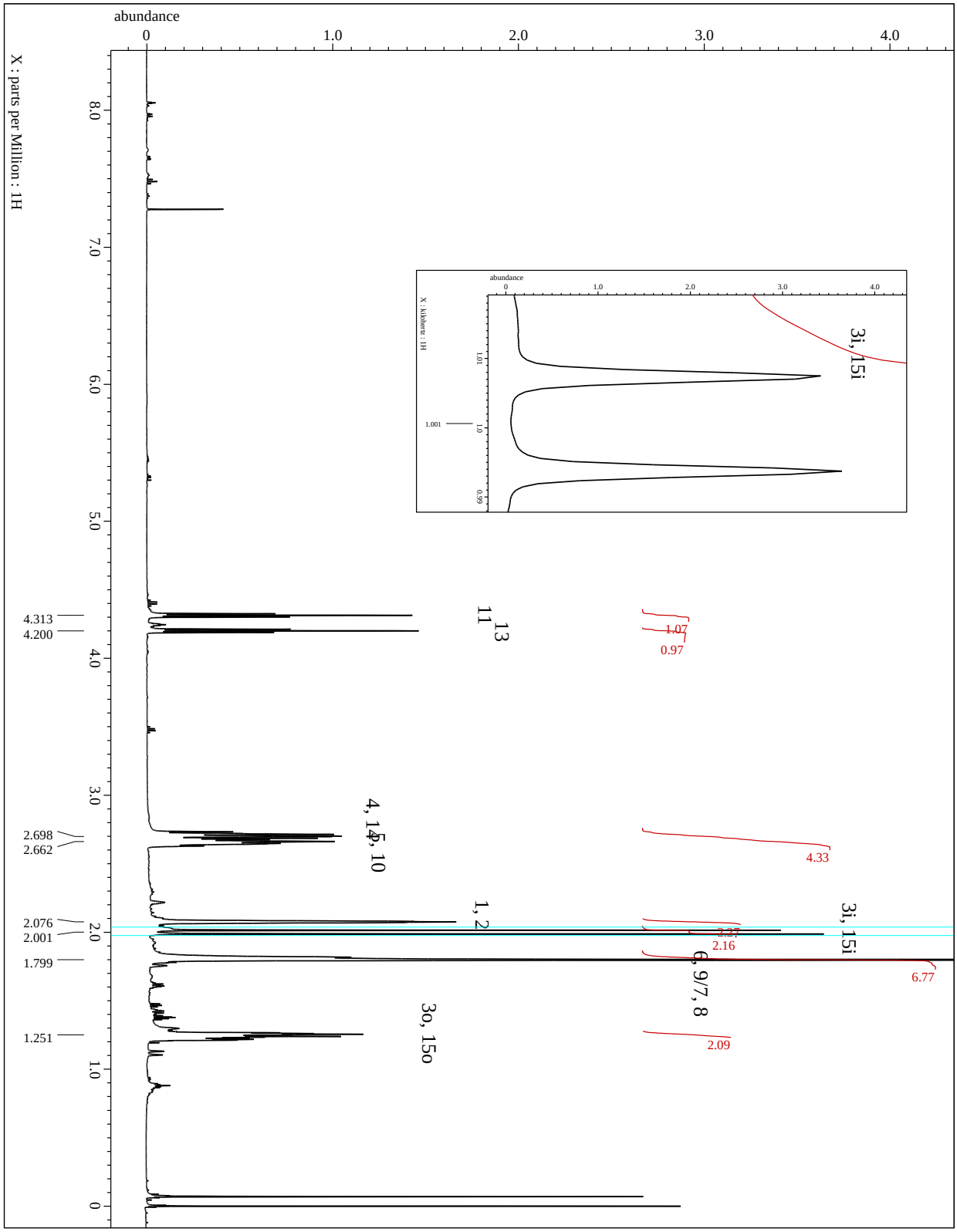
abundance
0
1.0
2.0
3.0
4.0
X : parts per Million : 1H
8.0
7.0
6.0
5.0
4.0
3.0
2.0
1.0
0
4.313
4.200
2.698
2.662
2.076
2.001
1.799
1.251
11
13
4, 14, 5, 10
1, 2
3o, 15o
6, 9/7, 8
3i, 15i
1.07
0.97
4.33
3.27
2.16
6.77
2.09
abundance
X : kilohertz : 1H
1.001
3i, 15i

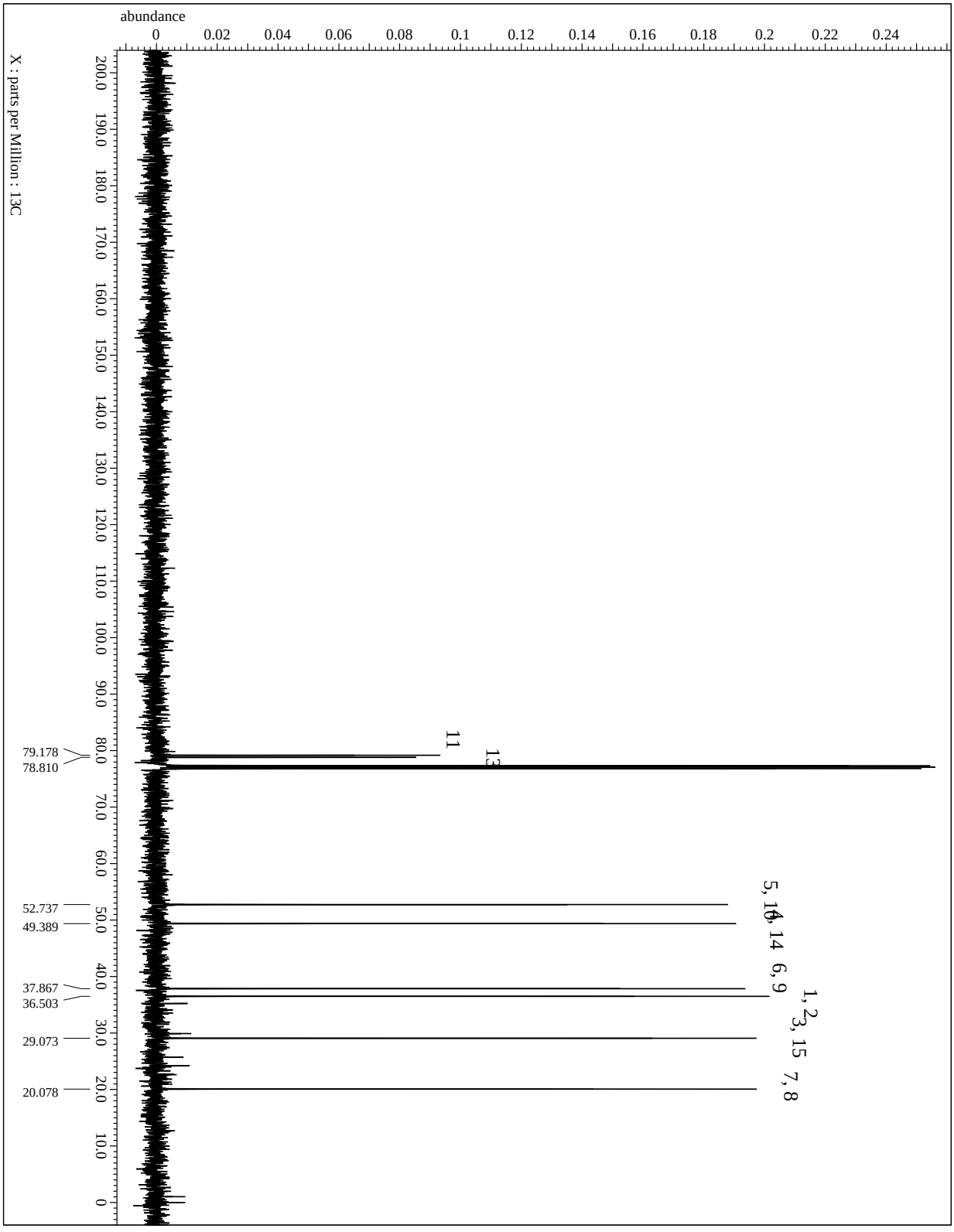
abundance
0
0.02
0.04
0.06
0.08
0.1
0.12
0.14
0.16
0.18
0.2
0.22
0.24
X : parts per Million : 13C
200.0
190.0
180.0
170.0
160.0
150.0
140.0
130.0
120.0
110.0
100.0
90.0
80.0
70.0
60.0
50.0
40.0
30.0
20.0
10.0
0
79.178
78.810
52.737
49.389
37.867
36.503
29.073
20.078
11
13
5, 10
4
14
6, 9
1, 2
3, 15
7, 8

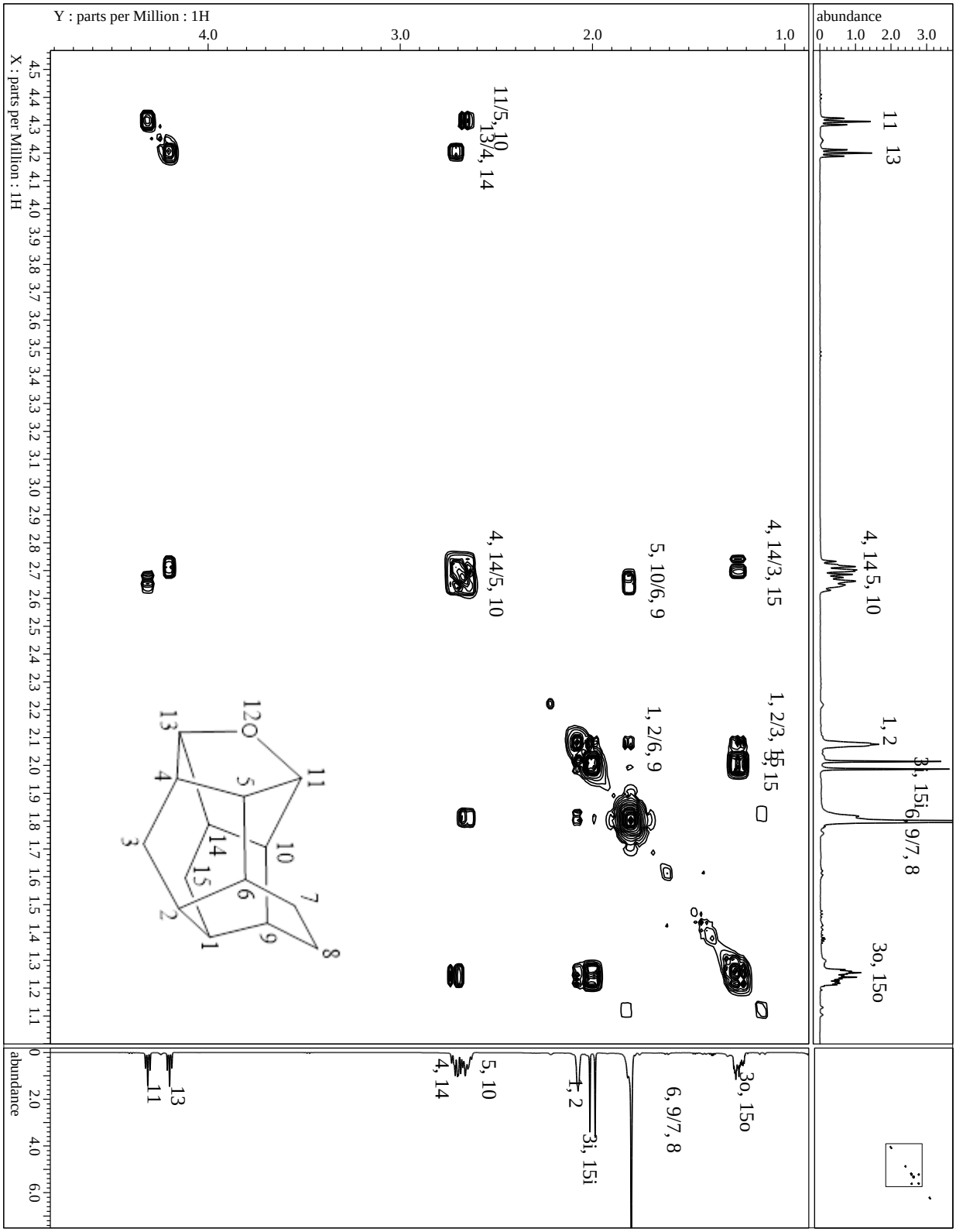
abundance
0 1.0 2.0 3.0
11 13
4, 14
5, 10
1, 2
3i, 15i
6, 9/7, 8
3o, 15o
Y : parts per Million : 1H
4.0 3.0 2.0 1.0
4, 14/3, 15
1, 2/3, 15
5, 10/6, 9
1, 2/6, 9
11/5, 10
13/4, 14
4, 14/5, 10
12
13
11
5
4
10
14
15
6
7
9
3
2
1
8
X : parts per Million : 1H
4.5 4.4 4.3 4.2 4.1 4.0 3.9 3.8 3.7 3.6 3.5 3.4 3.3 3.2 3.1 3.0 2.9 2.8 2.7 2.6 2.5 2.4 2.3 2.2 2.1 2.0 1.9 1.8 1.7 1.6 1.5 1.4 1.3 1.2 1.1
3o, 15o
6, 9/7, 8
1, 2
3i, 15i
5, 10
4, 14
13
11
0 2.0 4.0 6.0
abundance

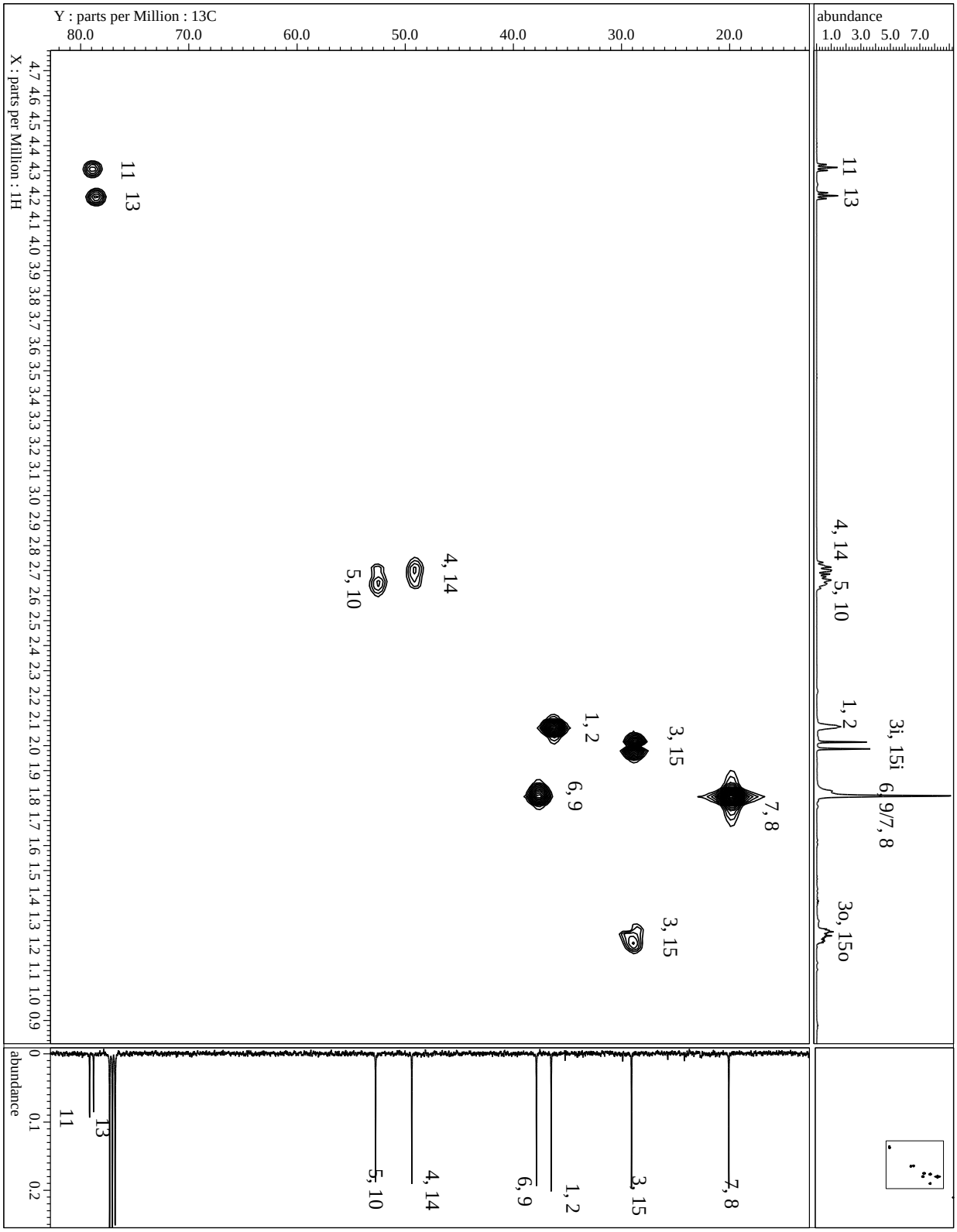
Y : parts per Million : 13C
X : parts per Million : 1H
abundance
11
13
4, 14
5, 10
1, 2
3i, 15i
6, 9/7, 8
3o, 15o
7, 8
3, 15
1, 2
6, 9
3, 15
4, 14
5, 10
11
13
7, 8
3, 15
1, 2
6, 9
4, 14
5, 10
11
13
abundance

15-Oxahexacyclo[6.6.1.$0^{2,7}$.$0^{3,12}$.$0^{6,11}$.$0^{9,14}$]pentadecane (158)

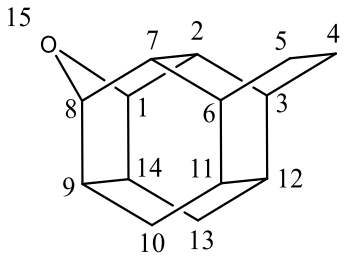

$C_{14}H_{18}O$ (202)

MP = 159.5-162.0 °C ($CHCl_3$)

IR (AT-IR): $\tilde{\nu}$ = 2930 (4, C-H), 2968 (s, C-H), 1446 (w, C-C), 1342 (w), 1257 (m), 1021 (s), 931 (s), 820 (s) cm^{-1}.

^{1}H-NMR ($CDCl_3$, 500 MHz): δ = 4.24 (s_{app}, 2H, H-1, -8), 2.22 (s_{app}, 2H, H-9, -14), 2.03(s_{app}, 2H, H-2, -7), 1.82 (d, 2H, H-10i, -13i), 1.75 (s_{app}, 2H, H-11, -12), 1.61 (d, 2H, H-4i, -5i), 1.42 (d, 2H, H-4o, -5o), 1.30 (s_{app}, 2H, H-3, -6), 1.11 (d, 2H, H-10o, -13o) ppm;

$^2J_{H\text{-}10i,\ -10o} = {}^2J_{H\text{-}13i,\ -13o}$ = 13.7, $^2J_{H\text{-}4i,\ -5i,H\text{-}4o,\ -5o}$ = 7.8 Hz.

^{13}C-NMR ($CDCl_3$, 100.7 MHz): δ = 79.8 (C-1, -8), 40.9 (C-2, -7), 35.2 (C-9, -14), 30.7 (C-3, -6), 29.9 (C- 11, -12), 25.7 (C-4, -5), 24.2 (C-10, -13) ppm.

MS (EI, 70 eV): *m/z* (%) = 203 (15.6) [$M^{\cdot+}$+1], 202 (100.0) [$M^{\cdot+}$], 184 (7.7), 169 (9.8), 158 (7.7), 156 (9.4), 145 (7.5), 143 (10.4), 142 (10.2), 141 (7.8), 132 (11.9), 131 (25.4), 130 (19.7), 129 (20.9), 128 (11.7), 117 (20.6), 115 (14.2), 105 (12.2), 104 (13.8), 93 (10.5), 92 (12.3), 91 (49.0), 81 (8.1), 80 (13.5), 79 (31.3), 78 (13.2), 77 (30.3), 67 (9.2), 65 (12.7), 53 (8.0).

Spectra:

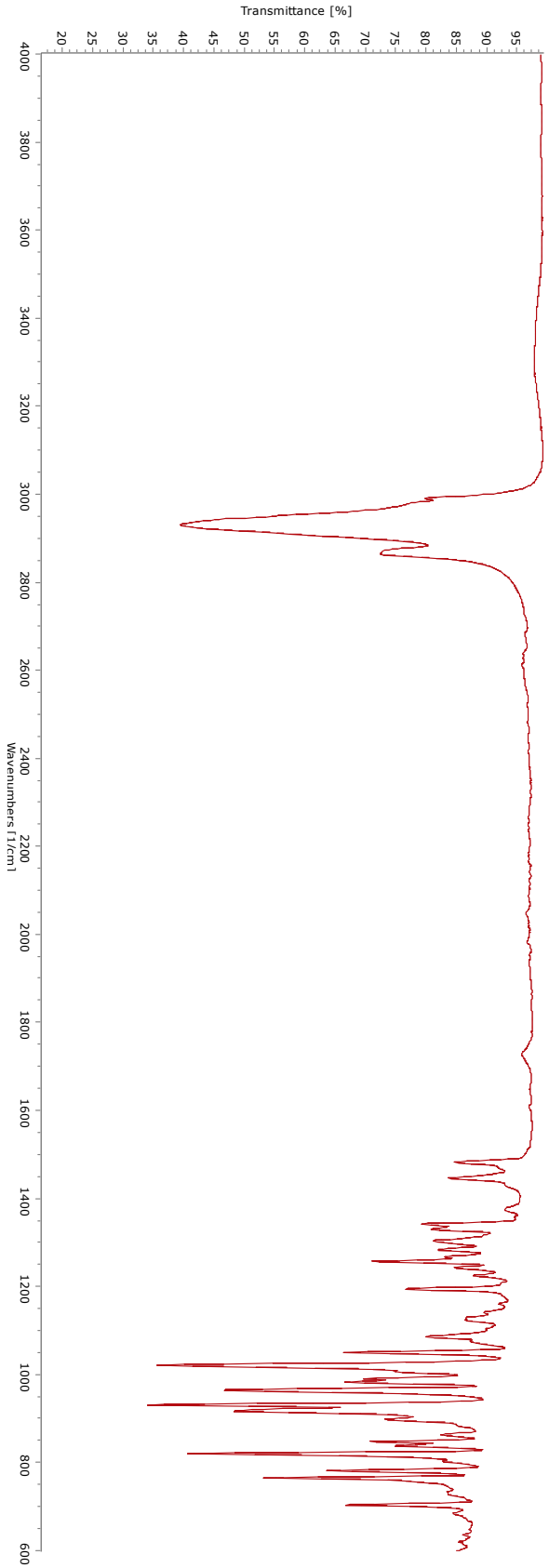
Transmittance [%]
Wavenumbers [1/cm]

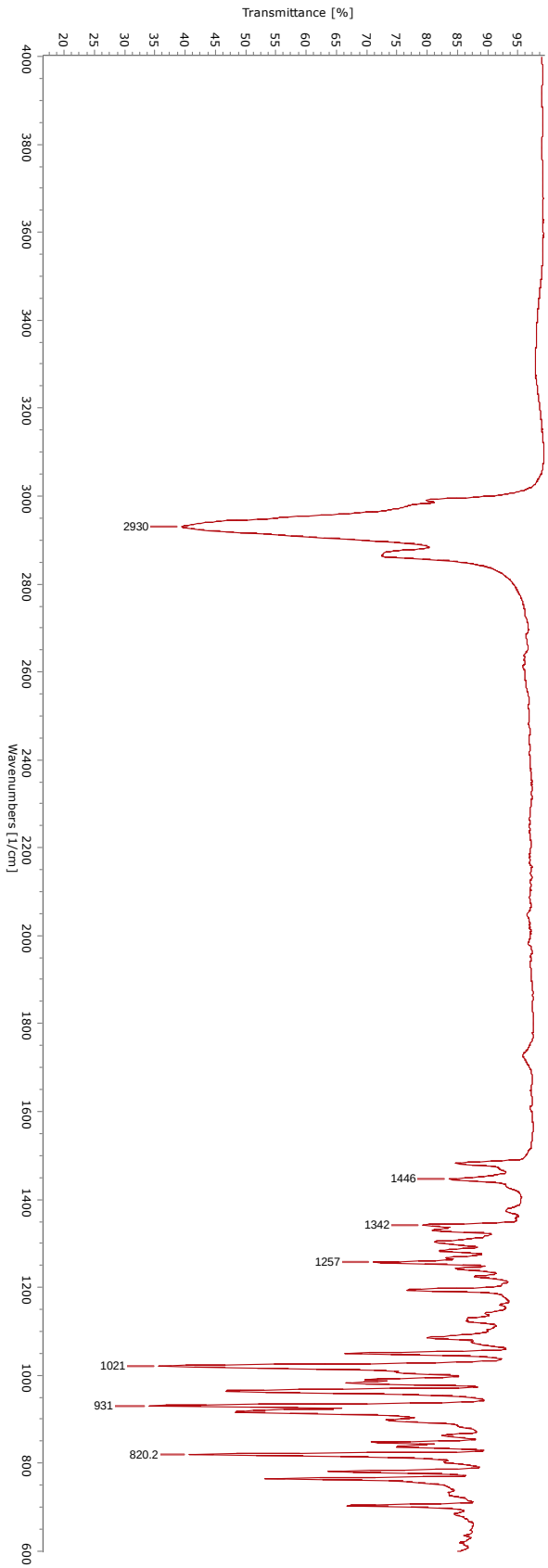
Transmittance [%]
Wavenumbers [1/cm]
2930
1446
1342
1257
1021
931
820.2

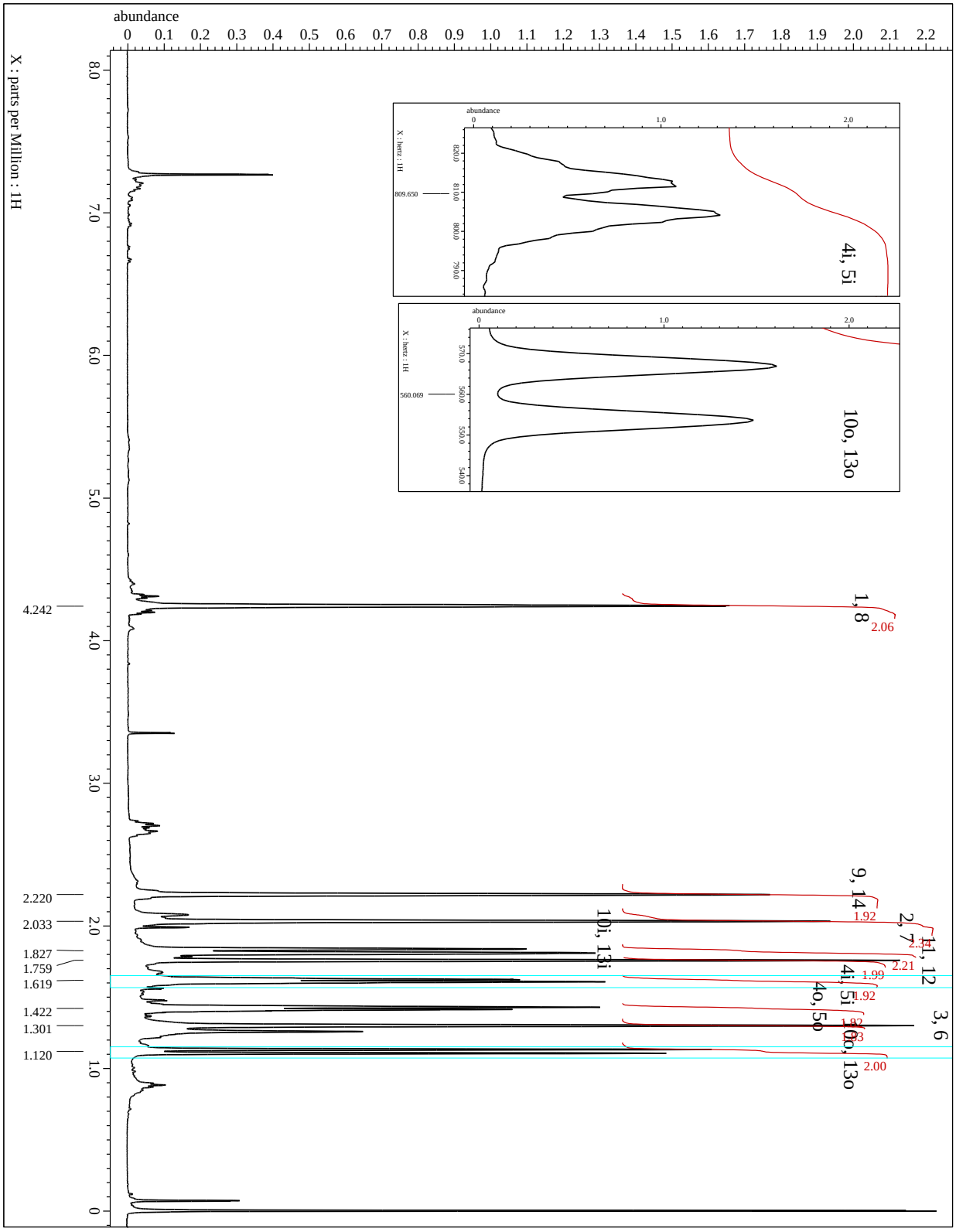
abundance
X : parts per Million : 1H
4.242
2.220
2.033
1.827
1.759
1.619
1.422
1.301
1.120
1, 8
2.06
9, 14
1.92
10i, 13i
2, 7
11, 12
2.21
4i, 5i
1.99
1.92
4o, 5o
3, 6
10o, 13o
2.00
X : hertz : 1H
809.650
4i, 5i
560.069
10o, 13o

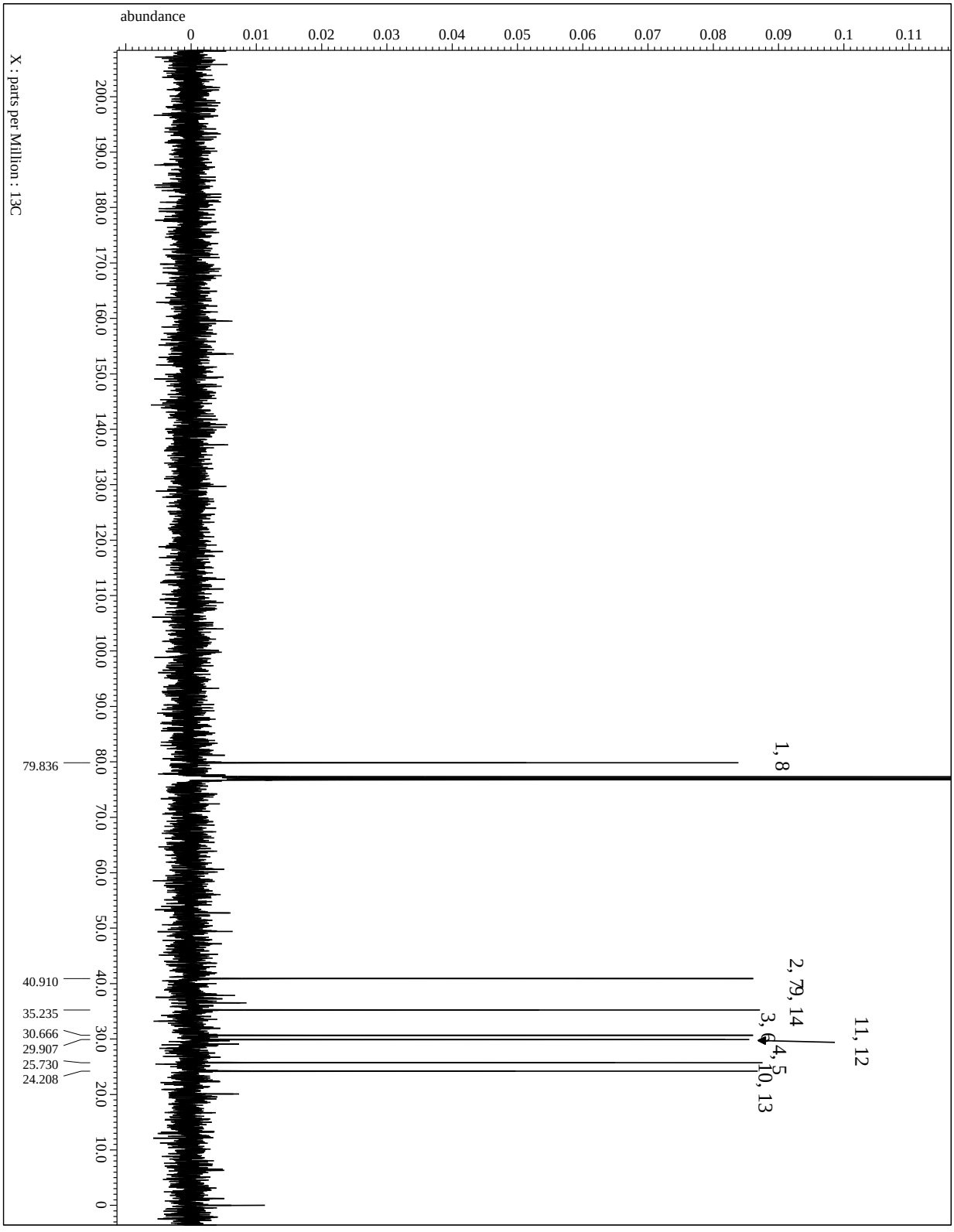
abundance
0
0.01
0.02
0.03
0.04
0.05
0.06
0.07
0.08
0.09
0.1
0.11
X : parts per Million : 13C
200.0
190.0
180.0
170.0
160.0
150.0
140.0
130.0
120.0
110.0
100.0
90.0
80.0
70.0
60.0
50.0
40.0
30.0
20.0
10.0
0
79.836
40.910
35.235
30.666
29.907
25.730
24.208
1, 8
2, 7, 9, 14
3, 6
4, 5
10, 13
11, 12

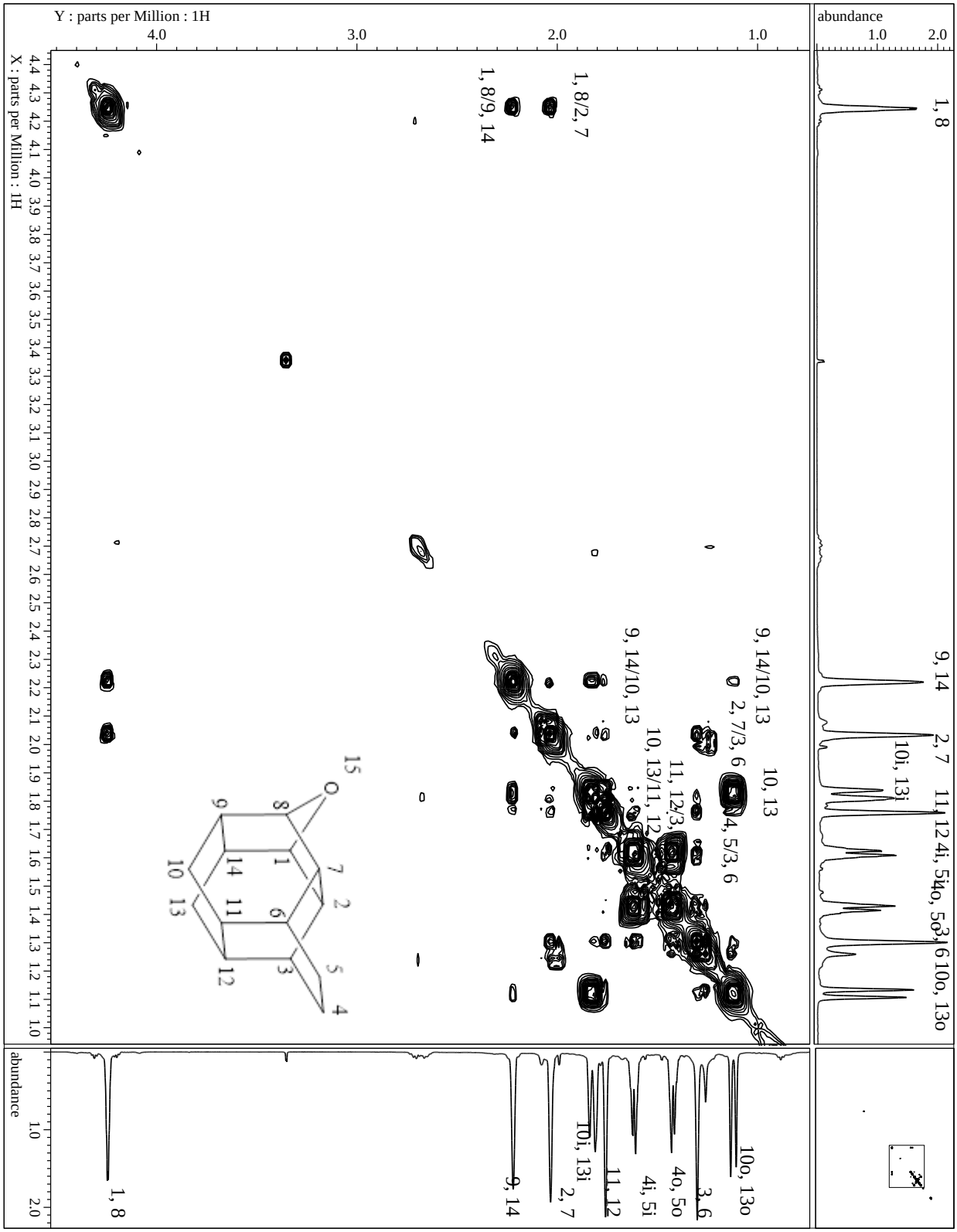
abundance
1.0
2.0
1, 8
9, 14
2, 7
10i, 13i
11, 12
4i, 5i
4o, 5o
3, 6
10o, 13o
Y : parts per Million : 1H
4.0
3.0
2.0
1.0
1, 8/2, 7
1, 8/9, 14
9, 14/10, 13
10, 13
2, 7/3, 6
4, 5/3, 6
11, 12/3, 6
10, 13/11, 12
9, 14/10, 13
X : parts per Million : 1H
4.4 4.3 4.2 4.1 4.0 3.9 3.8 3.7 3.6 3.5 3.4 3.3 3.2 3.1 3.0 2.9 2.8 2.7 2.6 2.5 2.4 2.3 2.2 2.1 2.0 1.9 1.8 1.7 1.6 1.5 1.4 1.3 1.2 1.1 1.0
abundance
1.0
2.0
10o, 13o
3, 6
4o, 5o
4i, 5i
11, 12
10i, 13i
2, 7
9, 14
1, 8
15
O
8
9
10
13
1
14
11
12
6
3
7
2
5
4

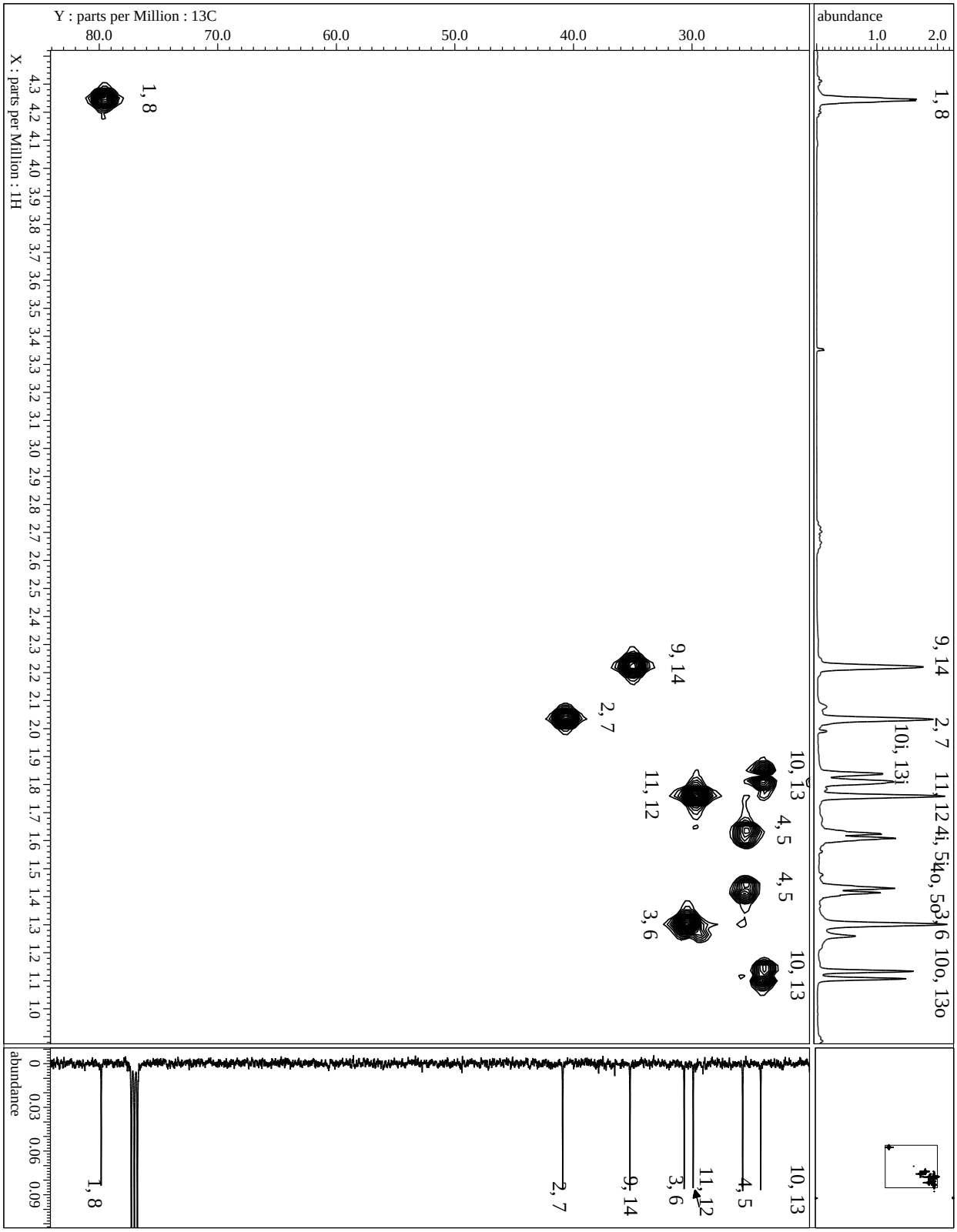
abundance
1.0
2.0
1, 8
9, 14
2, 7
10i, 13i
11, 12
4i, 5i
4o, 5o
3, 6
10o, 13o
Y : parts per Million : 13C
80.0
70.0
60.0
50.0
40.0
30.0
X : parts per Million : 1H
4.3 4.2 4.1 4.0 3.9 3.8 3.7 3.6 3.5 3.4 3.3 3.2 3.1 3.0 2.9 2.8 2.7 2.6 2.5 2.4 2.3 2.2 2.1 2.0 1.9 1.8 1.7 1.6 1.5 1.4 1.3 1.2 1.1 1.0
1, 8
9, 14
2, 7
10, 13
4, 5
4, 5
10, 13
11, 12
3, 6
10, 13
4, 5
11, 12
3, 6
9, 14
2, 7
1, 8
abundance
0
0.03
0.06
0.09

4.3 Experimental: Oxidation Chemistry

5.5 Experimental: Multistep Synthetic Approach Towards the Preparation of a Novel Tetraoxacage

5.5.1 Preparation of Ene-Diol **174** and Saturated Diol **219**

*cis-Dihydroxylation Protocol **O-A**:* Diene **1** (200 mg, 0.543 mmol) was dissolved in THF (4.04 mL) and water (0.476 mL), then cooled to 0 °C. To the stirring solution, acetic acid (1.24 mL) and Me_3NO (526.56 mg, 7.01 mmol) were added, followed by careful addition of 2% OsO_4 solution in ^tBuOH (1.087 mL, 0.068 mmol). The solution was stirred at room temperature for 48 hours then quenched with careful addition of solid K_2CO_3 (2.4 g) followed by saturated $NaHSO_3$ solution (50 mL). This was allowed to stir an additional 15 minutes then stretched with water and extracted with DCM (4x30 mL). The combined organic phase was washed with water (1x30 mL) and brine (3x30 mL), dried ($MgSO_4$) and concentrated to afford a green powdery solid. The solid was triturated with *n*-pentane (5x3 mL) to remove unreacted starting material to give clean osmate ester **217** (74 mg, 31% yield).

*cis-Dihydroxylation Protocol **O-B**: D*iene **1** (50 mg, 0.272 mmol) was dissolved in THF (1.4 mL) and water (0.30 mL) and cooled to 0 °C. To the cooled stirring solution NMO (183 mg, 1.56 mmol) was added, followed by careful addition of 2% OsO_4 solution in ^tBuOH (0.36 mL, 0.0225 mmol). The solution was stirred at room temperature for 7 days then quenched with careful addition of solid K_2CO_3 (1.2 g) and stirred for 16 hours. Saturated $NaHSO_3$ solution (20 mL) was then added stirred an additional 2 days, stretched with water, and extracted with DCM (5x30 mL). The combined organic phase was washed with water (1x30 mL), dried ($MgSO_4$), and concentrated to afford a green powdery solid (97 mg). The solid was triturated with *n*-pentane (5x3 mL) to remove

unreacted starting material. The residue was then triturated again with $CHCl_3$ (3x2 mL) to give clean diol **174** (29 mg, 49% yield).

*cis-Dihydroxylation Protocol **O-C**:* Diene **1** (100 mg, 0.543 mmol) and K_2OsO_4 (100 mg, 0.271 mmol) were dissolved in acetone (10 mL), water (5 mL), and ^tBuOH (5 mL). To the stirring solution, NMO (318 mg, 2.7 mmol) was added and stirred at room temperature for 15 days. The solvent was then removed by vacuum distillation giving a green residue (323 mg). The residue analyzed by ^1H-NMR and ^{13}C-NMR showing primarily osmate ester **217**. The residue was then treated with K_2CO_3 (1.2 g) and sat. $NaHSO_3$ solution according to *Protocol **O-B***. The solution was then extracted with DCM (5x30 mL). The combined organic phase was washed with brine (1x30 mL), dried ($MgSO_4$), and concentrated to afford a green solid with very poor solubility (535 mg). No product could be identified.

*cis-Dihydroxylation Protocol **O-D**:* The diene **1** (100 mg, 0.543 mmol) was dissolved in benzene (20 mL) and crystalline OsO_4 (≈ 100 mg, 0.393 mmol) was added. The solution was stirred at room temperature for 5 days, forming a green precipitate. After all diene **1** was consumed by TLC the supernatant was removed and the remaining benzene removed by vacuum distillation to dryness. The green powdery solid was triturated with *n*-pentane (5x3 mL) to remove unreacted starting material (15 mg, 15%). The residue (216 mg) contained 91% osmate ester **217** and 9% diol **174**.

Osmate Ester LAH Reduction: To a suspension of the above mixture (91% **217**, 320 mg, 0.664 mmol) in dry THF (70 mL), LAH (358.5 mg, 9.447 mmol) was added in portions over 3 hours until all the green color disappeared. The suspension was allowed to stir an additional 1 hour then carefully quenched with wet THF (10 mL THF, 0.5 mL water) and EtOAc (10 mL) added dropwise. Water (0.4 mL) was carefully added followed by 15% NaOH solution (1.2 mL) and water (1.0 mL). $MgSO_4$ was then added to the suspension and stirred an additional 15 minutes

before filtering over celite (or a short pad of silica gel). The filtrate was then dried ($MgSO_4$) and concentrated to afford an off-white crystalline solid (277 mg). The crude material was triturated with chloroform (5x2 mL) to give clean diol **174** (80 mg, 50% yield).

*Hydrogenation of **174***: To a solution of diol **174** (127 mg, 2.717 mmol) in EtOAc (20 mL), a catalytic amount of 5% Pt/C was added. To the suspension H_2 gas was bubbled until the reaction reached 100% conversion (based on GC/MS). The catalyst was filtered off through a plug of silica gel and the filtrate concentrated give a colorless crystalline solid. The solid was shown to be clean saturated diol **219** (127 mg, 99% yield).

14,14-dioxo-13,15-dioxa-14-osmahexacyclo[8.7.0.0^{3,8}.0^{4,17}.0^{7,11}.0^{12,16}]heptadec-5-ene (217)

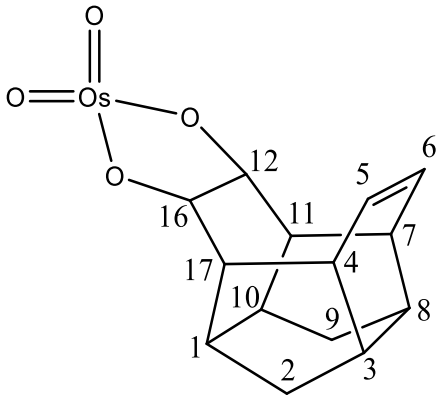

$C_{14}H_{16}O_4Os$ (438)

^{1}H-NMR ($CDCl_3$, 500 MHz): δ = 6.24 (m, 2H, H-5, -6), 5.06 (s_{app}, 2H, H-12, -16), 2.81 (m, 2H, H-11, -17), 2.79-2.74 (m, 2H, H-4, -7), 2.34 (s_{app}, 2H, H-3, -8), 2.02 (s_{app}, 2H, H-1, -10), 1.87 (d, 2H, H-2i, -9i), 0.79 (d, 2H, H-2o, -9o) ppm;

$^2J_{H\text{-}2i,\ -2o} = {}^2J_{H\text{-}9i,\ -9o} = 11.7$ Hz.

^{13}C-NMR ($CDCl_3$, 100.7 MHz): δ = 134.1 (C-5, -6), 90.1 (C-12, -16), 54.1 (C-11, -17), 40.2 (C-4, -7), 37.2 (C-1, -10), 33.0 (C-3, -8), 28.7 (C-2, -9) ppm.

Spectra:

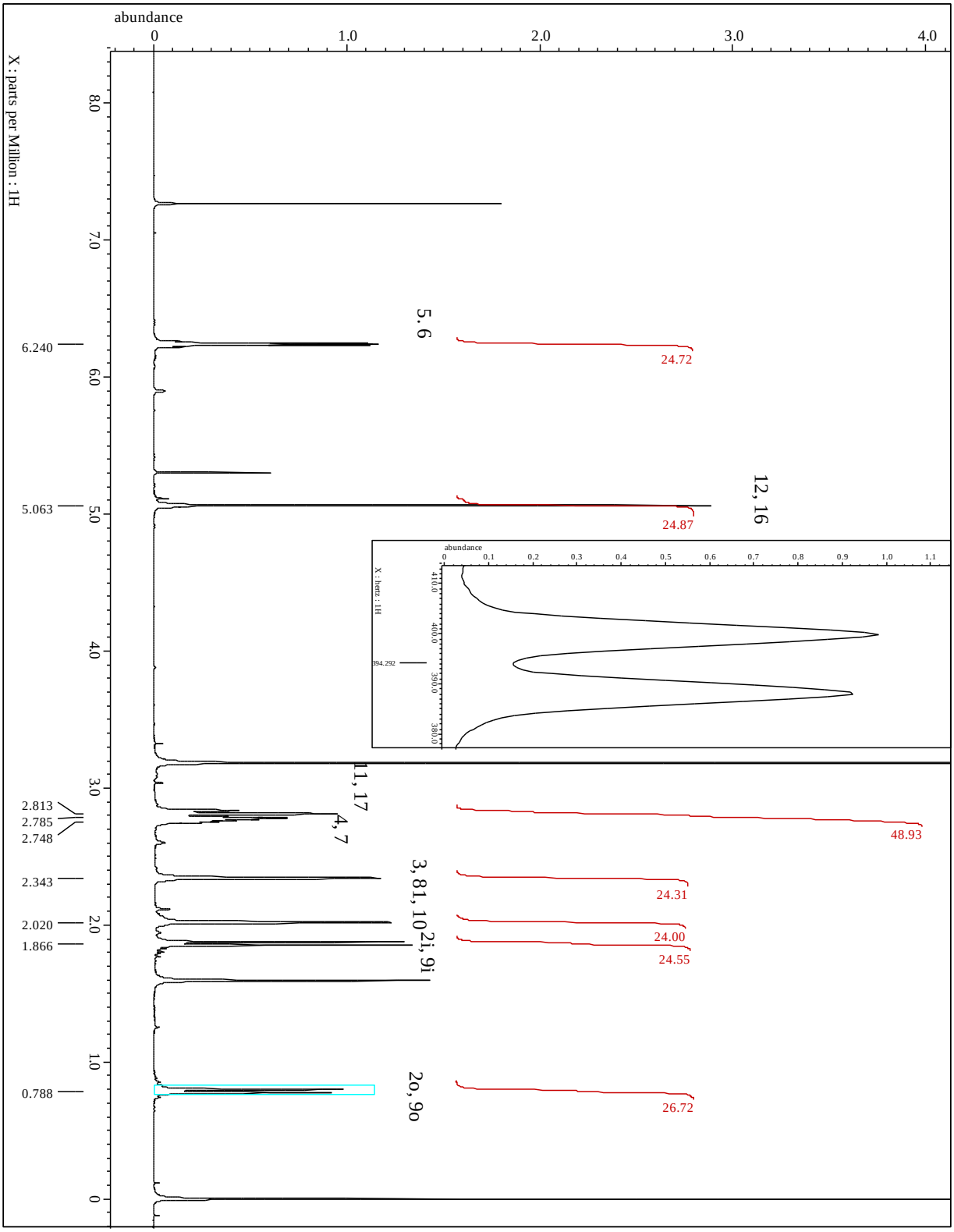
abundance
0
1.0
2.0
3.0
4.0
X : parts per Million : 1H
8.0
7.0
6.0
5.0
4.0
3.0
2.0
1.0
0
6.240
5.063
2.813
2.785
2.748
2.343
2.020
1.866
0.788
5, 6
24.72
12, 16
24.87
11, 17
4, 7
48.93
3, 8
1, 10
2i, 9i
24.31
24.00
24.55
2o, 9o
26.72
abundance
X : hertz : 1H
394.292

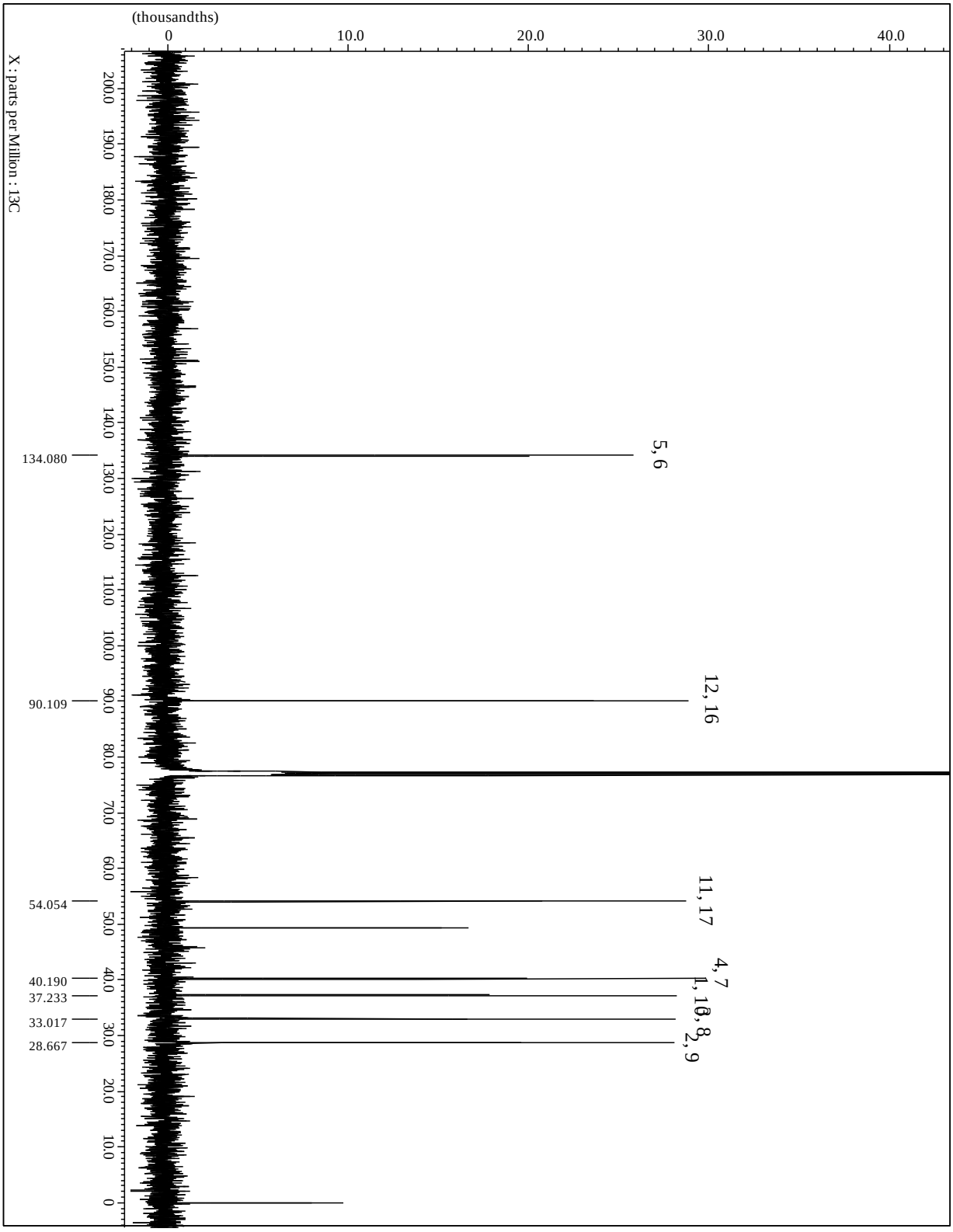
(thousandths)
0
10.0
20.0
30.0
40.0
X : parts per Million : 13C
200.0
190.0
180.0
170.0
160.0
150.0
140.0
130.0
120.0
110.0
100.0
90.0
80.0
70.0
60.0
50.0
40.0
30.0
20.0
10.0
0
134.080
90.109
54.054
40.190
37.233
33.017
28.667
5, 6
12, 16
11, 17
4, 7
1, 10
3, 8
2, 9

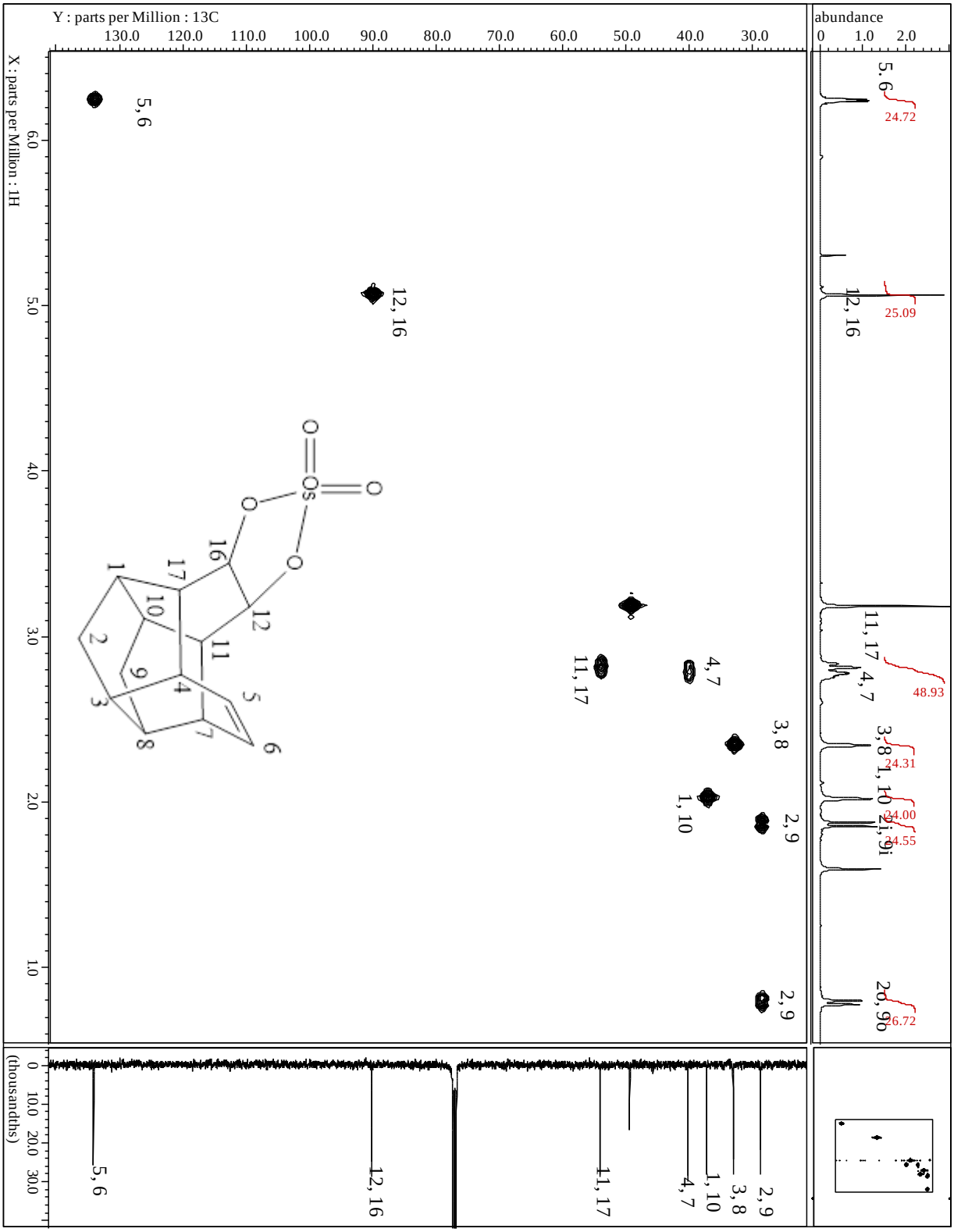
Y : parts per Million : 13C
X : parts per Million : 1H
abundance
(thousandths)
5, 6
12, 16
11, 17
4, 7
3, 8
1, 10
2, 9
24.72
25.09
48.93
24.31
24.00
24.55
26.72
Os
O

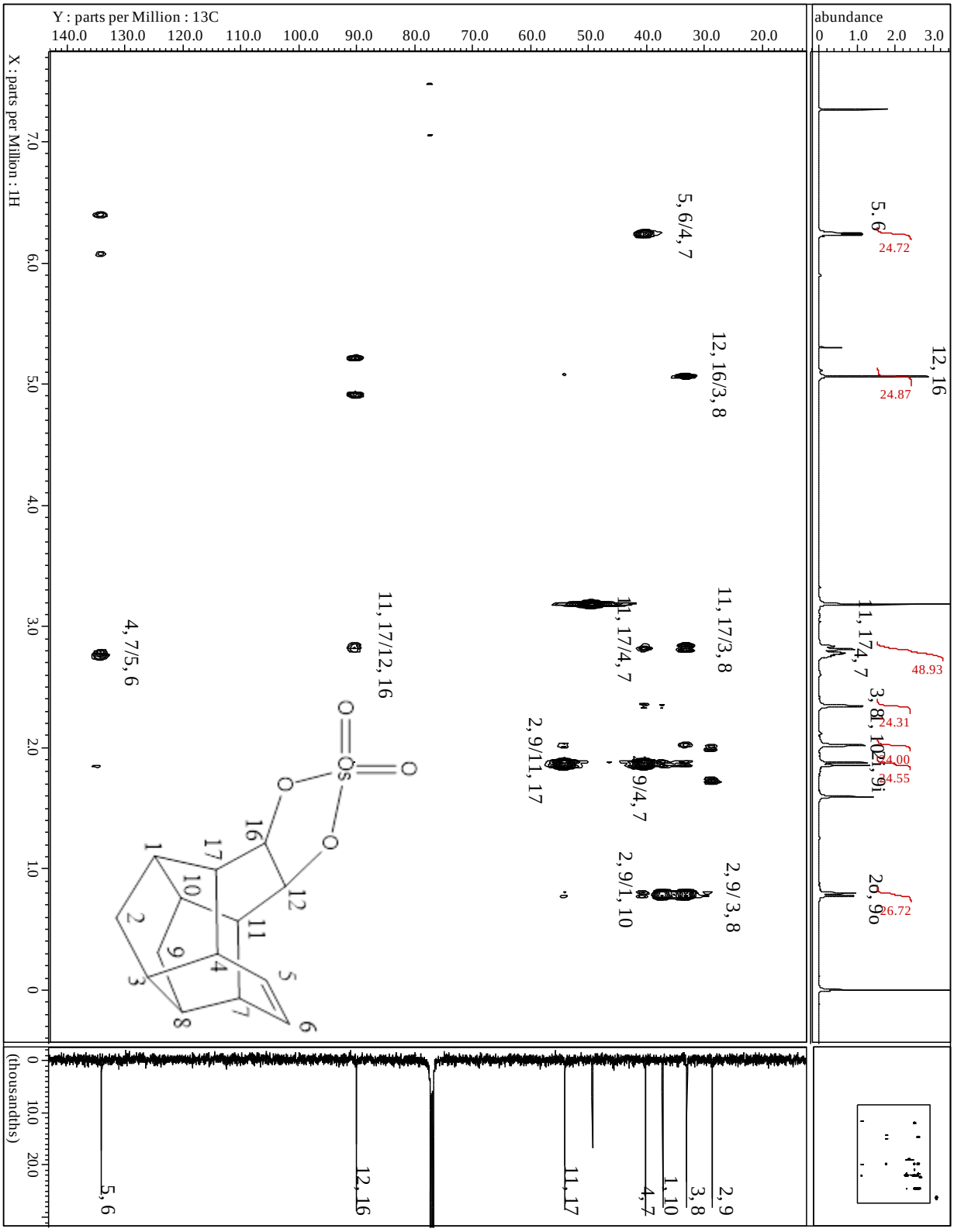
abundance
0 1.0 2.0 3.0
5, 6
24.72
12, 16
24.87
11, 17/4, 7
48.93
3, 8, 10/2, 9i
24.31
24.00
24.55
2o, 9o
26.72
Y : parts per Million : 13C
140.0 130.0 120.0 110.0 100.0 90.0 80.0 70.0 60.0 50.0 40.0 30.0 20.0
X : parts per Million : 1H
7.0 6.0 5.0 4.0 3.0 2.0 1.0 0
5, 6/4, 7
12, 16/3, 8
11, 17/3, 8
11, 17/4, 7
2, 9/11, 17
9/4, 7
2, 9/ 3, 8
2, 9/1, 10
11, 17/12, 16
4, 7/5, 6
O
Os
O
O
O
1
2
3
4
5
6
7
8
9
10
11
12
16
17
2, 9
3, 8
1, 10
4, 7
11, 17
12, 16
5, 6
0 10.0 20.0
(thousandths)

Pentacyclo[8.4.0.0^{3,8}.0^{4,14}.0^{7,11}]tetradec-12-ene-5,6-diol (174)

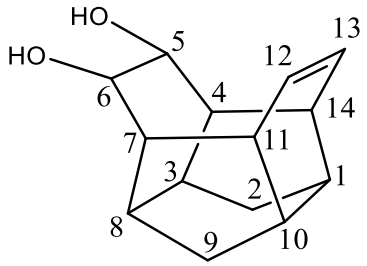

$C_{14}H_{18}O_2$ (218)

MP = 224.5-225.3 ° C (DCM)

IR (AT-IR): $\tilde{\nu}$ = 3334 (br m, O-H), 2929 (s, C-H), 1256 (w), 1015 (s), 790 (s) cm^{-1}.

^{1}H-NMR ($CDCl_3$, 500 MHz): δ = 6.14 (m, 2H, H-12, -13), 3.83 (s_{app}, 2H, H-5, -6), 2.65-2.59 (m, 2H, H-11, -14), 2.46 (d_{app}, 2H, H-4, -7), 2.38 (s_{app}, 2H, H-3, -8), 2.21 (br s, 2H, O-H), 2.01 (s_{app}, 2H, H-1, -10), 1.86 (d, 2H, H-2i, -9i), 0.76 (d, 2H, H-2o, -9o) ppm;

$^2J_{\text{H-2i, -2o}} = {}^2J_{\text{H-9i, -9o}} = 11.7$; $^3J_{\text{H-4, -7, H-5, -6}} = 11.7$ Hz.

^{13}C-NMR ($CDCl_3$, 100.7 MHz): δ = 134.0 (C-12, -13), 65.4 (C-5, -6), 53.6 (C-4, -7), 39.3 (C-11, -14), 38.0 (C-3, -8), 32.5 (C-1, -10), 28.3 (C-2, -9) ppm.

MS (EI, 70 eV): *m/z* (%) = 216 (0.02), 203.1 (15.6), 202.1 (100.0), 184.1 (7.7), 169.1 (9.8), 158.1 (7.7), 156.1 (9.4), 145.1 (7.5), 143.1 (10.4), 142.1 (10.2), 141.1 (7.8), 132.1 (11.9), 131.1 (25.4), 130.1 (19.7), 129.1 (20.9), 128.1 (11.7).

Spectra:

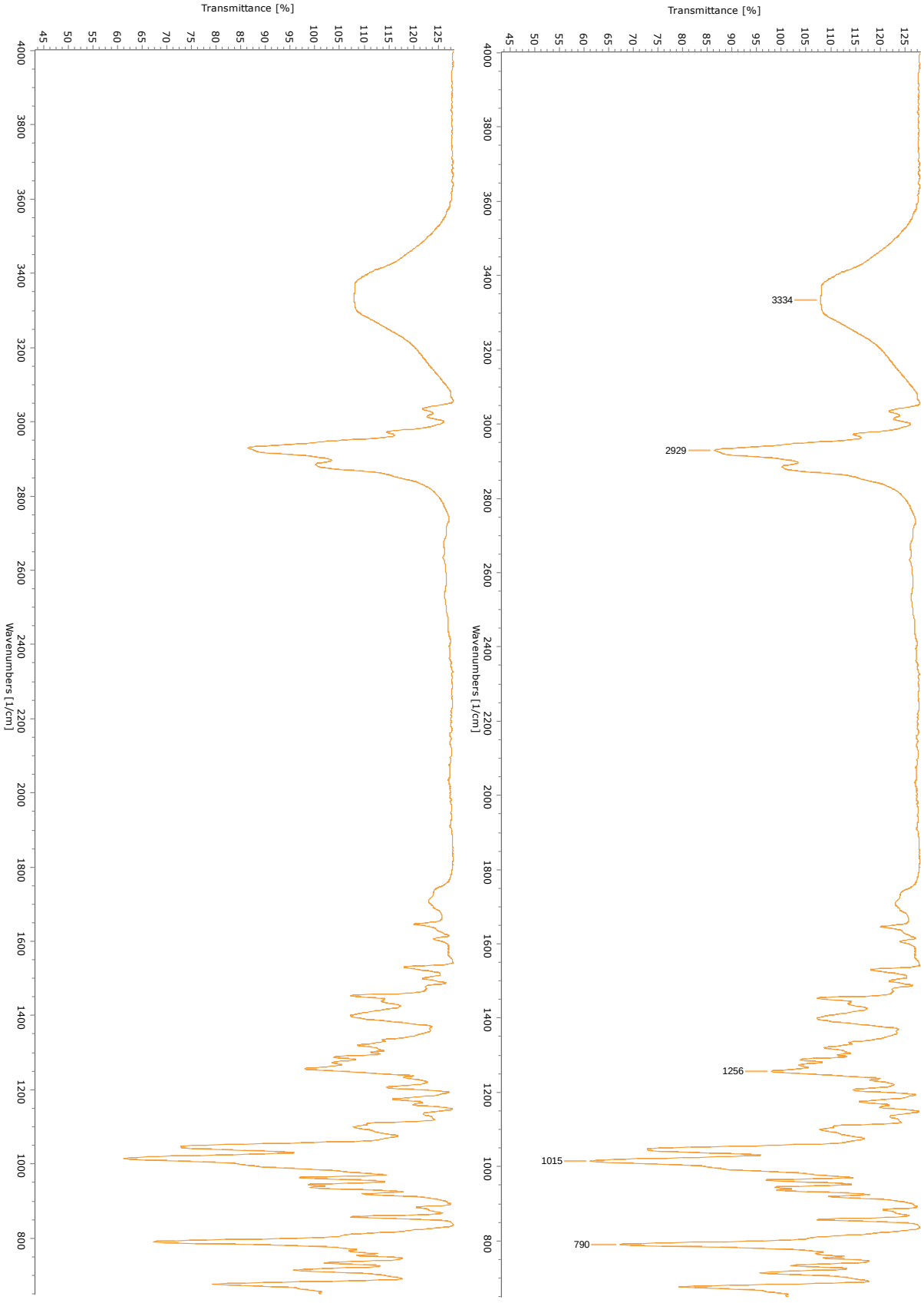
Transmittance [%]
Wavenumbers [1/cm]
3334
2929
1256
1015
790

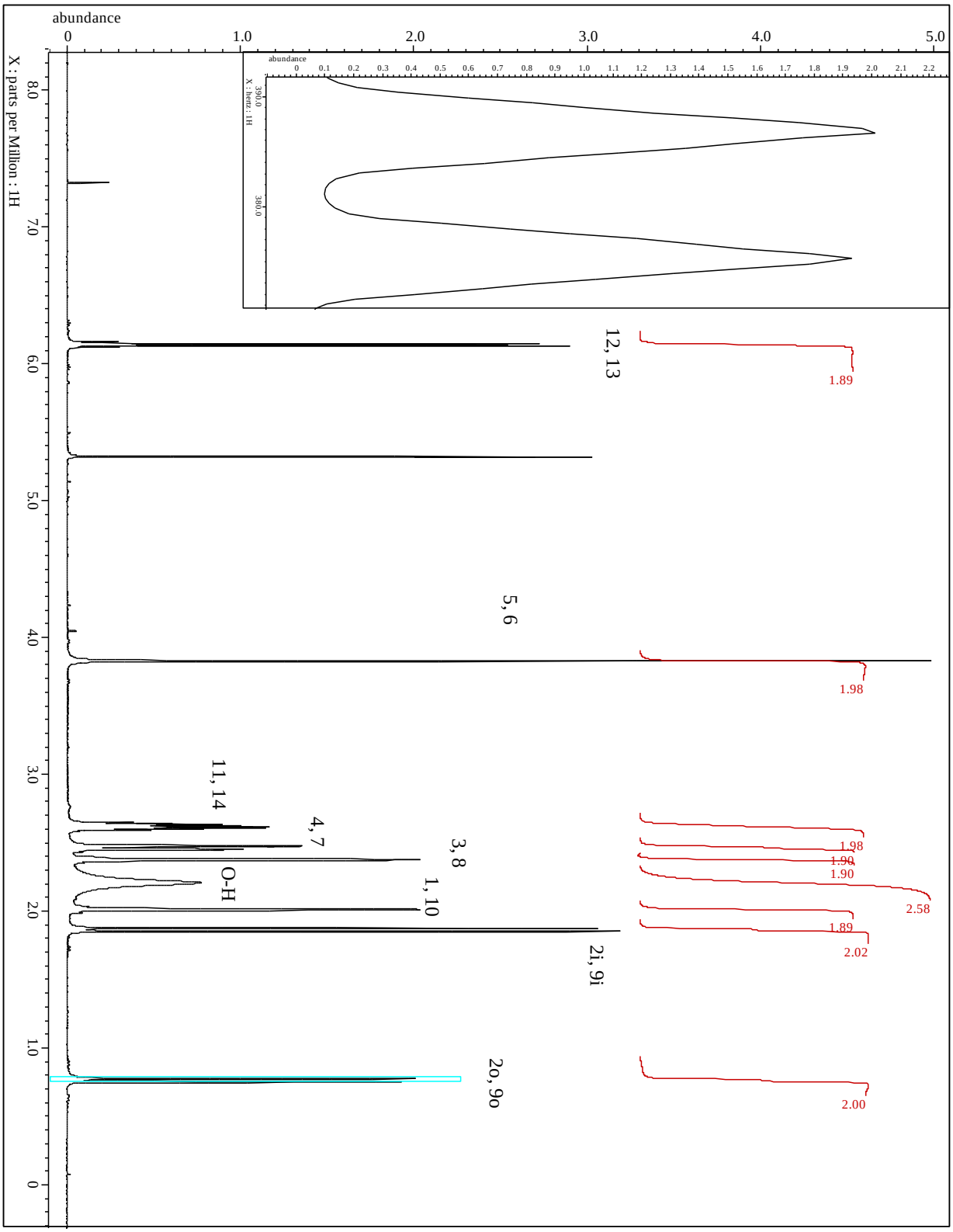
abundance
X : parts per Million : 1H
12, 13
5, 6
11, 14
4, 7
3, 8
O-H
1, 10
2i, 9i
2o, 9o
1.89
1.98
1.98
1.90
1.90
2.58
1.89
2.02
2.00
abundance
X : hertz : 1H
390.0
380.0

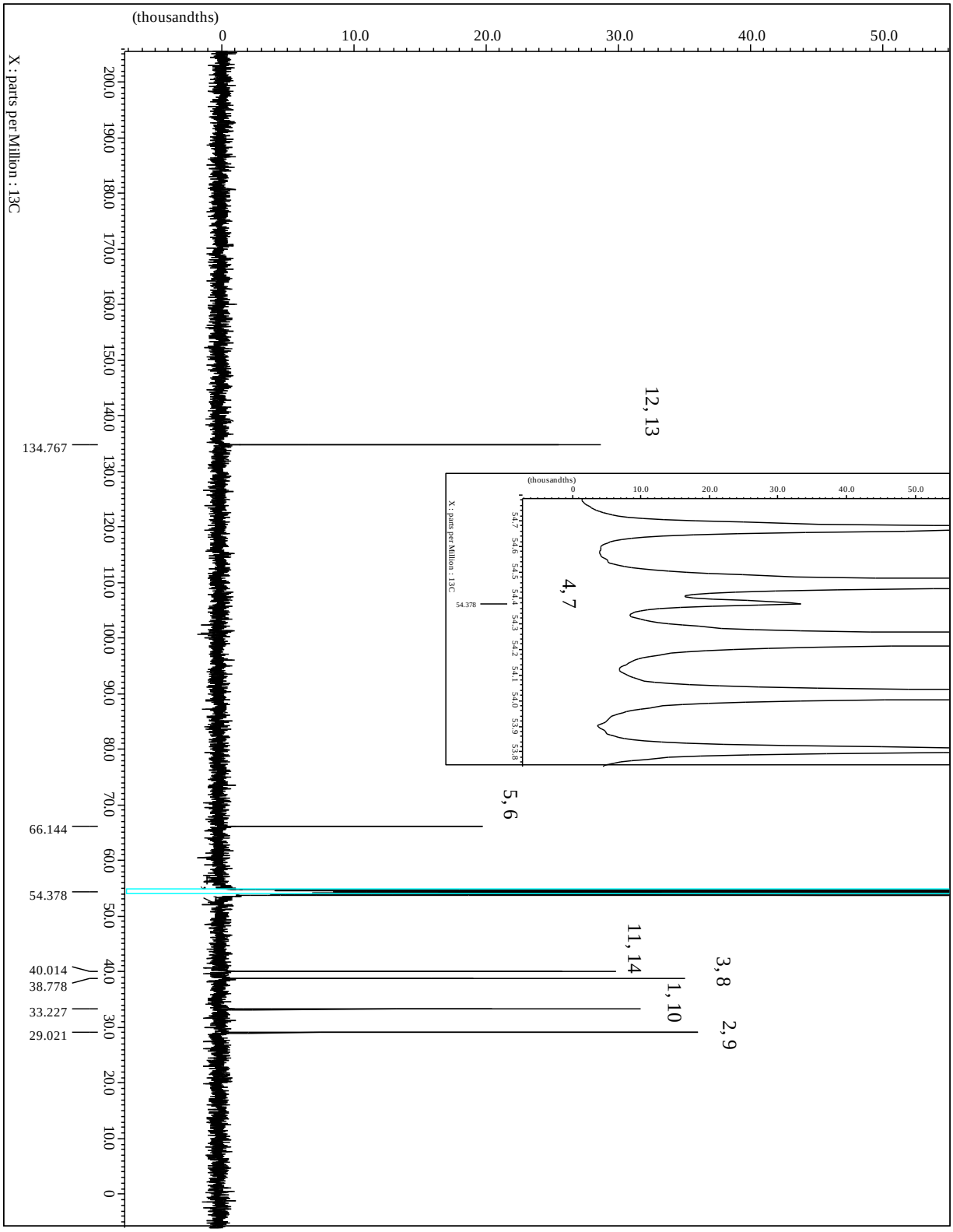
(thousandths)
0
10.0
20.0
30.0
40.0
50.0
X : parts per Million : 13C
200.0
190.0
180.0
170.0
160.0
150.0
140.0
130.0
120.0
110.0
100.0
90.0
80.0
70.0
60.0
50.0
40.0
30.0
20.0
10.0
0
134.767
66.144
54.378
40.014
38.778
33.227
29.021
12, 13
4, 7
5, 6
11, 14
3, 8
1, 10
2, 9
54.378

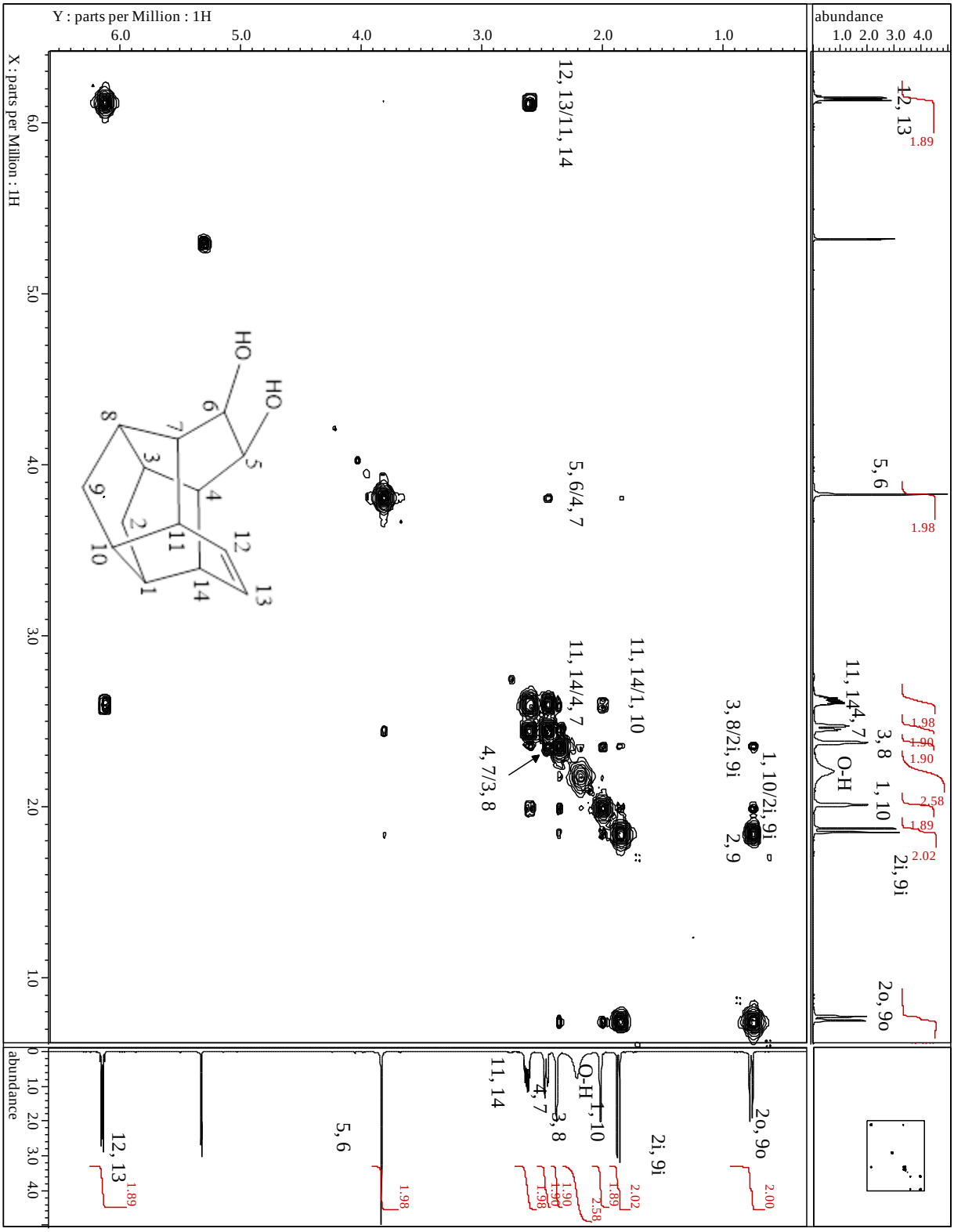
Y : parts per Million : 1H
X : parts per Million : 1H
abundance
12, 13
1.89
5, 6
1.98
11, 14
4, 7
3, 8
1, 10
O-H
2.58
1.89
2.02
2i, 9i
2o, 9o
12, 13/11, 14
5, 6/4, 7
11, 14/1, 10
1, 10/2i, 9i
3, 8/2i, 9i
2, 9
11, 14/4, 7
4, 7/3, 8
HO
HO
1
2
3
4
5
6
7
8
9
10
11
12
13
14

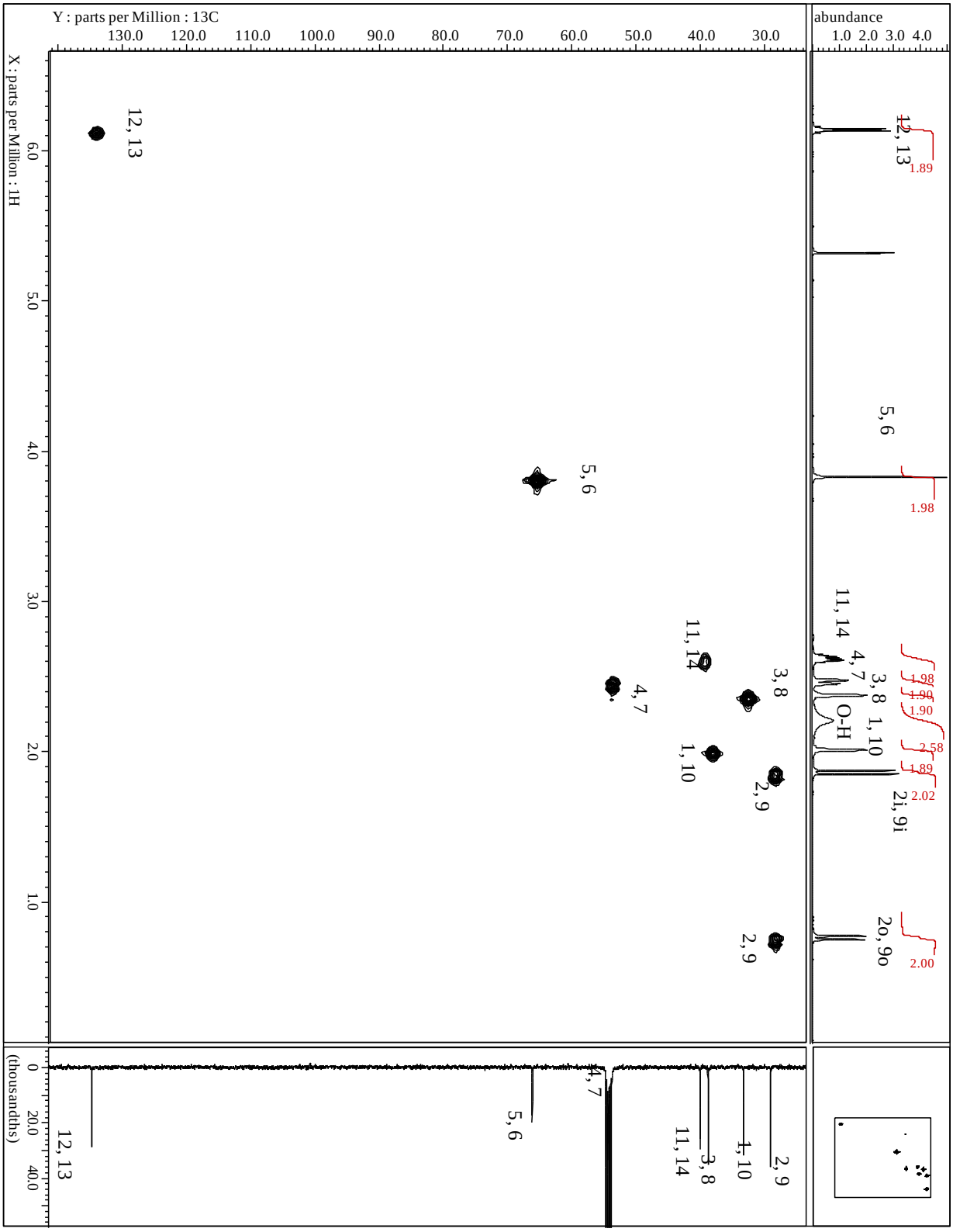
abundance
1.0 2.0 3.0 4.0
12, 13
1.89
5, 6
1.98
11, 14
4, 7
3, 8
1, 10
O-H
1.98
1.90
1.90
2.58
1.89
2i, 9i
2.02
2o, 9o
2.00
Y : parts per Million : 13C
130.0 120.0 110.0 100.0 90.0 80.0 70.0 60.0 50.0 40.0 30.0
X : parts per Million : 1H
6.0 5.0 4.0 3.0 2.0 1.0
12, 13
5, 6
4, 7
11, 14
3, 8
1, 10
2, 9
(thousandths)
0 20.0 40.0

Pentacyclo[8.4.0.0^{3,8}.0^{4,14}.0^{7,11}]tetradecane-5,6-diol (219)

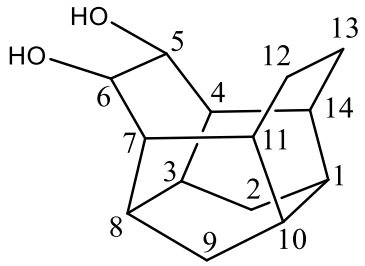

$C_{14}H_{20}O_2$ (220)

MP = Decomposition at at 260.0 °C (decomposition product(s) melted at 269.0-270.0 °C) (DCM)

IR (AT-IR): $\tilde{\nu}$ = 3342 (br m, O-H), 2918 (s, C-H), 1705 (w), 1453 (m), 1261 (m), 1038 (s), 805 (m) cm^{-1}.

^{1}H-NMR ($CDCl_3$, 500 MHz): δ = 4.18 (s_{app}, 2H, H-5, -6), 2.63 (br s, 2H, O-H), 2.35 (s_{app}, 2H, H-3, -8), 2.17 (s_{app}, 2H, H-1, -10), 1.99 (s_{app}, 4H, H-4, -7; H-11, -14), 1.84 (d, 2H, H-2i, -9i), 1.68 (s_{app}, 4H, H-12, -13), 0.62 (d, 2H, H-2o, -9o) ppm;

$^{2}J_{H\text{-}2i,\ -2o} = {}^{2}J_{H\text{-}9i,\ -9o}$ = 11.5 Hz.

^{13}C-NMR ($CDCl_3$, 100.7 MHz): δ = 66.0 (C-5, -6), 45.1 (C-4, -7), 37.2 (C-1, -10), 35.9 (C-11, -14), 32.8 (C-3, -8), 27.9 (C-2, -9), 19.1 (C-12, -13) ppm.

MS (EI, 70 eV): *m/z* (%) = 220 (20.0) [M$^{\cdot+}$], 202 (33.2), 201 (10.1), 174 (8.9), 173 (16.7), 169 (7.7), 161 (9.6), 159 (12.3), 147 (11.4), 146 (13.9), 145 (26.3), 144 (8.5), 143 (12.1), 142 (8.3), 137 (13.3), 135 (8.6), 134 (10.3), 133 (17.5), 132 (14.0), 131 (25.8), 130 (13.4), 129 (24.3), 128 (12.0), 124 (30.5), 123 (20.3), 122 (15.2), 121 (19.5), 120 (23.1), 119 (22.1), 118 (13.5), 117 (38.2), 116 (9.9), 115 (18.4), 111 (19.0), 110 (33.6), 109 (17.2), 108 (30.9), 107 (33.8), 106 (14.9), 105 (31.4), 104 (18.5), 103 (9.8), 97 (19.0), 96 (16.7), 95 (40.0), 94 (30.4), 93 (43.9), 92 (33.6), 91

(100.0), 83 (21.2), 82 (8.6), 81 (33.6), 80 (27.9), 79 (84.7), 78 (25.3), 77 (64.5), 70 (17.0), 69 (12.4), 67 (34.8), 66 (14.7), 65 (23.9), 57 (10.7), 55 (29.2), 53 (21.1), 51 (10.6).

Spectra:

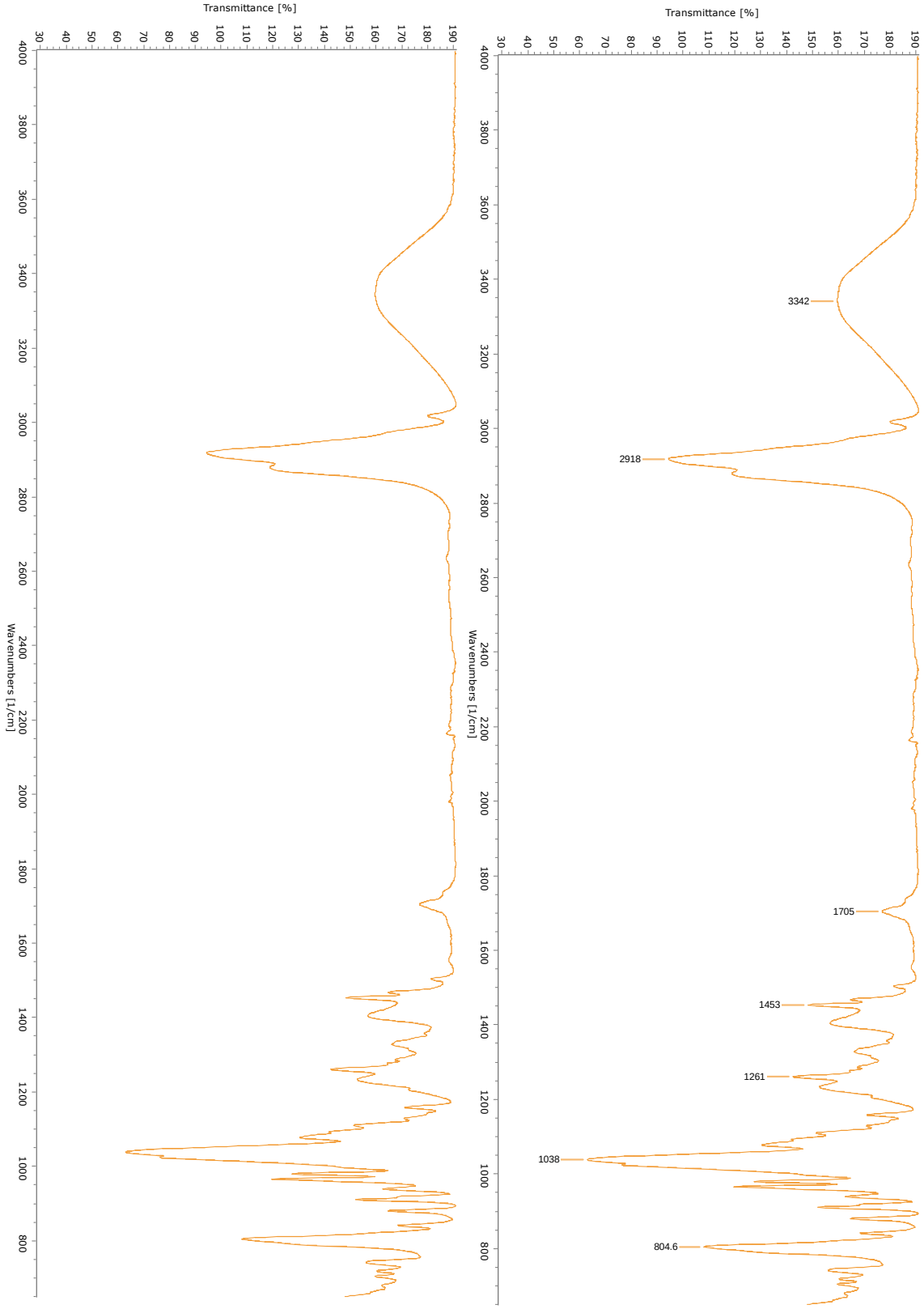
Transmittance [%]
Wavenumbers [1/cm]
3342
2918
1705
1453
1261
1038
804.6

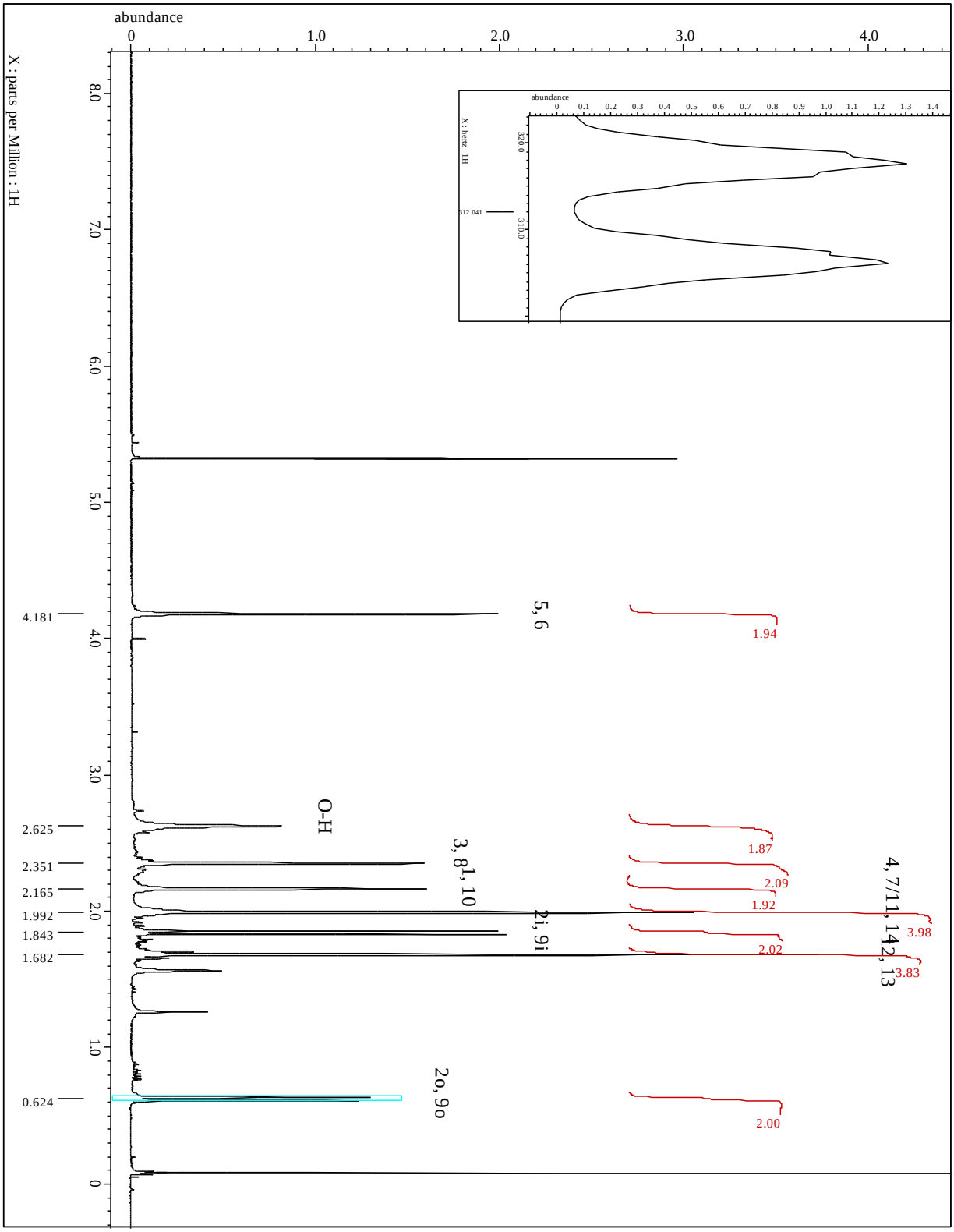
abundance
X : parts per Million : 1H
4.181
2.625
2.351
2.165
1.992
1.843
1.682
0.624
5, 6
O-H
3, 8
1, 10
2i, 9i
2o, 9o
4, 7/11, 12, 13
1.94
1.87
2.09
1.92
3.98
2.02
3.83
2.00
X : hertz : 1H
320.0
312.041
310.0

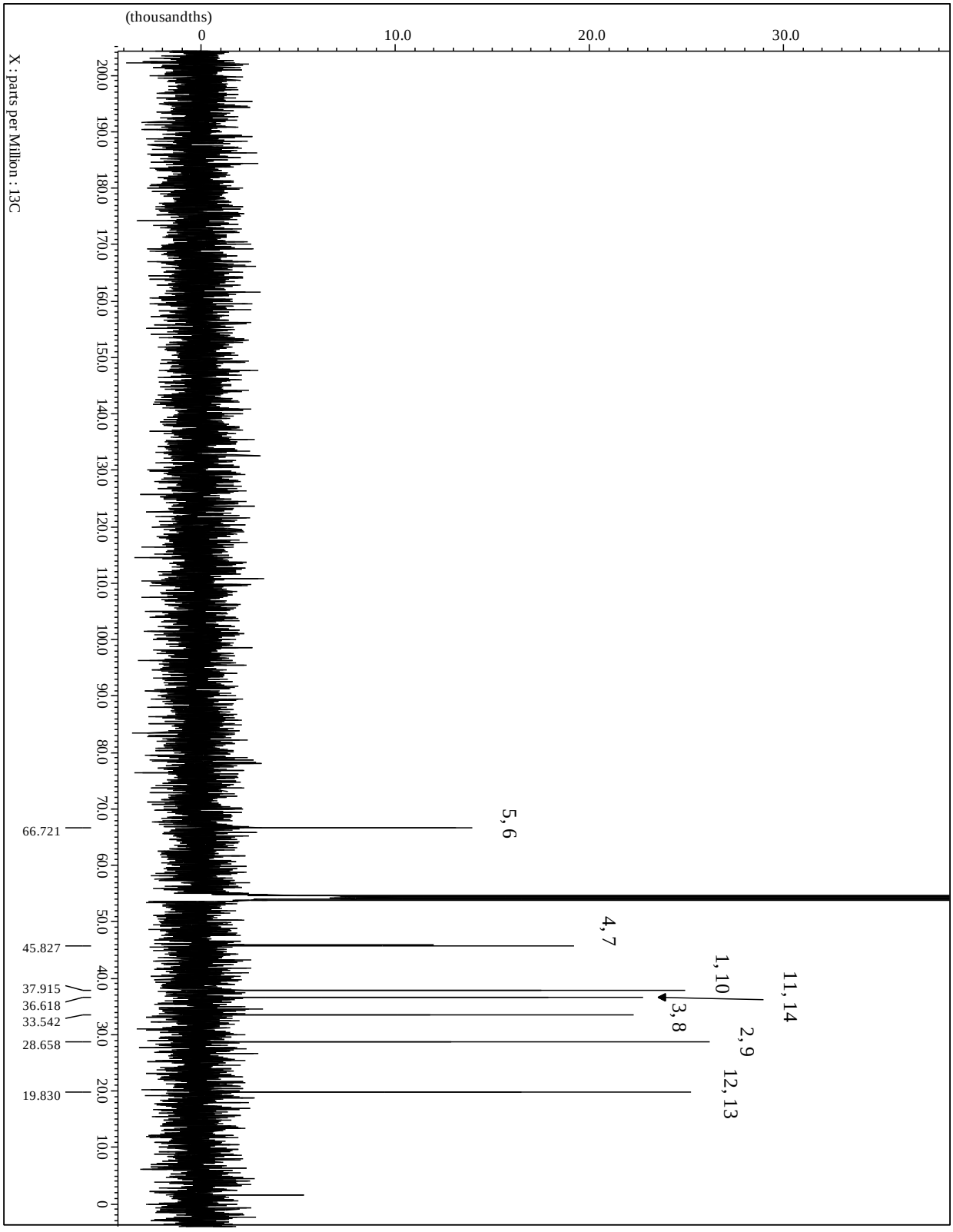
(thousandths)
0
10.0
20.0
30.0
X : parts per Million : 13C
200.0
190.0
180.0
170.0
160.0
150.0
140.0
130.0
120.0
110.0
100.0
90.0
80.0
70.0
60.0
50.0
40.0
30.0
20.0
10.0
0
66.721
45.827
37.915
36.618
33.542
28.658
19.830
5, 6
4, 7
1, 10
3, 8
11, 14
2, 9
12, 13

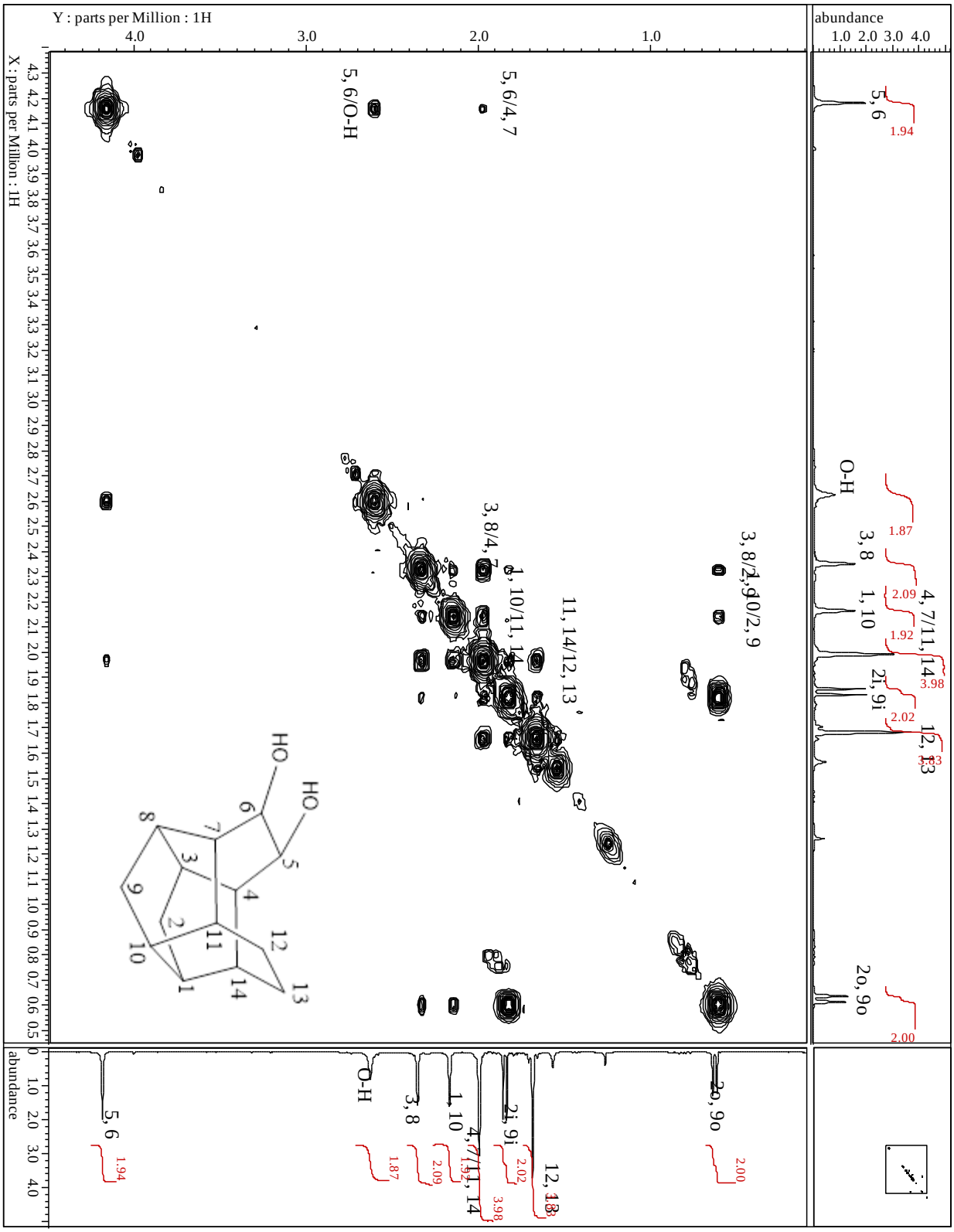
abundance
1.0 2.0 3.0 4.0
5, 6
1.94
O-H
1.87
3, 8
2.09
1, 10
1.92
4, 7/11, 14
3.98
2i, 9i
2.02
12, 13
2o, 9o
2.00
Y : parts per Million : 1H
4.0
3.0
2.0
1.0
5, 6/O-H
5, 6/4, 7
3, 8/4, 7
1, 10/11, 14
11, 14/12, 13
3, 8/2, 9
1, 10/2, 9
HO
HO
1
2
3
4
5
6
7
8
9
10
11
12
13
14
X : parts per Million : 1H
4.3 4.2 4.1 4.0 3.9 3.8 3.7 3.6 3.5 3.4 3.3 3.2 3.1 3.0 2.9 2.8 2.7 2.6 2.5 2.4 2.3 2.2 2.1 2.0 1.9 1.8 1.7 1.6 1.5 1.4 1.3 1.2 1.1 1.0 0.9 0.8 0.7 0.6 0.5
abundance
0 1.0 2.0 3.0 4.0

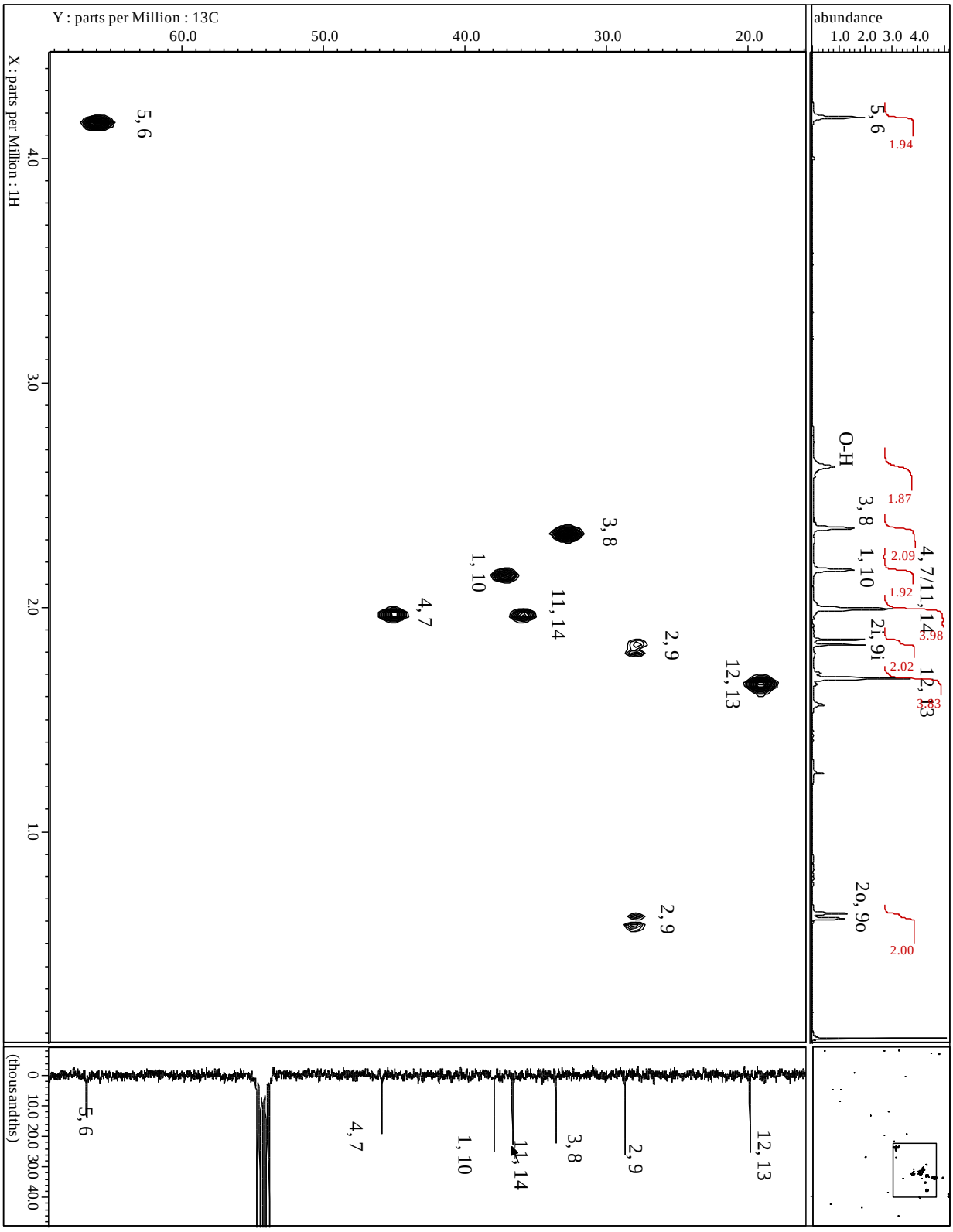
Y : parts per Million : 13C
60.0
50.0
40.0
30.0
20.0
X : parts per Million : 1H
4.0
3.0
2.0
1.0
abundance
1.0 2.0 3.0 4.0
5, 6
1.94
O-H
1.87
3, 8
1, 10
2.09
4, 7/11, 14
1.92
3.98
2i, 9i
2.02
12, 13
1.83
2.00
2o, 9o
(thousandths)
0 10.0 20.0 30.0 40.0

5.5.2 Preparation of Ene-Dione **222** and Saturated Dione **225**

General procedure for Swern Oxidation: Under inert atmosphere, DMSO (0.699 mL, 0.275 mmol) in DCM (1.71 mL) was cooled to -78 °C. TFAA (0.120 mL, 0.816 mmol) was added and stirred for 15 minutes. To the cooled solution, **174** (60 mg, 0.275 mmol) in DCM (0.57 mL) was added and stirred for 2 hours at -78 °C. Et_3N was then added and stirred an additional 2 hours at -78 °C. The reaction was then warmed to room temperature, stretched with water, and extracted with EtOAc (3x20 mL). The combined organic phase was washed with water (15 mL) and sat. $NaHCO_3$ solution (2x15 mL). The organic phase was dried ($MgSO_4$) and concentrated to afford yellow crystalline material (153 mg). Purification by column chromatography (SiO_2, 5:1 Hexanes: EtOAc) yielded pure dione **222** (30 mg, 51%). Mixed fractions containing dione **222** and tautomers **223** and **224** were also collected (30 mg).

Pentacyclo[8.4.0.0^{3,8}.0^{4,14}.0^{7,11}]tetradec-12-ene-5,6-dione (222)

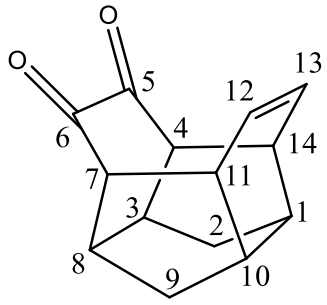

$C_{14}H_{14}O_2$ (214), R_f = 0.35 by SiO_2-TLC; visualized by UV or vanillin stain

MP = decomposition at 230.0 ° C (decomposition product(s) melted at 248.8-249.0 ° C) ($CDCl_3$)

IR (AT-IR): $\tilde{\nu}$ = 2958 (m, C-H), 1706 (s, C=O), 1456 (w, C-C), 1140 (m), 686 (m) cm^{-1}.

^{1}H-NMR ($CDCl_3$, 500 MHz): δ = 6.24 (m, 2H, H-12, -13), 3.14 (s_{app}, 4H, H-4, -7; H-11, -14), 2.79 (s_{app}, 2H, H-3, -8), 2.36 (s_{app}, 2H, H-1, -10), 2.05 (d, 2H, H-2i, -9i), 1.04 (d, 2H, H-2o, -9o) ppm;

$^{2}J_{\text{H-2i, -2o}} = {}^{2}J_{\text{H-9i, -9o}} = 12.1$ Hz.

^{13}C-NMR ($CDCl_3$, 100.7 MHz): δ = 198.0 (C-5, -6), 130.1 (c-12, -13). 56.6 (C-4, -7), 41.1 (C-11, -14). 39.2 (C-3, -8), 37.6 (C-1, -10). 29.3 (C-2, -9) ppm.

MS (EI, 70 eV): *m/z* (%) = 216 (47.0) [$M^{\cdot+}$+2], 214 (31.1) [$M^{\cdot+}$], 158 (10.4), 145 (9.2), 143 (8.2), 142 (8.9), 132 (9.8), 131 (22.8), 130 (35.9), 129 (33.2), 128 (16.6), 120 (20.1), 119 (8.8), 118 (12.0), 117 (38.0), 116 (11.6), 115 (27.0), 108 (9.7), 107 (21.0), 106 (17.2), 105 (21.2), 104 (21.3), 103 (9.4), 96 (14.0), 95 (38.3), 94 (21.9), 93 (19.8), 92 (77.9), 91 (100.0), 83 (12.4), 82 (18.9), 81 (12.1), 80 (30.5), 79 (57.5), 78 (24.6), 77 (47.1), 68 (13.9), 67 (16.6), 66 (24.0), 65 (24.3), 63 (8.2), 55 (9.4), 53 (16.3), 52 (9.7), 51 (15.6).

Spectra:

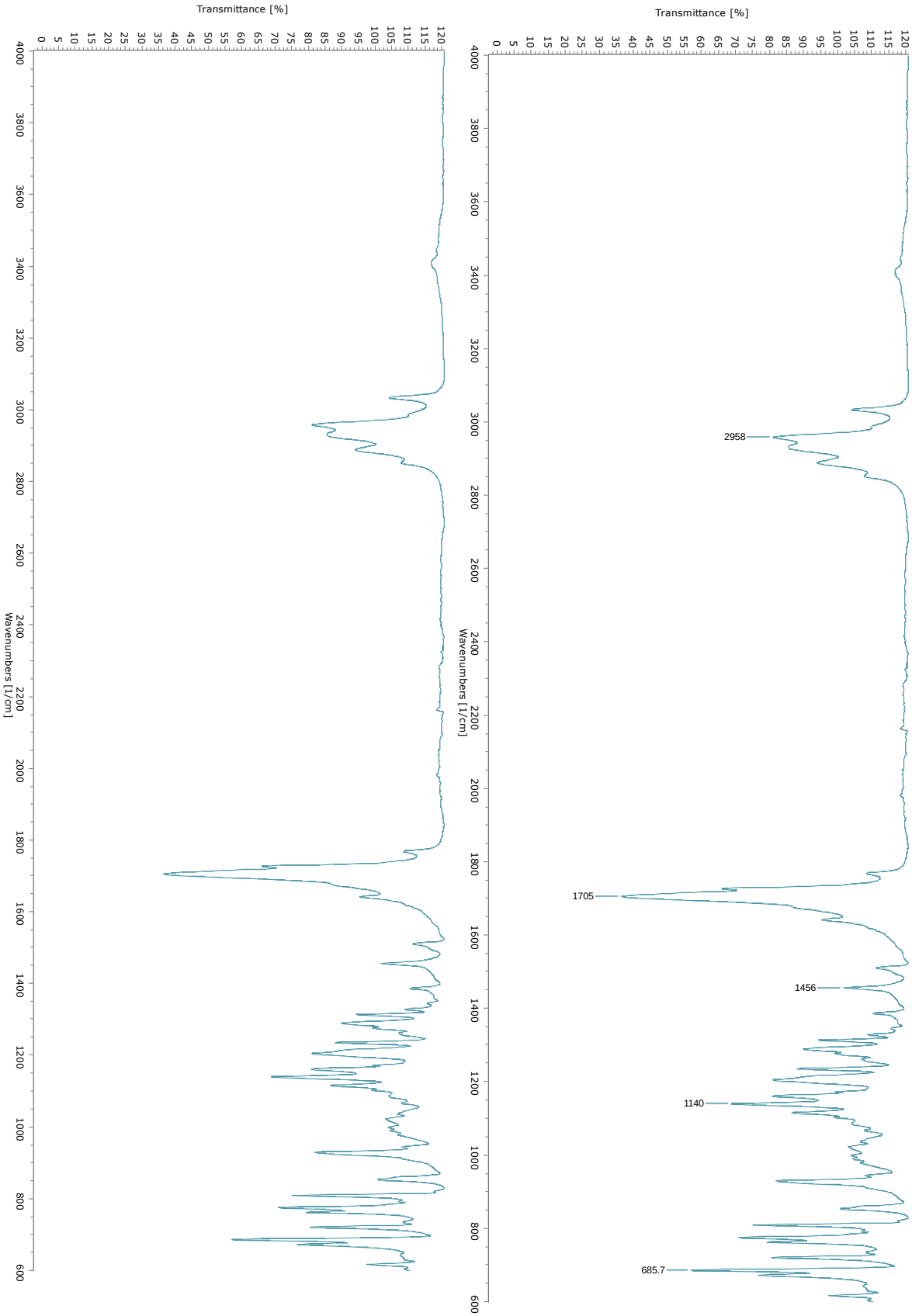
Transmittance [%]
Wavenumbers [1/cm]
2958
1705
1456
1140
685.7

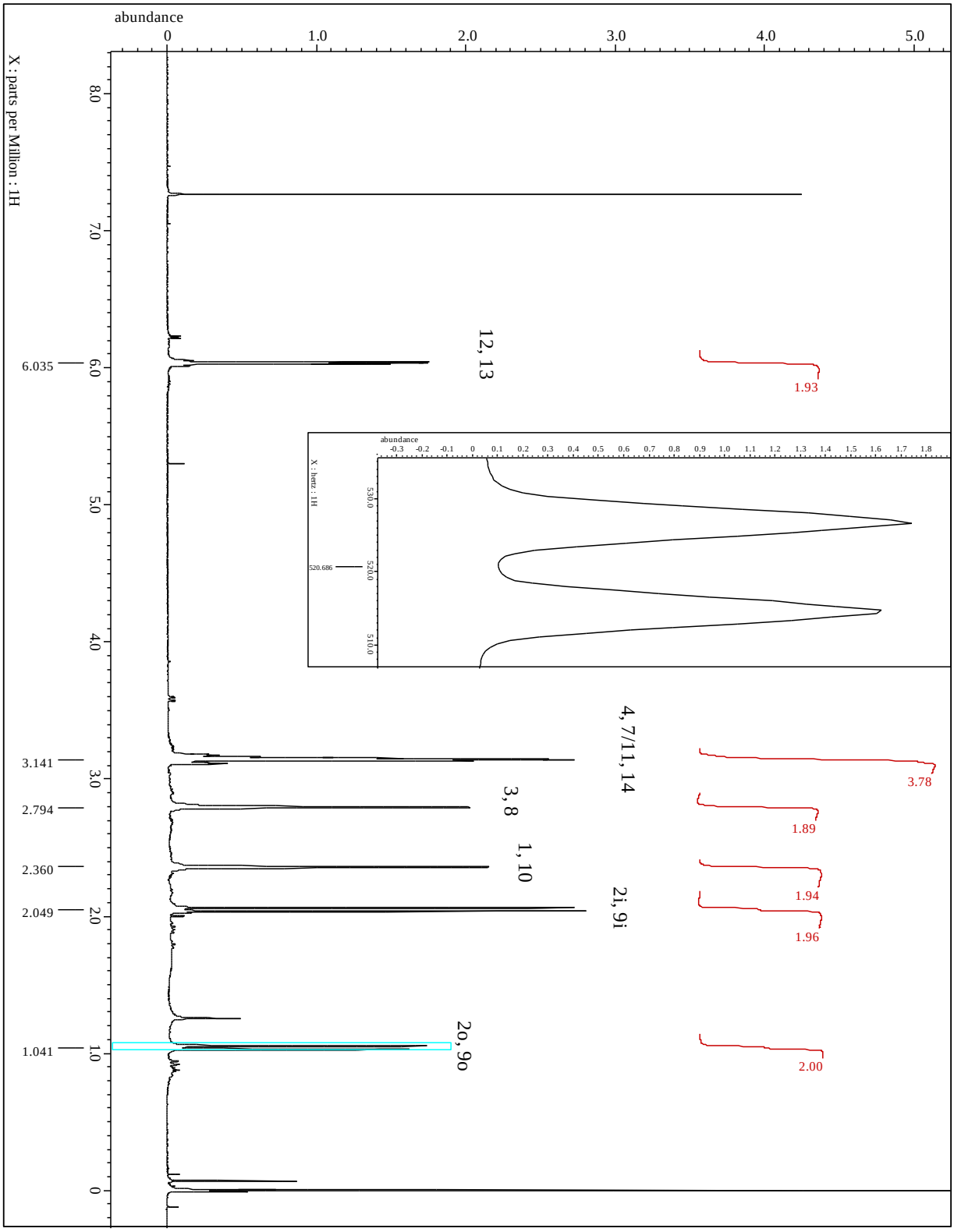
abundance
0
1.0
2.0
3.0
4.0
5.0
X : parts per Million : 1H
8.0
7.0
6.0
5.0
4.0
3.0
2.0
1.0
0
6.035
3.141
2.794
2.360
2.049
1.041
12, 13
1.93
4, 7/11, 14
3.78
3, 8
1.89
1, 10
1.94
2i, 9i
1.96
2o, 9o
2.00
abundance
X : hertz : 1H
530.0
520.686
520.0
510.0

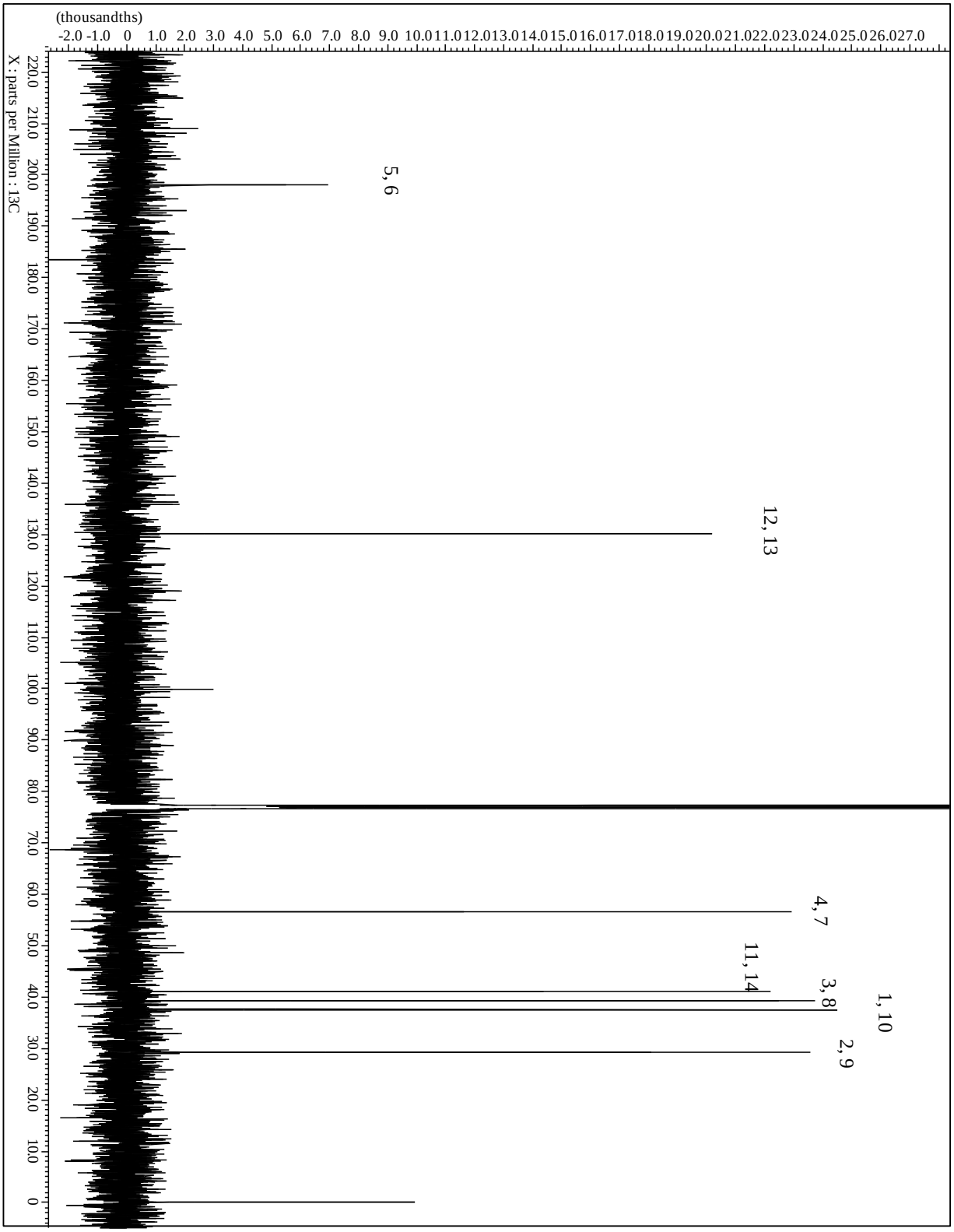
(thousandths)
-2.0 -1.0 0 1.0 2.0 3.0 4.0 5.0 6.0 7.0 8.0 9.0 10.0 11.0 12.0 13.0 14.0 15.0 16.0 17.0 18.0 19.0 20.0 21.0 22.0 23.0 24.0 25.0 26.0 27.0
X : parts per Million : 13C
220.0 210.0 200.0 190.0 180.0 170.0 160.0 150.0 140.0 130.0 120.0 110.0 100.0 90.0 80.0 70.0 60.0 50.0 40.0 30.0 20.0 10.0 0
5, 6
12, 13
4, 7
11, 14
3, 8
1, 10
2, 9

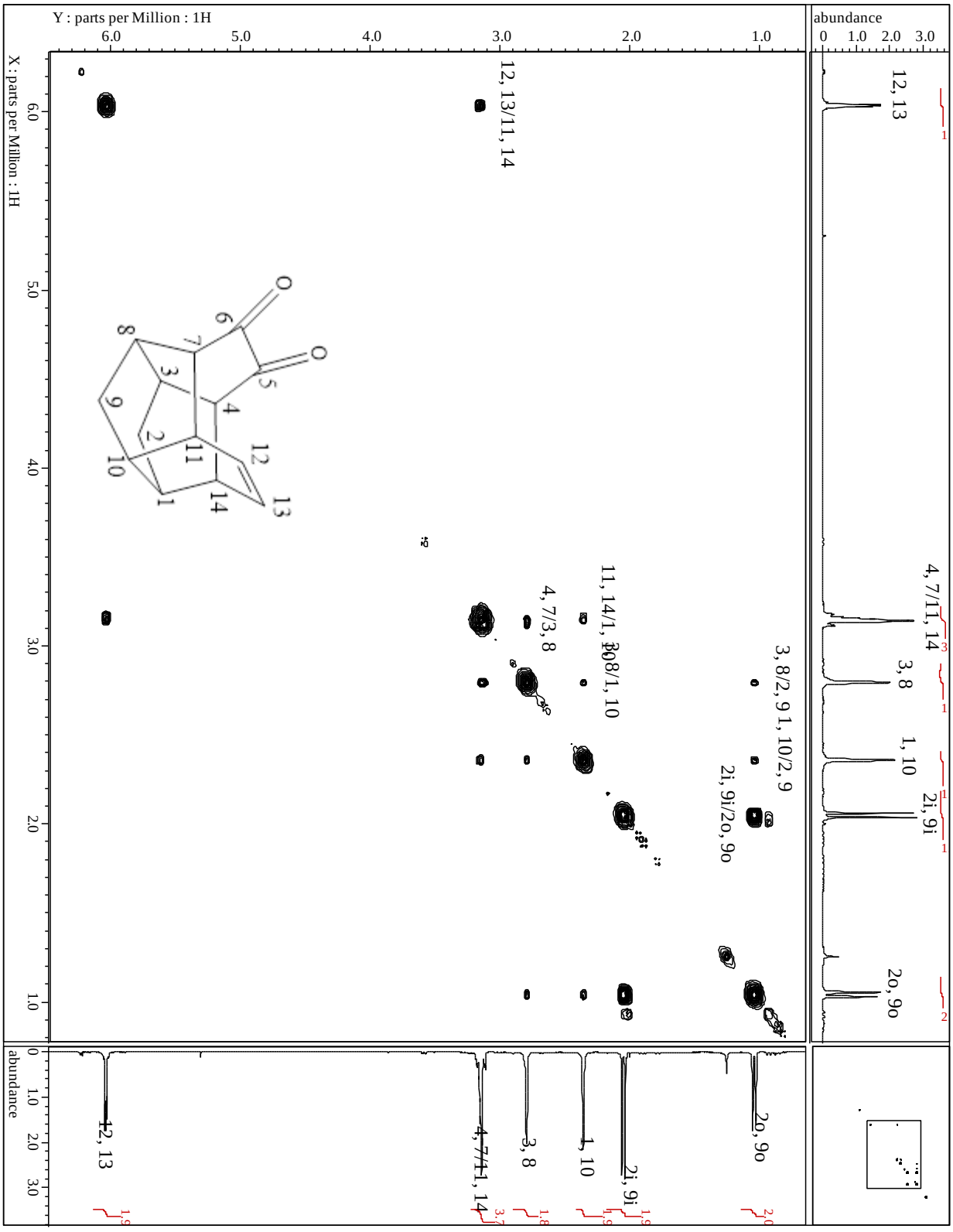
abundance
0 1.0 2.0 3.0
12, 13
4, 7/11, 14
3, 8
1, 10
2i, 9i
2o, 9o
Y : parts per Million : 1H
6.0 5.0 4.0 3.0 2.0 1.0
X : parts per Million : 1H
6.0 5.0 4.0 3.0 2.0 1.0
12, 13/11, 14
4, 7/3, 8
11, 14/1, 10
3, 8/2, 9
1, 10/2, 9
2i, 9i/2o, 9o
O
O
1
2
3
4
5
6
7
8
9
10
11
12
13
14
abundance
0 1.0 2.0 3.0
2o, 9o
1, 10
2i, 9i
3, 8
4, 7/11, 14
12, 13

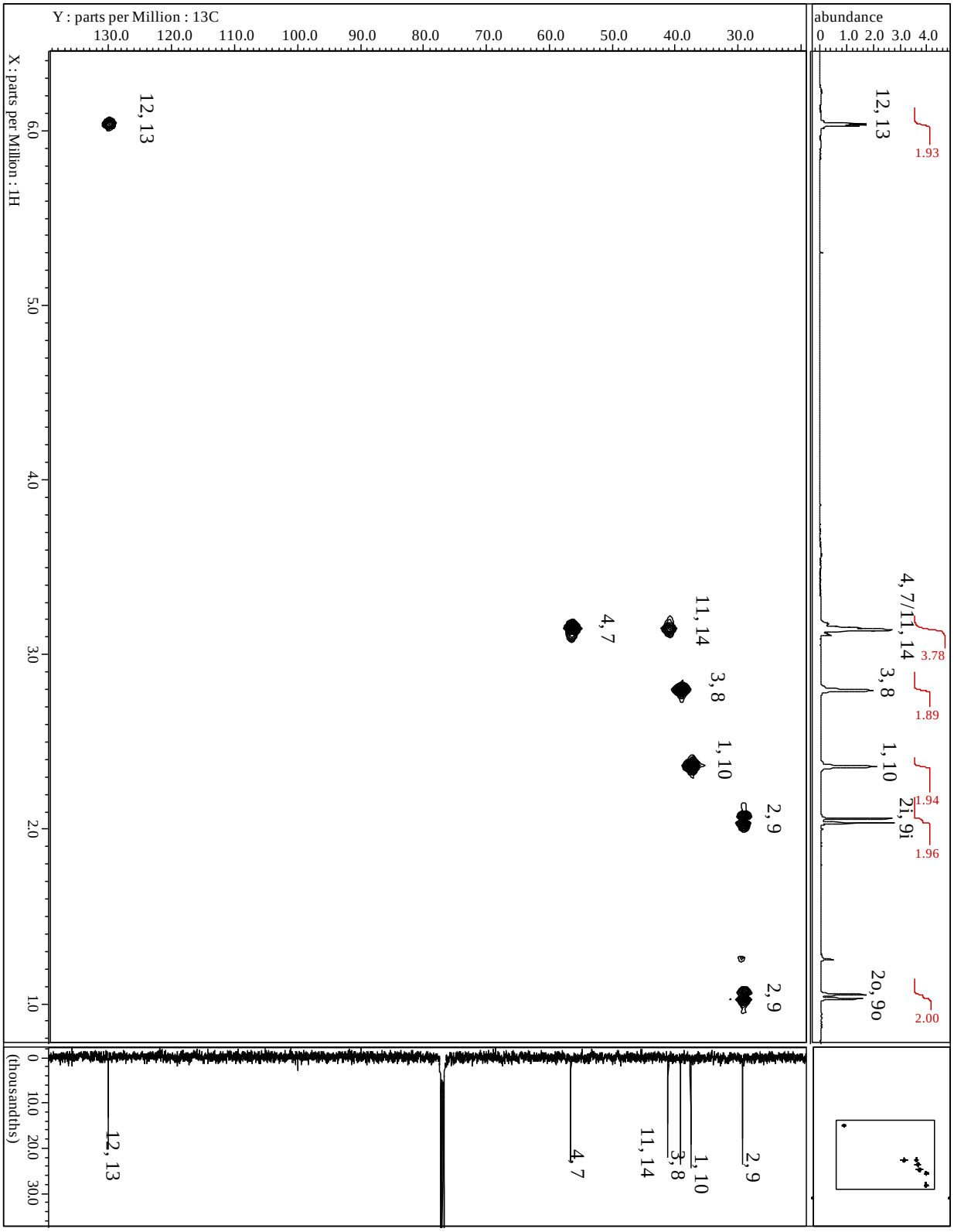
Y : parts per Million : 13C
X : parts per Million : 1H
abundance
(thousandths)
12, 13
4, 7/11, 14
3, 8
1, 10
2i, 9i
2o, 9o
2, 9
4, 7
11, 14
1.93
3.78
1.89
1.94
1.96
2.00

Pentacyclo[8.4.0.0^{3,8}.0^{4,14}.0^{7,11}]tetradecane-5,6-dione (225)

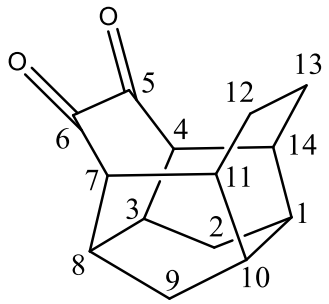

$C_{14}H_{16}O_2$ (216), R_f = 0.40 by SiO_2-TLC; visualized by UV or vanillin stain

MP = Decomposition at 201.0 °C (Decomposition product(s) melted at 285.7-286.4 ° C) ($CDCl_3$)

IR (AT-IR): $\tilde{\nu}$ = 2929 (m, C-H), 1706 (s, C=O), 1455 (w, C-C), 1132 (m), 800 (m) cm^{-1}.

^{1}H-NMR ($CDCl_3$, 500 MHz): δ = 3.00 (d, 2H, H-4, -7), 2.76 (s_{app}, 2H, H-3, -8), 2.46 (s_{app}, 4H, H-1, -10; H-11, -14), 2.05 (d, 2H, H-2i, 9i), 1.83 (d, 2H, H-12i, -13i), 1.48 (d, 2H, H-12o, -13o), 0.93 (d, 2H, H-2o, 9o) ppm;

$^2J_{H\text{-}2i,\,\text{-}2o} = {}^2J_{H\text{-}9i,\,\text{-}9o}$ = 12.1 Hz.

^{13}C-NMR ($CDCl_3$, 100.7 MHz): δ = 200.4 (C-5, -6), 56.3 (C-4, -7), 39.0 (C-3, -8), 38.9 (C-11, -14), 35.8 (C-1, -10), 29.3 (C-2, -9), 18.9 (C-12, -13) ppm.

MS (EI, 70 eV): *m/z* (%) = 217 (14.4) [$M^{\cdot+}$+1], 216 (92.3) [$M^{\cdot+}$], 188 (13.2), 160 (8.7), 146 (8.1), 145 (14.3), 144 (7.7), 142 (10.7), 134 (7.6), 132 (15.7), 131 (36.9), 130 (50.9), 129 (29.7), 128 (10.8), 120 (34.5), 119 (15.5), 118 (15.5), 117 (40.5), 116 (9.8), 115 (17.9), 108 (14.4), 107 (36.0), 106 (30.3), 105 (23.1), 104 (18.9), 103 (10.0), 97 (11.3), 96 (28.6), 95 (57.9), 94 (38.3), 93 (24.5), 92 (39.9), 91 (100.0), 83 (25.2), 82 (38.4), 81 (19.4), 80 (27.5), 79 (87.7), 78 (31.0), 77 (66.5), 68 (13.4), 67 (22.6), 66 (24.6), 65 (31.9), 63 (8.3), 55 (14.9), 53 (24.0), 52 (10.3), 51 (17.5).

Spectra:

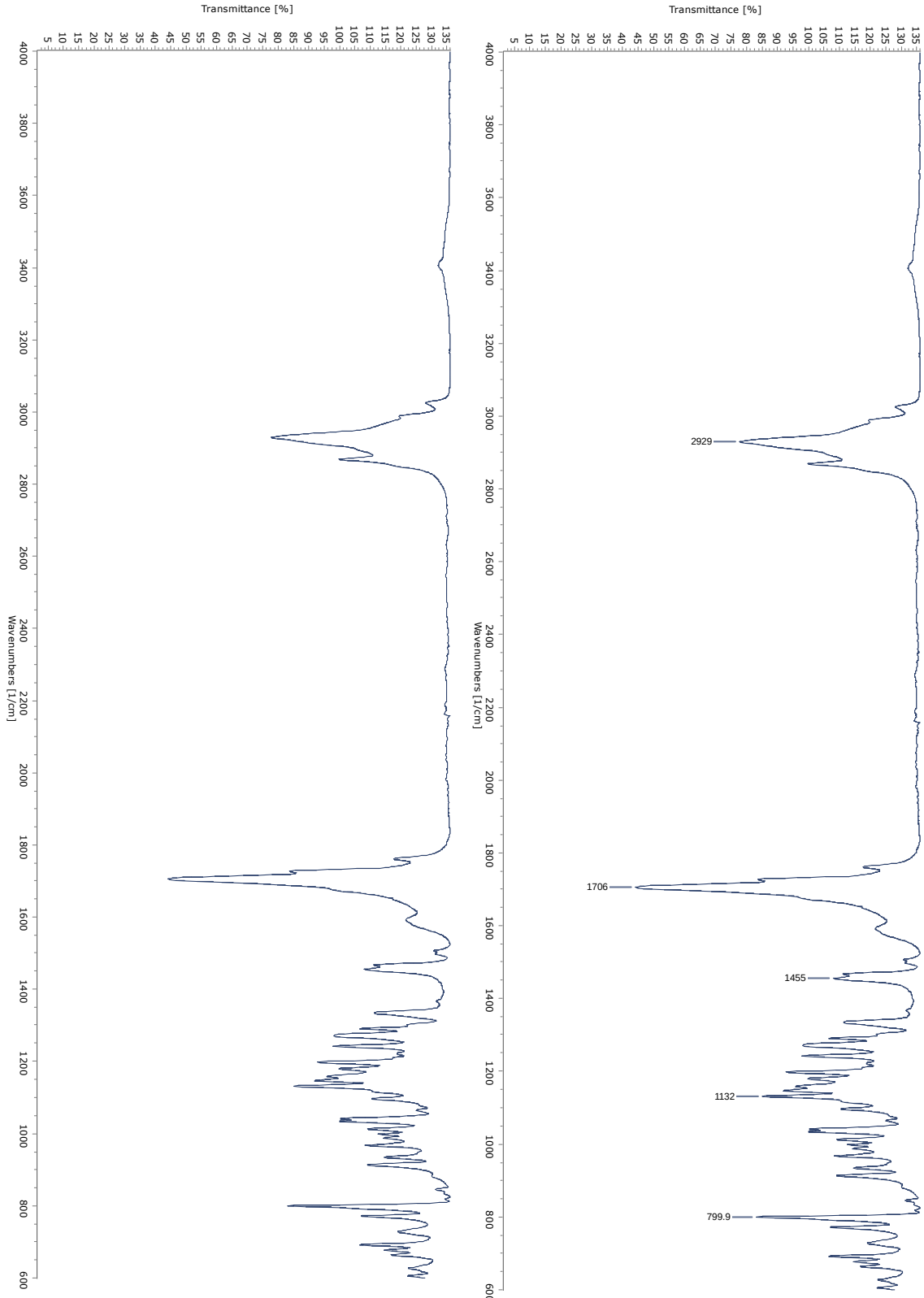

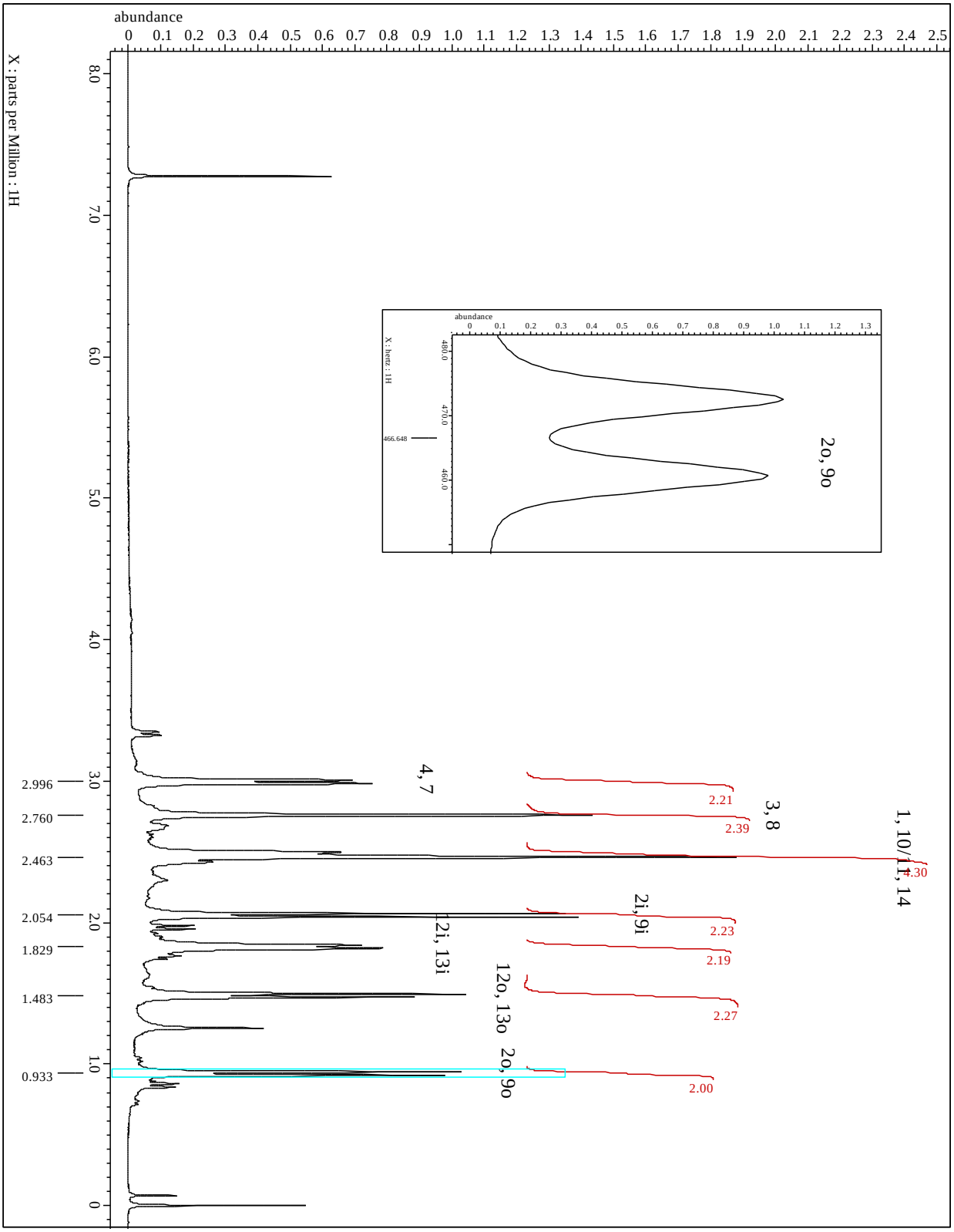
abundance
X : parts per Million : 1H
2.996
2.760
2.463
2.054
1.829
1.483
0.933
4, 7
12i, 13i
12o, 13o
2o, 9o
2i, 9i
3, 8
1, 10/11, 14
2.21
2.39
4.30
2.23
2.19
2.27
2.00
abundance
X : hertz : 1H
466.648
2o, 9o

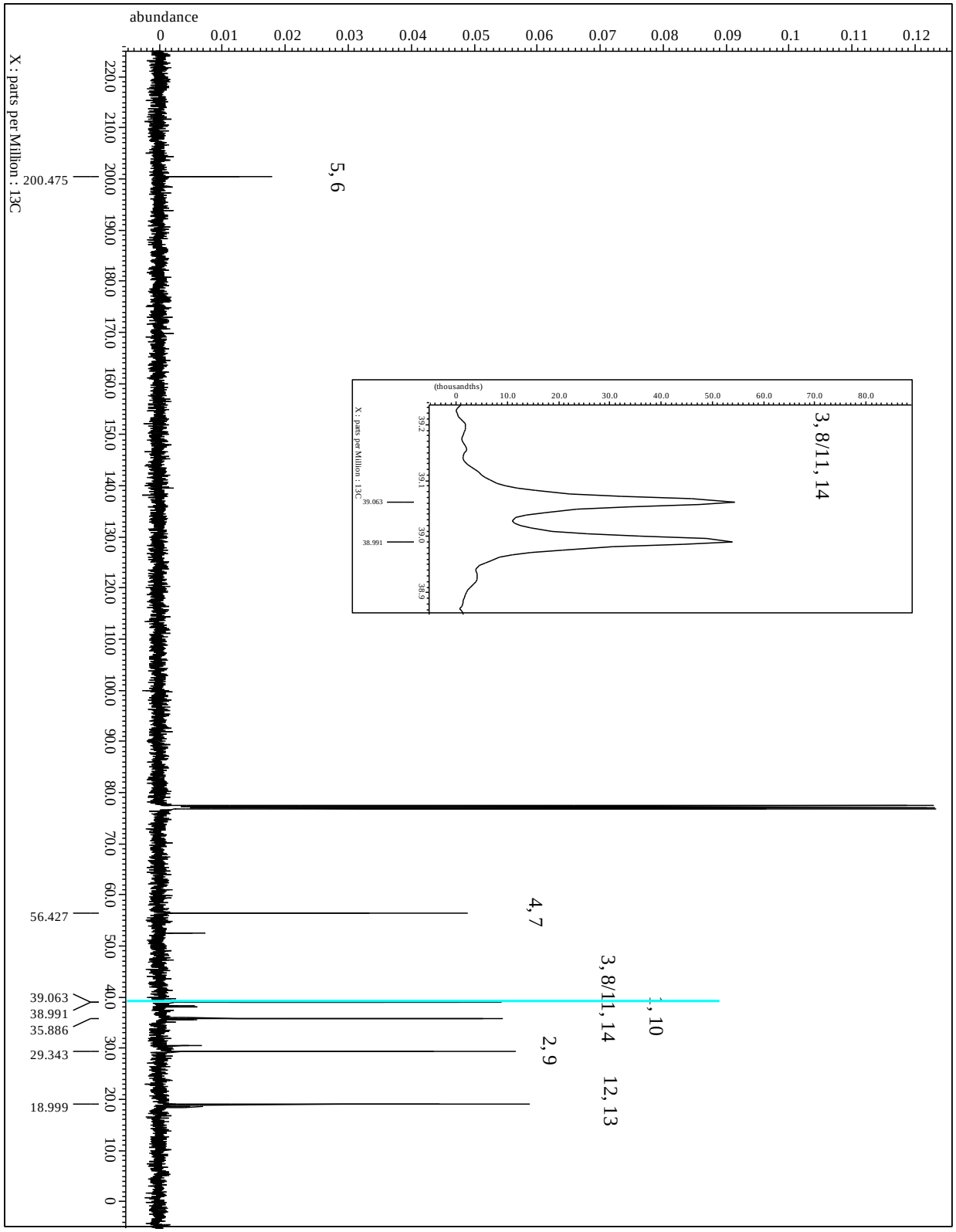
abundance
0
0.01
0.02
0.03
0.04
0.05
0.06
0.07
0.08
0.09
0.1
0.11
0.12
X : parts per Million : 13C
200.475
56.427
39.063
38.991
35.886
29.343
18.999
5, 6
4, 7
3, 8/11, 14
1, 10
2, 9
12, 13
(thousandths)
39.063
38.991

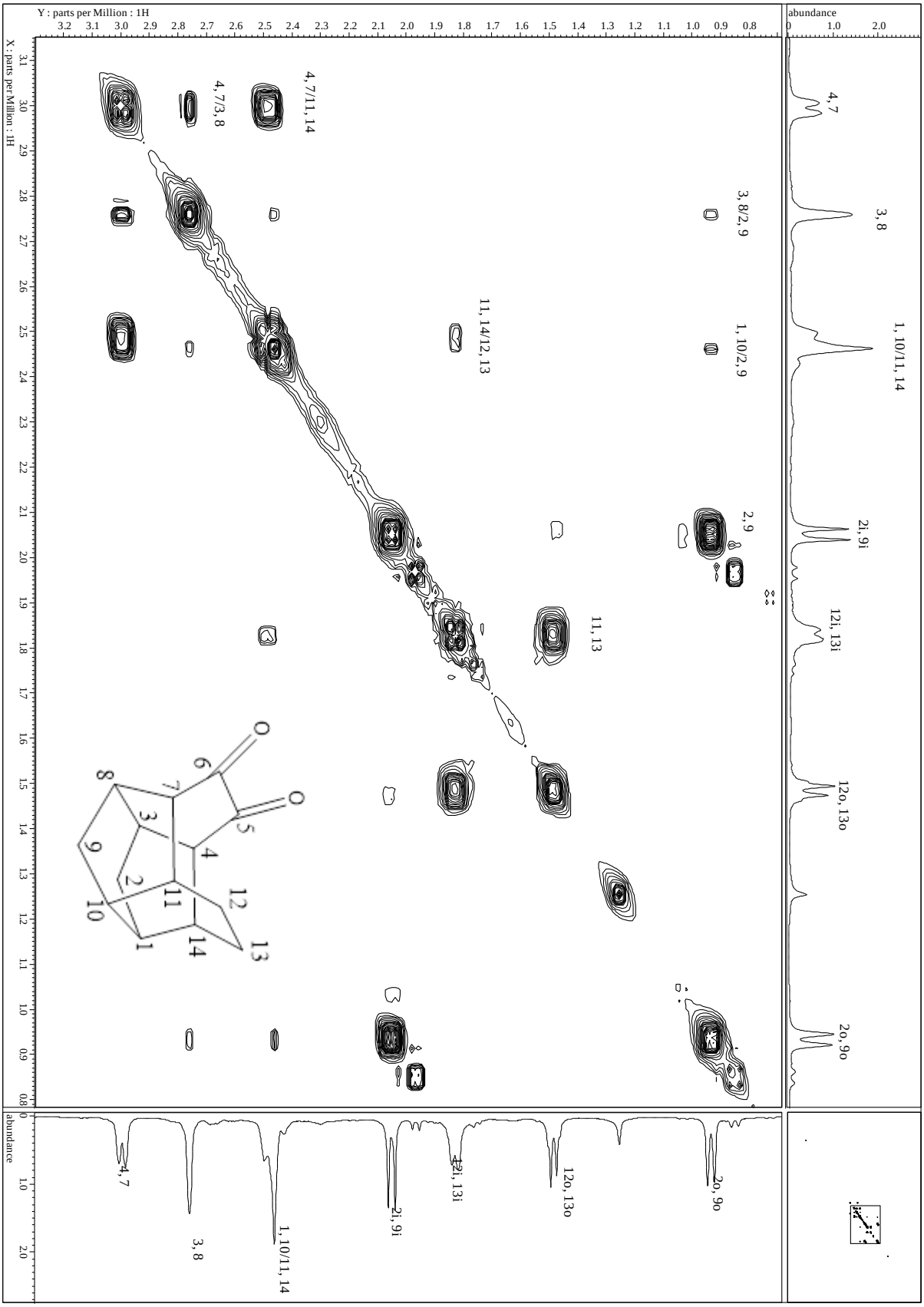
Y : parts per Million : 1H
X : parts per Million : 1H
abundance
4, 7
3, 8
1, 10/11, 14
2i, 9i
12i, 13i
12o, 13o
2o, 9o
3, 8/2, 9
1, 10/2, 9
2, 9
11, 13
11, 14/12, 13
4, 7/11, 14
4, 7/3, 8
O
O
1
2
3
4
5
6
7
8
9
10
11
12
13
14

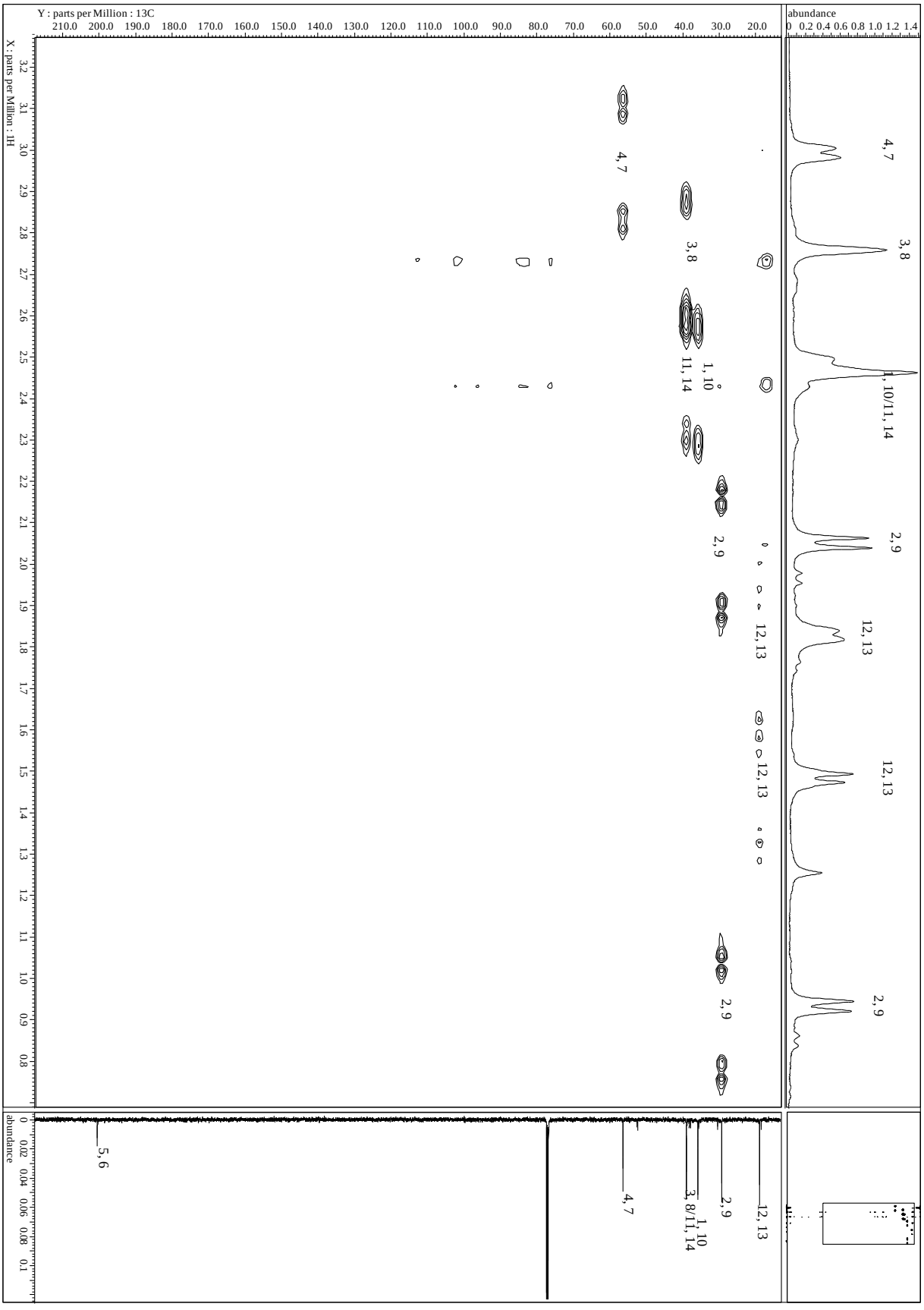
Y : parts per Million : 13C
X : parts per Million : 1H
abundance
4, 7
3, 8
1, 10/11, 14
2, 9
12, 13
5, 6

5.5.3 Preparation of Ene-Anhydride **228** and Saturated Anhydride **229**

General procedure for Baeyer-Villiger Oxidation: To a solution of dione **222** (16 mg, 0.074 mmol) in $CDCl_3$ (1.5 mL), MCPBA (16.6 mg, 0.096 mmol) was added and stirred for 1 hour until full conversion of **222** (based on GC/MS). The solution was stretched with water (10 mL) and extracted with DCM (3x10 mL). The combined organic phase was washed with $NaHCO_3$ (2x10 mL), dried ($MgSO_4$), and concentrated to give 95% clean anhydride **228** (17 mg, 95% yield).

13-oxapentacyclo[8.5.0.0^{3,8}.0^{4,15}.0^{7,11}]pentadec-5-ene-12,14-dione (228)

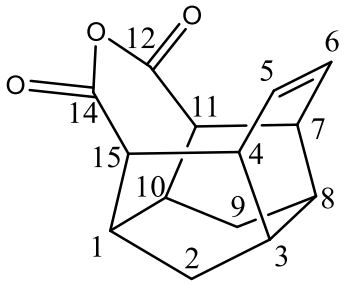

$C_{14}H_{14}O_3$ (230)

MP = 150.6-151.0 °C ($CDCl_3$)

IR (AT-IR): $\tilde{\nu}$ = 2930 (m, C-H), 1731 (s, C=O), 1460 (w, C-C), 1166 (s), 1020 (s), 783 (m) cm^{-1}.

^{1}H-NMR ($CDCl_3$, 500 MHz): δ = 6.23 (m, 2H, H-5, -6), 3.58 (dt, 2H, H-11, -15), 3.23 (m, 2H, H-4, -7), 2.81 (s_{app}, 2H, H-1, -10), 2.35 (s_{app}, 2H, H-3, -8), 2.01 (d, 2H, H-2i, -9i), 0.93 (s, 2H, H-2o, -9o) ppm;

$^2J_{H\text{-}2i,\ -2o} = {}^2J_{H\text{-}9i,\ -9o}$ = 12.3 Hz.

^{13}C-NMR ($CDCl_3$, 100.7 MHz): δ = 167.9 (C-12, -14), 131.9 (C-5, -6), 57.3 (C-11, -15), 40.2 (C-4, -7), 38.3 (C-1, -10), 36.6 (C-3, -8), 30.3 (C-2, -9) ppm.

Spectra:

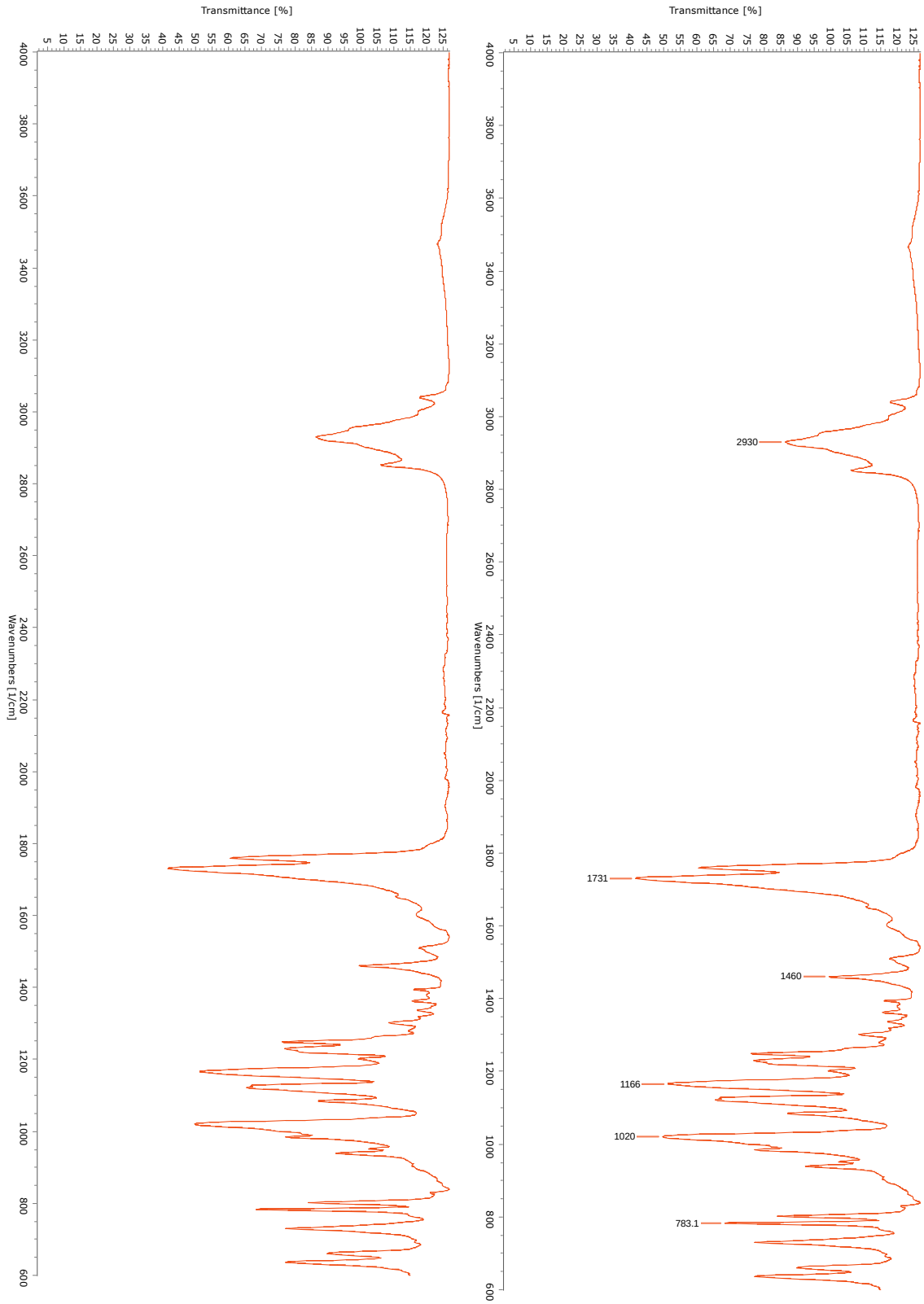
Transmittance [%]
Wavenumbers [1/cm]
2930
1731
1460
1166
1020
783.1

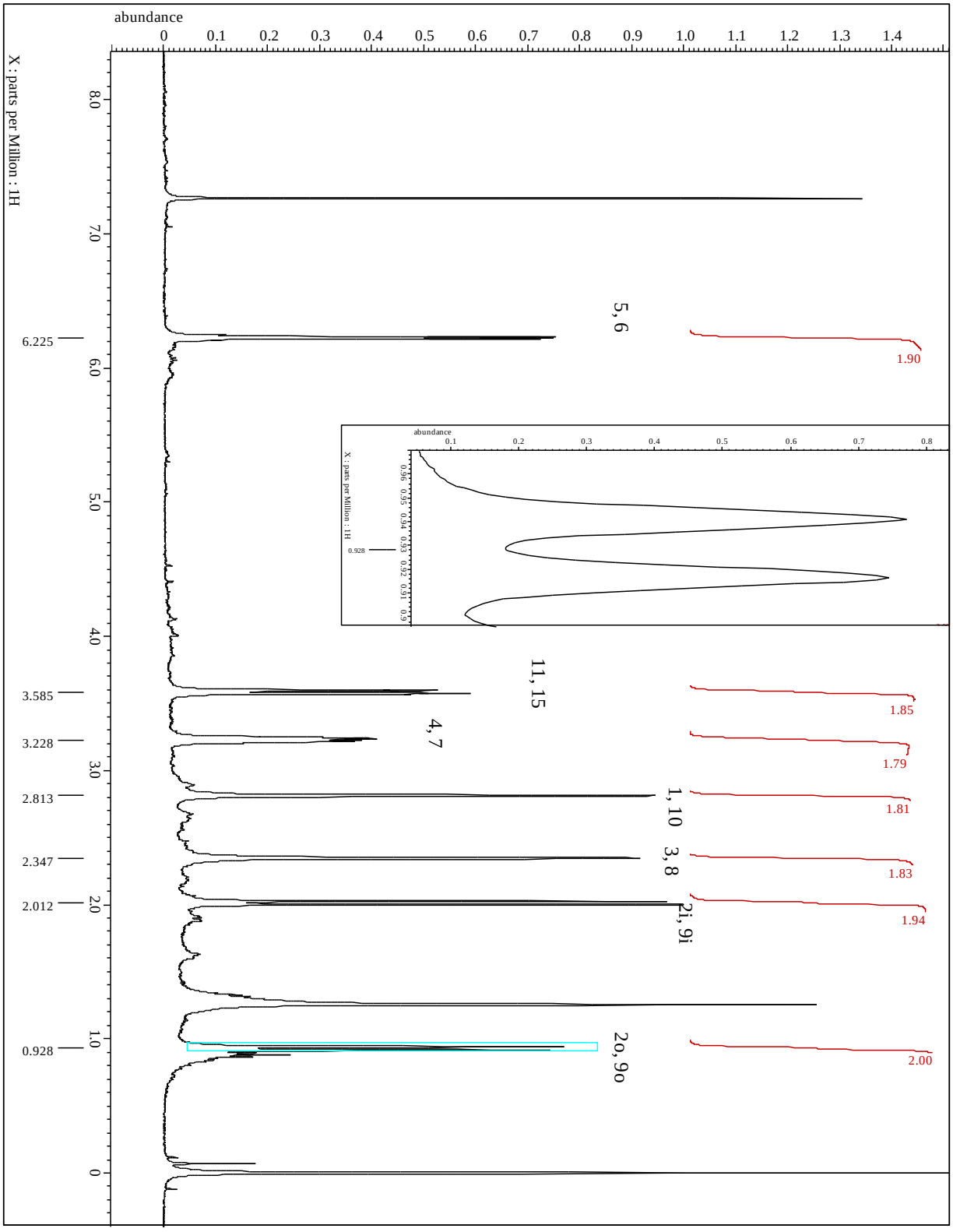
abundance
X : parts per Million : 1H
6.225
3.585
3.228
2.813
2.347
2.012
0.928
5, 6
11, 15
4, 7
1, 10
3, 8
2i, 9i
2o, 9o
1.90
1.85
1.79
1.81
1.83
1.94
2.00

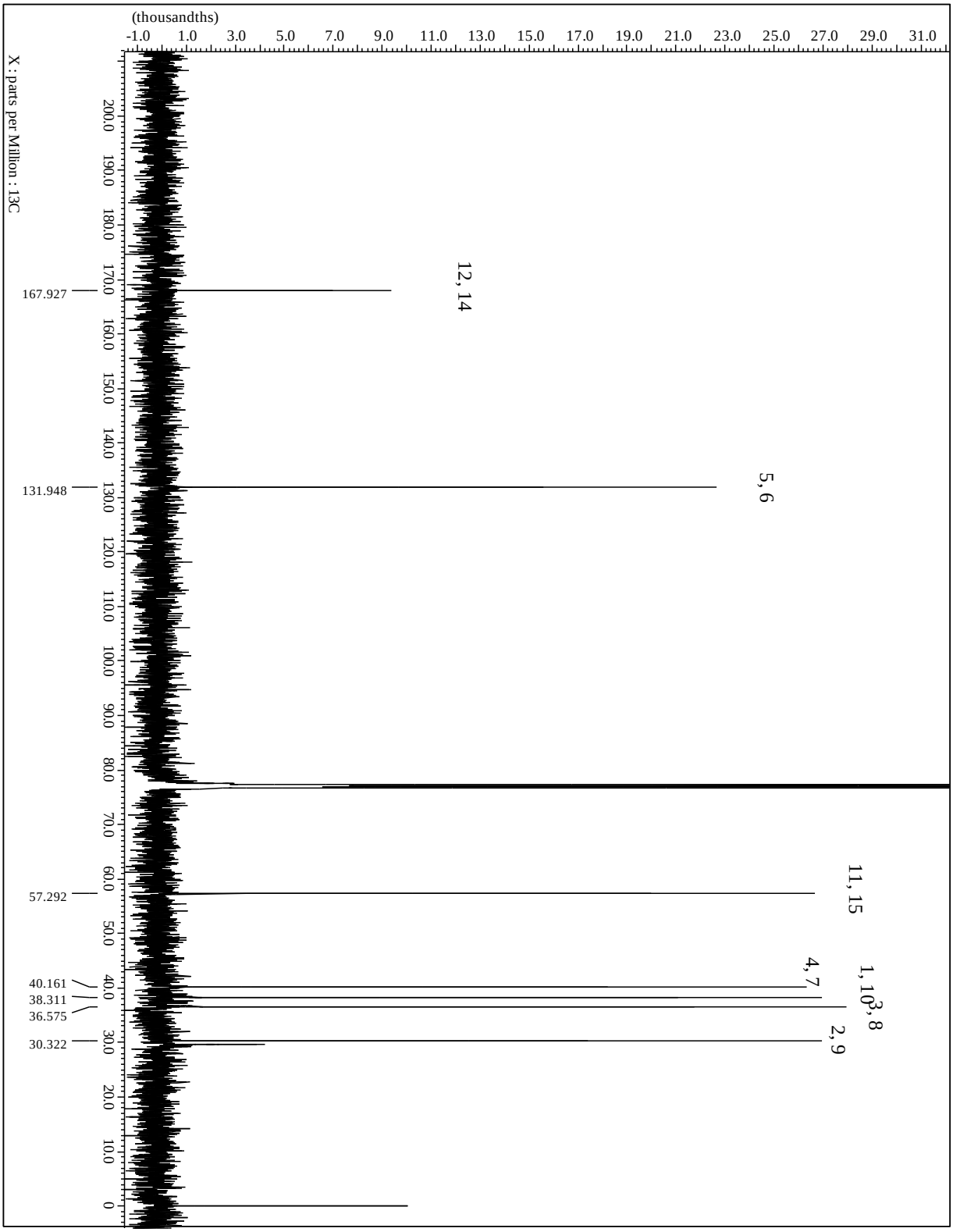
(thousandths)
-1.0 1.0 3.0 5.0 7.0 9.0 11.0 13.0 15.0 17.0 19.0 21.0 23.0 25.0 27.0 29.0 31.0
X : parts per Million : 13C
200.0 190.0 180.0 170.0 160.0 150.0 140.0 130.0 120.0 110.0 100.0 90.0 80.0 70.0 60.0 50.0 40.0 30.0 20.0 10.0 0
167.927
131.948
57.292
40.161
38.311
36.575
30.322
12, 14
5, 6
11, 15
4, 7
1, 10
3, 8
2, 9

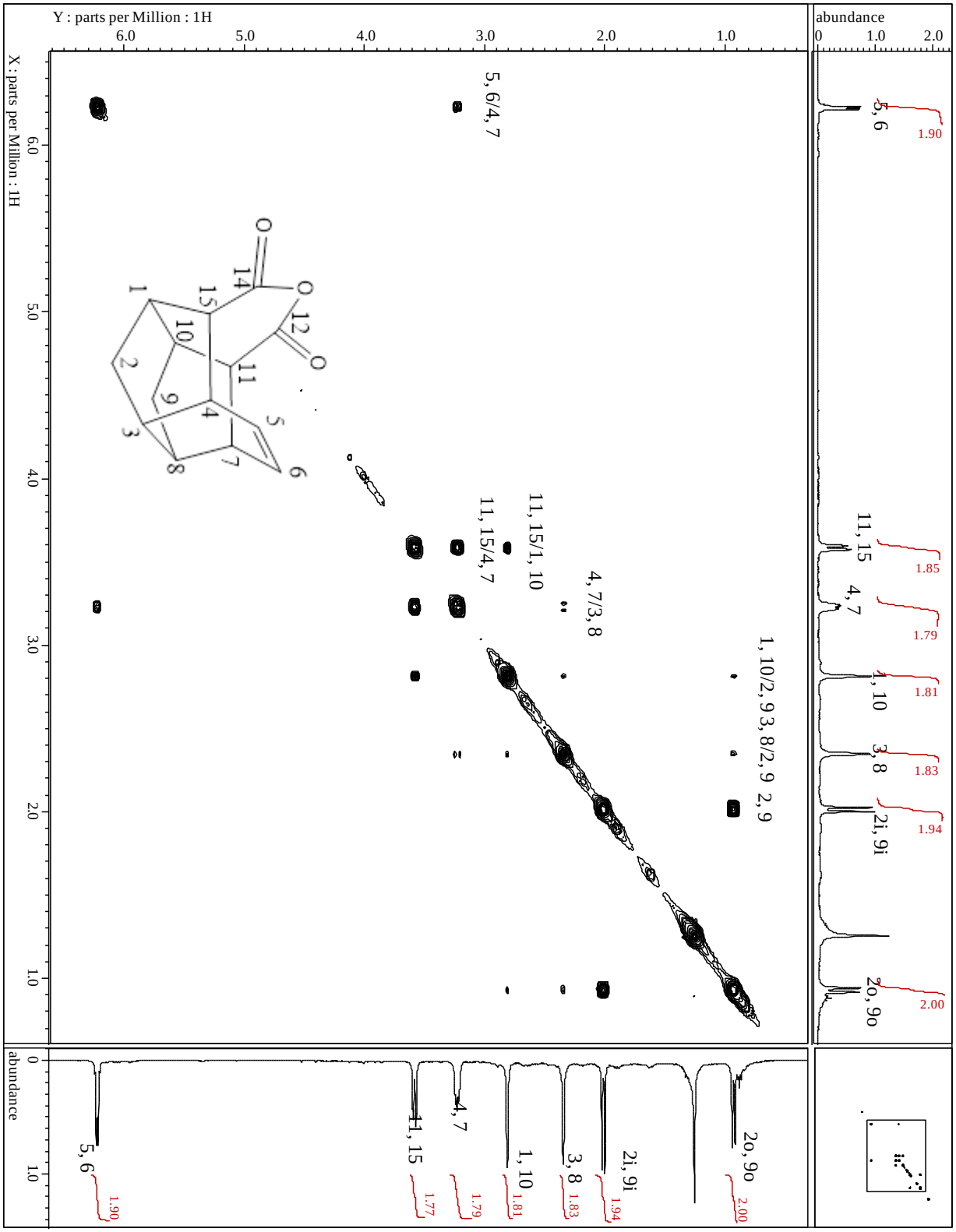
abundance
0
1.0
2.0
5, 6
1.90
11, 15
1.85
4, 7
1.79
1, 10
1.81
3, 8
1.83
2i, 9i
1.94
2o, 9o
2.00
Y : parts per Million : 1H
6.0
5.0
4.0
3.0
2.0
1.0
X : parts per Million : 1H
5, 6/4, 7
11, 15/1, 10
11, 15/4, 7
4, 7/3, 8
1, 10/2, 9 3, 8/2, 9 2, 9
O
O
O
O
1
2
3
4
5
6
7
8
9
10
11
12
14
15
abundance
0
1.0
2o, 9o
2.00
2i, 9i
1.94
3, 8
1.83
1, 10
1.81
4, 7
1.79
11, 15
1.77
5, 6
1.90

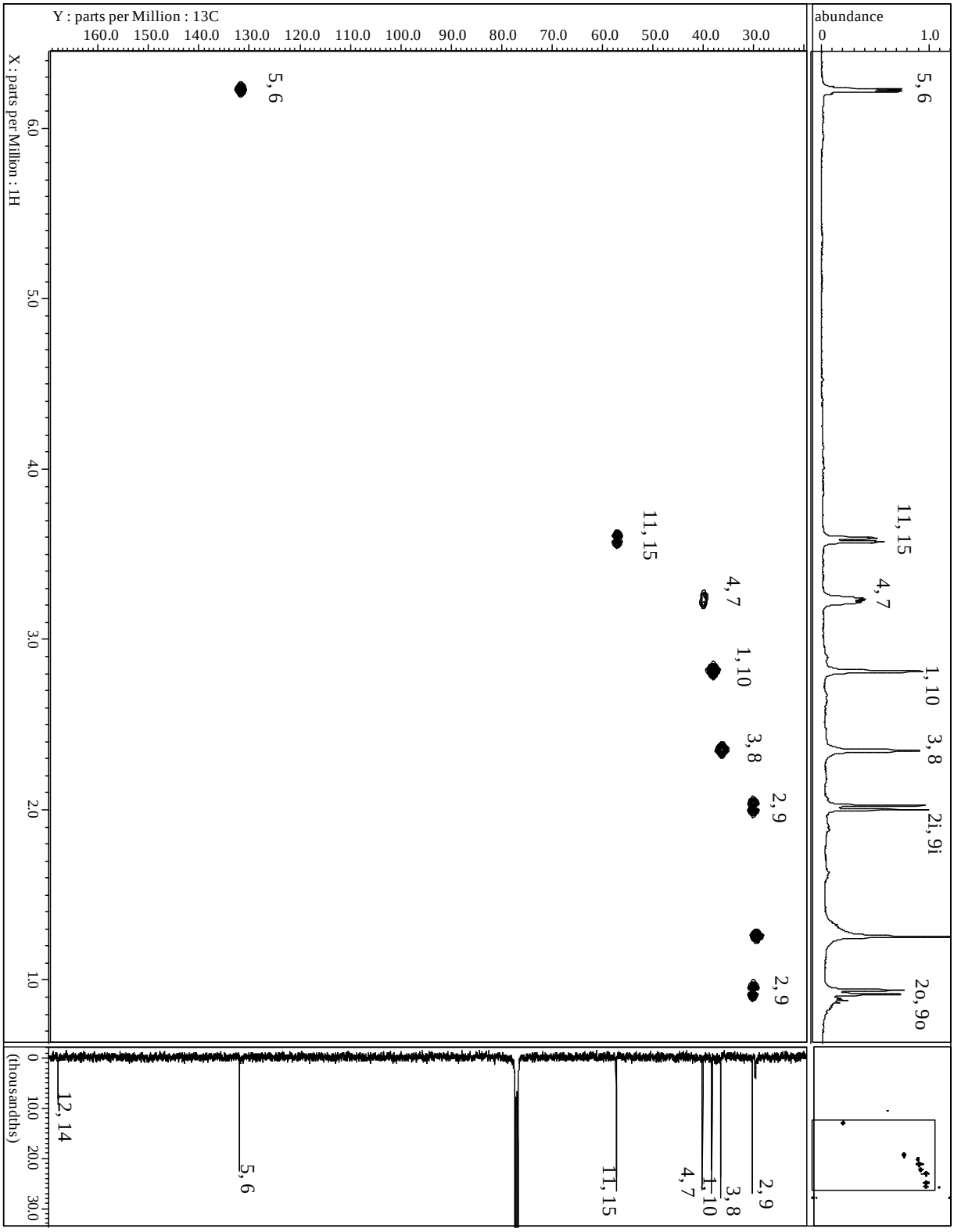
abundance
0
1.0
5, 6
11, 15
4, 7
1, 10
3, 8
2i, 9i
2o, 9o
Y : parts per Million : 13C
160.0 150.0 140.0 130.0 120.0 110.0 100.0 90.0 80.0 70.0 60.0 50.0 40.0 30.0
X : parts per Million : 1H
6.0 5.0 4.0 3.0 2.0 1.0
5, 6
11, 15
4, 7
1, 10
3, 8
2, 9
2, 9
(thousandths)
0 10.0 20.0 30.0
12, 14
5, 6
11, 15
2, 9
3, 8
1, 10
4, 7

13-oxapentacyclo[8.5.0.0^{3,8}.0^{4,15}.0^{7,11}]pentadecane-12,14-dione (229)

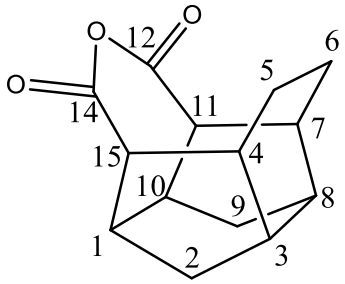

$C_{14}H_{16}O_3$ (232)

MP = Decomposition at 228.3 °C (decomposition product(s) melted at 234.4-235.2 ° C) ($CDCl_3$)

IR (AT-IR): $\tilde{\nu}$ = 2927 (m, C-H), 1729 (s, C=O), 1460 (w, C-C), 1161 (s), 1008 (s), 772 (m), 622 (w) cm^{-1}.

^{1}H-NMR ($CDCl_3$, 500 MHz): δ = 3.33 (dt, 2H, H-11, -15), 2.76 (s_{app}, 2H, H-1, -10), 2.67 (m, 2H, H-4, -7), 2.43 (s_{app}, 2H, H-3, -8), 1.96 (d, 2H, H-2i, -9i), 1.82 (m, 2H, H-5i, -6i), 1.76 (m, 2H, H-5o, -6o), 0.85 (d, 2H, H-2o, -9o) ppm;

$^2J_{\text{H-2i, -2o}} = {}^2J_{\text{H-9i, -9o}} =$ 12.1; $^3J_{\text{H-11, -15, H-1, -10}}$ = 12.5 Hz.

^{13}C-NMR ($CDCl_3$, 100.7 MHz): δ = 169.7 (C-12, -14), 52.4 (C-11, -15), 38.2 (C-1, -10), 37.9 (C-4, -7), 35.5 (C-3, -8), 30.4 (C-2, -9), 18.5 (C-5, -6) ppm.

Spectra:

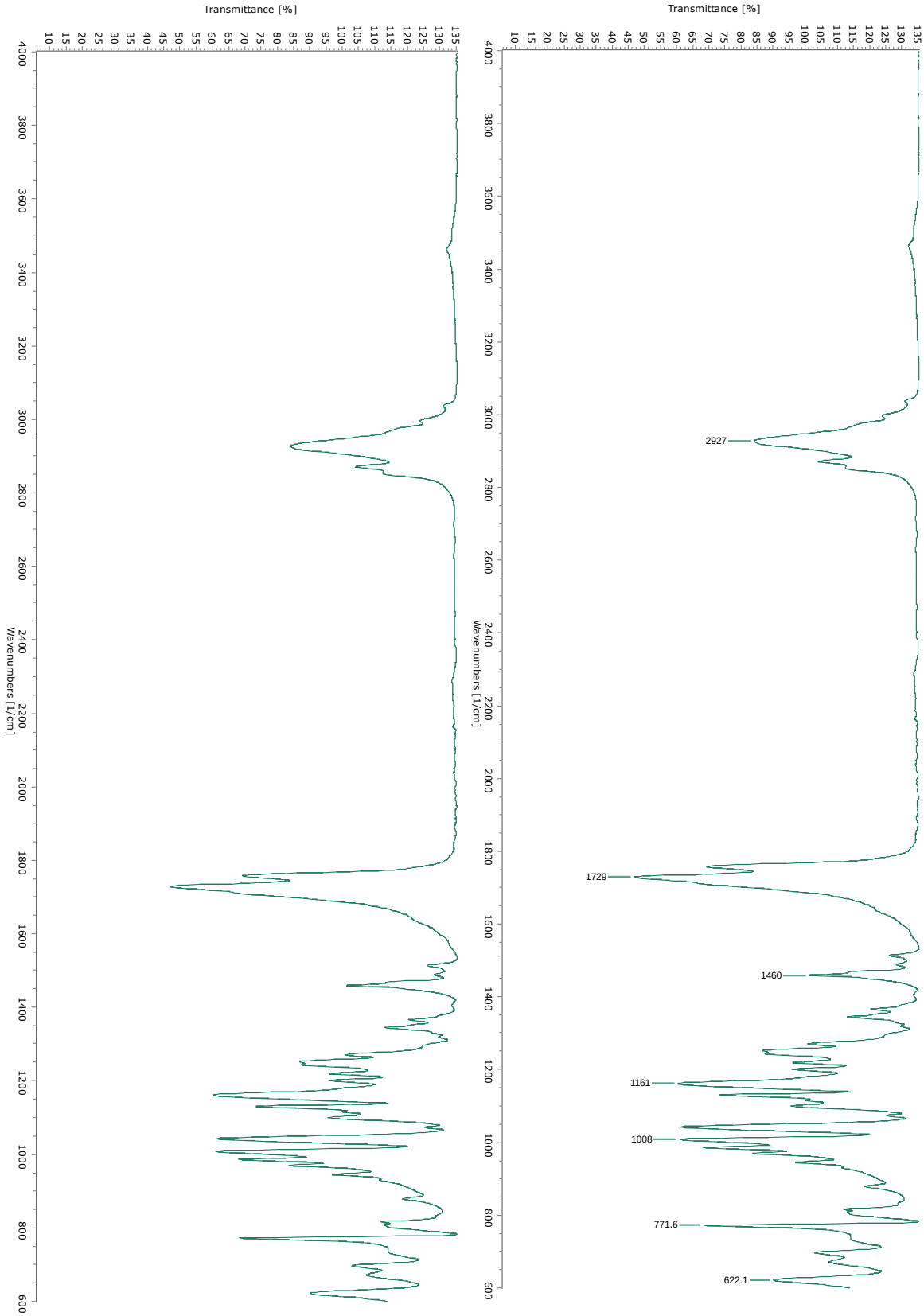
Transmittance [%]
Wavenumbers [1/cm]
2927
1729
1460
1161
1008
771.6
622.1

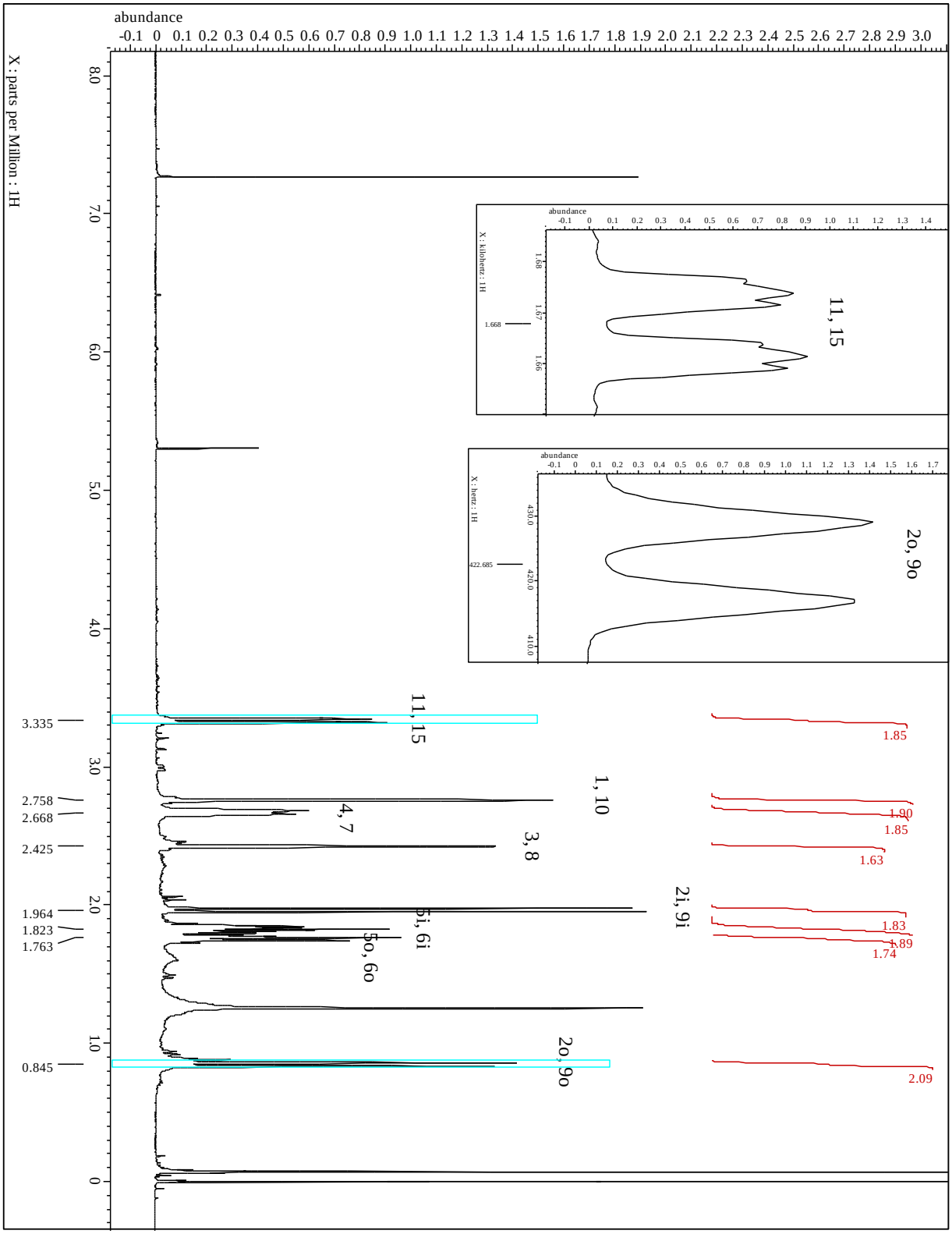
abundance
X : parts per Million : 1H
11, 15
1, 10
4, 7
3, 8
5i, 6i
5o, 6o
2o, 9o
2i, 9i
3.335
2.758
2.668
2.425
1.964
1.823
1.763
0.845
1.85
1.90
1.85
1.63
1.83
1.89
1.74
2.09
X : kilohertz : 1H
1.668
X : hertz : 1H
422.685

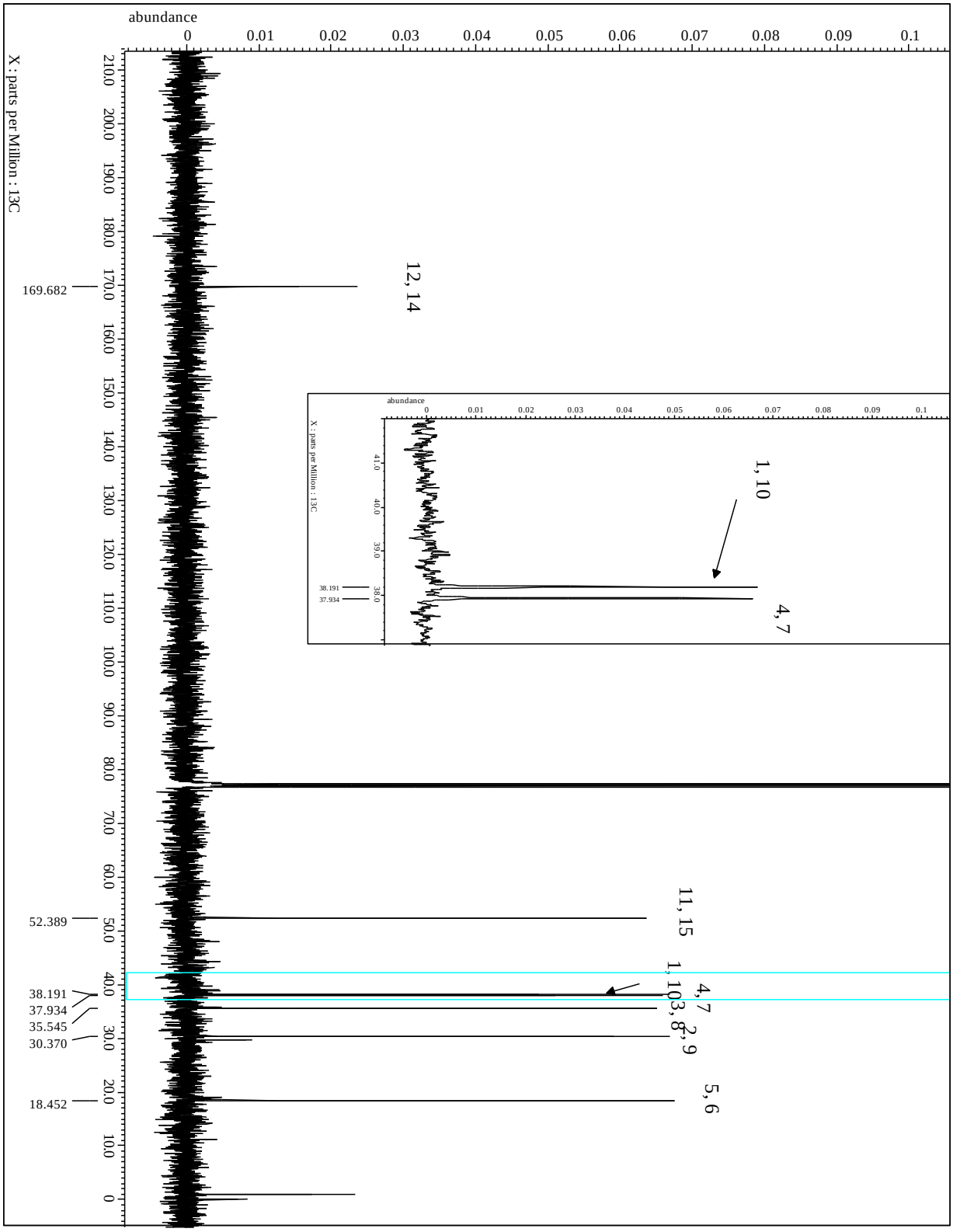
abundance
X : parts per Million : 13C
169.682
52.389
38.191
37.934
35.545
30.370
18.452
12, 14
11, 15
1, 10
4, 7
3, 8
2, 9
5, 6
1, 10
4, 7
38.191
37.934

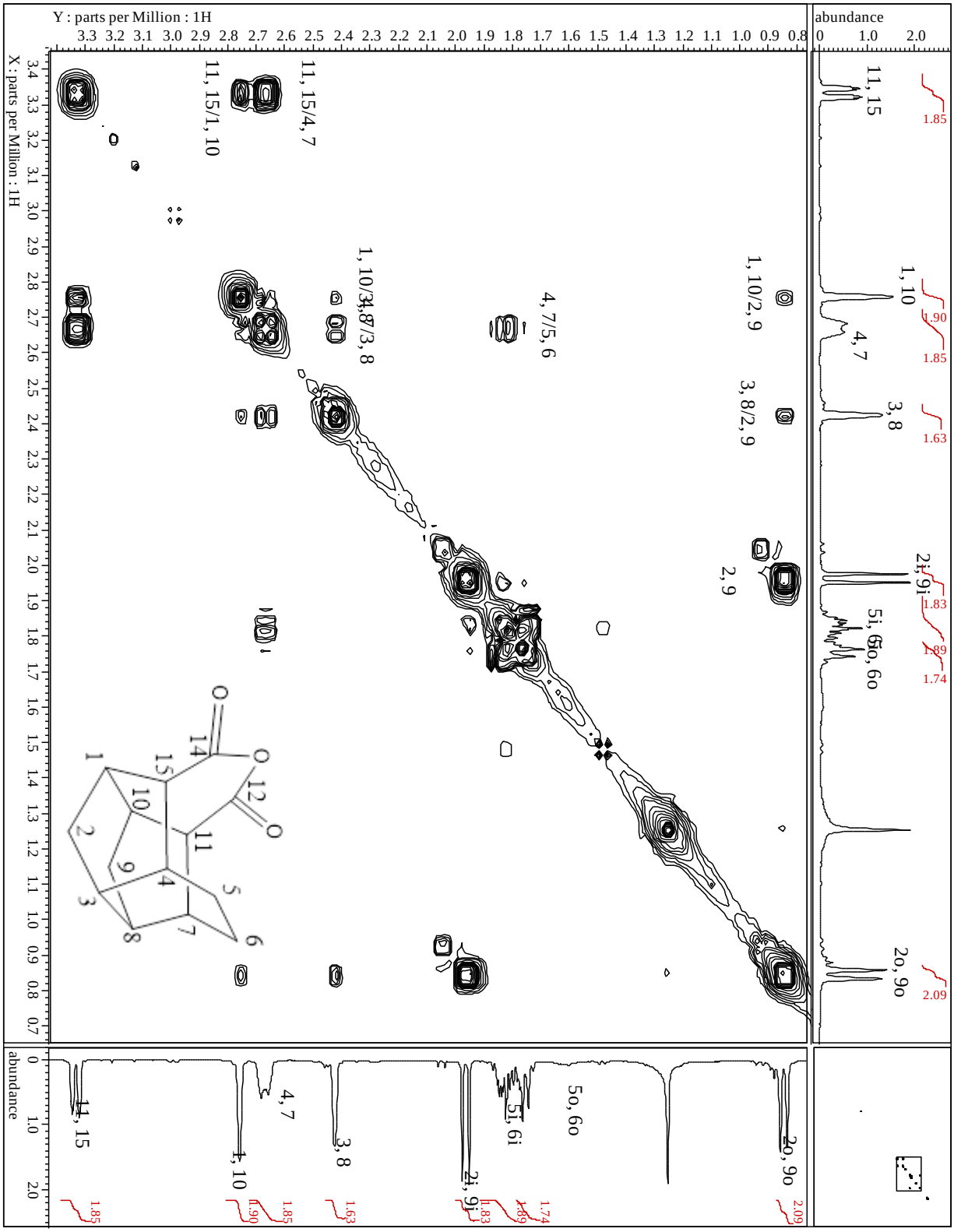
Y : parts per Million : 1H
X : parts per Million : 1H
abundance
11, 15
1, 10
4, 7
3, 8
2i, 9i
5i, 6i
5o, 6o
2o, 9o
1, 10/2, 9
3, 8/2, 9
2, 9
4, 7/5, 6
1, 10/3, 8
4, 7/3, 8
11, 15/4, 7
11, 15/1, 10
1.85
1.90
1.85
1.63
1.83
1.89
1.74
2.09
O
O
O
O
1
2
3
4
5
6
7
8
9
10
11
12
14
15

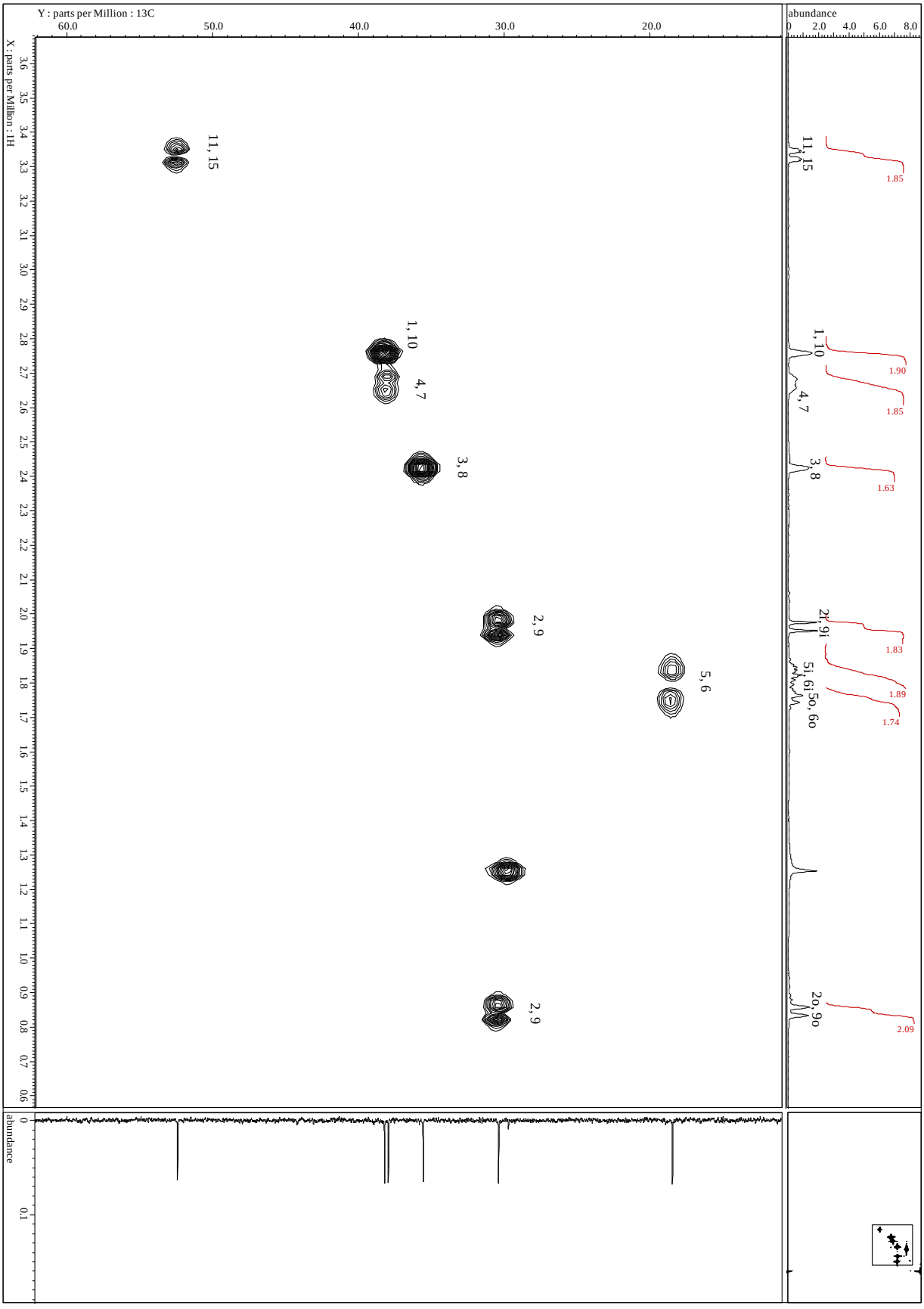
Y : parts per Million : 13C
60.0
50.0
40.0
30.0
20.0
X : parts per Million : 1H
3.6
3.5
3.4
3.3
3.2
3.1
3.0
2.9
2.8
2.7
2.6
2.5
2.4
2.3
2.2
2.1
2.0
1.9
1.8
1.7
1.6
1.5
1.4
1.3
1.2
1.1
1.0
0.9
0.8
0.7
0.6
11, 15
1, 10
4, 7
3, 8
2, 9
5, 6
2, 9
abundance
0
2.0
4.0
6.0
8.0
11, 15
1.85
1, 10
1.90
4, 7
1.85
3, 8
1.63
2f, 9i
1.83
5i, 6i
5o, 6o
1.89
1.74
2o, 9o
2.09
abundance
0
0.1

6 REFERENCES

1. Olah, G. A.; von R. Schleyer, P., *Cage Hydrocarbons*. Wiley: 1990.
2. Hoffmann, R.; Hopf, H., Learning from molecules in distress. *Angew. Chem. Int. Ed.* **2008,** *47* (24), 4474-81.
3. Srikrishna, A.; Sunderbabu, G., Hexacyclo[6.6.1.02,7.03,12.06,11.09,14]pentadecane and pentacyclo[8.4.0.03,8.03,14.07,11]tetradecane systems from decahydro[1,4;5,8]dimethanoanthracene-11,12-dione. *J. Org. Chem* **1987,** *52* (22), 5037-5039.
4. Chou, T.-C.; Lin, G.-H.; Wu, S.-C.; Bahekar, S. S., Synthesis of Endo,Endo-2.9-Dihydroxypentacyclo-[8.4.0.03,8.04,14.07,11]Tetradeca-5,12-Diene. *J. Chin. Chem. Soc.* **2008,** *55* (1), 171-182.
5. Mehta, G.; Padma, S., Synthetic studies towards prismanes: Seco-[6]-prismane. *Tetrahedron* **1991,** *47* (37), 7783-7806.
6. Mehta, G.; Padma, S.; Osawa, E.; Barbiric, D. A.; Mochizuki, Y., Strain energy considerations in the photochemical [π2 + π2] cage cyclisations. A case study en route to [6]-prismane. *Tetrahedron Lett.* **1987,** *28* (12), 1295-1298.
7. Mehta, G.; Padma, S., D2h-bishomohexaprismane ("garudane"). Design of the face-to-face 2 + 2 dimer of norbornadiene. *J. Am. Chem. Soc.* **1987,** *109* (23), 7230-7232.
8. Golobish, T. D.; Dailey, W. P., Synthesis and structure of bishomohexaprismanedione. *Tetrahedron Lett.* **1996,** *37* (19), 3239-3242.
9. Golobish, T. D. Synthetic approaches toward hexaprismane and heptaprismane (synthesis of bishomohexaprismanedione): Synthesis and structural properties of two biscyclopropenes. Ph.D., University of Pennsylvania, Ann Arbor, 1996.

10. Khoury, P. R.; Goddard, J. D.; Tam, W., Ring strain energies: substituted rings, norbornanes, norbornenes and norbornadienes. *Tetrahedron* **2004,** *60* (37), 8103-8112.

11. Duong, L.; Karanikas, H. C.; Watson, A. J.; Etzkorn, M.; Jones, D. S., Dichloro[(5,6:12,13-[eta]4)-pentacyclo[8.4.0.03,8.04,14.07,11]tetradeca-5,12-diene]platinum(II). *Acta Crystallogr., Sect. E.* **2006,** *62* (11), m2960-m2962.

12. Clarke, J. K. A.; McMahon, E.; Thomson, J. B.; Zeeh, B., Complexes of bicyclo [3.3.1]nona-2,6-diene with palladium(II), platinum(II) and rhodium(I). *J. Organomet. Chem.* **1971,** *31* (2), 283-287.

13. Lee, T. R.; Wierda, D. A.; Whitesides, G. M., The reduction of C* bonds proceeds with retention of configuration: stereochemical investigation of the heterogeneous reduction by dideuterium of (homohypostrophene)neopentyl(2-norbornyl)platinum(II) complexes on platinum black. *J. Am. Chem. Soc.* **1991,** *113* (23), 8745-8753.

14. carbenes. In *The IUPAC Compendium of Chemical Terminology*, 2014.

15. Skell, P. S.; Woodworth, R. C., Structure of Carbene, CH2. *J. Am. Chem. Soc.* **1956,** *78* (17), 4496-4497.

16. Xu, L.; Smith, W. B.; Brinker, U. H., Carbene rearrangements. 38. Functionalization of saturated hydrocarbons: selective insertion reactions of dihalocarbenes into carbon-hydrogen bonds adjacent to cyclopropane rings. *J. Am. Chem. Soc.* **1992,** *114* (2), 783-784.

17. Nemirowski, A.; Schreiner, P. R., Electronic Stabilization of Ground State Triplet Carbenes. *J. Org. Chem.* **2007,** *72* (25), 9533-9540.

18. Lee, E. P. F.; Dyke, J. M.; Wright, T. G., The lowest singlet–triplet gap in CCl2, CBr2 and CI2. *Chem. Phys. Lett.* **2000,** *326* (1), 143-150.

19. Wang, F.; Luo, T.; Hu, J.; Wang, Y.; Krishnan, H. S.; Jog, P. V.; Ganesh, S. K.; Prakash, G. K.; Olah, G. A., Synthesis of gem-difluorinated cyclopropanes and cyclopropenes: trifluoromethyltrimethylsilane as a difluorocarbene source. *Angew. Chem. Int. Ed.* **2011,** *50* (31), 7153-7.

20. von E. Doering, W.; Hoffmann, A. K., The Addition of Dichlorocarbene to Olefins. *J. Am. Chem. Soc.* **1954,** *76* (23), 6162-6165.

21. Lengel, R. K.; Zare, R. N., Experimental determination of the singlet-triplet splitting in methylene. *J. Am. Chem. Soc.* **1978,** *100* (24), 7495-7499.

22. Paquette, L. A.; James, D. R.; Klein, G., Impact of high-lying .sigma. orbitals and extensive through-bond interaction on chemical reactivity. 1. Convenient syntheses of hypostrophene and its susceptibility to rearrangement under electrophilic conditions. *J. Org. Chem.* **1978,** *43* (7), 1287-1292.

23. Klein, G.; Paquette, L. A., Impact of high-lying .sigma. orbitals and extensive through-bond interaction on chemical reactivity. 2. Solvolytic studies of hypostrophene derivatives. *J. Org. Chem.* **1978,** *43* (7), 1293-1298.

24. Brown, J. M., Long-range interactions. Part II. A model system for σ-interaction between allylic anion and olefin. *J. Chem. Soc. B* **1969,** (0), 868-872.

25. Elsässer, D.; Hassenrück, K.; Martin, H.-D.; Mayer, B.; Lutz, G.; Prinzbach, H., Small and Medium Rings, 771) Nonconjugated π,π Interactions Approaching Classical π,π Conjugation – PE-Spectroscopical Investigation of the 7,8;12,19-Diseco-1,16-dodecahedradiene System. *Chem. Ber.* **1991,** *124* (12), 2863-2869.

26. Sedelmeier, G.; Prinzbach, H.; Martin, H.-D., Cheminform Abstract: Homoconjugation And Photoreactivity In Fixed 1,5-Diene Structures. *Chem. Inf.-Dienst.* **1980,** *11*.

27. Yoshida, Z.; Tabushi, I.; Takahashi, N., Dichloromethyladamantanes. Formation via carbene insertion and hydrolytic rearrangement to homoadamantanone. *J. Am. Chem. Soc.* **1970,** *92* (22), 6670-6672.

28. Dehmlow, E. V.; Fastabend, U., Do the structures of phase-transfer catalysts influence dihalogenocarbene–carbenoid selectivities? *J. Chem. Soc., Chem. Commun.* **1993,** (16), 1241-1242.

29. Tabushi, I.; Aoyama, Y.; Takahashi, N.; Gund, T. M.; Schleyer, P. v. R., Dichloromethyldiamantanes, homodiamantanones, and homodiamantane. *Tetrahedron Lett.* **1973,** *14* (2), 107-110.

30. Goh, S.; Chan, K.; Kam, T.; Chong, H., Dihalocarbene insertions into carbon-hydrogen bonds of hydrocarbons and ethers. *Aust. J. Chem.* **1975,** *28* (2), 381-384.

31. Brinker, U. H.; Lin, G.; Xu, L.; Smith, W. B.; Mieusset, J.-L., Dihalocarbene Insertion Reactions into C−H Bonds of Compounds Containing Small Rings: Mechanisms and Regio- and Stereoselectivities. *J. Org. Chem.* **2007,** *72* (22), 8434-8451.

32. Goh, S. H., Dihalocarbene insertion experiment. *J. Chem. Educ.* **1975,** *52* (6), 399.

33. Dehmlow, E. V.; Gröning, C., Dioxa-cage and bridged compounds as possible precursors for tricyclo[5.5.0.04,10]dodeca-2,5,8,11-tetraene. *Tetrahedron* **1992,** *48* (1), 111-116.

34. Jefford, C. W.; Rossier, J.-C.; Zuber, J. A., A Simple Synthesis of Di- and Trihalobarbaralanes. *Angew. Chem. Int. Ed.* **1982,** *21* (7), 549-549.

35. Ni, C.; Hu, J., Recent Advances in the Synthetic Application of Difluorocarbene. *Synthesis* **2014,** *46* (07), 842-863.

36. Mąkosza, M.; Wawrzyniewicz, M., Reactions of organic anions. XXIV. Catalytic method for preparation of dichlorocyclopropane derivatives in aqueous medium. *Tetrahedron Lett.* **1969,** *10* (53), 4659-4662.

37. Preda, D. V. New chemistry and annulations of corannulene. Ph.D., Boston College, Ann Arbor, 2001.

38. Orpen, A. G.; Brammer, L.; Allen, F. H.; Kennard, O.; Watson, D. G.; Taylor, R., Appendix A: Typical Interatomic Distances in Organic Compounds and Organometallic Compounds and Coordination Complexes of the d- and f-block metals. In *Structure Correlation*, Volume 1, VCH Publishers, Inc., 1994; pp 752-858.

39. Van Der Waals Radius for all the elements in the Periodic Table. https://periodictable.com/Properties/A/VanDerWaalsRadius.an.html (accessed 01/18/22).

40. von R. Schleyer, P., A Simple Preparation Of Adamantane. *J. Am. Chem. Soc.* **1957,** *79* (12), 3292-3292.

41. von R. Schleyer, P.; Donaldson, M. M., The Relative Stability of Bridged Hydrocarbons. II. endo- and exo-Trimethylenenorbornane. The Formation of Adamantane1,2. *J. Am. Chem. Soc.* **1960,** *82* (17), 4645-4651.

42. Moore, R. E., Encyclopedia of chemical technology. Supplement volume: Adamantane to units. In *Encyclopedia of chemical technology. Supplement volume: Adamantane to units*, Vol. Supplement Volume: Adamantane to units; Interscience Publishers, 1971, pp 1-15.

43. Verevkin, Sergei P.; Kümmerlin, M.; Hickl, E.; Beckhaus, H.-D.; Rüchardt, C.; Kozhushkov, Sergei I.; Haag, R.; Boese, R.; Benet-Bucholz, J.; Nordhoff, K.; Meijere, Armin d., Thermochemical and X-ray Crystallographic Investigations of Some (CH)10

Hydrocarbons: Basketene, Nenitzescu's Hydrocarbon, and Snoutene. *Eur. J. Org. Chem.* **2002,** *2002* (14), 2280-2287.

44. Arts, N. B. M.; Klunder, A. J. H.; Zwanenburg, B., Chemistry of strained polycyclic compounds—IX11Part VIII, N.B.M. Arts, A.J.H. Klunder and B. Zwanenburg, Tetrahedron Letters 2359 (1976).: The synthesis and homoketonization of 4-substituted homocuneane acetates. *Tetrahedron* **1978,** *34* (8), 1271-1279.

45. Eaton, P. E.; Cassar, L.; Halpern, J., Silver(I)- and palladium(II)-catalyzed isomerizations of cubane. Synthesis and characterization of cuneane. *J. Am. Chem. Soc.* **1970,** *92* (21), 6366-6368.

46. Paquette, L. A.; Stowell, J. C., Silver ion catalyzed rearrangements of strained .sigma. bonds. Application to the homocubyl and 1,1'-bishomocubyl systems. *J. Am. Chem. Soc.* **1970,** *92* (8), 2584-2586.

47. Eaton, P. E.; Cassar, L.; Hudson, R. A.; Hwang, D. R., Synthesis of homopentaprismane and homohypostrophene and some comments on the mechanism of metal ion catalyzed rearrangements of polycyclic compounds. *J. Org. Chem.* **1976,** *41* (8), 1445-1448.

48. Dauben, W. G.; Schallhorn, C. H.; Whalen, D. L., Synthesis and rearrangement of strained cage molecules. *J. Am. Chem. Soc.* **1971,** *93* (6), 1446-1452.

49. Wiberg, K. B., Small Ring Bicyclo[n.m.0]alkanes. In *Advances in Alicyclic Chemistry*, Vol. 2; Elsevier, 1968; pp 185-254.

50. Paquette, L. A.; Boggs, R. A.; Ward, J. S., Silver(I) ion catalyzed rearrangements of strained .sigma. bonds. XXX. Rhodium(I)- and palladium(II)-promoted rearrangements of homocubanes. Comparison of kinetic reactivity and product distribution with substituent alteration. *J. Am. Chem. Soc.* **1975,** *97* (5), 1118-1124.

51. Marchand, A. P.; Chou, T.-C.; Ekstrand, J. D.; Van der Helm, D., Synthesis of tetracyclo[6.3.0.04,11.05,9]undeca-2,6-diene, 10-oxatetracyclo[6.3.0.04,11.05,9]undeca-2,6-diene, and hexacyclo[5.4.0.02,6.04,11.05,9.08,10]undecane. Structure of syn-4, syn-7-diiodopentacyclo[6.3.0.02,6.03,10.05,9]undecane. Synthesis and rhodium(I)-promoted rearrangement. *J. Org. Chem.* **1976,** *41* (8), 1438-1444.

52. Dong, D. C., An easy synthesis of two cage hydrocarbons. *J. Chem. Educ.* **1982,** *59* (8), 704.

53. Stille, J. K.; Kasper, P. R.; Witherell, D. R., Tetracyclic Dienes. II. Acid-catalyzed Rearrangement of 1,4,4a,5,8,8a-Hexa-hydro-exo-endo-1,4,5,8-dimethanonaphthalene (I)1. *J. Org. Chem.* **1963,** *28* (3), 682-686.

54. De Vries, L.; Winstein, S., Neighboring Carbon and Hydrogen. XXXIX.1 Complex Rearrangements of Bridged Ions. Rearrangement Leading to the Bird-cage Hydrocarbon1. *J. Am. Chem. Soc.* **1960,** *82* (20), 5363-5376.

55. Dong, D. C.; Edward, J. T., The reaction of potassium iodide in polyhydrogen fluoride – pyridine with two cage diols. A simple synthesis of tetracyclo[6.3.0.04,11. 05,9]undeca-2,6-diene ("homohypostrophene"). *Can. J. Chem.* **1980,** *58* (13), 1324-1326.

56. Fukunaga, T.; Clement, R. A., Thermal and base-catalyzed isomerizations of birdcage and half-cage compounds. *J. Org. Chem.* **1977,** *42* (2), 270-275.

57. Perni, R. B., Amberlyst-15 as a Convenient Catalyst for Chemoselective Thioacetalization. *Synth. Commun.* **1989,** *19* (13-14), 2383-2387.

58. Ballini, R.; Bosica, G.; Maggi, R.; Mazzacani, A.; Righi, P.; Sartori, G., Amberlyst® 15 as a Mild, Chemoselective and Reusable Heterogeneous Catalyst for the Conversion of Carbonyl Compounds to 1,3-Oxathiolanes. *Synthesis* **2004,** *2001* (12), 1826-1829.

59. Maerker, G.; Haeberer, E. T., Direct cleavage of internal epoxides with periodic acid. *J. Am. Oil Chem. Soc.* **1966,** *43* (2), 97-100.

60. Mehta, G.; Vidya, R., Oxa Bowls: Synthesis of New Tetraoxa-Cages and Their C−H···O-Mediated Solid-State Architecture. *J. Org. Chem.* **2000,** *65* (11), 3497-3502.

61. D. Gernon, M.; Wu, M.; Buszta, T.; Janney, P., Environmental benefits of methanesulfonic acid . Comparative properties and advantages. *Green Chem.* **1999,** *1* (3), 127-140.

62. Paquette, L. A.; Balogh, D. W., An expedient synthesis of 1,16-dimethyldodecahedrane. *J. Am. Chem. Soc.* **1982,** *104* (3), 774-783.

63. Bosse, D.; de Meijere, A., Bridgehead Cations of Tricyclo[5.2.1.04, 10]deca-2,5,8-triene (Triquinacene). *Angew. Chem. Int. Ed.* **1976,** *15* (9), 557-558.

64. Bischof, P., Stability of Triquinacenyl Cations and Triquinacenyl Radicals. *Angew. Chem. Int. Ed.* **1976,** *15* (9), 556-557.

65. Schleyer, P. V. R.; Bingham, R. C., Calculation of bridgehead reactivities. *J. Am. Chem. Soc.* **1971,** *93* (13), 3189-3199.

66. Paquette, L. A.; Begley, W. J.; Balogh, D.; Wyvratt, M. J.; Bremner, D., Topologically spherical molecules. Rearrangement reactions of functionalized C2-symmetric hexaquinane systems and synthesis of (C2)-dioxa-C20-octaquinane, a heterocyclic trisecododecahedrane. *J. Org. Chem.* **1979,** *44* (21), 3630-3638.

67. Marchand, A. P.; Alihodžić, S.; Ganguly, B., Photochemical Chlorocarbonylation of HCTD by Oxalyl Chloride. Carbocation-Mediated Rearrangement of HCTD Derivatives to Novel, Substituted Heptacyclopentadecanes. *J. Org. Chem.* **1998,** *63* (23), 8390-8396.

68. Prinzbach, H.; Sedelmeier, G.; Martin, H.-D., Geometrical Dependence of [2π+2σ]Photocycloaddition. *Angew. Chem. Int. Ed.* **1977,** *16* (2), 103-104.

69. Stuparu, M.; Gramlich, V.; Stanger, A.; Schlüter, A. D., Double-Stranded Cycles: Toward C84's Belt Region. *J. Org. Chem.* **2007,** *72* (2), 424-430.

70. Karakaya, B.; Claussen, W.; Gessler, K.; Saenger, W.; Schlüter, A. D., Toward Dendrimers with Cylindrical Shape in Solution. *J. Am. Chem. Soc.* **1997,** *119* (14), 3296-3301.

71. Gharpure, S. J.; Porwal, S. K., Synthesis of Oxa-, Aza- and Thia-Bowls and Cages. *Org. Prep. Proced. Int.* **2013,** *45* (2), 81-153.

72. Lin, C.-C.; Wu, H.-J., Formation of Tetraacetal Oxa-Cages and Convex Oxa-Cages on Ozonolysis of Bicyclo[2.2.2] Octenes. *J. Chin. Chem. Soc.* **1995,** *42* (5), 815-820.

73. Mehta, G.; Vidya, R., Oxa-bowls: The pentaoxa[5]peristylane. *Tetrahedron Lett.* **1997,** *38* (23), 4173-4176.

74. Mehta, G.; Vidya, R., Oxa Bowls: Studies Toward Hexaoxa-[6]-peristylane. Synthesis of a Seco-Derivative of Hexaoxa-[6]-peristylane. *J. Org. Chem.* **2001,** *66* (21), 6913-6918.

75. Zhang, G.; Mastalerz, M., Organic cage compounds--from shape-persistency to function. *Chem. Soc. Rev.* **2014,** *43* (6), 1934-47.

76. Wu, C.-Y.; Lin, C.-C.; Lai, M.-C.; Wu, H.-J., Synthesis of Novel Triacetal Trioxa-Cage Compounds by Ozonolysis of Bicyclo[2.2.1]Heptenes and Bicyclo[2.2.2]Octenes. *J. Chin. Chem. Soc.* **1996,** *43* (2), 187-194.

77. Schroeder, M., Osmium tetraoxide cis hydroxylation of unsaturated substrates. *Chem. Rev.* **1980,** *80* (2), 187-213.

78. VanRheenen, V.; Kelly, R. C.; Cha, D. Y., An improved catalytic OsO4 oxidation of olefins to cis-1,2-glycols using tertiary amine oxides as the oxidant. *Tetrahedron Lett.* **1976,** *17* (23), 1973-1976.

79. Tomioka, K.; Nakajima, M.; Iitaka, Y.; Koga, K., Mechanistic aspects of asymmetric cis-dihydroxylation of olefins with osmium tetroxide employing a C2-symmetric chiral diamine. *Tetrahedron Lett.* **1988,** *29* (5), 573-576.

80. Murty, B. A. R. C.; Pinkos, R.; Spurr, P. R.; Fessner, W.-D.; Lutz, G.; Fritz, H.; Hunkler, D.; Prinzbach, H., The Pagodane Route to Dodecahedranes Unsaturated (Hyperstable) and Saturated Bissecododecahedranes. *Chem. Ber.* **1992,** *125* (7), 1719-1739.

81. Suzuki, T.; Iida, K.; Wada, K.; Kondo, T.; Mitsudo, T.-a., Catalytic oxidation of pentacyclo[6.6.02,6. 03,13. 010,14]tetradeca-4,11-diene. Syntheses of novel polyfunctional half-open cage compounds. *Tetrahedron Lett.* **1999,** *40* (15), 2997-3000.

82. Isono, N.; Mori, M., Total Synthesis of (-)-Cephalotaxine. *J. Org. Chem.* **1995,** *60* (1), 115-119.

83. J. Chow, T.; Hon, Y.-S.; Jen, C.-C.; Liu, S.-S.; Chern, J.-H.; Lin, K.-J., Chemistry of cage-shaped hydrocarbons. Reactions of pentacyclo[6.6.0.02,6.03,13.010,14]tetradecane-4,11-diene. *J. Chem. Soc., Perkin Trans. 1* **1998,** (6), 1095-1100.

84. Kobayashi, T.; Kobayashi, S., Cyclovoltammetric Investigation into the Homoconjugation of Plural Pyrazine Rings Linked by Bicyclo[2.2.2]octadiene Spacers. *Eur. J. Org. Chem.* **2002,** *2002* (13), 2066-2073.

85. Hirao, K.-i.; Miura, H.; Hoshino, H.; Yonemitsu, O., Baeyer-villiger oxidation via carbocations in a strained cage system. *Tetrahedron Lett.* **1976,** *17* (43), 3895-3898.

86. Mehta, G.; Pandey, P. N.; Ho, T.-L., Regiospecific Baeyer-Villiger oxidation of polycyclic ketones with ceric ion. *J. Org. Chem.* **1976,** *41* (6), 953-956.

87. Acar, H. Y.; Jensen, J. J.; Thigpen, K.; McGowen, J. A.; Mathias, L. J., Evaluation of the Spacer Effect on Adamantane-Containing Vinyl Polymer Tg's. *Macromolecules* **2000,** *33* (10), 3855-3859.

88. Zu, S.-Z.; Sun, X.-X.; Liu, Y.; Han, B.-H., Supramolecular Surface Modification and Solubilization of Single-Walled Carbon Nanotubes with Cyclodextrin Complexation. *Chem.: Asian J.* **2009,** *4* (10), 1562-1572.

89. Evtushenko, A. V.; Molchanova, M. S.; Smirnov, B. B.; Shlyapochnikov, V. A., Computer generation and theoretical study of alicyclic caged structures without small-size cycles. *Russ. Chem. Bull.* **1996,** *45* (10), 2302-2308.